

THE UNIVERSITY OF HULL

*"IR LASER PHOTOCHEMISTRY OF ALKANOLS  
AND 3,3-DIMETHYLOXETANE"*

being a Thesis submitted for the Degree of  
Doctor of Philosophy  
in the University of Hull

by

Margaret Bishop, B.Sc.

August 1991

**To my husband, Gary**

**Summary of the Thesis submitted for the Ph.D. Degree in Chemistry**

**by**

**Margaret Bishop, B.Sc.**

**on**

**"IR Laser Photochemistry of Alkanols and 3,3-Dimethyloxetane"**

In this work, a pulsed CO<sub>2</sub> laser was used to excite methanol, ethanol, propan-2-ol, butan-2-ol, *t*-butanol, pentan-2-ol, hexan-2-ol, and 3,3-dimethyloxetane in order to study how these molecules absorb laser energy and decompose. The dependence of absorbed energy and fractional yield on laser parameters such as irradiating wavelength, fluence and pulse type, and on reactant molecular size, pressure and diluent, was examined.

The absorbed energy was measured using the optoacoustic (OA) technique. A new method for calibrating the OA cell was developed and is described in full in the thesis. The approach enables calibration to be extended to lower absorption levels (about 200 μJ for a signal-to-noise ratio of six) than is possible with the more usual transmission methods, and was found to be capable of measuring as little as 5 μJ. A particular advantage of the technique, is that it is simple, rapid, and provides an immediate visual indication of the absorption level.

It is observed, for all reactants studied, that the absorption cross-section at low pressure was less than at high pressure, but that the difference diminishes with molecular size with the absorption cross-section taking on a value comparable to that of the small signal, broadband cross-section. These findings are consistent with the explanation that rotational hole-burning exists, but decreases in importance as the molecular size, and hence density of states, increases. As the fluence is varied, the absorption cross-section is found to increase with decreasing fluence towards the small signal, broadband value. With increasing molecular size the increase is less noticeable, and the absorption cross-section takes on the value comparable to that of the small signal, broadband cross-section.

With increasing alkanol molecular size, it is observed that the major decomposition products can always be explained in terms of a molecular elimination channel i.e. one of dehydration. Also, the number of minor products and their yields both increase. It is believed that most of the minor products arise as a consequence of carbon-carbon fission processes, with minor contributions due to molecular elimination.

## ACKNOWLEDGEMENTS

Firstly, I should like to thank my supervisors Dr. G.A. Oldershaw, Dr. K.A. Holbrook, and Prof. P.E. Dyer for their guidance throughout my work. I extend special thanks to Mr. B.L. Tait, Mr. P. Monk, and the Applied Physics Mechanical and Electronic Workshops for their much appreciated and greatly valued technical support.

I also thank: Mr. G. Slater of the University of Hull Computer Centre, to whom I am much indebted for compiling the data analysis program; Mr. R. Teal for preparing the 3,3-dimethyloxetane, and for trying so hard to prepare sufficiently pure samples of other oxetanes; and Mr. A. Sinclair for producing the sputtered coatings for the 'identical' joulemeters.

I would like to thank Dr. R. Back of the National Research Council of Canada for his willingness to enter into discussions with a foreign student, and to thank my current employer, CAL Corporation, and my colleagues for their immense patience and generous support and encouragement.

Finally, I would like to acknowledge and thank my husband, Gary, for his artistic input, and, especially, for his support and encouragement during the course of this work.

# IR LASER ABSORPTION AND DECOMPOSITION OF ALKANOLS AND 3,3-DIMETHYLOXETANE

## CONTENTS

	PAGE
SUMMARY	(i)
ACKNOWLEDGEMENTS	(ii)
CONTENTS	(iii)
<b>1. INTRODUCTION</b>	<b>1</b>
1.0 RESEARCH AIMS AND THESIS LAYOUT	1
1.1 IR PHOTOCHEMISTRY - AN HISTORICAL OVERVIEW	2
1.1.1 The Role of Collisions	6
1.2 THE OPTOACOUSTIC TECHNIQUE - AN HISTORICAL REVIEW	12
1.3 OPTOACOUSTIC PROCESS - THEORY	13
1.3.1 Optoacoustic System Responsivity	15
1.3.2 Oscillatory Substructure	17
1.3.3 Frequency of Oscillatory Substructure	18
1.4 UNIMOLECULAR THEORY	19
1.4.1 Lindemann Theory	20
1.4.2 Hinshelwood Modification	23
1.4.3 Miscellaneous Developments	24
<b>2. EXPERIMENTAL SET-UP AND METHODOLOGY</b>	<b>30</b>
2.1 THE LASER	30
2.1.1 Single Longitudinal Mode Operation	31
2.1.2 Temporal Beam Profiles	32
2.1.3 Spatial Beam Profiles	36

2.1.4	Deconvolution	42
2.2	DESCRIPTION OF REACTION CELLS	43
2.2.1	Cell Alignment	48
2.3	OPTOACOUSTIC CELL CALIBRATION	48
2.3.1	The Differential Subtraction Method	50
2.3.2	Validity of Calibration Factor under Experimental Conditions	54
2.4	OPTICAL SET-UP	57
2.5	GAS ANALYSIS AND HANDLING	60
2.6	MATERIALS	61
2.6.1	Reactant Diluents	61
2.7	DATA ANALYSIS	63
<b>3.</b>	<b>ABSORPTION RESULTS</b>	<b>65</b>
3.1	METHANOL	68
3.2	ETHANOL	69
3.3	PROPAN-2-OL	72
3.4	BUTAN-2-OL	73
3.5	PENTAN-2-OL	74
3.6	PENTAN-3-OL	75
3.7	HEXAN-2-OL	76
3.8	3,3-DIMETHYLOXETANE	78
3.9	DECONVOLUTION	81
3.10	DISCUSSION	82
<b>4.</b>	<b>DECOMPOSITION RESULTS</b>	<b>92</b>
4.1	ETHANOL	96
4.1.1	Fluence Dependence	97
4.1.2	Pressure Dependence	98

4.1.3	Effect of Diluent	102
4.1.4	Effect of Pulse Type	103
4.1.5	Effect of Irradiating Wavelength	104
4.1.6	Minor Products	104
4.1.7	Discussion	106
4.2	PROPAN-2-OL	114
4.2.1	Fluence Dependence and Effect of Diluent	115
4.2.2	Pressure Dependence and Effect of Diluent	116
4.2.3	Discussion	116
4.3	BUTAN-2-OL	122
4.3.1	Fluence Dependence	123
4.3.2	Minor Products	127
4.3.3	Effect of Diluent	128
4.3.4	Pressure Dependence	128
4.3.5	Discussion	128
4.4	<i>tert</i> -BUTANOL	136
4.5	PENTAN-2-OL	138
4.5.1	Fluence Dependence	138
4.5.2	Effect of Diluent	140
4.5.3	Pressure Dependence	141
4.5.4	Discussion	143
4.6	PENTAN-3-OL	150
4.6.1	Fluence Dependence	150
4.6.2	Pressure Dependence	152
4.6.3	Discussion	152
4.7	HEXAN-2-OL	157
4.7.1	Fluence Dependence	157
4.7.2	Pressure Dependence	158
4.7.3	Discussion	159

4.8	3,3-DIMETHYLOXETANE	168
4.8.1	Fluence Dependence	169
4.8.2	Effect of Diluent	171
4.8.3	Effect of Pulse Type	171
4.8.4	Pressure Dependence	172
4.8.5	Discussion	174
<b>5. SUMMARISING DISCUSSION</b>		<b>177</b>
5.1	FUTURE WORK	180
<b>REFERENCES</b>		<b>183</b>
<b>APPENDICES</b>		
A1	Determination of the Speed of Sound from Optoacoustic Traces	A-1
A2	Energy Absorbed (Differential Ratio Method)	A-4
A3	Molecular Diffusion from the Focal Volume	A-5
A4	The Group Contribution Method	A-7
A5	Effect of Collisions on Absorption Linewidth	A-9

# 1. - INTRODUCTION

## 1.0 RESEARCH AIMS AND THESIS LAYOUT

This thesis documents the results of experiments carried out over the period October 1983 to October 1986 at the Departments of Chemistry and Applied Physics of the University of Hull, England.

The prime objective of this research was not one of developing a synthetically useful procedure, but rather to further the general understanding of photochemistry by studying the details of molecular interaction with pulsed infrared (IR) laser radiation. The dependence of absorbed energy and fractional yield on laser parameters such as irradiating wavelength, fluence and pulse type, and on reactant parameters such as pressure and diluent, were to be examined. The IR source was to be a tuneable, pulsed, hybrid, transversely excited atmospheric CO<sub>2</sub> laser. The energy absorbed by the reactant was to be measured optoacoustically, and the products were to be determined through gas chromatography.

It was further intended to see how molecular size affects photochemistry, so the majority of the reactants have been chosen from the same homologous series; the aliphatic alkanols. It was also intended to study several oxetanes, but only 3,3-dimethyloxetane was made with sufficient purity to be tested. Because of the intent to study as many molecules in the series as possible, no one molecule could be studied as exhaustively as is sometimes done in other studies.

For the remainder of this chapter, general theoretical and experimental concepts are introduced for; laser photochemistry (an historical overview, a

discussion on the role of collisions on the effect of an exciting IR field, and a description of the three stage multiphoton absorption model); the optoacoustic technique for measuring IR absorption (an historical review and a discussion of its mode of operation); and, finally, background to unimolecular theory. The actual experimental set-up and methodology is described in detail in Chapter 2 which includes descriptions of; the IR laser and its output beam properties; the reaction cells; a new optoacoustic calibration technique; and gas and data analysis. Chapter 3 is the first of the two results chapters, and is devoted to the presentation of absorption data, one section per molecule; methanol, ethanol, propan-2-ol, butan-2-ol, pentan-2-ol, hexan-2-ol, and 3,3-dimethyloxetane. The chapter ends with a general discussion. The decomposition data constitutes the fourth chapter where information pertaining to the product yields is presented. The chapter is again broken-up into sections, one for each reactant; ethanol, propan-2-ol, butan-2-ol, *t*-butanol, pentan-2-ol, hexan-2-ol, and 3,3-dimethyloxetane. At the beginning of each of these sub-sections, experimental conditions and a list of detected products specific to that reactant are presented, before the results are shown in detail. To conclude each sub-section, *a priori* reaction paths are proposed and briefly discussed, while a summarising discussion completes the chapter. The final chapter primarily consists of recommendations for further work.

## 1.1 LASER PHOTOCHEMISTRY - AN HISTORICAL OVERVIEW

The invention of the laser provided chemists with an alternative method of supplying energy to gases. The attraction of the method is that energy is absorbed directly by the molecules rather than indirectly through, for example, the thermal transfer of energy from the walls of a heated container. Excitation can be 'directed' either at the sample's electronic or vibrational molecular levels, by using UV or IR radiation respectively. IR laser

photochemistry is thus the photochemistry of highly vibrationally excited molecules in the ground electronic state, and remains a well researched and reviewed topic of interest(49-53). It has also become known as 'multiphoton vibrational photochemistry': The concept of a *multiphoton* absorption (MPA) process was introduced to help explain how the energy of IR laser photons (typically ~3kcal/mol) could ever cause dissociation of molecules whose activation energies are roughly twenty times the energy of the laser photon (i.e. ~60kcal/mol); by 1981 alone, over 100 molecules, of sizes varying from 3 to 62 atoms, had been demonstrated to be susceptible to IRMPA of laser radiation leading to dissociation (IRMPD)(49). To date, molecules successfully studied include alkanols (6-10,23,71,80,81,101), esters (22), halocarbons (75) and oxetanes (6).

Some of the earliest experiments which illustrated dissociation through IR absorption were carried out by Ambartzumian *et al.* (63) and Isenor *et al.* (64) in the early 1970s. They studied  $\text{BCl}_3$  and  $\text{SiF}_4$  decomposition respectively by monitoring the fluorescence of the electronically excited products. They were able to distinguish between collisionless photodissociations (instantaneous fluorescence peak), and collision dependent dissociations (delayed peak). The former was said to be representative of multiphoton absorption of IR radiation.

It was at this time that the three stage absorption model illustrated in Fig.1.1-1 began its development. It is now commonly used, although it was developed specifically for use with the  $\text{SF}_6$  molecule. Based on the knowledge that the density of states in a polyatomic molecule increases with energy, the model uses three regions to attempt to describe the change in absorption processes as the deposited energy increases. Basic methods of molecular vibrational level excitation and required laser intensities are shown in

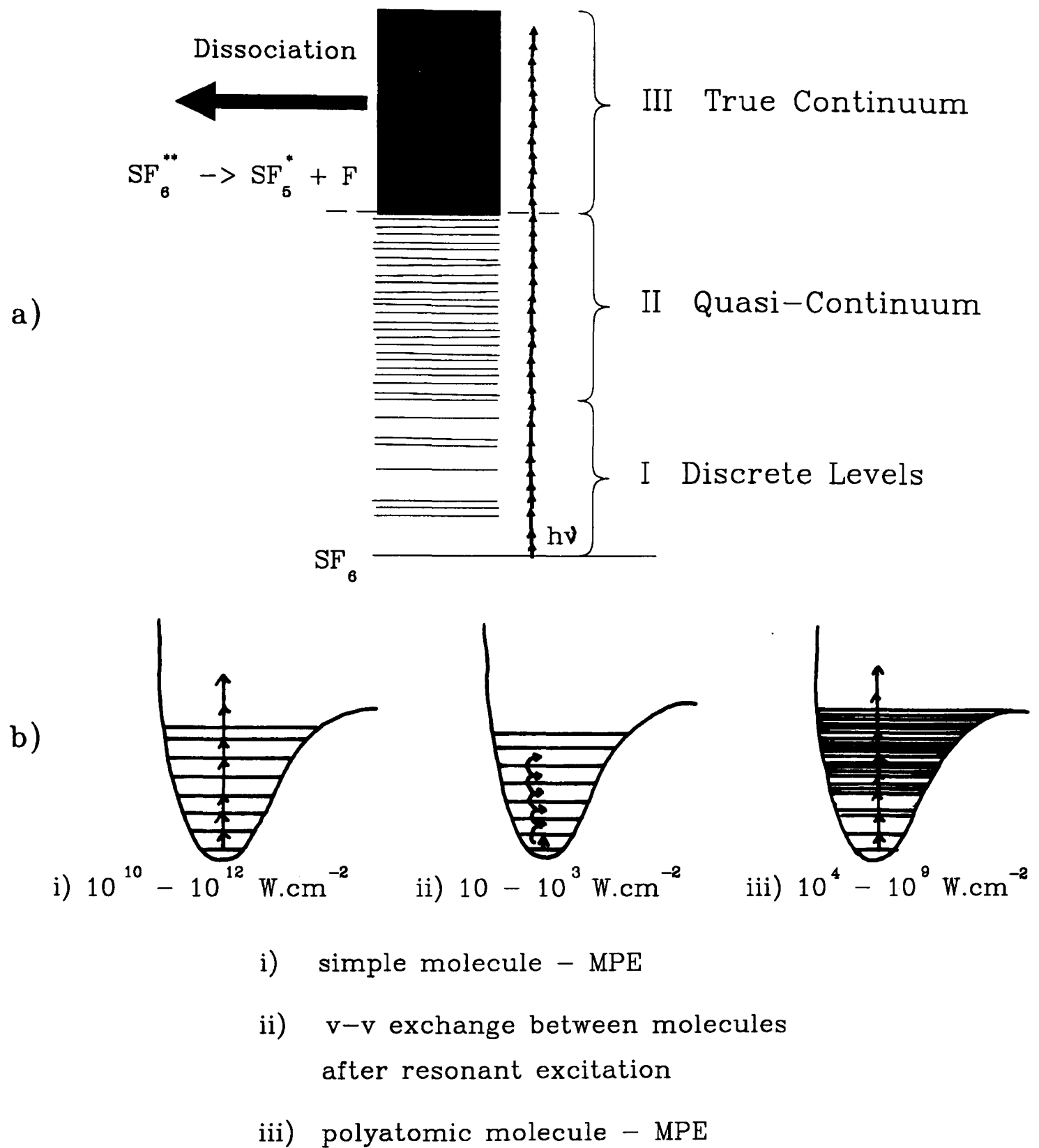


Fig. 1.1-1 (a) three stage absorption model;  
 (b) basic methods of molecular vibrational level excitation and required intensities

Fig.1.1-1(b). The discrete levels of region I contain anharmonicities which can only be overcome by multi- (rather than single-) photon absorption (64). Absorption becomes easier once region II is reached, where the density of states is so high that it can be described as a quasi-continuum. According to statistical theory (RRKM), which is described in Section 1.4, dissociation occurs in the true continuum of region III only after vibrational energy has redistributed to the weakest bond i.e. the bond which defines the dissociation energy. Obviously, further absorption occurs during the time it takes for this intramolecular vibrational energy distribution, therefore 'overexcitation' can be attained before dissociation.

Studies have been made on polyatomic molecules (65,66) illustrating that within the bounds of the model, the relative importance of each of the three stages depends on the molecule; for example, the larger the molecule the less significant is region I, and in  $S_2F_{10}$  this stage was shown to be nearly non-existent (65). Multiphoton absorption by a gas is best investigated by widely varying the laser intensity and frequency.

Danen (76) generalised that a 'large' molecule is one that has at least 5 or 6 atoms other than H or halogens, and that 'large' molecules all behave in a similar manner, this manner being different for 'small' molecules. However, Jang-Wren *et al.* (75a) have shown that this manner of classification (i.e. 5 or 6 non-H or -halogen atoms) does not always hold; 2-bromopropane,  $C_3H_7Br$  (3 atoms); 2-chloropropane,  $C_3H_7Cl$  (3 atoms); 2-chlorobutane,  $C_4H_9Cl$  (4 atoms) behave like 'large' molecules, while  $CH_3CF_3$  (2 atoms) and  $C_2H_5F$  (2 atoms) do behave as 'small', with  $CF_3CH_2Cl$  (2 atoms) being a transition molecule. Generally, a 'small' molecule has a low density of vibrational states, meaning that the laser excitation has to be coherent with the first few discrete levels for absorption to occur. Consequently excitation has been

found to be dependent on laser power rather than energy. Rotational structure and anharmonic splitting can sometimes compensate for anharmonicity in the laser excitation. Reaction thresholds are typically high, so high fluences are required to cause decomposition. Because of the high energy, decomposition lifetimes are short (fast decomposition rates). Conversely, for large molecules, the density of states is high, and the molecule may already lie in the quasi-continuum. Consequently, reaction threshold energies are low and decomposition lifetimes are long (slow decomposition rates). Jang-Wren *et al.* (75a) classified the size of the molecules according to their absorption characteristics: for example, for 'small' molecules the absorption cross-section increased with pressure (demonstrating rotational hole-filling), and decreased sharply with fluence, reaching a constant at high fluence (as the fluence approached zero, the cross-section became equal to the broadband cross-section). Conversely, the absorption cross-section of the large molecules was independent of pressure (no collision enhancement was observed), and was only weakly dependent on fluence.

In the earlier years of IR laser photochemical research, there was some hope that irradiation by a laser of a specific wavelength could cause the exclusive excitation of a molecular bond, or functional group, if the absorbed energy remained isolated in the excited mode; hence, there existed the exciting prospect that selective excitation (mode-selectivity) and decomposition of a molecule might be achievable. It had been established that mode selectivity was impossible with chemical activation, because of a very high rate of intramolecular energy relaxation ( $\sim 10^{12} \text{s}^{-1}$ ) (97). IRMD experiments using two widely separated frequencies have been carried out to explore mode selectivity in cyclobutanone (106a) and methanol (107). While results were particularly encouraging for cyclobutanone (106a), in that the product

distribution was different at each excitation frequency, it has since been argued (106b) that the differences surfaced because one of the excitation lines had a much higher intensity and was likely accessing the higher energy reaction channel; consequently mode selectivity was ruled out. The product distributions observed for methanol were found to be similar for both frequencies so also finding no evidence of mode-selectivity. It is now generally understood that rapid intramolecular energy relaxation also occurs for laser induced systems, and that this energy randomisation does not require the help of collisions.

Actual industrial application, of the knowledge gained from the years of research into the field of laser photochemistry, has so far been restricted to the atomic vapour isotope separation of uranium (67). A programme at the University of South Wales, Australia (67) has been working to investigate other potential areas such as coatings, surface treatments and printing.

### 1.1.1 The Role of Collisions

The ultimate effect of the exciting IR field is governed by the relationship between the excitation rate and the molecular vibrational relaxation time. If, for example, the relaxation rate is slow compared to the dissociation time, then it should be possible to excite selectively one particular vibrational mode, or even one particular type of molecule in a mixture.

Consider the following variables relating to the competing processes involved in energy absorption.

$\tau_{VV}^{in}$  = intramolecular transfer time of vibrational energy between different vibrational modes

$\tau_{VV}$  = intermolecular transfer time of vibrational energy between different molecules in a mixture

$\tau_{VT}$  = vibrational-translational energy relaxation time ie. time to complete thermal equilibrium

$W_{exc}$  = vibrational excitation rate of a molecule due to multi-photon absorption

where  $\tau_{VV}^{in} \ll \tau_{VV} \ll \tau_{VT}$

The second and third processes are collision dependent and will therefore come into play during the length of the exciting pulse only under 'non-collision-free' conditions. Since a system is considered to be 'collision-free' when the number of collisions during the laser pulse are insignificant, post-pulse photochemistry can be modified by the second and third processes even under collision-free conditions. For example, in this research, reactants were diluted with gases of good collision efficiency, and mixture at 'collision-free' pressures were tested to determine the role of post-pulse thermal reactions, the results being compared to the pure reactant data.

The most interesting experimental conditions to achieve would be when the excitation rate is much greater than intramolecular vibrational relaxation ( $W_{exc} \gg 1/\tau_{VV}^{in}$ ) because then mode-selective chemistry should be possible. Mode-selectivity would be best demonstrated on large molecules with well separated polyatomic functional groups to minimise vibrational relaxation between the groups (53). It might then be possible to achieve a non-equilibrium distribution of energy within the molecule in times shorter than collisions. Mode selectivity would be suggested if, for the same absorbed energy, dissociation yields at different exciting frequencies were not identical. However, the commonly best achieved conditions are when  $1/\tau_{VV}^{in} \gg W_{exc} \gg 1/\tau_{VV}$ , in which case a dissociating molecule will have intramolecular vibrational equilibrium, and RRKM theories (discussed in

Section 1.4) can be applied. Other conditions are of course possible, particularly when low fluence experiments are carried out. Non-selective photochemical reactions will also occur if  $1/\tau_{vV} \gg W_{exc} \gg 1/\tau_{vT}$ , because vibrational equilibrium is almost complete, but relaxation to heat has not occurred. Finally, thermal equilibrium is achieved when  $1/\tau_{vT} \gg W_{exc}$  and standard thermal chemistry occurs, with perhaps the only advantage that the photolysis volume can be heated while keeping the container walls at room temperature.

The discussion would not be complete without considering the rotational relaxation rate. There is, as one would expect, a Boltzmann distribution of molecules over the rotational levels of the ground vibrational state. The monochromatic laser radiation can have a sufficiently narrow linewidth to excite selectively molecules that lie within a particular rotational sublevel. The excitation rate is increased by using larger intensities, though a limit is reached when it becomes greater than the rotational relaxation rate. Under such a situation, depopulation of the lower sublevel occurs, thus preventing any further excitation until rotational relaxation depletes the upper excited sublevel. Rotational 'hole-burning' (or 'bottleneck') is the expression that has been given to this state of restricted absorption. At high pressures, collisions re-establish rotational equilibrium, by hole-filling; levels are refilled through collision induced rotational transitions from populations outside the initial laser bandwidth. So, further excitation (and hence absorption) is then allowed during the remainder of the pulse. At low pressures (and collision-free conditions), the first part of the pulse selectively excites a rotational level to saturation, so that the remainder of the pulse passes through unabsorbed because it is unable to excite any further.

The addition of a non-absorbing, vibrational energy deactivating gas to the reactant will have an effect which will depend on whether, for example, the reactant molecule is large or small, because rotational hole-burning should not be apparent for a molecule with a sufficiently high density of states. It will also depend on whether the excitation is collision-free for both pure and dilute cases, because then the degree of rotational hole-burning (and hence absorption and yield) can not be modified by collisions. Thus, the possible effects of an added diluent are:

- (i) Rotational relaxation will be made more efficient, thus increasing the absorption cross-section and increasing the yield, but this will only be noticeable for small molecules, and when the pure and dilute samples are not at collision-free pressures.
- (ii) Excited by-products will be deactivated more quickly (by randomisation and quenching of vibrational energy), thus causing a reduction in the yield of secondary products. The effect on the primary product yield will depend on the unimolecular reaction rate; the slower the rate (e.g. at lower fluences), the more collisions will compete effectively with the reaction, and a consequent decrease in primary product yield may occur. Clearly, for sufficiently fast reactions, no change in yield will be observed. A decrease in primary product yield may also be observed, however, if post-pulse thermal reaction is a product source for the case of the pure reactant.
- (iii) Diffusion and thermal properties will be controlled: diffusion control may either enhance or hinder the decomposition yield (see below).

These processes will be competitive and may result in no observable change in total product yield, although an altered product ratio would be an indication that the controlling processes had been modified. For non-collision-free conditions, for example, the effect of diluent will be the

result of two opposing effects; collisional deactivation, and absorption enhancement caused by rotational hole-filling. Whether or not the result is an enhanced product yield will depend on the collision rate and fluence i.e. on the down-pumping versus up-pumping. A few results from previous 'diluent' experiments are given below.

Quick and Wittig (68) found that dissociation yields were enhanced by the addition of an inert gas to a non-collision-free pressure of reactant, and concluded that "If the pulses are too long, or if the fluence is too low to cause saturation in the first place, or if the bath pressure is too high, only collisional deactivation causing a decrease in reaction probability will be observed." In cyclobutanone (17), the addition of a bath gas made the contributions from the channel with higher activation energy more effective, although the total yield did decrease. Whilst some workers (12b,13,14) reported a decrease of the SF<sub>6</sub> dissociation yield (after diluting the reactant with H<sub>2</sub>, noble gases and other SF<sub>6</sub> molecules), Lin *et al* (15) observed small enhancements of <20% (diluting with noble gases). Use of a time resolved luminescence/fluorescence method, eliminates the uncertainty as to whether reactions occur between irradiation and product analysis (16,17). In this manner, the addition of buffer gas was shown to increase the dissociation yields of C<sub>2</sub>H<sub>4</sub> (16), and fluorinated ethanes and ethenes (17).

Using a uniform beam, a decrease in yield was observed for dilution of 2,2-dimethyloxetane (with n-C<sub>6</sub>H<sub>14</sub>) (6). Because, in this case, the pressure of both the pure and dilute mixture was such that excitation was collision-free, the decrease was attributed to post-pulse collisional deactivation of the excited molecules.

Wittig (68) used a focussed system and pointed out that, at low pressures and at such sharp focussing conditions, the buffer gas inhibits molecular diffusion from the focal volume. As a result, it could be argued that dissociation enhancement is likely; however, the dissociation times must be considered. If they are much smaller than the length of the irradiating pulse, the diffusion hindered molecule may suffer from dissociation saturation, hence hindering yield enhancement.

For most of the diluent activities of this thesis, the total pressure was collision-free (50mtorr), and thus modification of the yield by (intra-pulse) rotational hole-filling was not a consideration.

The effects of pressure of *pure* reactant on primary product yield will also be wide ranging: The yield may drop as the pressure rises if the collision time is effectively competing with the decomposition time, by deactivating the molecule (such a drop is not a suitable measure or indication of post-pulse thermal activity; as discussed earlier, post-pulse activity is better investigated by adding a diluent and exciting a collision-free sample). A yield enhancement may indicate that inter-molecular vibrational energy transfer occurs to reactant molecules and to such a degree, that partially excited molecules are boosted up and over an anharmonic bottleneck(89): if at the lowest vibrational levels, they are already in resonance with the laser, then after some absorption (prior to reaching the quasi-continuum) they could become out of resonance at some higher level, so preventing further absorption and hence decomposition. If two such warm molecules were to collide, one could be 'lifted' over the barrier, while the other cools to a lower level, where (during a pulse) further absorption would be possible. McRae *et al.* have shown that excitation by collision is important for chloroform-*d*,  $\text{CDCl}_3$  (89). This effect may be less noticeable at high fluences, when the energy input

itself is high enough to overcome any such bottleneck. Furthermore, the effect may be enhanced as the pressure (and number of energy transfer collisions) is further increased, or suppressed if the time between collisions becomes too short, compared to the rate of absorption.

## 1.2 THE OPTOACOUSTIC TECHNIQUE - AN HISTORICAL REVIEW

Bell (54) and Tyndall (14) were the innovators of the optoacoustic (OA) technique (which is described in the following section) discovering that solids, liquids and gases emitted sound after visible radiation absorption. The spectrophone was developed (56,57) to measure the concentration of absorbing gas molecules and the vibrational-translational energy transfer rates; such information was gleaned from the sound trace.

Interest in the technique was recently revived with the development of lasers. These more powerful radiation sources (coupled with improved microphones) have dramatically increased the overall sensitivity of the method.

Pollution monitoring by detecting trace levels of vapour in air, has benefited greatly from the sensitive OA techniques (58), with noise limited sensitivities for detection now being in the region of a few parts in  $10^9$  for many pollutant gases (59). In 1982 (43) a deuterium fluoride laser (mid-IR) was used to establish a prototype OA laboratory system capable of measuring atmospheric HCl at a level of 50 parts in  $10^9$ . Previous best reported limits available from *in situ* methods, ranged between 5 and 10 parts in  $10^9$ . Extensive spectroscopic work by Beadle (69) has produced OA spectra of a selection of gases.

On a more theoretical level, the OA technique remains a useful tool in the field of photochemistry, since the microphones can be calibrated to measure the energy absorbed by the reactant. Cox (70), using SF<sub>6</sub>-argon mixtures and a high power CO<sub>2</sub> laser, showed that a single pulse OA detection technique could be used to identify the intensity regions for small signal absorption, saturation, and multiphoton excitation (MPE). Multiphoton absorption (MPA) is now commonly monitored in this way (6,9,11,36,71-74,78) particularly in order to supplement multiphoton decomposition (MPD) data.

### 1.3 OPTOACOUSTIC PROCESS - THEORY

Incident radiation excites the vibrational modes of the molecules within the irradiated volume. This absorption process is followed by V-T relaxation, releasing kinetic energy. Assuming that the rate of energy deposition and relaxation to heating (V-T) is fast compared with the rate of any subsequent pressure release by expansion, the irradiated volume is thus heated and experiences an instantaneous pressure rise. The result of this is a temperature and pressure step over the irradiated volume (Fig.1.3-1(a)). The core, of higher pressure, excited gas, relaxes its pressure through rarefaction and compression waves which travel radially to the walls (compression travelling outwards and rarefaction travelling inwards (Fig.1.3-1(b))); radial modes result from reflection of these waves at the walls. If thermal conduction on the time scale of the wave propagation is neglected, then the irradiated volume is not significantly cooled, and a temperature step will still exist.

A detailed Fourier analysis (38) shows that the initial pressure distribution is composed of a d.c. level plus superimposed higher frequencies of opposite phase that cancel each other out; in other words, the final pressure is as though the initial pressure step has been evenly distributed over the cell volume (the d.c. level). This pressure gradually falls as the molecules

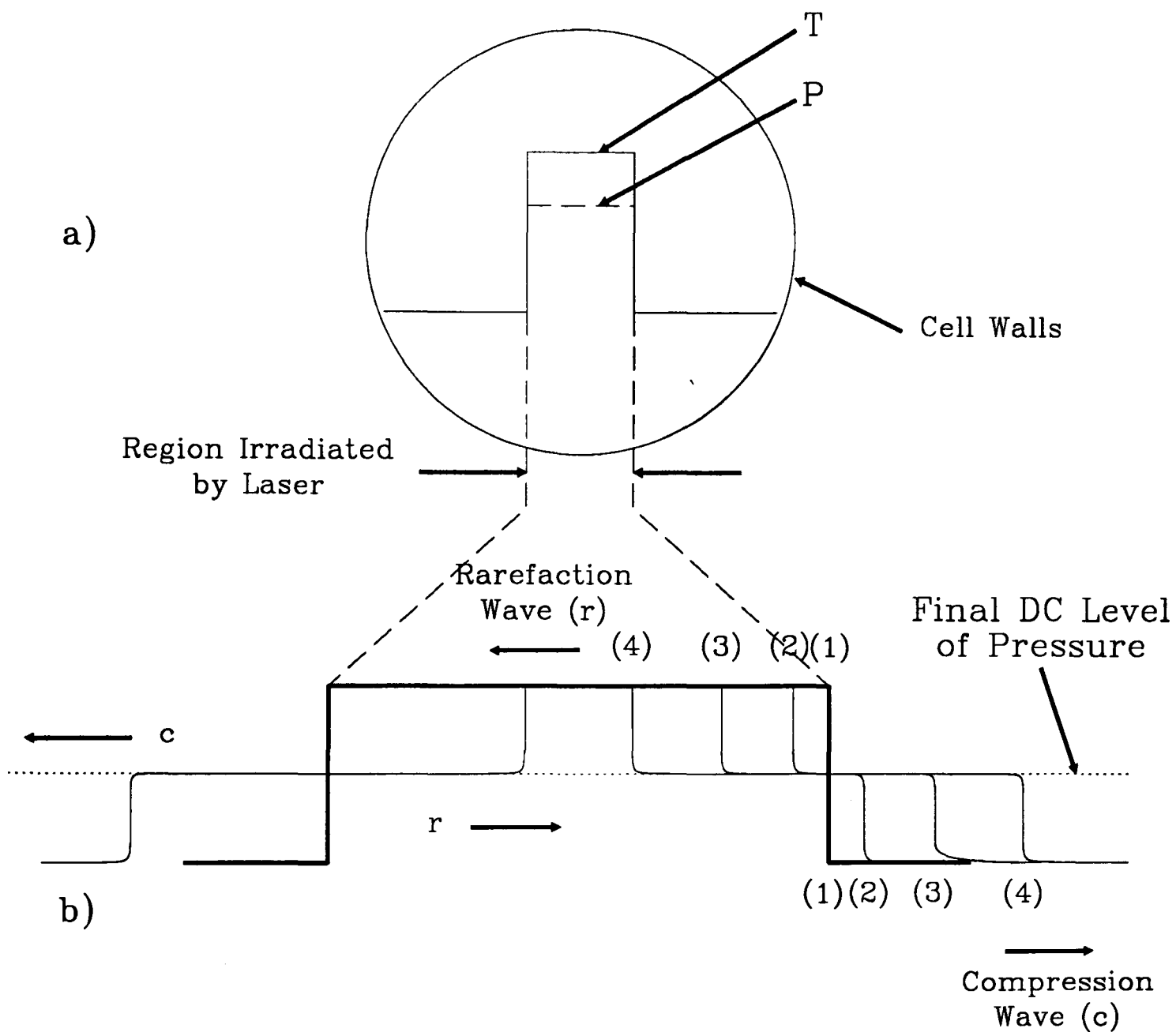
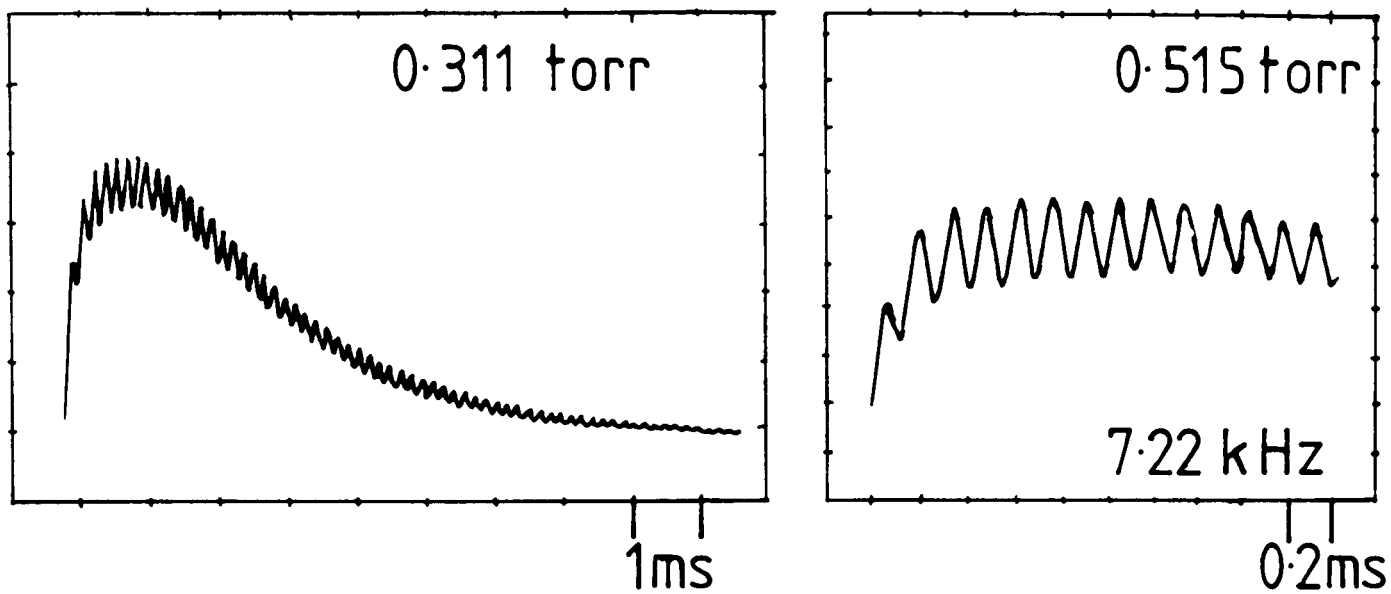


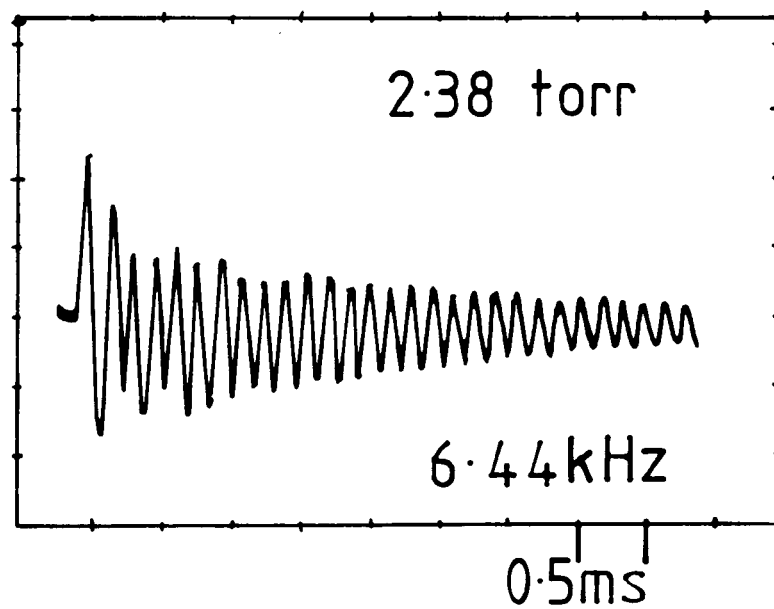
Fig.1.3-1 Cross-section of the reaction cell showing: a) the initial temperature ( $T$ ) and pressure ( $P$ ) profiles; and b) the development of the OA pulse

thermalise with the cell walls; the rise and fall of pressure is seen by the microphone (44,45). The acoustic oscillations (as discussed further in Section 1.3.1) are superimposed on this pressure pulse. If thermal relaxation is on a time-scale comparable to that of V-T relaxation, then the signal is weakened.

A sufficiently sensitive microphone, situated within the cell in a radial position, will pick up the resultant d.c. signal. If it has a limited bandwidth, the radial modes might not be resolved. Even if the response time was fast enough, some modes are not sustained and not every mode will be picked up. Unless electrically filtered, or damped by high pressures, the resonant frequencies of the microphone membrane will also be superimposed on the pressure pulse. When displayed on an oscilloscope, measurement of the first acoustic peak provides a sensitive absorption measurement. Leo *et al.* (40) showed that only under conditions of constant beam geometry, position and direction, could the relative amplitude and temporal features of the fine structure can be taken as a register of the absorbed energy. For their measurements Weulersse *et al.* (39) on the other hand, filtered out both acoustic and microphone resonances to use the peak of the pressure pulse. This achieves the same objective of integrating an unfiltered signal, in that the resultant signal is no longer dependent on the beam-cell alignment and beam geometry (40). An integrated signal is also invariant of relative amplitude and temporal features. OA signals vary in appearance with different cell dimensions and microphones. The traces of Fig. 1.3-2 are from two different cells (1.5 and 8cm long) using different microphones - both contained 2,2-dimethyloxetane. The first trace clearly shows resonant frequencies superimposed on the OA signal.



a) 1.5 cm cell



b) 8 cm cell

Fig. 1.3-2 Optoacoustic signals for  
2,2-dimethyloxetane

### 1.3.1 Optoacoustic System Responsivity

It will be shown that the microphone output voltage is proportional to the rise in pressure in the gas caused by the OA process,  $\Delta p$ . Assuming an ideal gas of pressure  $p$  and at temperature  $T$ , enclosed in cell of volume  $V$

$$pV = nRT \quad (1.3-1)$$

where  $n$  and  $R$  take on their standard meaning of number of moles and universal gas constant respectively. The cell volume is a constant, and the  $n$  is also a constant if there is negligible reaction during the measurement time. Then differentiating Eq.(1.3-1), for a temperature rise  $\delta T$  the pressure rise  $\delta P$  is

$$\delta p = \frac{nRV \delta T}{V^2} = \frac{p \delta T}{T} \quad (1.3-2)$$

Now the absorbed energy,  $\Delta E_{\text{abs}}$  (J) given in terms of the specific heat at constant volume,  $C_v$  ( $\text{J} \cdot \text{mol}^{-1} \text{K}^{-1}$ ), is

$$nC_v \delta T = \Delta E_{\text{abs}} \quad (1.3-3)$$

Combining equations (1.3-2) and (1.3-3)), the pressure rise beginning at an initial temperature,  $T$  is;

$$\delta p = \frac{R \Delta E_{\text{abs}}}{V C_v} = \frac{p \Delta E_{\text{abs}}}{n C_v T} \quad (1.3-4)$$

giving the responsivity of the gas to the optoacoustic process,  $R_g$  (torr/J):

$$R_g = \frac{\delta p}{\Delta E_{\text{abs}}} = \frac{\gamma - 1}{V} \quad (1.3-5)$$

The microphone responds to the pressure impulse with a sensitivity  $S$  (V/torr), and for a microphone operated in its linear region, the output voltage  $V_o$  will be proportional to the pressure change  $\delta p$ , so from Eqs.(1.3-4,5) the optoacoustic system responsivity,  $R_{oa}$  (V/J) (equal to the product  $R_g S$ ) is:

$$R_{oa} = \frac{V_o}{\Delta E_{abs}} \propto \frac{\gamma-1}{V} \quad \text{and} \quad \frac{p}{nC_v T} \quad (1.3-6)$$

where  $R = (C_p - C_v)$ , and  $\gamma = C_p/C_v$

Hence, it has been shown that if all the absorbed energy leads to heating of the gas, the optoacoustic system responsivity is proportional to  $(\gamma-1)$ , therefore is dependent on the gas mixture. A discussion, on the effect of gas mixture on the optoacoustic system responsivity (V/J) and on the subject of microphone sensitivity (V/torr) under experimental conditions, is presented in Section 2.3.2.

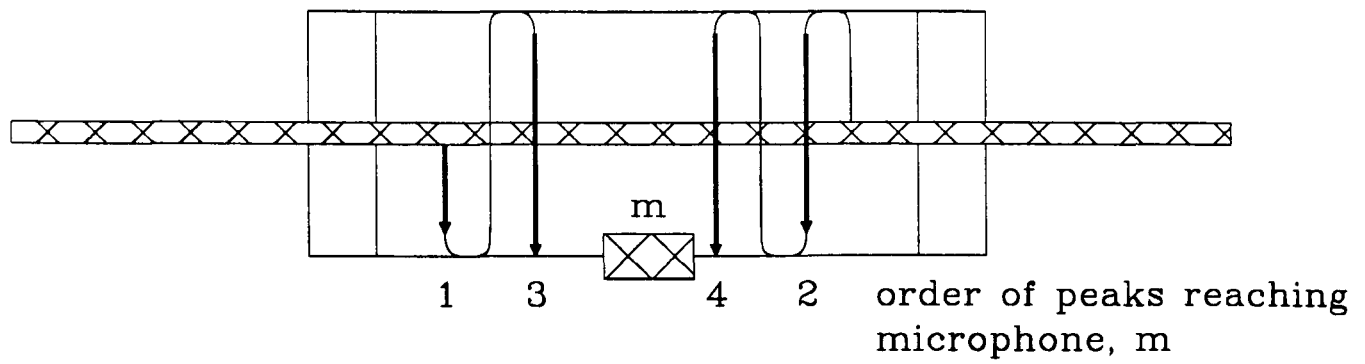
At very low pressures, the V-T relaxation time may be of the same order as, or even greater than, the time scale for cooling by thermal diffusion. The amplitude of the pressure pulse is then no longer directly related to the amount of energy absorbed, because some energy is transferred directly to the walls without first heating the gas. Furthermore, the first acoustic peak might not occur before contributions from other sources arrive at the microphone. For example, if the cell length is of a comparable dimension to the cell radius, then the first acoustic peak can become distorted by signals attributable to window effects.

### 1.3.2 Oscillatory Substructure

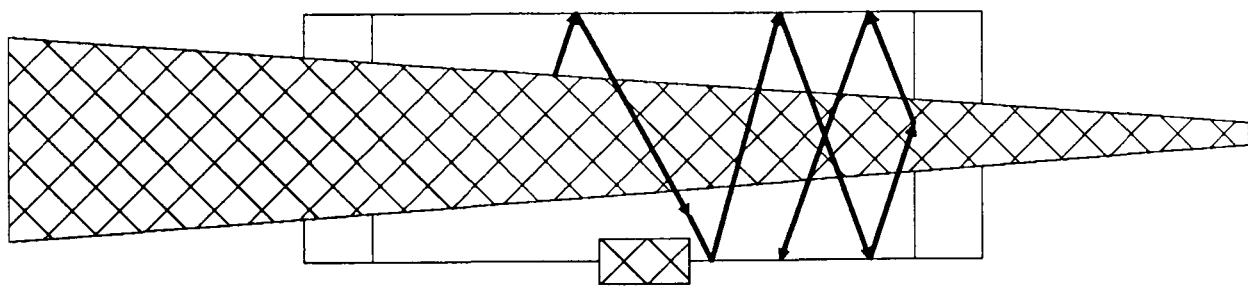
The oscillatory substructure can be interpreted as follows (42): If the beam travels centrally through the cell, the first few peaks arrive at the microphone in the order shown in Fig. (1.3-3a). The smooth sinusoidal oscillations can be easily perturbed. In one such case, the excited volume may not be cylindrical as in Fig. (1.3-3b). Since the pulses travel normal to the excited volume boundary, after several rebounds, the acoustic wave will reflect off the windows, and distortion of the later pulses will occur because of interference.

A second case arises when the beam does not travel centrally through the cell (Fig.1.3-3c). The pressure peaks will not arrive at regular time intervals, and eventually superposition occurs leading to a distorted signal.

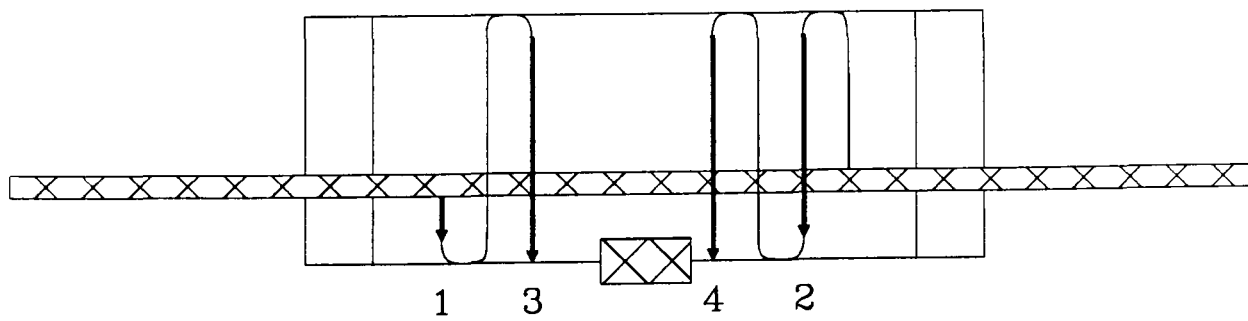
It has been noted (39,41,43,44,45,61) that there is a low pressure sensitivity limitation to the optoacoustic technique seen as spurious OA signals. This background noise has been attributed to window effects (41), specifically inner surface absorption at the windows (39,61); bulk absorption of the windows (39,44,61); and light scattering from the windows (45) towards the cell walls and microphone (44,45) where absorption takes place. The signals were found to be both pressure and fluence dependent (39,61), and also time dependent (61) since surface contaminants such as particulates and surface films accumulate with time. Some authors (39,43,45) recommend the use of Brewster windows to reduce noise caused by scattering. However, although the Brewster windows may solve this problem, another may occur since the signal from the excited volume immediately below (or above) the angled window, will be reflected from the window at an odd angle. Distorted acoustic signals will result, the effect being particularly noticeable in small cells, especially if the beam is not cylindrical or travelling centrally. Signals



a) On-axis, cylindrical, excited volume



b) Non-cylindrical excited volume



c) Off-axis excited volume

Fig. 1.3-3 Effect of beam geometry

caused by window absorption have been found to originate predominantly from absorption of a surface film rather than from bulk absorption (61). Furthermore, such a signal was found to be in-phase with the primary signal, and inversely proportional to the cell length (61). Finally there can be background signal caused by ablation of the window surface film. Longitudinal modes are initiated if the gas absorption length is about the same as the cell length, and therefore can occur at high cell pressures when there is a non-constant absorption over the cell length. Molecules ablated from the windows add to the local molecular concentration and can similarly cause longitudinal modes (if not already in motion) even if the high pressure gas is non absorbing; Parker *et al.* (41) detected an oscillatory signal corresponding to the primary longitudinal mode when the cell was filled with 35 atm. of  $N_2$ . Generally though only radial modes are excited, as discussed in Section 1.3.3.

It is because of the increased probability of distortion with time into the pulse that it has become customary to take measurements of the first signal peak, for the purpose of both quantitative and qualitative calculations of absorbed energy. Leo *et al.* (40) have shown that it is immaterial which part of the pulse is selected for measurement so long as the position/feature is consistently chosen and the beam geometry *etc.* is unchanging; measurements of any spike or the envelope were equally valid.

### 1.3.3 Frequency of the oscillatory substructure

OA traces can be used to establish the speed of sound  $v_s$ , through the gas. Radially the acoustic wave fits into the cell at a frequency described by a Bessel function. If the beam passes through the cell centrally, then usually  $J_0$  is excited, such that one of the nodes coincides with the boundary wall.

For off-centred beams the azimuthal mode is also probably excited and the cell resonances will be described by a series of Bessel functions.

The resonant angular frequencies  $\omega_j$  of the cell are given by (60):

$$\omega_j = 2\pi f_j = v_s \sqrt{K_z^2 + K_r^2} \quad (1.3-1)$$

$$K_z = (\pi/l) n_z \quad (n_z = 1, 2, 3, \dots); l = \text{cell length} \quad (1.3-2)$$

$$K_r = \pi \alpha_{mn}/a \quad a = \text{cell radius} \quad (1.3-3)$$

where  $n_z$ ,  $m$  and  $n$  are the longitudinal, azimuthal, and radial mode numbers.  $\alpha_{mn}$  is the  $n$ th root of the following equation involving the  $m$ th order Bessel function tabulated in reference (47).

$$[dJ_m(\pi\alpha)/d\alpha] \Big|_{\alpha=\alpha_{mn}} = 0 \quad (1.3-4)$$

The speed of sound (through the gas under scrutiny) can be found using the above equations, and the resonant frequency (calculated from the OA trace).

For the radial resonance only, equation 1.3-1 becomes:

$$\omega_j = cK_r = (c\pi/a) \alpha_{mn} \quad (1.3-5)$$

with  $m=0$  for a centred beam.

#### 1.4 UNIMOLECULAR THEORY

Previous work has shown that the primary reaction channels resulting from IR laser photochemistry are unimolecular, and this includes alkanols (6-10,23,71,80,81,101) and oxetanes (6). In addition, with the failure of CO<sub>2</sub> lasers of 'standard' pulse length (ns) to cause mode-selective decomposition (106b,107), it is generally assumed that vibrational energy is redistributed prior to dissociation of the molecule; since this is an essential, basic assumption of the RRKM unimolecular reaction theory (49,62,97), the theory can also adequately describe the dissociation of molecules that have

been excited through IRMPA. RRKM theory has been used successfully to model the decomposition of some alkanols and oxetanes (6).

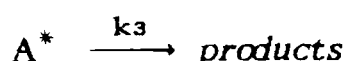
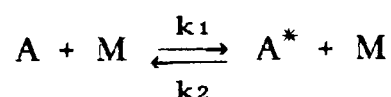
Through excitation, a *single* reactant molecule, A, can form an activated complex  $A^+$ . This activated complex will decay, resulting in either decomposition or isomerisation of A (or even relaxation back to a stable (original) molecule). Such a reaction is said to be unimolecular.

The activated complex is an energized molecule (with enough internal energy for reaction) which, through essential internal energy redistribution, has reached a critical configuration appropriate for decomposition or isomerisation. In thermal systems, energy redistribution is caused by collisions.

The theory of unimolecular reactions is not trivial and has been extensively covered in the literature, particularly by Robinson and Holbrook (62). Nevertheless, for the integrity of the thesis it is applicable to present a summary here.

#### 1.4.1 Lindemann Theory

Lindemann offered an explanation to a paradox; how is it that excitation by collisions in thermal systems (ie a bimolecular process) could result in first order kinetics? His answer has since become the foundation for all the recent (more accurate) unimolecular reaction theories. The reaction scheme proposed by Lindemann is as follows:



where A is a reactant molecule (represented by A\* after excitation), and M may be either a second reactant molecule, or one of an inert (diluent) gas, or a product molecule. For his theory, Lindemann assumes that  $k_1$ ,  $k_2$  and  $k_3$  are not energy dependent. By applying the steady state hypothesis to the rate of formation of excited reactant molecules ( $d[A^*]/dt = 0$ ), it can be shown that the overall rate of reaction is:

$$v = \frac{-d[A]}{dt} = k_3[A^*] = \frac{k_1 k_3 [A][M]}{(k_2[M] + k_3)} \quad (1.4-1)$$

First order kinetics occur at high pressures since then  $k_2[M] \gg k_3$ , therefore;

$$v_{\infty} = (k_1 k_3 / k_2)[A] = k_{\infty}[A] \quad (1.4-2)$$

whilst at low pressures  $k_2[M] \ll k_3$ , and the rate of reaction is equal to the second order rate of energization.

$$v_{\text{bim}} = k_1[A][M]$$

Thus, Lindemann predicted that the order of the initial rate of unimolecular reactions depends on the reactant concentration (and therefore pressure). The rate of reaction may be written with a pseudo-first-order rate constant,  $k_{\text{uni}}$ , to describe the fall-off with decreasing concentration (pressure); see Fig.1.4-1:

$$v_{\text{uni}} = \frac{-d[A]}{dt} = k_{\text{uni}}[A]$$

Combining this with equations (1.4-1) and (1.4-2), and noting that [M] may be replaced by the total pressure, we have:

$$k_{\text{uni}} = k_1 [M] / (1 + k_2 [M]/k_3) \quad (1.4-3)$$

$$= k_{\infty} / (1 + k_{\infty}/k_1 p) \quad (1.4-4)$$

The above equation leads to a few important conclusions concerning the effects of a diluent (inert) gas:

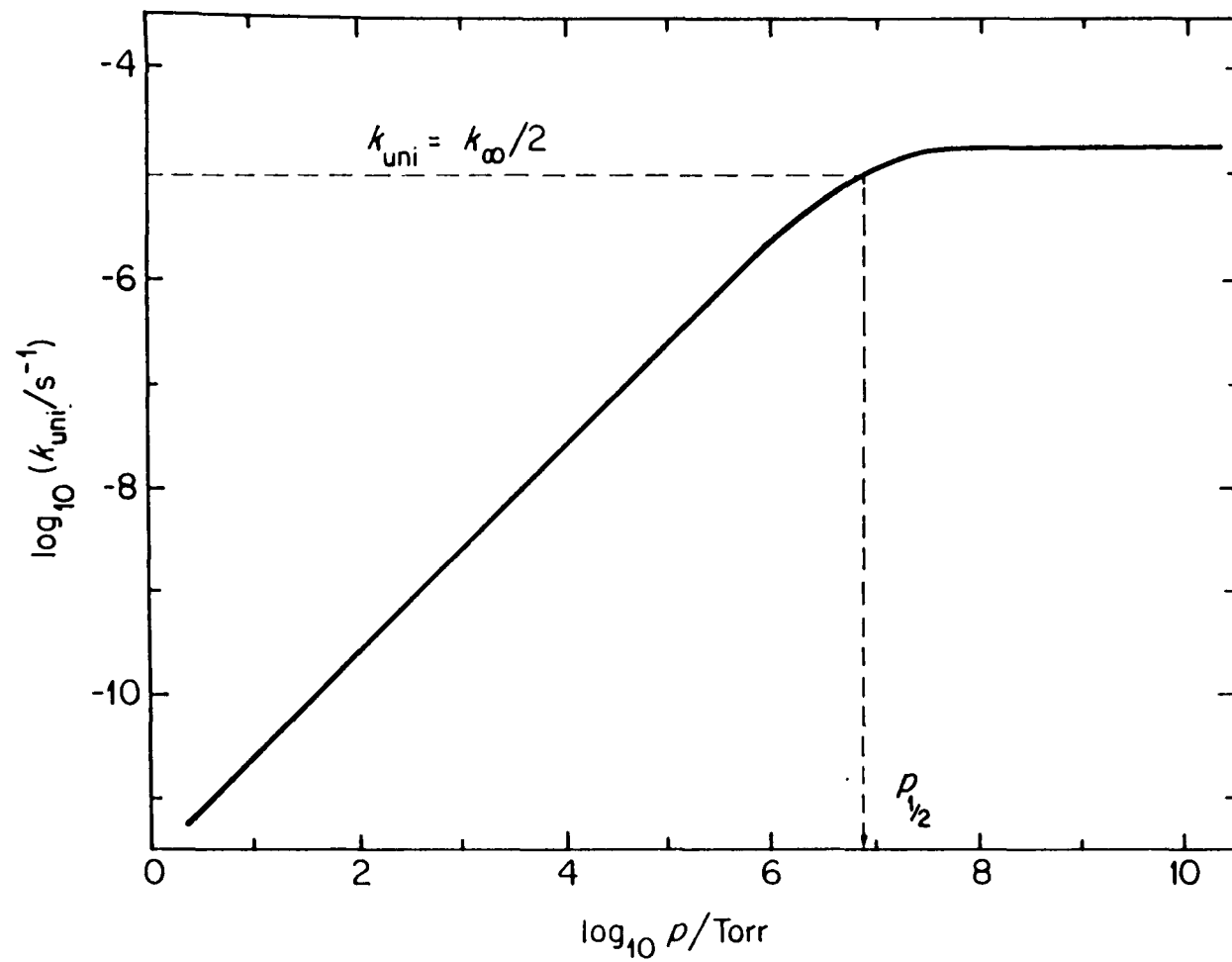


Fig. 1.4-1 Schematic of a Lindemann plot (from Ref. (62))

- (i) There will be no effect on the rate constant of a unimolecular reaction if an inert gas is added to a pressure of reactant for which the unimolecular reaction is in the first order region.
- (ii) An added diluent will increase the rate constant towards the high pressure (first-order) value if the initial pressure of reactant is such that the unimolecular reaction is in the second-order (fall-off) region.
- (iii) The result of point (ii) will clearly be a higher product yield. The amount of increase will not only depend on the pressure of diluent, but on the efficiency of collisional energy transfer.

The fall-off may be evaluated in terms of the ratio  $k_{uni}/k_{\infty}$ , and the pressure  $P_{1/2}$  at which this ratio is 0.5, i.e. when  $k_3=k_2[M]$ . Since  $[M]$  may be replaced by the total pressure, and by incorporating equation (1.4-2), it immediately follows that;

$$P_{1/2} = k_3/k_2 = k_{\infty}/k_1 \quad (1.4-5)$$

Since Lindemann's theory is based on collision theory,  $k_1$  was calculated using;

$$k_1 = Z_1 \exp(-E_0/kT) \quad (1.4-6)$$

where the collision number

$$Z_1 = (\sigma_d^2 N_A / R) (8\pi N_A k / \mu)^{1/2} (1/T)^{1/2} \quad (1.4-7)$$

and  $E_0$  = high pressure activation energy,  $E_{\infty}$

$\sigma_d$  = collision diameter

$N_A$  = Avagadro's Number

$R$  = gas constant

$k$  = Boltzmann constant

$\mu$  = reduced molar mass

$T$  = temperature

Using  $k_1$  calculated in this manner, and experimental data for  $k_\infty$ , the predicted  $p_{1/2}$  is found to be vastly different (too high) from the experimentally determined value:  $k_1$  must be larger than that calculated with equation (1.4-6).

#### 1.4.2 Hinshelwood Modification

Lindemann's collision theory treatment was shown not to be completely effective in describing unimolecular reactions *viz.* theoretical values of  $p_{1/2}$  were much higher than experimentally determined values. Hinshelwood developed Lindemann's theory to take into account molecular internal energy, particularly taking into consideration that prior to dissociation, the energy may need to take on a certain distribution over the molecule's  $s$  internal degrees of freedom. As for equation (1.4-6), Hinshelwood described  $k_1$  as being the product of the collision number and the probability of a molecule containing energy equal to, or in excess of  $E_0$ . The probability term is derived from statistical mechanics.

$$k_1 = Z_1 \exp(-E_0/kT) (E_0/kT)^{s-1} / (s-1)! \quad (1.4-8)$$

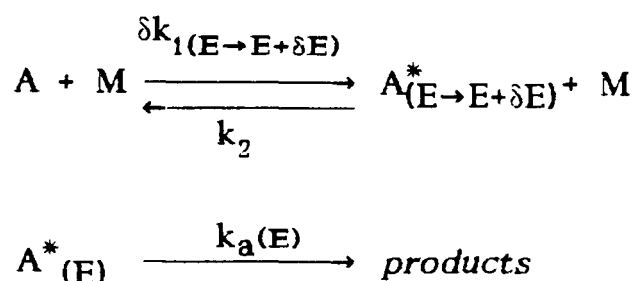
Clearly, the more complex the molecule, the more the degrees of freedom that are available, and hence  $k_1$  takes on larger and larger values *ie.* unlike before,  $k_1$  is now energy dependent.

Calculations of  $P_{1/2}$  using equation (1.4-8) are now in good agreement with experimentally determined values. However, the theoretical curve of  $k_{uni}$  (Eq.(1.4-4)) does not fit well to the experimental data over the rest of the pressure range. One other disadvantage of the Hinshelwood-Lindemann theory, is that it is not possible to predict  $s$ : it is approximately equal to half of the total number of modes of vibration.

Further equations (for  $k_{\infty}$  and  $E_{\infty}$ ) in the Hinshelwood-Lindemann theory can be used to demonstrate that the lifetimes of the energized molecules ( $k_3^{-1}$ ) increases when the internal energy can be stored among more degrees of freedom.

### 1.4.3 Miscellaneous Developments

The fit problem exhibited by the Hinshelwood-Lindemann theory is resolved by making both  $k_1$  and  $k_3$  energy dependent viz.  $\delta k_{1(E \rightarrow E+\delta E)}$  and  $k_a(E)$  respectively. The reaction scheme is thus:



The total rate constant is obtained by integrating the expression which represents the contribution to the unimolecular constant from energized molecules in the energy range  $E \rightarrow E+\delta E$  (the steady state hypothesis is applied this time to  $[A^*_{(E \rightarrow E+\delta E)}]$ ):

$$k_{\text{uni}} = \int_{E=E_0}^{\infty} \delta k_{\text{uni}(E \rightarrow E+\delta E)} = \int_{E=E_0}^{\infty} \frac{k_a(E) dk_{1(E \rightarrow E+dE)}/k_2}{1 + k_a(E)/k_2[M]} \quad (1.4-9)$$

The rate  $k_a(E)$  in Rice, Ramsperger and Kassel theories (RRK) is considered to be related to the probability that the critical energy  $E_0$  is concentrated in one part of the molecule. Both classical statistical mechanics and quantum approaches were covered.

The quantum approach (used only by Kassel) is the most realistic of the two (the classical equations have since been found to give poor approximations). In it, one of the molecule's  $s$  identical oscillators (all of frequency  $\nu$ ) must attain a critical energy, corresponding to  $m=E_0/h\nu$  quanta. The rate constant  $k_1(E)$  now refers to energization into a specific quantum state, rather than into an energy range  $E \rightarrow E+\delta E$ , and is given as:

$$k_1(nh\nu) = k_2 \left( \exp(-h\nu/kT) \right)^n \left( 1 - \exp(-h\nu/kT) \right)^s \frac{(n+s-1)!}{n!(s-1)!} \quad (1.4-10)$$

where  $n$  is the total number of quanta contained within the  $s$  oscillators (ie  $n=E/h\nu$ ). As for the high pressure rate constant  $k_\infty$ , Eq(1.3-11), summation over all the discrete energy levels must be carried out, in order to find the overall rate constant.

$$k_\infty = \sum_{n=m} \frac{k_1(nh\nu) k_\infty(nh\nu)}{k_2} \quad (1.4-11)$$

It is of interest to note that it can be shown that equation (1.4-11) may be represented in Arrhenius form:

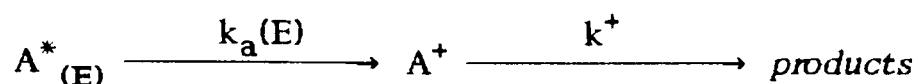
$$k_\infty = A \exp(-E_0/kT) \quad (1.4-12)$$

with  $A$  representing the reaction's high pressure A-factor.

A useful and more accurate modification to the *classical* approach of this RRK theory is discussed later.

Further treatment by Marcus of the RRK theories has led to the more complete RRKM theory: quantum mechanics is used to calculate  $k_1$ , and  $k_2$  can be equated to the collision number  $Z$  (of equation (1.4-7)) or  $Z\lambda$ , where  $\lambda$  is the collision deactivation frequency.  $k_a$  is calculated using ideas related to

the Absolute Rate theory. It is this RRKM theory which introduces the concept of an activated complex  $A^\ddagger$  (last mentioned at the beginning of this section on unimolecular theories). The last line of the reaction scheme thus becomes:



In addition, the energy terminology is refined in order to make a distinction between fixed and non-fixed energies. In RRKM theory, concentrations of  $A^*$  and  $A^\ddagger$  are calculated using statistical mechanics, since the aim is to investigate intramolecular energy distribution over the degrees of freedom. Only the non-fixed energy  $E^*$  is allowed to redistribute itself, and is comprised of the sum of vibrational  $E_v^*$  and rotational  $E_r^*$  components only. Molecular translation and zero point energies, for example, are fixed energies. Once an energized molecule  $A$  reaches its intermediate state (activated complex  $A^\ddagger$ ) the fixed energy is reduced to  $E^\ddagger$  by the critical energy  $E_0$  that was required to get over the energy barrier. Thus

$$E^\ddagger = E^* - E_0$$

and also

$$E^\ddagger = E_r^\ddagger + E_v^\ddagger + \kappa$$

where  $\kappa$  is associated with the translational motion of  $A^\ddagger$ . These energies are illustrated in Fig. 1.4-2.

*All of the  $E$ s in the current reaction scheme should now be replaced with  $E^*$ . The overall rate constant given by (1.4-9) is also rewritten with  $E^*$  instead of  $E$ .*

Because of the complexity of the RRKM theory it is often easier to use earlier theories as long as their limitations are realised, and only estimates

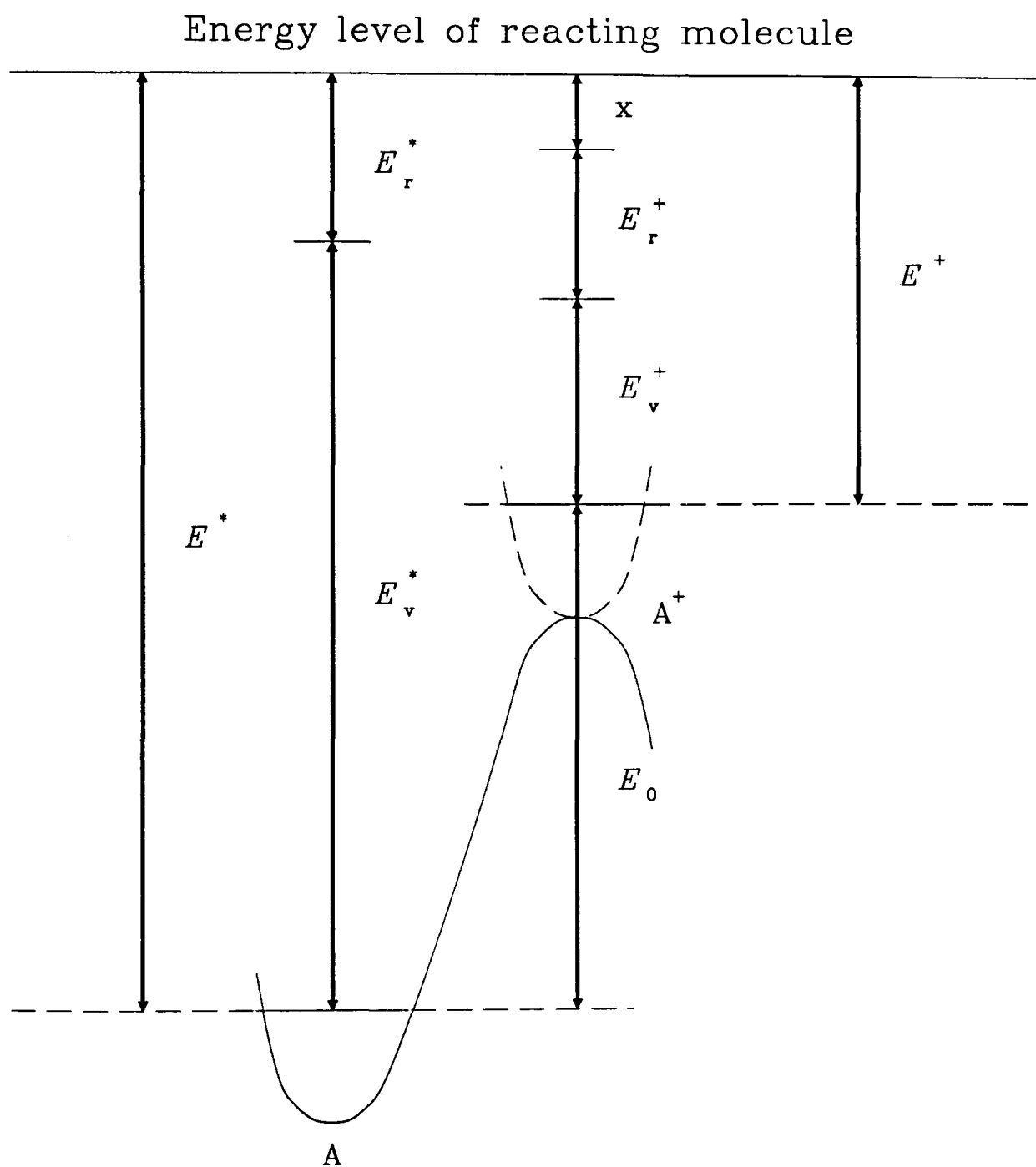


Fig. 1.4-2 Illustration of energy terminology for a unimolecular reaction; adiabatic and inactive degrees of freedom are excluded (from Ref. (62))

are required. For example, for even greater accuracy, a modification of the classical approach to the RRK theory takes into consideration that all the oscillator frequencies of the energised molecule and the activated complex are **not** identical. More specifically, the energized molecule has  $s$  oscillators of frequencies  $\nu_j$  ( $j=1$  to  $s$ ), and the activated complex  $s-1$  oscillators of frequencies  $\nu_i^+$  ( $i=1$  to  $s-1$ ). The rate of formation of products using classical statistical mechanics in this way is:

$$k_a(E^*) = \left( L \prod_{j=1}^s \nu_j / \prod_{i=1}^{s-1} \nu_i^+ \right) \left( (E^* - E_0) / E^* \right)^{s-1} \quad (1.4-13)$$

where  $L$  is the number of decay channels (reaction path degeneracy). Now the Arrhenius high pressure A-factor may be equated with the first bracketed term of Eq.(1.4-13), which has a numerical value in the order of one vibrational frequency *viz.* of the order of  $10^{13}$ - $10^{14}$ s<sup>-1</sup>. The second term may be abbreviated to  $f(E)$ , so Eq.(1.4-13) becomes:

$$k_a(E^*) = A f(E) \quad (1.4-14)$$

The term  $f(E)$  describes the relative number of ways of distributing the energy (of the excited molecule) among the vibrational modes of the reactant and activated complex.

ie. 
$$f(E) = \frac{\left( \text{Energy available for distribution in activated complex} \right)^{s-1}}{\left( \text{Energy available for distribution in molecule} \right)}$$

Hence:

$$f(E) = \left( E^+ / E^* \right)^{s-1}$$

Although this classical expression is still inaccurate, it is excellent for quickly giving an estimate for the amount by which a molecule can be excited over the dissociation limit (ie.  $E^* - E_0$ ), under nominal experimental

conditions. The number of absorbed quanta ( $E_0/h\nu$ ) is typically 20-50, as long as the threshold energy is not exceeded by the laser flux. An assumption is made that the decomposition rate is equal to the rate of absorption of those quanta ie.  $k_a(E^*) = E_0/(h\nu\tau)$ , where  $\tau$  is the pulse length (say 100 ns).  $k_a$  is thus evaluated as  $(2-5)\times 10^8 \text{ s}^{-1}$ , which then gives (from Eq.(1.4-14))  $f(E)\approx 10^{-4}$ . It is clear from equation (1.4-13) that for a constant value of  $f(E)$ , larger and larger molecules ( $s$  increasing) will support greater extents of overexcitation ( $E^*-E_0$ ). The dependence of  $f(E)$  on  $E^*/E_0$  as  $s$  changes is illustrated by Fig.1.4-3. In Fig.1.4-4  $E^*/E_0$  is plotted against the number of atoms in a molecule for a fixed value of  $f(E) = 10^{-4}$ .

Calculated  $k_a(E^*)$  values could be combined with assumed energy distributions to predict product yields in pulsed IR laser experiments(6). Typically, these predictions are made for dilute reactants(6) because of the complications that ensue in trying to model the result of the collision between two excited molecules(35): A collision between a diluent molecule and a reactant molecule may be regarded as a simple deactivating collision, whereas that between two excited molecules will cause a redistribution of energy leaving the absorbed energy as excitation energy. This energy eventually redistributes itself through all the molecules in the irradiated volume, at which point the gas is at a sufficiently high temperature for thermal reactions to occur. It takes a few  $\mu\text{s}$  for the thermal reactions to stop(35). The precise time is difficult to estimate and yet the predicted reaction yields are strongly dependent on this thermal component, particularly for low amounts of absorbed energy. Thus, analysis of dilute reactants, where this thermal component is not anticipated, is preferable.

In order to exclude the possibility of energy being transferred to the diluent molecules during excitation, modelling is carried out and compared against

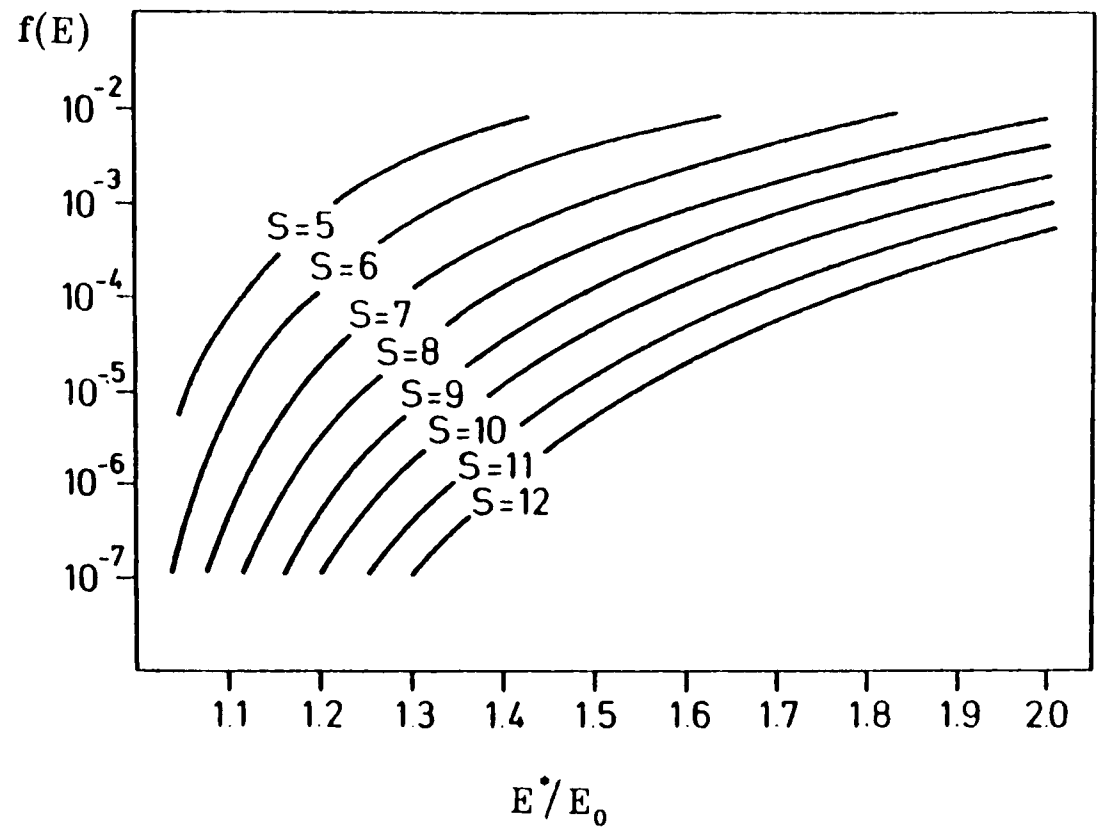
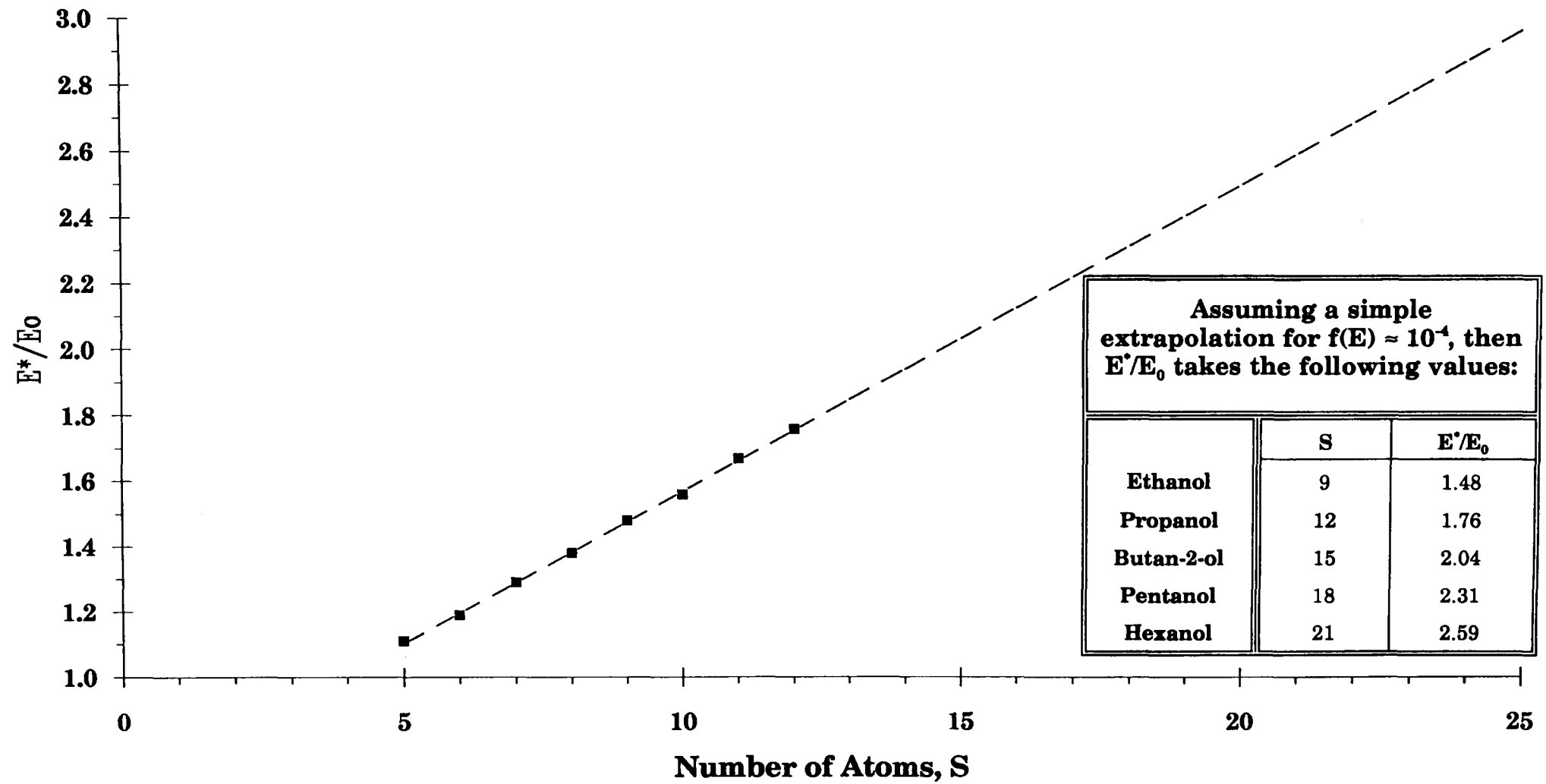


Fig. 1.4-3 Dependence of  $f(E)$  on the ratio between the vibrational energy  $E^*$  and the dissociation energy  $E_0$  for molecules with different number of atoms  $S$  (from Ref. (63))

**Fig. 1.4-4 Dependence of  $E^*/E_0$  on the number of atoms in a molecule for a fixed value of  $f(E) = 10^{-4}$**



experimental data gathered from collision-free conditions. Yield predictions are made by first taking the *measured* average absorbed energy per molecule in the irradiated volume, and assuming that it (together with the initial absorbed energy prior to absorption) is redistributed as vibrational energy among all the molecules in the irradiated volume. The final energy distribution is examined by assuming different distributions (e.g. Boltzmann for a wide distribution, and Poisson for a narrow distribution) and comparing the predicted yields with the experimental values: RRKM theory is used to calculate the rate coefficients for particular levels of vibrational energy within the reactant molecule, and taking the assumed energy distribution, and assuming that all collisions are deactivating, the product yields are predicted. As an example, if the collisions are assumed to be strong (i.e. on the first collision, the excited molecule is completely deactivated) with a collision frequency  $\omega$  ( $s^{-1}$ ), for RRKM rate constants of the two paths at energy  $E_v^*$  of  $k_a(E_v^*)$  and  $k_b(E_v^*)$ , and for the assumed energy distribution function of  $f(E_v^*)$ , the fractional decompositions for paths 'a',  $FD_a$ , and 'b',  $FD_b$ , are given by;

$$FD_a = \int_0^{\infty} \frac{k_a(E_v^*)}{k_a(E_v^*) + k_b(E_v^*) + \omega} f(E_v^*) dE^*$$

$$FD_b = \int_0^{\infty} \frac{k_b(E_v^*)}{k_a(E_v^*) + k_b(E_v^*) + \omega} f(E_v^*) dE^*$$

Predictions carried out on 2,2-dimethyloxetane, oxetane, 2-methyloxetane, ethanol and *t*-butanol yielded fractional decompositions less than those actually observed(6), leading to the conclusion that some molecules in the irradiated volume do not interact with the laser irradiation.

## 2. - EXPERIMENTAL SET-UP AND METHODOLOGY

### 2.1 THE LASER

Molecular gas lasers exploit transitions between energy levels of a molecule (94): Where the transitions are between different vibrational levels of the same (ground) electronic state (VIB-ROT), the energy difference  $-\Delta E$  is such that the laser oscillates in the middle to far-IR (5-300  $\mu\text{m}$ ). For transitions between vibrational levels of different electronic states, the emission is in the visible/uv, and far IR radiation (25  $\mu\text{m}$ -1mm) results from transitions between different rotational levels of the same vibrational state.

The  $\text{CO}_2$  laser falls into the first group, and Fig. 2.1-1 schematically illustrates the energy-levels. The lasing medium is a mixture of  $\text{CO}_2$ ,  $\text{N}_2$  and He, with population inversions being produced between the 001 and 100 or 020 levels shown.  $\text{N}_2$  and He serve to improve the lasing efficiency; vibrationally excited nitrogen has its  $v=1$  level in close co-incidence with the  $\text{CO}_2$  (001) state and assists upward pumping of the  $\text{CO}_2$  molecules through collisional energy transfer, while the inclusion of helium encourages a large population inversion by providing an additional path for relaxation of the (100) level to ground <sub>$\lambda$</sub>  <sup>or 020</sup>. Laser action in  $\text{CO}_2$  can be obtained on a continuous (cw) or pulsed basis.

For this work, a UV preionised, pulsed, hybrid, Transversely Excited Atmospheric (TEA)  $\text{CO}_2$  laser was used as the IR source (29,30,31)(Fig.2.1-2 ); it was discretely tunable to 70 transitions between 9 and 11  $\mu\text{m}$  and produced short pulses ( $\sim 50\text{ns}$  pulse length (FWHM) and  $\sim 600\text{ns}$  base width). Such tunability provides flexibility when choosing an irradiation wavelength which lies within the absorption band of the sample molecule: In this work the intention was to use a line which coincided with the peak of the absorption

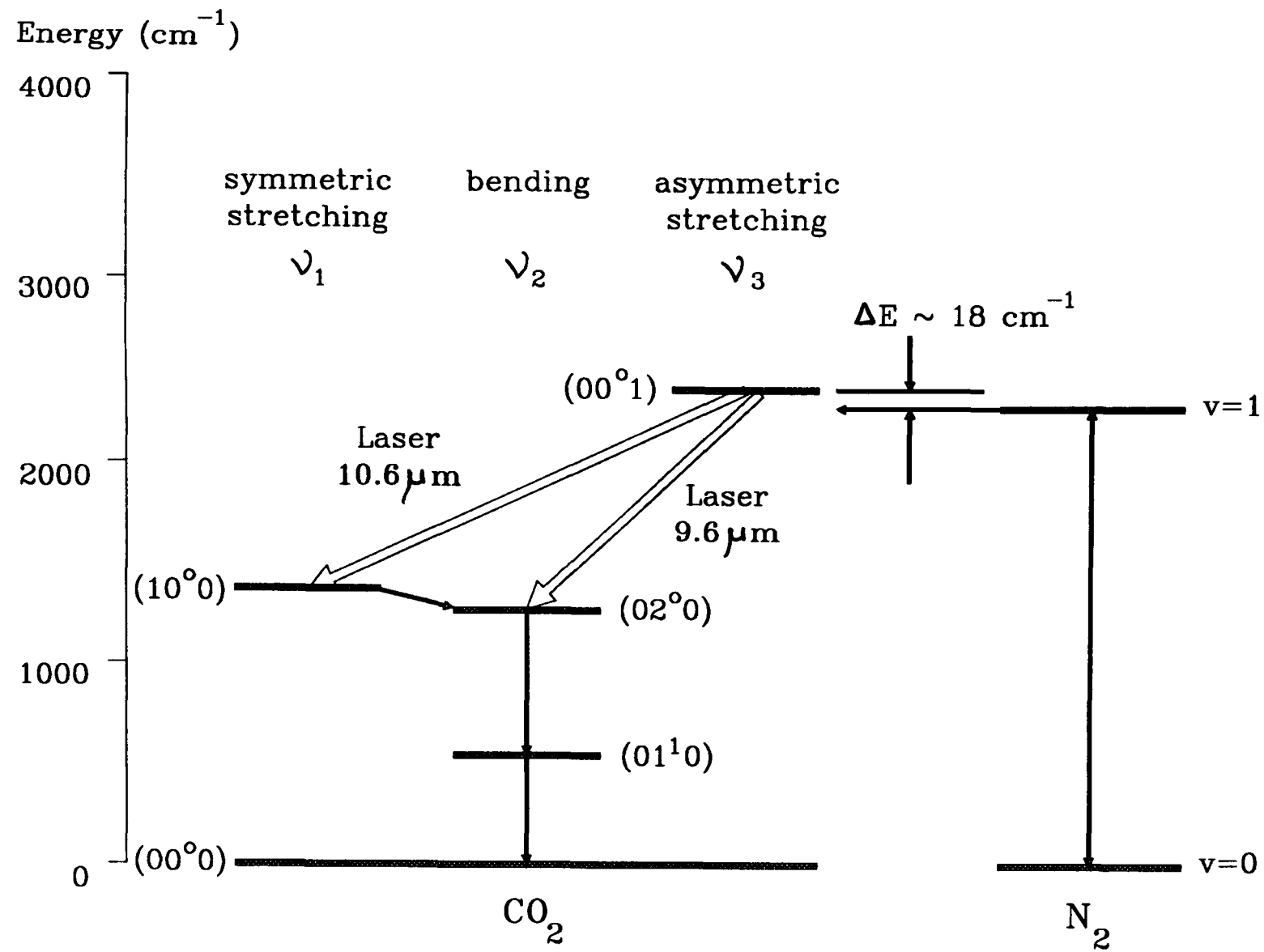


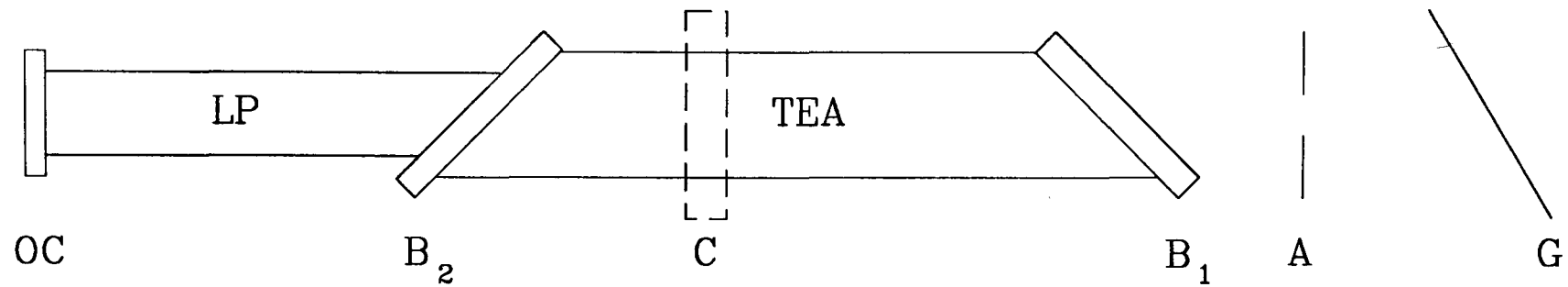
Fig. 2.1-1 CO<sub>2</sub> Laser energy level diagram

band. This was not usually possible, and instead a balance had to be struck between strong absorption of the sample and a strong laser fluence (energy per unit area).

Adjustment and measurement of the laser output was achieved as follows: Wavelength tuning was accomplished by altering the angle of a Littrow mounted diffraction grating that formed one mirror of the CO<sub>2</sub> laser resonator. The wavelength was monitored on an Optical Engineering Inc. spectrum analyser, and a Gentec pyroelectric Joulemeter was used to measure the output energy. Sometimes it was necessary to improve the beam quality by adjusting the alignment of the output coupler. Fluences were calculated after determining the laser beam radius in the region of interest, and Section 2.1.3 describes the methods used to establish a dependable value for this.

### 2.1.1 Single Longitudinal Mode Operation

A hybrid CO<sub>2</sub> laser (29) includes in its optical cavity a low pressure gas discharge tube (Fig.2.1-2) that is operated either in cw or pulsed mode. The tube has a narrow gain bandwidth by virtue of the low pressure (at ~10torr, there is 50MHz doppler broadening and ~50MHz of collision broadening -see calculations in Appendix 5) and provides gain for one longitudinal mode out of the many that normally exist within the high pressure TEA laser gain profile. The separation of longitudinal modes is given by  $c/(2L)$  (where L is the separation of the cavity mirrors, and c is the velocity of light) which, for this laser, gives 94 MHz. The FWHM bandwidth of the TEA gain section is found to be made up of 50 MHz doppler broadening and 4GHz pressure broadening (see Appendix 5 for calculation details). The small additional gain, provided by the low pressure section, enhances the growth of one longitudinal mode while others are suppressed because of gain competition:



TEA = pulsed TEA CO<sub>2</sub> laser

LP = pulsed low pressure section

C = coupling to original  
laser body

G = grating

A = aperture

B<sub>1,2</sub> = Brewster windows

OC = plane/plane

60% reflecting

Ge output coupler

$\overline{\overline{GA}} = 7\text{cm}$

$\overline{\overline{AB_1}} = 5\text{cm}$

$\overline{\overline{GC}} = 87\text{cm}$

$\overline{\overline{CB_2}} = 6\text{cm}$

$\overline{\overline{B_2OC}} = 66\text{cm}$

Fig. 2.1-2 Schematic diagram of a hybrid TEA CO<sub>2</sub> laser

operating conditions can thus be chosen to give single longitudinal mode output (Fig.2.1-3).

For this work, a premix of 10% CO<sub>2</sub>: 20% N<sub>2</sub>: 70% He was admitted to the previously evacuated low pressure gain section. The optimum discharge tube pressure was about 10 torr for main cavity flow rates (in litres per minute) of 1.2 N<sub>2</sub>: 2.4 CO<sub>2</sub>: 9 He; a spark gap pressure of 20 lb/in<sup>2</sup>; and a charging voltage of 19 kV .

Synchronisation of the pulsed low pressure section with the TEA discharge was achieved as follows: The discharge in the low pressure section was pulsed first, and the resultant discharge current sensed with a ferrite core transformer in one of the discharge leads. The core had a step-up transformer configuration, and its output was fed to a Farnell PG101 pulse delay generator (using a 50Ω terminator on the input) the output of which was used to trigger the TEA discharge current. A delay of 70 μs was found to provide optimal performance in terms of producing reliable, smooth pulse output which is a manifestation of single longitudinal mode operation (29).

### 2.1.2 Temporal Beam Profiles

Dyer *et al.* (37) performed a detailed study of the operation characteristics of a volume excited TEA CO<sub>2</sub> laser. Energy and power measurements were made as a function of the molecular gas flow ratio  $\gamma$  on various systems incorporating different capacitors and cavity mirrors.  $\gamma$  is defined as :

$$\gamma = \frac{\text{CO}_2 \text{ flow rate}}{\text{sum of CO}_2 \text{ and N}_2 \text{ flow rates}}$$

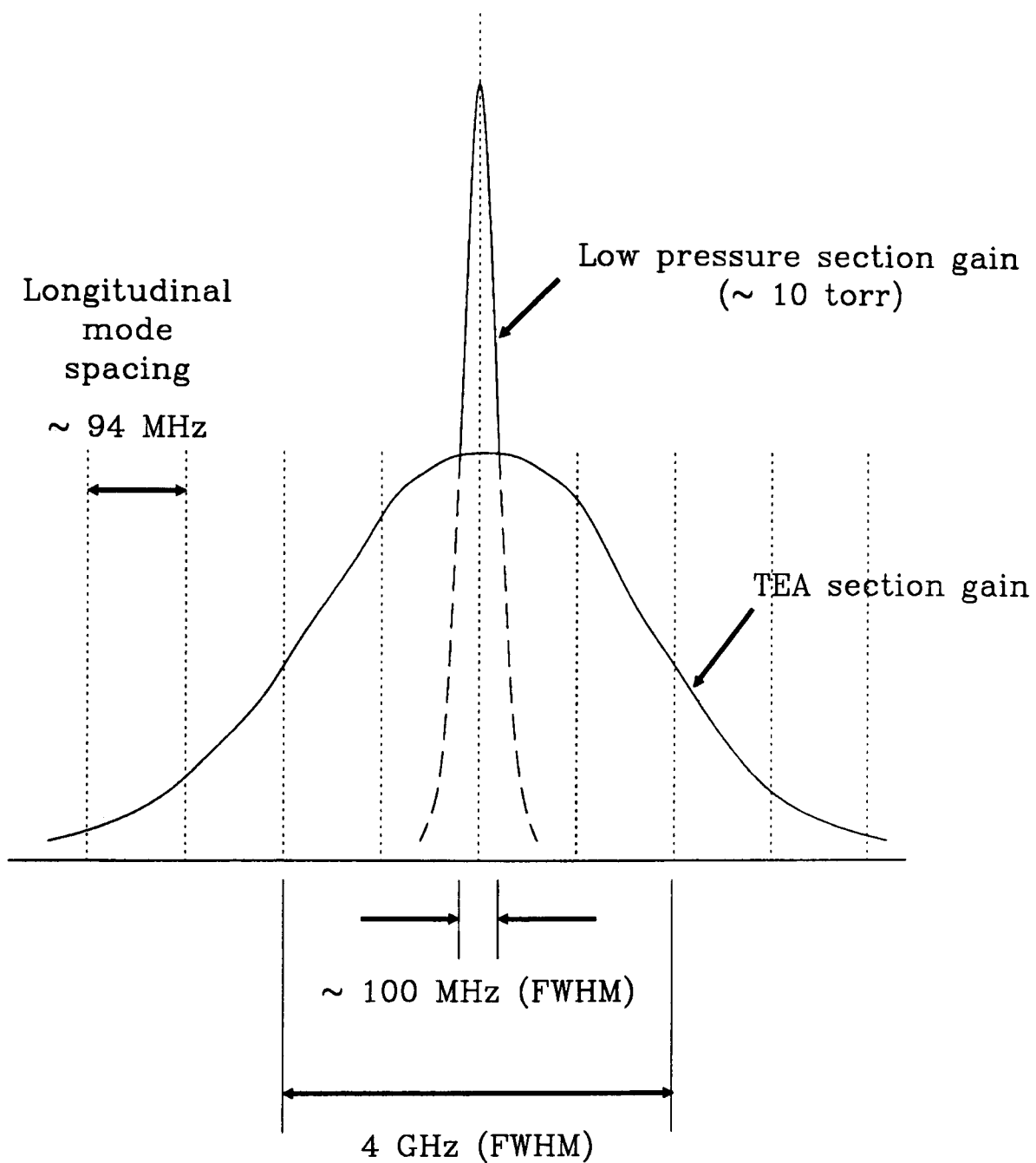


Fig. 2.1-3 Suppression of longitudinal modes by the addition of a low pressure gas discharge tube

For a helium concentration of 80%, maximum power occurred for a  $\gamma$  of approximately 0.6, and maximum energy for a  $\gamma$  of roughly 0.5. The maxima were fairly broad. They further observed that a decrease in He concentration increased the laser output energy, but in the system used the lower limit was set at 60% with the onset of arcing. At maximum power, the pulse consisted of an initial spike of 100 ns (FWHM), and a tail of lower amplitude lasting for several microseconds, containing a large fraction of the total energy. It was noted that a reduction in  $N_2$  transferred more energy into the initial spike.

Only a brief study was attempted for this research, first to verify the above observations for this particular laser, and to look specifically at the effect of lower charging voltages. Pulse shapes were monitored using a Rofin photon drag detector and displayed on a Tektronix 7834 oscilloscope using the 7A19 plug-in module. Pulse-to-pulse stability was not studied. A study of the pulse shape was embarked upon because over the course of the research, the gas mix was varied to achieve different performance requirements. For example, for optoacoustic cell calibration a highly stable output was required, whereas for 'normal' absorption and decomposition work, optimal energy output combined with reasonable stability was acceptable. Furthermore, as the laser 'lived' (over a period of many months), adjustments in the gas mix and spark gap pressure were required. For this work, the two most typically used  $N_2:CO_2:He$  gas mixtures had flow rates in litres per minute of 1.2: 2.4: 9 ( $\gamma=0.67$ , He=71%), and 1.2: 2.2: 6.0 ( $\gamma=0.65$ , He=64%).

Firstly,  $\gamma$  was varied by adjusting the  $N_2$  flow rate (X) only ...clearly this also had the effect of changing the He concentration (as well as  $CO_2$  and  $N_2$  concentrations); the gas flow rates were X:2.2:6.2 with units of litres/min. The laser was tuned to the  $R_{20}(9\mu m)$  transition, and the power supply was

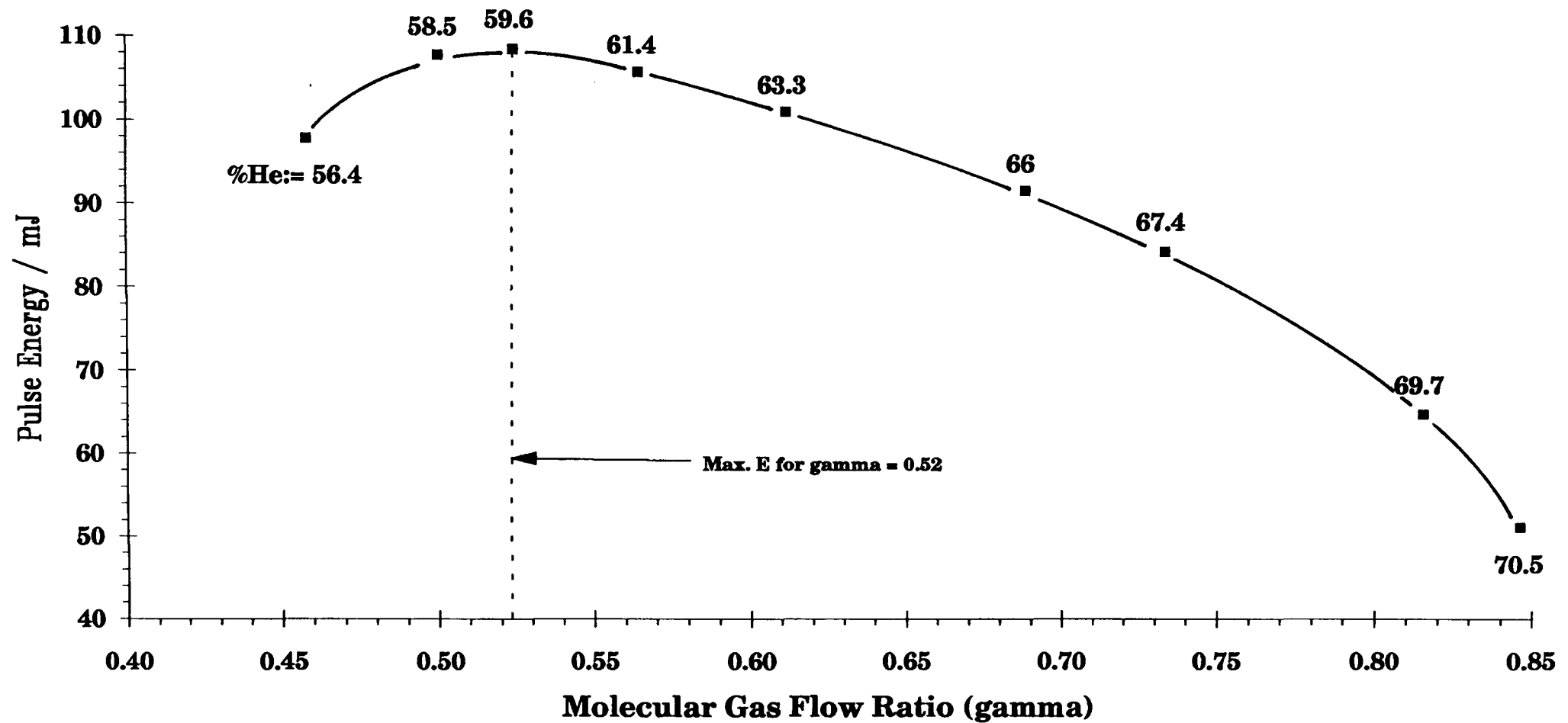
set at 19kV. The results shown in Fig.2.1-4 show that maximum energy output occurred for a  $\gamma$  of 0.52. The traces were not of sufficient clarity to study the effect on power, but the duration of the gain-switched spike was estimated to be of the order of 40 to 50 ns (FWHM). Secondly,  $\gamma$  was kept constant and the He concentration was changed, by altering both the N<sub>2</sub> and CO<sub>2</sub> flow rates. The results in Fig.2.1-5 show that maximum energy output occurred for a He concentration of 61%.

Examples of the pulse shape taken for Fig.2.1-4 are presented in Fig.2.1-6; there is an initial gain-switched spike of 40 ns (FWHM) followed by a very low amplitude tail. None of the pulse shapes in this series altered significantly with the simultaneous change in He concentration and  $\gamma$ .

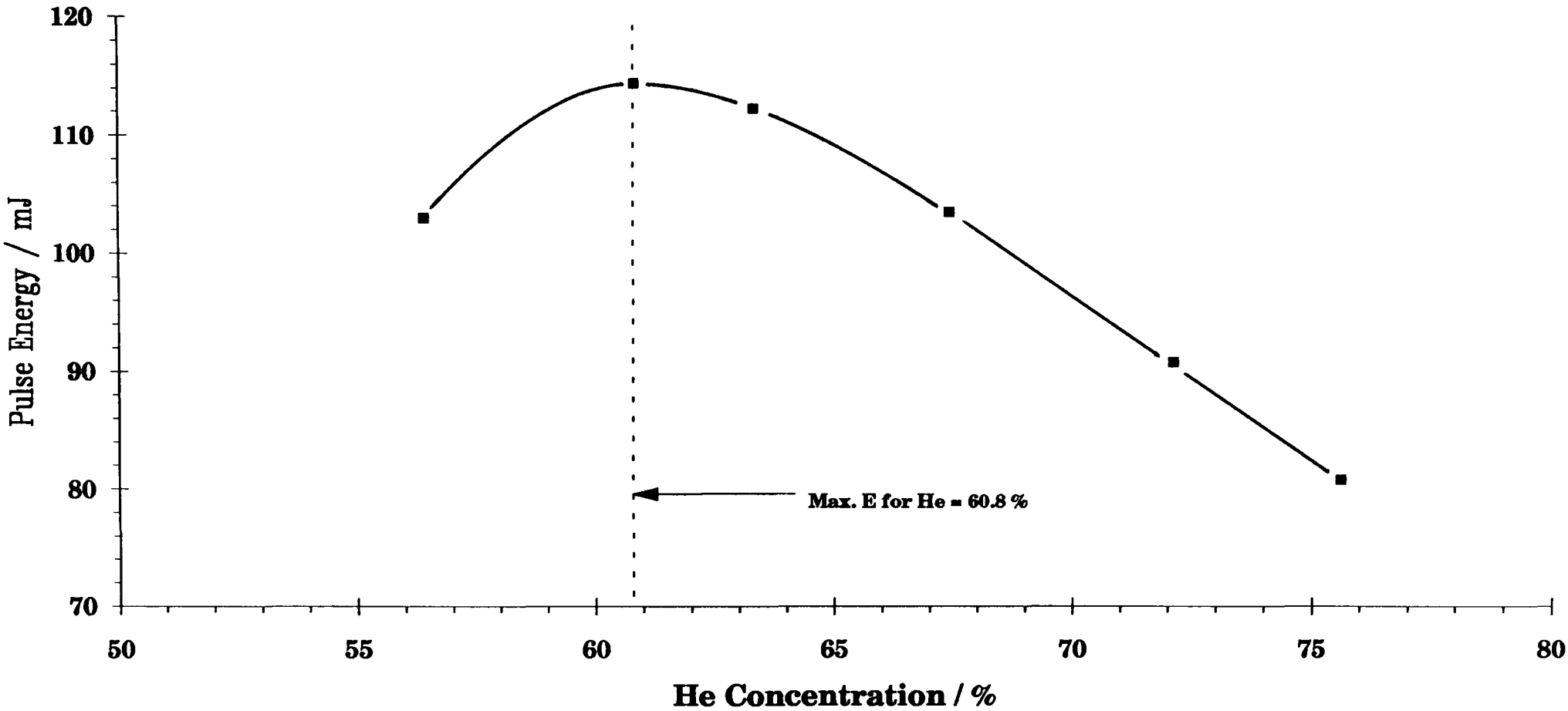
A comparison of the pulse shapes for two of the gas mixes used in this work is made in Fig.2.1-7a for a charging voltage of 19kV. For  $\gamma$  of 0.65 and 59% He concentration (case i), the width of the gain-switched spike is 43 ns (FWHM) and the base width is 486 ns, while for  $\gamma$  of 0.65 and 64% He concentration (case ii - most commonly used) the pulse length parameters are 49 ns (FWHM) and 486 ns. The tail contains roughly a quarter of the energy of the initial spike. The only noticeable difference between the two cases is that the spike of case (ii) is slightly longer.

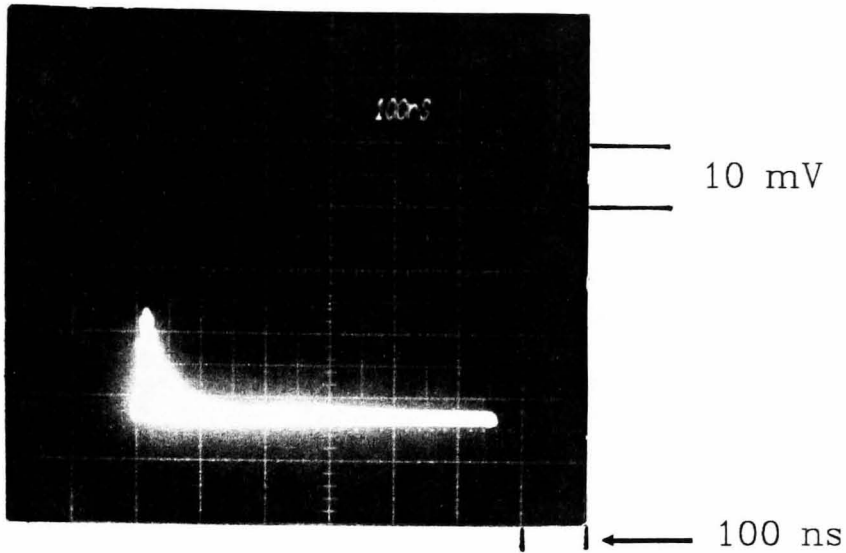
In Fig.2.1-7b the effects of charging voltage and He concentration on the pulse shape are explored. The charging voltage is 17.5kV compared to 19kV of Fig.2.1-6a. In case (i),  $\gamma$  is 0.65 with 64% He concentration, and a pulse length of 60 ns (FWHM) and base width of 600 ns is produced. For case (ii), a  $\gamma$  of 0.65 with 70% He concentration produces a 57 ns pulse with a base width of 600 ns. There is less than a quarter of the spike energy in the tail. The increase in the He concentration is seen to increase the separation of the

**Fig. 2.1-4** Variation of pulse energy with molecular gas flow ratio for the TEA CO<sub>2</sub> laser (19 kV charging voltage). The R20 (9 μm) transition was used in multimode configuration. The N<sub>2</sub> : CO<sub>2</sub> : He gas flow rates were X : 2.2 : 6.2 in l/min



**Fig. 2.1-5 Variation of pulse energy with %He for the TEA CO<sub>2</sub> laser (19 kV charging voltage) at a constant molecular gas flow ratio of 0.5. R20 (9 μm) transition was used in multimode configuration. The N<sub>2</sub> : CO<sub>2</sub> : He gas flow rates were X : X : 6.2 l/min**





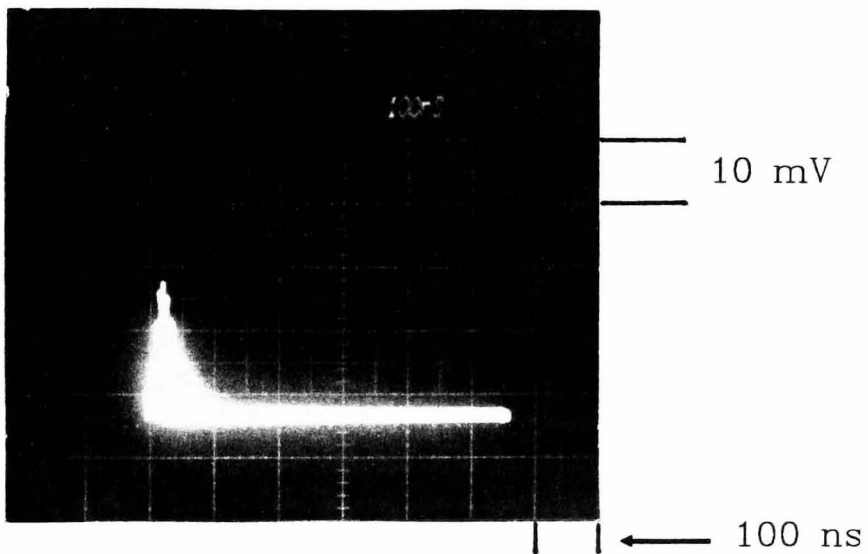
N<sub>2</sub> : CO<sub>2</sub> : He = 2.6 : 2.2 : 6.2 l/min

He content = 56.4 ± 0.6 %

Gamma = 0.458

Pulse energy = 97.8 ± 1.2 mJ

FWHM pulse length = 40 ns



N<sub>2</sub> : CO<sub>2</sub> : He = 0.5 : 2.2 : 6.2 l/min

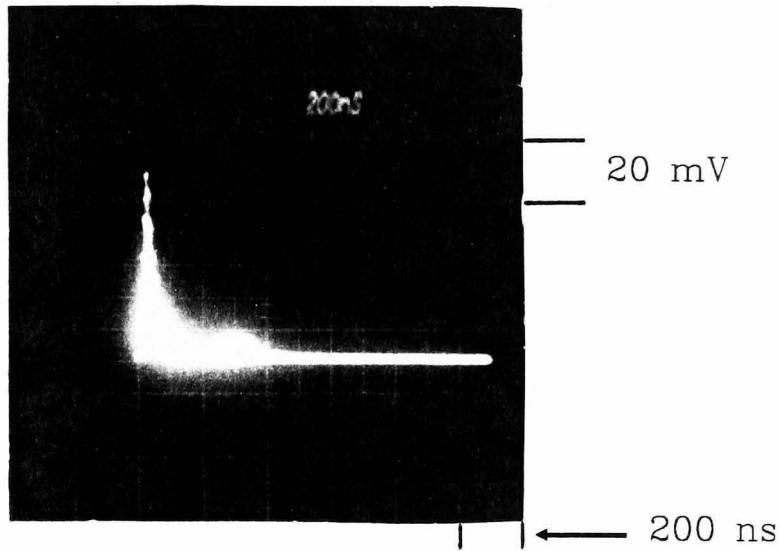
He content = 69.7 ± 0.6 %

Gamma = 0.815

Pulse energy = 64.8 ± 0.2 mJ

FWHM pulse length = 40 ns

Fig. 2.1-6 Rofin drag detector temporal profiles - R20 (9µm) multimode pulses



N<sub>2</sub> : CO<sub>2</sub> : He = 1.1 : 2.0 : 4.5 l/min

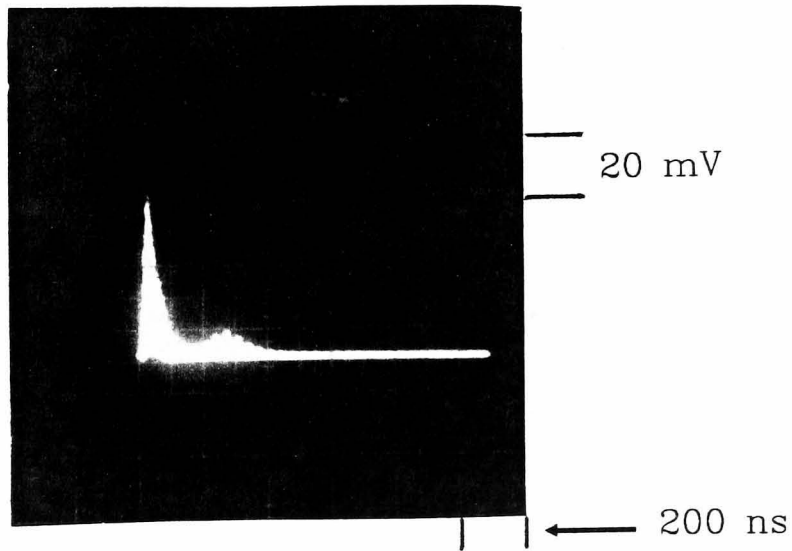
Charging voltage = 19 kV

He content = 59.2 +/- 0.6 %

FWHM pulse length = 43 ns

Gamma = 0.65

Base width = 486 ns



N<sub>2</sub> : CO<sub>2</sub> : He = 1.2 : 2.2 : 6.0 l/min

Charging voltage = 19 kV

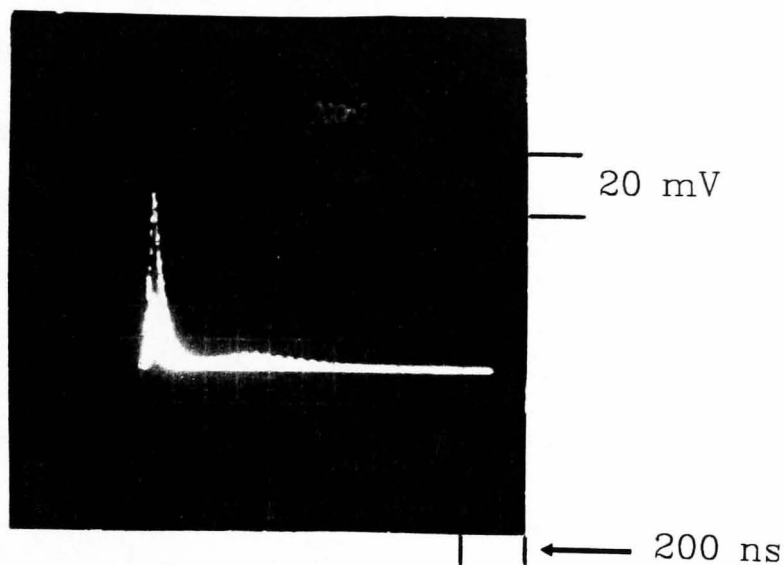
He content = 63.8 +/- 0.6 %

FWHM pulse length = 49 ns

Gamma = 0.815

Base width = 486 ns

Fig. 2.1-7a) Temporal profiles using typical conditions - R24 (10 μm) multimode pulses



N<sub>2</sub> : CO<sub>2</sub> : He = 1.2 : 2.2 : 6.0 l/min

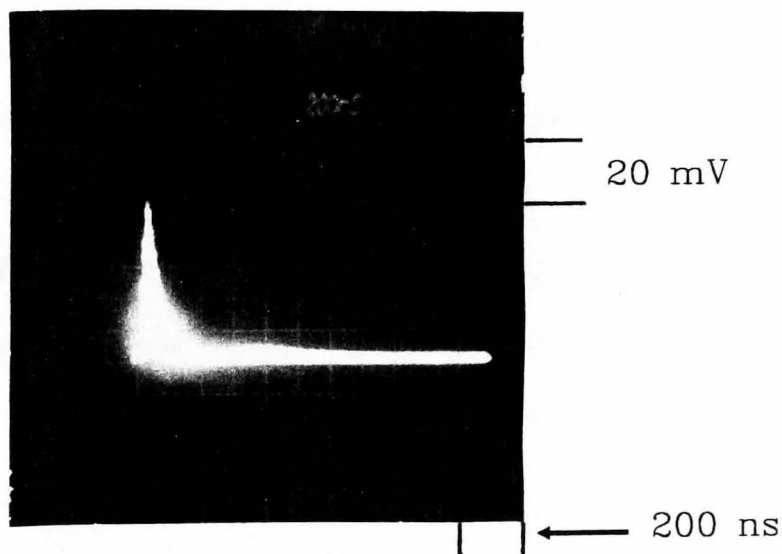
He content = 63.8 +/- 0.6 %

Gamma = 0.65

Charging voltage = 17.5 kV

FWHM pulse length = 60 ns

Base width = 600 ns



N<sub>2</sub> : CO<sub>2</sub> : He = 1.2 : 2.2 : 8.0 l/min

He content = 70.2 +/- 0.6 %

Gamma = 0.65

Charging voltage = 17.5 kV

FWHM pulse length = 57 ns

Base width = 600 ns

Fig. 2.1-7b) Temporal profiles for:  
 (i) reduced charging voltage; and (ii) reduced charging voltage and compensating increase in flow rate - R24 (10  $\mu$ m) multimode pulses

spike and tail. The 'secondary' pulse seen in the tail of each trace is likely due to repumping from  $N_2^*$ ;  $N_2^* + CO_2 \longrightarrow CO_2^* + N_2$ . The peak power of the tail drops with the charging voltage and shifts further from the main pulse, but is not affected by small changes in the gas mix. Furthermore, a reduction in charging voltage also reduces the peak power of the initial pulse while both pulse length and base width increase. As discussed in detail in Section 4.3.1, there was an experimental requirement to reduce the pulse energy beyond what could be achieved by the sole use of attenuators. The pulse energy drop was achieved with a simple decrease in power supply voltage and an increase in He concentration from 64% to 70% to optimise fluence stability (reference Fig.2.1-5).

A comparison of pulse shapes for multi-axial mode (multimode) and single-axial mode (singlemode) operation is made in Fig.2.1-8. One might expect single-axial mode pulses, which have a smooth temporal envelope (Fig.2.1-8a), to have different effects in multiphoton decomposition to the multi-axial mode case, where strong axial mode beating occurs (Fig.2.1-8b). Switching between these two cases was relatively easy with the hybrid TEA  $CO_2$  laser and simply required evacuation of the low pressure section: the pulse energy was found to be constant when switching in this manner.

In summary, the results show that there is maximum energy for  $\gamma$  of roughly 0.5; that energy decreases with increasing He concentration above 60%; and that arcing is observed as the energy decreases with decreasing He concentration below 60%: these results are supported by the previous empirical findings of Dyer *et al.* (37). The data were insufficient to verify that a reduction in  $N_2$  concentration (i.e. increasing  $\gamma$ ) transferred more energy into the spike (37), but it was assumed to be true. In this instance, the gain switched spikes were roughly 50 ns long, and the pulse base width was about

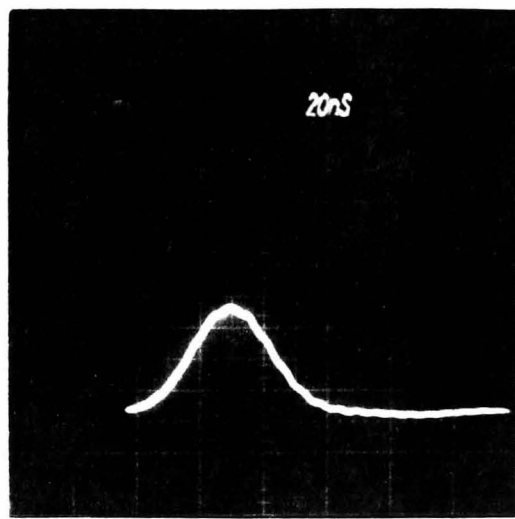
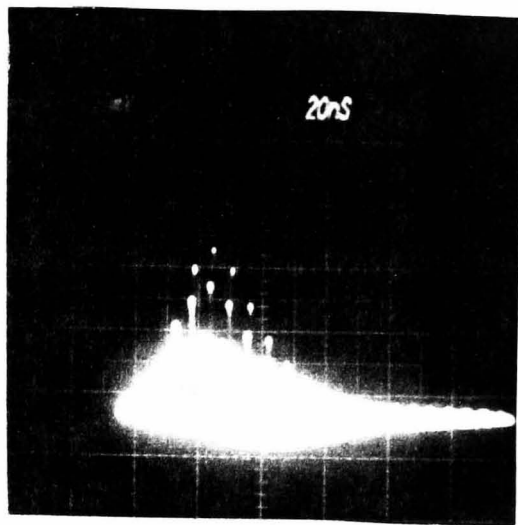


Fig. 2.1-8 Multimode and singlemode pulse temporal profiles (equal pulse energies)

600 ns. Flow rates were chosen (for absorption and decomposition work) to minimise the tail pulse (making  $\gamma > 0.5$ ), maximise the energy (obtained at  $\gamma = 0.5$ , He=60%) and maximise stability (making He concentration  $> 60\%$ ): the conditions used were  $\gamma = 0.65$ , He=64%. The concentration of He was further increased during times of calibration to gain extra stability when high energy was not required; the conditions then were  $\gamma = 0.67$ , He=71%. In the one instance that particularly low fluence was required, the charging voltage was dropped from 19 kV and the He concentration was raised to 70%; raising the He concentration further reduced the output, but was also required to optimise fluence stability.

### 2.1.3 Spatial Beam Profiles

For simplicity and reliability, the laser was operated on the TEM<sub>00</sub> transverse mode by using an aperture within the optical cavity. The resulting spatial irradiance distribution (or fluence distribution for a pulsed laser) in a plane normal to propagation is then Gaussian, and described by (98,99):

$$I = I_0 \exp(-r/r_0)^2 \quad (2.1-1)$$

where  $I_0$  is the maximum irradiance (power per unit area) at the beam centre;  $r_0$  is the Gaussian beam radius given by the radius at  $I = I_0/e$ ; and  $r$  is the radial co-ordinate.

It is well known that photochemical processes are strongly dependent upon the irradiating fluence. It was therefore necessary to establish that the fluence gradient across the length of the cell was negligible. The actual value of the irradiated volume is also required, in order to calculate the fractional decomposition. For these purposes, spatial beam profiles were taken, and a value for the Gaussian radius calculated. The Gaussian beam

assumption was verified by plotting theoretical profiles using the experimental  $r_0$ .

There exist several methods for measuring the spatial profile of a beam. Three procedures were utilised during the course of this work, one method being succeeded by another as the need for greater accuracy and reliability was realised.

Initially the profiles were found by scanning a sensitive joulemeter across the beam. Two sharp blades, forming a narrow slit aperture, were attached to the detector's face, and the detector head sat on a micropositioner, which could be adjusted along two axes. For a well defined beam, measurements were to be taken at intervals less than 0.5mm with an aperture width less than this value. However, more generous slit sizes were found to be necessary in order to provide readings with favourable signal-to-noise ratios. This technique was clearly not satisfactory but the best possible with the available instrumentation.

An SBRC (Santa Barbara Research Centre) photoconductive Au-Ge detector, cooled to liquid nitrogen temperature (77K), was then used to improve the measurement technique. This was fitted with a 0.35mm diameter pinhole to restrict the sample beam size. The equipment was highly sensitive, and the beam was attenuated to avoid damaging the detector element. This detector was mounted on a platform, which could be scanned using microadjusters along two axes, and was placed at the planes of interest (front and back faces, and the central plane of the sample cell). The detector signal was fed to a Tektronix 556 oscilloscope. Care had to be taken to keep the detector at a constant temperature, since its sensitivity was strongly dependent on temperature.

Reasonable profiles were obtained using this method, and astigmatism (caused by the inverse telescope described later in Section 2.4) was quite evident. However, it was time consuming to obtain a complete scan and, because it was known that the laser output would alter slightly with time, a faster technique was desirable. For example, profiles taken (and repeated within a few hours), at two separate planes within the expected region of negligible change, indicated a 30% difference in the radius. It was not possible to say whether this was a real effect, or a result of the slow scanning; the profiles take the passing of several hundred pulses to complete (at 1Hz pulse-repetition-rate), and as already mentioned the laser output was known to change over such periods of continuous use.

A 25mm linear pyroelectric detector manufactured by Delta Developments became available; the array being made up of 50, 0.5mm square detectors. It provided a means of measuring the full profile of each pulse, at any angle between the vertical and horizontal axes. A Tektronix oscilloscope was used to display the profiles (Fig. 2.1-9). To use the full size of the array, the beam was expanded using a long focal length Ge convex lens. Experimental imaging of crosswires (placed at the "centre-of-cell" position), enabled the focal length,  $f$ , of the lens to be established at 10.6 $\mu$ m using

$$\frac{1}{f} = \frac{1}{v} + \frac{1}{u} \quad (2.1-2)$$

where  $v$  and  $u$  were the measured image and object distances respectively;  $f$  was found to be 60.8cm.

The image planes of the internal faces of the front ( $v_1$ ) and back ( $v_2$ ) of

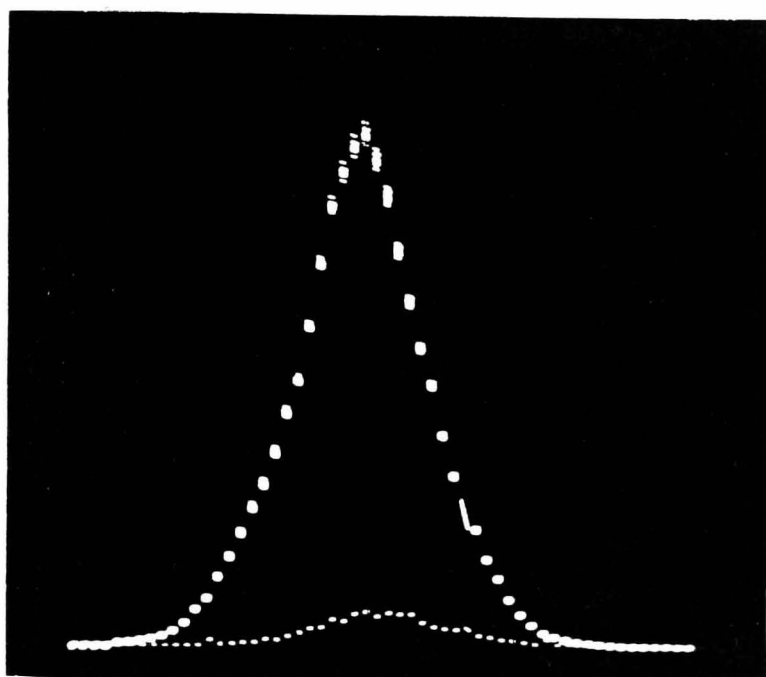


Fig. 2.1-9 Spatial beam profile using the array profiler (10 pulses are superimposed)

the cell were then located by calculation using

$$\frac{1}{v_{2,1}} = \frac{1}{f} - \frac{1}{(u \pm k)} \quad (2.1-3)$$

where  $k = \text{cell length}/2$

The Gaussian radii established at the image planes are magnifications of those at the object planes. The magnification factors are given by:

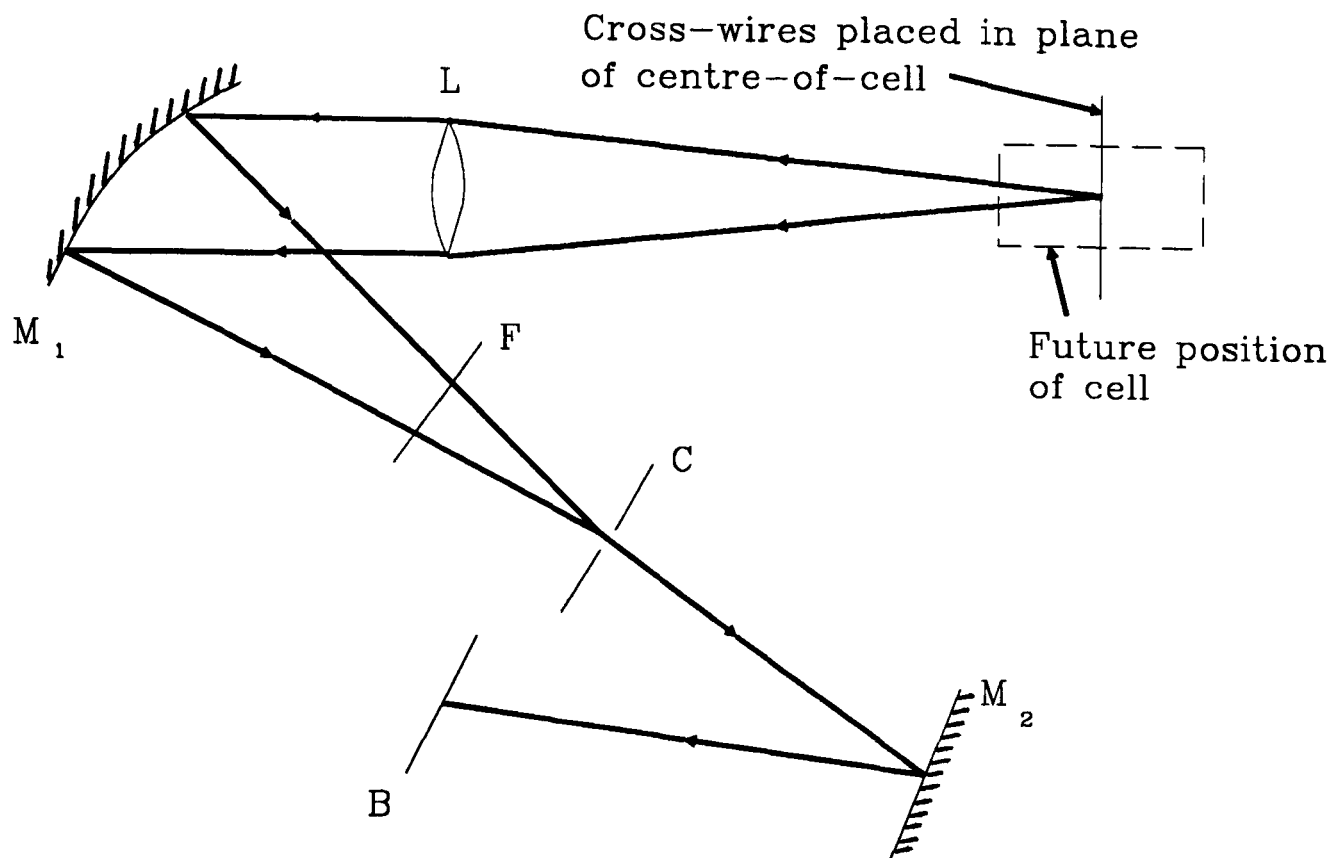
$$M = \frac{v}{u} \quad (2.1-4a)$$

$$M_{\text{backface}} = \frac{f}{(u - k - f)} \quad (2.1-4b)$$

$$M_{\text{frontface}} = \frac{f}{(u + k - f)}$$

where  $u$  refers to the "object distance" to the "centre-of-cell". Figure 2.1-10 illustrates the set-up used.

The method for calculating the measurement error of the Gaussian radii at cell front, back, and centre in object space is summarised as follows: Firstly, from the crosswire imaging of cell-centre,  $u$  and  $v$  are measured with errors  $\delta u$  and  $\delta v$ , then the error in the magnification factor (to be applied to the measured cell-centre Gaussian radius) is calculated from Eq. 2.1-4a. Furthermore, the measurements of  $u$  and  $v$  give  $f$  (Eq. 2.1-2), and  $\Delta f/f$  is determined. This  $f$  with its error is then used to predict the position of the image planes ( $v_{1,2}$ ) of the front and back of the cell (Eq. 2.1-3) which are located with an inaccuracy  $\delta v$ . This  $\delta v$  leads to an uncertainty in stating that the  $u \pm k$  Gaussian radii are actually at the cell faces;  $\Delta u'/u'$  is determined, where  $u'$  is the object distance corresponding to the  $v_{1,2}$  planes. Using this  $\Delta u'/u'$  and  $\delta v$ , the error in determining the magnification factor (to be applied to the "end-of-cell" Gaussian radii measured in the image plane) is calculated *viz.*  $\Delta M/M$ . Finally, the fractional errors of the Gaussian radii at the cell are



$M_1$ & $M_2$ – brass mirrors	$F$ = 345.2 cm
$L$ – Ge convex lens; f.l. = 60.80 cm @ 10.6 $\mu\text{m}$	$LC$ = 462.5 cm
$F, C, B$ – Profiles taken in these image planes of the front face, centre and back face of the cell	$LF$ = 807.7 cm
	$M_2 B$ = 118.5 cm
	$LB$ = 745.4 cm

Fig. 2.1–10 Schematic of the optical set-up for taking spatial beam profiles with the array detector

established using  $\Delta M/M$  and the measurement error of the Gaussian radius at the image plane.

In this section, the details of the calculation are given: The error in M from Eq. 2.1-4 for the "centre-of-cell" plane is

$$\Delta M = \frac{u \delta v}{u^2} - \frac{v \delta u}{u^2}$$

and 
$$\frac{\Delta M}{M} = \left( \frac{\delta v}{v} \right) - \left( \frac{\delta u}{u} \right)$$

from which the fractional error  $\Delta M/M$  was found to be 3.0%.

From Eq. 2.1-2, the error in the calculated f caused by measurement errors,  $\delta u$  and  $\delta v$ , of u and v is given as

$$\Delta f = \frac{u(u+v) - vu}{(u+v)^2} \delta v + \frac{v(v+u) - vu}{(u+v)^2} \delta u$$

and 
$$\frac{\Delta f}{f} = \left( \frac{u}{u+v} \right) \left( \frac{\delta v}{v} \right) + \left( \frac{v}{u+v} \right) \left( \frac{\delta u}{u} \right)$$

from which the fractional error  $\Delta f/f$  was found to be 0.9%.

Similarly, from Eq. 2.1-2 the fractional error(s) in  $u'$  ( $u'=u \pm k$ ) (the object distances calculated from the "end-of-cell" image plane distances  $v'$  ( $v_1$  and  $v_2$ )) are:

$$\frac{\Delta u'}{u'} = \left( \frac{f}{v-f} \right) \left( \frac{\delta v'}{v'} \right) + \left( \frac{v'}{v'-f} \right) \left( \frac{\delta f}{f} \right)$$

and were found to be 1.3% for  $v_1$  (cell-front), and 1.2% for  $v_2$  (cell-back).

From Eq. 2.1-4b, the fractional error of M for the cell-ends is

$$\frac{\Delta M}{M} = \left( \frac{u'}{u'-f} \right) \left( \frac{\delta f}{f} - \frac{\delta u'}{u'} \right)$$

and was found to be 2.3% for the cell-front and 3.7% for the back, and the root sum squared (rss) error over the entire cell length is  $\sqrt{(2.3\%^2 + 3.0\%^2 + 3.7\%^2)} \approx 5\%$ , while the average is 3%.

Finally, the Gaussian diameter in the image plane,  $D_{oI}$ , is determined from the oscilloscope photograph to better than 0.5mm ( $\delta D_{oI}$ ). Since the Gaussian radius in the object plane,  $r_o$  is  $D_{oI}/2M$ , the fractional measurement error is

$$\frac{\Delta r_o}{r_o} = \frac{1}{2Mr_o} \left( \delta D_{oI} - \left( D_{oI} \frac{\delta M}{M} \right) \right)$$

and was determined to be 8%, 4% and 0.005% for radii at the cell front, centre, and back respectively.

However, experiments showed that;

- (i) a  $\pm 12\%$  change in  $r_o$  can occur if the laser is run continuously for half an hour (the longest experiments were carried out for 20 minutes).
- (ii) differences in  $r_o$  of upto 12% were noted between consecutive attempts at realigning the laser to re-establish the best laser output.
- (iii) consecutive shot-to-shot profile reproducibility was excellent as shown in Fig.2.1-9 which shows superimposed exposures of 10 pulses.
- (iv) switching from multimode to singlemode operation of the laser produces no more than a 5% change in  $r_o$  (which includes a measurement fractional error of only 0.005%).
- (v) There was an average change of  $\leq 0.01$  mm in radius between the cell centre and its windows:

Three profiles taken at  $45^\circ$  to each other in each plane showed that

the inverse telescope arrangement introduced astigmatism at the focal region where the cell was situated; the shortest length was about 80% of the longest. Averaging the Gaussian radii over the cell length gave a value of  $0.52 \pm .01\text{mm}$ .

These errors (determined by monitoring fluctuations in the radius), will be called 'experimental' errors, since they arise through changes in the experimental equipment.

Since, the measurement fractional error of the Gaussian radius is <8% (as demonstrated earlier) and is included in the experimental fractional errors tabulated above (in parts i, ii, and iv), the confidence in  $r_0$  will be given as the most probable error  $\sqrt{(12\%^2 + 12\%^2 + 5\%^2)} \sim 18\%$  using those experimental values.

#### 2.1.4 Deconvolution

The yield and absorption parameters measured are a function of fluence under certain experimental conditions. Clearly, the difficulty in interpreting the results will be compounded by the fact that the laser beam intensity (and therefore fluence) is not a constant across its cross-section. Black *et al.* (32) used the following equation to deconvolute their results, that is, to predict experimental values that would have been observed if the beam had had a 'top hat' fluence profile. The value of any fluence-dependent quantity  $f$  corresponding to the uniform fluence  $F$  is :

$$f_D(F) = \frac{d(\ln f_G(F))}{d(\ln F)} \times f_G(F) \quad (2.1-4)$$

where  $f_D(F)$  is the deconvoluted value corresponding to a uniform fluence, and  $f_G(F)$  is the experimental value of  $f$  for a Gaussian beam with nominal fluence  $F$ , as given by the measured energy divided by the nominal cross sectional area of the Gaussian beam  $\pi r_0^2$ .

## 2.2 DESCRIPTION OF REACTION CELLS

Experimentation began with an OA cell 1.5cm in length and of volume  $12.78 (\pm 0.26)\text{cm}^3$ , fitted with a Tandy electret microphone element (6). An electret is a piece of permanently charge-polarized dielectric (usually Mylar), manufactured by cooling the material (from high temperatures) within a strong electric field. One side is coated with metal to form an electrode, and a small air gap ( $\sim 20\mu\text{m}$ ) separates the dielectric from the second electrode. When the electret is displaced, the capacitance of the device,  $C$ , changes and since the charge,  $Q$ , is fixed, the signal,  $V$ , changes ( $C=Q/V$ ): thus, it is seen that an electret-type microphone is a self-biased electrostatic or condenser transducer. Since this is a high impedance device, high input impedance amplifiers (eg. FET amplifiers) are required to avoid losses by impedance mismatching.

Unfortunately, for the 2,2-dimethyloxetane under scrutiny at that time, the low absorption (about 1%) was below the detection limit of the OA-calibrating differential joulemeter system; a more sensitive calibrating system, capable of measuring only  $5\mu\text{J}$  of absorbed energy, would not be developed until much later. Both calibrating systems are described in Section 2.3. A pressure of about 10 torr would have given more suitable absorption (10%), but at such pressures the OA signal became distorted. Although the cell was consequently abandoned for an 8cm cell in order to increase the absorption path, the clarity of the oscillatory substructure was such that the OA traces appeared to be adequate for calculating the velocity of sound in the gas, as described in Section 1.4.2. The frequency of the substructure is required for the calculation, and so care must be taken in choosing a trace unaffected by distortions. Since the determination of the velocity of sound is not directly relevant to the rest of the project, all further discussion on this occurs in Appendix A1. Calculations could not be attempted in this manner

for other sample gases because they did not exhibit clear resonances (though the signals were adequate for the required absorption measurements - see Fig.2.2-4). The oscillations (Fig.1.3-2) should be attributable to radial resonances of the cylindrical cell (Eq.1.3-5) because the work was carried out at relatively low pressures so that longitudinal resonances are negligible. However, the work discussed in Appendix A1 leads to the interesting conclusion that all the identifiable resonances were, in fact, microphone resonances. This method, for measuring the velocity of sound of a gas, might only be useable at very high pressures when these microphone resonances are damped.

Several problems were experienced with the original 8cm cell (Fig.2.2-1), (volume  $50.22 \pm 0.13 \text{ cm}^3$  (6)) which was also fitted with an electret microphone. These problems were namely OA signal saturation and distortion; reaction of the gas with the cell; and an unreliable microphone sensitivity:

(i) Saturation of the OA signal at low pressure was attributed to a poor quality FET amplifier (i.e. high noise and low gain bandwidth). A new x10.6 amplifier overcame this problem, allowing measurements to be made on 2,2-dimethyloxetane for pressures of up to 7.5 torr instead of only 0.9 torr.

(ii) Stray capacitance also limited the bandwidth and distorted the signal. This was corrected by feeding the signal to the Tektronix 556 oscilloscope via a x10 probe: the capacitance of the probe was adjusted until a square wave input pulse could be displayed without distortion.

(iii) Initial decomposition studies on butan-2-ol clearly indicated that reactions were being induced by the materials of the microphone (or its housing). Several products were being formed without any irradiation, including significant quantities of those expected as a consequence of irradiation. Thus, the potential to gather coincident absorption and decomposition data was lost.

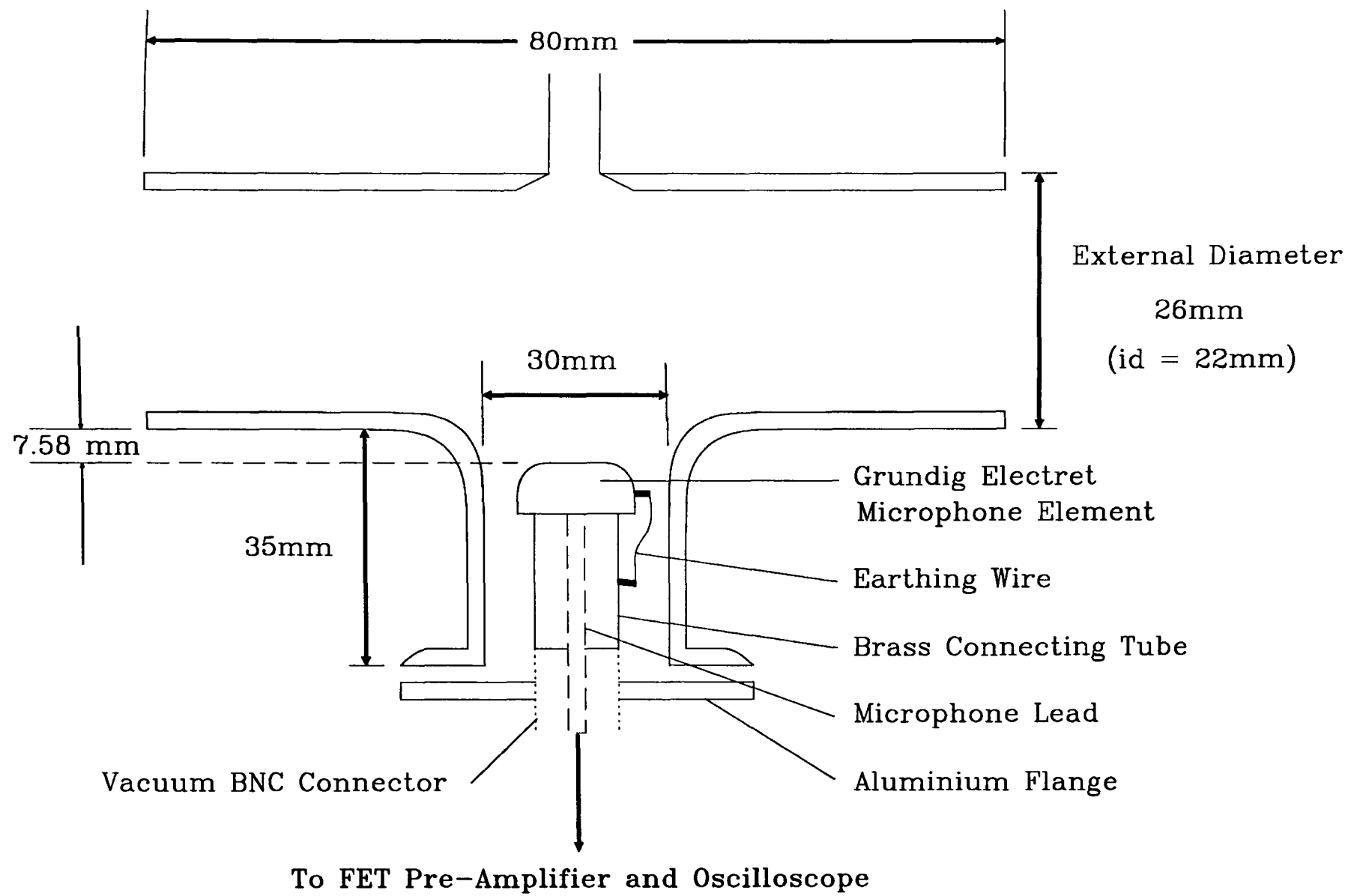


Fig. 2.2-1 Original 8cm optoacoustic cell

(iv) Because of the hygroscopic nature of the NaCl windows, the cell was stored in a heated optical cupboard. After one such occasion, the microphone sensitivity was found to be greatly reduced. The change was attributed to irreversible thermal diffusion of the electric polarisation, stimulated by too high an ambient temperature.

A second OA cell was designed with various improvements in mind (Fig.2.2-2):

(i) The previous microphone housing had been rather heavy, making it cumbersome. The new cell was therefore designed to be lighter, non-reactive and of a geometry favouring 'ideal' OA signals.

(ii) A demountable housing for the microphone was used allowing for easy change of the microphone should it be damaged, or have been unsuitable. In place of the electret device, an electromagnetic, metal diaphragm microphone (Advanced Acoustics Type 62A - Fig. 2.2-3a) was used, with a manufacturer's specified responsivity of 0.56 mV/Pa, a diaphragm diameter of 1.6cm, and a flat frequency response from ~1500-3500 Hz. The microphone was modified by removing the front shield enclosure, aluminium plate and plastic membranes as in Fig.2.2-3b. This microphone has wider applications such as military fieldwork in which case the membranes provide a moisture barrier, protecting the internal mechanism from corrosion and contamination; the aluminium plate at the front and rear protects these thin membranes. Holes piercing the housing and plates/membranes allow for pressure equalisation. The signal was magnified (x100) and displayed on a Tektronix 556 oscilloscope. The metal diaphragm-type microphone was chosen in preference to the potentially more sensitive electret device and was used in the above configuration, because other work (38) indicated that it had better long-term stability and reproducibility. EMI screening was achieved by wrapping metal ribbon around the outside of the cell.

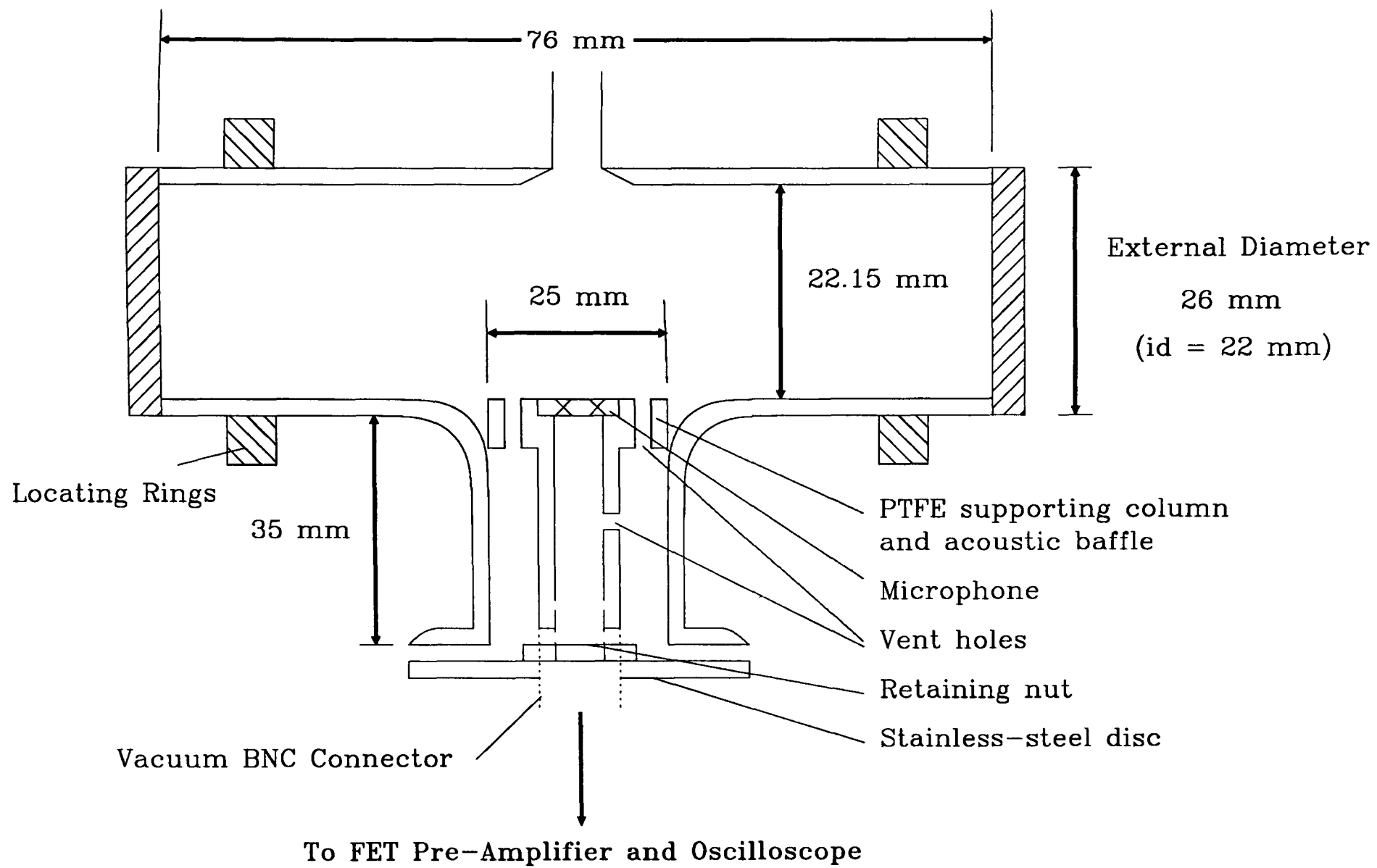
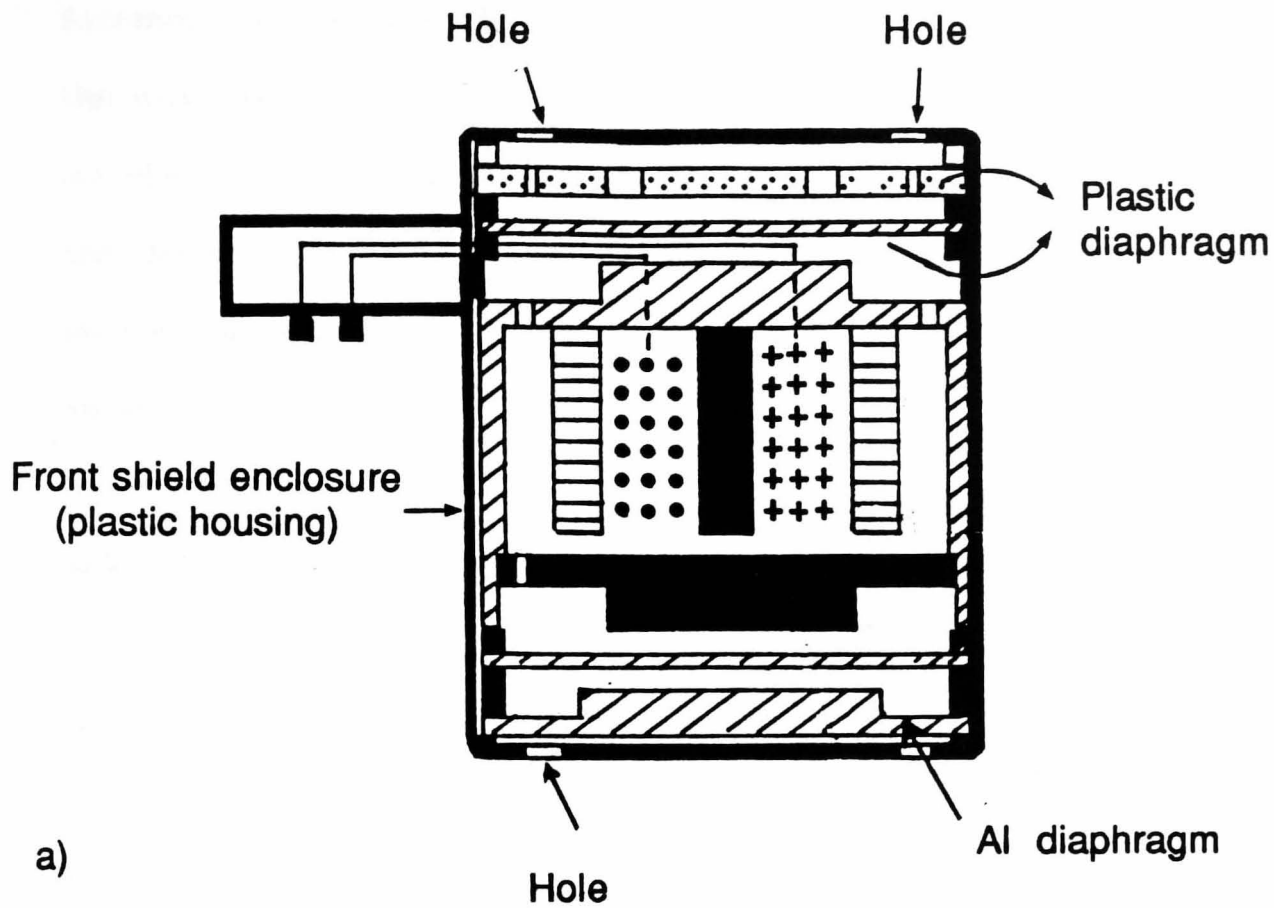
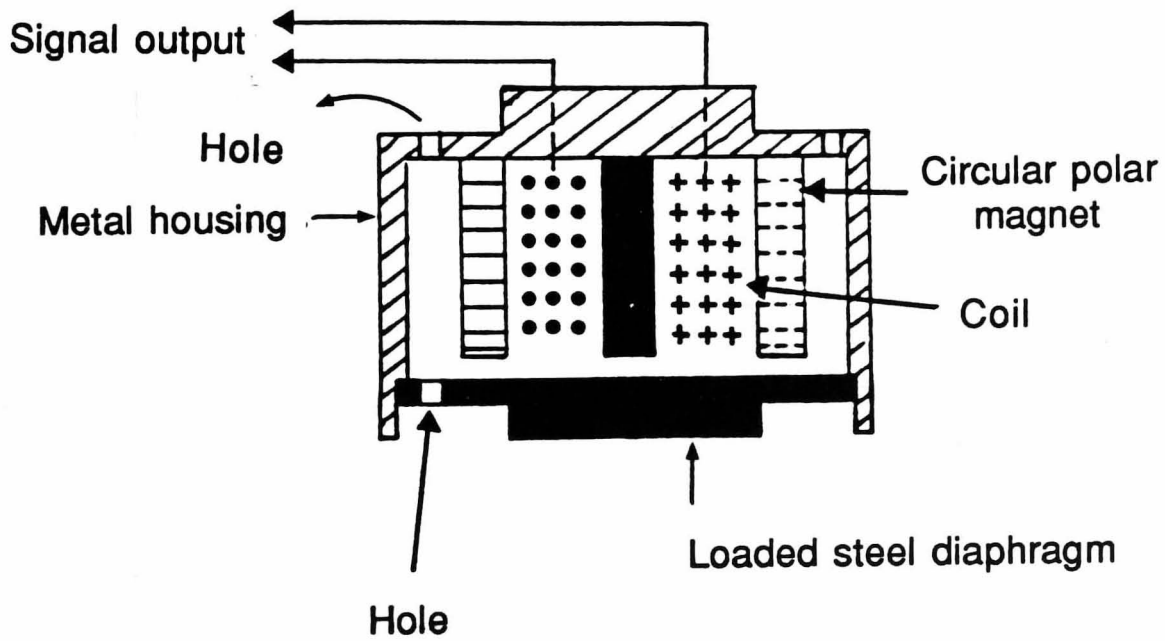


Fig. 2.2-2 Improved optoacoustic cell



a)



b)

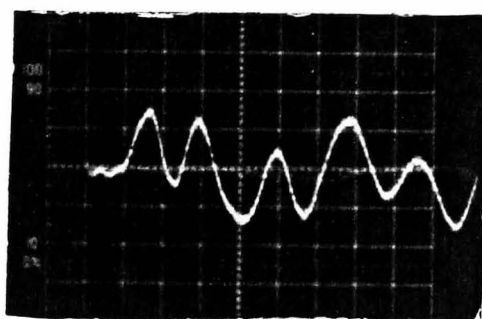
Fig. 2.2-3 Electromagnetic metal diaphragm microphone: a) as supplied; and b) as modified (from Ref. 38)

Attempts to optimise the coupling between the acoustic energy produced at the irradiated volume and the microphone, included specifying a perpendicular interface between the main body of the cell and the side-arms. Furthermore, the design included a facility for vertical positioning of the microphone. The microphone arm of the cell was filled with a PTFE core, which was to act as an acoustic baffle (hindering reflections from that area), and was threaded to allow for adjustment: thus the microphone could be fitted flush with the side of the cell. The PTFE core was pierced along its length in several places, to assist cell evacuation. Unfortunately, these attempts to preclude unwanted contributions to the OA signal were flawed because the pyrex cell was not made to specification; the junction of the microphone arm with the rest of the cell was very rounded and would cause complicated acoustic reflections (reference Section 1.3.2 on "Oscillatory Substructure"). The design would have been further improved (in terms of achieving a clean signal) if the gas input port was offset from its position opposite the microphone. The resulting signal substructure was too complicated to try speed of sound calculations using the resonant method of Section 1.4.2, (Fig.2.2-4), but was still adequate to proceed with absorption measurements. The first peak was very slight, occurring on a time scale of  $15\mu\text{s}$  even when the cell was evacuated; it was subsequently proved to be a window effect (that reached the microphone through the cell body) and was ignored.

The depression of the metal diaphragm by the incident pressure pulse disturbs the uniform radial field of the permanent magnetic which has circular poles. According to Faraday, an emf is induced in the coil which is directly proportional to the rate of change magnetic flux linking the coil. Consequently, the voltage output is dependent on the steel diaphragm velocity (and hence pressure gradient) rather than displacement as it would have been for a capacitance-type transducer.

96 mtorr of Bu-2-OH

0.1 V/div



50 μs/div

Fig. 2.2-4 Typical OA signal from the improved OA cell

The removal of the housing and diaphragms from the microphone, and operation at sub-atmospheric pressure, eliminated built-in damping mechanisms, so modifying the manufacturers specifications outlined above and allowing the metal diaphragm to resonate at the pressures used in this work. The microphone resonances are discussed in Section 2.3.2.

The new 7.6cm long OA cell (Fig.2.2-2) did not induce reactions in the absence of irradiation in butan-2-ol (or ethanol), so allowing absorption and decomposition data to be gathered from the same cell fill. It had a volume of  $4.039 \pm 0.20 \text{ cm}^3$  and an irradiated volume of  $0.06456 \text{ cm}^3$ . However, reactions of varying degrees (but all less than originally experienced with butan-2-ol), were found to occur for other molecules, so the decision was made to carry out the remainder of the decomposition experiments (which included further work on butan-2-ol) in a separate 8.0cm long, non-OA cell of cell volume  $30.41 \pm 0.38 \text{ cm}^3$  (irradiated volume  $0.06796 \text{ cm}^3$ ). The cell was based on the design of the OA cell, but without the microphone port.

A further non-OA cell was designed to test the effect of NaCl surfaces on the sample gas. It had been concluded for some gases that condensation was occurring when the gas was admitted to the cell; particles of condensed matter ablated from the NaCl window surfaces, may have been an explanation of the phenomenon observed by Shaw (6) *viz.* whilst studying ethanol, he monitored  $\text{C}_4$  hydrocarbon production even from an apparently evacuated cell. To exaggerate any surface stimulated effects, the cell was designed to hold several NaCl windows (Fig.2.2-5), the results of which are discussed in the decomposition results chapter under ethanol (see Section 4.1.6).

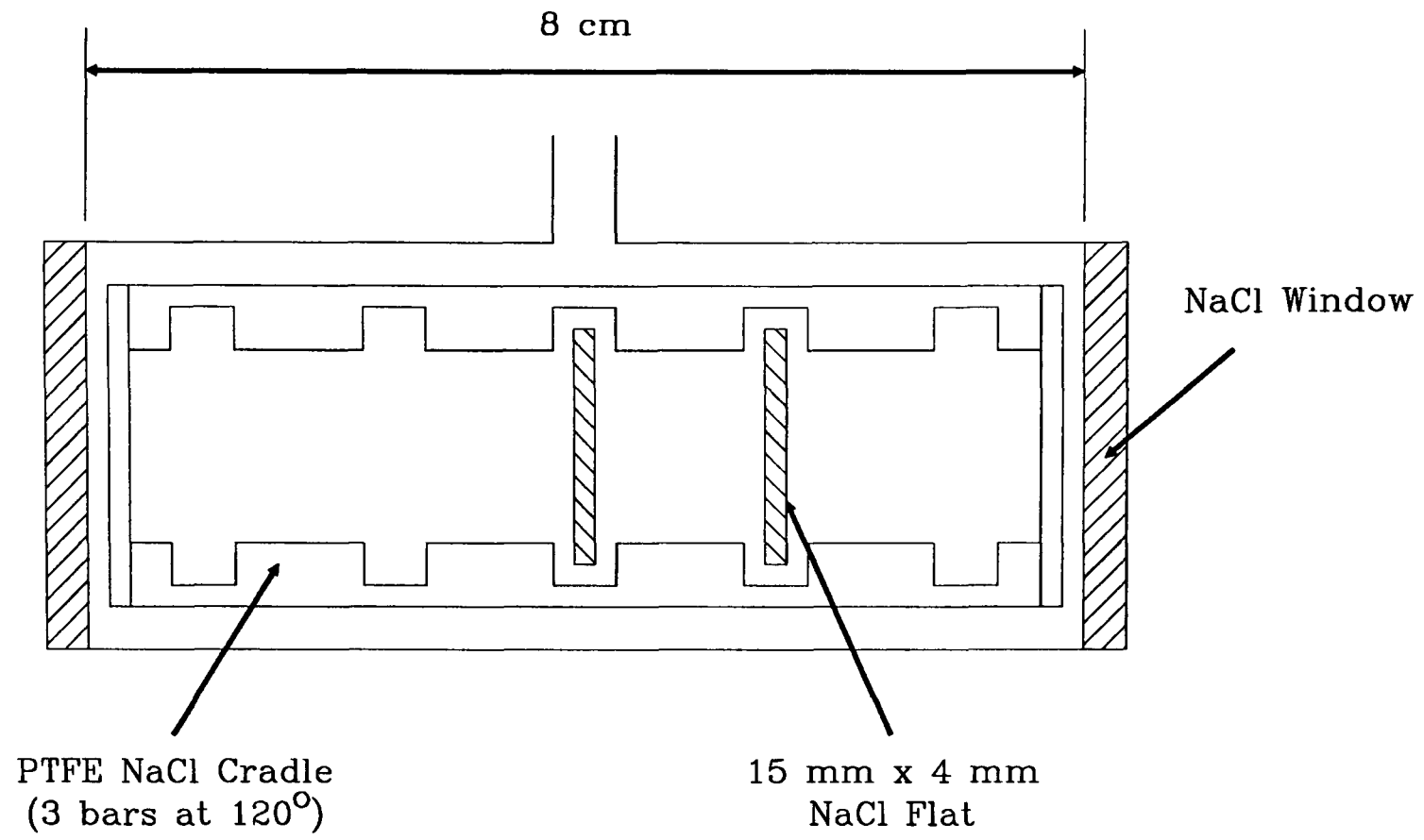


Fig. 2.2-5 Schematic diagram of the salt flat cell

As a standard procedure, the reaction cell (and vacuum line) was flushed with nitrogen before each cell fill, and the NaCl windows were replaced whenever clouding was noticed.

### 2.2.1 Cell Alignment

Certain precautions were taken to ensure constant geometrical conditions from experiment to experiment for reasons explained in Section 1.3. A permanent pointer marked the axial "centre-of-cell" position. Movement of the cell was made possible with the installation of a Cajon stainless steel flexible coupling between the cell and vacuum system. The pointing angle of the laser is not stable over long periods of time, and it was considerably simpler to align the cell to the beam than vice versa. The cell was cradled on a device which permitted both macro and microadjustments in all directions. The cell was firmly held in position once external metal rings sat flush with stops on the cradle. A ring fixed with a centralised carbon target, and of the same diameter as the locating rings on the cell, was moved to several places on the vacant cradle; adjustment of the cradle, until the laser beam fell on the centre of the target in each plane, ensured a central passage of the beam through the cell.

## 2.3 OPTOACOUSTIC CELL CALIBRATION

In order to relate the OA voltage signal to the energy absorbed, it was necessary to calibrate the cell. The procedure has in itself been a subject for development in this work (34).

Transmission techniques are often used for this purpose and rely on the difference between two transmitted signals with and without the gaseous sample present. Since the photochemical experiments were to be carried out under collision free conditions, low absorption was expected ( $<0.5$  mJ), and it

was felt necessary to calibrate in the range of the lowest detectable absorption. For such low absorption, the desired signal is the small difference between two large values, so that high quantitative accuracies in measured signal intensities are essential.

The most common method uses a differential ratio system (6, 35, 36). Figure 2.3-1 illustrates the set-up, and defines the variables; the variable attenuator is only relevant to Section 2.3.1. Voltages from joulemeters  $J_1$  and  $J_2$ , are connected through an amplifier to a digital display where there is simultaneous measurement of the incident and transmitted energies. Pre-calibration of  $J_1$  was carried out with a third joulemeter  $J_3$ , in the absence of the cell and the second beam splitter. The transmissivity for each of the cell windows,  $T_3$ , was established with a Perkin-Elmer 580B IR spectrophotometer by testing a freshly purged, then evacuated reaction cell. This transmission technique is independent of laser shot to shot intensity variation,  $E_0$ , and of beam reflectance,  $R$ , beam splitter transmissions,  $T_{1,2}$ , and joulemeter sensitivities,  $S_{1,2}$ , all of which would be difficult to measure: Appendix A2 shows the absorbed energy

$$E_{\text{abs}} = E_{\text{in}} \{ 1 - [(V_2/V_1)_F / (V_2/V_1)_E] \}$$

The subscripts F and E refer to the situation when the cell is full and empty respectively.

However, under conditions of low absorption, the small change in  $V_2$  is hidden by the total error accumulated from the (noise) uncertainties in each of the four voltage terms. Calibration at higher values of  $E_{\text{abs}}$  was not acceptable, because there were indications that the OA signal was not a

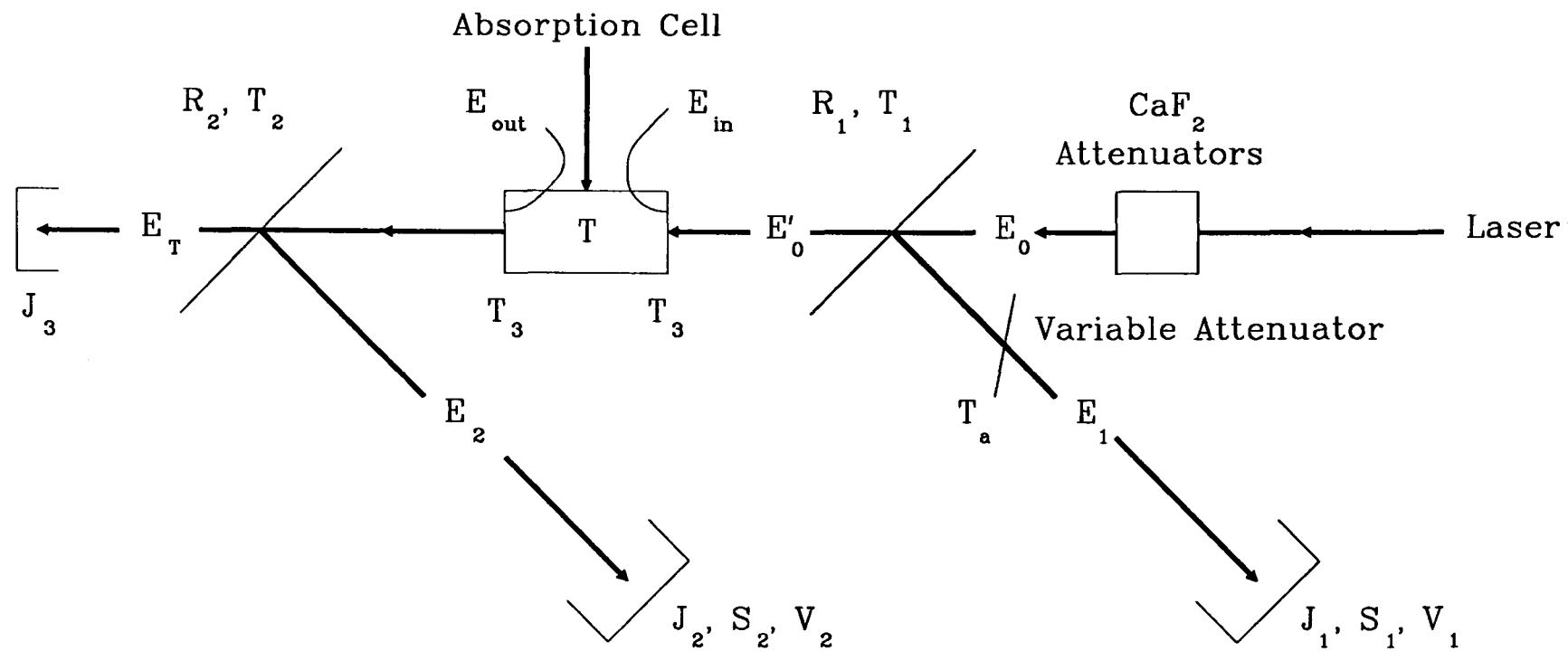


Fig. 2.3-1 Experimental arrangement for differential absorption measurements

linear function of absorbing energy, and therefore subsequent extrapolation to the lower  $E_{\text{abs}}$  region would introduce more serious errors.

### 2.3.1 The Differential Subtraction Method

A new, more sensitive technique was developed, which allows direct measurement of as little as 30  $\mu\text{J}$  absorbed from an incident 50-100mJ TEA  $\text{CO}_2$  laser pulse (the microphone can detect as little as 5 $\mu\text{J}$  ). This was a considerable improvement over previous results obtained using transmission methods that required repeated ratioing and averaging (35). Therefore, calibration over a wider than usual range was now feasible, giving a greater level of confidence when extrapolating the responsivity to the collision-free zone. In addition, it gives an immediate visual indication of the absorption level: In the previous technique, the degree of absorption was only evident after extensive calculation, and very often, a large amount of accumulated data was then found to be redundant. The new method was faster, a calibration procedure typically taking half an hour to complete compared to several hours for the other method.

The technique is again based on the arrangement of Fig.2.3-1. The key feature is the use of two closely matched, sensitive, pyroelectric joulemeters. The nearly identical detectors sample the input and output energy at the gas cell, and their signals are fed to a high sensitivity differential amplifier (Tektronix 7A22 plug-in module) where they are subtracted, then displayed on a Tektronix 7904 oscilloscope. With the cell evacuated, a continuously variable attenuator,  $T_a$ , (a pellicle polyethylene beam splitter situated at the face of  $J_1$  ) is adjusted until the resultant output voltage,  $\delta V_E$  is (ideally) zero. Assuming the joulemeters exhibit a linear energy responsivity, this voltage is:

$$\delta V_E = E_o (R_1 T_a S_1 - T_1 T_3^2 R_2 S_2) \quad (2.3-1)$$

and the responsivities,  $S_{1,2}$ , have units of V/J. On admitting an absorbing gas

(of transmission factor T) to the cell , the difference voltage becomes:

$$\delta V_F = E_o (R_1 T_a S_1 - T T_1 T_3^2 R_2 S_2) \quad (2.3-2)$$

Readings are taken of the deflection,  $\delta V$ , caused by the additional absorption, where:

$$\delta V = \delta V_F - \delta V_E = T_1 T_3^2 R_2 S_2 E_o (1 - T) \quad (2.3-3)$$

A third pyroelectric joulemeter,  $J_3$ , (Gentec) located behind the final beam splitter (in a low fluence region), is used to measure the transmitted energy,  $E_T$ , and to calibrate the system by providing a relationship between  $E_T$  and the voltage output,  $V_2$ , from  $J_2$ :

$$V_2 = R_2 S_2 E_T / T_2 \quad (2.3-4)$$

The expression for the energy absorbed in the gas sample,  $E_{abs}$ , is obtained by combining equations (2.3-1), (2.3-2) and (2.3-4):

$$E_{abs} = E_{in} - E_{out} = T_1 T_3 (1 - T) E_o = E_T \delta V / (T_2 T_3 V_2) \quad (2.3-5)$$

Thus, the absorbed energy is easily established by measuring the differential offset voltage,  $\delta V$ , the transmitted energy,  $E_T$ , and the corresponding output voltage,  $V_2$ , from joulemeter  $J_2$ ; the transmission factors for the beam splitter,  $T_2$ , and cell window,  $T_3$ , can be measured straightforwardly using standard techniques. By using  $J_3$  to measure the transmitted energy, the approach avoids the need for precise alignment of the ingoing and outgoing beam samples on  $J_1$  and  $J_2$ , and does not rely on knowledge of the beam splitter reflectivities.

The pyroelectric joulemeters were fabricated from a poled PZT ceramic substrate (Vernitron PZT5A) of nominal thickness 0.5 mm, and were used with the 'as supplied' metallic face coatings. In order to achieve as near possible identical sensitivities and time responses, both detectors were cut into squares of 10 x 10 mm<sup>2</sup> from the same parent substrate. They were coated simultaneously on one face, by sputtering from a pure carbon rod.

thus producing a uniform IR absorbing film of roughly 100Å thickness. The elements were mounted onto brass heat-sinks using equal quantities of silver loaded epoxy. The heat-sinks also formed the earth connection, whilst a fine wire, soldered to the edge of each front face, served as the output voltage lead. The voltage responsivity for the finished detectors, was measured as 22 V/J at 10.6  $\mu\text{m}$ .

The individual joulemeter output signals and the differential signal obtained under balanced conditions are shown in Fig.2.3-2. Despite the precautions taken, there was a slight difference in the temporal response of the two detectors. Imperfect cancellation in the time domain, caused the differential signal to be bipolar at high amplification; hence a perfect balance was not possible. Instead, the balance condition was set so that;

(i) the zero-crossing occurred at the same time as the joulemeter output voltage reached its maximum value (roughly 150  $\mu\text{s}$  after the start of the laser pulse).

(ii) the voltage offset,  $\delta V$ , was measured at the corresponding point to (i).

The lower limit on the measurable absorbed energy (Eq. 2.3-5), was set by fluctuations in the differential voltage signal. These fluctuations were traced to shot-to-shot variations in the laser energy, and to noise on the joulemeter outputs caused by extraneous acoustic and optical sources. The former probably arise through residual non-linearities in the joulemeter energy responsivity, or through slight movements of the beams on the joulemeters (a result of laser 'misfires'). Laser output stability was maximised for calibration purposes (to approximately  $\pm 0.4\%$ ), by using a pulse repetition frequency of 1Hz and a gas mixture of 1:1:4 ( $\text{CO}_2:\text{N}_2:\text{He}$ ). Additional voltage fluctuations arose from stimulation of the piezoelectric effect by external acoustic signals. These were minimised by isolating each detector-head within a

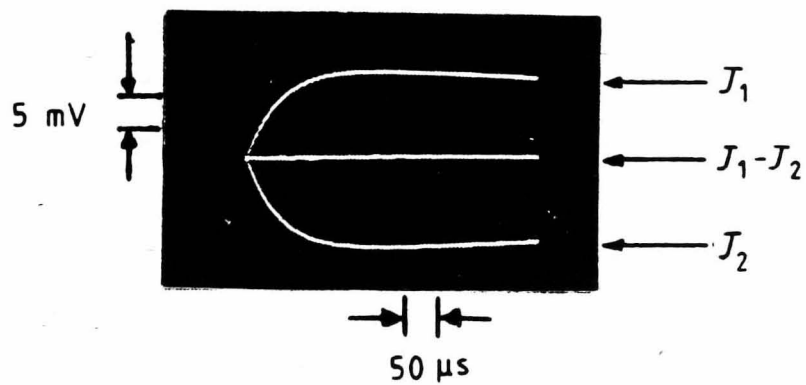
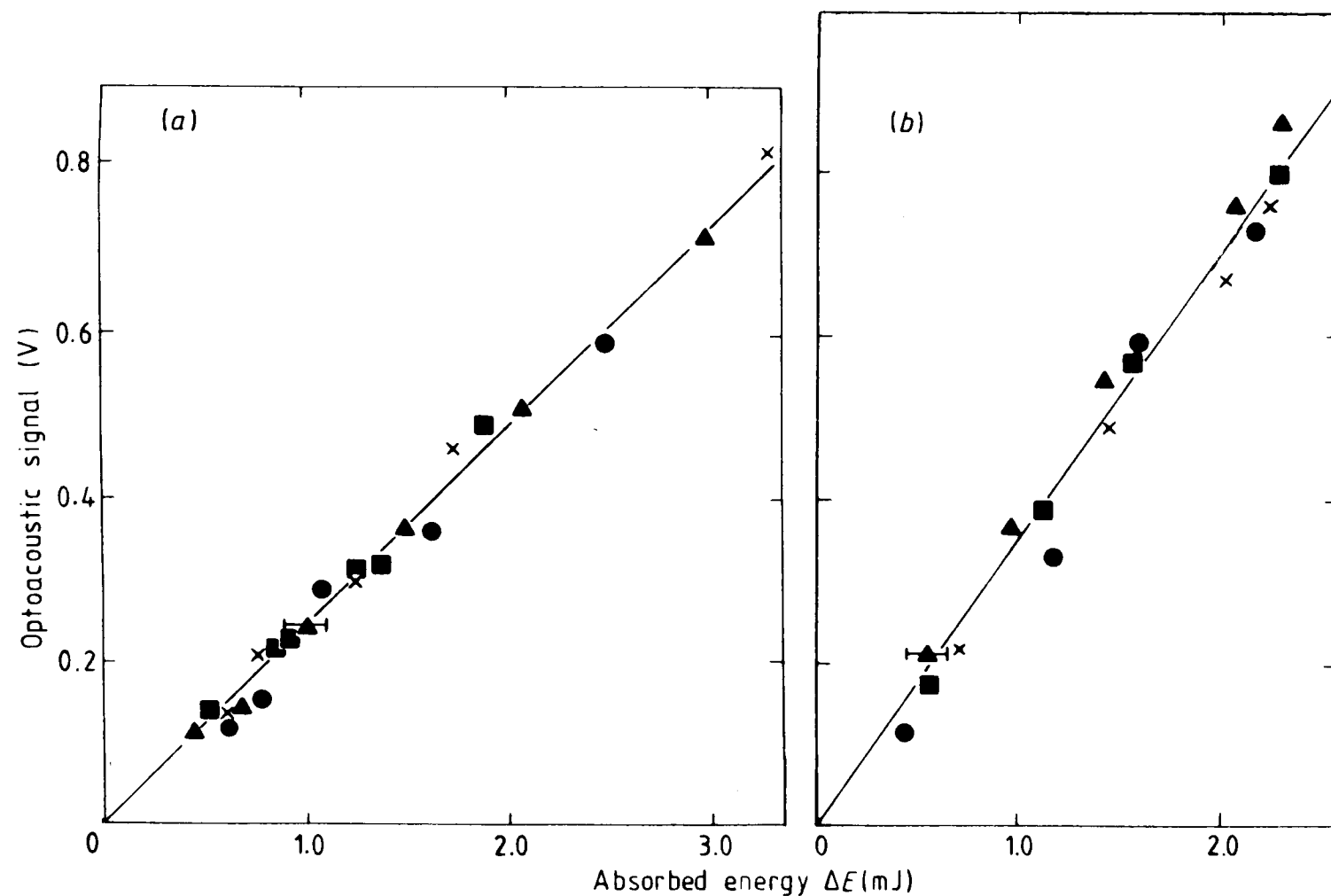


Fig. 2.3-2 Output voltage signals from the input,  $J_1$ , and output,  $J_2$ , joulemeter and the resultant difference signal,  $J_1 - J_2$

sound-dampening lead-lined foam sandwich (T Mat Engineering Ltd), and by fitting a NaCl window to each face. The salt flats reduced thermal perturbations (due to air currents) and airborne acoustic noise. Vibrational coupling of the vacuum pump through the system, was dampened by inserting a flexible rubber coupling near the pump. Elimination of some other extraneous frequencies was carried out during signal processing, for example, the differential amplifier was set to a bandwidth of 0-3kHz. These precautions, together with eliminating all unnecessary local acoustic noise sources and optical radiation sources (eg overhead lighting to which the detectors were sensitive), reduced the residual differential voltage fluctuations to approximately 60  $\mu$ V. The corresponding minimum detectable absorbed energy was about 30  $\mu$ J for a signal-to-noise ratio of unity.

Calibration results for butan-2-ol and ethanol are shown in Figs.2.3-3a and 2.3-3b; the amplitude of the first peak of the microphone signal (ignoring window effects), which provides a measure of the absorbed energy (Section 1.3), is plotted as a function of  $E_{\text{abs}}$  determined from Eq. 2.3-5).  $\text{CaF}_2$  attenuators, and changes in sample pressure, were used to vary the absorbed energy and, as can be seen, there is a linear dependence of the microphone signal on  $E_{\text{abs}}$ , allowing extrapolation through the origin. The calibration factors for the two gases were  $0.23 \pm 0.06$  V/mJ for butan-2-ol and  $0.34 \pm 0.07$  V/mJ for ethanol; the values remained unchanged when the calibrations were repeated several days later. It is of interest to note that over the limited pressure range studied (0.3torr - 3torr), the calibrations were independent of pressure; this differs from the behaviour previously reported by Chin *et al.* (36). However, the independence is consistent with the predictions of simple modelling (presented in Section 1.3.1) of the pressure pulse generated within the cell, assuming all the absorbed energy leads to



**Fig. 2.3-3** Microphone signal as a function of absorbed energy,  $\Delta E$ , for: (a) butan-2-ol irradiated using the  $R_{24}$  ( $10\ \mu\text{m}$ )  $\text{CO}_2$  laser transition; and (b) ethanol irradiated using the  $R_{20}$  ( $9\ \mu\text{m}$ )  $\text{CO}_2$  laser transition (34). The incident energy is indicated and in each case the pressure was varied in the range  $0.3 \rightarrow 3$  torr to change the absorbed energy.  $\blacksquare$ , indicates an incident energy of 39 mJ;  $\blacktriangle$ , an incident energy of 48 mJ;  $\bullet$ , an incident energy of 59 mJ; and  $\times$ , an incident energy of 70 mJ.

heating of the gas. This matter is further expanded upon in the following section.

In summary, the present approach enables calibration to be extended to considerably lower absorption levels (about  $200\mu\text{J}$  for a signal-to-noise ratio of six) than is possible with the more usual transmission methods (35). In the weakly absorbing regime ( $<200\mu\text{J}$ ), where the differential technique becomes inaccurate, the microphone signal can be used to determine  $E_{\text{abs}}$ , with a minimum detectable absorption in the present case of roughly  $5\mu\text{J}$ , set by noise levels.

An advantage of the differential absorption scheme is that once implemented it provides a rapid and simple means of measuring the absorbed energy and gives an immediate visual indication of the absorption level. Finally, in addition to its usefulness for direct measurements in gas phase samples, the technique can be employed for the calibration of various optoacoustic devices.

### 2.3.2 Validity of Calibration Factor under Experimental Conditions

Optoacoustic calibration was carried out for all the reactants presented in this research in the 7.6cm long cell which was fitted with the magnetic microphone. Pressures of the pure reactant were varied between roughly 0.3 and 3torr and the calibrations were all independent of pressure and incident energy. Consequently, each calibration factor ( $V/J$ ) was assumed to be valid for all experimental conditions using the same pure reactant gas. This calibration factor is also known as the optoacoustic system responsivity,  $R_{\text{Oa}}$ . In Section 1.3.1, a simple model is used to validate the assumption of pressure independence, but shows there is a dependence on  $\gamma$  ( $=C_p/C_v$ ) of gas responsivity (to the optoacoustic process),  $R_g$  (torr/J), and hence also of the optoacoustic system responsivity,  $R_{\text{Oa}}$  (V/J):  $R_{\text{Oa}}=R_g S$  where, as described

below,  $S$  is the microphone sensitivity. This dependence on gas mixture will be discussed further in this section using actual experimental data.

There also follows, a discussion about a model for the microphone sensitivity,  $S$  (V/torr), which initially predicts pressure effects, and also which considers the effect of changing specific heat ratios ( $\gamma$ ). However, using parameters specific to this research it is shown that these effects are negligible.

Wake and Amer (48) discuss a model proposed by Fraim (46) whereby the microphone sensitivity  $S$  is shown to be dependent on the gas pressure  $P_0$ , ratio of specific heats  $\gamma$ , and temperature  $T$ , according to:

$$S(P_0, \gamma, T) = 2S_r / (1 + (P_0 \gamma T_{stp} / P_a \gamma_a T)) \quad (2.3-6)$$

where  $S_r$  is the rated sensitivity at atmospheric pressure  $P_a$  (760 torr). Some values for  $\gamma$  are presented in Table 2.3-1. At constant temperature all over a pressure range of 7.6→0 torr of air, it is thus calculated that there should be <1% change in the microphone sensitivity. Furthermore, the same negligible order of percentage change (i.e. <1%) is found for the same pressure range if  $\gamma$  is 1.1 (approximate values for most of the alkanols used) The calibration data obtained in this work (Fig. 2.3-3) support this since, within the experimental scatter, the optoacoustic system responsivity (V/J) was shown to be constant over the range 0.3→3 torr (Fig. 2.3-3).

In some instances in this work, the reactant was diluted to a ratio one part reactant to nine parts diluent, as shown in Table 2.3-1. The specific heat of

Gas	molar mass /g.mole(-1) ref (1)	Cp /J.mole(-1).K(-1)	ref	gamma (Cp/Cv)	zeta (calibration correction factor)	speed of sound =(gamma.RT/m) Ref.: Appdx. A1 /m.s(-1)	Comments
methanol	32.04	43.89	96	1.23		309.91	
ethanol	46.07	65.44	96	1.15		249.04	
propan-2-ol	60.11	88.62	96	1.10		213.99	
butan-2-ol	74.12	113.19	96	1.08		190.58	
		113.80	1	1.08		190.54	
pentan-1-ol	88.15	132.76	96	1.07		173.74	
hexan-1-ol	102.18	147.32	96	1.06		160.84	
3,3-DMO	86.13	49.89	A1	1.2		186.41	
CO2	44.01	37.11	1	1.29		270.26	
cyclohexane	84.16	105.02	1	1.09		179.40	
		107.03	1	1.08		179.26	
ethanol:CO2 (1:8.96)	44.22	39.95		1.26	1.81	266.90	
ethanol:cycloC6H14(1:9)	80.35	101.06		1.09	0.62	183.92	
propanol:cycloC6H14 (1:9)	81.76	103.38		1.09	0.84	182.15	
butanol:cycloC6H14 (1:9.63)	83.22	105.85		1.09	1.08	180.36	
pentanol:cycloC6H14 (1:9.18)	84.55	107.74		1.08	1.25	178.79	
hexanol:CO2 (1:10.14)	49.23	47.94		1.21	3.51	247.58	
hexanol:CO2 (1:4.07)	49.72	58.85		1.16	2.75	241.69	
3,3DMO:cycloC6H14 (1:8.77)	84.36	99.38		1.09	0.46	179.63	

**Table 2.3-1** Values of: (i) ratio of specific heats; (ii) calibration correction factors; and (iii) speed of sound

the mix,  $C_p$ , with a fraction  $\chi$  of absorbing gas is

$$\bar{C}_p = \chi C_{p(\text{absorber})} + (1 - \chi) C_{p(\text{diluent})} \quad (2.3-7)$$

therefore in this work, typically

$$\bar{C}_p = \frac{1}{10} C_{p(\text{absorber})} + \frac{9}{10} C_{p(\text{diluent})} \quad (2.3-8)$$

Like the reactants, all the diluents were polyatomic, therefore, the ratio of the specific heats of the diluents will be comparable to those of the reactants, and  $\gamma$  of the mix should not be too dissimilar to that of the pure reactant. Take, for example, the experimental case where ethanol (one of the smallest reactant molecules) was diluted with  $\text{CO}_2$  (one of the smallest diluent molecules). Using Eq.(2.3-8) the specific heat of the mix is found to be about 10% larger than of the pure reactant. However, using Eq.(2.3-6) and substituting first for the pure reactant and then for the mix, it is calculated that the sensitivity of the microphone (V/torr) is only 0.001% greater for the mix than for the pure reactant. The ratio of specific heats for the pure reactants and the mixes are calculated in Table 2.3-1, and in most cases  $\bar{C}_p$  differs from  $C_p$  by only ~1%. In the absence of data on pentan-2-ol and hexan-2-ol, values of  $\gamma$  of the primary alkanols were used: very little difference is expected, if any, between the two values; for example for propan-1-ol  $C_p=87.45$  J/mole/K (1) while for propan-2-ol it is 88.62J/mole/K (96) ...there is even some spread in  $C_p$  for the same gas, as shown for butan-2-ol and cyclohexane in Table 2.3-1. Furthermore,  $\gamma$  for 3,3-dimethyloxetane was estimated from the results of 2,2-dimethyloxetane discussed in Appendix A1.

As already mentioned, the responsivity of the gas to the optoacoustic process  $R_g$  (torr/J) is dependent on gas mixture, being proportional to  $(\gamma-1)$  (Eq. 1.3-5b). For a fixed cell volume and the same absorbed energy, the gas responsivity for a mix will equal the gas responsivity of the pure sample multiplied by a correction factor  $\zeta$ , where from Eq. 1.4-5b:

$$\zeta = \frac{R_g[\text{mix}]}{R_g[\text{pure}]} = \frac{\gamma[\text{mix}] - 1}{\gamma[\text{pure}] - 1} \quad (2.3-9)$$

Hence the optoacoustic system responsivity (V/J)  $R_{Oa} = \zeta R_g S$  where  $\zeta$  is unity for a pure sample. Examples of correction factors are given in Table 2.3-1.

To further enhance Table 2.3-1, the velocity of sound in both the pure gases and mixtures is tabulated using Eq. A2. The equation requires the molar mass which, for the mixtures with a fraction  $\chi$  of absorbing gas, is:

$$\bar{M}_p = \chi M_{p(\text{absorber})} + (1 - \chi) M_{p(\text{diluent})} \quad (2.3-10)$$

In conclusion, it has been demonstrated theoretically and empirically, that with the conditions used for this work it is meaningful to apply the microphone responsivity found at calibration to microphone readings taken at the lower experimental pressures of pure reactants. However, a correction factor must be applied for dilute reactants.

## 2.4 OPTICAL SET-UP

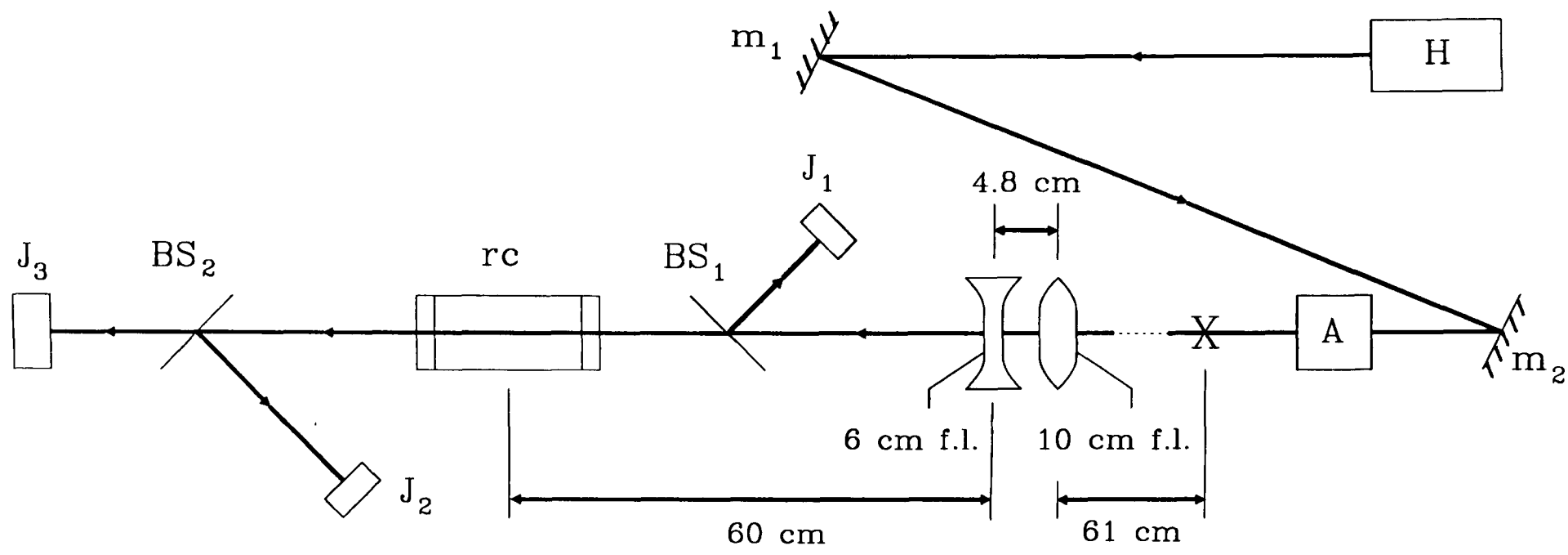
As mentioned before in Section 2.1.3, some photochemical processes are strongly dependent on the fluence. Consequently, one requirement was to design a laser beam delivery system that would minimise the longitudinal fluence gradient through the reaction cell. For most of the work, the

arrangement of figure (2.4-1) was used: The two element lens system was of an inverse Galilean telescope arrangement which produces a collimated beam of reduced size. Hence there was minimal beam divergence through the cell, and the fluence was of sufficient strength to cause measurable decomposition. A further advantage of this type of telescope is it avoids an intermediate focal point at which the fluence would certainly cause air-breakdown.

At the highest fluences produced by the system, the NaCl cell windows were near their damage threshold. It was discovered that their susceptibility to damage is reduced by following a preconditioning procedure: this involved gradually exposing the cell to higher fluences by appropriately varying the CaF<sub>2</sub> attenuators. This process was carried out immediately prior to sample gas injection into the cell. The fact that the damage threshold can be increased in this simple way is not common knowledge, and may be attributed to one or more of the following mechanisms:

- (i) There is localised (mechanical) stress relief caused by the gradual heating.
- (ii) Ablation of particulate and molecular surface contaminants occurs, which, if initially exposed at high fluence, would act as damage sites.

A few experiments required fluences that would have caused window damage despite preconditioning. For these occasions only, a focussed optical system was employed. By placing the reaction cell and focussing lens back towards the laser output, the double-lens system was left undisturbed. The lens (Ge) had an outer diameter of 2.5cm (clear aperture,  $D_a$ ,  $>2$ cm) a focal length,  $f$ , of 2.5cm, and was placed 61cm in front of the inverse telescope arrangement as shown in Fig.2.1-2. At this position the laser beam had a diameter,  $D$ , of approximately 10mm (estimated from a burn mark); by placing the cell



- |                                 |  |                    |   |
|---------------------------------|--|--------------------|---|
| H                               | - hybrid CO <sub>2</sub> laser   | G                  | - inverse Galilean telescope;<br>60 cm back f.l.          |
| m <sub>1</sub> , m <sub>2</sub> | - plane mirrors (brass)  | BS <sub>1,2</sub>  | - beam splitters (NaCl)                                   |
| A                               | - optical attenuators  | J <sub>1,2,3</sub> | - joulemeters   |
| X                               | - position of the 2.5 cm<br>focal length lens and cell<br>for 'focussed' experiments | rc                 | - reaction cell; centre<br>568.8 cm from the laser output |

Fig. 2.4-1 Schematic of the optical set-up

window flush with the lens, window damage was avoided, yet a high fluence of several thousand  $\text{J}/\text{cm}^2$  was achieved at the focal plane within the cell.

The Gaussian radius (and hence beam diameter) was not established accurately at the plane of the lens and using an estimate in the fluence calculation can lead to a high error; fluence is inversely proportional to the square of the radius, so errors in the radius are doubled in the fluence calculation. The spot size depends on the proportion of the clear aperture of the lens to the input beam radius ( $\omega$ ) at the  $1/e^2$  points of the irradiance. The diameter at the  $1/e^2$  points encompasses 87% of the beam energy, and since  $\omega/r_0 = \sqrt{2}$ , (where  $r_0$  is the radius at the  $1/e$  points of the irradiance) the diameter at the  $1/e$  points encircles 63% of the power. This  $D_a/\omega$  ratio must be greater than  $\pi$  for 99% of the laser energy to pass through the lens. However, even though a sharp edged aperture may be cutting off only a small fraction of the beam energy, diffraction effects can still be produced (Siegman), and for the  $D_a/\omega = \pi$  criterion diffraction ripples with a peak-peak intensity variation of  $\pm 17\%$  still exist in the near field, and a peak intensity reduction of  $\sim 17\%$  on axis in the far field results. To reduce diffraction ripple effects to  $\pm 1\%$ ,  $D_a \approx 4.6\omega$ . Therefore for this case, only if the input beam had a Gaussian radius  $\omega < 4.4 \text{ mm}$  and the lens spherical aberration was negligible, would the beam focus to a spot of diffraction limited radius  $1.27\lambda f/(2D)$ . Nevertheless, for  $4.4 \text{ mm} < \omega < 6.4 \text{ mm}$  (i.e.  $D_a/\pi$ ) the equation would be an excellent approximation. However, when  $\omega \gg 6.4 \text{ mm}$  the light forms an Airy-like distribution pattern, and an equation which gives the diameter of the central bright spot is more appropriate. The central spot contains 84% of the energy leaving the lens and its radius is given by  $1.22\lambda f/D_a$ .

For the experimental conditions under question,  $\omega < 6.4 \text{ mm}$  and so the diffraction limited equation may be used; thus, after a typical amount of

energy transmitted through the lens of 79.6 mJ has been focussed. the diffraction limited radius,  $r_0$ , at 1/e points is 15  $\mu\text{m}$ . for  $\omega$  of 4 mm, which leads to a fluence value of  $\sim 11300 \text{ J/cm}^2$ , while for  $\omega$  of 5 mm these radius and fluence values are 12  $\mu\text{m}$  and  $\sim 17600 \text{ J/cm}^2$ .

Therefore, despite the estimation, it is clear that the fluence values achieved in the focal plane were at least a factor of  $10^3$  greater than those with the collimated beam.

## 2.5 GAS ANALYSIS AND HANDLING

Analysis of both irradiated and unirradiated gas samples was carried out by gas chromatography. Over the course of the work two chromatographs were used; a Pye Unicam 104 (Pye) and a Carlo Erba 4200 (Carlo). Where possible they were used together; the Pye for resolving  $\text{C}_1$ - $\text{C}_4$  products, and the Carlo the heavier hydrocarbons. Various columns and flow rates were used for the Pye and are described for each applicable reactant section of Chapter 4. Gas pressures were maintained at 15 lb/in<sup>2</sup> for each of the columns used in the Carlo: carrier rates of 50 cc/min were used with the Chromosorb 101 (80- 100 mesh) and the Poropak QS columns, and 2 cc/min for the capillary column. For the Pye, optimum baseline conditions were maintained only by regularly baking the oven at roughly 200°C (to remove material which collected on the detectors) and by equally regular conditioning of the columns. Calibration of both instruments was performed regularly.

Two vacuum systems were available for gas handling, both of which contained rotary and diffusion pumps. The system associated with the GLC was the larger offering facilities for preparing and storing mixtures. Samples were taken from this line to calibrate the Pye and Carlo chromatographs, and to fill stock bulbs. Pressures were monitored with an MKS Baratron PDR-A

(0.01 - 100torr) pressure transducer. The other system permitted on-site filling of the reaction cell for the laser absorption and decomposition experiments. Pre-experiment N<sub>2</sub> purging of the reaction cell and vacuum line was also performed at this station. The pressure transducer was an MKS Baratron PDR-C-1B (0.001 - 10torr) which had to be screened to protect it from extensive electromagnetic interference from neighbouring lasers. Leak testing of the vacuum system and reaction cell was carried out with an Edwards type LT104 helium detector.

## 2.6 MATERIALS

The general practice was to distil new liquid samples, using the middle fraction for experimentation. All gas samples were checked for purity by gas chromatography, and if necessary further distillation was performed.

3,3-Dimethyloxetane was made within the Chemistry Department of the University of Hull and purified to 98% by preparative gas-liquid chromatography on a Pye 104: A 25m BP1 OV101 capillary column was kept at 30° C under 0.5 bar pressure and with a N<sub>2</sub> carrier flow of 40 ml/min. Hexan-2-ol was supplied by Koch-Light Laboratories and hex-1-ene from Fluka AG. ('PURUM'). Both samples were already distilled to >98% purity. AnalaR butan-2-ol was obtained from BDH chemicals. Its purity was better than 99%. Matheson gases supplied but-1-ene, *trans* but-2-ene and *cis* but-2-ene. *t*-Butanol and *iso*-butene had been obtained by Shaw (6), while Dr. P. Francis of the Chemistry Department (University of Hull) supplied distilled ethanol.

### 2.6.1 Reactant Diluents

Interest in the effects of adding a diluent, were stimulated by results obtained by Shaw (6) for 2,2-dimethyloxetane which showed that the extent

of decomposition may be greatly reduced by the addition of an inert gas. The behaviour was attributed to the suppression of thermal reaction occurring after the initial laser-induced decomposition. The addition of a diluent to a pure reactant can reveal other important information about the photochemistry. For example a diluent which is a radical scavenger (eg.  $O_2$ ) will quite clearly suppress the products which derive from reaction paths that involve bond fission and thus will aid in the identification of the reaction mechanism. Although not carried out in this work, reference is made to the results of other researchers that have used this method. The role of collisions is discussed in Section 1.2.

In choosing a diluent for the experiments described in this thesis, the aim was to make inter-molecular vibrational-vibrational energy transfer efficient, thus hindering (or even preventing) thermal reactions particularly in the instance of the post-pulse, or post-first-collision phase of a 'collision-free' experiment. This function is best performed by large molecules; cyclohexane and n-hexane were always considered (although n-hexane was never actually selected as a diluent). It is obviously important that the diluent experiences negligible absorption during irradiation, otherwise it too may undergo decomposition. For some reactant molecules, the excitation wavelength was also absorbed by both cyclohexane and n-hexane, as shown by OA tests. In this case  $CO_2$  was used as the diluent. In all other cases, cyclohexane was found to be the most satisfactory diluent. The hexanes were both of 'spectroscopic' quality, and were further purified by distillation. The majority of the 'dilute' experiments were for 'collision-free' conditions *viz.* a total pressure of 50 mtorr, provided by partial pressures of 5 and 45 mtorr respectively of reactant and diluent. A few select data were taken for larger partial pressures of diluent to increase the total pressure into the region where collisions are important, but the emphasis was always intended to be

on the effect of diluent in a 'collision-free' environment. To make the stock bulb mixture, the diluents were added to the reactants by slow seepage. Most of the dilute work is presented in the decomposition results chapter (Ch. 4). There is also some discussion in Ch. 3 (eg. under hexanol).

## 2.7 DATA ANALYSIS

A complex Fortran program was developed to aid in the analysis of both absorption and decomposition data. Graphical or tabulated output was available. The following points summarise the program's content and capabilities.

1/ The program was run on the ICL 2900 mainframe computer and accessed graphical and curve fitting library programs.

2/ The program was menu driven.

3/ The input datafile contained raw yield and/or absorption data, room temperature, irradiated volume, the number of pulses, sample pressure, cell input energy, and a header summarising the experimental conditions. Yield data was given as the peak height of the chromatograph trace, and the calibration factor.

4/ Graphical output of the data, with or without deconvolution, could be selected from the following menu options:

Yield	vs	Fluence
Absorbed Energy	vs	Fluence
Yield	vs	Pressure
Absorption Cross-Section	vs	Fluence
Absorption Cross-Section	vs	Pressure
Yield	vs	Absorbed Energy

Polynomial curve fitting and analysis of the fit was possible. This was particularly important for the deconvolution procedure.

5/ Tabulated output included some of the input data plus the calculated fluence, absorbed energy per mole, absorption cross-section, total fractional decomposition, total fractional decomposition per pulse and the yield (fractional decomposition per pulse in the irradiated volume).

### 3. - ABSORPTION RESULTS

Absorption of laser radiation of frequency  $\nu$  by a molecule is defined in terms of the Beer-Lambert Law:

$$\log_e(E_I/E_T) = \sigma n' l \quad (3.0-1)$$

where  $\sigma$  is defined as the absorption cross-section ( $\text{cm}^2/\text{molec}$ ):  $E_I$  is the incident energy;  $E_T$  is the transmitted energy ( $E_I - E_{\text{abs}}$ );  $E_{\text{abs}}$  is the absorbed energy;  $n'$  is the number of molecules per unit volume; and  $l$  is the path length. Use of this equation requires calibration of the optoacoustic cell for the compound under study. The procedure for calibration has been discussed in Chapter 2.

Absorption can also be expressed in terms of the average number of absorbed photons per molecule,  $\langle n \rangle$ .

$$E_{\text{abs}} = \langle n \rangle x h \tilde{\nu} c \quad (3.0-2)$$

where  $x$  = number of molecules within the irradiated volume

$h$  = Planck's constant

$\tilde{\nu}$  = wavenumber of laser transition ( $\text{cm}^{-1}$ )

$c$  = speed of light

Consideration of the behaviour of  $\sigma$  and  $\langle n \rangle$  over various experimental conditions is an extension to Shaw's work (6) on ethanol, t-butanol, oxetane, 2-methyloxetane and 2,2-dimethyloxetane.

Measurements of  $\sigma$  and  $\langle n \rangle$  are reported in this chapter for a variety of experimental conditions (in particular as functions of pressure and laser fluence) on all the reactants which were studied for their decomposition behaviour *viz.* ethanol, propan-2-ol, butan-2-ol, pentan-2-ol, pentan-3-ol,

hexan-2-ol, and 3,3-dimethyloxetane. For completeness, methanol was also included in this absorption analysis, although it was not used for the decomposition measurements. There is a section devoted to each of these molecules in this chapter; data is always graphically presented in the order  $\sigma$  vs F,  $\langle n \rangle$  vs F,  $\sigma$  vs P then  $\langle n \rangle$  vs P. Despite the pressure range, all the absorption cross-section data are plotted with a linear pressure scale in order to discourage misinterpretation of the degree of fall-off that is shown to exist. Exploded views of the lowest pressures are provided. It has been noted that the shape of the curves of  $\langle n \rangle$  versus pressure look like those of  $\sigma$  versus pressure and since the fall-off rate is already clarified in the cross-section curves, the former are plotted with a logarithmic x-axis. Furthermore, it must be noted that all the data are presented in undeconvoluted form, while the deconvolution factors are tabulated in Section 3.9. Within each section is a summary of the main observations made for that molecule, and comparisons are made of the laser absorption cross-section with the small signal (i.e. low fluence), broadband value ( $\sigma_{\text{broadband}}$ ) established from data taken with an IR spectrometer. The final section of this chapter 3.10 is a general discussion in which the results are evaluated and compared with those of other workers, especially with the results of Shaw (6).

The "most probable" fractional errors for the values of fluence, average number of absorbed photons, and absorption cross-section are as follows:

$$\frac{\Delta F}{F} = \pm 36\% \qquad \frac{\Delta \langle n \rangle}{\langle n \rangle} = \pm 36\% \qquad \frac{\Delta \sigma}{\sigma} = \pm 20\%$$

while the error in the pressure readings is  $\pm 1$ mtorr. The F and  $\langle n \rangle$  errors are largely governed by the error in the calculated radius of the irradiating beam, which was determined in Section 2.1.3 to be  $\pm 18\%$ . The fractional errors quoted above have been established in the same manner as that used in Section 2.1.3. For those graphs plotted for constant fluence (and in some

instances constant pressure), the fluence uncertainty quoted in the text is indicative of the *stability* of the fluence over the length of the test: this value tends to be worse for absorption data gathered during decomposition work because of the extended experimental time.

It was initially intended to gather absorption data during the same laser runs that were used for analysis of decomposition products. However, as was explained in Section 2.2 on reaction cells, the optoacoustic cell caused some of the reactants to decompose within the cell without any obvious stimulant being applied. Time consuming tests showed that butan-2-ol and ethanol were not affected in this manner, and so decomposition and absorption data were gathered, for these reactants, from the same run. All other absorption work was carried out separately from the decomposition work.

Clearly, the laser wavelengths chosen for absorption measurements were ones used, or intended for use in the decomposition work. In a couple of instances, more than one laser line was used, and the absorption data reflects this (eg. ethanol and 3,3-dimethyloxetane). In addition, it was at these laser wavelengths, that the broadband, low intensity, absorption cross-section ( $\sigma_{\text{broadband}}$ ) for each reactant was determined: a Perkin Elmer 580B IR Spectrometer was used in order to obtain the broadband IR spectrum of a relatively high pressure sample of each reactant.

Another aspect of the research, was to look for the effects of pulse type (see Section 2.1) on decomposition and absorption. The behaviour of the absorption cross-section of 3,3-dimethyloxetane was observed in detail, using multimode and singlemode pulses, as first the fluence and then the reactant pressure was varied.

### 3.1 METHANOL

The small signal (broadband) absorption cross-section of methanol was evaluated from an IR spectrum, at the  $R_{32}(10\mu\text{m})$  wavelength ( $983.3\text{cm}^{-1}$ ):  $\sigma_{\text{broadband}}$  was found to be  $5.12 \times 10^{-20}\text{cm}^2/\text{molecule}$ . The optoacoustic cell was used to monitor the change in absorption cross-section with fluence at 0.982 torr and 8.09 torr (Fig.3.1-1), and with pressure at a fluence of  $7.56 \pm 0.01\text{J}/\text{cm}^2$  (Fig.3.1-3). The variation in the average number of absorbed photons per molecule with fluence is shown in Fig.3.1-2, while the variation with pressure is shown in Fig.3.1-4.

Within the range of the data taken, the main observations are:

- (i) There is no sharp contrast between the behaviour of  $\sigma$  with pressure at high and low pressures.
- (ii)  $\sigma$  falls off continuously towards zero with decreasing pressure (Fig.3.1-3).
- (iii) At all pressures studied (i.e.  $<8\text{torr}$ ), the  $\sigma$  values are less than the broadband absorption cross-section.
- (iv) There is little variation of  $\sigma$  with fluence above  $1.5\text{J}/\text{cm}^2$ , there being a very slight decrease with increasing fluence for both pressures.
- (v) For 8.09 torr, with decreasing fluence below  $1.5\text{J}/\text{cm}^2$ , there is a sharp rise (of rapidly increasing gradient) of  $\sigma$  towards the broadband value.
- (vi) Multiple-photon absorption is apparent for conditions of high pressure and high fluence. Since average  $n$  values are plotted i.e.  $\langle n \rangle$ , some multiphoton absorption occurs even when  $\langle n \rangle < 1$  at the lower pressures and fluences; indeed it is believed that only a low fraction of the molecules absorb, therefore multiphoton absorption must occur for many which do.

**Fig. 3.1-1 Methanol: Variation of absorption cross-section with fluence, at R32 (10  $\mu\text{m}$ )**

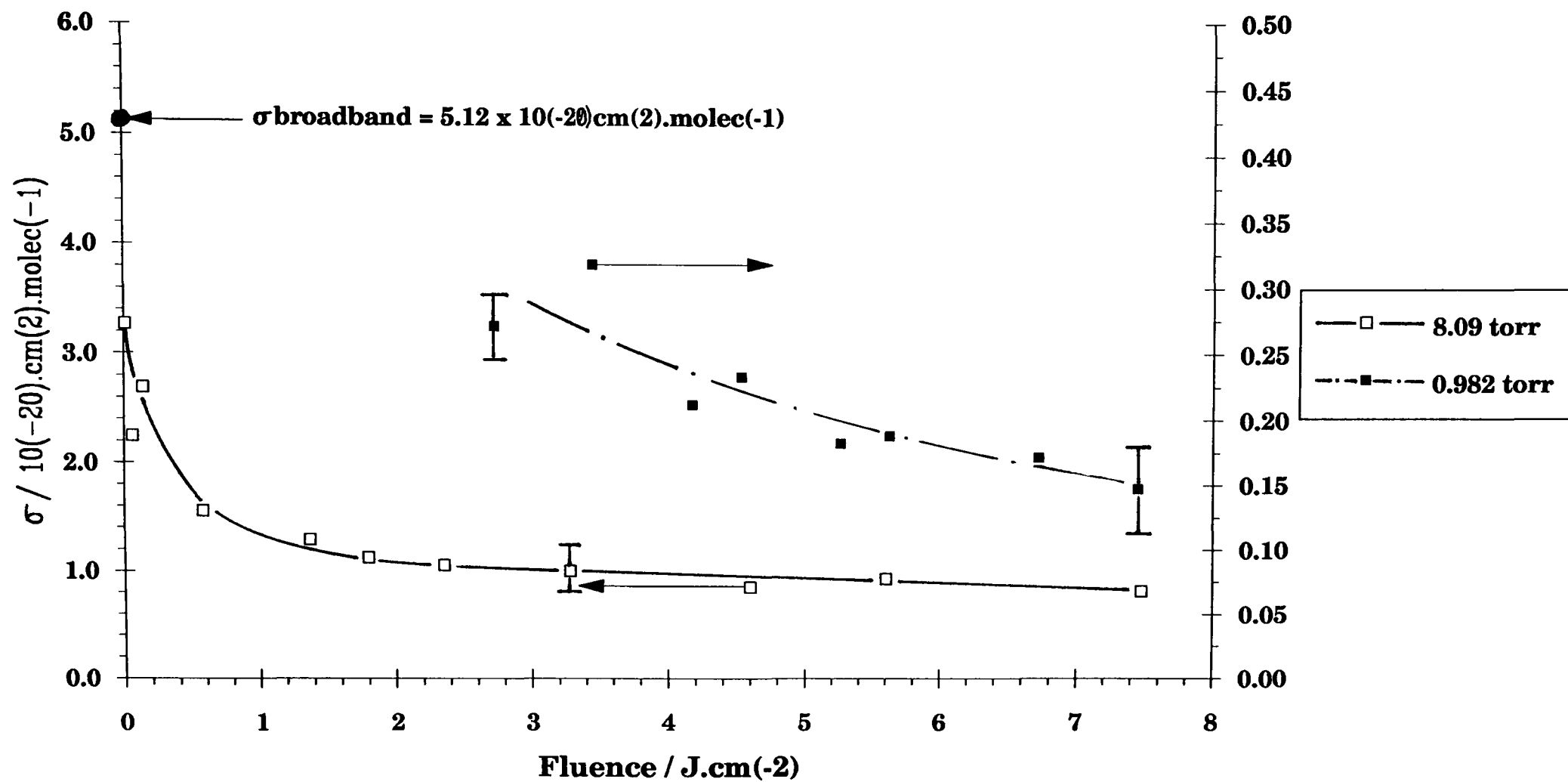


**Fig. 3.1-2 Methanol: Variation with fluence of the average number of absorbed photons per molecule, at R32 (10  $\mu\text{m}$ )**

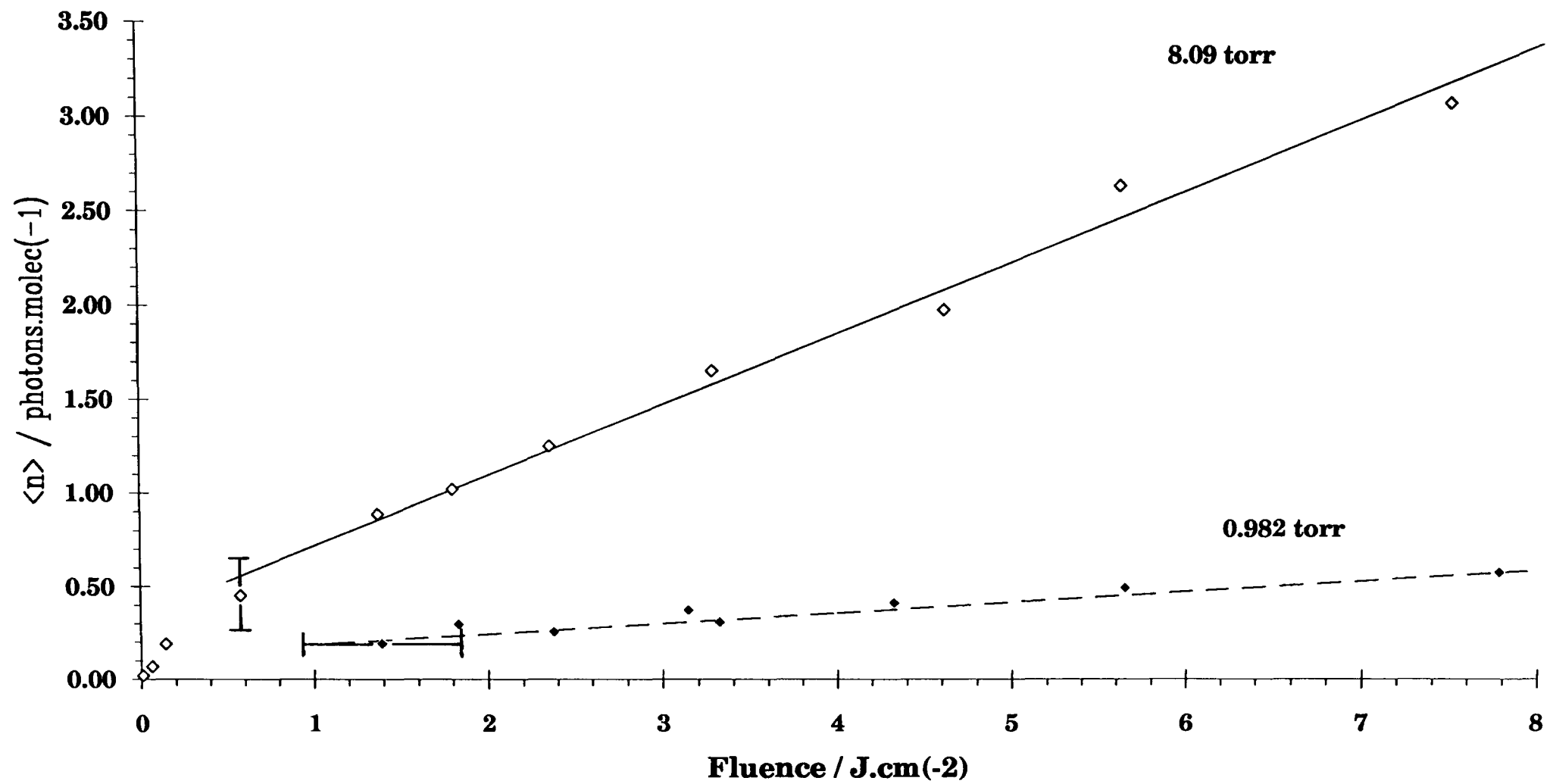


**Fig. 3.1-3 Methanol: Variation of  $\sigma$  with pressure at R32 (10  $\mu\text{m}$ ), and 7.56 J/cm(2)**

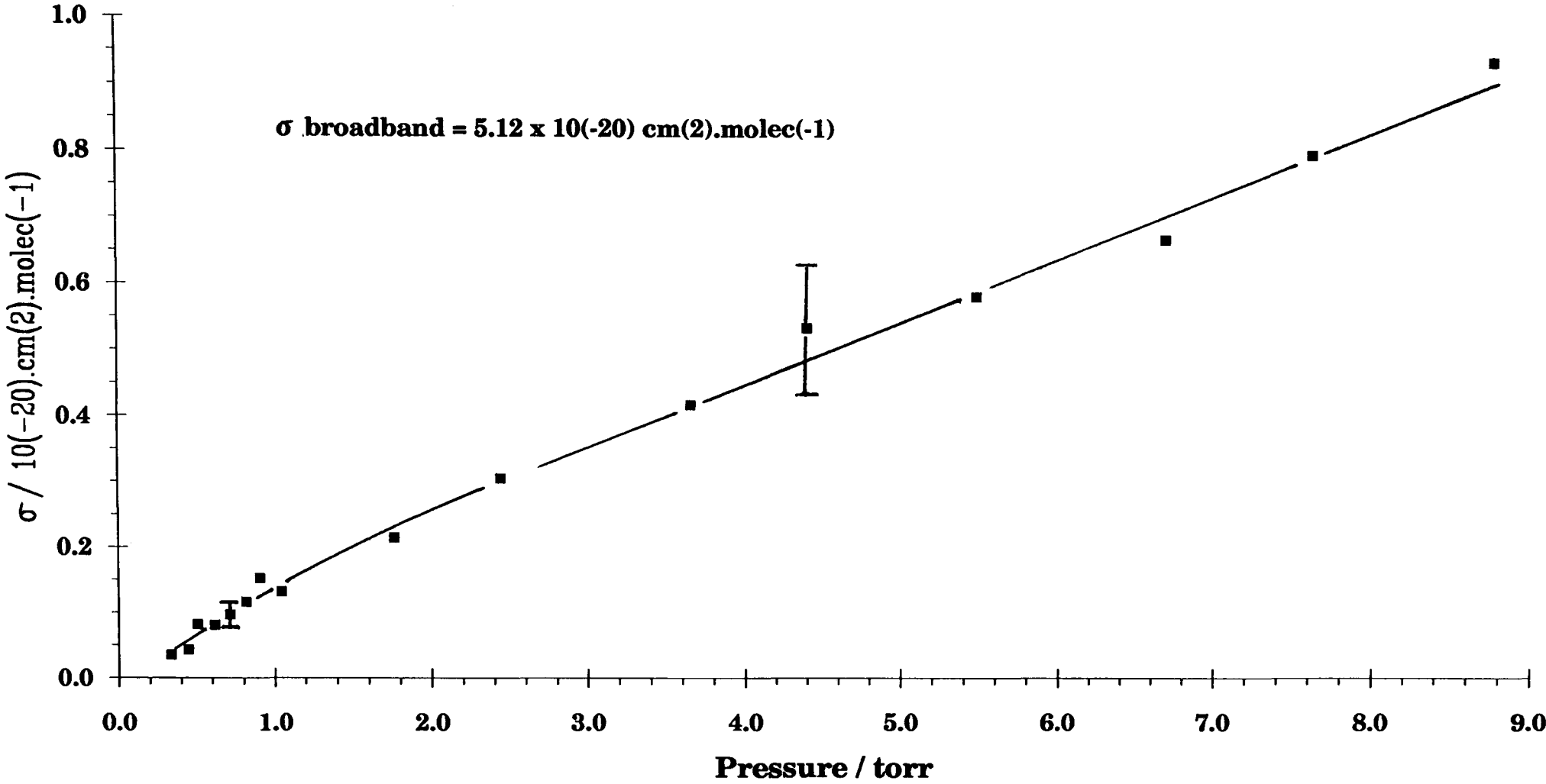
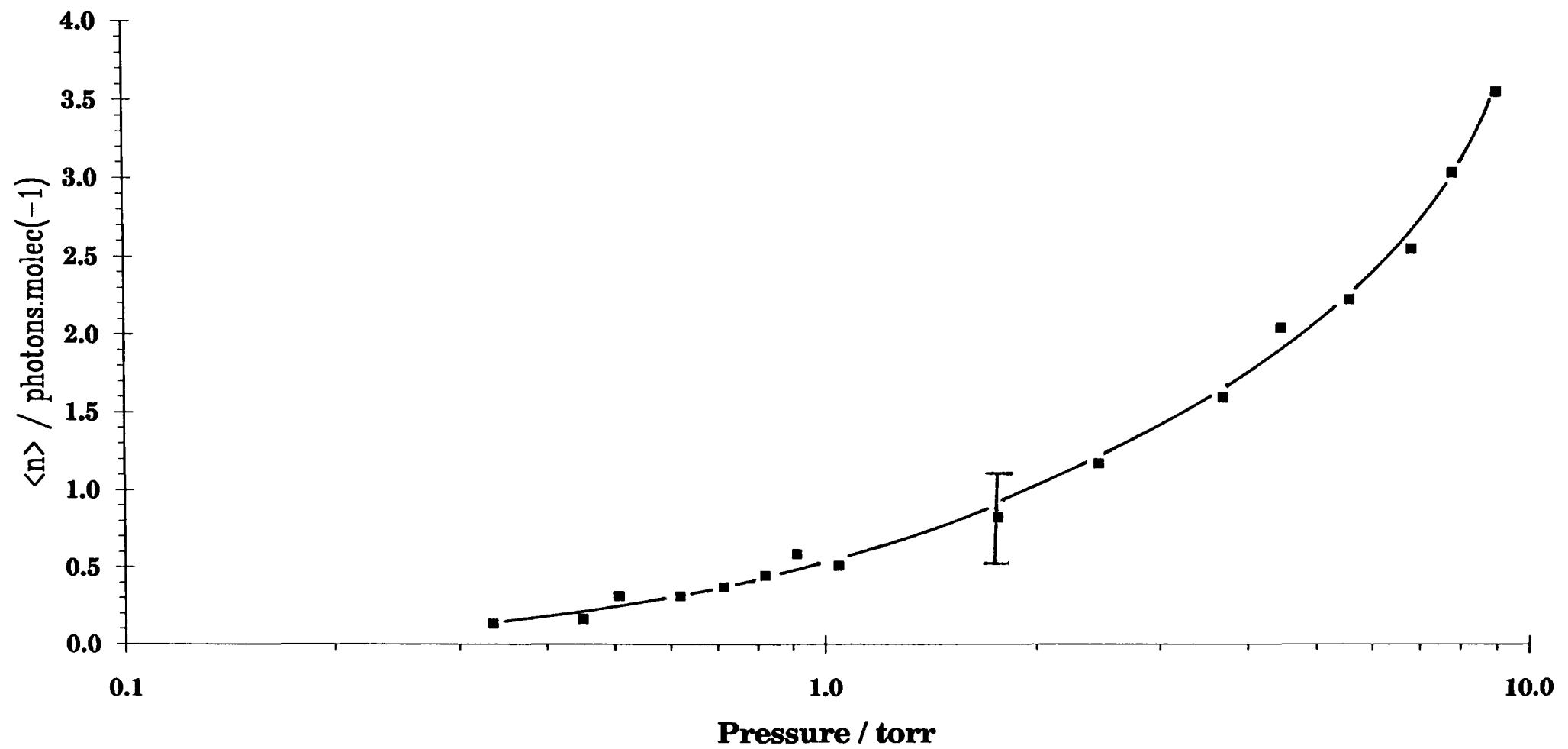


**Fig. 3.1-4 Methanol: Variation with pressure of the average number of absorbed photons per molecule, at a fluence of 7.56 J/cm(2) on R32 (10  $\mu$ m)**



## 3.2 ETHANOL

The small signal, broadband absorption cross-section,  $\sigma_{\text{broadband}}$ , of ethanol at a wavelength given by the  $P_{18}(9\mu\text{m})$  laser transition ( $1048.66\text{cm}^{-1}$ ) is  $23.0 \times 10^{-20}\text{cm}^2/\text{molecule}$ , and at the  $R_{20}(9\mu\text{m})$  transition ( $1078.59\text{cm}^{-1}$ ) it is  $23.3 \times 10^{-20}\text{cm}^2/\text{molecule}$ . These wavelengths were chosen in view of the previous work on ethanol (6,75) and correspond to the P and R branches respectively of a methyl rocking mode absorption band (78). The optoacoustic cell was used to monitor the change in absorption cross-section with fluence at these wavelengths at a nominal pressure of 50 mtorr, and the results are shown in Fig.3.2-1. The data was taken using both multimode and singlemode pulse types and the comparison is also given in Fig.3.2-1. The variation of absorption cross-section with pressure is shown in Fig.3.2-3 for high ( $8.6 \pm 0.1\text{J}/\text{cm}^2$ ) and low ( $3.8 \pm 0.1\text{J}/\text{cm}^2$ ) fluences of  $R_{20}(9\mu\text{m})$  irradiation. The variation with fluence of the average number of absorbed photons is shown in Fig.3.2-2, while the variation with pressure is given by Fig.3.2-4.

Ethanol was the first gas to be analysed for its absorption qualities, and some time was spent in determining the best experimental technique. To begin with, the absorption data was collected during a decomposition run. Each run typically lasted 10 to 25 minutes, and absorption data was gathered at least at the start and at the end of each run. It was discovered that the OA signal increased over the length of an experiment, but that the increase was not noticeable over a five minute run. There was however, no correlation between the amount of product produced with the percentage increase in the OA signal, so the signal change could not be attributed to the increase in the product quantity. Neither could the change be attributed to an increase in laser energy, since the data showed that to be slightly decreasing over the run-time. It was subsequently decided to use only the value attained at the start of any experiment. Furthermore, much of the absorption data presented

**Fig. 3.2-1 Ethanol: Comparison of the effect of multimode and singlemode pulses on the variation with fluence of the absorption cross-section, at two wavelengths**

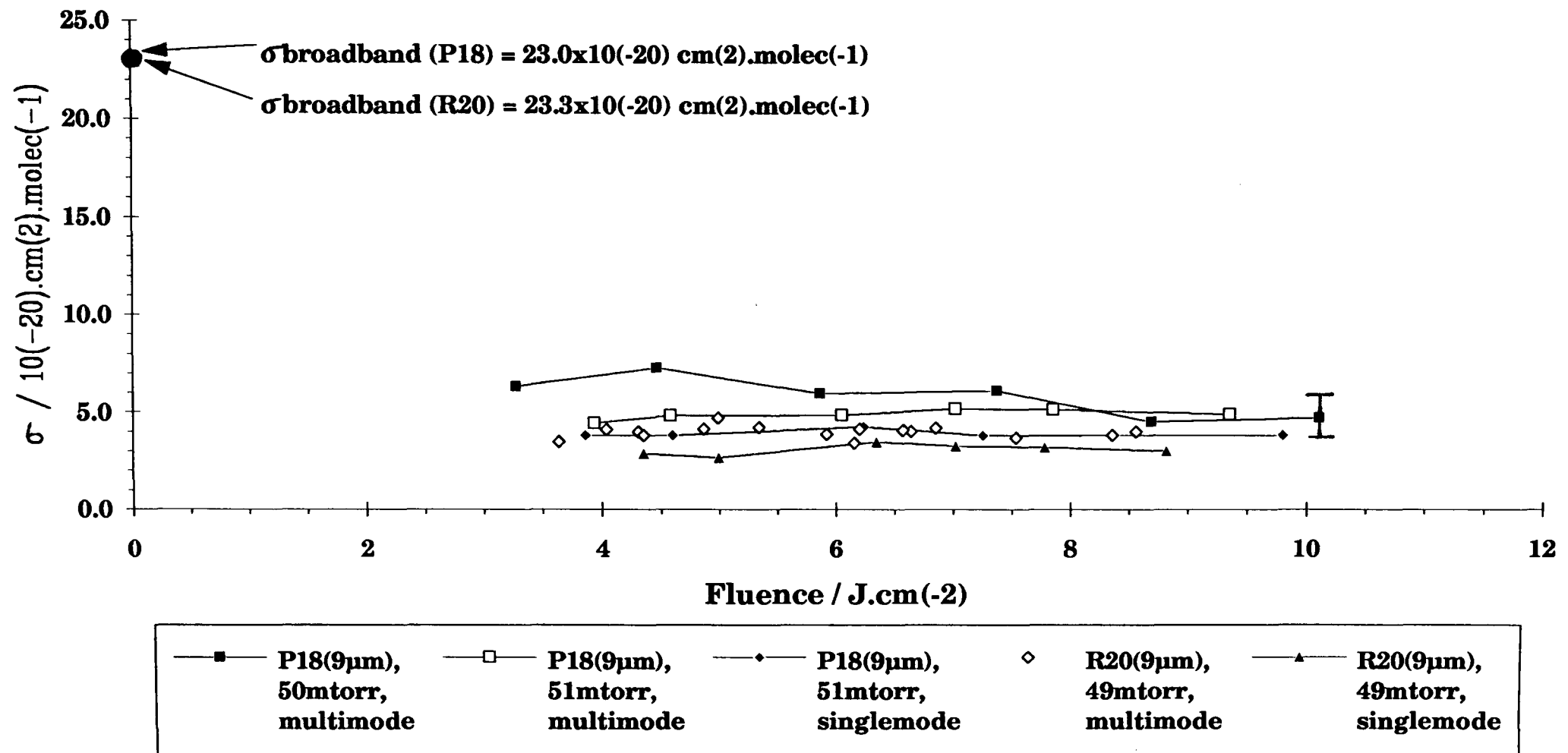


**Fig. 3.2-2 Ethanol: Comparison of the effect of multimode and singlemode pulses on the variation with pressure of the average number of absorbed photons per molecule, at two wavelengths**

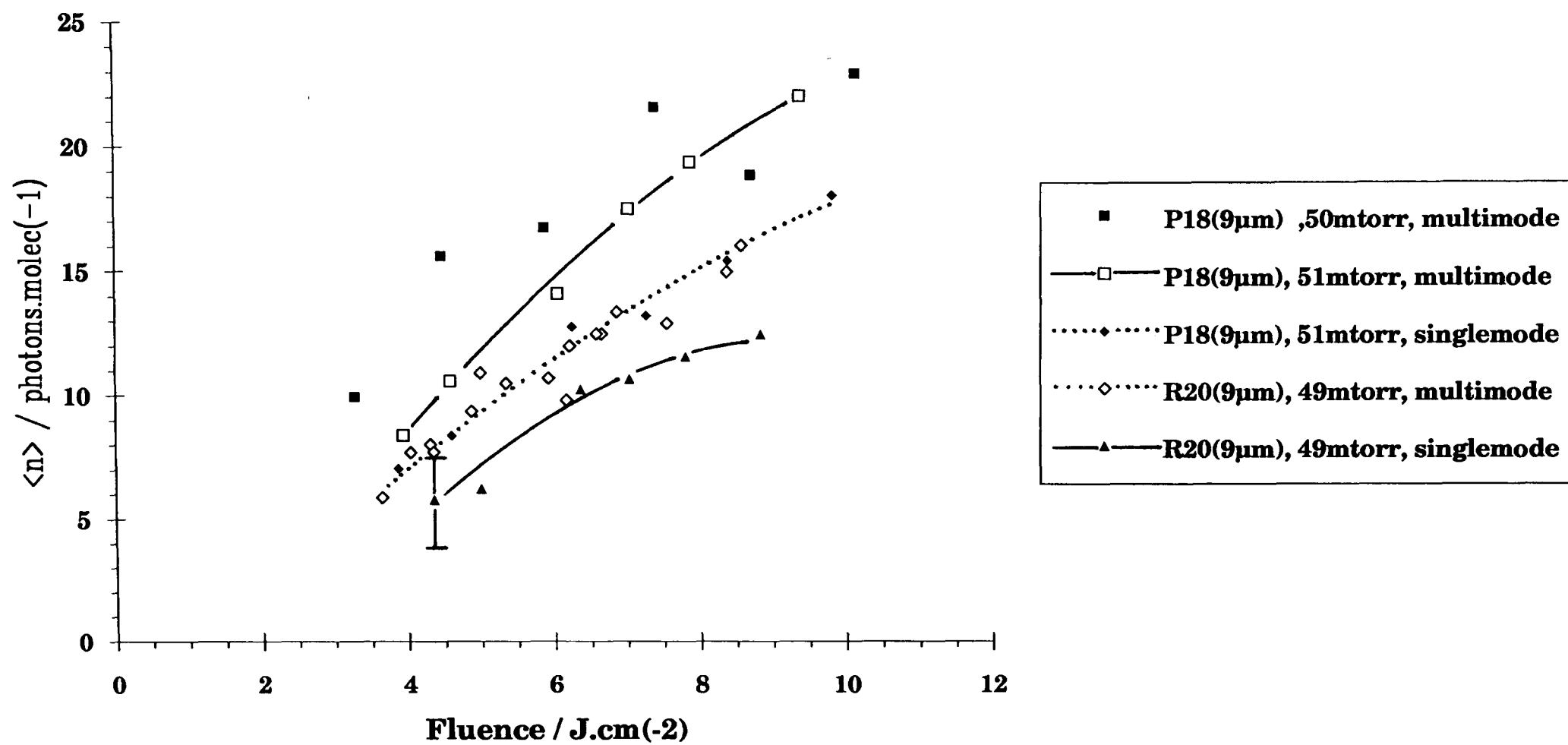


**Fig. 3.2-3 Ethanol: Variation of absorption cross section with pressure.  
Comparison of the effect of fluence on R20 (9  $\mu\text{m}$ )**

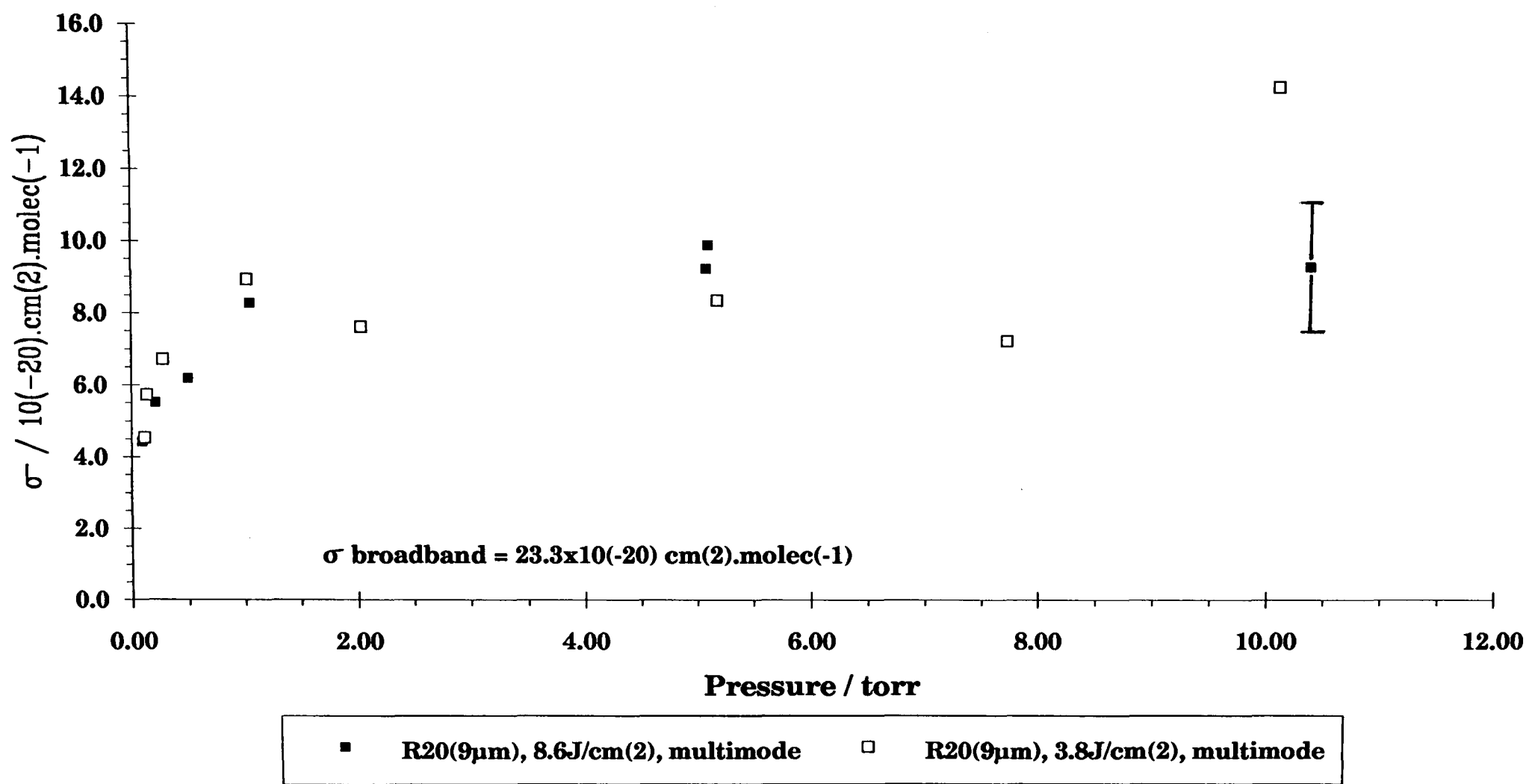
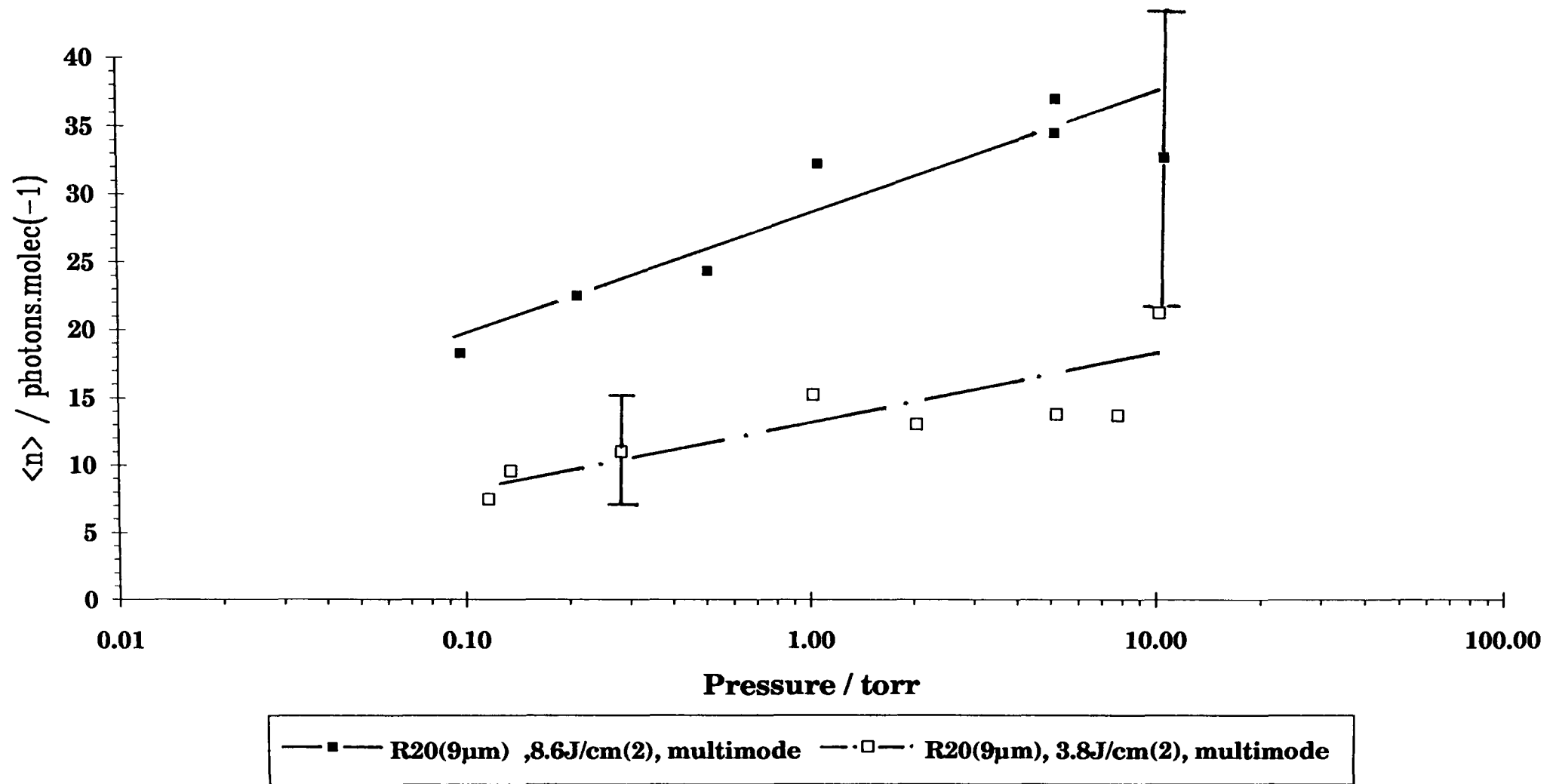


**Fig. 3.2-4 Ethanol: Variation with pressure of the average number of absorbed photons per molecules. Comparison of the effect of fluence on R20 (9  $\mu\text{m}$ )**



here was accumulated during 'absorption only' experiments. The time lapse between the first and last data point was minimised, as was the potential for error in maintaining a constant cell pressure over the entire duration. These specifications were achieved by using one single cell-fill, and proceeding with the predetermined sequence of fluence/pulse-type change and data acquisition as rapidly as possible. Irradiation of the gas was only permitted with the pulses selected for OA measurement (three for each experimental condition), and the highest fluences were preserved until last. In this way, trend aberrations caused by decomposition-induced pressure changes were also minimal. The first set of data, and part of the fourth, described in the graph legends of Figs. 3.2-1 and 3.2-2 were taken during a 'decomposition' run, while the others were of the type just described. The scatter shown by the first set (i.e.  $P_{18}(9\mu\text{m})$  multimode) was typical of data taken in that manner. The  $R_{20}(9\mu\text{m})$  decomposition run data however, showed much reduced scatter and has been incorporated into the equivalent set taken during the 'absorption only' run.

In this instance the 'absorption only' procedure was primarily applied to study the effect of pulse-type. The gas sample was changed between conditions of different wavelengths. There is an indication that at both wavelengths, the singlemode pulse-type shows a drop in absorption cross-section of roughly 20% of the multimode value, and consequently a drop in the average number of absorbed photons per molecule.

Regardless of whether the first or second set of  $P_{18}$  data is used for a wavelength comparison of multimode pulses, the conclusion is that for both pulse-types, the absorption cross-section and average number of absorbed photons per molecule are smaller for the  $R_{20}(9\mu\text{m})$  than for the  $P_{18}(9\mu\text{m})$  laser transition. The drop is about 20% for both singlemode and multimode

pulses. This effect is despite the fact that the broadband cross-sections for both lines are similar and it may well be indicative of a shift to longer wavelengths of the absorption features. Fig. 3.2-5 illustrates that a moderate red-shift will bring the peak of the P-branch of the methyl rocking mode closer to the  $P_{18}(9\mu\text{m})$  wavelength, while at the same time moving the peak of the R-branch further off that of the  $R_{20}(9\mu\text{m})$  transition. Such shifts have been observed for  $\text{SF}_6$  and  $\text{OsO}_4$  (53), and alkanol and oxetane molecules (6). It was observed that the shifts were also accompanied by a broadening of the spectrum. The red shift can be explained in terms of vibrational anharmonicity; with increasing fluence, multiphoton absorption is more effective and higher vibrational levels are reached. Because of anharmonicity, whereby the vibrational levels become more closely spaced, each contribution of a new vibrational transition is shifted towards longer wavelengths. However, the observed trend of  $\sigma$  with fluence (see notes (iv) and (v) below) might be considered incompatible with the occurrence of red-shifting which causes the irradiation to sample larger and larger absorptive regions of the spectrum ...an increase in  $\sigma$  with fluence could be expected in such instances, as the red-shifting becomes more and more prominent.

The remaining main observations are:

- (i) Above and below 1.0 torr, there is a contrast in the dependence of  $\sigma$  on pressure: Above 1 torr  $\sigma$  is virtually independent of pressure (Fig.3.2-3).
- (ii) There is a fall off of  $\sigma$  with decreasing pressure below 1 torr (Fig.3.2-3).
- (iii) The value of  $\sigma$  is less than the broadband cross-section for all pressures (Fig.3.2-3), and there is no marked dependence on fluence (Fig. 3.2-1 and -3) at any of the pressures measured. A consequent increase of  $\langle n \rangle$  with fluence is noted for pressures of 50 mtorr

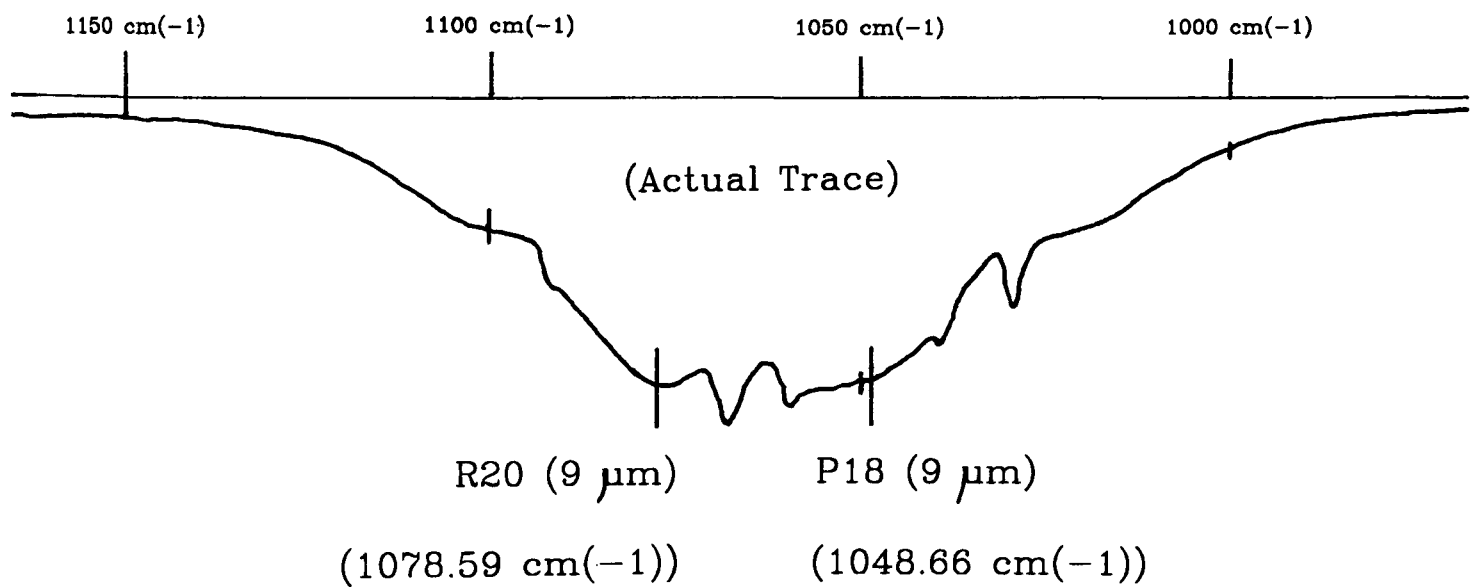
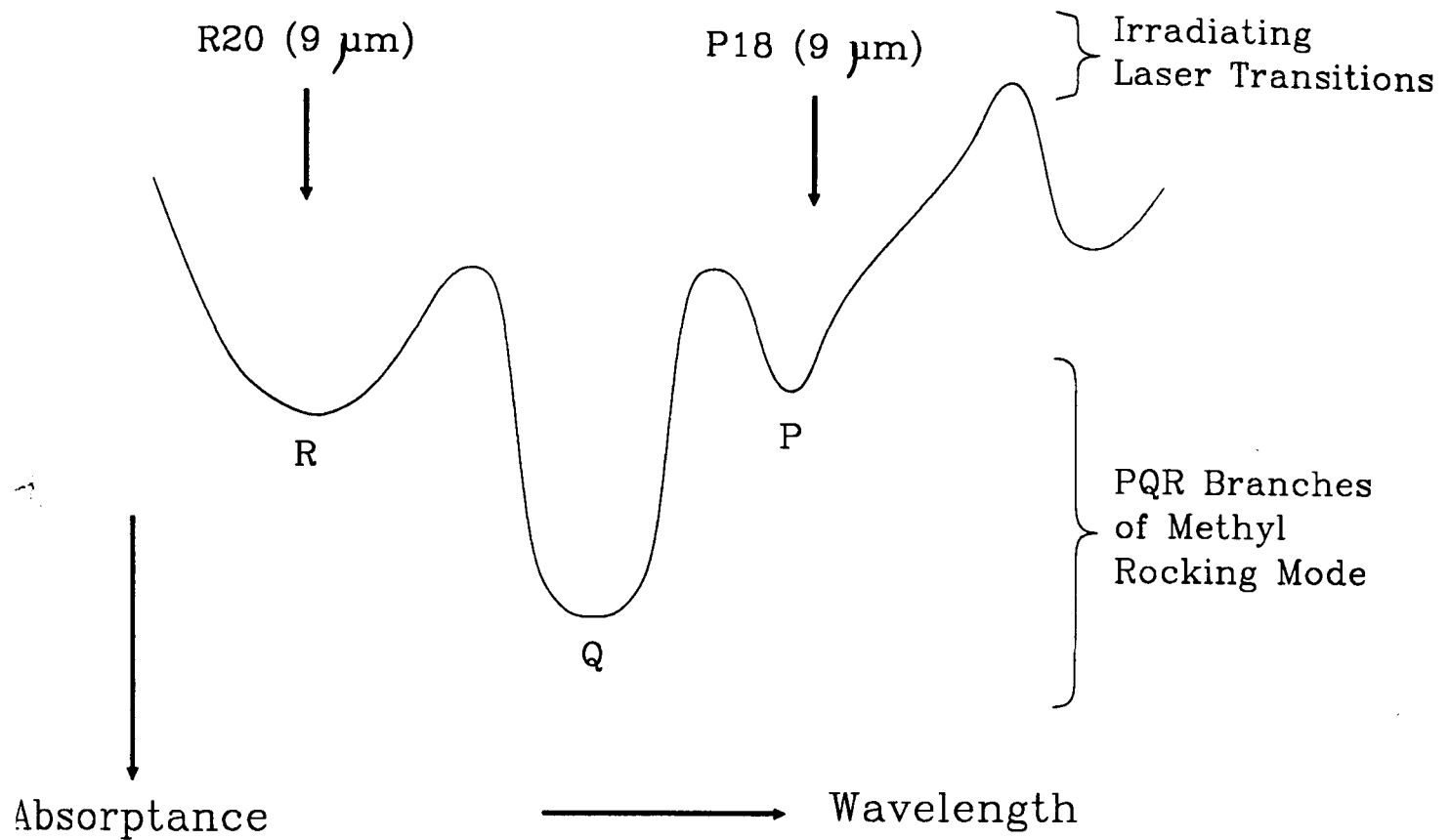


Fig. 3.2-5 Ethanol: Schematic of the broadband absorption spectrum, showing the relative positions of the laser transitions used for experimentation

(Fig.3.2-2) and for the measured pressures greater than 0.1 torr (Fig. 3.2-4).

- (iv) There is very little variation of  $\sigma$  with fluence above  $4\text{J}/\text{cm}^2$  for a nominal pressure of 50 mtorr (Fig.3.2-1).
- (v)  $\sigma$  at zero fluence (broadband value) is much larger than  $\sigma$  at the lowest fluence measured (Fig.3.2-1).
- (vi) Multiple-photon absorption is achieved fairly readily for both pulse-types and at both wavelengths.

### 3.3 PROPAN-2-OL

The small signal, broadband spectrum of propan-2-ol at the wavelength of  $R_{14}(9\mu\text{m})$  ( $1074.6\text{cm}^{-1}$ ) gives a value of  $12.5 \times 10^{-20}\text{cm}^2/\text{molecule}$  for the absorption cross-section,  $\sigma_{\text{broadband}}$ . The optoacoustic cell was used to monitor the change in absorption cross-section with fluence at 51.5 mtorr and 1.009 torr (Fig.3.3-1), and with pressure at a fluence of  $9.2 \pm 0.1\text{J}/\text{cm}^2$  (Fig.3.3-3(a) & (b)). The variation of the average number of absorbed photons per molecule with fluence is shown in Fig.3.3-2, while the variation with pressure is shown in Fig.3.3-4.

The main observations are:

- (i) Above and below 0.8 torr there is a contrast in the dependence of  $\sigma$  on pressure: Above 0.8 torr  $\sigma$  is virtually independent of pressure (Fig.3.3-3(a)).
- (ii) There is a rapid fall off of  $\sigma$  with decreasing pressure below 0.2 torr and a more gradual fall off between 0.8 torr and 0.2 torr (Fig.3.3-3(b)).
- (iii) The value of  $\sigma$  is less than the broadband cross-section for all pressures.

**Fig. 3.3-1 Propan-2-ol: Variation of absorption cross-section with fluence at R14 (9  $\mu\text{m}$ )**

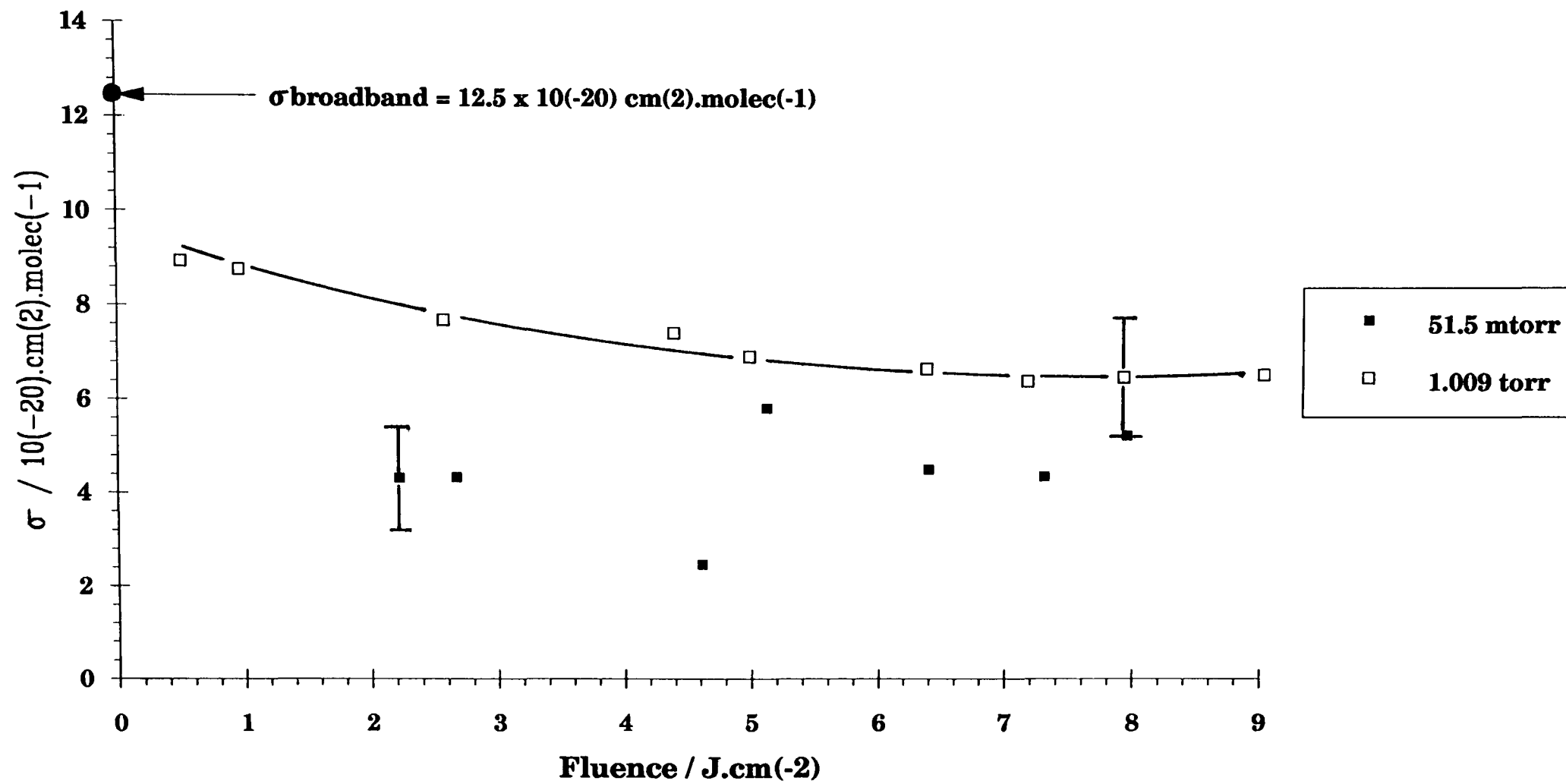


**Fig. 3.3-2 Propan-2-ol: Variation of the average number of absorbed photons per molecule with fluence at R14 (9  $\mu\text{m}$ )**

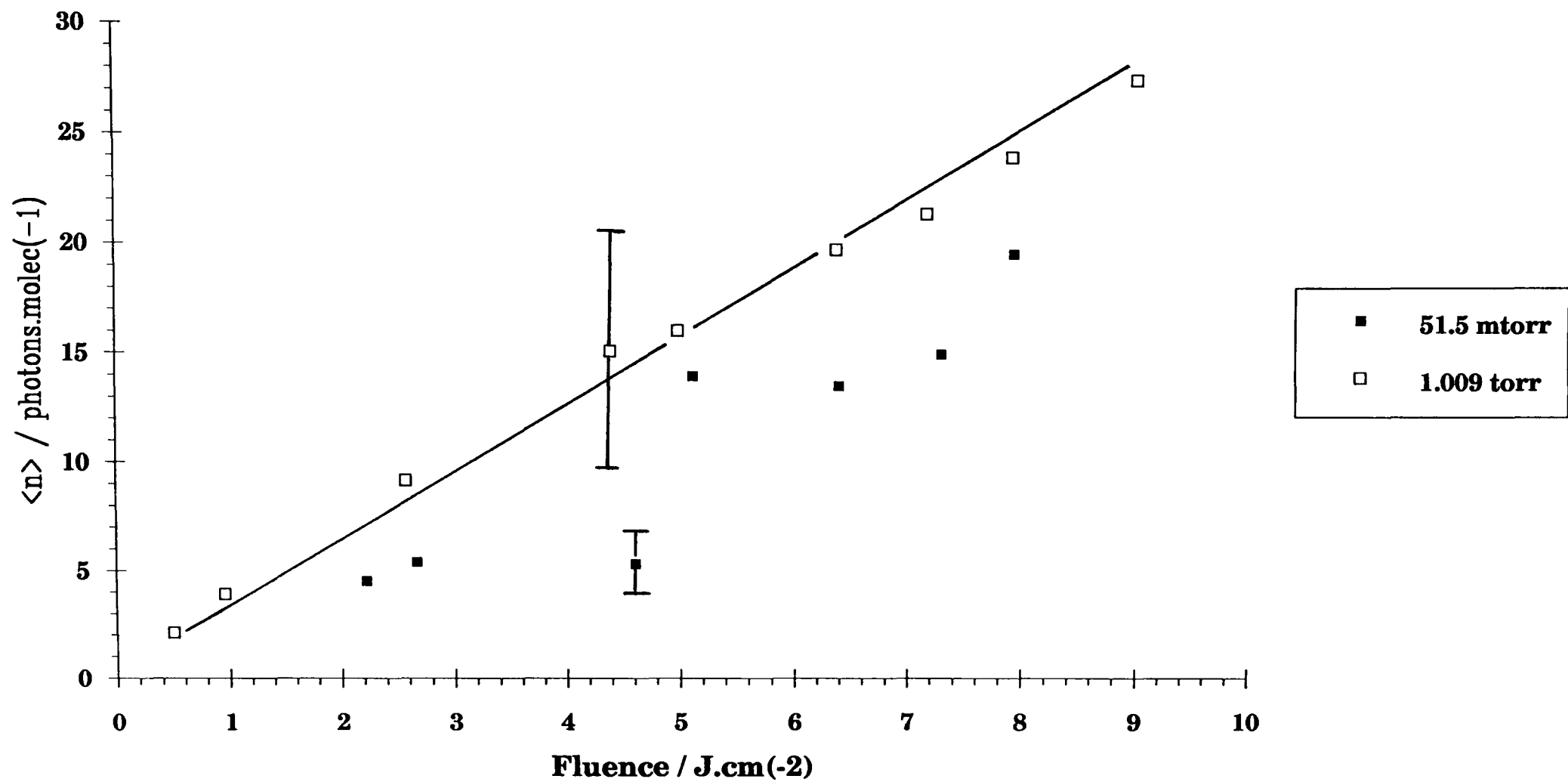


**Fig. 3.3-3(a) Propan-2-ol: Variation with pressure of the absorption cross-section, at a fluence of  $9.2 \text{ J.cm}^{-2}$  on R14 ( $9 \mu\text{m}$ )**

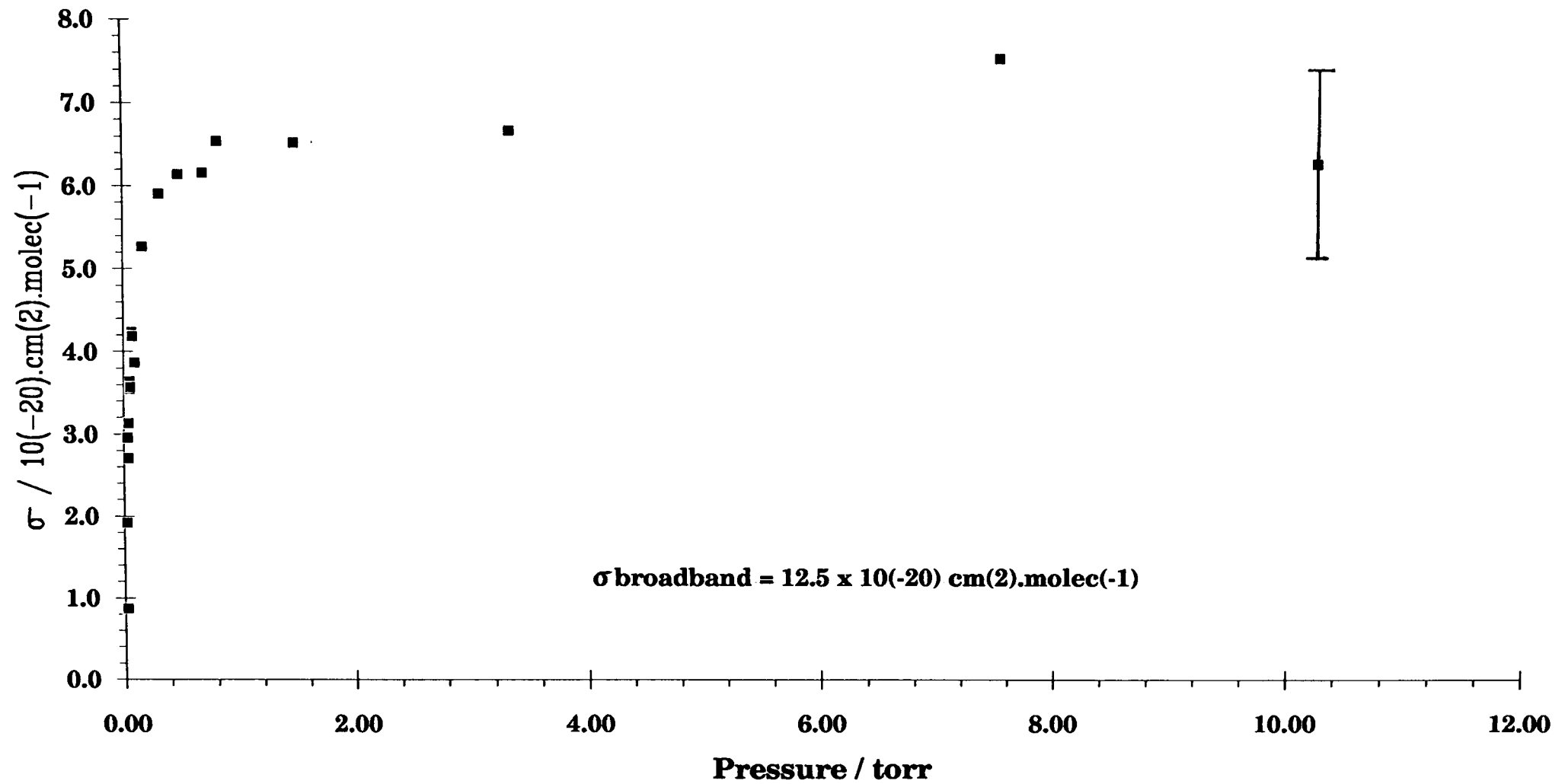


**Fig. 3.3-3(b) Propan-2-ol: Variation with pressure of the absorption cross-section, at a fluence of 9.2 J.cm(-2) on R14 (9 μm): P<1 torr**

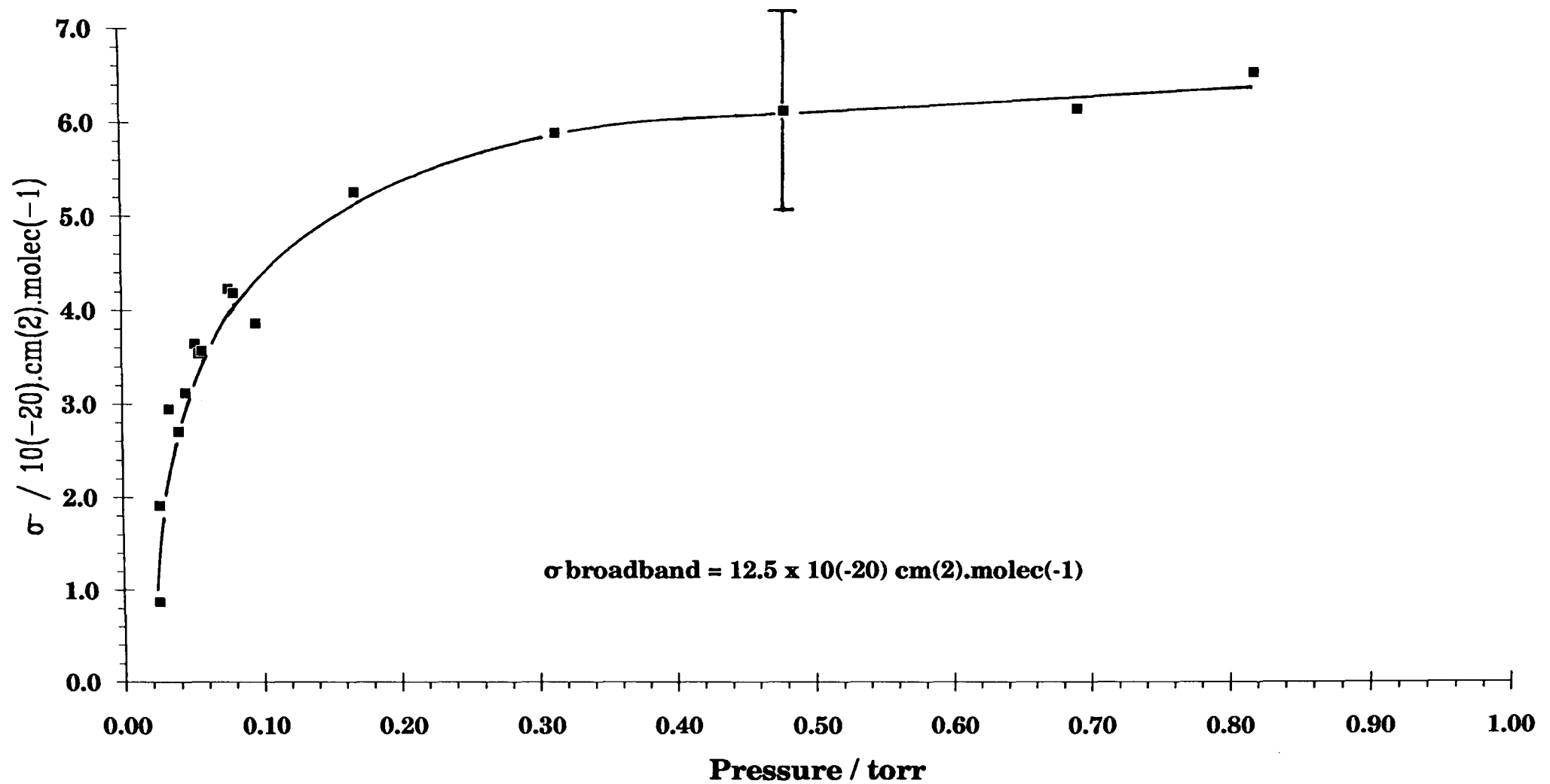
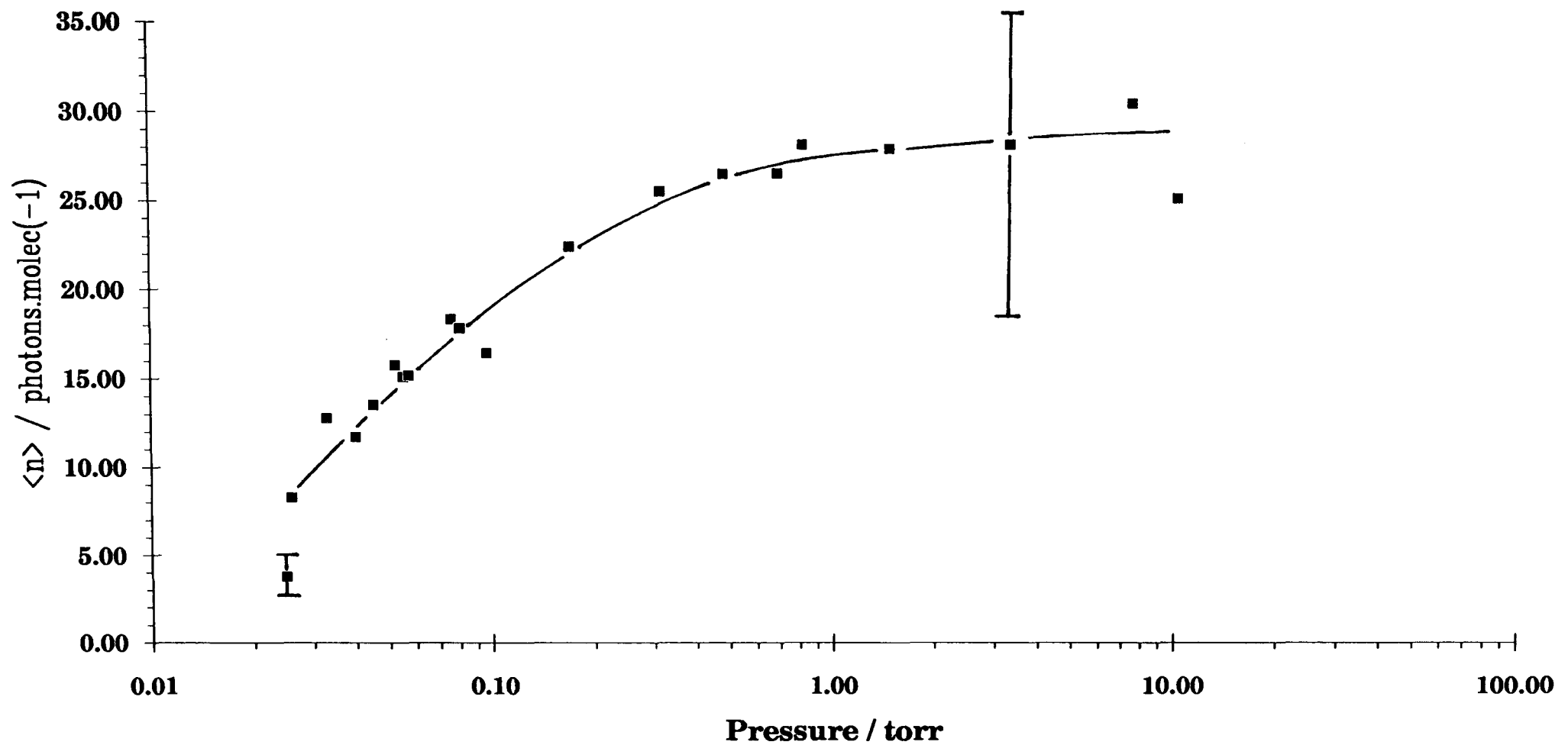


**Fig. 3.3-4 Propan-2-ol: Variation with pressure of the average number of absorbed photons per molecule, at a fluence of  $9.2 \text{ J.cm}^{-2}$  on R14 ( $9 \mu\text{m}$ )**



- (iv) There is very little variation of  $\sigma$  with fluence above  $6\text{J}/\text{cm}^2$  for a pressure of 1.009 torr, and also above  $2\text{J}/\text{cm}^2$  for a pressure of 51.5 mtorr.
- (v) For the 1.009 torr data there is a marked upward trend of  $\sigma$  with decreasing fluence.  $\sigma$  at zero fluence (broadband value) is larger than  $\sigma$  at the lowest fluence measured (Fig.3.3-1).
- (vi) Multiple-photon absorption is achieved fairly readily.

### 3.4 BUTAN-2-OL

The small signal (broadband) absorption cross-section,  $\sigma_{\text{broadband}}$ , was evaluated from an IR spectrum at the irradiating wavelength of  $R_{24}$  ( $10\ \mu\text{m}$ ) ( $978.47\text{cm}^{-1}$ ) and found to be  $7.88 \times 10^{-20}\ \text{cm}^2/\text{molecule}$ . The optoacoustic cell was used to monitor the change in absorption cross section with fluence at pressures of 53 mtorr, 55 mtorr, and 1.008 torr (Fig.3.4-1), and with pressure at three different fluences (Fig.3.4-3). The variation with fluence of the average number of absorbed photons per molecule is shown in Fig.3.4-2, while Fig.3.4-4 shows its dependence on pressure.

The three fluences used for the data of Figs.3.4-3(a-c) and 3.4-4 are  $9.59 \pm 0.15\ \text{J}/\text{cm}^2$ ,  $10.56 \pm 0.14\ \text{J}/\text{cm}^2$  and  $2.25 \pm 0.01\ \text{J}/\text{cm}^2$ . Apart from allowing an obvious high/low fluence comparison to be made, this data also shows that results are largely reproducible within the experimental scatter: Compare the graphical points which represent the two separate runs of near identical fluence.

The main observations are:

- (i) Above and below 0.1 torr, there is a sharp contrast in the dependence of  $\sigma$  on pressure (Fig.3.4-3(b)): The dependence is far greater below 0.1 torr.

**Fig. 3.4-1 Butan-2-ol: Variation of absorption cross-section with fluence at R24 (10  $\mu\text{m}$ ) and at high and low pressures**

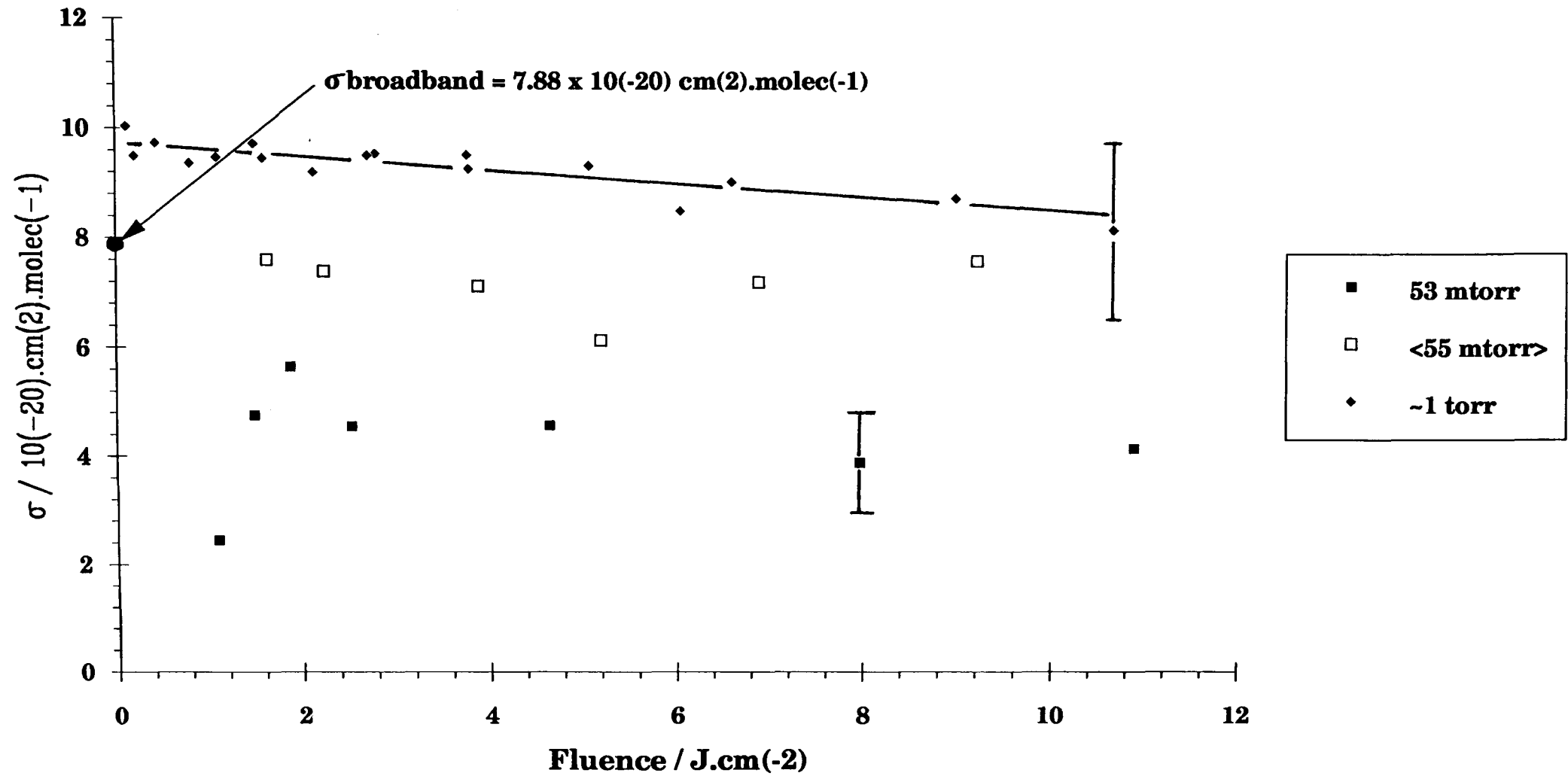


**Fig. 3.4-2 Butan-2-ol: Variation with fluence of the average number of absorbed photons per molecule at R24 (10  $\mu\text{m}$ ) and at high and low pressures**

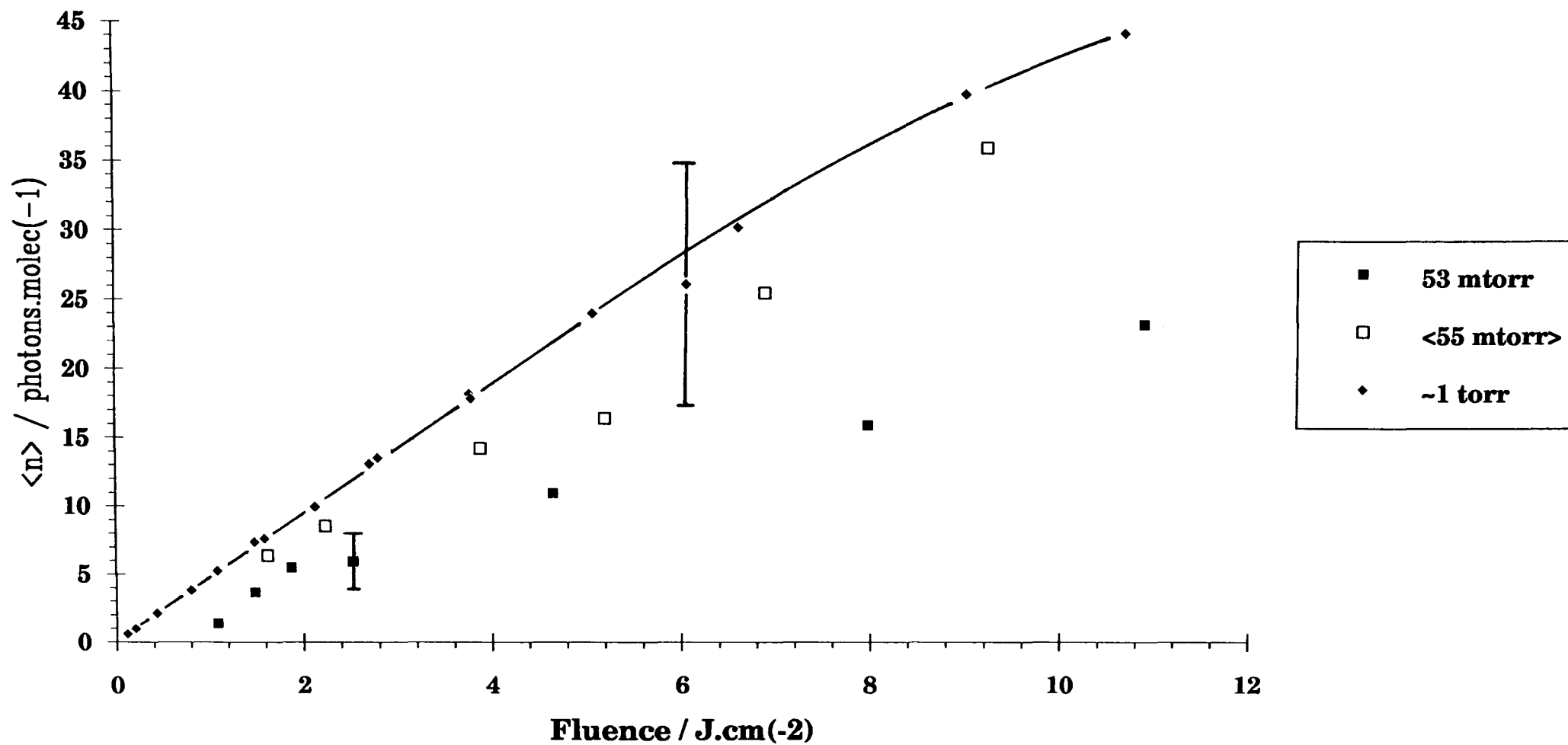


**Fig. 3.4-3(a) Butan-2-ol: Variation of absorption cross-section with pressure at R24 (10  $\mu\text{m}$ ) and at high and low fluences**

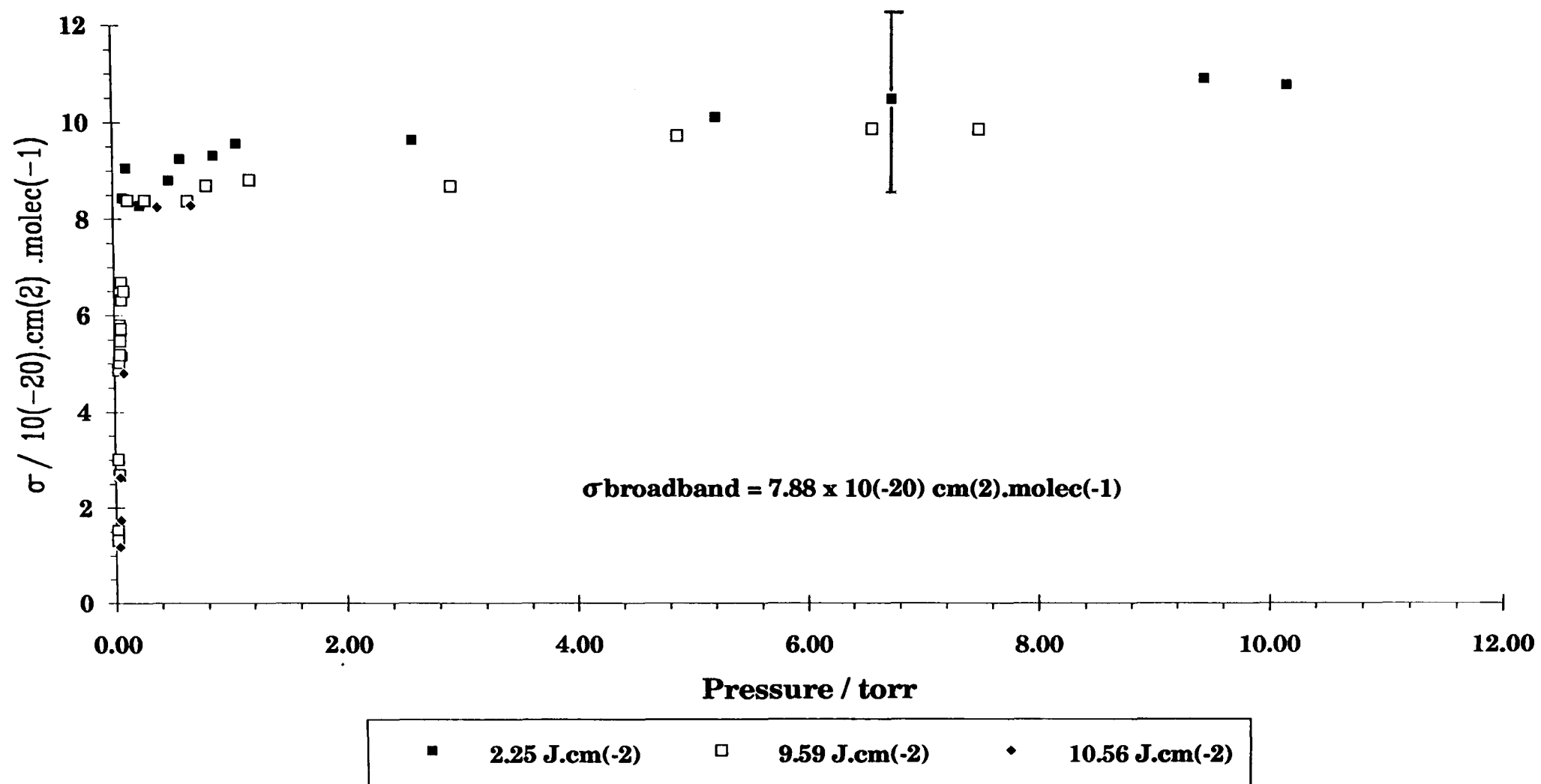


**Fig. 3.4-3(b) Butan-2-ol: Variation of absorption cross-section with pressure at R24 (10  $\mu\text{m}$ ) and at high and low fluences;  $P < 0.8$  torr**

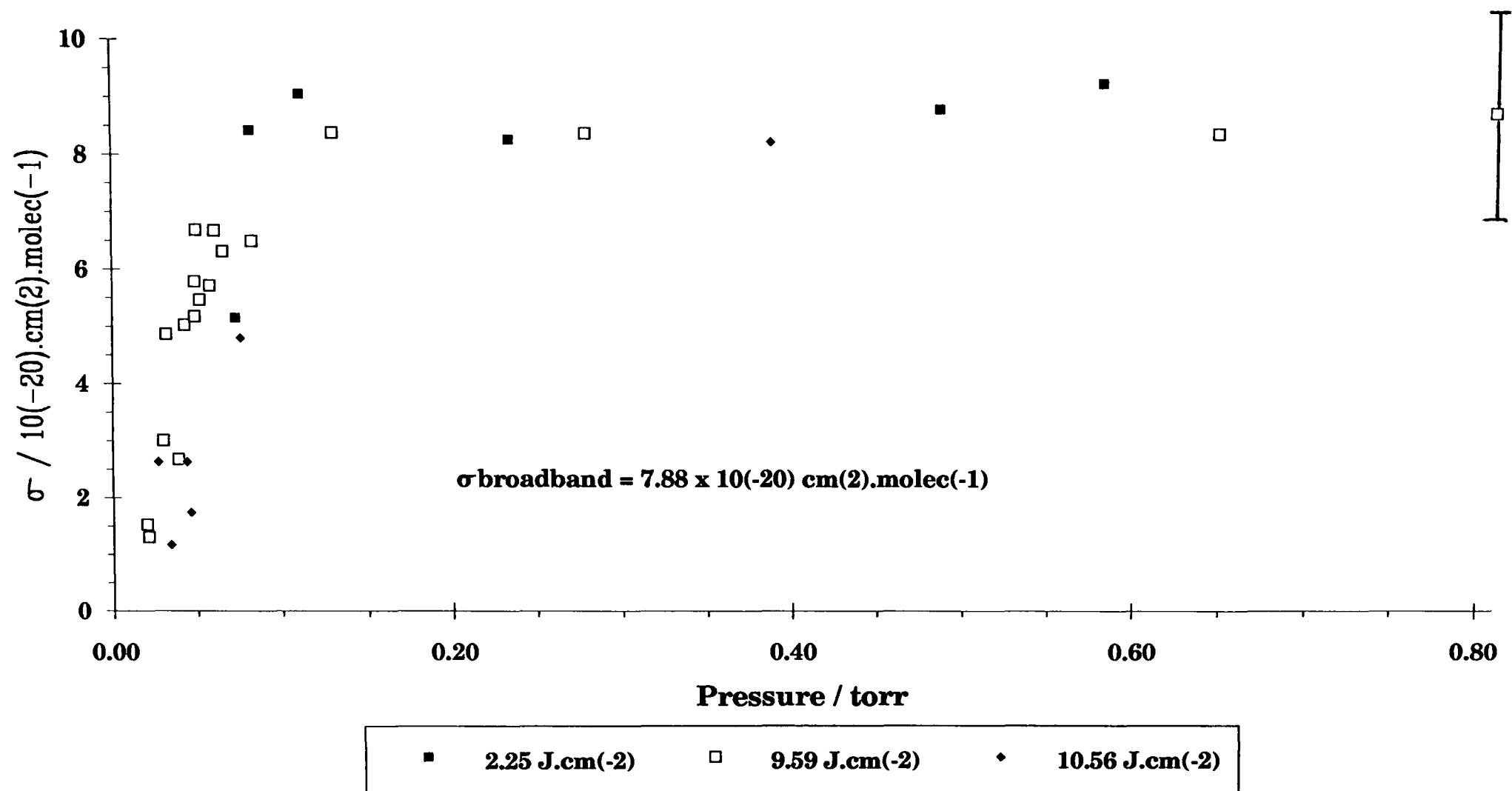


**Fig. 3.4-3(c) Butan-2-ol: Variation of absorption cross-section with pressure at R24 (10  $\mu\text{m}$ ) and at high and low fluences:  $P < 0.15$  torr**

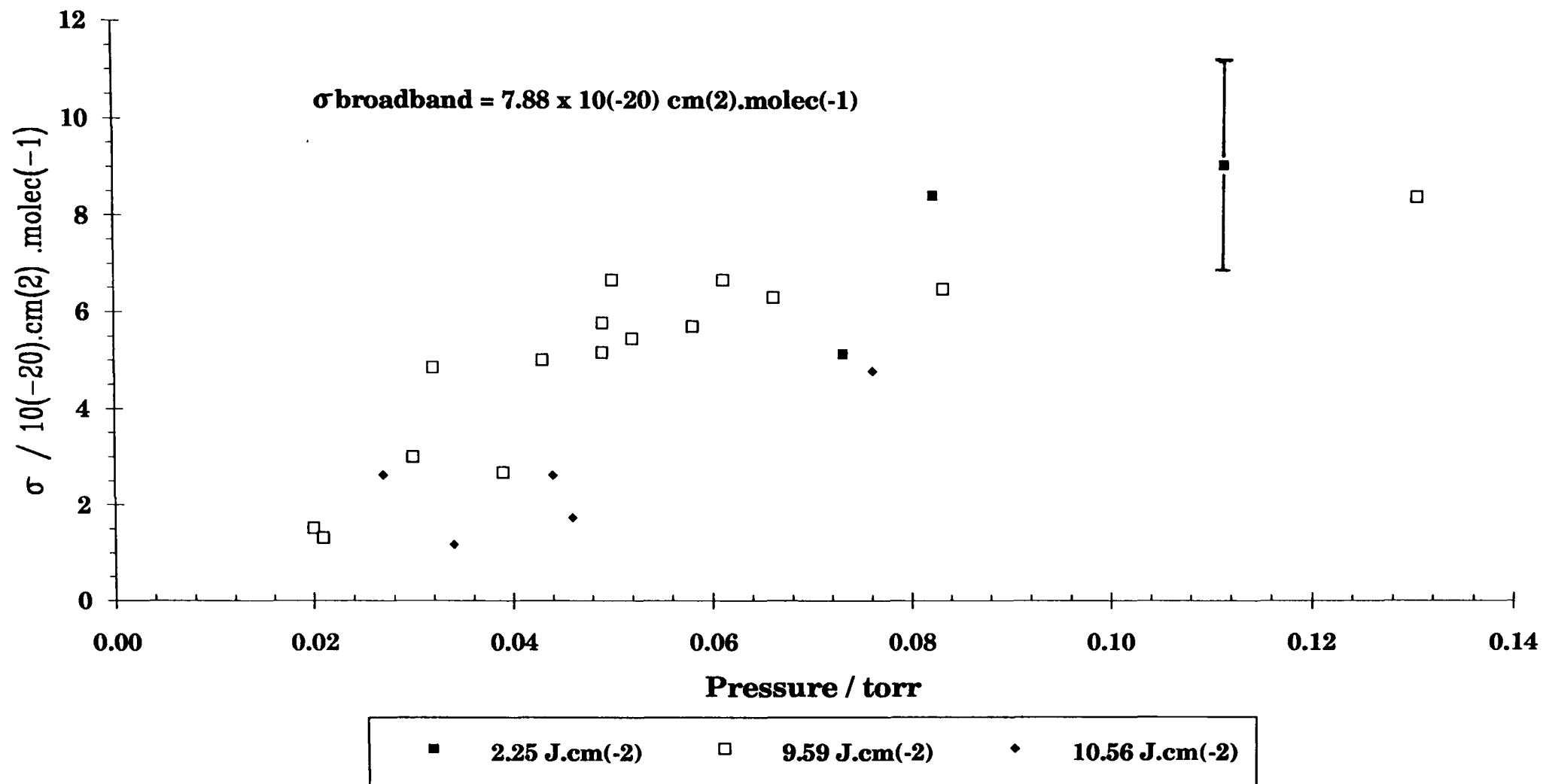
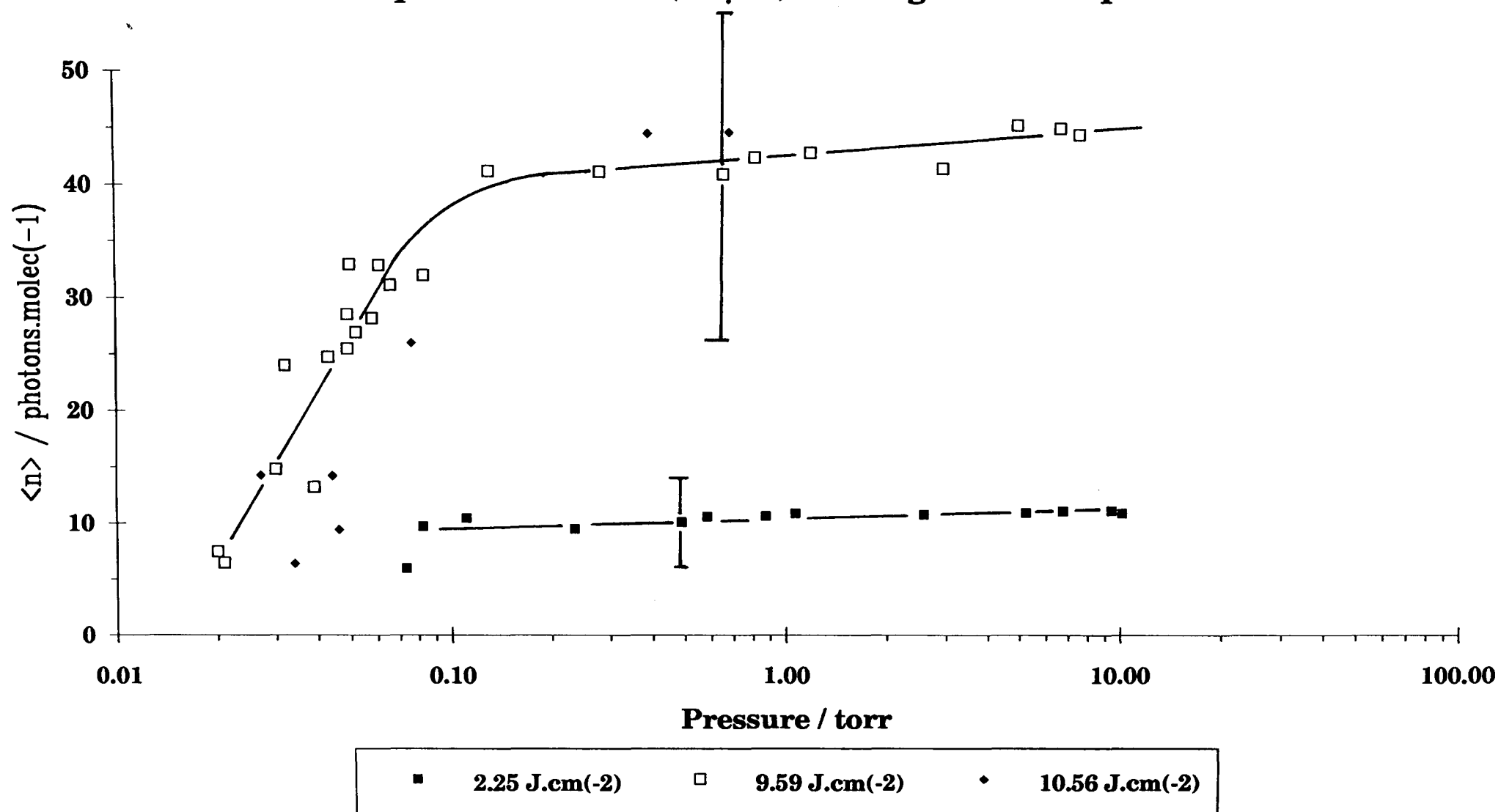


**Fig. 3.4-4 Butan-2-ol: Variation of average number of absorbed photons with pressure at R24 (10  $\mu\text{m}$ ) and high and low pressures**



- (ii) There is a rapid fall off below 0.1 torr of  $\sigma$  with decreasing pressure.
- (iii) The  $\sigma$  values of the more gently varying (higher pressure) section, are greater than that of the broadband absorption cross section.
- (iv) There is very little variation of  $\sigma$  with fluence for the observed pressures of 50 mtorr and 1 torr; there is a slight fall off with increasing fluence which is less noticeable for pressures of 50 mtorr (Fig.3.4-1).
- (v)  $\sigma$  at zero fluence (broadband value) is smaller than  $\sigma$  at the lowest fluence measured for a pressure of 1.008 torr, but larger than that for the 53 mtorr data, and approximately the same as that measured for the 55 mtorr data (Fig.3.4-1).
- (vi) Multiple-photon absorption is readily achievable, even at collision-free conditions. Results however, appear particularly sensitive to pressure in the collision free regime (Figs.3.4-2 and -4). At high pressures,  $\langle n \rangle$  is independent of pressure, and a four fold increase in fluence is seen to cause the same increase in  $\langle n \rangle$  (Fig.3.4-4).

### 3.5 PENTAN-2-OL

The small signal, broadband absorption cross-section,  $\sigma_{\text{broadband}}$ , of pentan-2-ol at the wavelength of  $R_{26}(9\mu\text{m})$  ( $1082.296\text{cm}^{-1}$ ) is  $5.83 \times 10^{-20}\text{cm}^2/\text{molecule}$ . The optoacoustic cell was used to monitor the change in  $\sigma$  with fluence at 50 mtorr (Fig.3.5-1) and with pressure at a fluence of  $6.65 \pm 0.05\text{J}/\text{cm}^2$  (Fig.3.5-3 (a-b)). The variation of the average number of absorbed photons per molecule with fluence is given in Fig.3.5-2, while Fig.3.5-4 shows its dependence on pressure. The data in Figs.3.5-1 and 3.5-2 include those from two separate sets of experiments.

The main observations are:

- (i) There is a contrast between the behaviour of  $\sigma$  versus pressure at high and low pressures (Fig.3.5-3(a)):

**Fig. 3.5-1 Pentan-2-ol: Variation of absorption cross-section with fluence at R26 (9  $\mu\text{m}$ ) and a pressure of 50 mtorr**

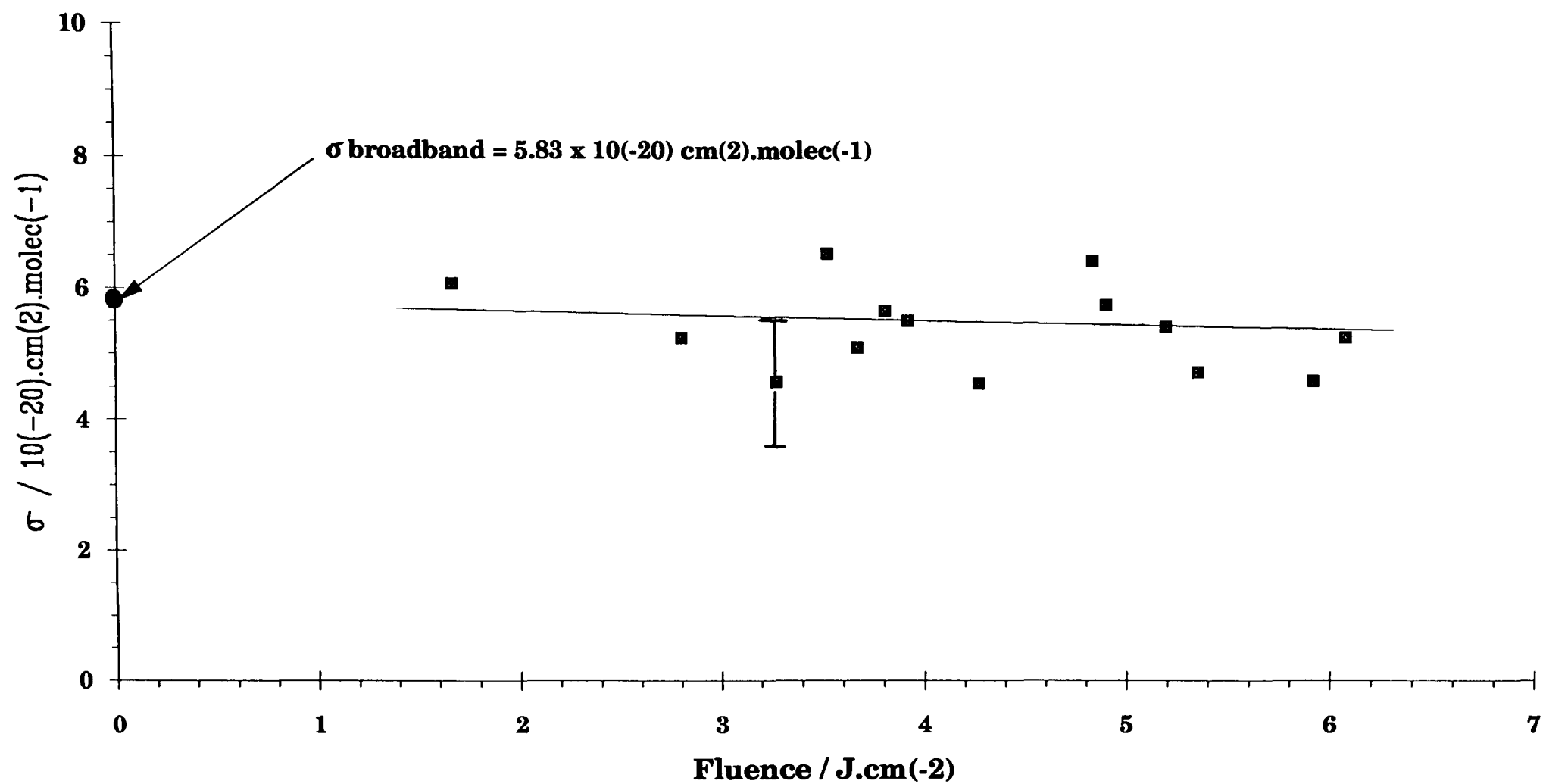


**Fig. 3.5-2 Pentan-2-ol: Variation of the average number of absorbed photons per molecule with fluence at R26 (9  $\mu\text{m}$ ) and a pressure of 50 mtorr**

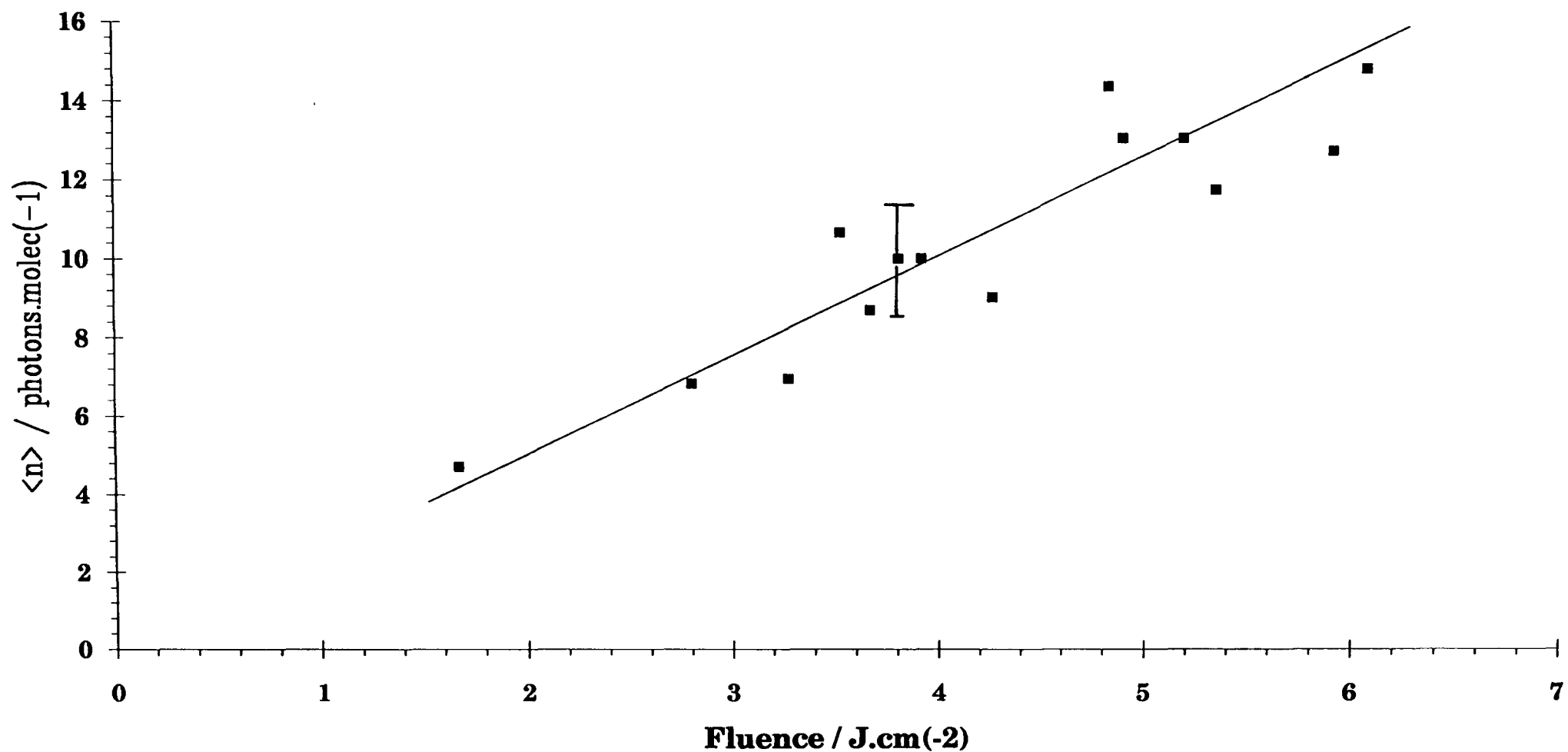


**Fig. 3.5-3(a) Pentan-2-ol: Variation of absorption cross-section with pressure at R26 (9  $\mu\text{m}$ ), and a fluence of 6.65  $\text{J}\cdot\text{cm}^{-2}$**

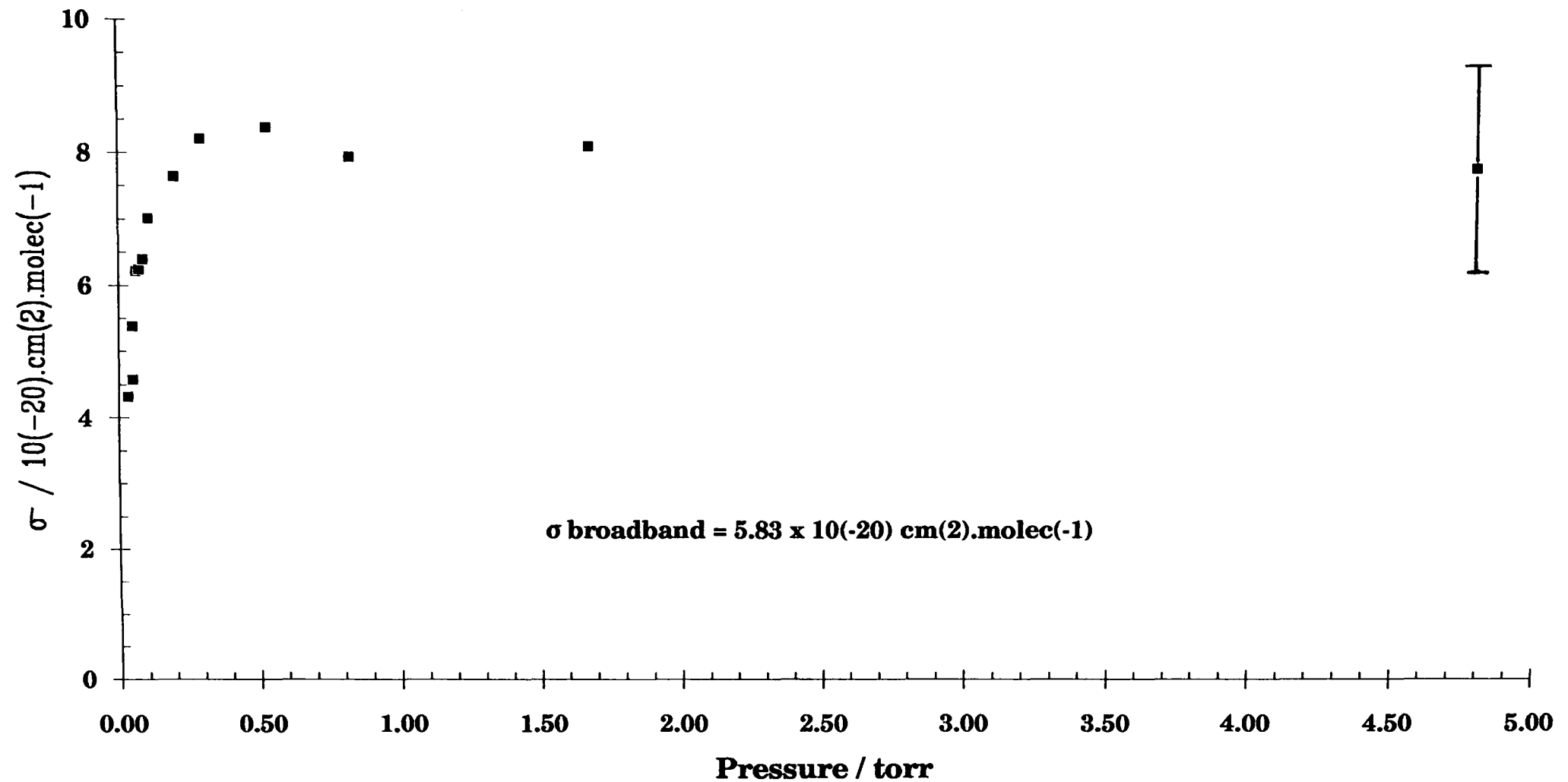


**Fig.3.5-3(b) Pentan-2-ol: Variation of absorption cross-section with pressure at R26 (9  $\mu\text{m}$ ) and a fluence of 6.65  $\text{J}\cdot\text{cm}^{-2}$ , for  $P < 1$  torr**

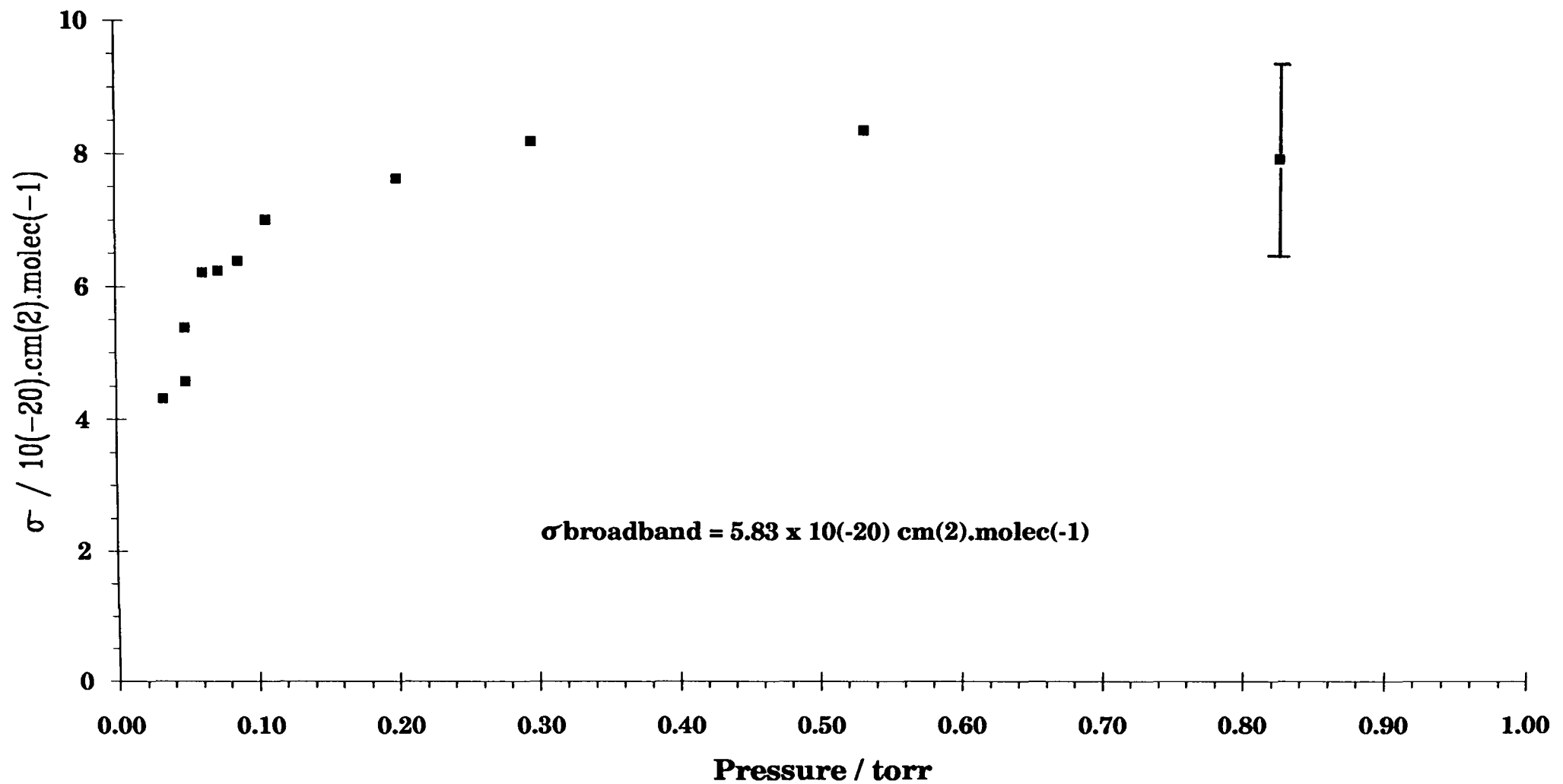
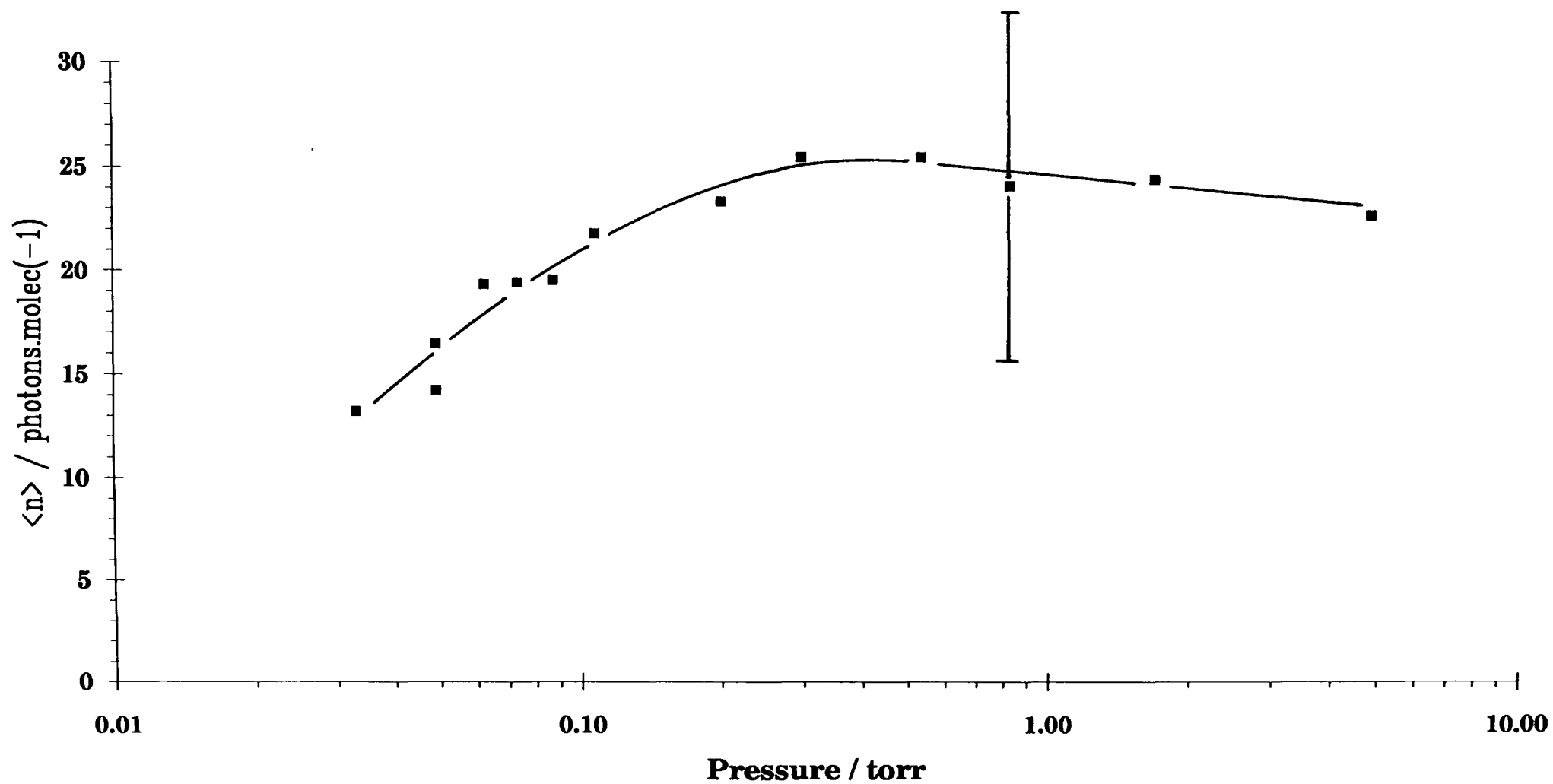


**Fig. 3.5-4 Pentan-2-ol: Variation of average number of absorbed photons per molecule with pressure at R25 (9  $\mu\text{m}$ ) and a fluence of 6.65 J.cm(-2)**



- (ii) There is a fall off of  $\sigma$  with decreasing pressure below 0.3 torr (Fig.3.5-3(b)).
- (iii) The value of  $\sigma$  over the more gently varying (higher pressure) section, is greater than that of the broadband absorption cross-section.
- (iv) There is no clear variation of  $\sigma$  with fluence.
- (v) It is possible, that within the experimental scatter, there is a very small and gradual upward trend of  $\sigma$  with decreasing fluence over the entire fluence range (Fig.3.5-1).  $\sigma$  at zero fluence (broadband value) lies within the range of the experimental data.
- (vi) Multiple-photon absorption is readily achievable even at collision-free pressures and at the lowest laser fluence.

### 3.6 PENTAN-3-OL

The small signal, broadband absorption cross-section,  $\sigma_{\text{broadband}}$ , at the wavelength of  $R_{14}$  ( $10\ \mu\text{m}$ ) ( $971.931\text{cm}^{-1}$ ) is  $16.9 \times 10^{-20}\ \text{cm}^2/\text{molecule}$ . Under laser irradiation at the same wavelength, the variation of  $\sigma$  with fluence at 49 mtorr and 0.995 torr, and with pressure at  $11.18 \pm 0.02\ \text{J}/\text{cm}^2$  is as shown in Figs.3.6-1 and 3.6-3(a-b). The variation of the average number of absorbed photons with fluence is shown in Fig.3.6-2, while the variation with pressure is given by Fig.3.6-4.

The main observations are:

- (i) Above and below 0.5 torr, there is a contrast in the dependence of  $\sigma$  on pressure: Above 0.5 torr,  $\sigma$  is virtually independent of pressure (Fig.3.6-3(a)).
- (ii) There is a rapid fall off of  $\sigma$  with decreasing pressure below 0.1 torr. Figs.3.6-3(a) and (b).
- (iii) The value of  $\sigma$  is less than the broadband cross-section for all pressures.

**Fig. 3.6-1 Pentan-3-ol: Variation of absorption cross-section with fluence at R14 (10  $\mu\text{m}$ ) and high and low pressures**

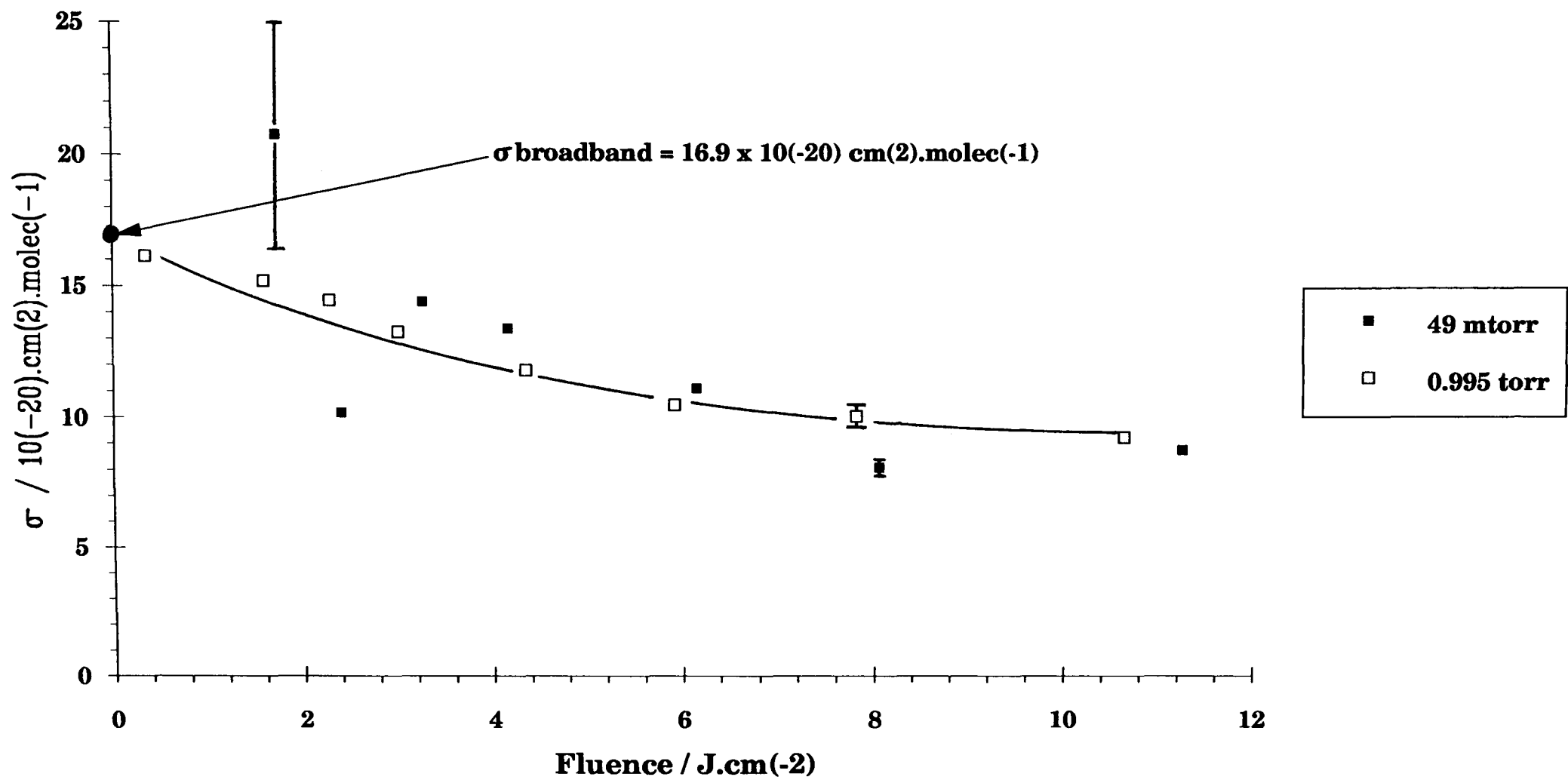


**Fig. 3.6-2 Pentan-3-ol: Variation of the average number of absorbed photons per molecule with fluence at R14 (10  $\mu\text{m}$ ) and high and low pressure**

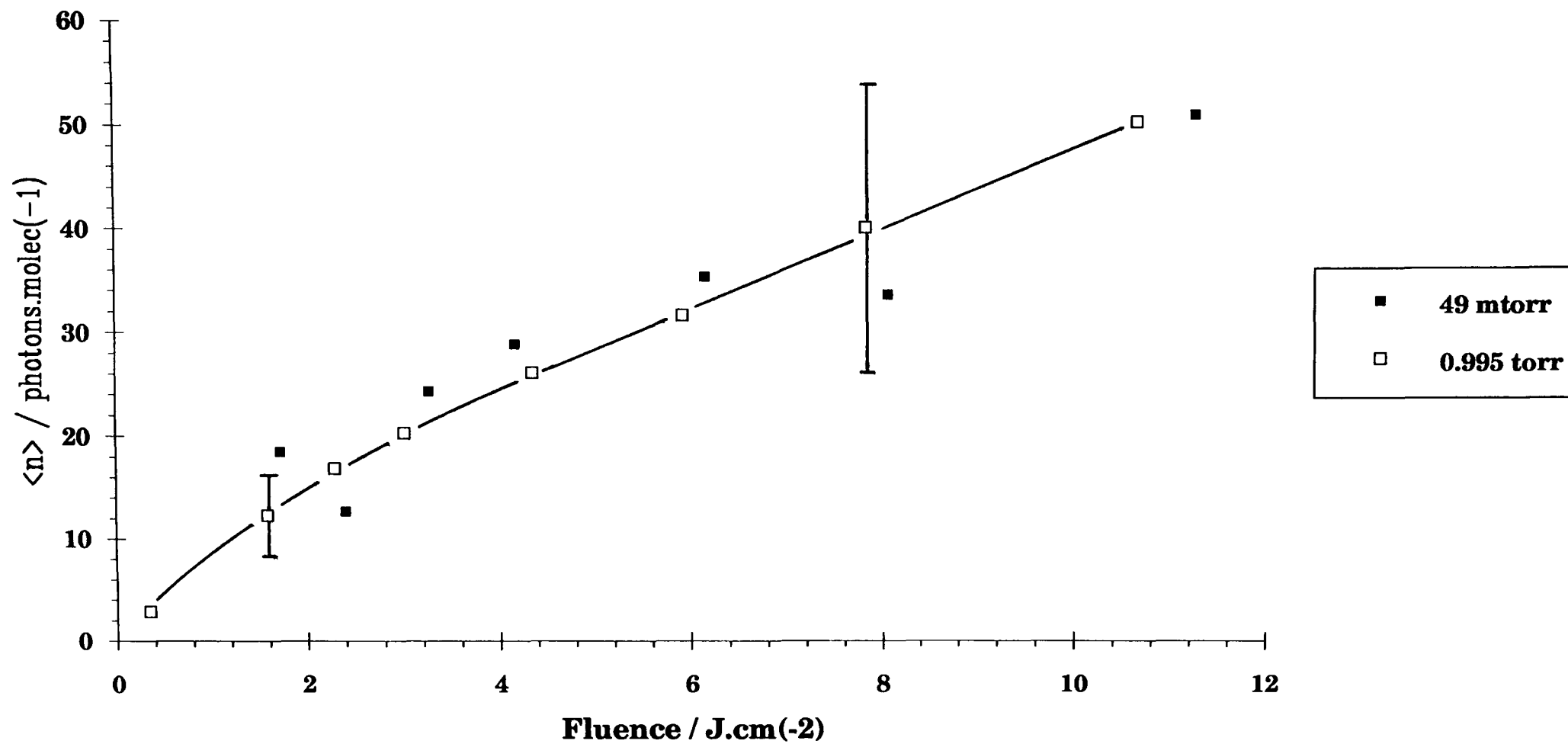


**Fig. 3.6-3(a) Pentan-3-ol: Variation of absorption cross-section with pressure at R14 (10  $\mu\text{m}$ ) and a fluence of 11.18  $\text{J}\cdot\text{cm}^{-2}$**

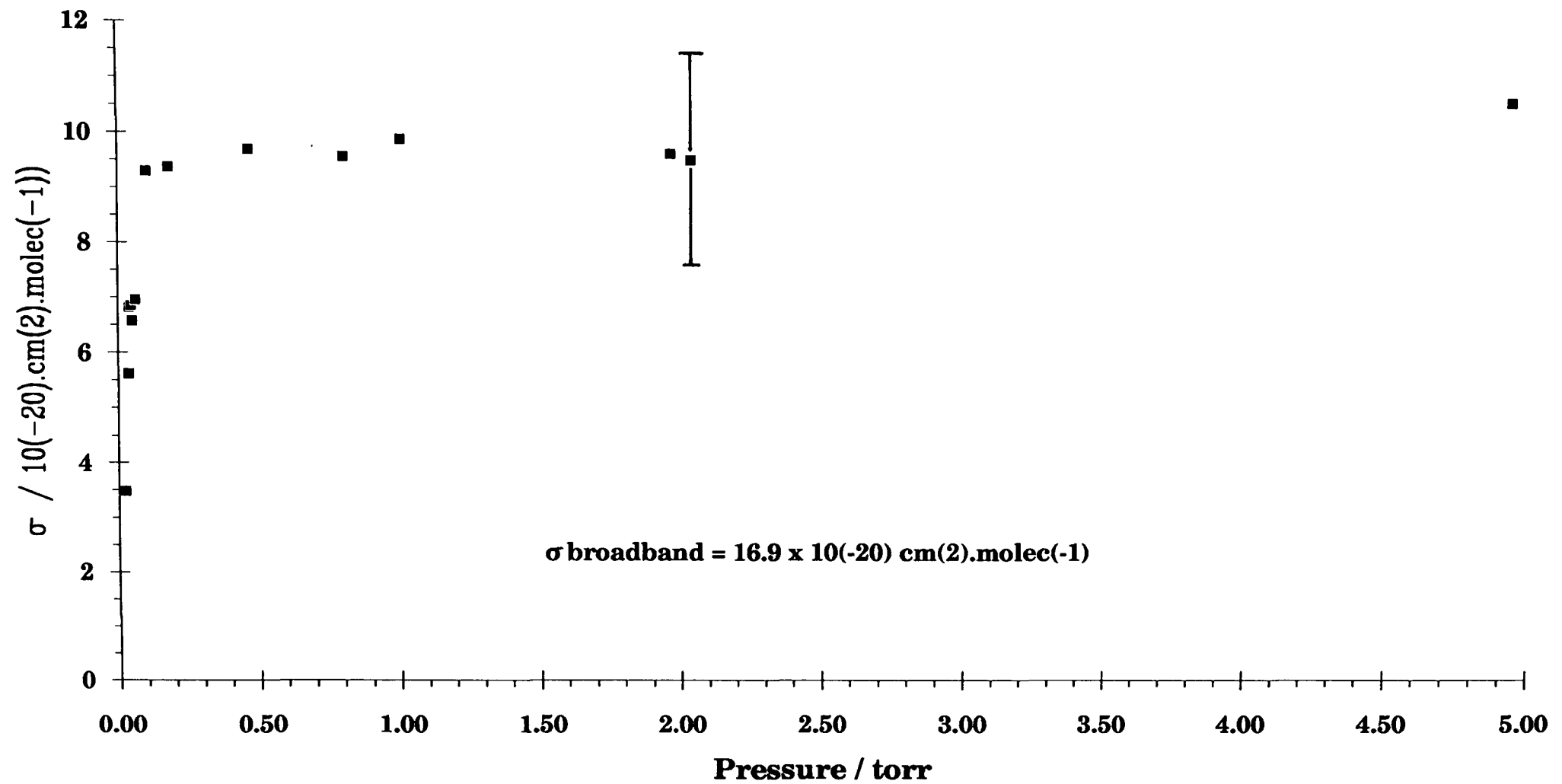


**Fig. 3.6-3(b) Pentan-3-ol: Variation of absorption cross-section with pressure at R14 (10  $\mu\text{m}$ ) and a fluence of 11.18  $\text{J}\cdot\text{cm}^{-2}$ , for  $P < 1$  torr**

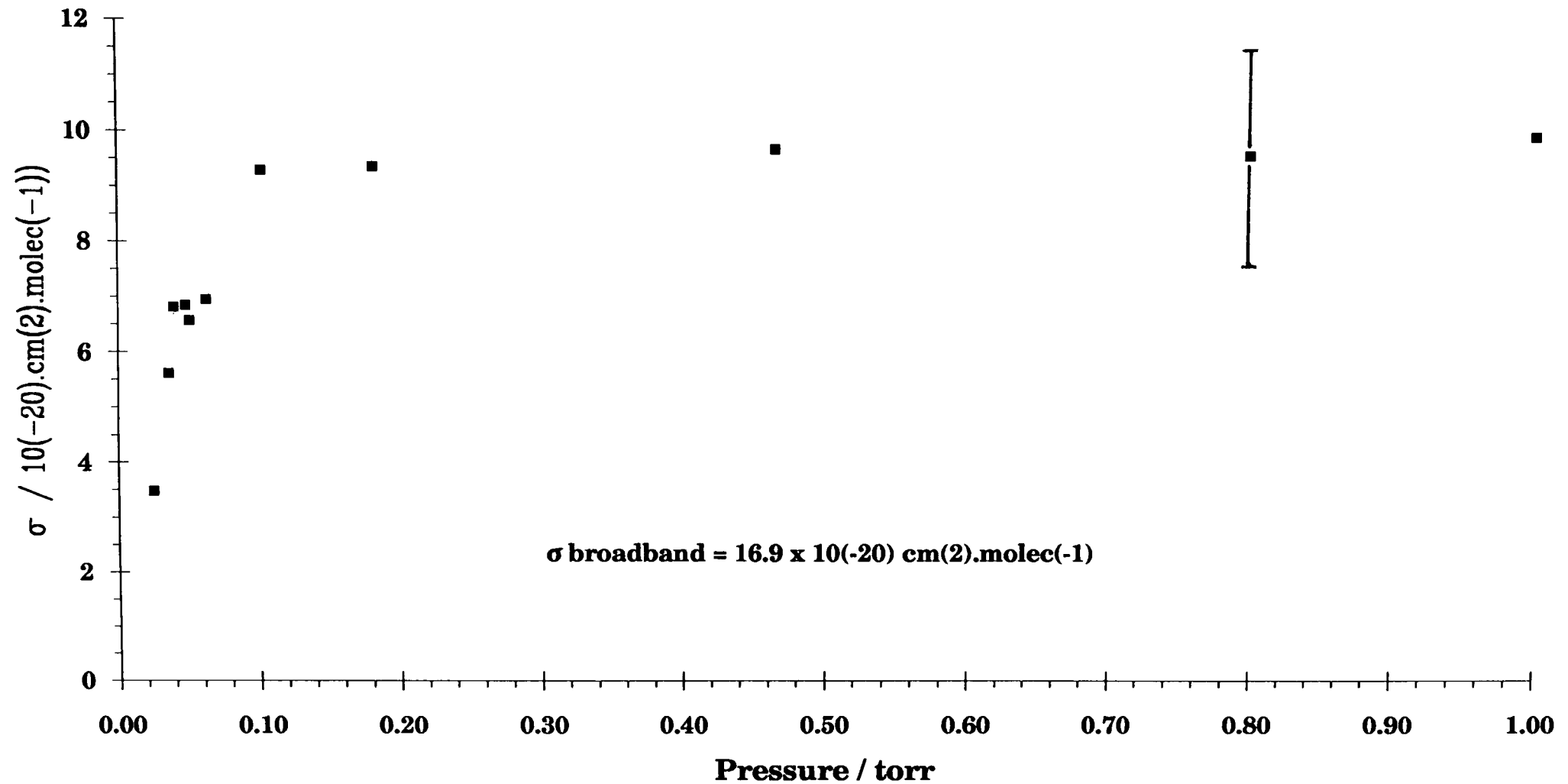
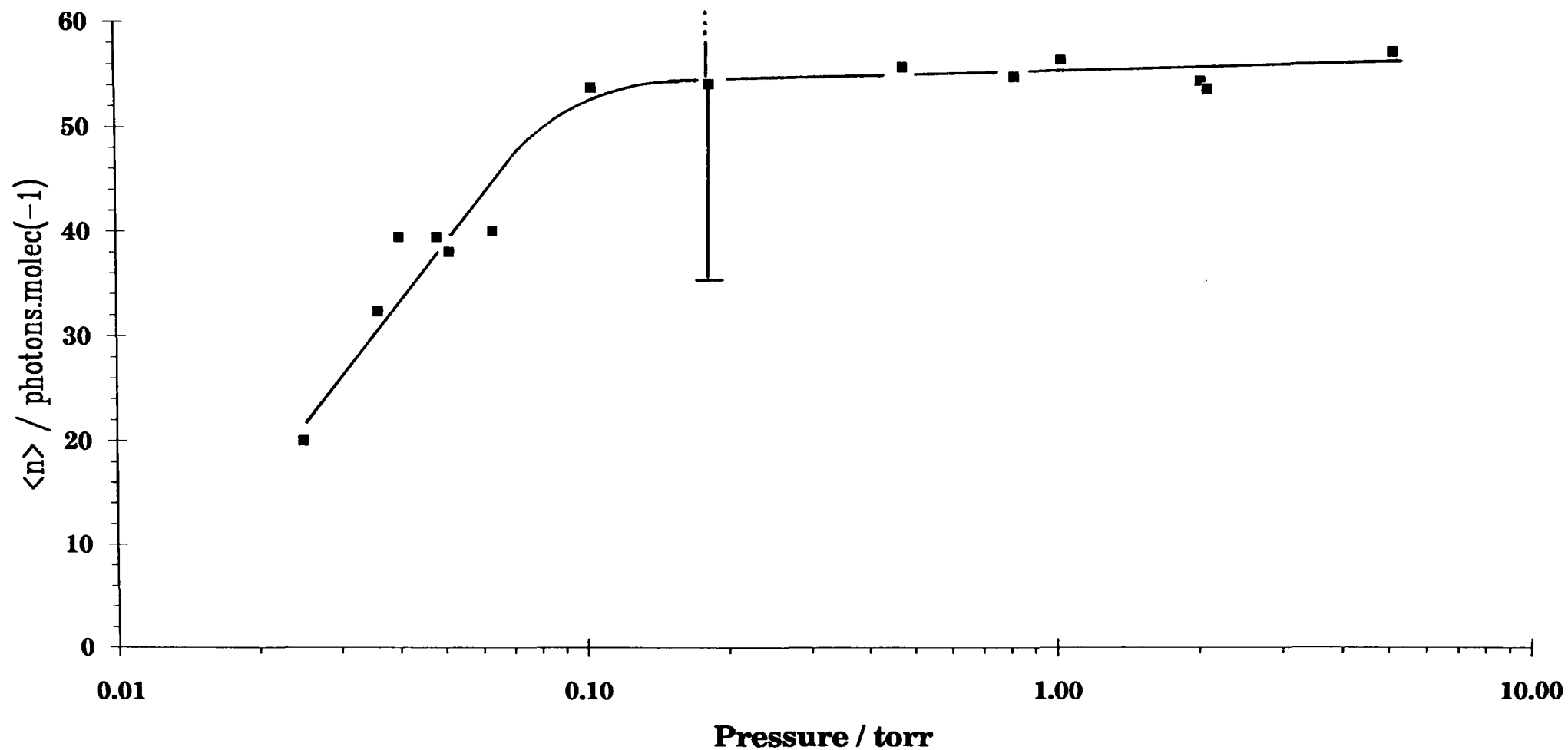


**Fig. 3.6-4 Pentan-3-ol: Variation with pressure of average number of absorbed photons per molecule at R14 (10  $\mu\text{m}$ ) and a fluence of 11.18  $\text{J}\cdot\text{cm}^{-2}$**



- (iv) There is a similar variation of  $\sigma$  with fluence for both the high and low pressures over the entire fluence range (Figs.3.6-1).
- (v) For both 49mtorr and 0.995torr there is a marked upward trend of  $\sigma$  with decreasing fluence towards the broadband value; the broadband value is only slightly greater than  $\sigma$  measured at the lowest fluence of the 0.995torr data (Fig.3.6-1). The rise below  $6\text{J}/\text{cm}^2$  is more rapid than at higher fluences, though the entire upward trend is particularly smooth and gradual for both pressures.
- (vi) Multiple-photon absorption is readily achievable. There is no apparent difference between the trend of  $\langle n \rangle$  with fluence at 49mtorr compared to that at 0.995torr.

### 3.7 HEXAN-2-OL

The small signal, broadband absorption cross-section,  $\sigma_{\text{broadband}}$ , at the wavelength of  $\text{P}_{20}(9\mu\text{m})$  ( $1046.85\text{cm}^{-1}$ ) is  $4.76 \times 10^{-20}\text{cm}^2/\text{molecule}$ . Under laser irradiation at the same wavelength, the variation of  $\sigma$  with fluence (at nominal pressures of 50mtorr and 1torr) and with pressure (at a fluence of  $9.0 \pm 0.25\text{J}/\text{cm}^2$ ) is shown in Figs.3.7-1 and 3.7-3. The variation with fluence of the average number of absorbed photons per molecule is shown in Fig.3.7-2, while Fig.3.7-4 shows the variation of  $\langle n \rangle$  with pressure.

The main observations are:

- (i) Above and below 0.2torr, there is a contrast in the dependence of  $\sigma$  on pressure: Above 0.2torr,  $\sigma$  is approximately independent of pressure.
- (ii) There is a rapid fall off of  $\sigma$  with decreasing pressure below 0.1torr.
- (iii) The value of  $\sigma$  for pressures over 0.1torr is greater than that of the broadband absorption cross-section.
- (iv) For both pressures studied, there is a fall off of  $\sigma$  with increasing

**Fig. 3.7-1 Hexan-2-ol: Variation of absorption cross-section with fluence at P20 (9  $\mu\text{m}$ )**

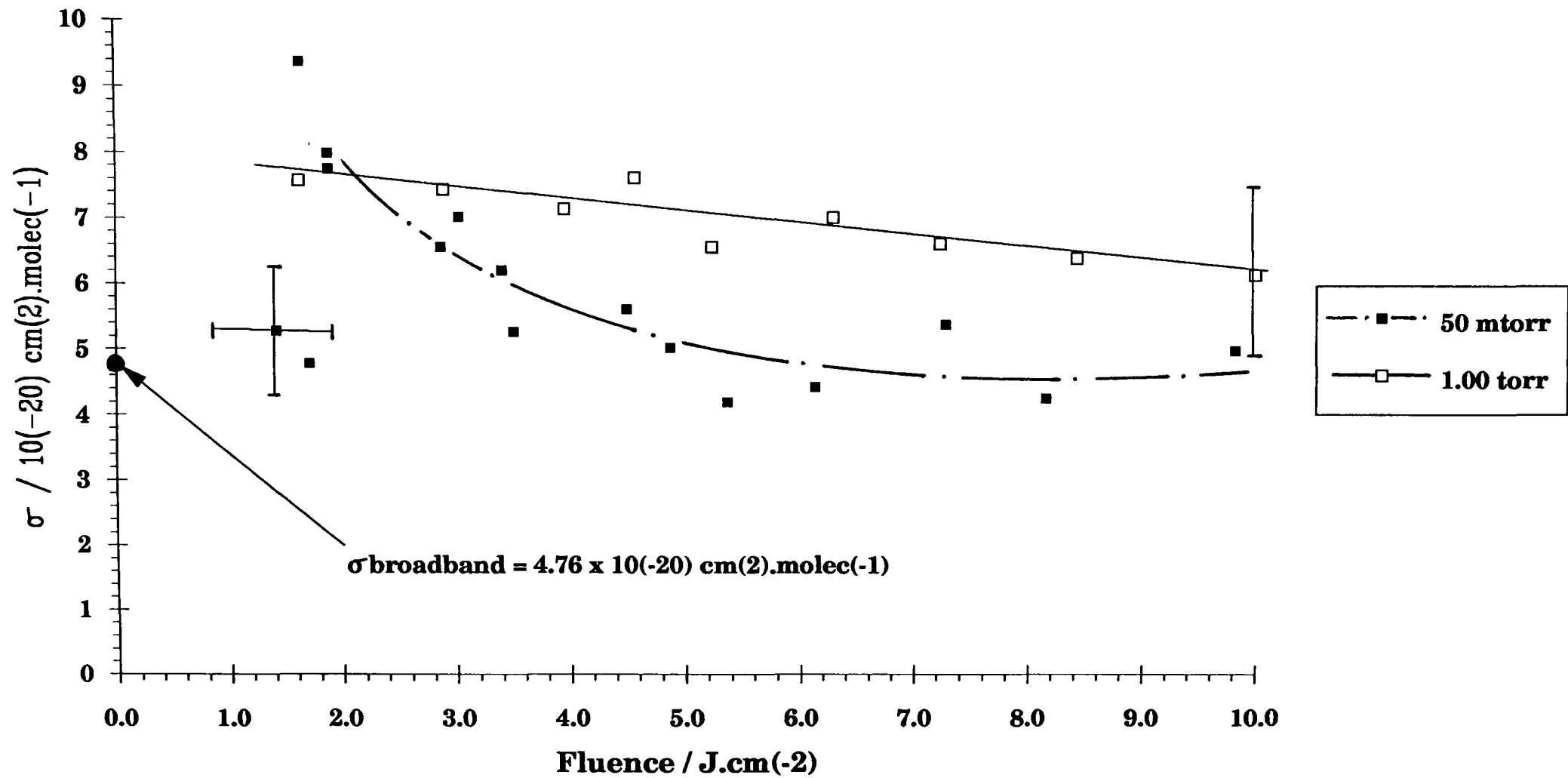


**Fig. 3.7-2 Hexan-2-ol: Variation of the average number of absorbed photons per molecule with fluence at P20 (9  $\mu\text{m}$ )**

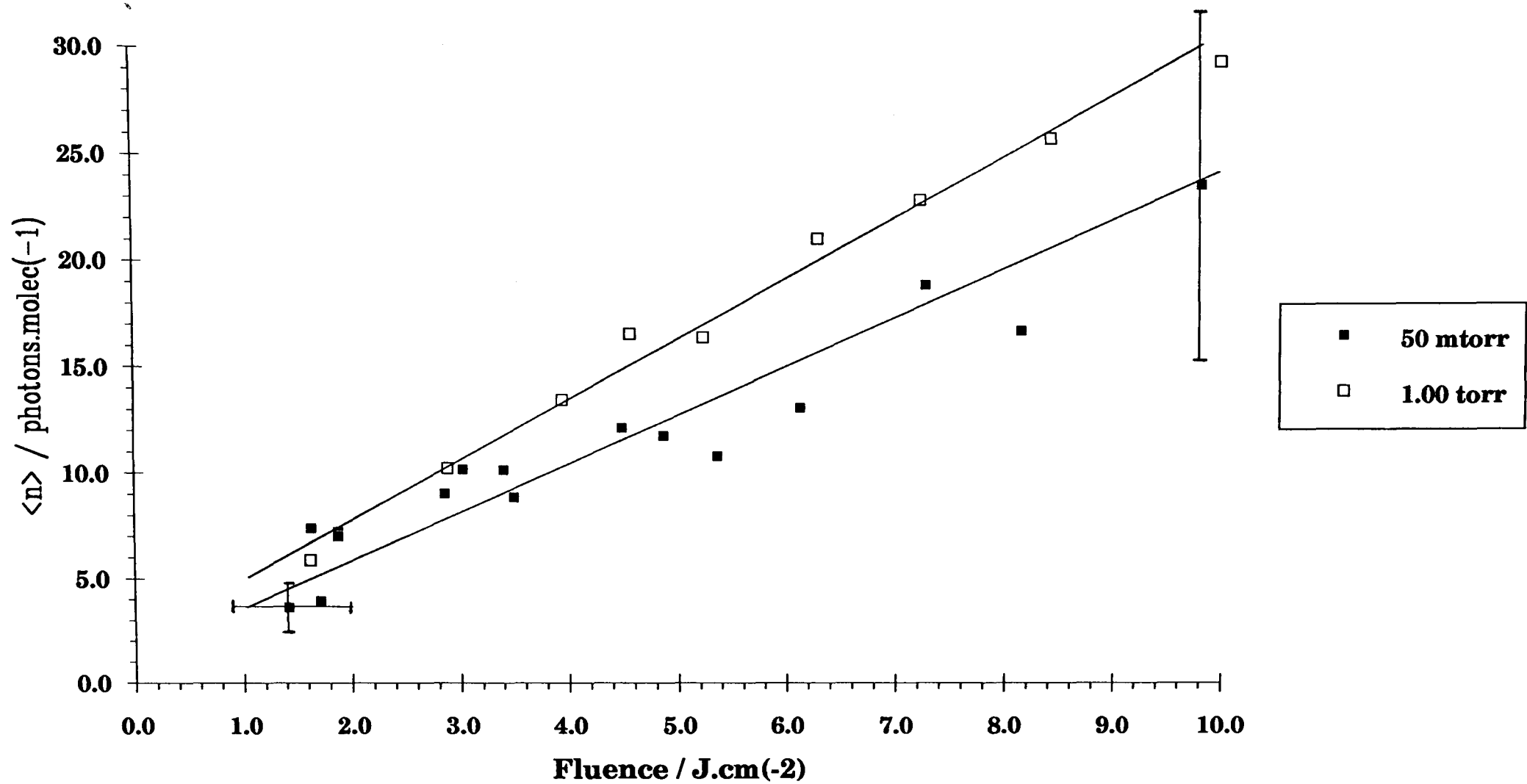


**Fig. 3.7-3 Hexan-2-ol: Variation of absorption cross-section with pressure at P20 (9  $\mu\text{m}$ ), and with a fluence of  $9.0 \text{ J.cm}^{-2}$**

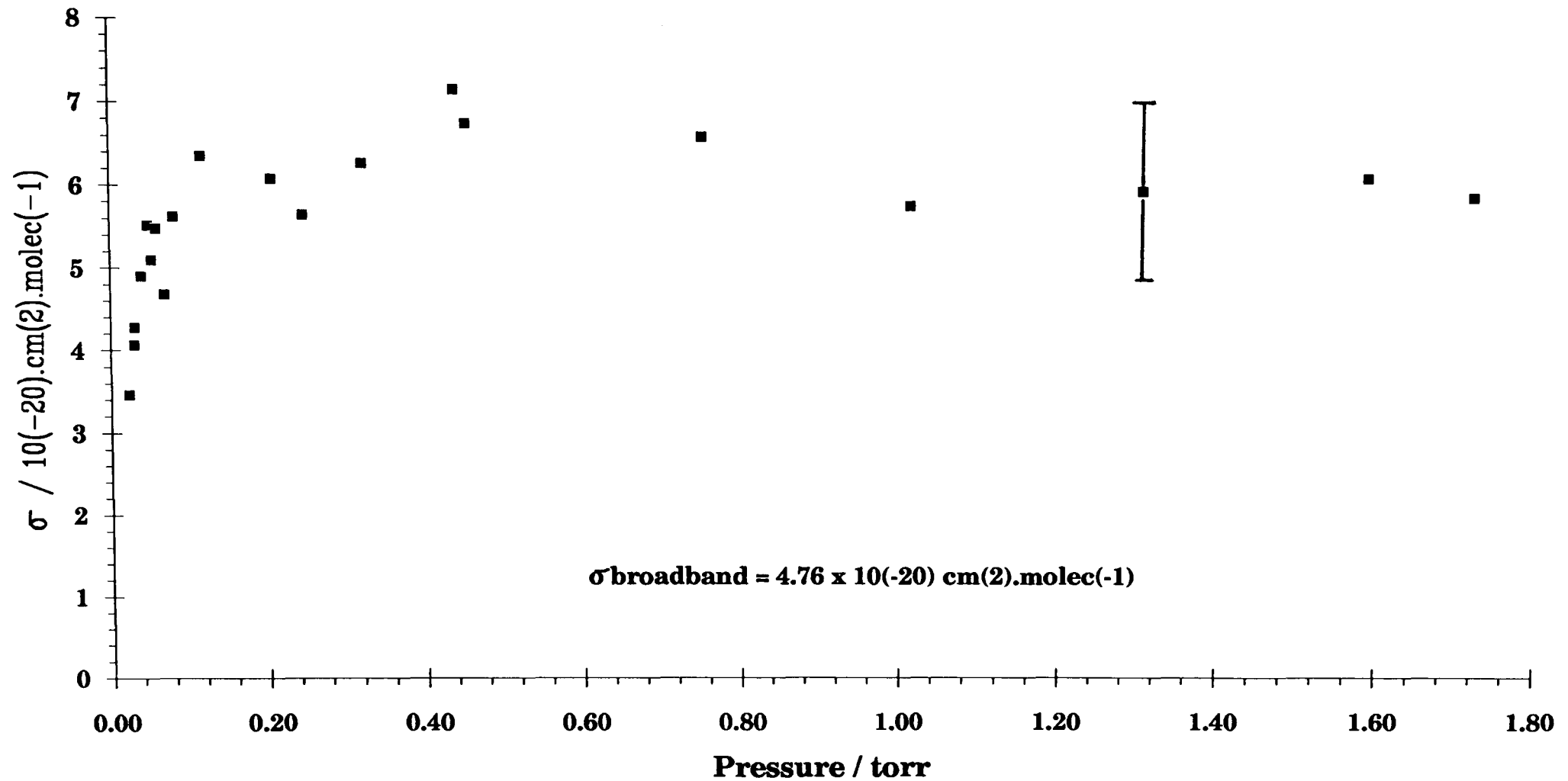
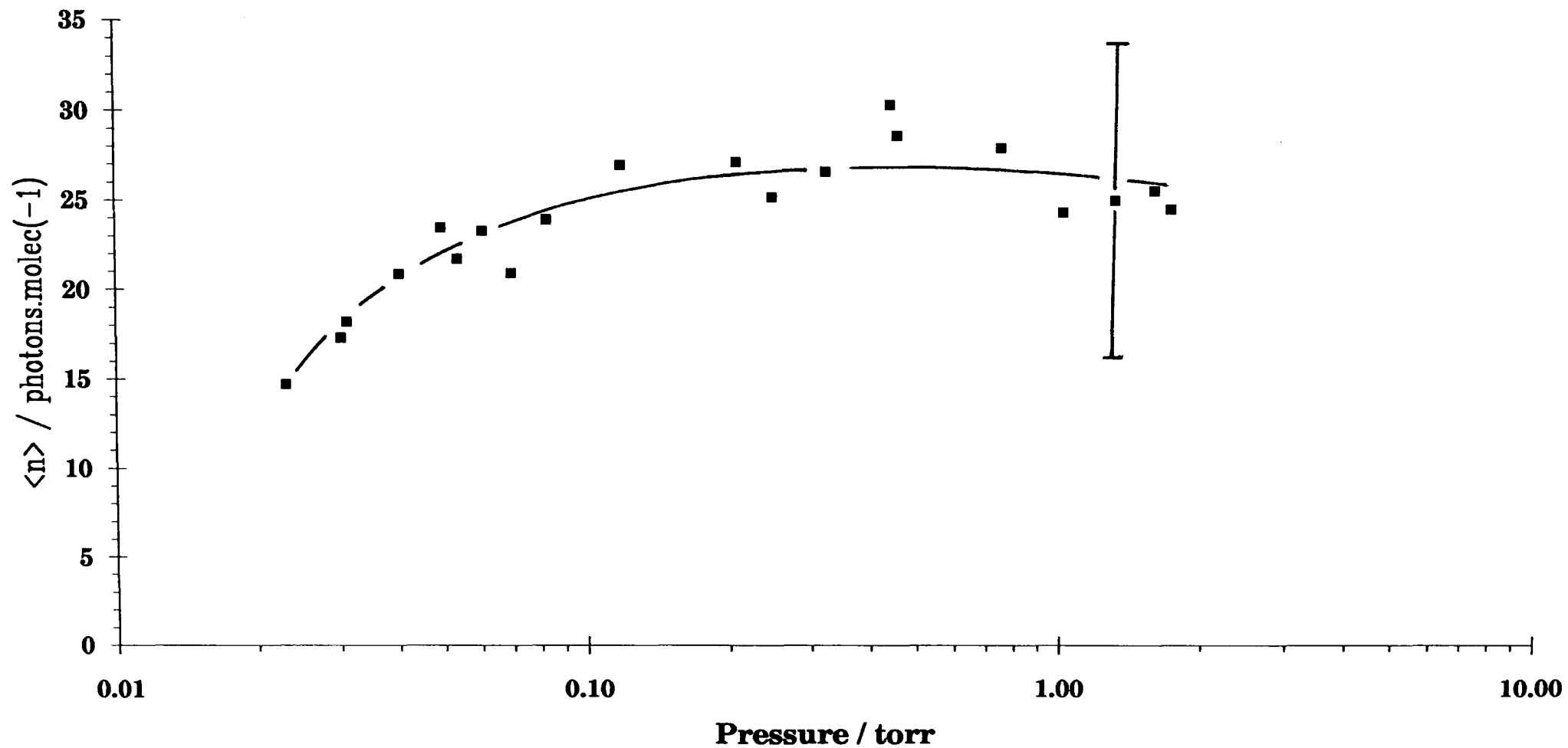


**Fig. 3.7-4 Hexan-2-ol: Variation of average number of absorbed photons per molecule with pressure at P20 (9  $\mu\text{m}$ ), and with a fluence of 9.0  $\text{J}\cdot\text{cm}^{-2}$**



fluence;  $\sigma_{\text{broadband}}$  is comparable to the high fluence values at 50 mtorr pressure.

- (v) Multiple-photon absorption is readily achievable even at low fluence, collision-free condition.

The drop in  $\sigma$  at low pressures is rapid, but small compared to the smaller molecules, falling by roughly 58% of the high pressure value over the range 0.1 torr to 25 mtorr. Apart from this small drop, it can be said that the absorption cross-section is independent of pressure and this may indicate an absence of rotational hole-burning, but only if the low pressure drop is an aberration of the experimental set-up; in Section 3.11 it is explained that the drop is caused by the set-up, specifically that vibrational energy relaxation is unlikely to be complete by the time the excited molecule reaches the microphone. It is very likely that for such a large polyatomic molecule as hexanol, the quasi-continuum starts at such a low vibrational level that rotational hole-burning does not develop.

A further experiment was proposed in order to help determine whether hexan-2-ol exhibits rotational hole-burning. Since for the smaller molecules it has been observed that increasing pressure (hence increasing collision frequency) causes an increase in  $\sigma$ , it was hoped that hole-burning effects would be highlighted by adding varying amounts of diluent to a constant pressure of hexanol. For this work with hexanol two different dilution ratios were used (1/10.14 and 1/4.07) and, together with a pure sample, their cross-sections were measured at three different fluences, each cell-fill containing the same amount of hexanol (0.2 torr). Both n-hexane and cyclohexane were found to absorb on  $P_{20}$  (9  $\mu\text{m}$ ), therefore  $\text{CO}_2$  was chosen as the diluent. Calibration correction factors were applied to the dilute data as determined in Ch. 2.

The results (Fig.3.7-5) show that as the amount of diluent increases, the dependence of absorption cross-section on fluence decreases. The dependence is such that for the cases of no or low dilution,  $\sigma$  decreases as the fluence increases; this dependence on fluence is consistent with the results of Fig.3.7-1.

In addition, Fig.3.7-5 shows a roughly 40% reduction in  $\sigma$  for both a four fold and ten fold dilution. This drop in  $\sigma$  as the collision frequency is increased is not easily explained, though it is not indicative of rotational hole-burning.

### 3.8 3,3-DIMETHYLOXETANE

The small signal, broadband absorption cross-section,  $\sigma_{\text{broadband}}$ , of 3,3-dimethyloxetane at the wavelength of  $R_{24}(10\mu\text{m})$  ( $978.47\text{cm}^{-1}$ ) is  $15.7 \times 10^{-20}\text{cm}^2/\text{molecule}$ , while at  $P_{24}(10\mu\text{m})$  ( $940.5\text{cm}^{-1}$ ) it is  $5.51 \times 10^{-20}\text{cm}^2/\text{molecule}$ . The optoacoustic cell was used to monitor the change in absorption cross-section with fluence at 51mtorr (Fig.3.8-1), and with pressure at a fluence of  $11.0 \pm 0.3\text{J}/\text{cm}^2$  (Fig.3.8-3(a) & (b)), for  $P_{24}(10\mu\text{m})$ . Similar measurements were made at  $R_{24}(10\mu\text{m})$ , for  $\sigma$  versus fluence at 50mtorr and 1.048torr, and for  $\sigma$  versus pressure at  $9.65 \pm 0.03\text{J}/\text{cm}^2$  (Figs.3.8-1 and 3.8-3 respectively). The variation with fluence of the average number of absorbed photons is given in Fig.3.8-2, while Fig.3.8-4 shows its variation with pressure.

The main observations from this set of data for the effect of irradiating wavelength are:

- (i) Above and below about 1torr, there is a contrast in the dependence of  $\sigma$  on pressure (Fig.3.8-3): For  $R_{24}$  this value is 1.15torr, above which,  $\sigma$  is virtually independent of pressure. For  $P_{24}$  the change occurs at

**Fig. 3.7-5 Hexan-2-ol: Variation of absorption cross-section with fluence and with CO2 overpressure on 0.2 torr of reactant**

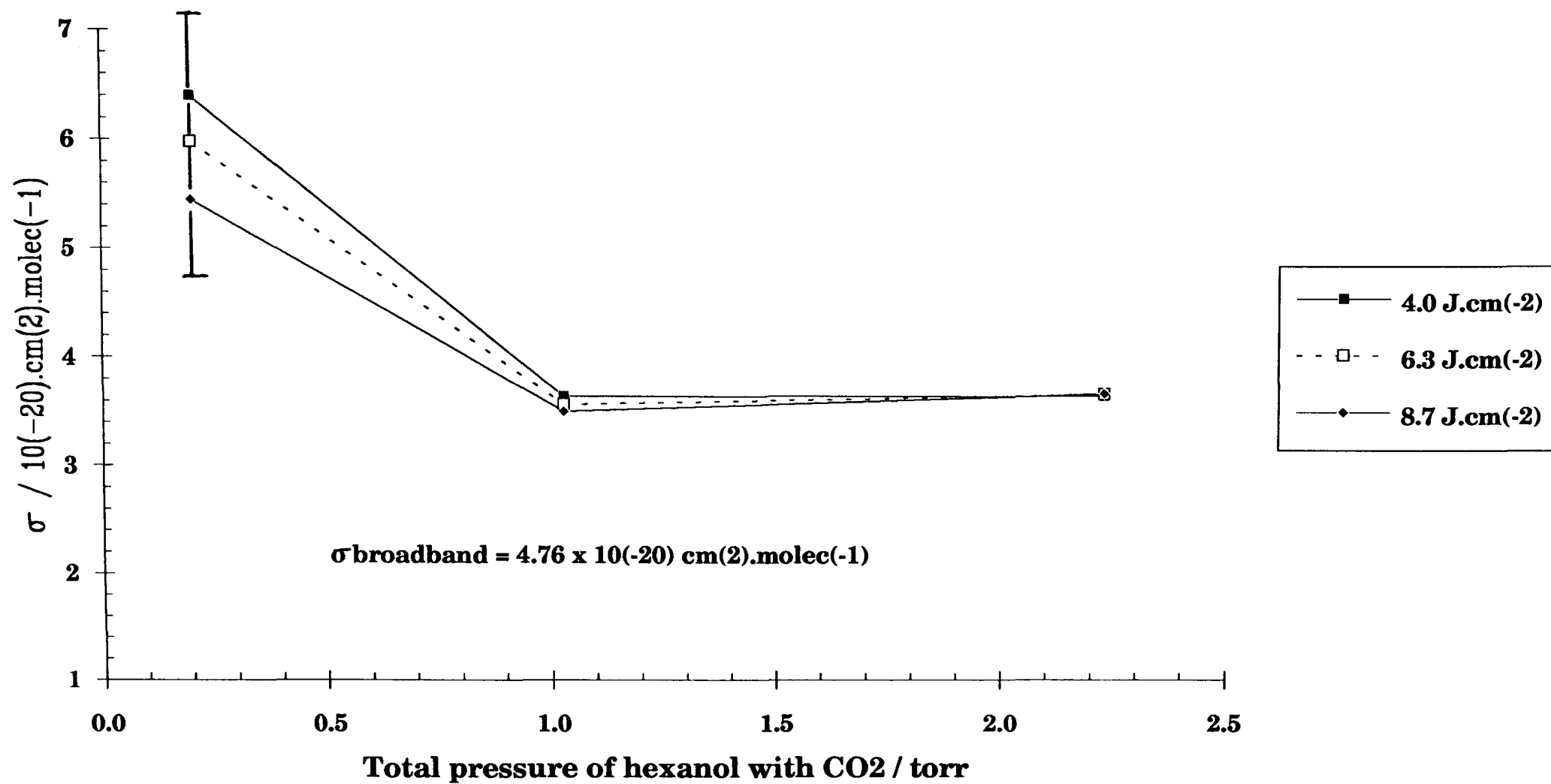
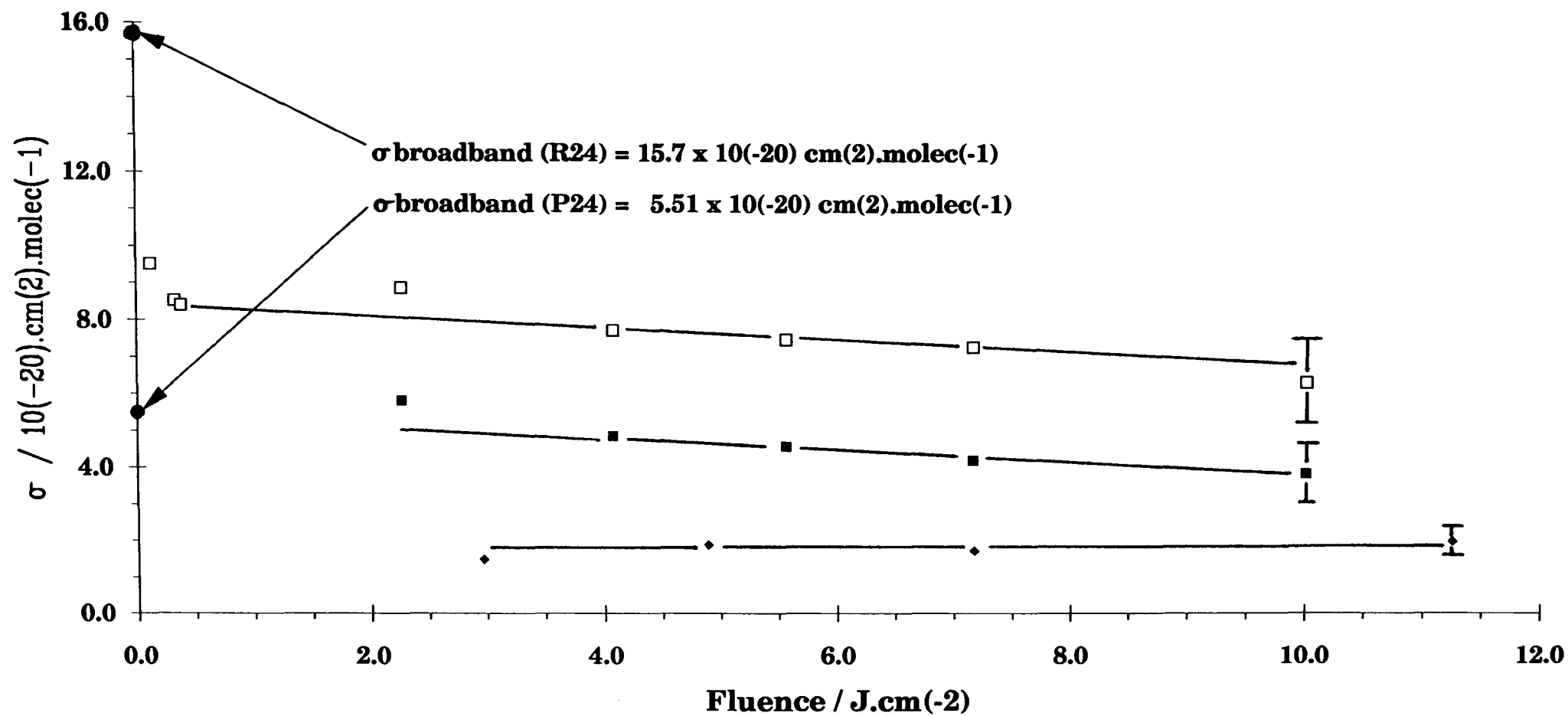


**Fig. 3.8-1 3,3-dimethyloxetane: Variation of absorption cross-section with fluence at different wavelengths and pressures.**



■ R24 (10  $\mu\text{m}$ ), 50 mtorr    □ R24 (10  $\mu\text{m}$ ), 1.048 torr    ♦ P24 (10  $\mu\text{m}$ ), 51 mtorr

**Fig. 3.8-2 3,3-dimethyloxetane: Variation with fluence of the average number of absorbed photons per molecule at different wavelengths and pressures**

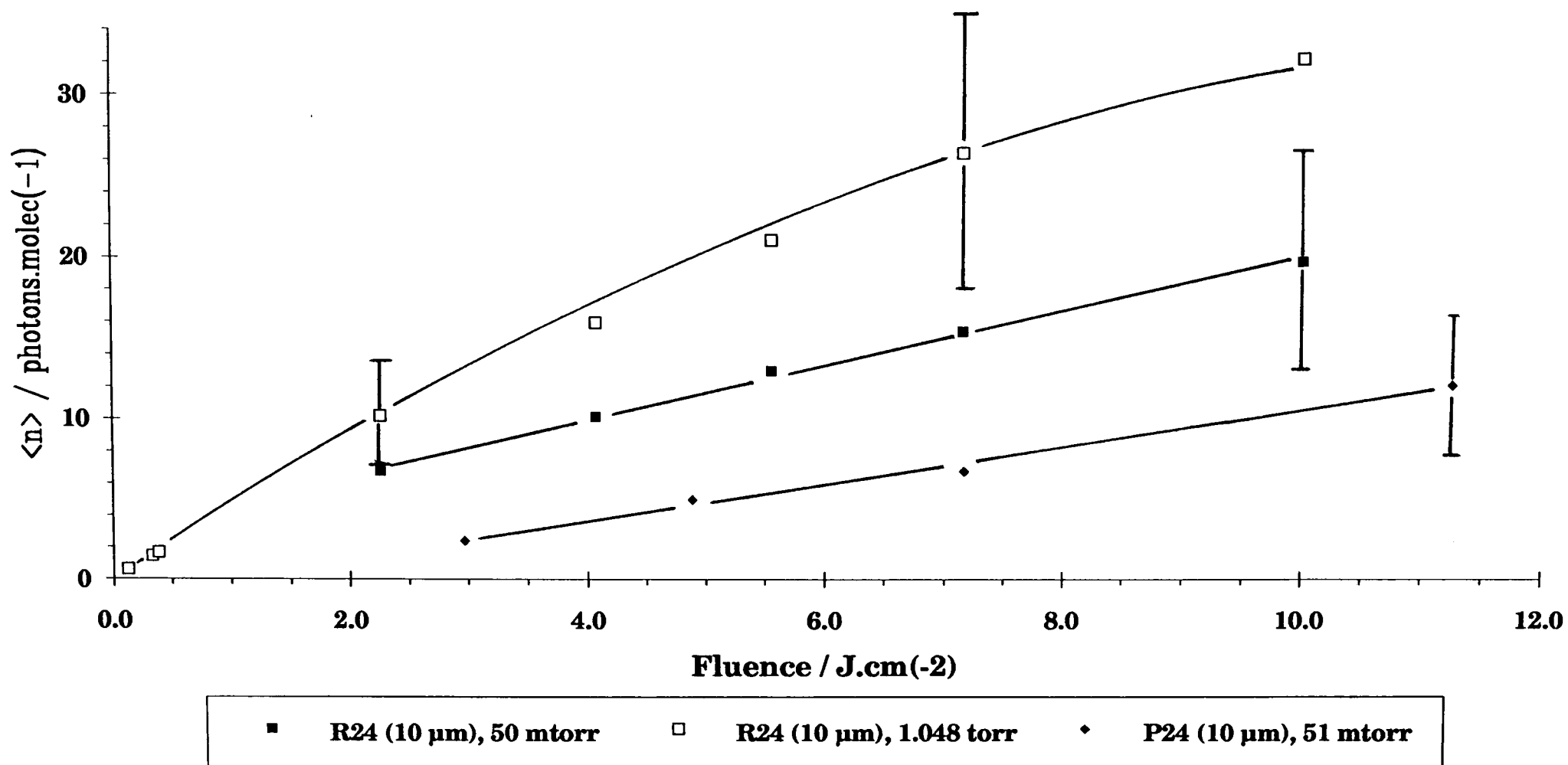


**Fig. 3.8-3(a) 3,3-dimethyloxetane: Variation with pressure of the absorption cross-section at a fluence of 11.0 (+/- 0.3) J.cm(-2) on P24 (10 μm), and 9.65 (+/- 0.03) J.cm(-2) on R24 (10 μm)**

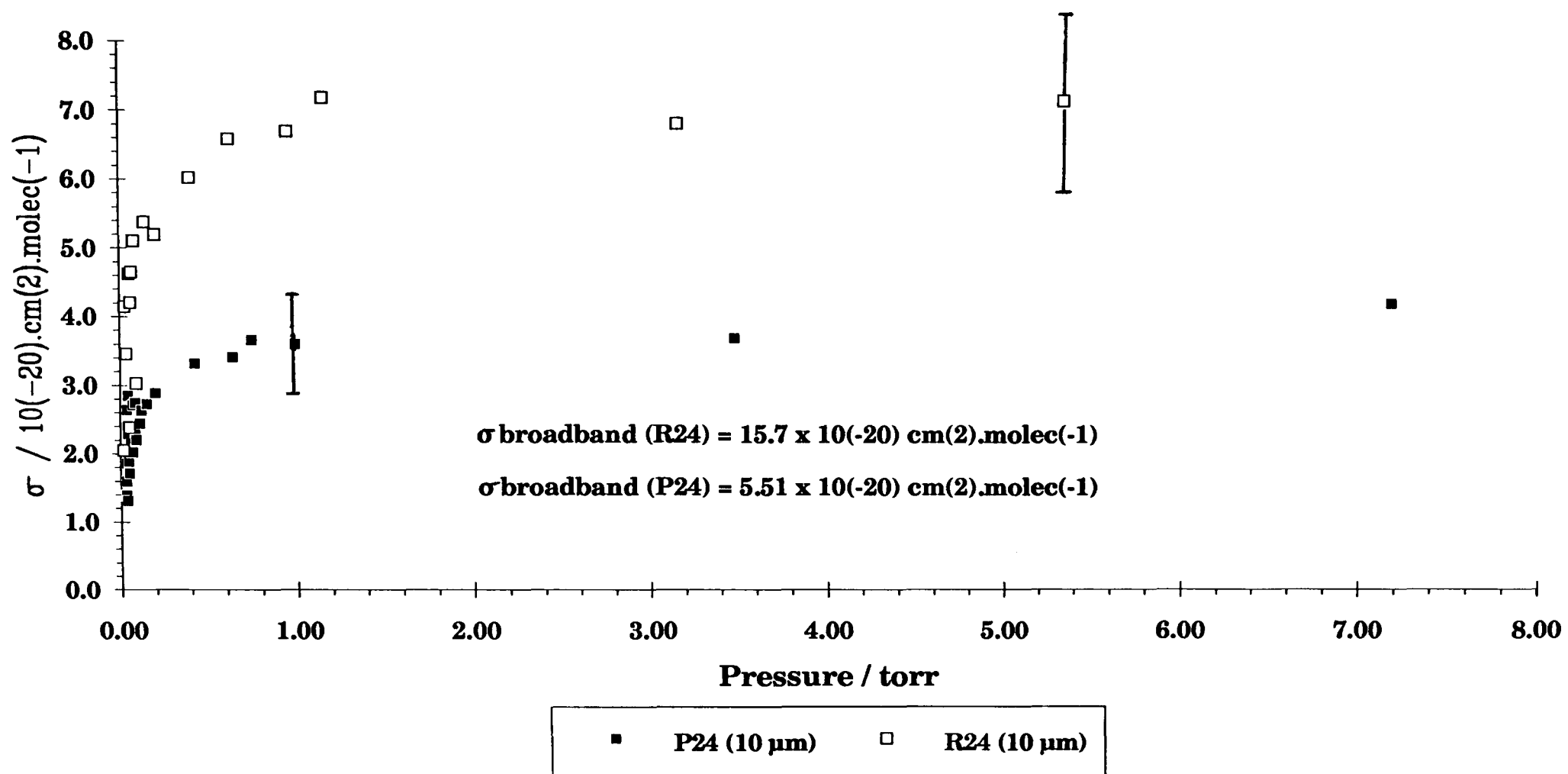


**Fig. 3.8-3(b) 3,3-dimethyloxetane: Variation with pressure of the absorption cross-section at a fluence of 11.0 (+/- 0.3) J.cm(-2) on P24 (10 μm) and 9.65 (+/- 0.03) J.cm(-2) on R24 (10 μm), for P<1 torr**

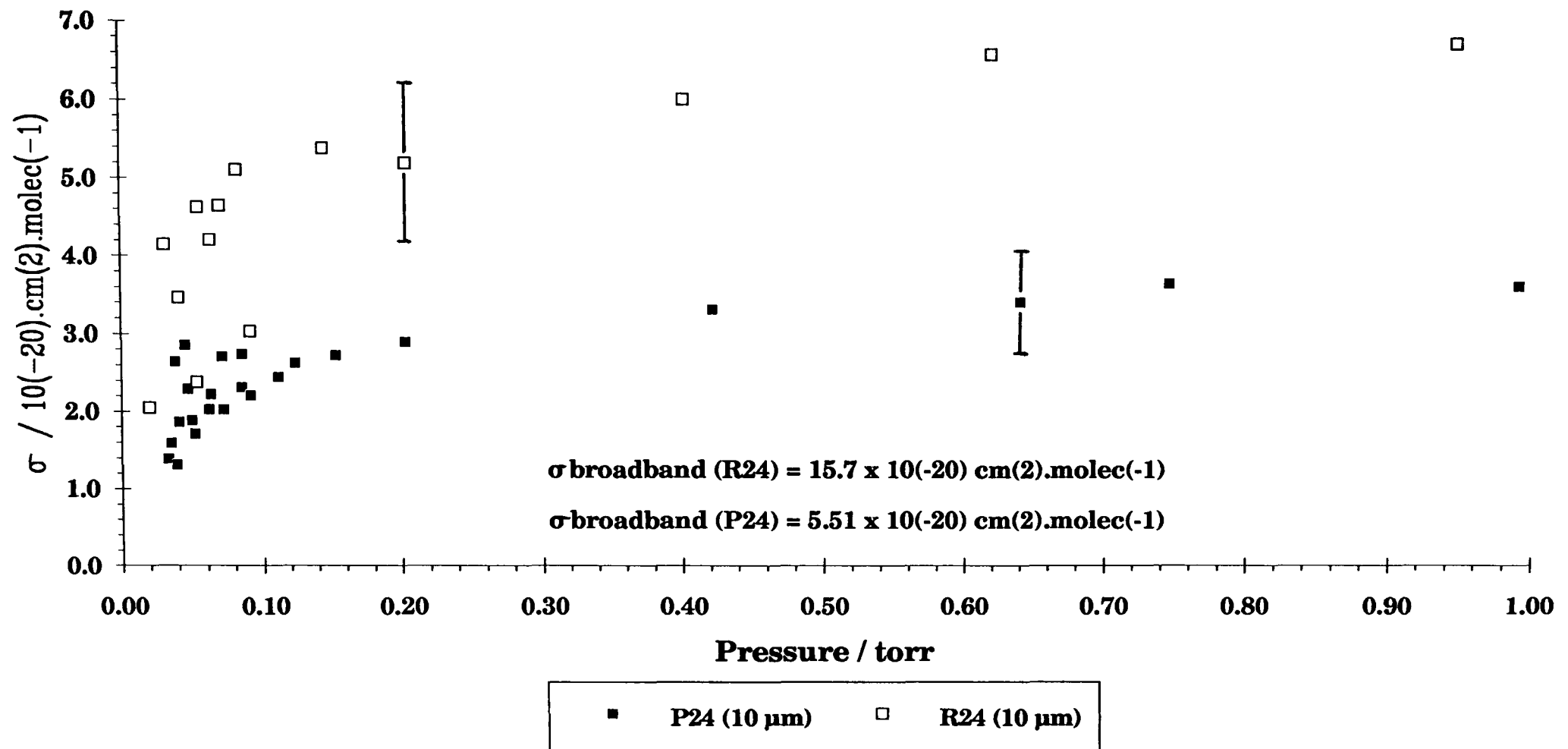
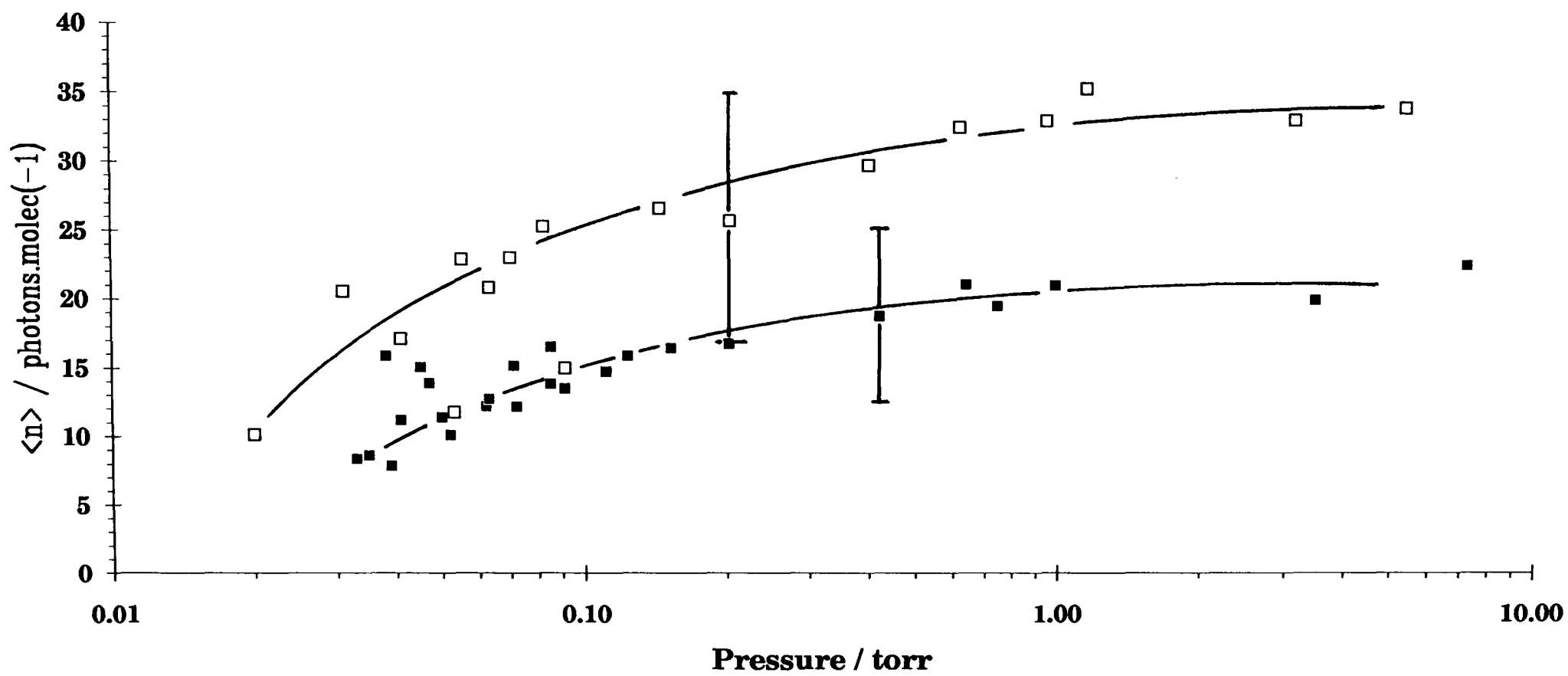


**Fig.3.8-4 3,3-dimethyloxetane: Variation with pressure of the average number of absorbed photons per molecule at high fluence and at two different wavelengths**



■ P24 (10 μm), 11.0 ± 0.3 J.cm <sup>-2</sup>	□ R24 (10 μm), 9.65 ± 0.03 J.cm <sup>-2</sup>
--	---

0.7 torr, above which there is only a small dependence on pressure (increasing very slightly with pressure).

- (ii) For  $R_{24}$ , there is a rapid fall off of  $\sigma$  with decreasing pressure below 0.15 torr, and a more gradual fall off between 1.15 torr and 0.15 torr (Fig. 3.8-3). Similarly for  $P_{24}$ , the rapid fall off occurs below 0.1 torr, whilst the more gradual fall off is between 0.7 torr and 0.1 torr (Fig. 3.8-3).
- (iii) The value of  $\sigma$  is less than the broadband cross-section for all pressures, and for both lines (Fig. 3.8-3).
- (iv) There is very little variation of  $\sigma$  with fluence above  $0.5 \text{ J/cm}^2$  for a pressure of 1.048 torr, and above  $2 \text{ J/cm}^2$  for a pressure of 51 mtorr using the  $R_{24}$  radiation; both sets of data show a slight decrease with fluence (Fig. 3.8-1). However, on  $P_{24}$ , the data collected at 51 mtorr shows no variation with fluence; the data is for fluences greater than  $3 \text{ J/cm}^2$ .
- (v) For all fluences and both irradiating wavelengths, the broadband cross-section is greater than the measured cross-sections for pressures of 50 mtorr and 1.048 torr (Fig. 3.8-1).
- (vi) Multiple-photon absorption is readily achievable. At 50 mtorr pressure,  $\langle n \rangle$  is greater for  $R_{24}(10 \mu\text{m})$  radiation than for  $P_{24}(10 \mu\text{m})$  (Fig. 3.8-2).

Some of the above experiments were repeated at a much later date, when the effect of pulse type on absorption cross-section was studied in detail.  $R_{24}(10 \mu\text{m})$  was the chosen wavelength, and the optoacoustic signal was monitored as the pulse type was switched in turn between one of a longitudinal multimode, M, to one of a longitudinal singlemode, S, (eg. S,M,M,S,S,M,M, etc). For each new pair of pulses, either the fluence was altered, or the reactant pressure was changed, depending on which trend was under observation at that particular time. Singlemode/multimode operation is

described in Section 2.1. A  $\text{CO}_2:\text{N}_2:\text{He}$  (10:20:70) premix pressure of 7.5 torr was used in the low pressure gain section of the laser during singlemode operation, and the tube was evacuated for multimode operation.

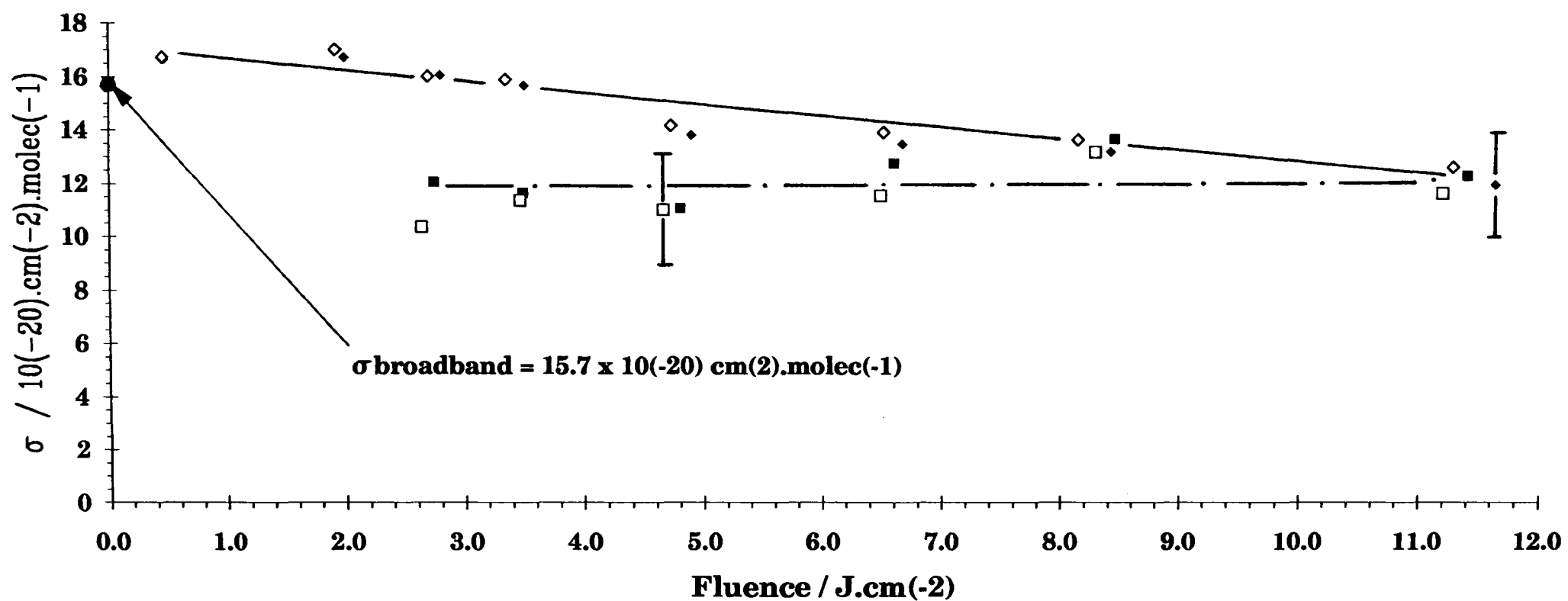
A comparison of the effect of pulse type on the variation of absorption cross-section with fluence is given in Fig.3.8-5. Results are taken at the nominal pressures of 50 mtorr and 1 torr. The associated variation of the average number of absorbed photons with fluence is given in Fig.3.8-6.

The singlemode/multimode comparison for  $\sigma$  versus pressure, at an average incident fluence of  $10.0 \pm 0.4 \text{ J/cm}^2$ , is made in Fig.3.8-7. An exploded view of the data within the range 0 to 1 torr is presented in Fig.3.8-7(b). The variation with pressure of the average number of absorbed photons per molecule is given in Fig.3.8-8. It is immediately apparent, that the cross-sectional values in Fig.3.8-7 are not consistent with those taken earlier and illustrated in Fig.3.8-3: For this new set of data, the cross-section at higher pressures are comparable to the broadband absorption cross-section. Since good procedural reproducibility has been proven in the work on butan-2-ol and pentan-2-ol, this discrepancy is not explicable. Whilst there is now some uncertainty about the absolute values of  $\sigma$  (for 3,3-dimethyloxetane at  $R_{24}(10\mu\text{m})$ ), there is no need to doubt the value of the difference in  $\sigma$  between the two types of pulses. Furthermore, the main conclusions on the trend of the absorption cross-section are still valid.

The main observations concerning the effect of pulse type are:

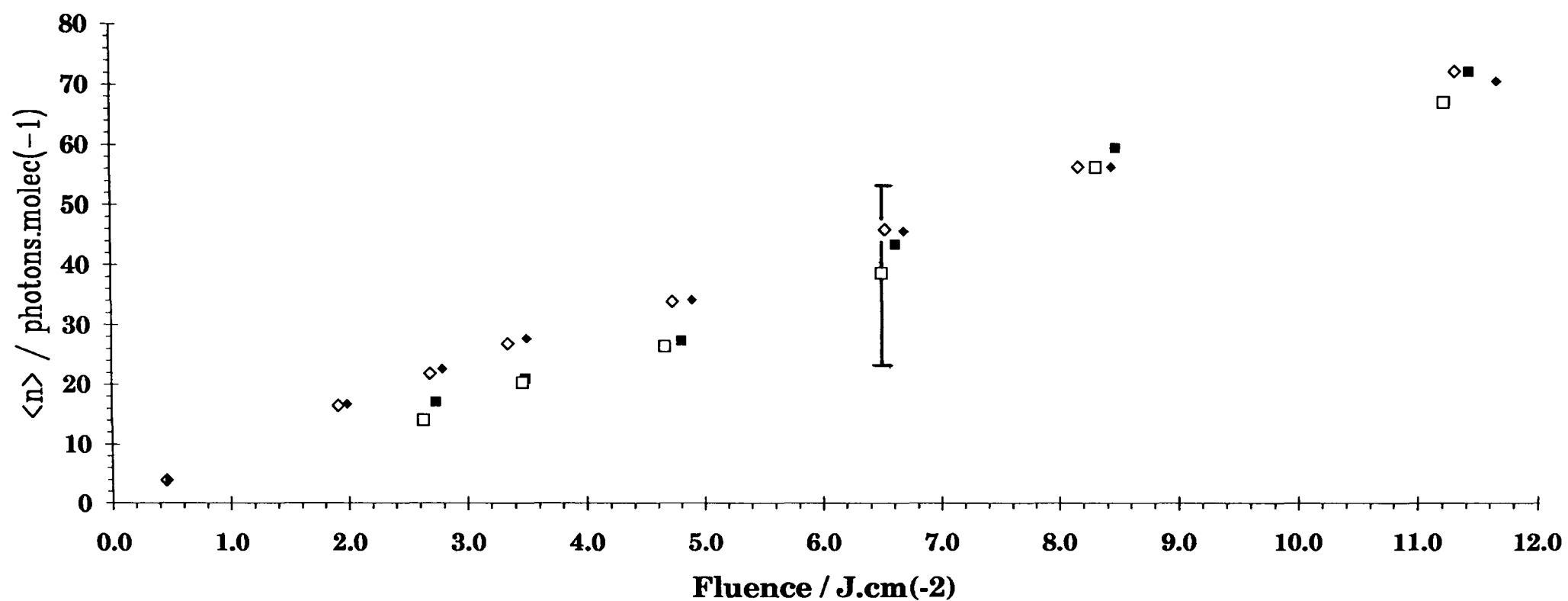
- (i) As both pressure and fluence are varied, the values of  $\sigma$  are comparable (ie. within a ratio of  $\sigma_{\text{multimode}}:\sigma_{\text{singlemode}}$  of 1:0.83 and 1:1.07) (Fig.3.8-5).

**Fig. 3.8-5 3,3-dimethyloxetane: Comparison of the effect of multimode and singlemode pulses on the variation with fluence of absorption cross-section at two different reactant pressures using R24 (10  $\mu\text{m}$ ) radiation**



52 mtorr, multimode
 
 52 mtorr, singlemode
 
 0.997 torr, multimode
 
 0.997 torr, singlemode

**Fig. 3.8-6 3,3-dimethyloxetane: Variation with fluence of the average number of absorbed photons per molecule at R24 (10  $\mu\text{m}$ ). Comparison of the effect of multimode and singlemode pulses at two different reactant pressures**



■	52 mtorr, multimode	□	52 mtorr, singlemode	◆	0.997 torr, multimode	◇	0.997 torr, singlemode
---	---------------------	---	----------------------	---	-----------------------	---	------------------------

**Fig. 3.8-7(a) 3,3-dimethyloxetane: Variation with pressure of the absorption cross-section at a fluence of 10.0 (+/- 0.4) J.cm(-2) on R24 (10 μm). Comparison of the effect of multimode and singlemode pulses**

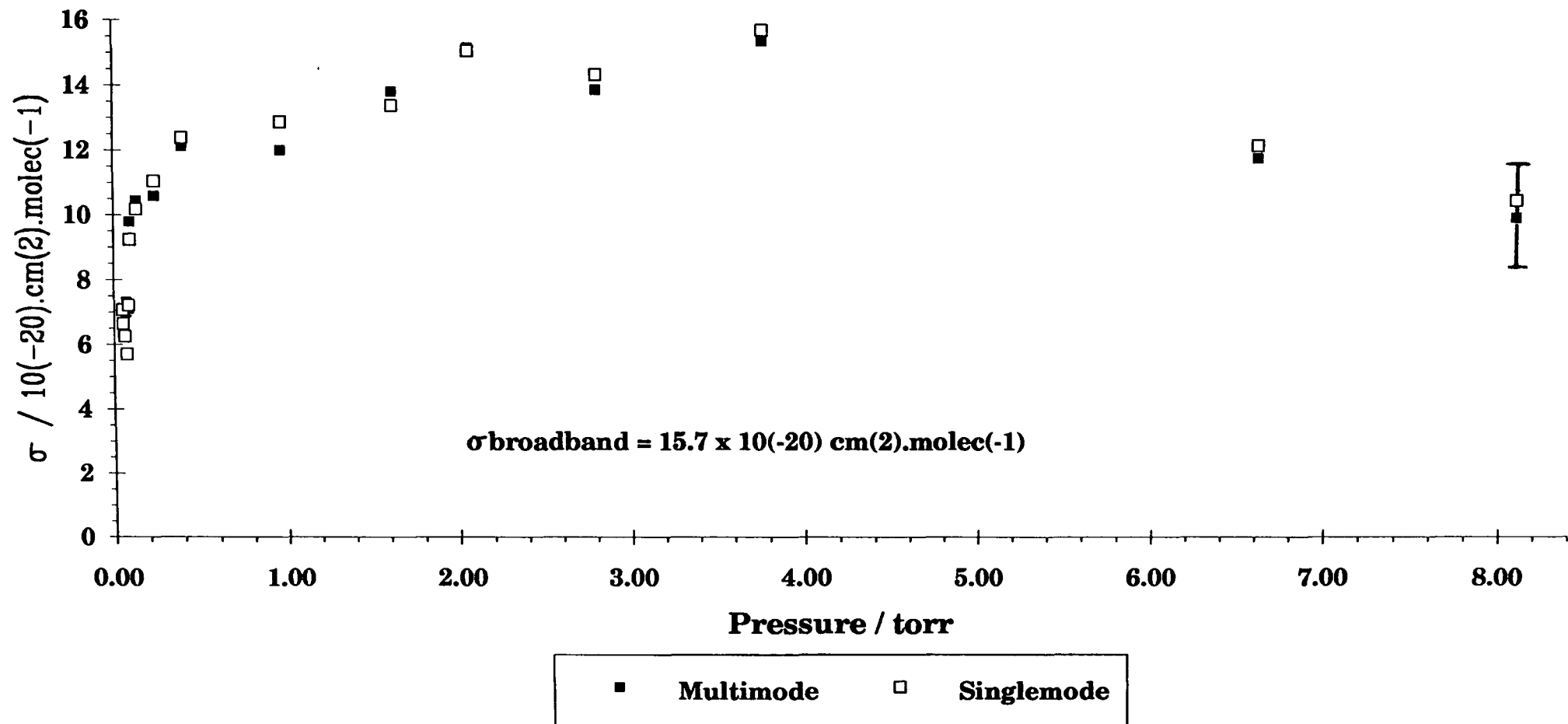
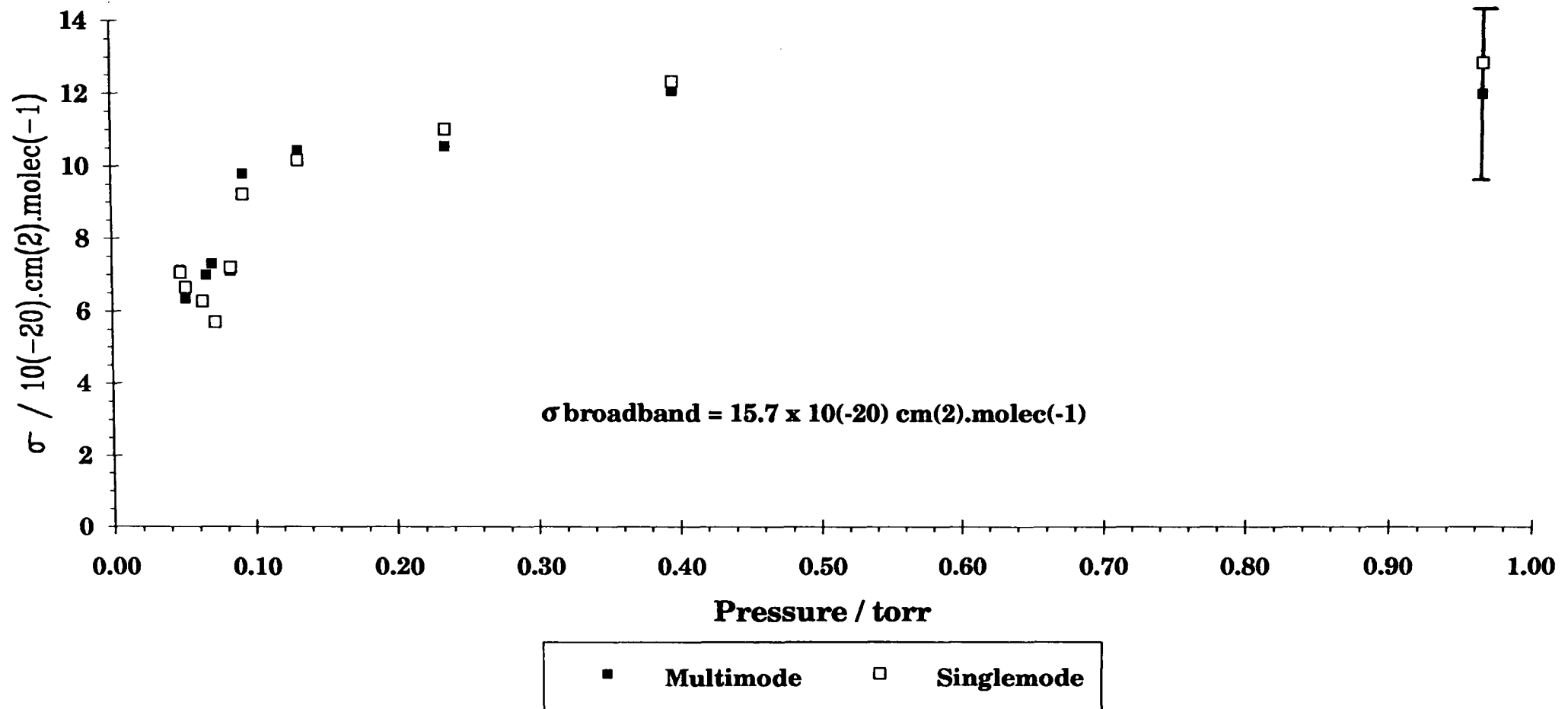


**Fig. 3.8-7(b) 3,3-dimethyloxetane: Variation with pressure of the absorption cross-section at a fluence of 10.0 (+/- 0.4) J.cm(-2) on R24 (10 μm). Comparison of the effect of multimode and singlemode pulses for P<1 torr**



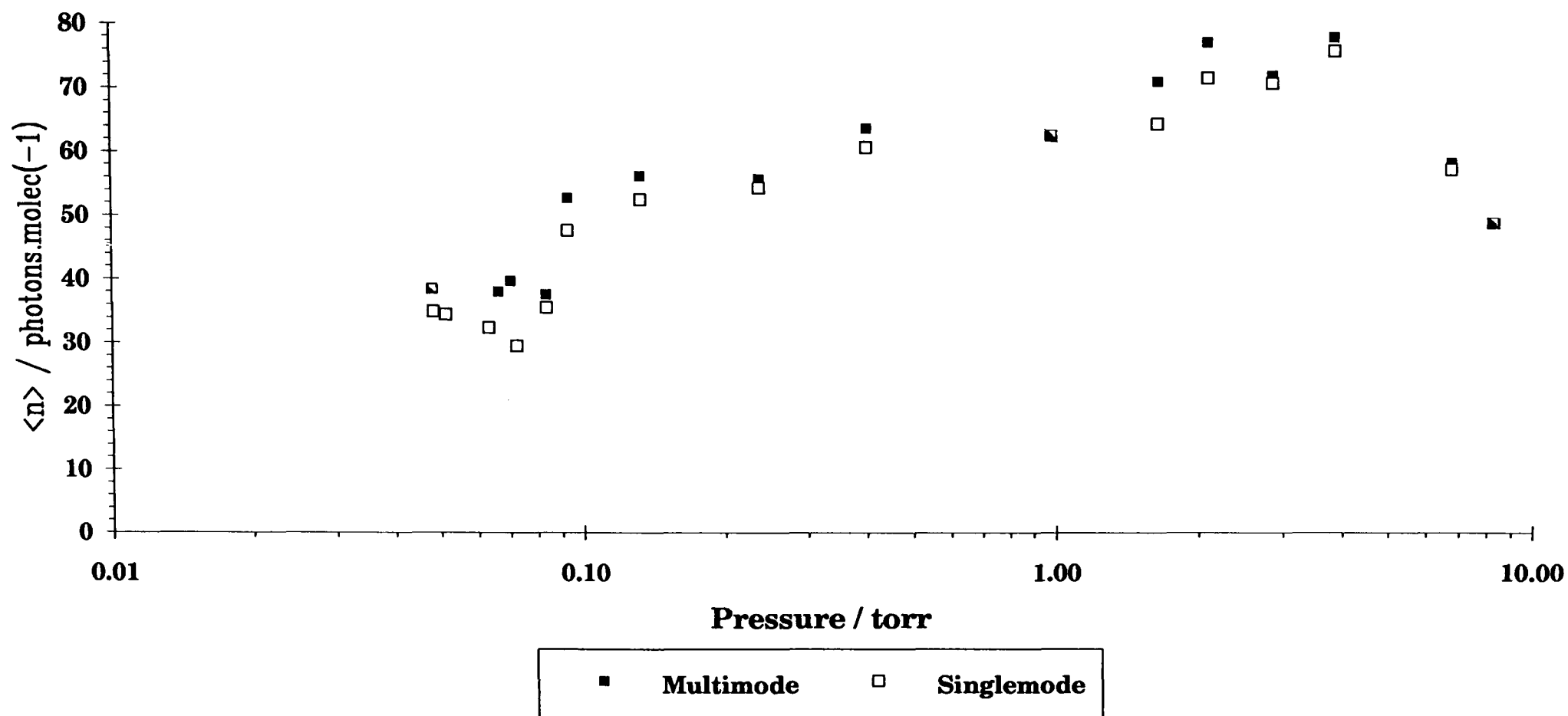
- (ii) At any fluence at low pressure (52 mtorr), the value of  $\sigma$  for the singlemode pulse is slightly less than that for the multimode pulse (Fig. 3.8-5): The difference reaches a minimum at about  $4 \text{ J/cm}^2$ .
- (iii) For a middle pressure (0.997 torr) the value of  $\sigma$  for the singlemode pulse is slightly **larger** than that for the multimode pulse: As the fluence increases the difference increases (Fig. 3.8-5).
- (iv) In general, as the pressure varies above 0.2 torr (for high fluence) the value of  $\sigma$  for the singlemode pulse is larger than that for the multimode pulse (Fig. 3.8-7). Below 0.2 torr the opposite is true. The change occurs close to the change in the gradient of  $\sigma$  versus pressure.
- (v) For fluences less than  $7 \text{ J/cm}^2$  the roughly linear trend of  $\langle n \rangle$  with fluence depends on pressure but not pulse-type (Fig. 3.8-6). The variation of  $\langle n \rangle$  with pressure does not reach a stable plateau, but at all times, the multimode values are larger than the singlemode (Fig. 3.8-8).

One might conclude from point (ii) above, that for fluences upto  $4 \text{ J/cm}^2$  and for low pressure, there is some increase of  $\sigma$  and  $\langle n \rangle$  with power. The  $R_{24}(10\mu\text{m})$  laser absorption cross-section is more than three times that for  $P_{24}(10\mu\text{m})$  no matter which series is considered, and since the equivalent factor is only three for the broadband cross-sections, this is possible evidence that red-shifting occurred. Fig. 3.8-9 shows the broadband absorption spectra and the relative positions of the two irradiating wavelengths.

### 3.9 DECONVOLUTION

So far, all of the data presented has been in its raw, or undeconvoluted form. The concept of deconvolution was explained in Section 2.1.4. When  $\log_{10}\langle n \rangle$  vs  $\log_{10}$  fluence is plotted, it is noted that in all cases the data

**Fig. 3.8-8 3,3-dimethyloxetane: Variation with pressure of the average number of absorbed photons per molecule at a fluence of 10.0 (+/- 0.4) J.cm(-2) on R24 (10 μm). Comparison of the effect of multimode and singlemode pulses**



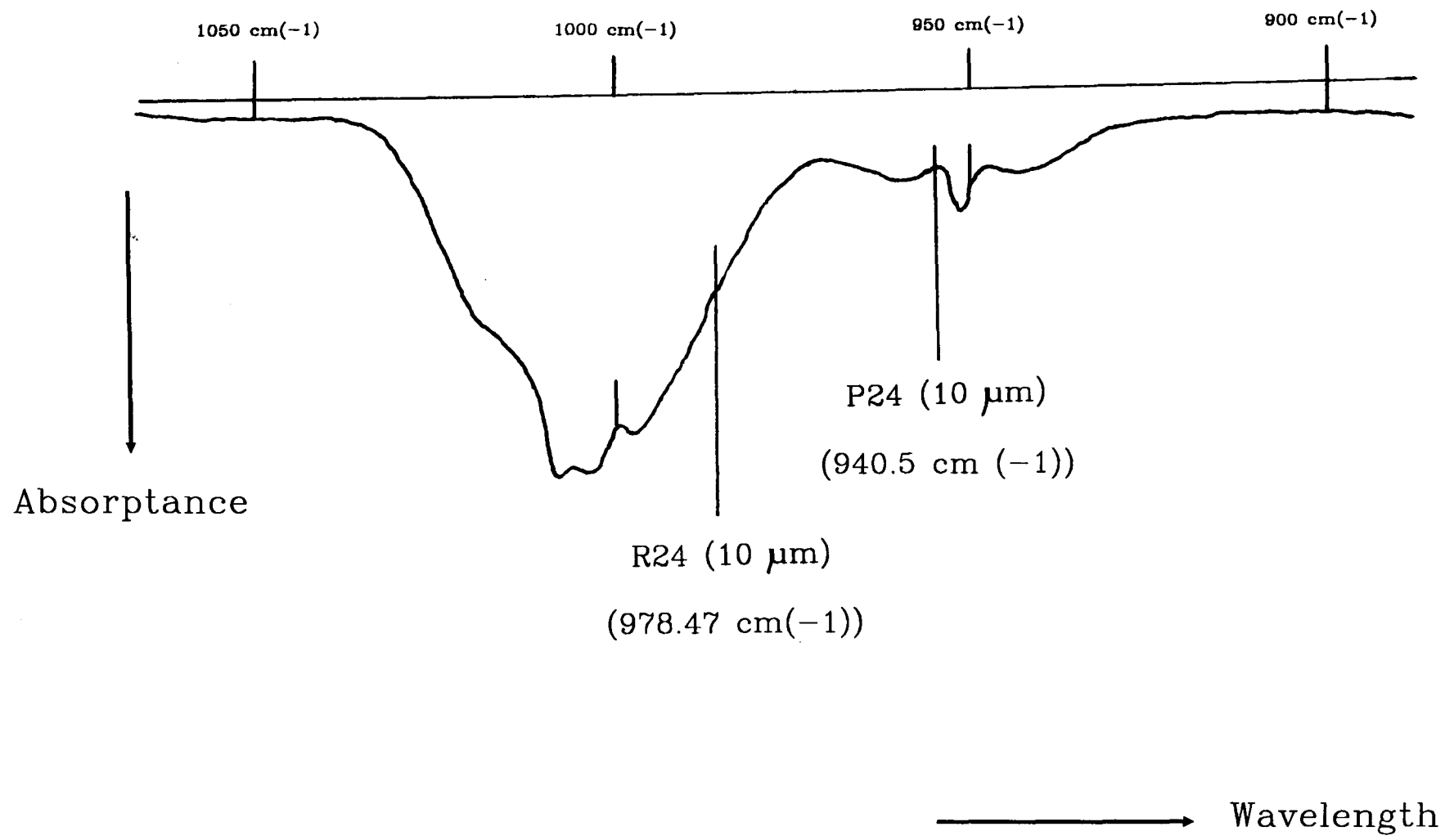


Fig. 3.8-9 3,3-dimethyloxetane: Broadband absorption spectrum, showing the relative positions of the laser transitions used for experimentation

will fit to a straight line; the graph for methanol has been included as an example (Fig.3.9-1). As a consequence, for each raw set of data, each data point will be corrected by the same amount *viz.* by the gradient of the line. Note that  $d(\log_{10}\langle n \rangle)/d(\log_{10} \text{ fluence})$  and  $d(\ln\langle n \rangle)/d(\ln \text{ fluence})$  are equivalent because  $2.303 \cdot \log_{10}(x) = \ln(x)$ . None of the previously illustrated graphs will therefore change in general appearance if represented in deconvoluted form. Table 3.9-1 contains the deconvolution factors obtained by a least squares fit to a line through each  $\log_{10}\langle n \rangle$  vs  $\log_{10}$  fluence plot. It is noted that many of the factors are close to unity. Applying factors less than one to the raw form will reduce all  $\sigma$  and  $\langle n \rangle$  values and gradients, and will contract the value axis range. In other words, presentation of the data in raw form can serve to magnify any fluence dependency.

### 3.10 DISCUSSION

In this section, the findings of the variation of absorption with fluence; the variation of absorption with pressure; and the effects of pulse type and irradiating wavelength on absorption, are discussed.

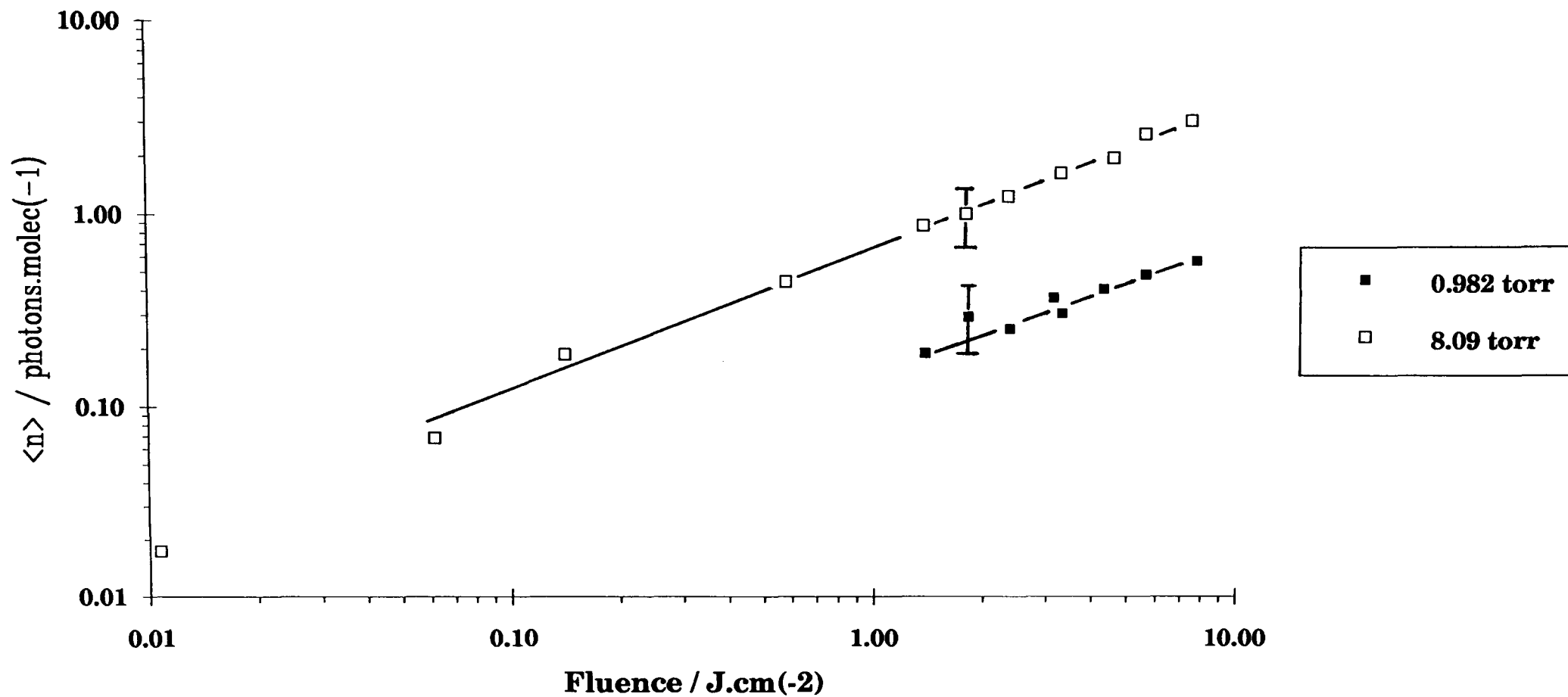
Detailed work on methanol, ethanol, butan-2-ol, pentan-3-ol, and 3,3-dimethyloxetane has confirmed one general observation made by Shaw (6): The small signal, broadband absorption cross-section is much greater than the cross-section obtained under high fluence (narrow laser linewidth), low pressure conditions. However, for the larger alkanols this is not true, because for hexan-2-ol and pentan-2-ol the values are comparable. As can be seen from Table 3.10-1, the difference is somewhat dependent on molecular size; generally reducing as the molecular size increases. The difference in behaviour shown by the two pentanols indicates that there is also a dependence on hydroxyl site. The large value for 3,3-dimethyloxetane (16 atoms) compared to butan-2-ol (15 atoms) may be due to the ring nature of

the molecule, or due to the definition of molecular size; it has been said that the size of the molecule should be determined by the number of atoms other than carbon or halogens (18), in which case the sizes would be 6 atoms and 5 atoms respectively (see Table 3.10-2), and 3,3-dimethyloxetane should then be compared to pentanol. The percentages still do not equate, which further indicates that the ring may reduce the 'effective' size of the molecule.

The change observed in the functional form of  $\sigma$  with fluence as one progresses through the homologous series is similar to that of  $\sigma$  with pressure, *viz.* with increasing molecular size, the dependence of  $\sigma$  on fluence and pressure appears to decrease and  $\sigma$  itself takes on a value closer to the broadband value (Table 3.10-1). Furthermore, as the fluence approaches zero, the absorption cross-section appears to tend towards the small-signal, broadband value, which for the smaller molecules involves an increase in  $\sigma$  with decreasing fluence. Jang *et al.* (11) found no fluence dependence with  $\text{CH}_3\text{CF}_3$  and  $\text{C}_2\text{H}_5\text{F}$ , but found a similar behaviour to that just mentioned with 2-bromopropane, 2-chloropropane, 2-chlorobutane and 1,1,1-trifluoro-2-bromoethane.

This functional form of  $\sigma$  against fluence is to be expected: At high fluence, it is likely that the quasi-continuum is accessed, and since the laser linewidth is small relative to the 'merged' absorption linewidths of the transitions within the quasi-continuum, the bulk absorption cross-section is small. Once the quasi-continuum has been reached, the fluence is not expected to alter the ratio of laser linewidth to the effective absorption bandwidth, and hence the absorption cross-section is expected to remain constant. At low laser fluence, however, the molecule is not excited beyond the discrete levels, and the narrow laser linewidth will see an absorption linewidth considerably reduced from that of the quasi-continuum: thus the

**Fig. 3.9-1 Example of the variation with fluence of the average number of absorbed photons per molecule when plotted as log  $\langle n \rangle$  against log F: the data are that of methanol irradiated with R32 (10  $\mu\text{m}$ ) radiation (ref. Fig. 3.1-2)**



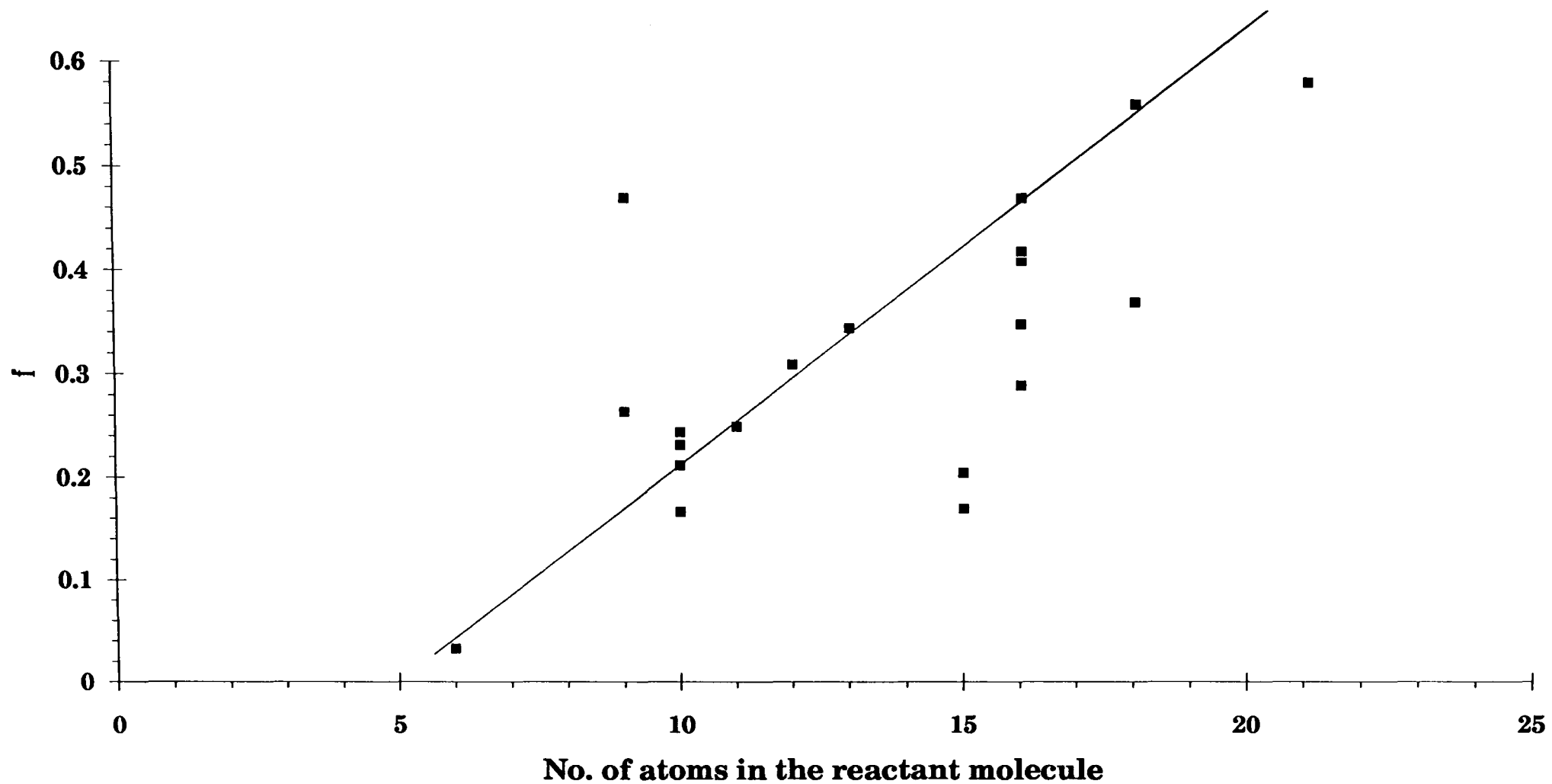
<b>Reactant</b>	<b>Figure Reference</b>	<b>Data Identification</b>	<b>Deconvolution Factor</b>
<b>Methanol</b>	3.1-2	0.982 torr	0.6
		8.09 torr	0.8
<b>Ethanol</b>	3.2-2	1st set	0.7
		2nd set	1.1
		3rd set	1.0
		4th set	1.0
		5th set	1.2
<b>Propanol</b>	3.3-2	(50 mtorr	1.1
		(1 torr	0.9
<b>Butan-2-ol</b>	3.4-2	53 mtorr	1.1
		<55 mtorr>	1.0
		~1 torr	1.0
<b>Pentan-2-ol</b>	3.5-2	50 mtorr	0.9
<b>Pentan-3-ol</b>	3.6-2	51.5 mtorr	0.6
		0.995 torr	0.8
<b>Hexan-2-ol</b>	3.7-2	50 mtorr	0.8
		1.00 torr	0.9
<b>3,3-dimethyloxetane</b>	3.8-2	R24 (10 $\mu$ m), 50 mtorr	0.7
		R24 (10 $\mu$ m), 1.048 torr	0.9
		P24 (10 $\mu$ m), 51 mtorr	1.2
	3.8-6	52 mtorr, multimode	1.1
		52 mtorr, singlemode	1.1
		1 torr, multimode	0.9
1 torr, singlemode	0.9		

**Table 3.9-1 Deconvolution Factors**

Reactant	$\frac{\sigma_{highF,lowp} - \sigma_{broadband}}{\sigma_{broadband}}$ (%)
Methanol	96
Ethanol	78
Propan-2-ol	68
Butan-2-ol	50
Pentan-2-ol	8
Pentan-3-ol	47
Hexan-2-ol	0
3,3-dimethyloxetane	78 R24 (Fig. 3.8-1)
	73 P24 (Fig. 3.8-1)
	24 (Fig. 3.8-5)

**Table 3.10-1** Comparison of the difference of  $\sigma_{broadband}$  to  $\sigma_{high\ fluence, low\ pressure}$

**Fig. 3.10-1 Variation of the fraction of absorbing molecules,  $f$ , with size of molecule:  $f$  is determined using the lowest pressure for which there is a data point. Fluences and pulse type are mixed**



effective laser cross-section is seen to increase. The lack of dependence on fluence for the larger molecules (such as hexan-2-ol) is not surprising, since the density of states is greater and the quasi-continuum lies at much lower excitation levels; hence, the first fluence dependent stage of the absorption ladder becomes less significant.

It is, however, recognised though, that different variations of  $\sigma$  with fluence might have been observed if different excitation lines had been used. It has been shown (11) that excitation near the edge of an excitation band will produce no dependence of  $\sigma$  on fluence. This is because the flattening of the absorption bands as the fluence increases is most pronounced towards band centre. Lack of time prevented investigation of the variation of absorption cross-section with wavelength, so the presence of red-shifting could not be proved for each molecule (the results for ethanol suggest that there may be some effect). There is, however, experimental evidence (11) to suggest that red-shifting occurs for molecules exhibiting a variation of  $\sigma$  with pressure which can be interpreted as the existence of hole-burning. These types of molecules have been described as "small". For  $C_2H_5F$  and  $CH_3CF_3$  the red-shift was in the order of  $10\text{ cm}^{-1}$ , and was approximately the same for all fluences.

Finally with respect to effects of fluence; as observed, the average number of absorbed photons per molecule is expected to rise with fluence. Further, because of the energy gap between rotational levels, absorption bottlenecks may appear in the  $\langle n \rangle$  versus fluence graph as points of inflection, or regions of zero gradient (105); there may be evidence of this for methanol at  $4.5\text{ J/cm}^2$  (Fig. 3.1-2), propan-2-ol at  $\sim 4.5\text{ J/cm}^2$  (Fig. 3.3-2), butan-2-ol at  $\sim 5\text{ J/cm}^2$  (Fig. 3.4-2), hexan-2-ol at  $\sim 5.5\text{ J/cm}^2$  (Fig. 3.7-2), and 3,3-dimethyloxetane at  $\sim 5.5\text{ J/cm}^2$  (Fig. 3.8-6). While it is recognised that the

experimental proof is weak, and requires further investigation, the observations are pointed out because of similar anomalous observations, previously made, of the yield against pressure data of oxetane(6) and cyclobutanone(28) and of the  $\langle n \rangle$  versus fluence data of  $\text{OsO}_4$  (105).

Another general observation is the absorption cross-section pressure dependence, and in particular the presence of a fall-off at low pressures: Methanol, ethanol, propan-2-ol, and possibly pentan-2-ol show an increase of effective absorption cross-section with pressure, for pressures above 0.1torr (the remainder of the molecules are largely independent of pressure above 0.1torr). Except for methanol, the absorption cross-sections eventually reach a plateau. The absorption cross-section gradient is most simply explained in terms of rotational hole-burning and hole-filling, with the effect being greatest in molecules with the lowest density of rotational states. To reiterate the description of rotational hole-burning given in Section 1.1, at high pressures, collisions reestablish rotational equilibrium, so allowing further excitation (and hence absorption) during the remainder of the pulse. At low pressures (and collision-free conditions), the first part of the pulse selectively excites a rotational level to saturation, so that the remainder of the pulse passes through unabsorbed because it is unable to excite any further.

In addition to any gradient caused by hole-burning, the observed independence of cross-section with pressure is to be expected for the pressures used in this work. Broadening of the absorption lines by collisions is not a dominant effect for such pressures (Appendix A5). Rather, the absorption lines are effectively determined by the amount of Doppler broadening which is pressure independent (Appendix A5). Consequently, the absorption cross-section

(related to the ratio of the irradiating laser linewidth to that of the absorption linewidth) also remains constant with pressure.

Shaw had established that at the lowest pressures (0-0.1torr), there exists a constant absorption cross-section consistent with the pressure independence of the Beer-Lambert Law (Eq.3.0-1). Because of the scattered nature of data at the lowest pressures in this research, it was not possible to verify this behaviour. There were, however, some instances of continued pressure dependency at the lowest pressures. It was initially proposed that this might only be as a consequence of a limitation in microphone responsivity rather than of any micro-physical action, but it was shown in Sections 1.3 and 2.3 that any change in responsivity is negligible; a discussion follows of the probable reason for these results.

The following is a discussion which proposes that incomplete relaxation of the molecules arriving at the microphone is the reason why no low pressure plateau was observed for the absorption data of this work. Table A5-1 shows that collision intervals for 0.1torr will be 670→1190ns depending on the molecule and mixture. A typical value of 800ns will be used for further calculation. The probability of collision during the laser pulse (~50ns FWHM and ~600ns base width) is consequently low, both at 0.1torr and at vanishingly low pressure: Table A5-1 shows that the pressure for which the collision interval is as long as the pulse base width, varies from 0.20torr for methanol, to 0.12torr for the larger molecules of this work; for these pressures only one collision may occur during the base width of the pulse. More significantly, much of the absorption will occur during the gain-switched spike (~50ns FWHM) which is considerably shorter than the base width, and thus the probability of collision during this time will also be

much reduced. Relaxation times for vibration-translation energy transfer at 1atm are:

CH <sub>4</sub>	~ 1μs
CH <sub>3</sub> Br	70 ns
C <sub>2</sub> H <sub>6</sub>	20 ns
C <sub>4</sub> H <sub>10</sub>	<1.5 ns
CH <sub>3</sub> OCH <sub>3</sub>	4 ns

Thus for the alkanols, the relaxation times, t, are probably in the range 1-20ns at 1atm, and at 0.1torr, they are probably in the range 7600ns to twenty times this value i.e. ~8μs to 150μs. Now a typical value (2-methyloxetane) for the diffusion coefficient, D, at 1torr is 60cm<sup>2</sup>/s, so this will be 600cm<sup>2</sup>/s at 0.1torr. Therefore, the distance travelled, x, in the relaxation time by the diffusing molecule is:

$$x = \sqrt{2Dt} = \sqrt{2 \times 600 \times 8 \times 10^{-6}} \quad \text{to} \quad \sqrt{2 \times 600 \times 150 \times 10^{-6}}$$

$$= 0.1\text{cm} \rightarrow 0.4\text{cm} \quad \text{at } 0.1 \text{ torr}$$

The relaxation time is taken at 1/e of the time for 'complete' relaxation, so 'complete' relaxation takes about 3 relaxation times (3t). Since 'complete' relaxation can be considered to have occurred after >95% relaxation (95% = 1 - e<sup>-3</sup>), then for complete relaxation x increases by √3 and is thus found to lie in the range 0.17cm → 0.73cm; this should be compared with a beam-centre to microphone distance of 1.115cm (Fig.2.2-2).

Thus, with the microphone 1.115cm from the irradiated region, non-relaxation may be a problem as the pressure starts to fall below 0.1torr; for example, at 20mtorr both D and t are five times larger than at 0.1torr. So the distance required for 'complete' relaxation is five times as long, i.e. 0.85 → 3.7 cm.

Clearly, the order of magnitude of pressure, where incomplete relaxation is expected to start, agrees with the sharp fall in  $\sigma$  below about 0.1torr that was measured in all cases except methanol and ethanol; for these last cases, signals, for pressures 0.1torr and below, were not detectable.

Because of the non-relaxation, values of  $\sigma$  at about 0.1torr and below are suspect: If 't' is closer to 150 $\mu$ m than 8 $\mu$ m (i.e. the worst case), the pressure, for which complete relaxation requires the entire beam-to-microphone distance, is  $\sim$ 70mtorr. A procedure for estimating  $\sigma$  at zero pressure was attempted as follows: Let  $\sigma$  at 0.2torr, zero pressure, and infinite pressure be known as  $\sigma_{0.2}$ ,  $\sigma_0$ , and  $\sigma_\infty$  respectively. Table 3.10-2 lists the experimental cross-sectional values at high pressure; 0.2torr of this, and previous (6) work on similar molecules; and at the low pressure plateau (i.e.  $\sigma_0$ ) for previous (6) work. From these results of similar molecules (6), the percentage, P, that  $\sigma_{0.2} - \sigma_0$  constitutes of  $\sigma_\infty - \sigma_0$  was established. It was then intended to estimate  $\sigma_0$ , for the current data, using this knowledge. However, P was not a constant, varying between 0% (oxetane) and 56% (ethanol). It was determined that this method was unsuitable, and no alternative method was found.

As previously discussed, it is observed for all reactants analysed in this work, that the value of  $\sigma$  at low pressure is less than that at high pressure; that the difference diminishes with increasing molecular size; and consequently that for the largest molecule analysed (hexanol), the difference is barely noticeable.

While it is clear that  $\sigma_0$  has not been accurately predicted, use of the experimental values of  $\sigma$  at 50mtorr, and at the lowest pressures used, will allow a rough estimate to be made of the fraction of molecules initially capable of absorbing radiation, f, for the fraction is the ratio  $\sigma_0/\sigma_\infty$ . For

Reactant	No. of atoms (minus H atoms)	Laser Line	$\sigma / 10(-20).cm(2).molec(-1)$				at ~50 mtorr		at lowest measured p			Comments M=longitudinal multimode S=longitudinal singlemode P=pressure
			broad-band	at high P	at 0.2 torr	measured at low P plateau	f	fluence / J.cm(-2)	f	p /mtorr	fluence / J.cm(-2)	
methanol	6 (2)	R32(10)	5.123	> 0.94	0.02		< 0.085	7.56	< 0.032	33	7.56	M. No plateau at high P.
ethanol	9 (3)	R20(9)	23.25	10	5.6				0.47	100	4 & 9	M. Plateaux not clear.
		P18(9)	23	21	11.2	5.75	0.264	4.8	0.264	50	4.8	M (6)
cyclobutanone	11 (5)	P20(9)							0.25	2500	0.5 & 1.0	S. 10ns and 40ns FWHM pulses.(73)
propan-2-ol	12 (4)	R14(9)	12.366	6.6	5.4		0.52	9.2	0.31	25	9.2	M. Low P plateau not clear.
butan-2-ol	15 (5)	R24(10)	7.883	10.7	8.3		0.56	2.3 & 10.56	0.17	20	2.3 & 10.56	M. Low P plateau not clear.
butanol	15 (5)	P30(10)	13	> 17	4.25	3.5	< 0.194	5.9	< 0.205	34	5.9	M. No high P plateau.(6)
pentan-2-ol	18 (6)	R26(9)	5.834	8	7.6		0.56	6.65	0.56	50	6.65	M. Low P plateau not clear.
pentan-3-ol	18 (6)	R14(10)	16.94	10.3	9.5		0.72	11.18	0.37	25	11.18	M. Low P plateau not clear.
hexan-2-ol	21 (7)	P20(9)	4.762	6.1	6.1		0.83	9	0.58	23	9	M. Low P plateau not clear.
3,3-dimethyloxetane	16 (6)	R24(10)	15.694	7.2	5.2		0.61	9.65	0.29	20	9.65	M. Low P plateau not clear.
		R24(10)	15.694	12.5	10.05		0.47	10	0.47	50	10	M. High P plateau not clear.
		P24(10)	5.513	4.25	2.8		0.61	11	0.41	33	11	M. Low P plateau not clear.
		R24(10)	15.694	12.5	10.05		0.47	10	0.47	50	10	S. High P plateau not clear.
2,2-dimethyloxetane	16 (6)	R20(10)	37	> 21.3	11.5	9.5	< 0.419	6.5	< 0.419	50	6.5	M. High P plateau not clear.(6)
		R20(10)		> 21.3	9.3	7.3	< 0.349	3.5	< 0.349	50	3.5	S. High P plateau not clear.(6)
oxetane	10 (4)	R20(10)	13	19	4.25	4.25	0.232	6.2	0.232	50	6.2	M (6)
		R20(10)		23.7	6				0.244	100	3.2	M (6)
		R20(10)		29.3	7.5				0.212	100	1.8	M (6)
		R20(10)		11.5	no data below 0.4 torr				<< 0.167	400	3.7	S. No plateaux. (6)
2-methyloxetane	13 (5)	R34(10)	29	20	11	6.3	0.345	5.5	0.345	50	5.5	M (6)

**Table 3.10-2** Summary of the fraction of absorbing molecules f, and broadband cross-section for different reactants. Experimental data such as the laser line and fluence (for f) are included.

comparison, Table 3.10-2 summarises the fraction of excited molecules observed at low fluences for IR laser pulses by several researchers (6,73 and this work). Previously, values for  $f$  have been predicted in the range 0.1 to 0.001 (53). Very few of the tabulated values lie in this range. It is possible that the temperature of the reactant gases varied sufficiently, that the strong dependence on temperature (observed by Letokhov (53)) affected the ratios. Of immediate note is that many of the ratios are approximations (for both current and other work), for a reason in addition to the 'incomplete relaxation' problem outlined earlier: As described in the comments column of the Table, not all the reactants had well defined plateaux at either (or both) the high or low pressures. Consequently the actual ratios may be considerably less than the calculated values if either the high pressure plateau is not clear or if the low pressure plateau is not reached, and more if the low pressure plateau has been modified by lack of complete intermolecular vibrational-vibrational energy relaxation. The tabulated data (current work and other) is represented in graphical form (Fig.3.10-1) to see the extent of correlation between the fraction of excited molecules,  $f$ , and the size of reactant molecule; the fraction is determined using the lowest pressure for which there was a measurement. It is noted that there is some correlation.

The experimental conditions associated with each value of  $f$  vary in fluence and pulse type. The current work on ethanol and butan-2-ol, and the past work on cyclobutanone, and oxetane leads one to conclude that the fraction of excited molecules does not depend on fluence for either type of pulse. However, the dependence on pulse type is not clear: The data on oxetane (6) shows that the value of  $f$  for a multimode pulse is more than 1.4 times that for a singlemode pulse, but for 3,3-dimethyloxetane, there was no measureable difference.

The effect of pulse type was studied for ethanol and 3,3-dimethyloxetane. In both cases there is evidence that multimode pulses cause an increase in the average number of absorbed photons per molecule, and hence that there is some increase of  $\langle n \rangle$  with power. This same conclusion, generalised for all pressures and fluences, was drawn by Shaw (6) for 2,2-dimethyloxetane.

Ethanol and 3,3-dimethyloxetane were also used to study the effect of irradiating wavelength. In both cases, the difference in laser absorption cross-sections of the different wavelengths did not coincide with that of the low fluence, broadband cross-sections. As discussed in those sections (3.2 and 3.8), it is proposed that this is evidence that the absorption spectrum shifts to the red with increasing fluence. Such shifts have previously been observed for  $\text{SF}_6$  and  $\text{OsO}_4$  (53), and alkanol and oxetane molecules (6).

In summary, for the smaller molecules studied, the small signal, broadband absorption cross-section is much greater than that measured when irradiating with the laser. This difference diminishes with molecular size and was not significant for the larger molecules of this study, the 'laser' cross-section being of a value comparable to that of the small signal, broadband measurement.

Furthermore, it is observed for all the reactants analysed in this work, that the value of  $\sigma$  at low pressure is less than at high pressure. This is consistent with the findings of previous work (6), and with the explanation that the drop is caused by rotational hole-burning. Moreover, as one progresses through the alkanol homologous series, a general trend is observed in the change of this variation of  $\sigma$  with pressure: The decrease at low pressure becomes less obvious and the value approaches the broadband value. This behaviour would indicate a lessening importance of the rotational

hole-burning mechanism, and is to be expected since the density of states increases with increasing molecular size. Indeed, the hexan-2-ol data although a little scattered, suggest complete pressure independence, for the low pressure drop is barely noticeable. For this work, a further, more rapid decrease observed at the lowest pressures has been attributed to incomplete inter-molecular vibrational-vibrational energy relaxation.

## 4. - DECOMPOSITION RESULTS

The effects, on product yield, of laser fluence, reactant pressure, laser pulse type and added diluent, have been studied to varying extents on ethanol, propan-2-ol, butan-2-ol, pentan-2-ol, pentan-3-ol, hexan-2-ol, and 3,3-dimethyloxetane. The results are presented in this chapter with a section being devoted to each molecule. Typically the data are plotted against fluence and pressure either as 'yield',  $Y_F$ , or 'yield Ratio',  $Y_{FR}$ , (i.e. the yield of a product relative to the yield of the primary product(s)). Unless otherwise stated, the yields discussed in this thesis are the *fractional product yields per laser pulse* given by:

$$\frac{\text{pressure of product}}{\text{reactant pressure}} \times \frac{\text{vol. of cell}}{\text{irradiated vol.}} \times \frac{1}{\text{number of pulses}}$$

Any values quoted for the purpose of comparing the magnitude of yields formed under different conditions, are interpolated from graphs to which a computer least squares fit has been formed.

The "most probable" fractional errors, typical for the values of fluence, yield, and yield ratio, are tabulated below, while the error in the pressure readings is  $\pm 1$ mtorr:

$\frac{\Delta F}{F}$	$\frac{\Delta Y_F}{Y_F}$	$\frac{\Delta Y_{FR}}{Y_{FR}}$	COMMENTS
$\pm 36\%$	$\pm 31\%$	$\pm 44\%$	{ "clean" GLC signal single primary product
"	$\pm 40\%$	$\pm 57\%$	{ "trace" GLC signal single primary product
"	$\pm 31\%$	$\pm 62\%$	{ "clean" GLC signal 3 primary products
"	$\pm 40\%$	$\pm 80\%$	{ "trace" GLC signal 3 primary products

These tabulated fractional errors are largely governed by the error in the calculated radius of the irradiating beam, which was determined in Section 2.1.3 to be  $\pm 18\%$ . Furthermore, the errors have been established in the same manner as that used in Section 2.1.3. Other factors of note are that; i) for products occurring as trace amounts, the GLC peaks were consequently small and often superimposed on a noisy baseline, or perhaps at the shoulder of a more dominant peak (product); and ii) there is only one primary product for ethanol, propanol, and 3,3-dimethyloxetane, while there are two for pentan-3-ol, and three each for butan-2-ol, pentan-2-ol, and hexan-2-ol. The effect of these factors has been taken into account in the typical values quoted in the above table. For those graphs plotted for constant fluence (and in some instances constant pressure), the fluence uncertainty quoted in the text is indicative of the *stability* of the fluence over the length of the test.

It was anticipated that differences between sets of data could be small (if at all present): to reduce uncertainties brought about through lapses of time, certain precautions were taken, *viz.* for the comparison of pulse effects, the pulse type was swapped at each new cell fill, and in order to collate diluent data, those experiments were run immediately after completing the associated 'pure' set. Interest in the effects of a diluent derives from the findings of Shaw (6) with 2,2-dimethyloxetane: he showed that yields decreased in the diluted sample. The behaviour was attributed to the suppression of post-first-collision thermal reactions by deactivating collisions of the excited 2,2-dimethyloxetane molecules with the more abundant diluent molecules.

Calculation (for the experiments which used a uniform beam) shows that the effect of diffusion on yield is insignificant under collision free, high focus conditions, and therefore also for all other conditions (see Appendix A3).

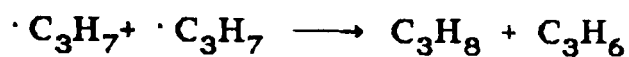
Thus the remaining possible effects of adding a diluent are points (i) and (ii) as discussed in Section 1.1.1: i.e. that rotational relaxation will become more efficient, increasing both the absorption cross-section and yield; and that excited by-products will be deactivated more quickly, so reducing the yields of secondary products.

At the onset of this work, the primary reaction channel for the alkanols was expected to be one of unimolecular dehydration, through a four-centred transition state, while bond fission was expected to almost exclusively deliver any other product. This expectation was derived from the literature available at that time (1983) (6,7,8). For example Bialkowski (80) redemonstrated proof of C-O bond fission of high pressure methanol: the resultant OH occurred in both ground and excited state. The same path is less likely for heavier hydrocarbons, because C-C fission is easier. Articles exploring the possibility of further unimolecular channels were just surfacing (8). Gandini and Back (8) suggested that excess methane found after decomposition of ethanol, may have come from a unimolecular channel that formed  $\text{CH}_4 + \text{CH}_2\text{O}$ . Later, this was also proposed by Leite *et al.* (10).

The heats of reaction for decomposition via molecular elimination and via formation of free radicals are compared in this thesis for each alkanol under analysis. Where possible, heats of formation for the products were taken from standard sources (2a),(2b),(1). If necessary, they were calculated using the group contribution method (2a) as described in Appendix A4.

Radicals resulting from the breaking of the bonds, would be expected to undergo recombination possibly followed by disproportionation. To help give an indication of whether a certain radical pair would prefer a recombination path to one of disproportionation, values have been included in the tables

wherever possible for  $\Delta$ ; the ratio of the rate of the disproportionation reaction to that of the recombination reaction. The possibility is therefore immediately evident for one particular product to be formed in more than one way (as a result of the breaking of more than one bond-type): For example, propane could be formed as follows:



The combination and permutation of reactions following bond fission are so numerous, that both qualitative and quantitative analysis of the product yields is very awkward and complicated. It is consequently often impossible to conclusively show that a certain bond has fissioned.

## 4.1 ETHANOL

Investigation of the effects of laser radiation on ethanol, has already been carried out by other workers eg. Bhatnagar (7), Shaw (6), Back et al (8)(9)(9b), Leite et al (10). However, there was some conflicting and unusual data that could not be truly compared, since their experimental conditions were not identical. Some of the previous experiments have been repeated here in order to clarify some points, and to correct what is considered to be limitations of the systems used at the time: for example, extensive use has been made of focussed laser beams in order to achieve high fluences. This type of system is otherwise avoided in this thesis, because of the complications that ensue in defining the irradiated volume, and fluence. This series of experiments looks at the effect of irradiation line ( $R_{20}(9\mu\text{m})$  or  $P_{18}(9\mu\text{m})$ ), pulse type (multimode or singlemode) and diluent ( $\text{CO}_2$  or cyclohexane). A repetition rate of 65 pulses per minute was used.

The major product expected, as a result of unimolecular dehydration, is ethene. Over the course of this work, products were identified as methane, ethane, ethene, acetylene, propane, butane, *cis*- and *trans*-but-2-ene, and acetaldehyde ( $\text{CH}_3\text{CHO}$ ). Several heavy hydrocarbons remained unidentified, although it was established that they were not n-hexane, n-pentane or ethylene oxide ( $\text{C}_2\text{H}_5\text{O}$ ). The analysis eventually made use of both the GLC machines, however, at the beginning of the work, only the Pye GLC was available. At that time, it was fitted with the 6m long chromosorb P column, that had been especially made for the initial butan-2-ol work (see Section 4.3). Over the course of this column's use, the oven temperature was  $50^\circ\text{C}$ , but the  $\text{N}_2$  flow rate varied between 30 ml/min and 40 ml/min; most of the work was carried out with faster rate. When the Carlo oven became available, the Pye chromatograph was fitted with a 2.9m long column, of 3mm inner diameter, which was packed with 13.5% bis-2-methoxy-ethyl adipate and 6.5%

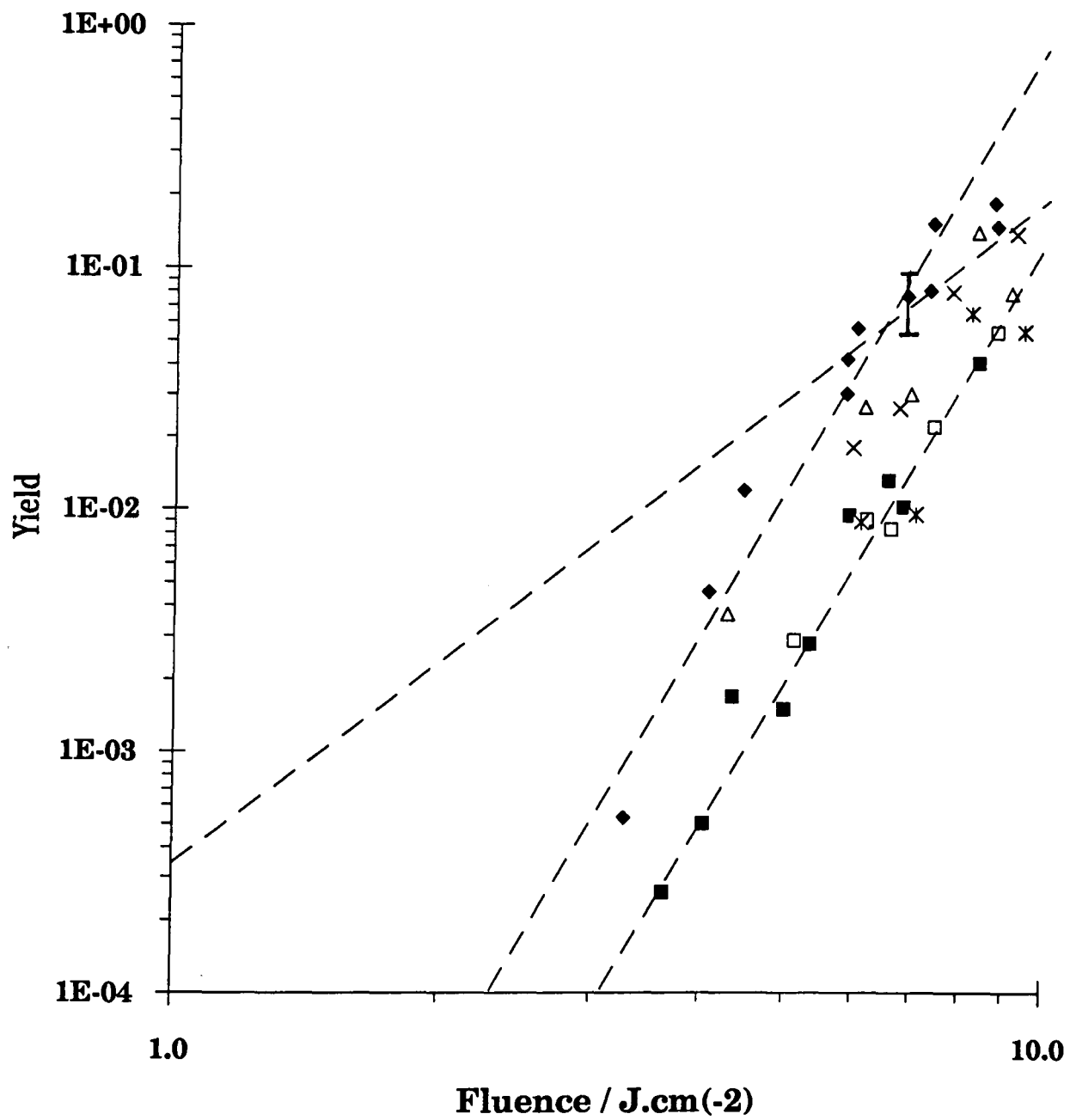
di-2-ethyl-hexyl sebacate on Chromosorb P (60/85 mesh); it was used with a carrier flow rate of 20 ml/min and a temperature of 40°C, and assisted, primarily, in the search for C<sub>4</sub> products. The Carlo oven was fitted with the chromosorb 101 column, and was used to resolve the C<sub>2</sub> hydrocarbons (oven temperature 40-43°C) and acetaldehyde (oven temperature 180°C). The two ovens were used one immediately after the other to test each sample.

#### 4.1.1 Fluence Dependence

C<sub>2</sub>H<sub>4</sub> production per pulse in the irradiated volume, increases rapidly with fluence under all conditions examined *viz.* laser wavelength, pure and diluted reactant, multi- and single-longitudinal mode pulses (Fig.4.1-1). The increase follows  $Y \propto F^{6.3}$  except above a fluence of about 6.3 J/cm<sup>2</sup> for multi-mode, pure reactant, P<sub>18</sub>(9μm) radiation conditions; the trend then follows  $Y \propto F^{2.8}$ ; for the P<sub>18</sub>(9μm) line, the variation agrees (within experimental scatter) with the undeconvoluted results of Shaw (6) taken over a more limited range of fluence.

The corresponding variations of C<sub>2</sub>H<sub>6</sub>/C<sub>2</sub>H<sub>4</sub> and CH<sub>4</sub>/C<sub>2</sub>H<sub>4</sub> with fluence are shown in Figs. 4.1-2 and 4.1-3 respectively. There is a general increase in the yield of C<sub>2</sub>H<sub>6</sub> and CH<sub>4</sub> with fluence, but not to the same degree as C<sub>2</sub>H<sub>4</sub>. Both C<sub>2</sub>H<sub>6</sub>/C<sub>2</sub>H<sub>4</sub> and CH<sub>4</sub>/C<sub>2</sub>H<sub>4</sub> are therefore seen to decrease as the fluence increases, however, around 8 (±2) J/cm<sup>2</sup> apparent minima are reached, and the ratios then show a slight increase to the highest fluence used of ~9 J/cm<sup>2</sup>; such behaviour was not observed by Back *et al.* (9). This implies a growing importance of the unimolecular dehydration channel, with fluence, upto roughly 8 J/cm<sup>2</sup>. Above that fluence, there is then increasing importance in the channels which generate methane and ethane as fluence is increased further. As is discussed more in Section 4.1.2, at collision-free pressures, the focussed system yields a higher proportion of both methane and ethane to

**Fig. 4.1-1 Ethanol: Comparison of the effect of a pure (P) & dilute (D) reactant on C<sub>2</sub>H<sub>4</sub> yield (raw data) as a function of fluence for both single (S) & multi (M) mode pulses**



■ P, R20(9)	□ D (cyclo C6H14), R20(9)	◆ P, P18(9)	◆ P, M, P18(9)
△ P, S, P18(9)	× D(CO2), M, P18(9)	× D(CO2), S, P18(9)	

**Fig. 4.1-2 Ethanol: Comparison of the effect of pure (P) & dilute (D) reactant on C<sub>2</sub>H<sub>6</sub>/C<sub>2</sub>H<sub>4</sub> (raw data) as a function of fluence for both single (S) & multi (M) mode pulses**

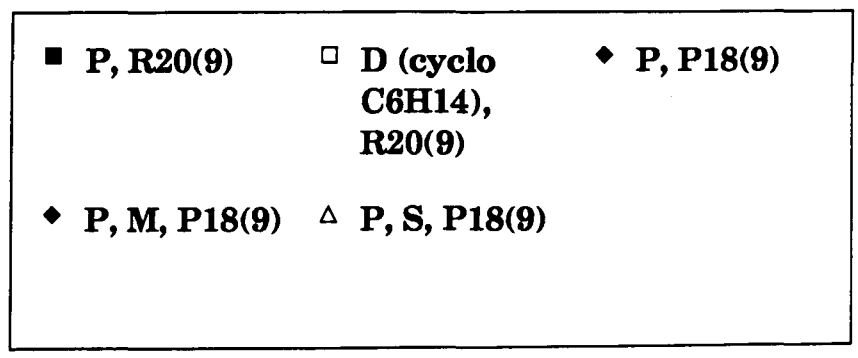
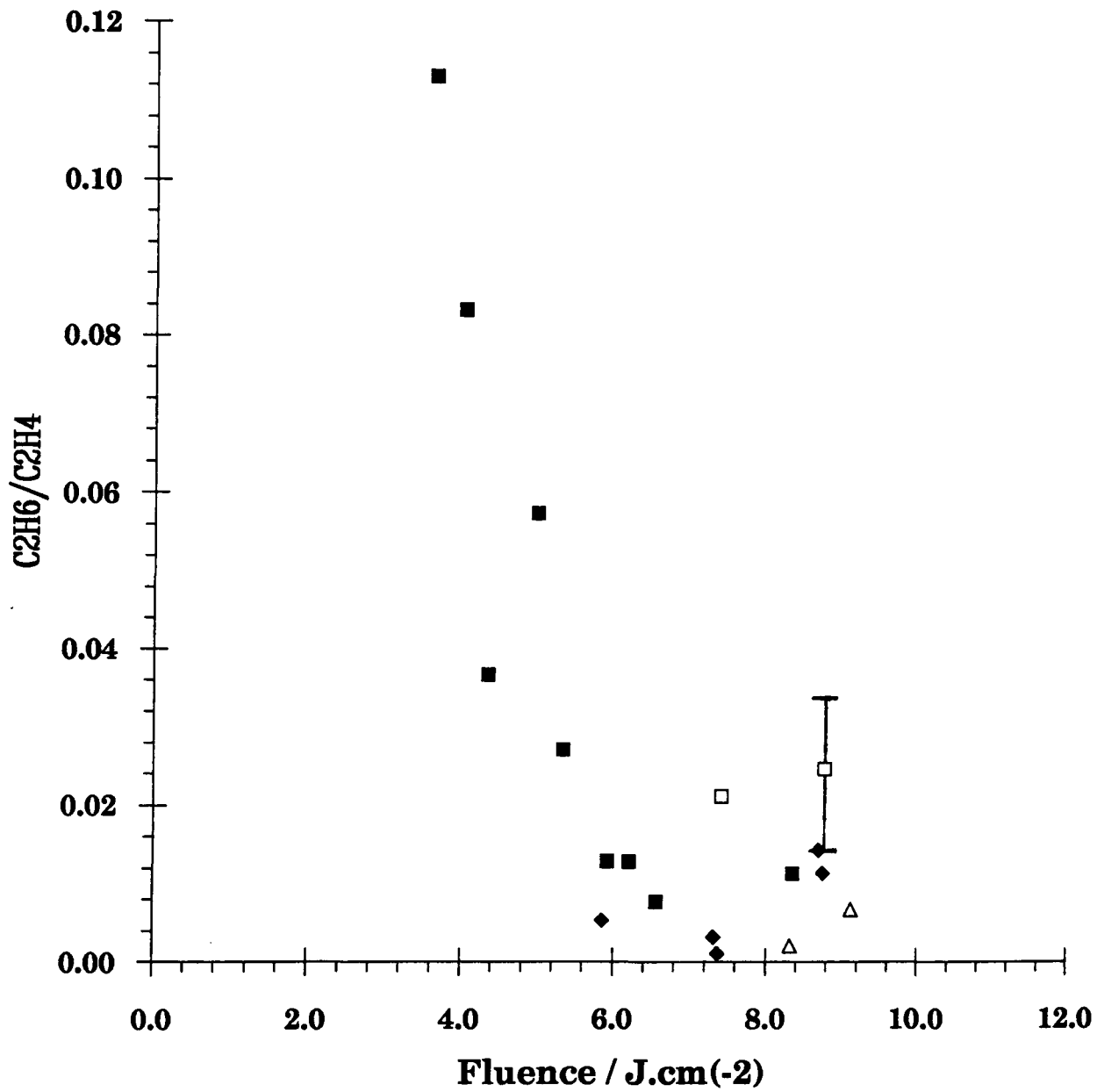
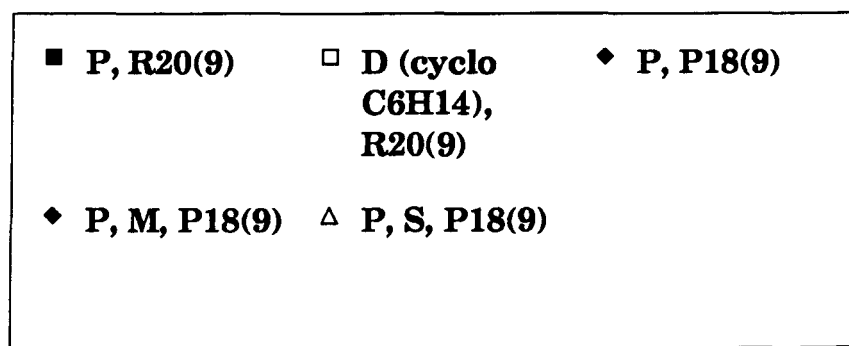
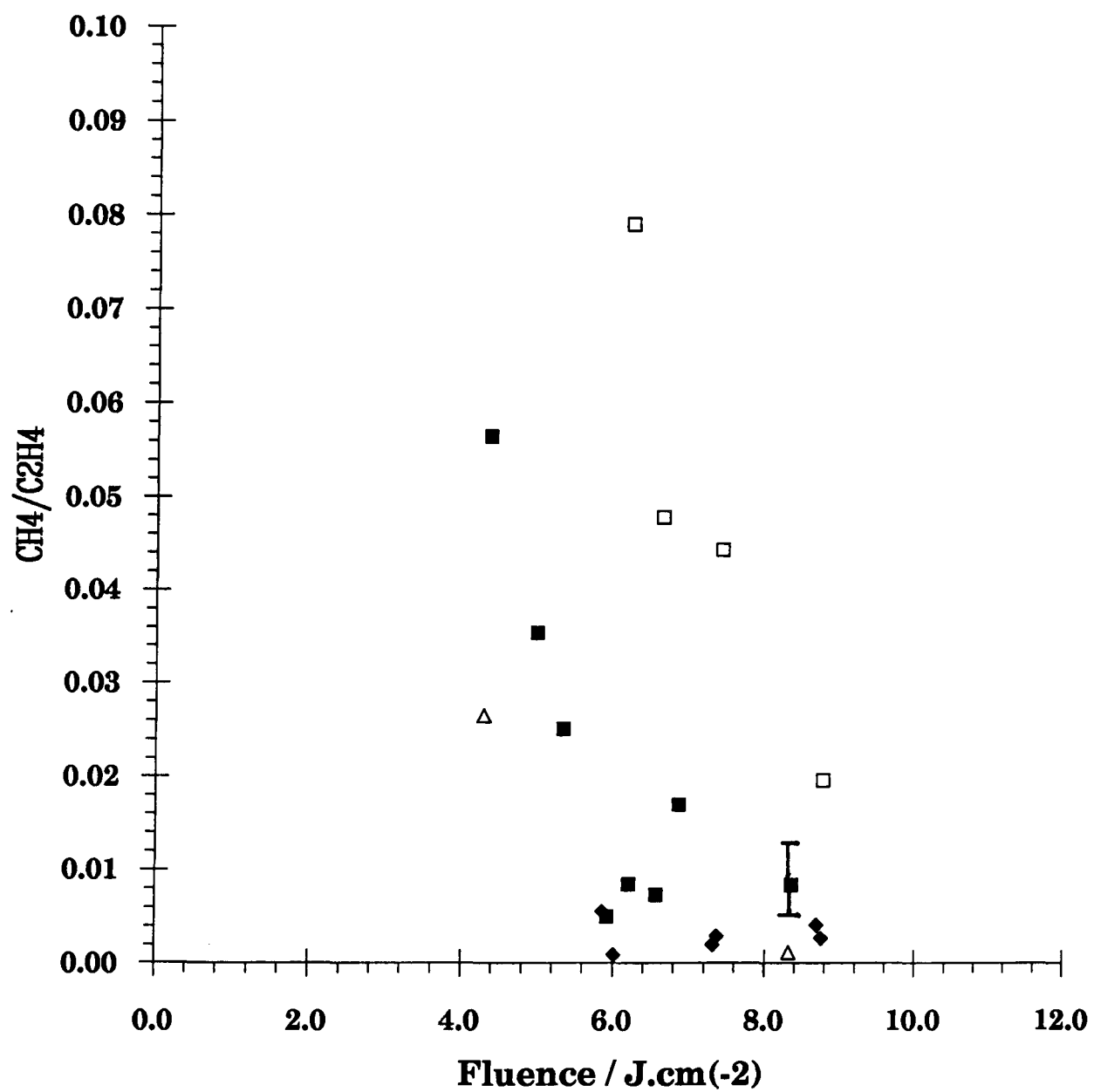


**Fig. 4.1-3 Ethanol: Comparison of the effect of pure (P) & dilute (D) reactant on CH<sub>4</sub>/C<sub>2</sub>H<sub>4</sub> (raw data) as a function of fluence for both single (S) & multi (M) mode pulses**



ethene: in a more general sense, this increase with fluence of methane and ethane agrees with the findings of Back *et al.* (9).

In general, the results imply that the channels leading to  $\text{CH}_4$  and  $\text{C}_2\text{H}_6$  have higher activation energies than the channel which leads to  $\text{C}_2\text{H}_4$ .

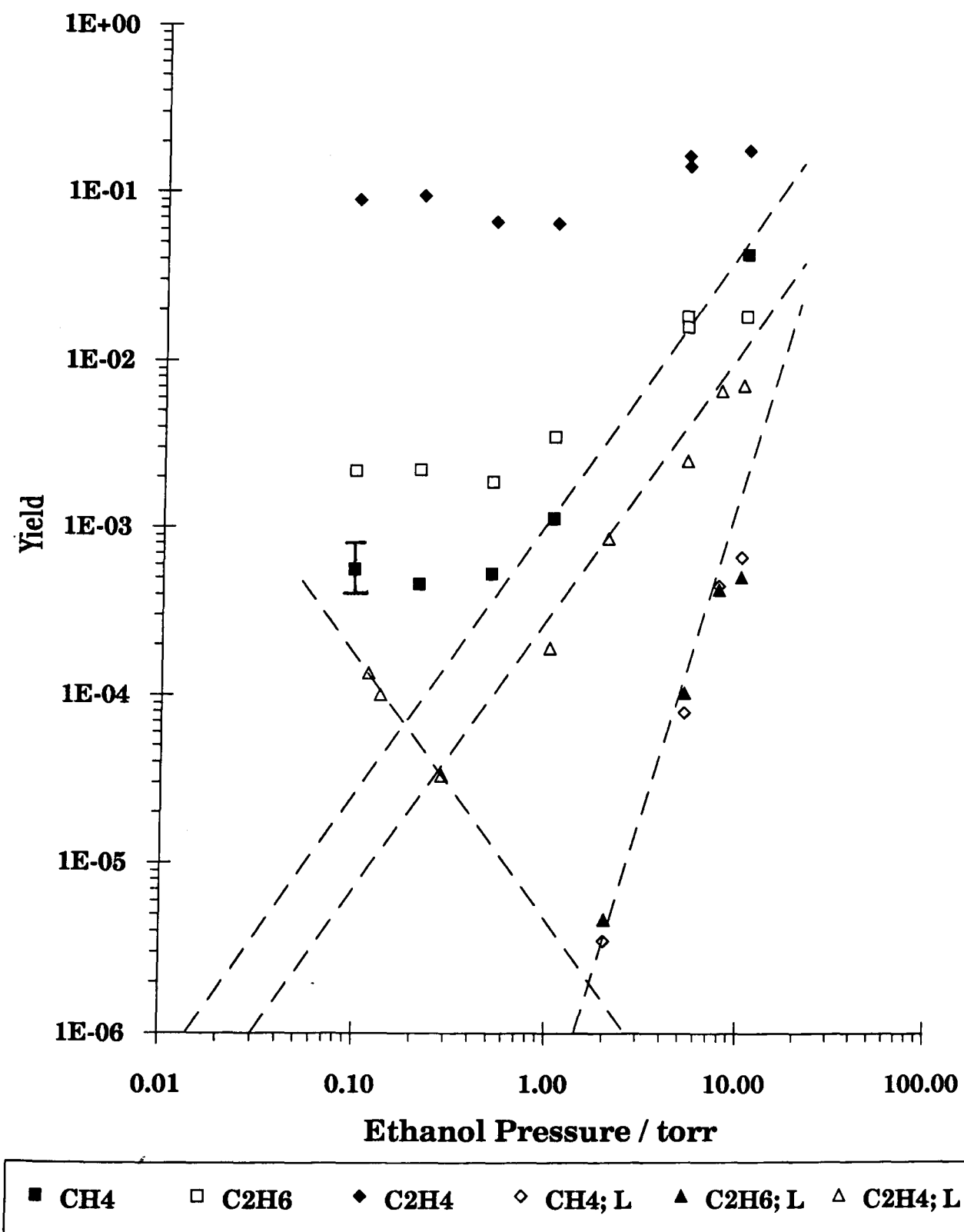
#### 4.1.2 Pressure Dependence

The variation with initial ethanol pressure of  $\text{CH}_4$ ,  $\text{C}_2\text{H}_6$  and  $\text{C}_2\text{H}_4$  production per pulse in the irradiated volume is illustrated in Fig.4.1-4 for two contrasting fluences on  $R_{20}(9\mu\text{m})$ . Back *et al* (9b) have observed, for focussed beam systems, that over the pressure range  $P < 1.2$  torr the yield of the main decomposition channel, ethene, is independent of pressure, while for  $1.2 \text{ torr} < P < 5 \text{ torr}$  the absolute yield decreases with increasing pressure. Likewise, Shaw (6) found the yield to be independent of pressure below 0.2 torr, and to rise with higher pressures. This work with a collimated beam and  $R_{20}(9\mu\text{m})$  (Fig.4.1-4) shows that the behaviour depends on fluence and pressure range; pressures up to 10 torr were used:

- i) Above 1 torr methane, ethane and ethene yields all increase with pressure for conditions of high and low fluence.
- ii) At low fluence and low pressures ( $< 0.3$  torr, ethene decreases as the pressure increases (methane and ethane were not measured).
- iii) At high fluence and low pressures ( $< 0.5$  torr methane decreases as the pressure increases to a minimum at 0.2 torr but ethane and ethene rise to local maxima at 0.2 torr before decreasing to minima at 0.5 torr. The changes in these yields over this range is, however, small.

The increase with pressure for any one product is less severe at the higher fluence. For ethene and low fluence conditions  $Y \propto P^{1.54}$  when the pressure is above 0.2 torr and  $Y \propto P^{-1.59}$  for pressures less than 0.2 torr.

**Fig. 4.1-4 Ethanol: Comparison of yield (raw data) as a function of pressure for pure reactant irradiated at 8.6J/cm(2) and 3.8J/cm(2) (products from the latter have an L suffix)**



For direct comparison of the effect of focussed versus collimated beams, the total amount of product produced in the cell volume per pulse is used, rather than the fractional yield per pulse (Fig.4.1-5). This is so as to avoid involving a value for the irradiated volume; a particularly difficult task for the focussed system. Furthermore the fluence value quoted for the focussed system is in the plane of the focussed spot only ( $\sim 17600 \text{ J/cm}^2$ ; greater than  $10^3$  times the fluence of collimated beam; see Section 2.4). The average fluence over the length of the irradiated volume will be less than this peak value, but is probably no more meaningful than the peak value when it comes to explaining the observed decomposition. The fluence for the collimated beam experiment was  $9.4 \pm 0.1 \text{ J/cm}^2$ . The collimated beam yields may be multiplied by 625 to get the product produced per pulse in the irradiated volume, and by 3218 for the fractional yield per laser pulse.

The total ethene yield per pulse (note, not fractional yield), for both focussed and high fluence, collimated beam conditions, increased with pressure according to  $Y \propto P^{1.1}$  i.e. below 10 torr, the ethene yield roughly proportional to the pressure of ethanol. Collimated beam conditions produced four times more yield (Fig.4.1-5), so, for ethene production, the higher fluence achieved by focussing was outweighed by the smaller effective irradiated volume.

The variations of  $\text{C}_2\text{H}_6/\text{C}_2\text{H}_4$  and  $\text{CH}_4/\text{C}_2\text{H}_4$  with pressure are shown in Figs. 4.1-6 and 4.1-7 respectively. Data are included for a focussed beam geometry (taken on  $P_{18}(9\mu\text{m})$  only), but will not be discussed immediately. Fig.4.1-4 shows that for both high and low fluence conditions  $\text{C}_2\text{H}_6$  dominates over  $\text{CH}_4$  below 6 torr only. It should be noted that the high and low fluence conditions lie either side of the minima described in the  $\text{C}_2\text{H}_6/\text{C}_2\text{H}_4$  and  $\text{CH}_4/\text{C}_2\text{H}_4$  curves versus fluence (Figs.4.1-2 and 4.1-3). The two ratios (to

**Fig. 4.1-5 Ethanol: Comparison of the effect of focussed (F) & collimated (C) beams on C<sub>2</sub>H<sub>4</sub> production as a function of reactant pressure**

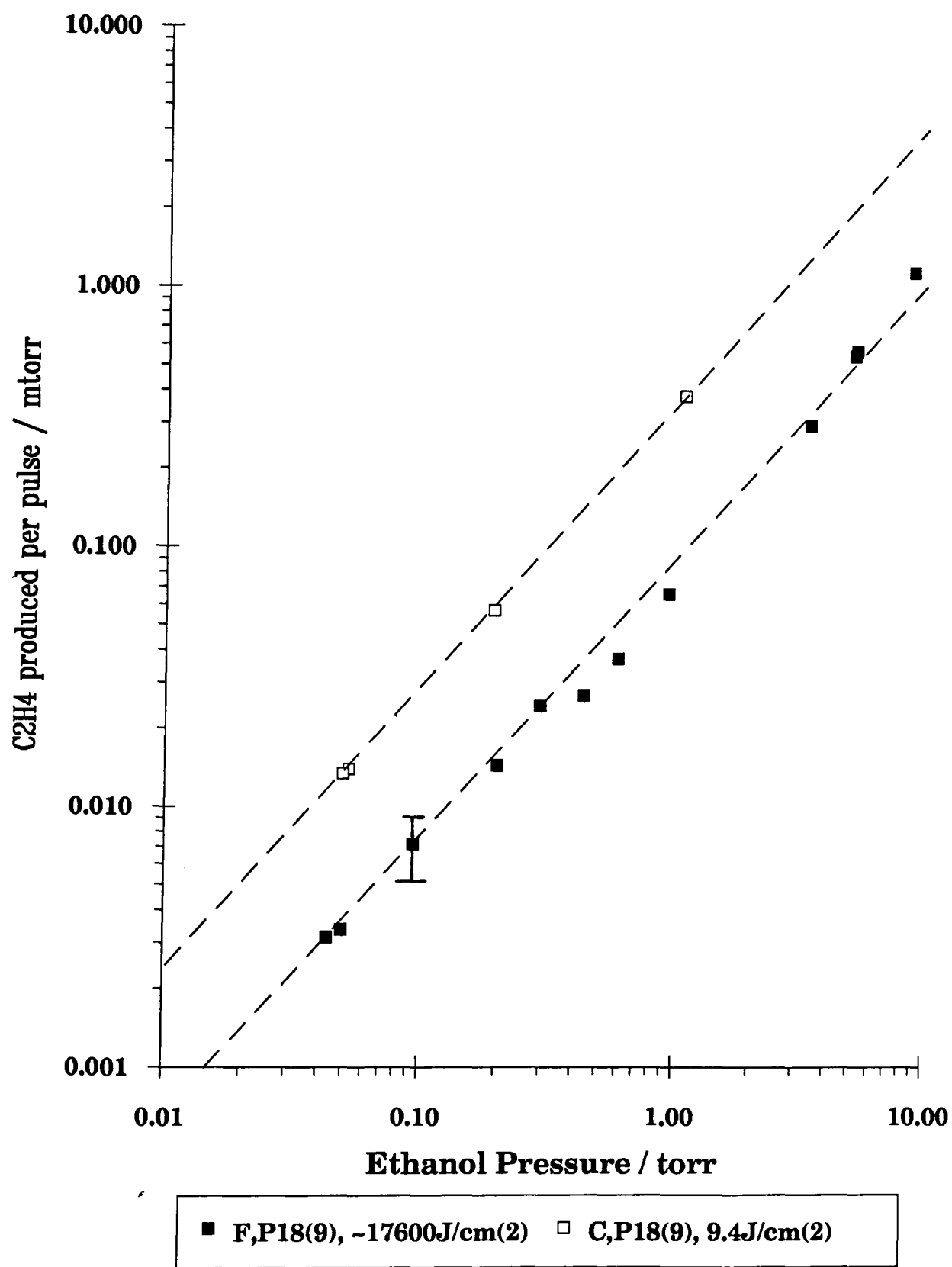
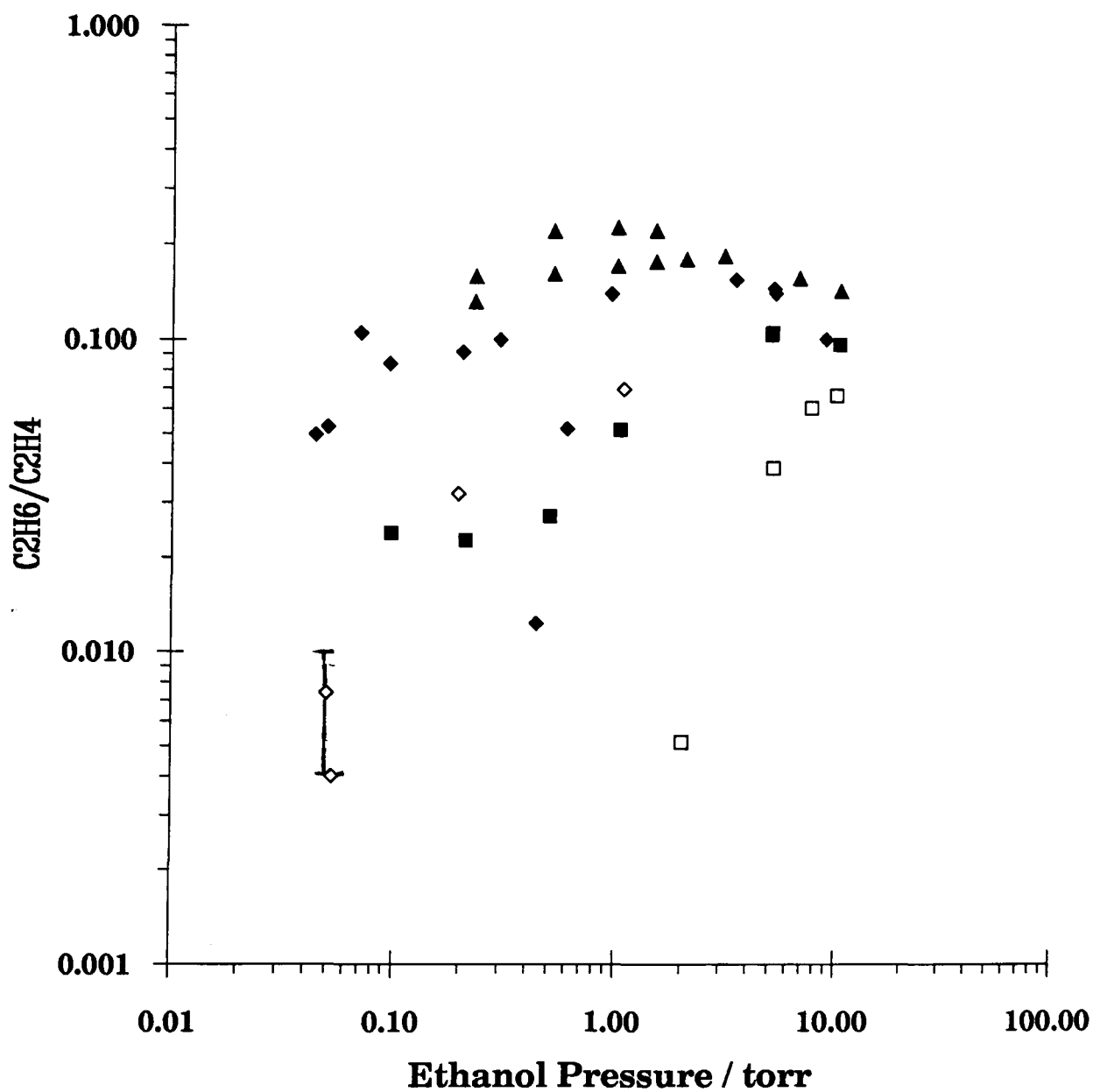
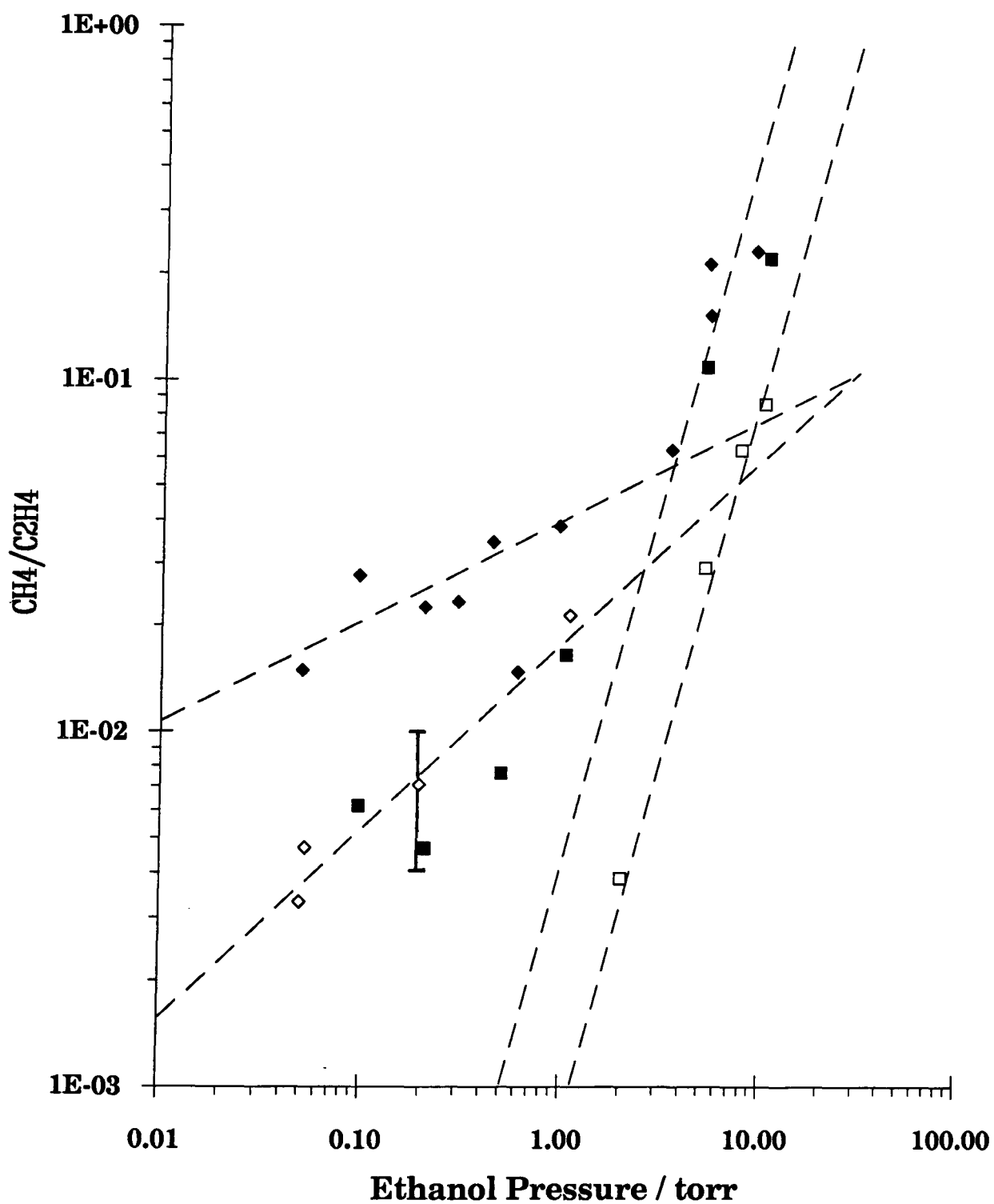


**Fig. 4.1-6 Ethanol: Comparison of the effect of focussed (F) & collimated (C) beams, irradiating wavelength, and fluence on C<sub>2</sub>H<sub>6</sub>/C<sub>2</sub>H<sub>4</sub> as a function of reactant pressure**



■ C, R20(9), 8.6J/cm(2)	□ C,R20(9), 3.8J/cm(2)	◆ F,P18(9), ~17600J/cm (2)
◇ C,P18(9), 9.4J/cm(2)	▲ F; R20(9): Ref.( 7 ).	

**Fig. 4.1-7 Ethanol: Comparison of the effect of focussed (F) & collimated (C) beams, irradiating wavelength, and fluence on CH<sub>4</sub>/C<sub>2</sub>H<sub>4</sub> as a function of reactant pressure**



$C_2H_4$ ) are very similar at all pressures for low fluence conditions, and increase quite steadily with pressure, to a plateau: this demonstrates an increasing importance with pressure on the reaction path which leads to  $C_2H_6$  and  $CH_4$  production. Under higher fluence conditions (which includes the focussed systems), the rise in  $C_2H_6/C_2H_4$  with pressure is considerably more rapid, the values are higher, and the plateau is reached at a lower pressure; in addition the plateau has a negative gradient. At any one pressure, focussed systems yield a higher proportion of ethane to ethene than the collimated systems (Fig.4.1-5). In addition, the initial rise with pressure is more severe in the focussed system.

Work with the focussed system was carried out on  $P_{18}(9\mu m)$ . Although methane was not measured on this line for pressures greater than 1 torr it would be reasonable to assume that the similarity between the trends of  $CH_4/C_2H_4$  for  $P_{18}(9\mu m)$  and  $R_{20}(9\mu m)$  observed for pressures less than 1 torr will continue at the higher pressures (Fig.4.1-7). Using this assumption, the following observation is true: the focussed system delivers a higher yield of  $CH_4/C_2H_4$  than the collimated beam (to about 2 torr, above which there is no difference between the systems).

Since the focussed system was detrimental to the production of ethene, it is clear that, in terms of maximising yields of particular products, achieving an extremely high fluence by focussing is not always the ultimate goal.

Whilst Fig. 4.1-2 indicates that  $C_2H_6/C_2H_4$  will be high at the lowest experimental fluence conditions and low at the highest fluence conditions, Fig. 4.1-6 appears to contradict; the ratio is larger for the higher fluence. There is a similar observation for  $CH_4/C_2H_4$ . It is not believed that this is a discrepancy, because the results of Fig. 4.1-2 are for collision-free conditions

(50 mtorr total), whereas the observations made from Fig. 4.1-6 are obviously made over a pressure range most of which cannot be considered collision-free. A reverse in fluence dependence has been observed for  $\text{CH}_3\text{CHO}/\text{C}_2\text{H}_4$  (9b): higher fluence conditions only increased the ratio when the reactant pressure was greater than 1 torr while at collision-free pressure, low fluence conditions yielded a larger  $\text{CH}_3\text{CHO}/\text{C}_2\text{H}_4$  than at high fluence conditions. The research for this thesis revealed the same reversal in fluence dependence for  $\text{C}_2\text{H}_6/\text{C}_2\text{H}_4$  and  $\text{CH}_4/\text{C}_2\text{H}_4$  although this trend was not observed for these same products in the research of ref. 9b. It should be remembered that both  $\text{C}_2\text{H}_6$  and  $\text{C}_2\text{H}_4$  absolute yields increase with fluence, so the reason for the increasing preference for the path leading to  $\text{C}_2\text{H}_4$  is not because of suppression of the  $\text{C}_2\text{H}_6$  channel. We know from the absorption results that, in the fluence range used,  $\sigma$  is independent of fluence, and  $\langle n \rangle$  increases. So as  $F$  increases, a particular molecule is excited to higher energies. The products will have more energy and the unimolecular decay rate will be faster. Furthermore, at low pressures, both  $\sigma$  and  $\langle n \rangle$  are less than at high pressures, so at high fluence and high pressure, as well as each molecule being excited to higher levels, the number of molecules being excited are more numerous: consequently yields will tend to increase.

The minimum at roughly 0.3 torr in low fluence yields of  $\text{C}_2\text{H}_4$  of Fig. 4.1-4, shifts very slightly to a higher pressure with increasing fluence and becomes less pronounced; it is seen as an inflection at 0.35 torr for the entirely independent set of focussed data of Fig. 4.1-5. Insufficient data was accumulated for the collimated system to be able to identify this anomaly. Such minima/inflections have been observed before in oxetane (6) and cyclobutanone (28), and it has been suggested that the cause may be restricted intramolecular relaxation. If this were a valid explanation, then in the same pressure region one might expect to see a reduction in yield of the

minor fragments both in absolute values and relative to  $C_2H_4$ , because restricted intramolecular relaxation favours mode-selectivity. While even the major fragments,  $C_2H_6$  and  $CH_4$ , are too low in concentration to be measured at the lowest fluence, data at higher fluence are compatible with the behaviour just described (Figs.4.1-4, -6, -7). The suggestion that a pronounced minimum exists for  $C_2H_6/C_2H_4$  under focussed conditions on  $P_{18}(9\mu m)$  is thus validated.

#### 4.1.3 Effect of Diluent

The effect on the yield by adding a diluent was first investigated for the  $R_{20}(9\mu m)$  line, where cyclohexane was found to be a suitable diluent ie. it did not absorb. However, when experiments were later carried out on the  $P_{18}(9\mu m)$  line, it was found that cyclohexane absorbed at an unacceptable level; for a 60mJ pulse,  $6.0 \times 10^{-4}$  mJ was absorbed by 45 mtorr of cyclohexane, whilst  $4.1 \times 10^{-3}$  mJ was absorbed by 5 mtorr of ethanol.  $CO_2$  was chosen as the diluent for this line, after it was demonstrated that there was no detectable absorption even at high pressures. Ethanol was diluted with  $CO_2$  to a ratio of 1/8.96 and with cyclohexane to a ratio of 1/9. Total pressures were limited to 50 mtorr so that excitation was 'collisionless'.

Under conditions of single longitudinal mode pulse and  $P_{18}(9\mu m)$  irradiation, the effect of the diluent is to decrease the  $C_2H_4$  fractional decomposition per pulse in the irradiated volume (Fig.4.1-1). The amount of decrease lessens as the fluence increases, varying from a 72% decrease of the 'pure' yield at low fluence, to 50% at high fluence. Using Xenon as the diluent, Shaw (6) found, for the same line, that little or no reduction in yield occurred except at the lowest fluence used.

A decrease in yield with the addition of a  $\text{CO}_2$  diluent is also observed under conditions of multilongitudinal mode pulses and  $P_{18}(9\mu\text{m})$  (Fig.4.1-1); a decrease of 70%. However, a cyclohexane diluent combined with multimode  $R_{20}(9\mu\text{m})$  pulses has no effect.

The results imply that there is a small thermal contribution to the reaction which is reduced by adding a diluent. The amount of contribution is wavelength dependent, being negligible for  $R_{20}(9\mu\text{m})$ . Under irradiation conditions of  $P_{18}(9\mu\text{m})$  singlemode pulses, the degree of contribution depends on the fluence, there being less of an effect at the highest fluences. This may indicate that at high fluence, reactant molecules achieve a high enough degree of over excitation that  $k_{\text{uni}}$  is fast enough to allow a high proportion of decomposition before the first neutralising collision; furthermore, the products produced may also have very little excess energy available for inter-molecular energy transfer.

The results of Figs.4.1-2 and 4.1-3 indicate that in the range of fluences measured on  $R_{20}(9\mu\text{m})$ , the addition of a cyclohexane diluent causes an increase in the  $\text{C}_2\text{H}_6/\text{C}_2\text{H}_4$  and  $\text{CH}_4/\text{C}_2\text{H}_4$  ratios. It has already been stated that under the same conditions the  $\text{C}_2\text{H}_4$  yield was not altered. Clearly then the increase is due to an increase in both  $\text{C}_2\text{H}_6$  and  $\text{CH}_4$  yields. Products other than ethene were not measured for conditions of  $P_{18}(9\mu\text{m})$  and  $\text{CO}_2$  diluent.

#### 4.1.4 Effect of Pulse Type

Comparison of the effect of pulse type on yields was carried out on line  $P_{18}(9\mu\text{m})$  (Figs. 4.1-1 to 4.1-3). A difference is noted, though not very dramatic: there is up to a two fold increase in  $\text{C}_2\text{H}_4$  yield with the multimode pulse (Fig. 4.1-1). This result is not surprising since, as already

discussed in Section 2.1.2 the multimode pulse actually consists of a train of high powered (very short) pulses, and, furthermore, the absorption results showed there to be greater absorption for multimode pulses. Since Back *et al.* (9) have shown that pulse length (and hence intensity) have no effect on decomposition on the  $P_{16}(9\mu\text{m})$  line (comparing 60 ns and 10 ns pulses), the small effect noted in this instance may be due to one of two things: i) the effect is not very sensitive to changes in pulse length, so is only noticeable when the pulse length reduction is much larger than that used by Back *et al.*; ii) the much higher repetition rate of the high power pulses within the multimode envelope causes a rapid, step-wise excitation of the molecule, resulting in more efficient up-pumping.

#### 4.1.5 Effect of Irradiating Wavelength

Comparisons of two wavelengths  $R_{20}(9\mu\text{m})$  and  $P_{18}(9\mu\text{m})$ , were only made for the most abundant products. The results are summarised in Table 4.1-1. For a given fluence,  $R_{20}(9\mu\text{m})$  causes substantially less decomposition than  $P_{18}(9\mu\text{m})$ . This is not a surprising result since  $R_{20}(9\mu\text{m})$  radiation is also more weakly absorbed, as shown in the comparison of cross-sections.

#### 4.1.6 Minor Products

The most important products other than ethene, measured in this work, were methane and ethane, and the behaviour of these has already been discussed. Products other than  $\text{CH}_4$ ,  $\text{C}_2\text{H}_4$  and  $\text{C}_2\text{H}_6$  were only measured during the series of experiments carried out to compare the decomposition behaviour versus pressure caused by a collimated irradiating beam, with one that was focussed. These products (as a ratio to  $\text{C}_2\text{H}_4$ ) are displayed in Table 4.1-2 (collimated beam) and Fig. 4.1-8 (focussed beam). It is immediately evident that, for conditions of a collimated beam irradiating at high fluence on  $P_{18}(9\mu\text{m})$ , additional products do not appear in the same abundance as for

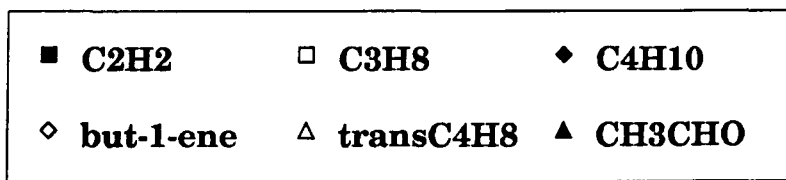
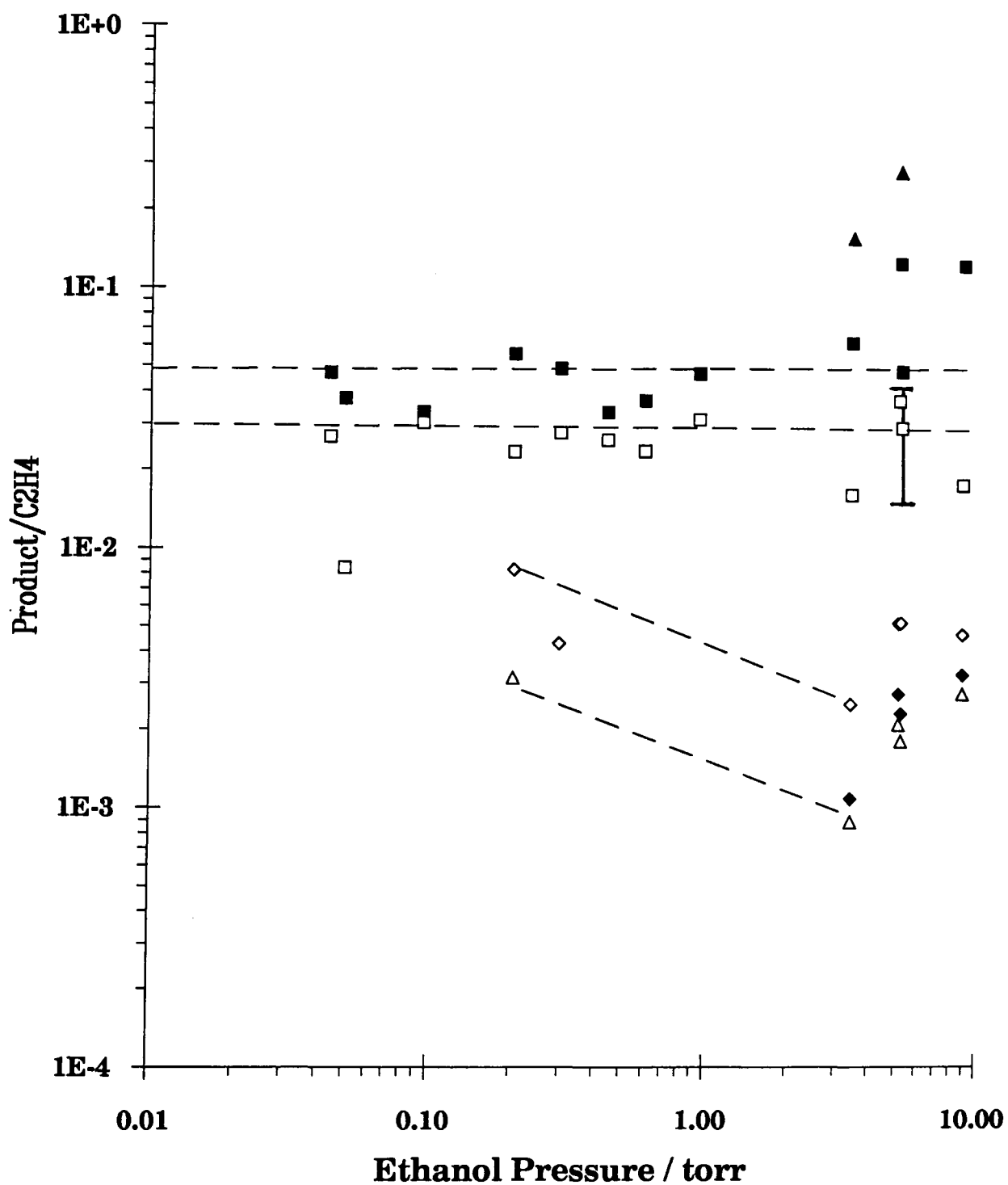
Product	Variation with F or P	Comparison of Yields	Figure Number	Comments
$C_2H_4$	F	$R_{20}(9) < P_{18}(9)$	4.1-1	$P_{18} = 10^{7.3}R_{20}$
$C_2H_6/C_2H_4$	F	$R_{20}(9) > P_{18}(9)$	4.1-2	
$CH_4/C_2H_4$	F	$R_{20}(9) > P_{18}(9)$	4.1-3	
$C_2H_6/C_2H_4$	F	$R_{20}(9) < P_{18}(9)$	4.1-6	
$CH_4/C_2H_4$	P	No Difference	4.1-7	

**Table 4.1-1** Ethanol: Summary of the effect of irradiating wavelength on yield

Reactant Pressure /torr	$C_2H_2/C_2H_4$	$C_3H_8/C_2H_4$	$C_4H_{10}/C_2H_4$	but-1-ene/ $C_2H_4$
0.050	-	$1.99 \times 10^{-2}$	-	-
0.053	-	$2.420 \times 10^{-2}$	-	$1.040 \times 10^{-2}$
1.082	$2.850 \times 10^{-3}$	$1.96 \times 10^{-2}$	$3.84 \times 10^{-4}$	$3.662 \times 10^{-4}$

**Table 4.1-2'** Ethanol: The effect of a collimated beam on the secondary products (as a ratio to ethene) as a function of reactant pressure. Fluence was constant at  $(9.4 \pm 0.1)J/cm^2$ .

**Fig. 4.1-8 Ethanol: Effect of pressure of the ratio on the product yield to that of C<sub>2</sub>H<sub>4</sub> for a focussed beam with a fluence of ~17,600 J/cm<sup>2</sup> at P18 (9 μm)**

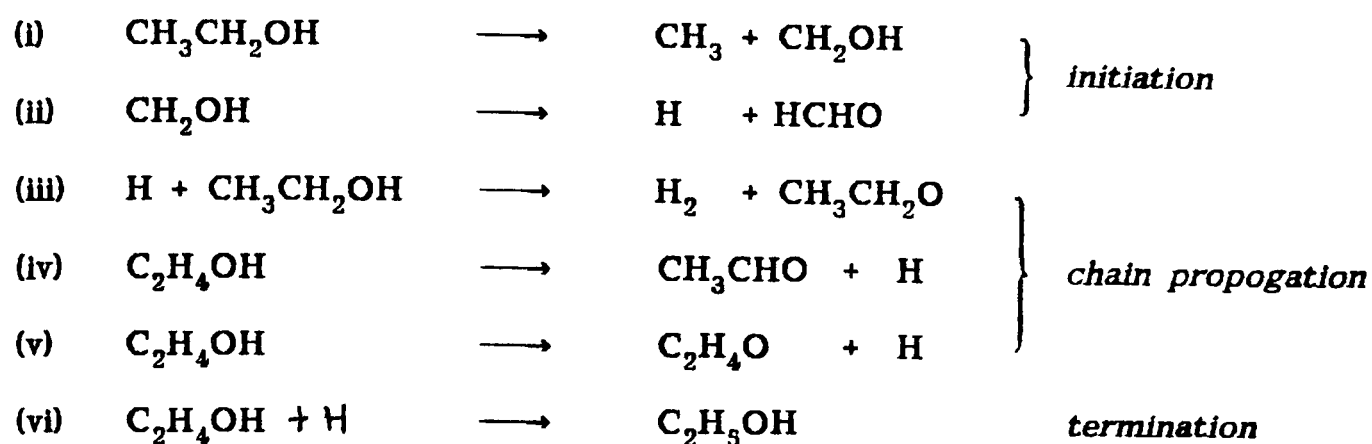


focussed conditions, although the values for the ratio  $C_3H_8/C_2H_4$  are approximately the same. For focussed conditions,  $C_4H_{10}/C_2H_4$ , but-1-ene/ $C_2H_4$ , and *trans*-but-2-ene/ $C_2H_4$ , follow the same trend. The path(s) leading to their production consequently have similar activation energies. The same observation is made for the path(s) leading to the production of  $C_3H_8$  and  $C_2H_2$ . Furthermore,  $C_3H_8/C_2H_4$  and  $C_2H_2/C_2H_4$  are independent of pressure: the  $C_3H_8$  yield is 56% of the  $C_2H_2$  yield. This implies that  $C_3H_8$  and  $C_2H_2$  production requires  $C_2H_4$ , and are formed via a process that is neither hindered nor accelerated by collisions to any other degree than that which affects  $C_2H_4$  production. It is of interest to note that Back *et al.* (8) detected both propane and propene (propane dominated), Bhatnagar (9) on the other hand, also measured only propane. Furthermore, there is cross agreement between all of us in that the proportion of propane to ethene at 1 torr is 43%.

For pressures greater than 2 torr and the focussed system,  $CH_3CHO$  (acetaldehyde),  $C_4H_{10}$ , but-1-ene, and *trans*- $C_4H_8$  increase with respect to  $C_2H_4$  with increasing pressure. This implies that these products which result from collision modified reactions have higher average energies (and hence faster  $k_{uni}$ ) than for collision-free decomposition.

The detection of acetaldehyde only at high pressures and high fluence, combined with the inability to detect ethylene oxide ( $C_2H_4O$ ), is consistent with the conclusion that laser pyrolysis of ethanol proceeds with a different mechanism than thermolysis. Barnard *et al.* (88) thermally excited ethanol, and detected hydrogen and acetaldehyde. They proposed the following mechanism; initiation by (i) then (ii), followed by a chain propagation (iii), (iv) or (v), and termination (vi). Ethylene oxide is a by-product of (iii). Detection of thermolysis products would only be expected perhaps at high pressures of

reactant undergoing laser pyrolysis, since the many collisions could provide thermalisation.



The results of Shaw (6) concerning C<sub>4</sub> hydrocarbon production on irradiation of an empty cell could not be repeated. For further exploration, ethanol was irradiated in the 8cm long, OA cell on R<sub>20</sub>(9 μm) and P<sub>18</sub>(9 μm), at various pressures and fluences (focussed and collimated systems). C<sub>4</sub> hydrocarbons were only detected following high fluence, high pressure conditions: the noise baseline was equivalent to 1.5 x 10<sup>-2</sup>mtorr of C<sub>4</sub>. To reveal whether or not surface reactions on the windows were the cause of C<sub>4</sub> production, the special cell described in Section 2.2 was irradiated at full fluence for 1260 pulses. The cell contained three, 15mm x 3mm, NaCl flats (increasing the NaCl surface area four times) and 50mtorr of ethanol. The fluence gradient over the length of the cell was of course greatly modified by absorption and reflection at the salt windows. The only measurable products were methane, ethane and ethene.

#### 4.1.7 Discussion

Listed below are some decomposition paths (molecular elimination [4.1-1] to [4.1-3], and bond fission [4.1-4] to [4.1-8]) with related heats of reaction for ethanol, which, *a priori*, may be accessible with IR irradiation. The threshold energies of the molecular elimination channels will be substantially higher

than the enthalpy changes, but for the bond fission channels, the thresholds will be close to the enthalpies. According to Fig.1.4-4, excitation to 1.5 times that of the dissociation energy is likely. Table 4.1-3 summarises the Arrhenius parameters found in the literature. The dehydration channel has the lowest activation energy, and so the allowable overexcitation is approximately 213kcal/mol. Hence, with no further reaction, all the listed reactions [4.1-1] through to [4.1-8] will be allowed. These and further reactions will be possible if the total activation energy does not exceed 213kcal/mol.

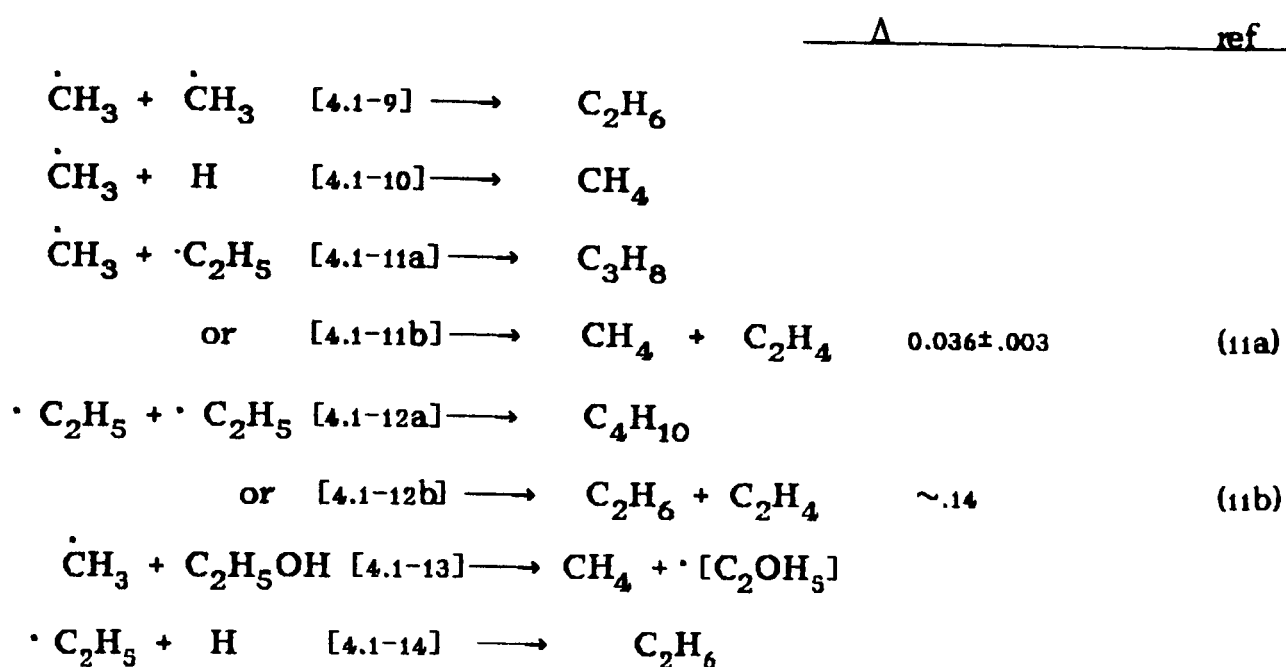
	$\Delta H_{300}^{\circ}$ kcal.mol <sup>-1</sup>		
<b>Molecular elimination:</b>			
$C_2H_5OH + nh\nu$ [4.1-1] $\longrightarrow$ $C_2H_4 + H_2O$	10.9		
[4.1-2] $\longrightarrow$ $CH_3CHO + H_2$	26.1	(9)	
[4.1-3] $\longrightarrow$ $CH_4 + HCHO$	11.6	(9)	
 <b>Bond fission:</b>			
[4.1-4] $\longrightarrow$ $\dot{C}H_3 + CH_2OH$	84.0		
	82.0	(9)	
[4.1-5] $\longrightarrow$ $H + \dot{C}H(CH_3)OH$	93.0 $\pm$ 1.0		
[4.1-6] $\longrightarrow$ $H + \dot{C}H_2CH_2OH$	98.1		
[4.1-7] $\longrightarrow$ $\cdot C_2H_5 + OH$	102.6 $\pm$ 1.4	(3)	
	102.4	(4)	
	100.1 $\pm$ 2.3	(1)	
	100.7	(2a)	
[4.1-8] $\longrightarrow$ $H + CH_3(CH_2)\dot{O}$	104.2 $\pm$ 1.0		

By comparing the magnitudes of the heats of formation of the bond fission channels, it must be expected that when the higher energy channels are accessed, there will be an abundance of methyl radicals: the activation energy for bond fission channels will be similar to their endothermicities.

REACTION	$E_{\text{act}} / \text{kcal.mol}^{-1}$	$A / \text{s}^{-1}$	REF
[4.1-1] $\text{C}_2\text{H}_4 + \text{H}_2\text{O}$	68.26	-	6
	71.00	-	23
	76.50	$10^{14}$	24
	71.20	$1.7 \times 10^{14}$	25
[4.1-2] $\text{CH}_3\text{CHOH} + \text{H}_2$	112.1	$3.1 \times 10^{14}$	25 (calculation)
[4.1-3] $\text{CH}_4 + \text{HCHO}$	~84	-	This work
[4.1-4] $\cdot\text{CH}_3 + \cdot\text{CH}_2\text{OH}$	82.0	$10^{16.4}$	9, 23

**Table 4.1-3** Summary of Arrhenius Parameters

Ethyl production will only be evident at the highest fluences. That is, when the population density of molecules with energies in the order of 100 kcal/mol becomes more significant. The possibility of the following radical reactions will be discussed.



Of the previous work on ethanol, and the work carried out concurrently with this research, Back *et al.* (9b) showed that reaction [4.1-7] existed by measuring OH at high fluence. Back (9) also proposed a unimolecular channel [4.1-2], after proving that the addition of an O<sub>2</sub> diluent did not inhibit acetaldehyde (CH<sub>3</sub>CHO) production: Arrhenius parameters as calculated by Ref. (25) are in Table 4.1-1. The diluent, however, did adversely affect the ethane yield, to which Back inferred that methyl radicals had been scavenged, so suppressing reaction [4.1-9].

The results have clearly demonstrated that the molecular elimination channel [4.1-1] is the least endothermic leading to preferential production of ethene, and that the extent of fragmentation increases at higher pressures (Fig. 4.1-4).

Ethene was by far the major product in all the work. Ethane yields were compared with those of ethene in both the focussed and unfocussed systems

(Figs. 4.1-2 and 4.1-6). Previous indications (7) were that for a focussed system, the ethane/ethene ratio might well decrease as the ethanol pressure tended towards the lowest pressures. Repetition under similar (but not identical) conditions confirmed the indication (Fig. 4.1-6). For the same pressures, the ratio is much reduced in the unfocussed system (ie. at lower peak fluence, higher average) and also demonstrates the decrease mentioned above. The ethene yield was also compared to methane, and it was observed that the ratio methane/ethene increased with both pressure (Fig. 4.1-7) and fluence (Fig. 4.1-3).

Ethane is expected to come from recombination of methyl radicals [4.1-9] and the radicals to come from fission of the high energy C-C bond [4.1-4]. Because of the strength of the C-C bond, products from the fission reaction (and hence methyl radicals) will be more abundant under high fluence conditions. It is therefore not surprising that the ethane yield increases with fluence.

Another suggestion for an additional ethane channel would be as follows. From the list of possible fission channels at the beginning of this section, other research has already pointed to the existence of reactions [4.1-1], [4.1-4] and [4.1-7]. By comparing the endothermicities (and hence activation energies) of the bond fission channels, the inference is that [4.1-5] and [4.1-6] also occur. If so, they will occur more than [4.1-7], and more H will be produced than  $\cdot C_2H_5$ . Thus [4.1-14] could statistically become more probable than [4.1-9]. Channels [4.1-5] and [4.1-6] can not be proven, however, since any products that might result from these steps (other than ethane) were not looked for.

Methane was also expected to come from methyl radicals, but via hydrogen abstraction [4.1-13]. However, if it is first assumed the only alkyl radicals present are  $\text{CH}_3$ , that methyl recombination is the sole source of ethane, and if the actual ethane yield is then used to calculate the initial methyl concentration (using known rate constants for methyl recombination *viz.*  $k_{\infty} = 2.78 \times 10^{11} \exp(154/T)$  Ref(3)), then we find that the observed methane yield is much greater than if all the methyl radicals went to form methane. The calculation treats the chemistry as being a competition between first order (producing  $\text{CH}_4$ ) and second order (producing  $\text{C}_2\text{H}_6$ ) reactions. The conclusion is true, whether or not it is assumed that the radicals remain in the irradiated volume. If the initial premises are wrong, and there is a further channel producing ethane, then the actual methyl concentration will be even less than that calculated here. It must be concluded that there is a further minor channel, possibly molecular [4.1-3]. The proposed molecular channel suggests the presence of formaldehyde ( $\text{HCHO}$ ), but detection of this product was not attempted in this work.

An alternative, viable, possibility is to consider that the reaction does not take place at room temperature, and is a non-equilibrium process. For example, cyclobutanone has been shown (17) to experience an A temperature of approximately 1600 K at low pressures (0.5 torr). The system was more thermally equilibrated at high pressures, where the A temperature was approximately 830 K. At low pressures of ethanol (50 mtorr) theoretical ratios become comparable to those observed if it is assumed that the temperature in the irradiated volume rises to 791 K, or 490 K if the radicals spread throughout the vessel. Temperatures in excess of 2500 K are calculated to be required at higher pressure (5.1 torr), but the calculation depends on a large, and therefore unreliable, extrapolation of the rate coefficients to these high temperatures.

There is no reason to select only one of the above possibilities, and in reality both elevated irradiated volume temperatures, and additional channels for  $\text{CH}_4$  may well exist.

Recently (1989/90), Goodale *et al.* (81) performed laser pyrolysis tests on deuterated ethanol,  $\text{CH}_3\text{CD}_2\text{OH}$ , in order to more effectively establish the decomposition mechanisms. They showed that all ethene came from dehydration [4.1-1], the water being formed <sup>from</sup> the hydroxyl group and an H from the methyl group. Further, that the isotopic form of acetaldehyde [4.1-2] indicated the occurrence of a concerted elimination of HD across the CO bond i.e. there is no involvement of the methyl hydrogens. Also, [4.1-3] occurs by a concerted molecular elimination of the methyl group with the hydrogen of the hydroxyl group. Finally, the fission reaction [4.1-4] was explained to produce only ethane [4.1-9], hence excluding ethane formation by [4.1-14], methane formation by hydrogen abstractions [4.1-10] and [4.1-13], and propane formation by recombination with ethyl radicals [4.1-11a]. Furthermore, deuterated forms of ethane ( $\text{CH}_3\text{CH}_2\text{D}$ ) were detected only at high pressures (together with  $\text{CH}_3\text{CH}_3$ ).

The similarity of the fluence dependence of  $\text{CH}_4/\text{C}_2\text{H}_4$  to that of  $\text{C}_2\text{H}_6/\text{C}_2\text{H}_4$  points to similar activation energies: with the assumption that  $\text{C}_2\text{H}_6$  primarily comes from methyl recombination, then the activation energies for the two paths will be similar to the endothermicity of path [4.1-4] i.e. 84 kcal/mol (according to Back (9), two paths whose activation energies were 60kJ/mol (14.3kcal/mol) apart were "similar"). This proposed value for the activation energy of channel [4.1-3] is in agreement with that suggested by Back *et al.* (9b).

In summary, the observed products may be explained as follows:

**Ethene** arises from the dehydration channel [4.1-1].

**Ethane**; it is difficult to suggest a source for this product other than the recombination of methyl radicals formed in [4.1-3]. The conclusion is supported by evidence that ethane formation is suppressed by radical scavengers (9).

**Methane** arises from the molecular elimination channel [4.1-3] rather than by H abstraction from ethanol by methyl radicals. Evidence for this was a lack of response of the methane yield to radical scavengers (9); and through the deuterated ethanol work of Goodale *et al.* (81). Calculations carried out in the present work supports this evidence, by showing that the observed  $\text{CH}_4/\text{C}_2\text{H}_6$  ratios are far higher than those expected on the assumption that both are formed from methyl radicals. Further, it is argued in this work, that the activation energy for this channel is in the order of 84 kcal/mol.

**Acetaldehyde** arises from a molecular, rather than a radical, channel since it has been shown that radical scavengers have no effect on its yield (9b); the proposed channel is [4.1-2].

**Acetylene** is thought to arise from secondary decomposition of hot ethene during a single pulse (9b).

**Propane**; it is difficult to suggest a source for this product other than perhaps through a reaction between hot ethene and methane.

**C<sub>4</sub>** products may arise from radical recombination as in step [4.1-12], and, analogously to steps proposed for ethene and propene in butan-2-ol and

ethene in propan-2-ol, may also arise via vinyl radicals ( $C_2H_3$ ) which form by water elimination from the  $CH(CH_3)OH$  and  $CH_2CH_2OH$  radicals of the carbon-carbon fission steps [4.1-5] and [4.1-6].

## 4.2 PROPAN-2-OL

Propan-2-ol was irradiated at 1.65 Hz using the  $R_{14}$  (9  $\mu$ m) line. All experiments were performed with multi-longitudinal mode pulses. The major product expected, as a result of unimolecular dehydration, is propene. The products were found to be methane, ethane, ethene and propene. For completeness, both the Carlo Erba and Pye Unicam gas chromatographs were used in the analysis. The Carlo chromatograph ran on a programme: 80°C for 6 minutes, followed by a 20°C/min rise to 150°C where it was held for 7 minutes, after which there was a 5 minute cooltime. The Chromosorb column was used with 50ml/min flow rates, and the Poropak column with the same flow rates but a different programme: 70°C for 13 minutes, followed by a 20°C/min rise to 200°C where it remained for 10 minutes, after which there was a 5 minute cool time. The conditions for the Pye chromatograph were the same as those for hexan-2-ol. Propanol was checked for purity on both columns and was found not to need additional purification. Cyclohexane was chosen as the diluent (n-hexane was found to absorb strongly on this line); the sample/diluent ratio was 1/9.

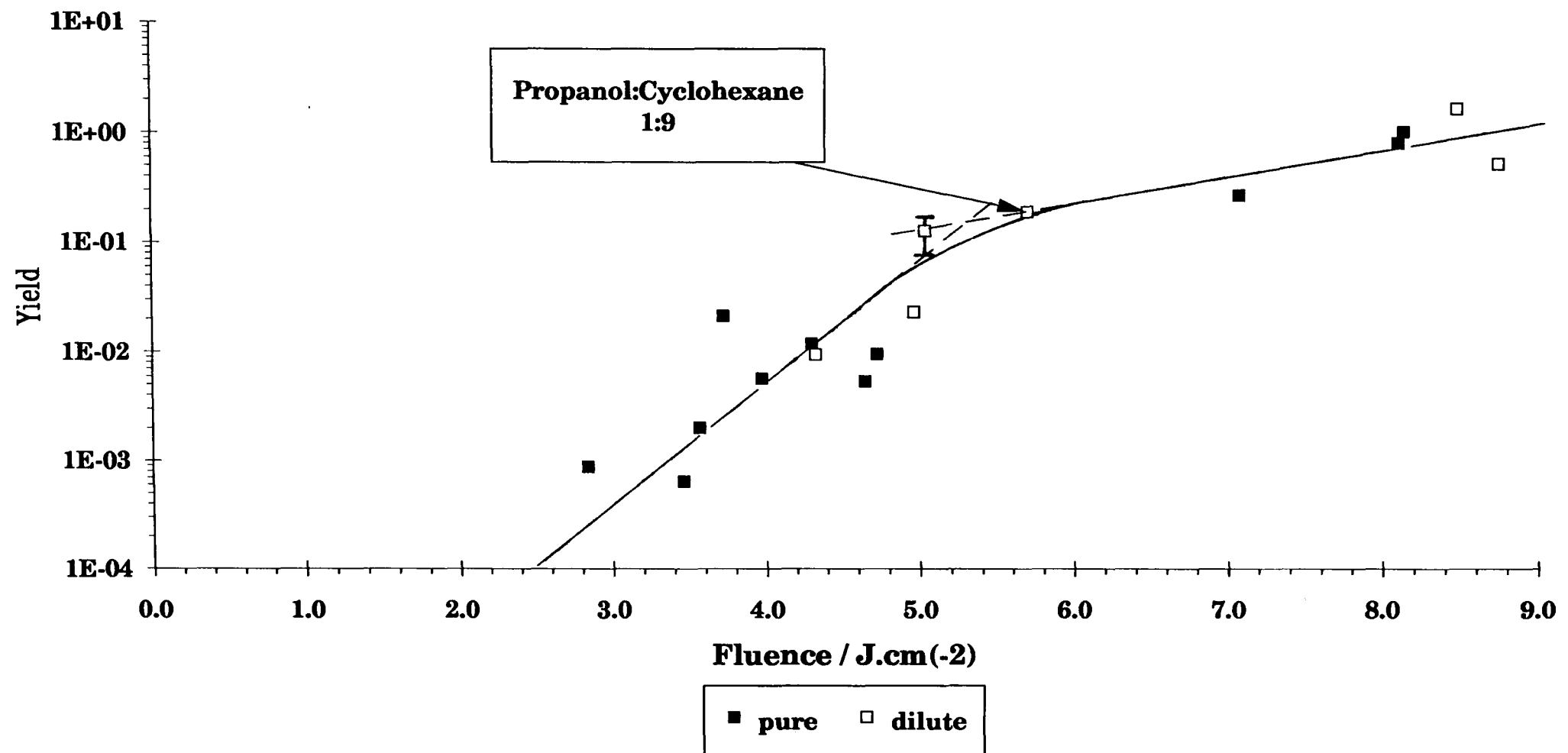
The second Carlo column (Poropak QS) was introduced in order to establish whether any propane was present; neither of the other columns resolved propane and propene. Furthermore, there had been occasional traces of a product in the  $C_6$  region, and it was wondered whether  $i$ - $C_3H_7$  radical reactions were creating 2,3-dimethylbutane and propane (see Discussion). However, propane was not detected, and the retention times of 2,3-dimethylbutane and the unidentified product did not coincide: The trace remained unidentified.

#### 4.2.1 Fluence Dependence and Effect of Diluent

Product yields were monitored as the fluence was varied for pure (50 mtorr) and dilute (5mtorr propanol plus 45mtorr cyclohexane) cases: The deconvoluted yields are compared in Fig.4.2-1 and Table 4.2-1.  $C_3H_6$  is the major product at all fluences and within the experimental scatter, it can be said that the dominant propene yields of the pure and dilute reactant were similar. This indicates that the extent of post-pulse, quasithermal reaction, following the first few collisions, is small.  $C_3H_6$  production per pulse in the irradiated volume increases with fluence (Fig.4.2-1). For fluences (F) less than  $5.4 J/cm^2$  the yield (Y) variation is approximately  $Y \propto 10^{1.1F}$ , while for higher fluences the fluence dependency reduces to approximately  $Y \propto 10^{0.23F}$ .

The yields of the other products, methane, ethane and ethene, are given as a fraction of  $C_3H_6$  (Table 4.2-1). Methane was only measured under high fluence, pure reactant conditions. Of these minor products, for all fluences, using the pure reactant, ethane was produced most abundantly. For the dilute reactant, the nature (of the most abundant of these other products) was dependent on fluence: *viz.* ethene at low fluence and ethane at high fluence. Of note, is that, at high fluence, unimolecular dehydration is most efficient for the dilute case: i.e. under collision-free conditions, the ratio  $C_2H_6/C_3H_6$  falls from  $8.37 \times 10^{-2}$  to  $6.48 \times 10^{-3}$  (deconvoluted data) when a mixture diluted in ratio 1:9 with cyclohexane is used. The ratio  $C_2H_4/C_3H_6$  also falls, but less steeply ( $7.63 \times 10^{-3}$  to  $2.79 \times 10^{-5}$ ). As has been discussed already, the addition of a diluent is only expected to have an effect if thermal effects were/are in any way contributing to the formation of the products. In such an event, the (inert) diluent will suppress thermal build-up of the yield. For propanol, the reduction of the relative yield of the higher energy channels is understandable in terms of being caused by a decrease in the average level of excitation of the decomposing molecules.

**Fig. 4.2-1 Propanol: Comparison of the effect of pure & dilute reactant on C<sub>3</sub>H<sub>6</sub> yield (deconvoluted data) as a function of fluence at 50 mtorr total pressure**



FLUENCE / J.cm(-2)	Pure Propanol, Deconvoluted Yields			
	Ratios To C3H6			TOTAL C3H6
	CH4	C2H6	C2H4	
2.84				8.696E-04
3.46				6.387E-04
3.56				1.993E-03
3.72				2.126E-02
3.97		4.696E-02		5.657E-03
4.29		3.072E-02		1.192E-02
4.64				5.335E-03
4.72				9.552E-03
7.05	2.624E-02	1.892E-01	6.765E-03	2.687E-01
8.07		1.006E-01	2.498E-03	7.914E-01
8.10	1.591E-02	8.373E-02	7.629E-03	1.000E+00
	Dilute Propanol, Deconvoluted Yields			
4.32			4.673E-03	9.430E-03
4.96				2.334E-02
5.02				1.276E-01
5.68				1.888E-01
8.44		6.484E-03	2.792E-05	1.627E+00
8.71		2.560E-02		5.104E-01

**Table 4.2-1** Propan-2-ol: The effect of fluence and cyclohexane diluent on the ratio of minor product to C3H6 yield (deconvoluted data) for 50 mtorr reactant irradiated with the R14 (9 μm) line.

There is very little else that can be noted apart from the fact that the total amount of product other than the primary product, is greater for the pure case, and that  $C_2H_4/C_3H_6$  (dilute case) decreases as the fluence increases.

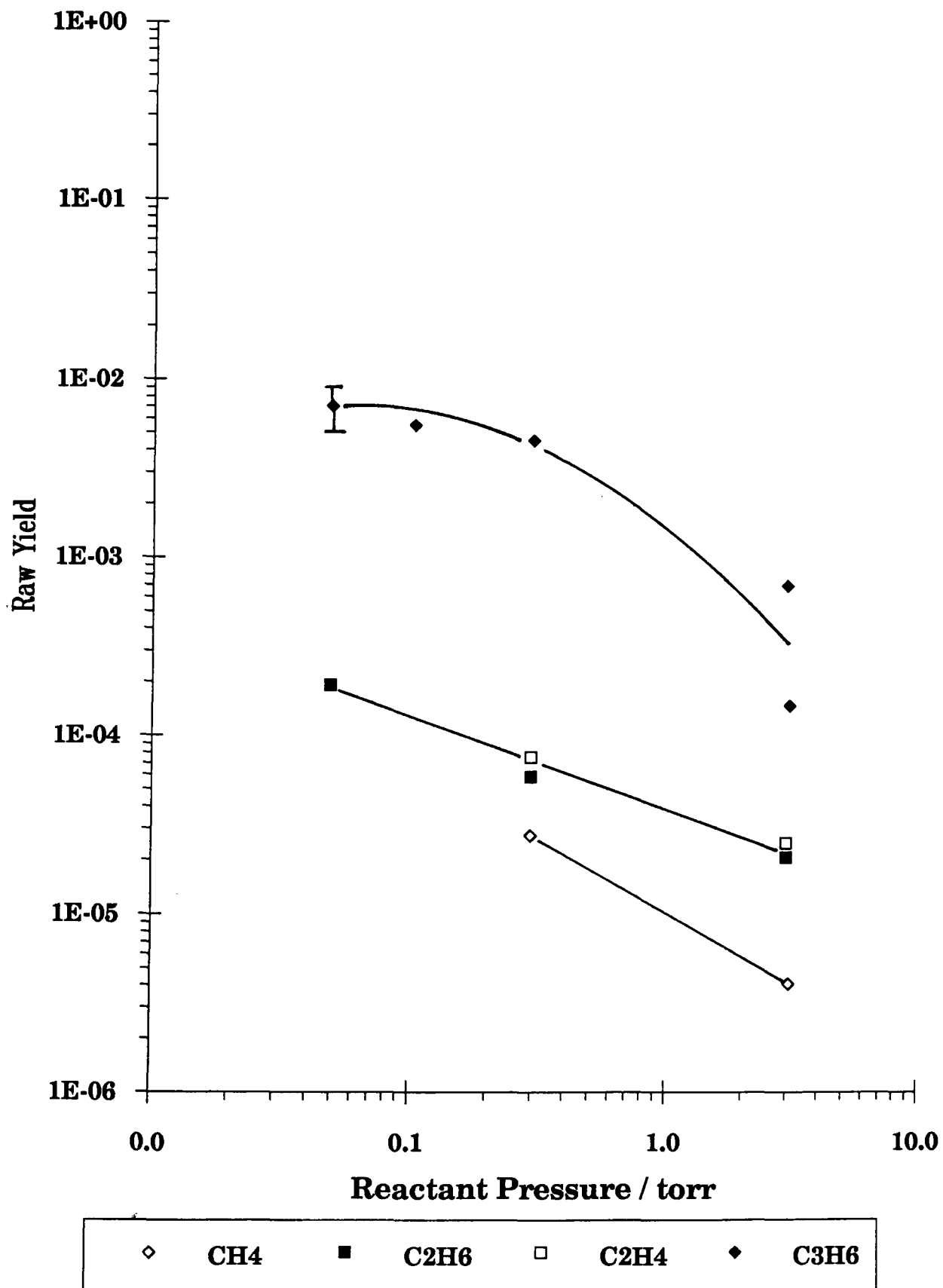
#### 4.2.2 Pressure Dependence and Effect of Diluent

From the graph of the undeconvoluted yields versus pressure (Fig.4.2-3), propene is seen to be the dominant product (over the range of pressure used). For the illustrated situation of varying pressure of pure reactant irradiated at constant medium fluence ( $4.8 \pm 0.1 \text{ J/cm}^2$ ), the yields are seen to decrease as the reactant pressure increases. This is an expected trend, when as the pressure increases, the role of collisions becomes more significant and large compared to the laser up-pumping: molecules are less likely to reach even the minimum activation energy, then, only those molecules with a fair excess in energy will have  $k_{uni}$  fast enough (compared to the collision frequency) to actually result in a product. For the dilute reactant,  $CH_4$  was not detected at all,  $C_2H_4$  was not measured for reactant pressures above 49 mtorr, and  $C_2H_6$  was only detected up to the 52 mtorr pressure data point.

#### 4.2.3 Discussion

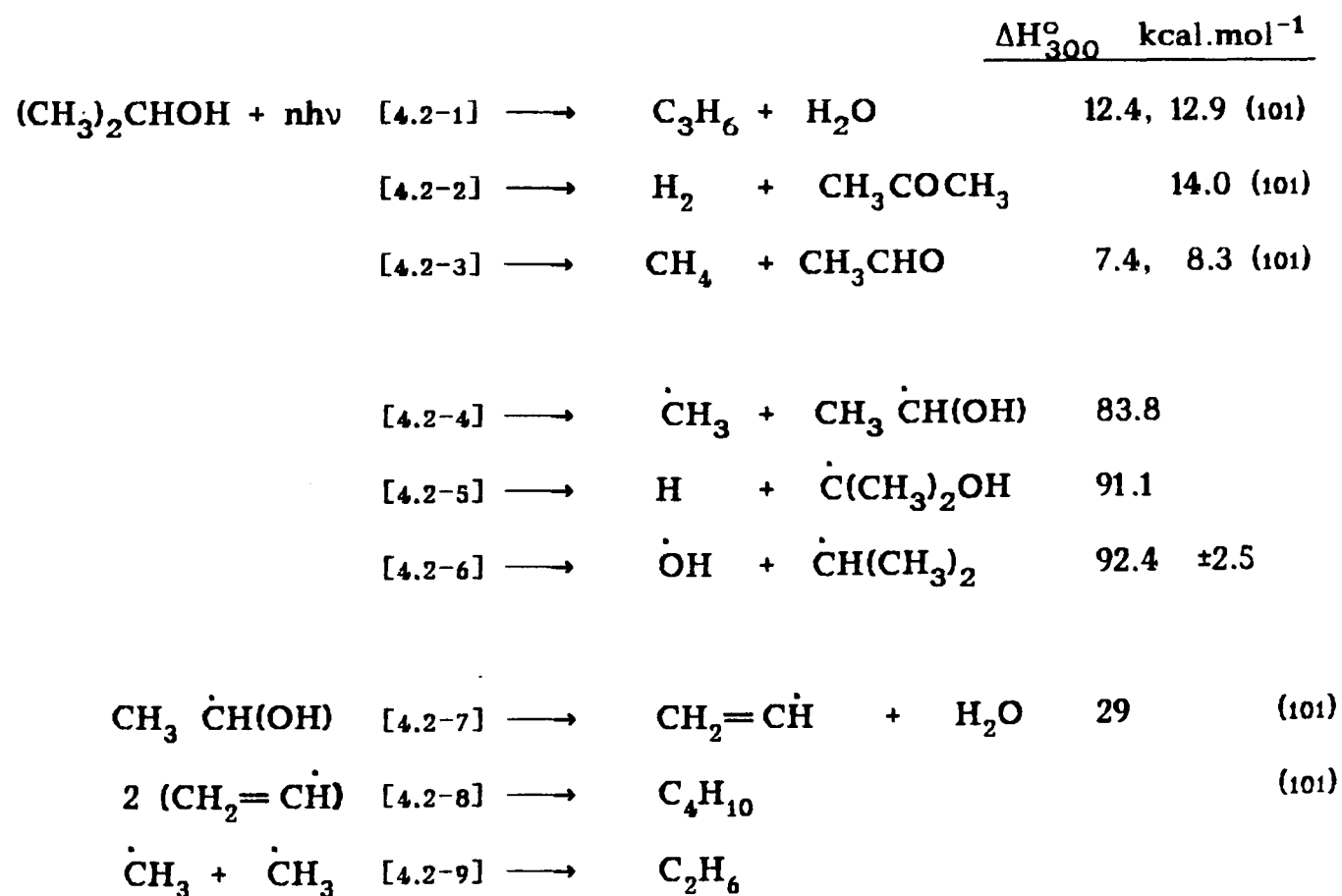
Listed below are some decomposition paths (molecular elimination and bond fission) with related heats of reaction for propan-2-ol, which, *a priori*, may be accessible with IR irradiation. According to Fig.1.4-4, excitation to 1.8 times that of the dissociation energy is allowable. Reference to the Arrhenius parameters for the least energetic (molecular dehydration) channel in the literature, have been made by Danen (23) and Zhitneva *et al.* (27). Danen estimated that  $E_a=67 \text{ kcal/mol}$ , by analysing the trend in activation energies for dehydrochlorination of 2-chloro-2-methylpropane, 2-chloropropane, and chloroethane, and extrapolating the same trend from the known activation energy of *t*-butanol ( $E_a=61.6 \text{ kcal/mol}$ ) (26). Zhitneva said that for *n*-propanol,

**Fig. 4.2-3 Propan-2-ol: Effect of pressure on yield (raw data) for pure reactant irradiated at a fluence of  $4.8 \pm 0.1 \text{ J.cm}^{-2}$**

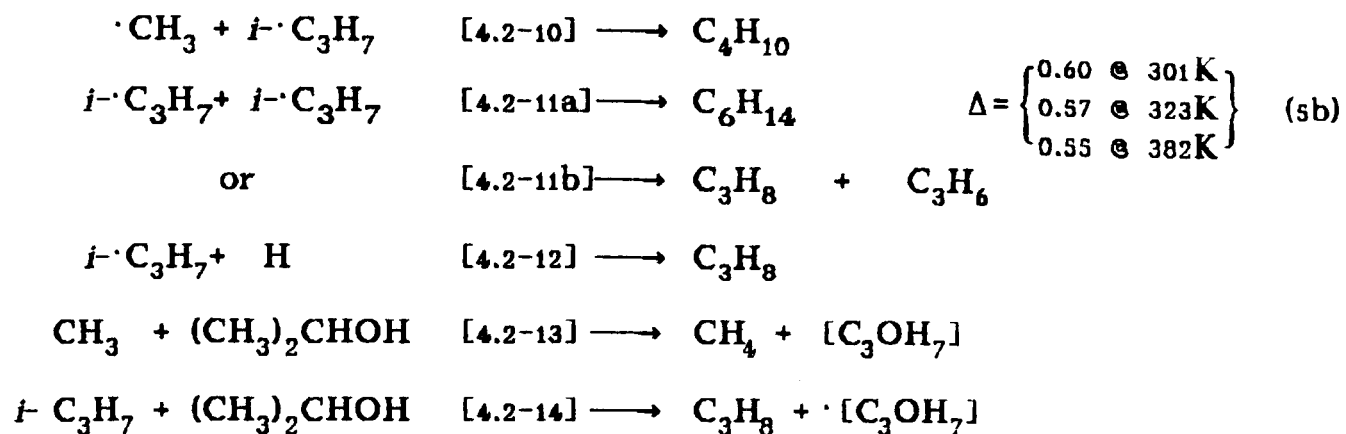


$k=10^{13.4}\exp(-68493/RT)s^{-1}$ , that the activation energy for propan-2-ol is about 3.82 kcal/mol less, and that  $A_{\text{iso-propanol}}/A_{\text{n-propanol}}$  is 3. Hence for propan-2-ol (*iso*-propanol)  $E_a=64673$  cal/mol. The value suggested by Zhitneva for the difference in activation energy is because  $\alpha$ -methylation has been shown to cause this level of decrease between 2,3-dimethylbutanol and 3,3-dimethylbutanol. The likely overexcitation thus becomes roughly 123 kcal/mol, theoretically permitting all the reactions [4.2-1] through [4.2-5] if there are no further reactions. These and further reactions, will be possible if the total activation energy does not exceed 123 kcal/mol.

By analogy with ethanol, three molecular decomposition channels may be relevant [4.2-1] to [4.2-3]. In addition, several bond fission ([4.2-4] to [4.2-6]) and radical recombination ([4.2-7] to [4.2-9]) processes can be considered.



Other paths that will be briefly discussed are:



Unimolecular dehydration described by [4.2-1] is the dominant process, and the effect of diluent on a collision free sample irradiated at high fluence is to reduce the yield of the products from the higher energy channels. Furthermore, minor product yields are not detected at low fluence, which is consistent with the idea that channels of higher energy than dehydration cannot be accessed at low excitation energy.

As mentioned earlier, an attempt was made to identify the product which caused occasional chromatograph traces in the  $\text{C}_6$  region. In doing so, the chance that  $i\text{-C}_3\text{H}_7$  [4.2-6] radical reactions were creating 2,3-dimethylbutane [4.2-11] and propane ([4.2-11b], [4.2-12] and [4.2-13]) was explored. However, propane was not detected, and the retention times of 2,3-dimethylbutane and the unidentified product did not coincide.

Lack of detection of these products is understandable for the following reasons: Because of molecular symmetry, there are two separate, but identical bonds that can break, each leading to reaction [4.2-4]. In addition, since the  $\Delta\text{H}$  of reaction [4.2-5] is much greater than that of [4.2-4] it is reasonable to assume that there will be an abundance of methyl radicals. Hence, if produced,  $i\text{-C}_3\text{H}_7$  would preferentially recombine with  $\cdot\text{CH}_3$  [4.2-10] (rather than with another  $i\text{-C}_3\text{H}_7$  radical), and production of 2,3-dimethylbutane

[4.2-11a], propane [4.2-11b] & [4.2-12] or propene (through [4.2-11b]) would be highly improbable anyway. However, since  $C_4H_{10}$  was not detected either, the evidence is particularly strong that propyl radicals were not produced.

Propyl radical production [4.2-6] cannot be completely ruled out without first considering its decomposition to give propene. The heat of reaction for this is estimated to be 47 kcal/mol (Table 4.2-2), and, as for radical recombination and disproportionation reactions, the heat of reaction is expected to be similar to the activation energy. It would therefore seem that this too is forbidden, at least at low fluences, since the combined heats of reaction are above the allowable overexcitation (total  $\Delta H = 92+47=139$  kcal/mol).

Thus, under pure, collision-free conditions, the absence of propane, and 2,3-dimethylbutane, as well as  $C_4H_{10}$ , indicates a lack of 2-propyl radical formation through reaction [4.2-6]. It may therefore be concluded that, for laser pyrolysis, under the conditions used, C-O fission (reaction [4.2-6]) is not significant, and furthermore, because of a similarity in  $\Delta H$  values, channel [4.2-5] is also improbable. Similarly, fission of the O-H bond of the hydroxyl group has a much higher  $\Delta H$  than [4.2-6] (104.6 kcal/mol), so is not a viable path.

The occurrence of channel [4.2-2] would not have been detected, since neither  $H_2$  nor  $(CH_3)_2CO$  were measured.

The products are thus explained as follows:-

**Propene** as with ethanol arises from elimination of water [4.2-1] and is the main decomposition channel.

Radical Dehydrogenation Reaction	$\Delta H^{(a)} / \text{kcal.mol}^{-1}$
$\text{C}_2\text{H}_5 \rightarrow \text{C}_2\text{H}_4 + \text{H}$	38.7 <sup>(b)</sup>
$\text{n-C}_3\text{H}_7 \rightarrow \text{C}_3\text{H}_6 + \text{H}$	34.3
$\text{i-C}_3\text{H}_7 \rightarrow \text{C}_3\text{H}_6 + \text{H}$	47.0
$\text{s-C}_4\text{H}_9 \rightarrow \text{C}_4\text{H}_8 + \text{H}$	-38.0 <sup>(c)</sup>
$\text{t-C}_4\text{H}_9 \rightarrow \text{C}_4\text{H}_8 + \text{H}$	-33.0 <sup>(c)</sup>

**Notes:**

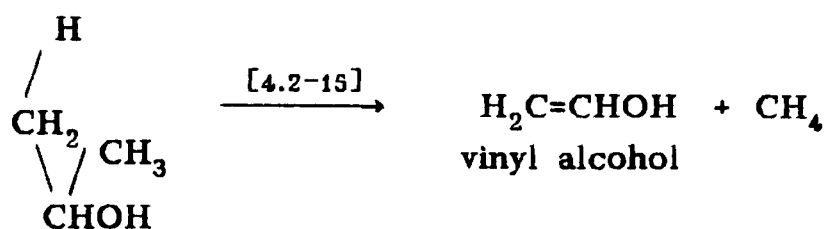
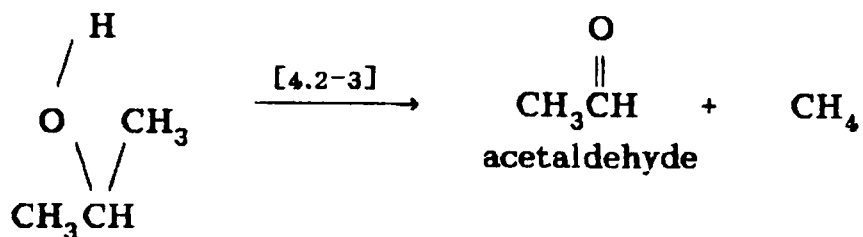
(a) Calculated using group contribution method (Appendix A3), and  $\Delta H_f^\circ$  values from Ref. (1).

(b)  $E_a = 42.2 \text{ kcal.mol}^{-1}$  (27)       $E_a = 42 \text{ kcal.mol}^{-1}$  (103)  
 $E_a = 41.8 \text{ kcal.mol}^{-1}$  (100)       $A = 10^{13.5} \text{ s}^{-1}$  (103)

(c) An average value of -1 is taken for  $\Delta H_f^\circ \text{ C}_4\text{H}_8$  since the actual value varies from 0 to -3 depending on the type of isomer.

**Table 4.2-2**      Estimated heat of reaction for radical dehydrogenation (for reference in later sections).

**Methane.** Under pure, collision-free conditions, methane was only detected at high fluence. One would expect, by analogy with the results from ethanol, that  $\text{CH}_4$  is formed in a molecular process [4.2-3] from a unimolecular channel of high activation energy. In addition [4.2-15] may be possible; both reactions are shown below;



No attempt was made though to detect either acetaldehyde or vinyl alcohol (this last product is unstable and rapidly isomerises to acetaldehyde). However, acetaldehyde was measured by Zhitneva *et al.* (101) from their focussed system. Because of the abundance of methyl radicals, the possibility of hydrogen abstraction between the radicals and reactant molecules, or reaction between the radicals and H, cannot be ignored.

**Ethane** is produced by process [4.2-4] followed by the recombination of  $\text{CH}_3$ . The extent of production of ethane shows that  $\text{CH}_3$  radical recombination (reaction [4.2-9]) dominates over hydrogen abstraction [4.3-13]. As to be expected, under collision-free conditions, fragmentation [4.2-4] does not occur at the lowest fluences where the higher energy channels cannot be accessed.

**Ethene.** No unimolecular source of ethene can be implied from these results, so the channel producing this product is not clear. However, Zhitneva *et al.*

(101), who used a focussed system, have proposed that ethene arises from vinyl radicals ( $C_2H_3$ ) produced from reaction [4.2-7]; as proof of this channel, they have measured butadiene ( $C_4H_6$ ) which is produced from two vinyl radicals [4.2-8].

### 4.3 BUTAN-2-OL

The major products, expected as a result of unimolecular dehydration, are but-1-ene, and *cis*- and *trans*-but-2-ene. Products were examined, following irradiation by multi-longitudinal mode pulses, of both pure and dilute (with cyclohexane) butan-2-ol on  $R_{24}$  (10 $\mu$ m) at a repetition rate of 2Hz. Both the Carlo and Pye chromatographs were used eventually, but when butan-2-ol was first analysed, only the Pye GLC was available. A new column was made to maximise the detectability of the  $C_2$ - $C_4$  hydrocarbons, while at the same time permitting reasonable resolution of the butene isomers. This column was 6m long, and was initially packed with 15.8% di-2-ethyl-hexyl sebacate and 8.6% bis-2-methoxy-ethyl adipate on chromosorb P (60/80 mesh); this column was then packed tighter, and a further 20cm of 30% sebacate was added. Optimum conditions were found to be a carrier flow rate of between 35 and 40ml/min, and an oven temperature of 37°C; resolution of the  $C_2$ s and also of the  $C_3$ s was very poor. After the Carlo oven became available, both ovens were used. The Carlo used the same flow rates and column as for the ethanol work (chromosorb 101 column, and an oven temperature of 40°C). It was used, primarily, to resolve the  $C_2$  hydrocarbons, but also as a cross check of the larger hydrocarbons. At this point, the column in the Pye oven was changed to the 2.9m column described in Section 4.1; the  $N_2$  flow rate was 20ml/min, and the oven temperature was 40°C.

Identification was made of methane, ethane, ethene, propane, propene, butane, but-1-ene, and *trans*- and *cis*-but-2-ene; an additional peak, occurring in the region of the  $C_5$  hydrocarbons, remained unidentified. A distribution of these product yields, as a result of irradiation of a collision-free sample, is shown in Fig. 4.3-1.

A further check was made on the possibility of the occurrence of radical

reactions (also see propanol). 3,4-Dimethylhexane would be the expected result of  $\cdot\text{C}_4\text{H}_9$  recombination, and its presence was searched for using a programme and the capillary column of the Carlo chromatograph. The oven was held at 40°C for 5 minutes, followed by a 10°C/min rise to 120°C where it was held for 10 minutes before starting a 5 minute cooltime. A sample of 3,4- dimethylhexane (117°C boiling point) was not available, so a sample of n- octane (126°C boiling point) was used as a reference instead. By comparing boiling points, one would expect the 3,4-dimethylhexane peak to occur between that of butan-2-ol (99.5°C boiling point) and n-octane ...no such peak was detected and it was concluded that 3,4-dimethylhexane was not a product.

#### 4.3.1 Fluence Dependence

Product yields were monitored as the fluence was varied for the irradiation of collision free (50 mtorr) samples. Several series of data were built up by re-examining pure butanol several times over a couple of years. The data has not been integrated into one set and are referred to subsequently as follows:

SERIES 1 - The original data made up of data taken from two sets of runs, carried out several weeks apart.

Series 2 and 3 were obtained at later stages in the work.

SERIES 2 - are the results of dilution experiments shown in Fig.4.3-2; data were gathered for both pure and dilute gas mixtures.

SERIES 3 - A series which used differing charging voltages (in combination with the  $\text{CaF}_2$  attenuators) in an attempt to accumulate more low fluence results. A straightforward reduction in the voltage (from 19kV to 17.5kV)

yielded lower but erratic fluences. The fluence was stabilised by increasing the helium flow rate so that the N<sub>2</sub>, CO<sub>2</sub>, He laser cavity rates were 1.2, 2.2, 8.0 litres/min rather than the nominal 1.2, 2.2, 6.0 litres/min. Photon-drag photographs were taken in order to determine the extent of pulse temporal changes. The results were presented and discussed in Section 2.1.2 (and Fig. 2.1-6). It was shown that a reduction in voltage lengthens the pulse (both FWHM and basewidth) and reduces the energy in the tail. Because of this change, the Series 3 experimental results should be considered with low weighting since this effect alone may change the photochemistry (the effect on photochemistry by changing the pulse shape is studied for a few of the molecules in this thesis). This method of fluence reduction is not recommended, but was nevertheless the only experimental technique available at the time which could hope to achieve the objective.

Absolute raw yields for the butenes and other products of the first series are displayed in Fig. 4.3-1. Absolute raw yields of Series 2 butene products are shown in Fig. 4.3-2.

The preliminary, entirely separate study of butanol which is known as Series 1, initiated extreme interest in the ratios of each butene to the sum of the butenes. The two sequences of experiments, that were carried out several weeks apart and which collectively form Series 1, concurred, demonstrating apparently anomalous behaviour at low fluence (Fig. 4.3-3). More specifically, the dominant *but-1-ene* decreases rapidly with *cis-but-2-ene* at low fluence as the fluence is decreased, such that *trans-but-2-ene* becomes dominant. A similar analysis of data (gathered during the main study) lacks clarity in the low fluence region, but hints at the same trend. While the Series 3 data tentatively show the same trend (but for the range 4.4 J/cm<sup>2</sup> to 4.7 J/cm<sup>2</sup> only), there is a higher, unknown degree of uncertainty in the data, because

**Fig. 4.3-1 Butan-2-ol: Variation of the yield (raw data - 1st series) as a function of fluence, for a (50 +/- 1) mtorr pure sample**

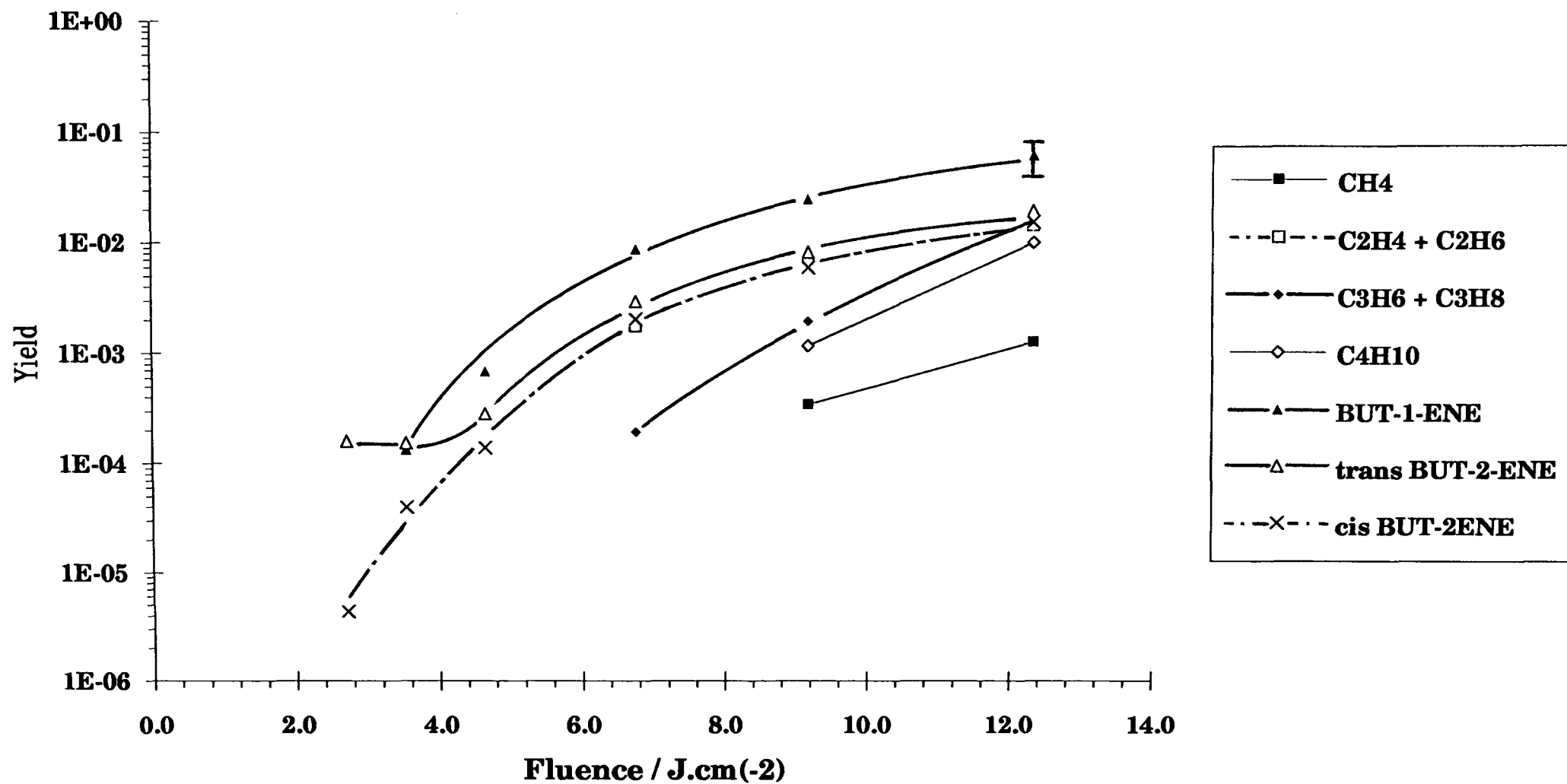


**Fig. 4.3-2 Butan-2-ol: Effect of an added diluent on yield (raw data - 2nd series) as a function of fluence at R24 (10  $\mu$ m). Reactant pressure was (50 +/- 2) mtorr for the pure series, and (4.7 +/- 1) mtorr for the dilute ('D' prefix)**

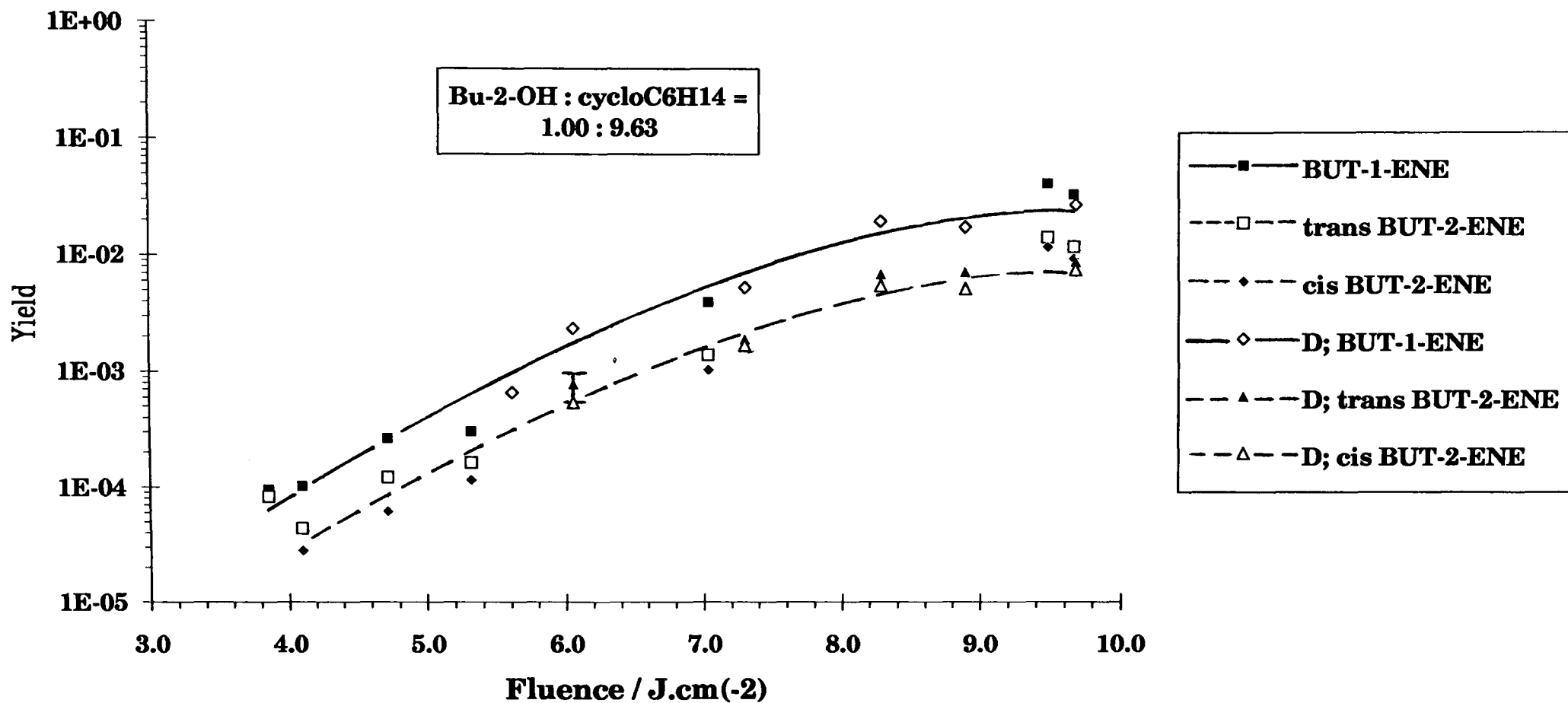
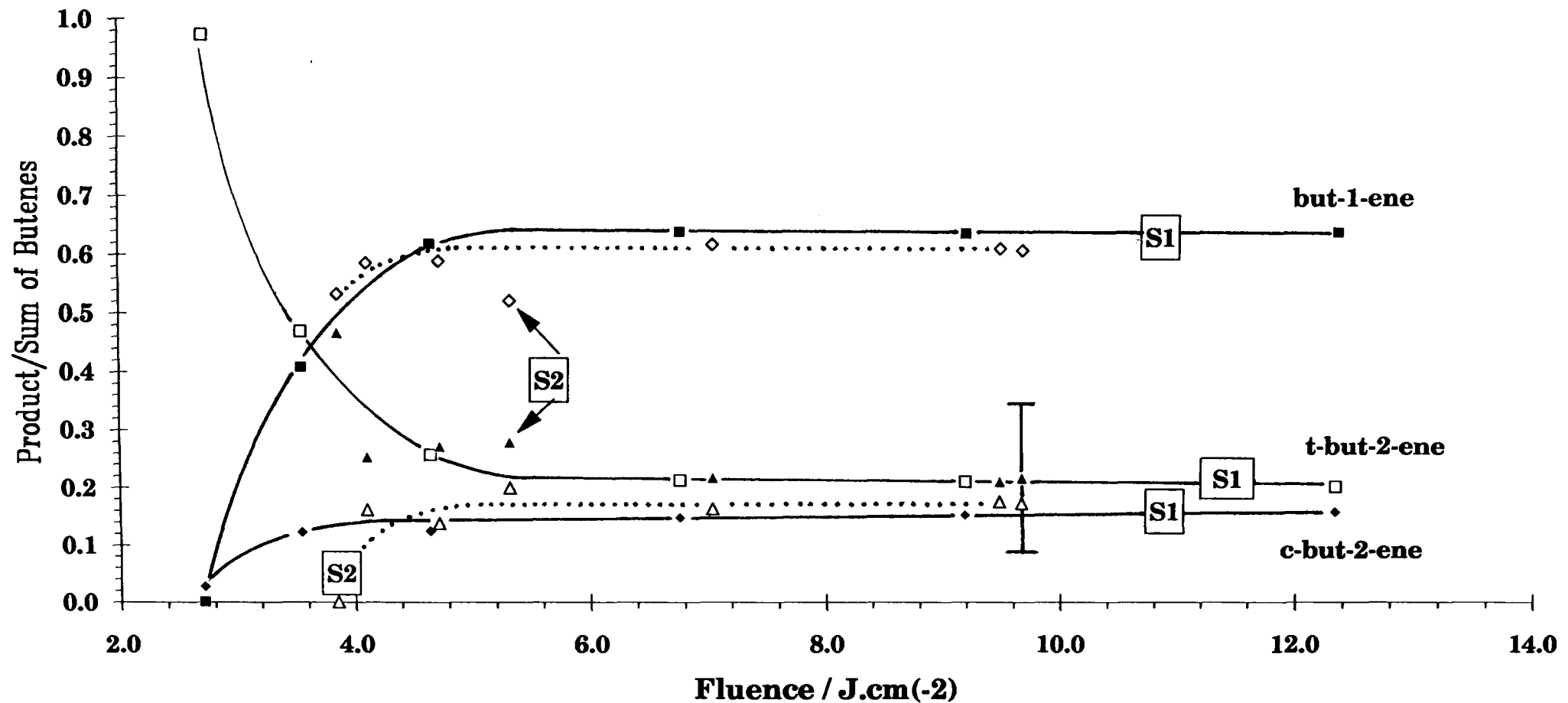


**Fig. 4.3-3 Butan-2-ol: Effect of diluent on the raw data yield ratio (product to the sum of butenes) as a function of fluence at R24 (10  $\mu\text{m}$ ). Reactant pressure was nominally 50 mtorr for the pure series S1 and S2**



of the manner in which the fluence was varied. Table 4.3-1 gives the ratios of each butene product to the sum of the butenes for each series; the  $N_2:CO_2:He$  flow rates used to vary the charging voltages in Series 3 are given, as are the resultant voltages.

A systematic error seems a likely explanation for the non-coincidence of the two "pure" series of absolute yield data (i.e. Series 1 data, and the "pure" data of Series 2; Figs. 4.3-1 and 4.3-2). The fluence stability for each data point of both series was better than  $0.05 J/cm^2$ . This would not account for the shift in data, even allowing for an additional 20% variation; a result of a combination of a different position of the input beam on the detecting crystal, and different calibration factors caused by ageing. Since the general trend of the ratios to total butene yield are similar versus fluence, the indication is that the systematic error lies in the yield values. It is entirely likely that it lies with the chromatograph detection system, since very frequent maintenance was required on this instrument. Furthermore, during the large time interval between the two series, the vacuum systems were given a major overhaul.

At high fluence, the ratio of but-1-ene to but-2-ene is about 3:2, as expected on the basis of free rotation about the  $C_1-C_2$  bond and about the  $C_2-C_3$  bond. This enables the formation of a planar, 4-centred transition state, involving either one of the three methyl H atoms or one of the methylene H atoms, leading to the production of but-1-ene or but-2-ene.

Conformational analysis offers further insight into the observed olefin ratios; the eclipsed and staggered conformations resulting from rotation about the  $C_2$  and  $C_3$  bond, and  $C_1$  and  $C_2$  bond, are illustrated in Figs. 4.3-4a and 4.3-5a respectively. In the transition state, the  $\pi$  bond is not yet complete allowing

Series	Fluence J/cm <sup>2</sup>	Ratio of Product to Sum of Butenes				comments e.g. charging voltage (+/- 0.2kV) & N <sub>2</sub> :CO <sub>2</sub> :He gas mix
		but-1-ene	trans but-2-ene	cis but-2-ene	fluence stability +/- J/cm <sup>2</sup>	
I Pure Butanol (raw data)	2.71	0.0000	0.9732	0.0268	0.09	
	3.54	0.4081	0.4694	0.1225	0.12	
	4.64	0.6186	0.2562	0.1252	0.10	
	6.75	0.6400	0.2124	0.1476		
	9.18	0.6376	0.2098	0.1526	0.37	
	12.33	0.6402	0.2012	0.1585	0.02	
II Pure Butanol (raw data)	3.85	0.5334	0.4666	0.0000		
	4.10	0.5863	0.2527	0.1610		
	4.72	0.5900	0.2716	0.1384		
	5.31	0.5219	0.2784	0.1996		
	7.03	0.6192	0.2177	0.1631		
	9.47	0.6132	0.2110	0.1758		
II Dilute Butanol (raw data)	6.61	1.0000	0.0000	0.0000		
	6.05	0.6404	0.2135	0.1461		
	7.30	0.5946	0.2151	0.1903		
	8.27	0.6116	0.2169	0.1715		
	8.89	0.5845	0.2417	0.1738		
	9.68	0.6245	0.2030	0.1725		

<b>II Pure Butanol (deconvoluted)</b>	3.85	0.6406	0.3594	0.0000	0.20	
	4.10	0.8089	0.1911	0.0000		
	4.72	0.6097	0.2200	0.1703		
	5.31	0.5329	0.2393	0.2278	0.033	
	7.03	0.6281	0.2087	0.1632	0.062	
	9.47	0.6225	0.2189	0.1586	0.013	
	9.66	0.6185	0.2259	0.1555	0.060	
<b>II Dilute Butanol (deconvoluted)</b>	5.61	1.0000	0.0000	0.0000	0.018	
	6.05	0.6722	0.1854	0.1424	0.047	
	7.30	0.6106	0.2066	0.1887		
	8.27	0.6084	0.2187	0.1729		
	8.89	0.5634	0.2592	0.1774		
	9.68	0.5919	0.2350	0.1731		
<b>III Pure Butanol (raw data)</b>	4.15	0.727	0.273	0.000	.01	17.2kV; 1.2:2.2:8.0
	4.34	0.567	0.240	0.194	.02	17.5kV; 1.2:2.2:8.0
	4.43	0.533	0.219	0.248	.01	17.8kV; 1.2:2.2:8.0
	4.79	0.641	0.207	0.153	.01	18.0kV; 1.2:2.2:8.0
	5.55	0.589	0.218	0.193	.04	19.0kV; 1.2:2.2:6.0
	7.58	0.602	0.223	0.176	.01	19.0kV; 1.2:2.2:6.0

**Table 4.3-1** Butan-2-ol: Ratios of the primary products to the sum of the primary products resulting from irradiation of 50 mtorr total pressure of gas using the R<sub>24</sub> (10 μm) line.

STAGGERED / SKEWED CONFORMS

ECLIPSED CONFORMS

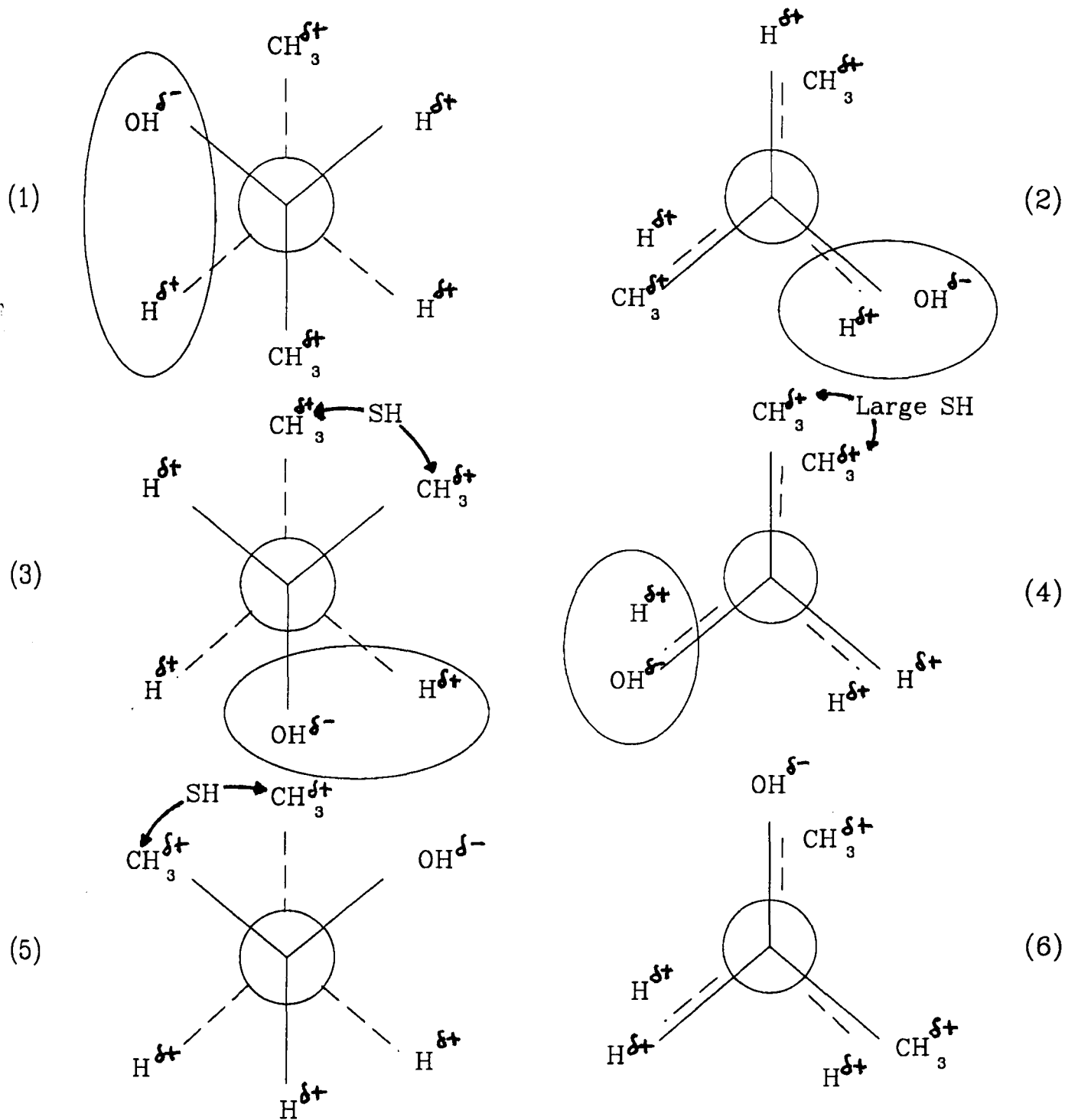


Fig. 4.3-4(a) Butan-2-ol: Eclipsed and staggered conforms resulting from rotation about the C<sub>2</sub> and C<sub>3</sub> bonds (SH = steric hindrance)

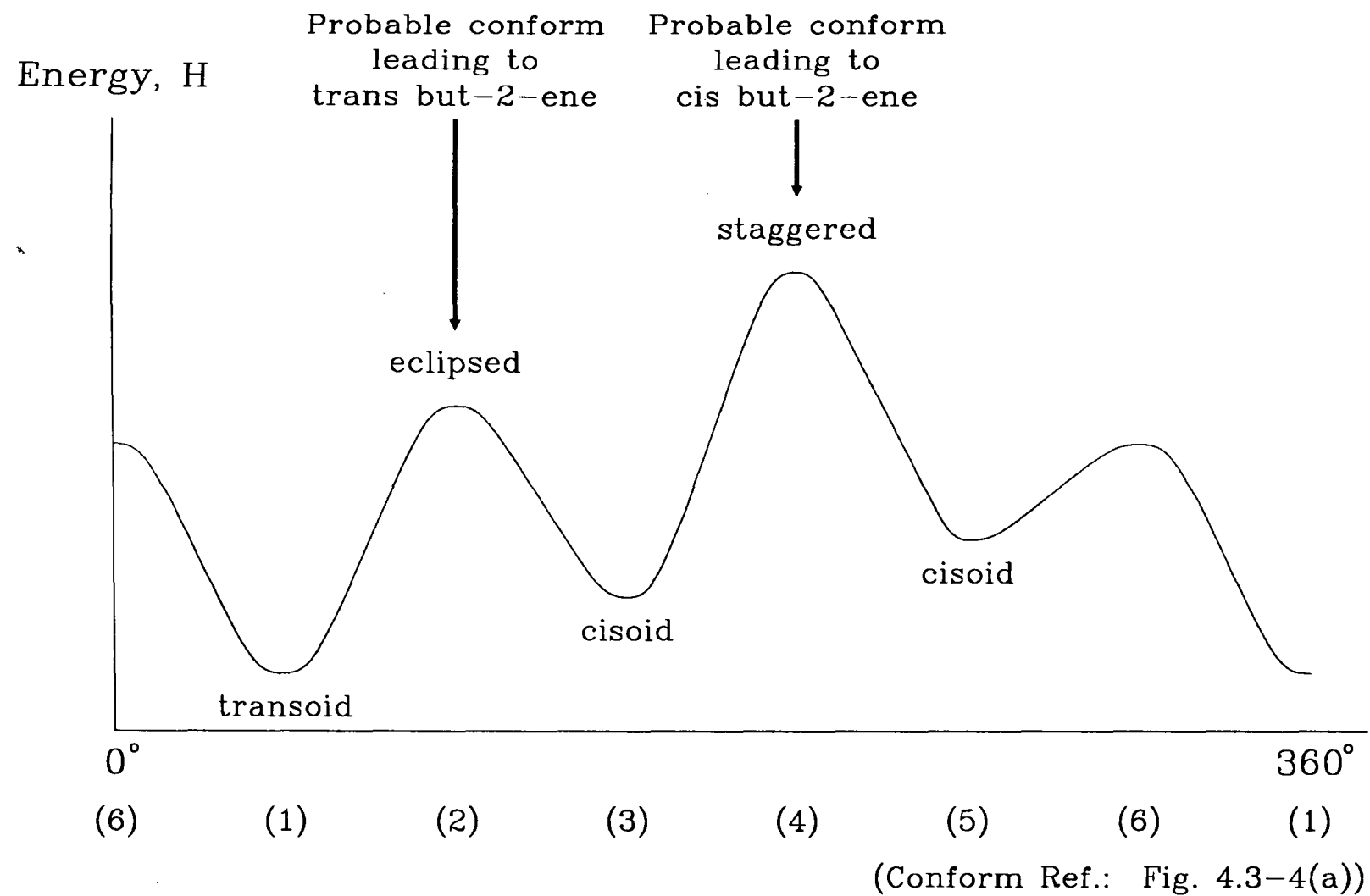


Fig. 4.3-4(b) Butan-2-ol: Schematic diagram showing energy as a function of rotation angle about the  $C_2$  and  $C_3$  bond

STAGGERED CONFORMS

ECLIPSED CONFORMS

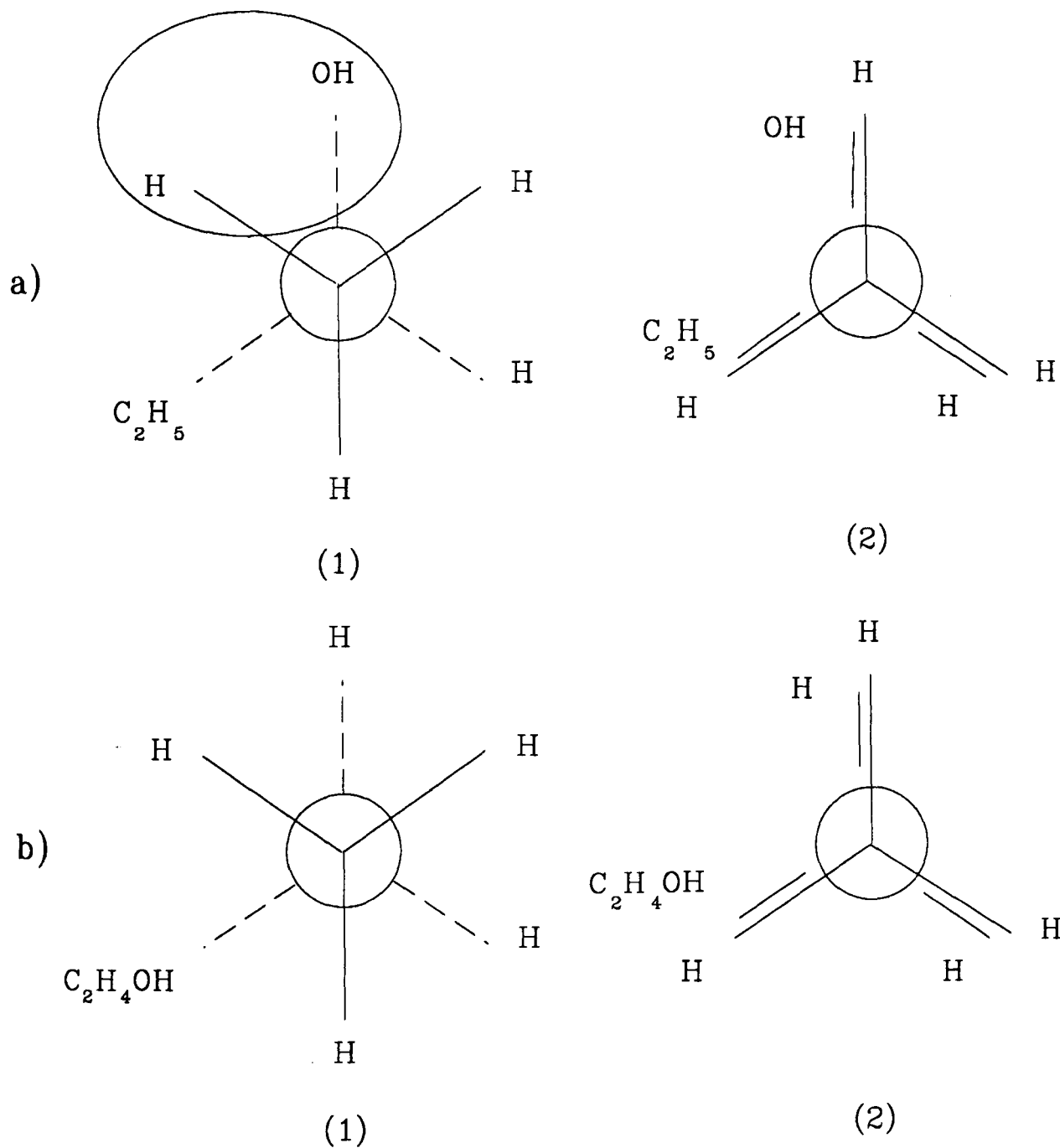


Fig. 4.3-5(a) Butan-2-ol: Eclipsed and staggered conforms resulting from rotation about a), the  $C_1$  and  $C_2$  bond, and b) the  $C_3$  and  $C_4$  bond

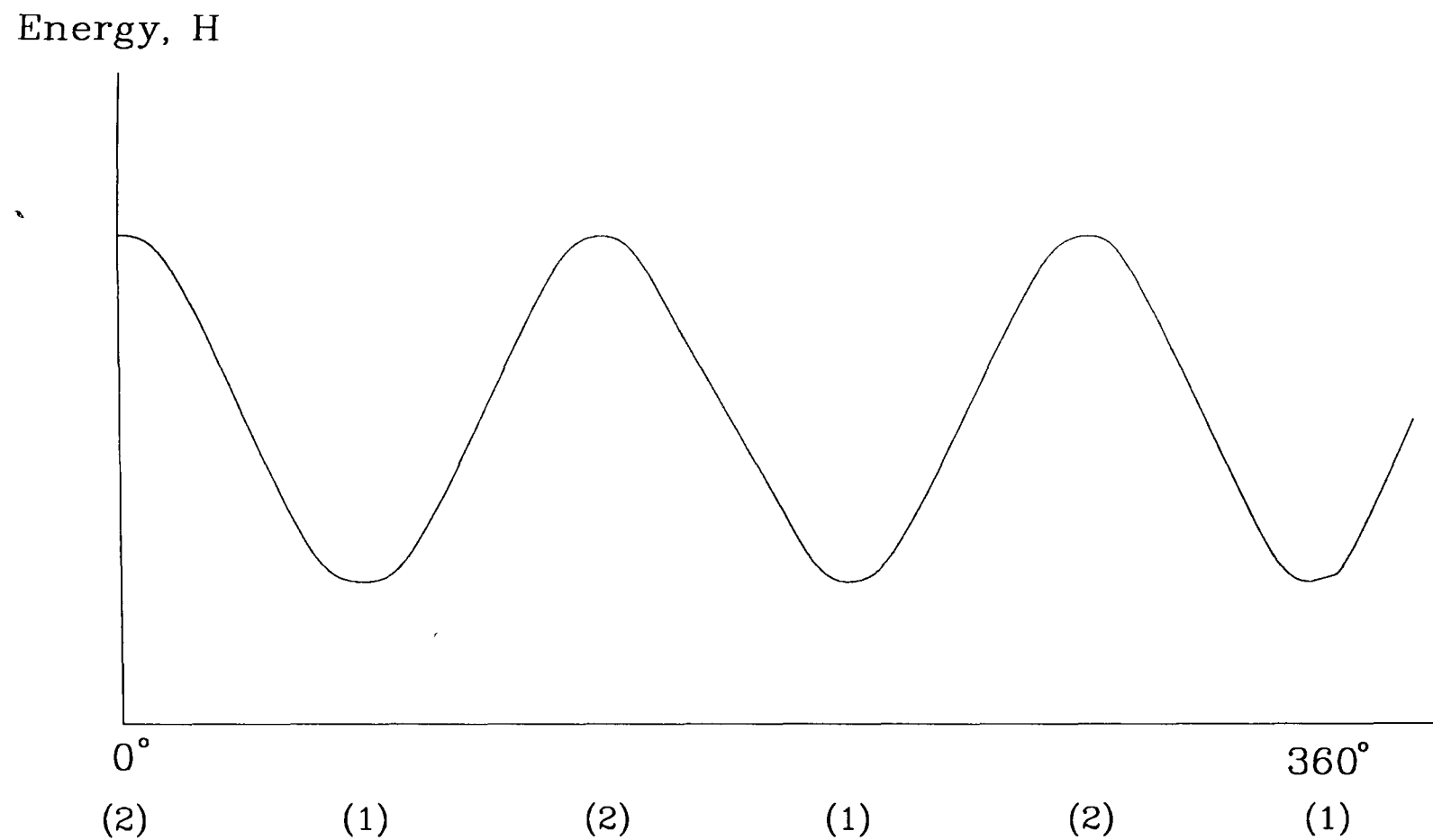


Fig. 4.3-5(b) Butan-2-ol: Schematic diagram showing energy as a function of rotation angle about either the  $C_1$  &  $C_2$  or the  $C_3$  &  $C_4$  bond

the free rotation. Furthermore, molecules in room temperature vapour have sufficient energy to traverse the energy barriers for all the conformational configurations; Figs. 4.3-4b and 4.3-5b are schematics of energy versus rotation angle, formulated by taking the following into consideration: i) staggered forms are more stable than eclipsed forms, since steric hindrance is reduced in the former (21). ii) there will be ionic repulsion between  $H^{\delta+} \dots H^{\delta+}$ , and  $H^{\delta+} \dots CH_3^{\delta+}$ , and ionic attraction for  $H^{\delta+} \dots OH^{\delta-}$ , and  $OH^{\delta-} \dots CH_3^{\delta+}$ . iii) there will be more steric hindrance between two methyl groups than between a methyl group and a hydroxyl group, because a methyl group occupies a larger volume than a hydroxyl group (20). The time at which the hydroxyl group is closest to a hydrogen is during an eclipsed configuration, and is also when dehydration is most likely to occur. Of the five  $\alpha$  hydrogens that can be expected to react with the hydroxyl during the four centred dehydration reaction, statistically there is clearly a 3:2 chance that the hydroxyl will react with a methyl hydrogen rather than one from the  $CH_2$  group. Because of isomeric forms, the resultant 60%:40% 1-ene/2-ene ratio, is predicted to be further statistically divided into 60%:20%:20% 1-ene:*trans*:*cis*. On dissociation, the product has some excess energy. Higher excitation levels will produce, on the whole, more highly excited products, and post decomposition isomerisation of *cis*  $\rightarrow$  *trans* is likely to occur (under collision-free conditions). This will manifest itself as the observed trend towards *trans/cis* 2-olefin ratios, differing from statistical predictions and nearer to the thermodynamic equilibrium values, as the fluence is increased. Direct *cis*  $\rightarrow$  *trans* isomerisation occurs by the uncoupling of the  $\pi$  bonds, so allowing free rotation and this freedom already exists in the transition state. Since the complete isomerisation process requires approximately 63 kcal/mole, even less is obviously required for an isomer still within the transition state. Furthermore, since isomerisation is catalysed by free radicals, it is reasonable

to expect more isomerisation at the highest fluences where radical formation is most likely.

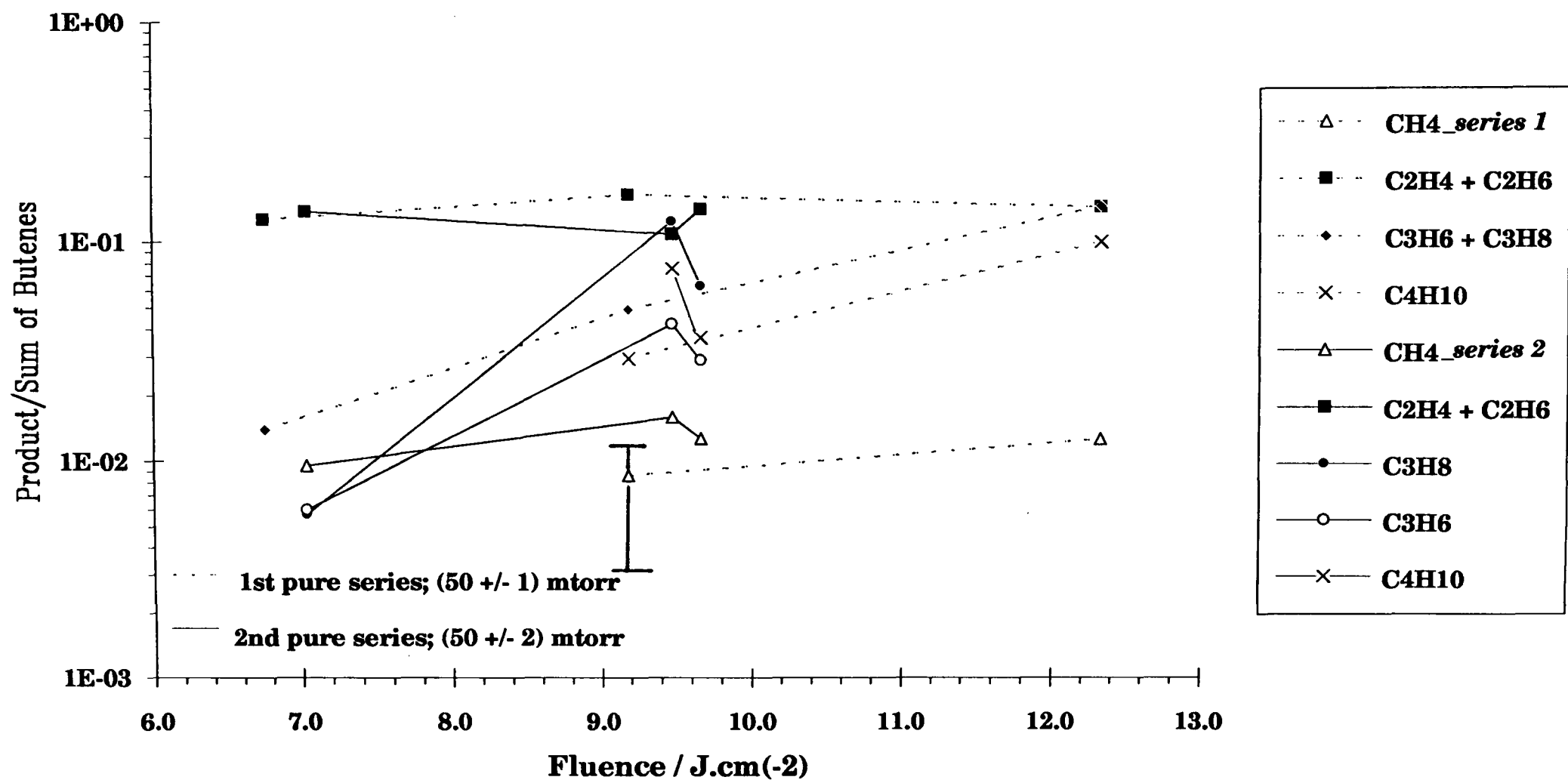
The appropriate temperature for calculating equilibrium ratios, applicable to these experimental conditions, is unknown. However, as the temperature is lowered, the thermodynamic equilibrium proportion of the *trans*-isomer increases (for example, at 500 K the molar fractions (102) are; *but*-1-ene 0.146; *cis*-*but*-2-ene 0.295; *trans*-*but*-2-ene 0.558). Some increase in the proportion of *trans*-isomer with decrease in fluence is therefore to be expected. At the lowest fluence investigated, an unexpectedly high preference for the *trans*-isomer was observed (97%; see Fig.4.3-3 and Table 4.3-1). This single observation has not been confirmed and, whilst of considerable interest, requires further investigation.

#### 4.3.2 Other Products

The products found that were not from the unimolecular dehydration channel that results in the butenes were; methane, ethane, ethene, propane, propene and butane (3,4-dimethylhexane was specifically looked for but not detected). Their yields are displayed in absolute form for the first series in Fig.4.3-1, and as a fraction of the sum of the dehydration channel products in Fig.4.3-6; the C<sub>2</sub> hydrocarbons and C<sub>3</sub> hydrocarbons were not resolved in these instances. The C<sub>2</sub> hydrocarbons are the most abundant of these 'other' products, followed by the C<sub>3</sub> hydrocarbons, butane, then methane.

It was not always possible to isolate propane from propene, but it was proven that both exist and that propane predominates. For the most part of the butanol study, it was also not possible to resolve ethane and ethene, and there is a lack of detail with respect to them in the 'pure' work. However, it was confirmed that both exist as products and in a ratio ethene/ethane of

**Fig. 4.3-6 Butan-2-ol: Variation of the yield ratio of product to butenes (raw data - Series 1 & 2) with fluence at R24 (10  $\mu\text{m}$ )**



1.77 at  $9.7\text{J}/\text{cm}^2$ . Only a few more points were taken in the dilute case, showing a similar ratio that increases slightly with fluence (from 2.14 at  $7.3\text{J}/\text{cm}^2$  to 2.52 at  $9.7\text{J}/\text{cm}^2$ ).

#### 4.3.3 Effect of Diluent

Butanol was diluted with cyclohexane to a ratio of 1/9.63, and was tested under constant pressure, collision-free conditions viz. 5mtorr partial pressure of butanol, and 50mtorr total. The results are presented in Figs.4.3-2 and Table 4.3-1. There is no apparent affect on the undeconvoluted yield of the major product (but-1-ene), whilst the majority of the other products exhibit a slight yield increase after dilution. More specifically, there is no more than a five fold increase in ethene (at high fluence), and no more than a two fold change in the but-2-enes. The reason for this pattern of observation is not clear.

#### 4.3.4 Pressure Dependence

The variation with pressure of the yield of each primary product to that of the sum of the dehydration products is given in Table 4.3-2 and Fig.4.3-7. The high fluences used are given for each pressure (Table 4.3-2).

These ratios are invariant with pressure for the most part, though there appears to be a convergent trend towards the highest pressures. Analysis was not carried out for any other product.

#### 4.3.5 Discussion

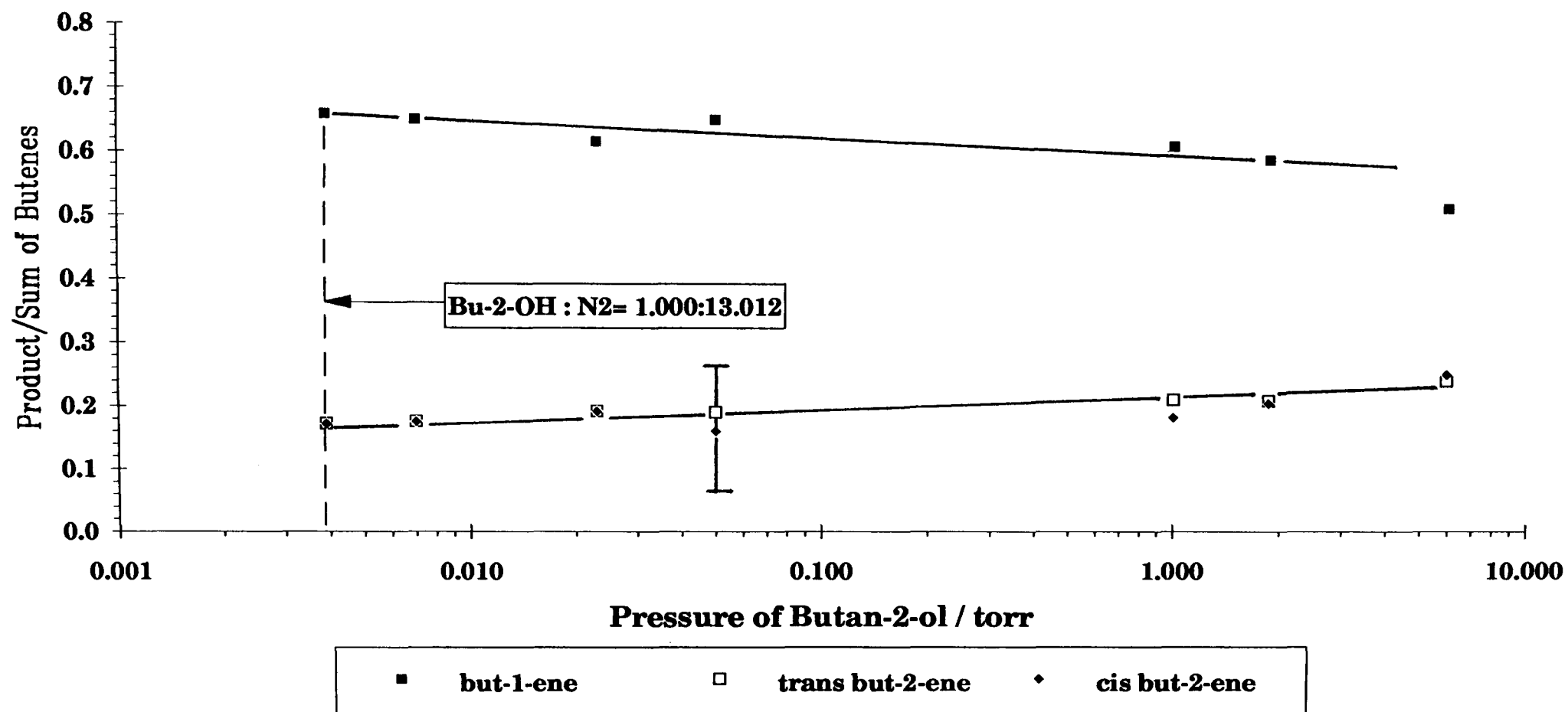
Listed below are some decomposition paths (molecular elimination and bond fission) with related heats of reaction for butan-2-ol, which, *a priori*, may be accessible with IR irradiation. According to Fig.1.4-4, excitation to twice that of the activation energy is allowable. An extensive literature search did not

Butanol Pressure / torr	Fluence / J.cm(-2)	Ratio of Product to Sum of Butenes		
		but-1-ene	trans but-2-ene	cis but-2-ene
0.004 *	9.1	0.658	0.171	0.171
0.007	8.8	0.650	0.175	0.175
0.023	9.8	0.616	0.192	0.192
0.050	8.4	0.650	0.190	0.160
1.001	9.5	0.608	0.210	0.182
1.862	9.3	0.587	0.208	0.205
5.925	9.3	0.510	0.240	0.250

\* Dilute mixture; Bu-2-OH : N<sub>2</sub> = 1.0 : 13.0

**Table 4.3-2** Butan-2-ol: Ratios of the primary products to the sum of the primary products resulting from irradiation at high fluence with the R24 (10µm) laser line (see Fig. 4.3-10)

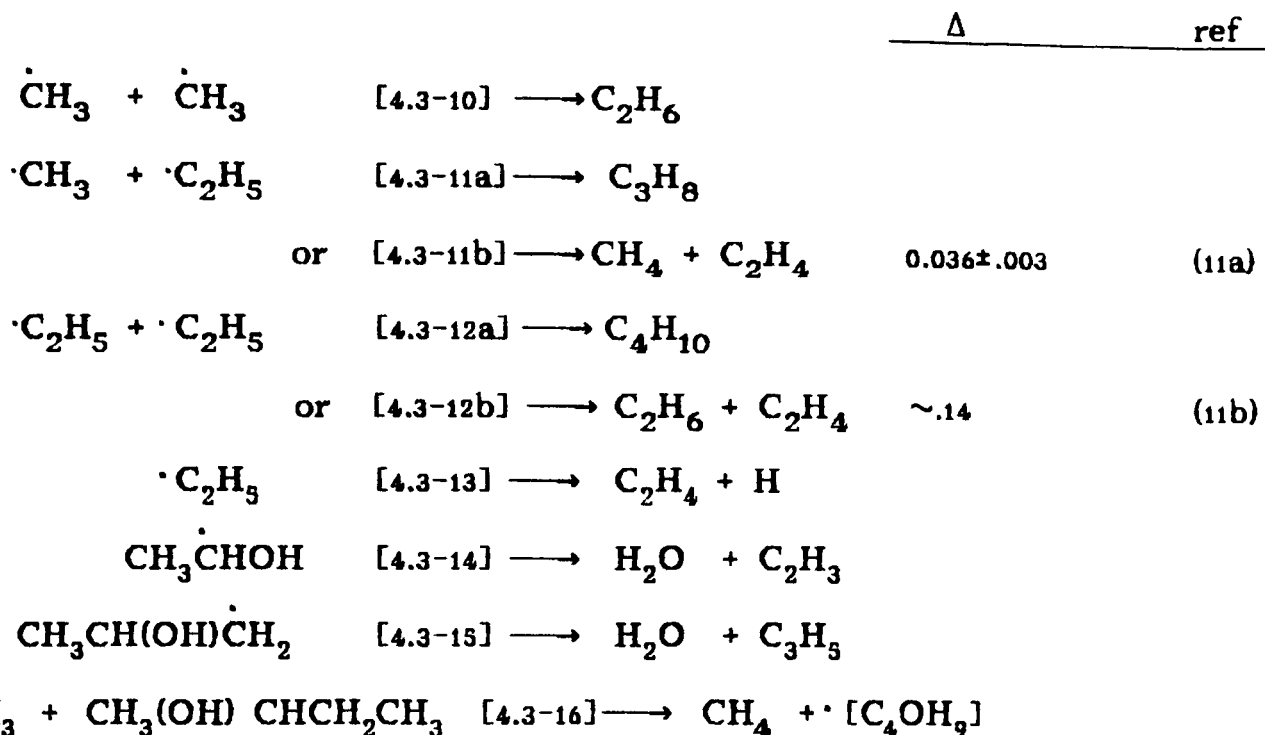
**Fig. 4.3-7 Butan-2-ol: Variation in the ratio of the yield of product to the sum of the butenes as a function of pressure. A high fluence of  $\sim 9 \text{ J/cm}^2$  at R24 ( $10 \mu\text{m}$ ) was used, and, as shown, in all but one case the reactant was pure**



yield Arrhenius parameters for butan-2-ol, though Shaw (6) estimated  $E_a=64.0$  kcal/mol, for the least energetic (dehydration) channel of t-butanol. For the same path Tsang (26) quoted  $\log_{10}k=13.4-(61600/2.303RT)$  s<sup>-1</sup>. 62 kcal/mol would also be a reasonable value to assume for butan-2-ol. The likely overexcitation thus becomes about 124 kcal/mol so with no further reactions, all the listed reactions [4.3-1] through to [4.3-9] will be allowed (since for bond fission reactions,  $\Delta H$  values are similar to the activation energies). These and further reactions will be possible if the total activation energy does not exceed 124 kcal/mol.

	$\Delta H_{300}^{\circ}$ kcal.mol <sup>-1</sup>
<b>Molecular Elimination:</b>	
$\text{CH}_3\text{CH}(\text{OH})\text{CH}_2\text{CH}_3$ [4.3-1] $\longrightarrow$ $\text{CH}_3\text{CH}=\text{CHCH}_3 + \text{H}_2\text{O}$	9.8 <i>trans</i>
	10.8 <i>cis</i>
[4.3-2] $\longrightarrow$ $\text{CH}_3\text{CH}_2\text{CH}=\text{CH}_2 + \text{H}_2\text{O}$	12.5
[4.3-3] $\longrightarrow$ $\text{CH}_3\text{CHO} + \text{C}_2\text{H}_6$	10.0
[4.3-4] $\longrightarrow$ $\text{CH}_3\text{OH} + \text{C}_3\text{H}_6$	26.9
[4.3-5] $\longrightarrow$ $\text{CHOCH}_2\text{CH}_3 + \text{CH}_4$	7.3
 <b>Bond Fission:</b>	
[4.3-6] $\longrightarrow$ $\cdot\text{C}_2\text{H}_5 + \text{CH}_3\dot{\text{C}}\text{HOH}$	83.2 (3)
	83.0 (4)
	80.7 (1)
[4.3-7] $\longrightarrow$ $\dot{\text{C}}\text{H}_3 + \dot{\text{C}}\text{H}_2\text{CH}(\text{OH})\text{CH}_3$	83.8
[4.3-8] $\longrightarrow$ $\dot{\text{C}}\text{H}_3 + \dot{\text{C}}\text{HOHCH}_2\text{CH}_3$	84.6
[4.3-9] $\longrightarrow$ $\dot{\text{O}}\text{H} + \text{CH}_3\dot{\text{C}}\text{HCH}_2\text{CH}_3$	91.5

Subsequent radical reactions may be expected to form the following products:



The  $\Delta\text{H}$  of the reactions forming  $\text{CH}_3$  and  $\text{C}_2\text{H}_5$  radicals are very similar, though one would expect methyl radical production to be favoured since there are two possible channels leading to their production Eqs. [4.3-7] & [4.3-8]: consequently one would expect reaction [4.3-10] to occur in statistical preference to reaction [4.3-11].

The observed product ratio  $\text{C}_2\text{H}_4/\text{C}_4\text{H}_{10}$  could be compared with the known theoretical ratio of disproportionation to recombination,  $\Delta$ , for  $k_{[4.3-12b]}/k_{[4.3-12a]}$ . Since, however,  $\text{C}_2\text{H}_4$  is likely to be formed in a number of other ways, this comparison is not profitable. The observed yield ratios  $\text{CH}_4/\text{C}_3\text{H}_8$  and  $\text{C}_2\text{H}_4/\text{C}_3\text{H}_8$  could likewise be compared with  $k_{[4.3-11b]}/k_{[4.3-11a]} = 0.036$  (11a). The fact that these observed ratios are not equal to each other implies that  $\text{C}_2\text{H}_4$  and  $\text{CH}_4$  do not solely arise by a common step such as [4.3-11b]. The fact that  $(\text{C}_2\text{H}_4/\text{C}_3\text{H}_8)_{\text{observed}} > 0.036$  suggests that  $\text{C}_2\text{H}_4$  arises from other steps as well as [4.3-11b].

If it is assumed that only [4.3-12b] and [4.3-11b] are responsible for  $\text{C}_2\text{H}_4$  production, then a further calculation of the expected ratios  $\text{C}_2\text{H}_4/\text{C}_3\text{H}_8$  and

$C_2H_4/C_4H_{10}$  may be carried out. For this purpose it is assumed that propane solely comes from [4.3-11a] and butane solely comes from [4.3-12a].

$$\text{From 4.3-12b} \quad \frac{C_2H_4}{C_4H_{10}} = 0.14 \quad \text{i.e.} \quad \frac{C_2H_4}{\chi} = 0.14$$

$$\text{From 4.3-11b} \quad \frac{C_2H_4}{C_3H_8} = 0.036 \quad \frac{C_2H_4}{y} = 0.036$$

Hence the total predicted ethene yield is given by;  $C_2H_4 = 0.14\chi + 0.036y$

Now, the expected ratio of

$$\frac{C_2H_4}{C_4H_{10}} = \frac{0.14\chi + 0.036y}{\chi} = 0.14 + 0.036\left(\frac{y}{\chi}\right)$$

Substituting the observed ratio of  $C_3H_8/C_4H_{10}$  for  $(y/\chi)$  gives a predicted value of 0.20 for  $C_2H_4/C_4H_{10}$ , and Fig.4.3-1 shows there to be far more ethene than this predicted value, thus supporting the idea for other routes to its formation.

Furthermore, all the aforementioned ratios decrease with increasing fluence, which may be interpreted as another clue to there being additional channels: if the biradical path were the only path, and the process was isothermal, then the ratios should be invariant of fluence, because the ratio of disproportionation to recombination ( $\Delta$ ) (which is a function of temperature) is invariant of fluence. On the other hand, the observed drop in values as the fluence is increased may be because the  $C_3H_8$  starts to (or always did) come from another channel. This discussion thus shows that bond fission processes alone do not explain the results.

In summary, the products may be explained as follows:

**Butenes:** The primary reaction paths have been shown to involve the concerted elimination of the hydroxyl with a C<sub>1</sub>, [4.3-2], or C<sub>3</sub>, [4.3-1], hydrogen; both paths occur, leading to but-1-ene and but-2-ene production. The dominant path is that which leads to the 1-olefin, even though this product is the least thermodynamically stable.

**Ethene** production is not easily explained, but may arise in one of three ways, all involving radicals:

(a) by disproportionation of ethyl radicals (produced in [4.3-6]) through reactions [4.3-12b] or [4.3-11b].

(b) by further decomposition of ethyl radicals as in [4.3-13] for which  $\Delta H^\circ \sim 40$  kcal/mol (see Table 4.2-1). The total energy requirement of the complete path ([4.3-6] followed by [4.3-13]) is  $\sim 123$  kcal/mol, just inside of the allowable limit as discussed earlier.

(c) by production via vinyl radicals, which arise, as in step [4.3-14], by water elimination from the CH<sub>3</sub>CHOH radicals generated by carbon-carbon fission in step [4.3-6]. This type of reaction was first proposed by Zhitneva *et al.* (101).

As discussed earlier, the experimental results show a proportion of C<sub>2</sub>H<sub>4</sub> that cannot be explained by method (a) alone.

**Ethane** is most obviously formed by recombination of methyl radicals [4.3-10] generated by the carbon-carbon fission processes [4.3-7] and [4.3-8]. By analogy to the production of methane from ethanol and propan-2-ol, which was via a unimolecular channels (reactions [4.1-3] and [4.2-3]), a possible path for butan-2-ol would be the four-centred, molecular elimination reaction [4.3-3]. As implied by the discussion of CH<sub>4</sub> production from butan-2-ol,

discussed below, it is likely that this molecular process only occurs to a small extent compared with methyl radical recombination.

**Propane** is probably formed by recombination of methyl radicals (produced in [4.3-7] and [4.3-8]) with ethyl radicals (from step [4.3-6]) through reaction [4.3-11a].

**Propene**, analogously to ethene, could arise from propenyl radicals generated, as in step [4.3-15], from  $\text{CH}_3\text{CH}(\text{OH})\text{CH}_2$  radicals produced in step [4.3-7]. Molecular elimination of methanol from butan-2-ol [4.3-4] may also be possible.

One other possible, but insignificant, source of propene is the butyl radical generated by the C-O fission in step [4.3-9]. This type of reaction is analogous to that first proposed by Danen *et al.* (81) for the pulsed laser decomposition of 2-iodobutane; it was proposed that propene derived from the butyl radicals which formed after fission of the C-I bond (Danen further argued that this channel could become the dominant channel at high levels of excitation, since compared to the primary HI elimination channels, this path has both a high A factor, and high activation energy). The absence of 3,4-dimethylhexane indicates that C-O fission by process [4.3-9], producing 2-butyl radicals, does not occur to any significant extent, and therefore fission of O-H is unlikely, since the  $\Delta H^\circ$  for that reaction is higher (103.0 kcal/mol).

**Butane** is most likely to be formed through reaction [4.3-12a] which involves recombination of ethyl radicals formed in step [4.3-6]. Since the yields are in the order  $\text{C}_2\text{H}_6 > \text{C}_3\text{H}_8 > \text{C}_4\text{H}_{10}$ , this is consistent with a greater production of

methyl radicals than ethyl radicals which is as to be expected on statistical grounds.

**Methane** could conceivably arise by methyl abstraction [4.3-16]. However, the concerted molecular elimination of the methyl group by the H of the OH group to give methane, was the reaction proven by Goodale *et al.* (81) to account for methane from doped ethanol: by analogy, the same molecular elimination process for butan-2-ol is more likely to be the source of methane also producing propanal ( $\text{CHOCH}_2\text{CH}_3$ ) [4.3-5]. Since this molecular channel is expected to contribute largely to the yield of methane, and since the analagous channel is expected to contribute to the same degree to the yield of ethene, then from the low amount of  $\text{CH}_4$  produced relative to  $\text{C}_2\text{H}_6$ , it is likely that this process is unimportant compared with carbon-carbon fission processes.

With the exception of the small observed amount of  $\text{CH}_4$  and possibly a small amount of  $\text{C}_2\text{H}_6$ , all these other products are well accounted for by the occurrence of carbon-carbon fission processes occurring alongside the main water elimination channel which produces the butenes.

According to Back *et al.* (9,9c), products exhibiting similar fluence dependency can be said to have come from reactions of similar activation energies (9), and this concept will be applied in the next two paragraphs. The degree of similarity is not quantified. Back (9) uses this analogy to show that two non bond-breaking channels had similar  $E_a$  to a bond-breaking channel, so  $E_a$  for those two were demonstrated to be similar to the endothermicity of the third channel (within 7 kcal/mole (30 kJ/mol)).

In this butanol work, the dependencies of propane with propene, and butane on fluence are similar for high fluences (Fig.4.3-1), and therefore, can be expected to have similar activation energies. All proposed bond-breaking channels have  $\Delta H^\circ (\sim E_a) \sim 84 \text{ kcal/mol}$  (351.46 kJ/mol) plus the  $\Delta H$  of the deactivation reaction of the radicals.

The *trans*-, *cis*-2-olefin and 1-olefin dehydration products all have similar trends with fluence, and in particular the 2-olefins. The simile breaks down only at very low fluences as discussed earlier. Furthermore, at high fluence, the sum of ethane and ethene appears to have the same trend as *cis*-but-2-ene (Fig.4.3-1) in which case the activation energy for each path will be in the region of that predicted for the primary dehydration channel i.e. 62kcal/mol. Such a low value is not consistent with the occurrence of bond fission and is therefore a further indication that ethene and ethane are products of molecular channels (eg. [4.3-3]).

Finally, heterogeneous effects have previously been shown to favour *cis*-but-2-ene formation over that of the *trans*-isomer (19), after pyrolysis of 2-chlorobutane. The fact that *trans*-but-2-ene is the favoured 2-olefin in this research acts as a check that laser decomposition under conditions described are homogeneous.

#### 4.4 *tert.*- BUTANOL

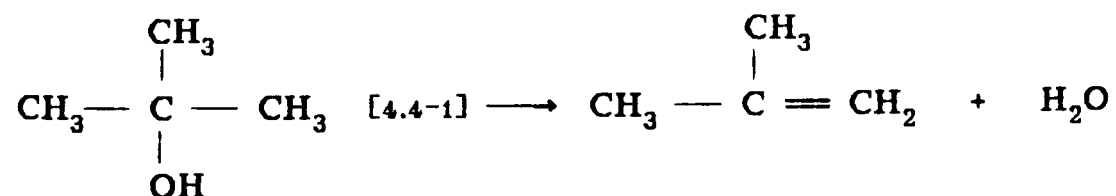
This molecule was studied only briefly. At a high fluence of  $8\text{J}/\text{cm}^2$  using  $\text{P}_{30}(10\mu\text{m})$  radiation, 50 mtorr of pure *t*-butanol decomposed to give ethane and/or ethene, propane and/or propene, and *iso*-butene, in proportions 10.3%:11.6%:78.1% respectively of the total product yield. No other products were detected which meant that any further products were at the most 0.5% of the total product yield. Chromatograph conditions were the same as those of the Pye during analysis of butan-2-ol.

Shaw (6) has reported the minor products  $\text{H}_2$ ,  $\text{C}_2\text{H}_4$ ,  $\text{CH}_4$ ,  $\text{CO}$ ,  $\text{C}_2\text{H}_6$  and  $\text{C}_2\text{H}_2$  in the laser photolysis of *t*-butanol, but only at pressures above 3 torr.

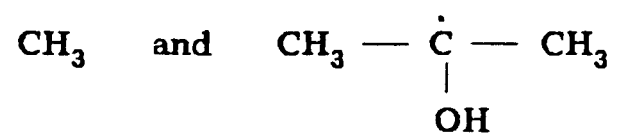
Barnard studied the thermal decomposition of *t*-butanol in the gas phase between 487 and  $620^\circ\text{C}$  (33). He concluded that the reaction proceeded mainly through unimolecular dehydration and that the *iso*-butene formed broke down further into methane, ethane, propane, ethene, propene and some solid polymer.

Some of the the products detected in this work may be explained as follows:

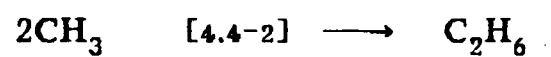
***iso-butene:*** The primary reaction path of laser photolysis, is one of unimolecular dehydration and results in the formation of *iso*-butene:



The minor products probably arise from carbon-carbon fission, which in all cases leads to the formation of the following two radicals:



**Ethane** would then form because of recombination of methyl radicals:



**Propene** may possibly be formed from  $\text{CH}_3\dot{\text{C}}(\text{OH})\text{CH}_3$  by the elimination of water to give  $\text{CH}_3\dot{\text{C}}=\text{CH}_2$  followed by hydrogen abstraction.

## 4.5 PENTAN-2-OL

Pentan-2-ol was irradiated at a frequency of 1.85 Hz using the  $R_{26}$  (9  $\mu$ m) line, and multi-longitudinal mode pulses. The major products expected, as a result of unimolecular dehydration, are pent-1-ene, and *cis*- and *trans*-pent-2-ene. Products were identified as methane, ethane, ethene, propane, propene, butane, but-1-ene, n-pentane, pent-1-ene, and *cis*- and *trans*-pent-2-ene: A further peak remained unidentified, but occurred at a retention time expected of a  $C_6$  hydrocarbon. No suitable conditions could be found for separating the pent-2-ene isomers or pent-1-ene on the Carlo GLC, using either the chromosorb or capillary columns. Difficulty in resolving the isomers arose from the small difference ( $<0.5^\circ\text{C}$ ) in their boiling points. Adequate conditions were eventually found on the Pye, using the same 2.9 m chromosorb column as for butanol, but with slightly higher carrier flow rates and a lower oven temperature of  $30^\circ\text{C}$ . To achieve this low temperature, the oven had to be vented; special care was taken over calibration, and to ensure constant temperature conditions. However, resolution of methane through to ethene was rather poor: for information on those products the Carlo GLC was used with the chromosorb 101 column, carrier flow rates of 50 ml/min and the oven at  $40^\circ\text{C}$ .

### 4.5.1 Fluence Dependence

For pentan-2-ol it was fairly easy to fit simple curves to the data to carry out deconvolution of the yields. Deconvoluted results given in Fig. 4.5-1(b) show that a substantial change occurs as a result of deconvolution. The data, however, were not sufficiently precise to permit this procedure to be adopted in all cases. Since, when a comparison is made with other results, the same form of data must be used, in general the raw data is presented.

The variation of yields versus fluence for nominally 50 mtorr of pure

**Fig. 4.5-1(a) Pentan-2-ol: Comparison of pentene yields (raw data) as a function of fluence for pure reactant, and reactant diluted with cyclohexane (D suffix), 50 mtorr total pressure**

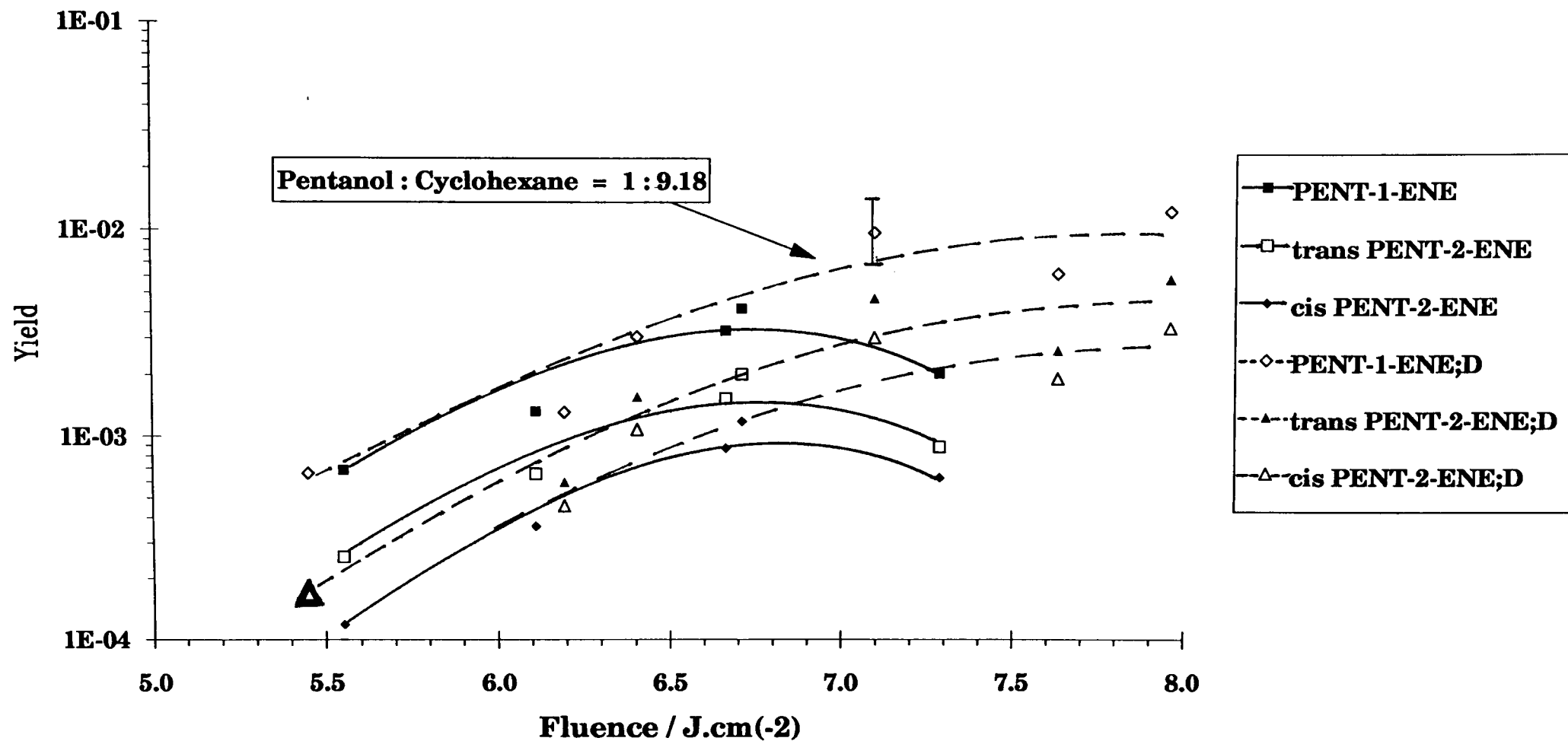
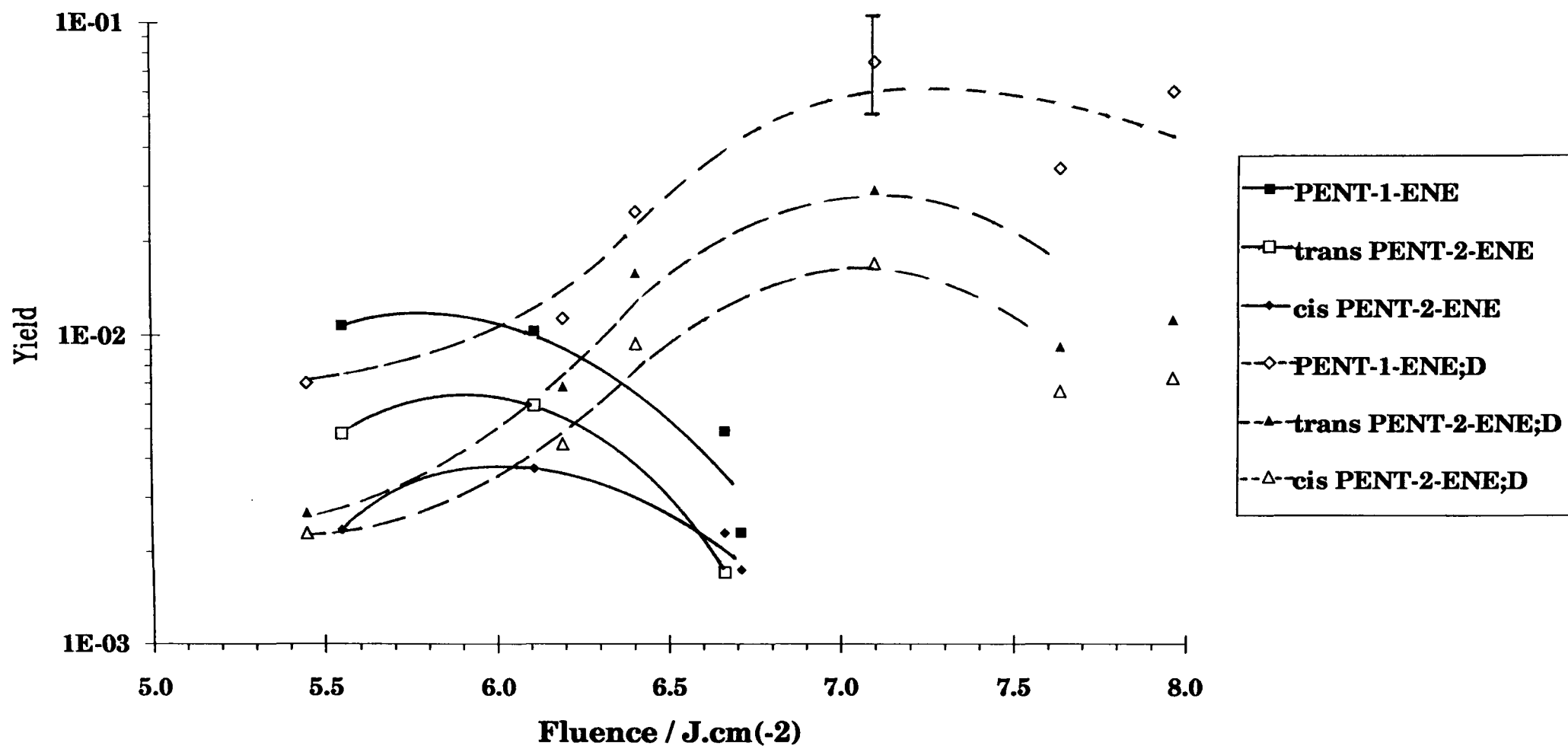


**Fig. 4.5-1(b) Pentan\_2\_ol: Comparison of pentene yields (deconvoluted data) as a function of fluence for pure reactant, and reactant diluted with cyclohexane (D suffix), 50 mtorr total pressure**



Series	Fluence J/cm <sup>2</sup>	Ratio of Product to Sum of Pentenes			
		pent-1-ene	trans pent-2-ene	cis pent-2-ene	fluence stability +/- J/cm <sup>2</sup>
<b>I</b> <b>Pure Reactant</b>  (48.6 ± 0.6) mtorr	5.55	0.6466	0.2413	0.1121	0.01
	6.11	0.5652	0.2792	0.1556	0.02
	6.66	0.5771	0.2686	0.1543	0.02
	6.71	0.5676	0.2717	0.1607	0.04
	7.29	0.5730	0.2502	0.1767	0.10
<b>II</b> <b>Dilute Reactant</b>  Reactant Partial Pressure of (4.98 ± 0.05) mtorr	5.45	0.6666	0.1650	0.1684	0.02
	6.19	0.7404	0.0008	0.2588	0.01
	6.40	0.5361	0.2749	0.1890	0.02
	7.10	0.5588	0.2686	0.1726	0.02
	7.63	0.5762	0.2449	0.1788	0.05
	7.96	0.5717	0.2719	0.1564	0.02

**Table 4.5-1** Pentan-2-ol: Ratios of the primary products to the sum of the primary products resulting from irradiation of nominally 50 mtorr total pressure of gas using the R<sub>26</sub> (10 μm) line.

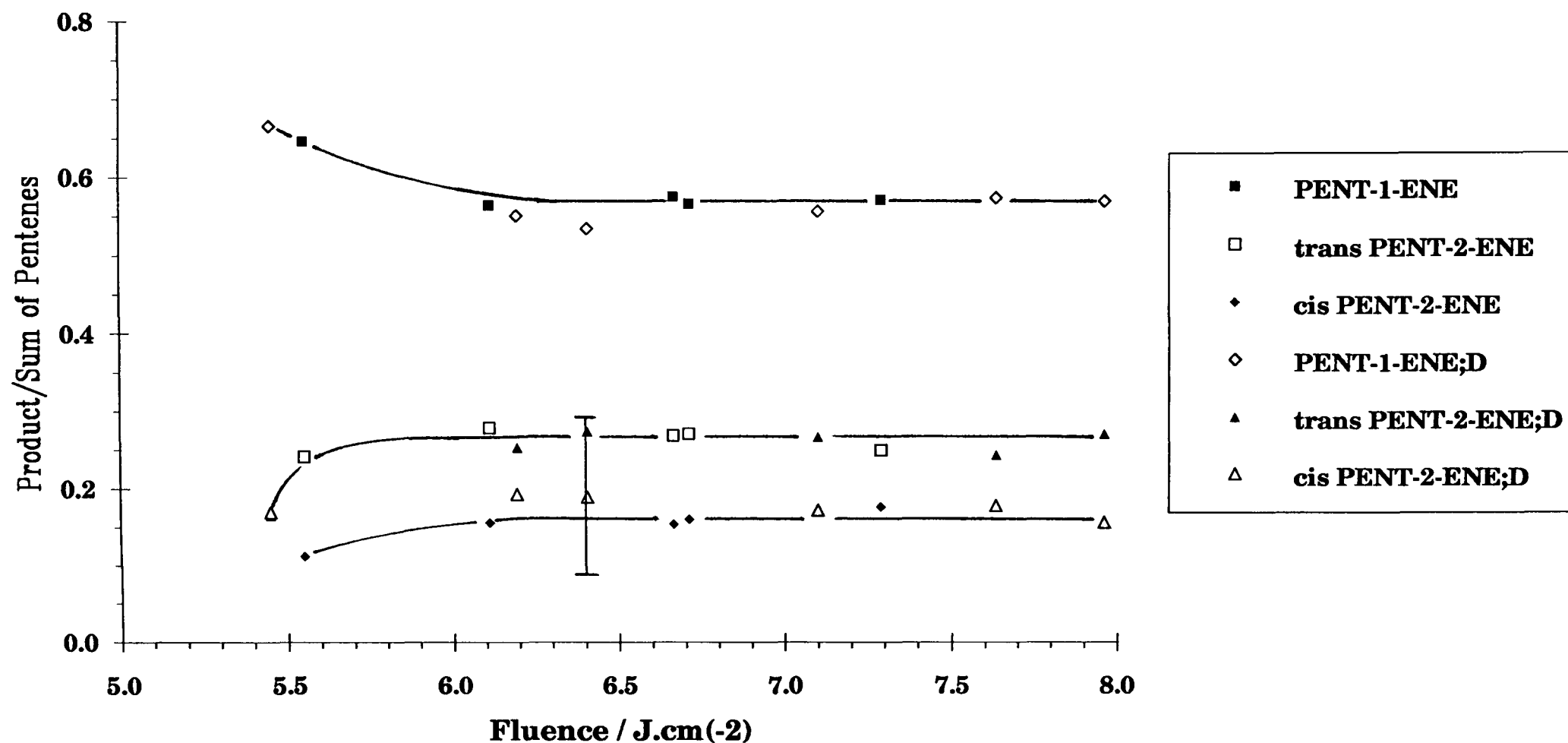
pentan-2-ol are presented in Figs.4.5-1 to 4.5-4 (the average pressure used for these constant pressure experiments was  $48.6 \pm 0.6$  mtorr). The product yields from the dehydration channel are presented in Fig.4.5-1. These and other product yields are represented as a fraction of the sum of the dehydration products in Figs.4.5-2 to 4.5-4.

Fig.4.5-2 shows that the olefin products of dehydration expressed as a ratio to the sum of the same products are approximately independent of fluence above  $6 \text{ J/cm}^2$ . The percentages of pent-1-ene, *trans*-pent-2-ene, and *cis*-pent-2-ene at the maximum fluence of  $7.3 \text{ J/cm}^2$  are 57%, 25% and 18%. Below  $6 \text{ J/cm}^2$  the 2-olefin values decrease as the fluence decreases, while that of pent-1-ene increases; the ratios of the individual pentenes to the sum of the pentenes are summarised in Table 4.5-1. As was discussed for butan-2-ol, these details can be explained by conformational and statistical analysis: Fig.4.5-5 illustrates the conforms and a schematic diagram of the variation of energy with angle of rotation about a specific C-C bond: the  $\text{C}_2\text{-C}_3$  bond. The ratio of pent-1-ene to pent-2-ene is generally close to the statistical value of 3:2 based on free rotation about C-C bonds in pentan-2-ol. The ratio of *cis*-pent-2-ene to *trans*-pent-2-ene differs significantly from the value of 1.0 expected on similar statistical arguments. Evidently pent-2-ene isomerises after decomposition of pentan-2-ol.

As explained earlier, the deconvoluted data are unreliable. Figs.4.5-2 and 4.5-3 show from raw data that over the fluence range  $5.5 \rightarrow 6.7 \text{ J/cm}^2$ :

- (i) the pentene ratios are approximately constant with change in fluence (apart from some deviation at fluences below  $6 \text{ J/cm}^2$ ).
- (ii) the ratios of minor products are again approximately constant with fluence but the scatter is greater (the  $\text{CH}_4$  point at  $7.3 \text{ J/cm}^2$  is anomalous and requires confirmation).

**Fig. 4.5-2 Pentan-2-ol: Comparison of yield ratio of product to the sum of pentenes (raw data) as a function of fluence for pure reactant, and reactant diluted with cyclohexane (D suffix), 50 mtorr total pressure**



**Fig.4.5-3 Pentan-2-ol: Ratio of product to the sum of pentenes (raw data) as a function of fluence for pure reactant**

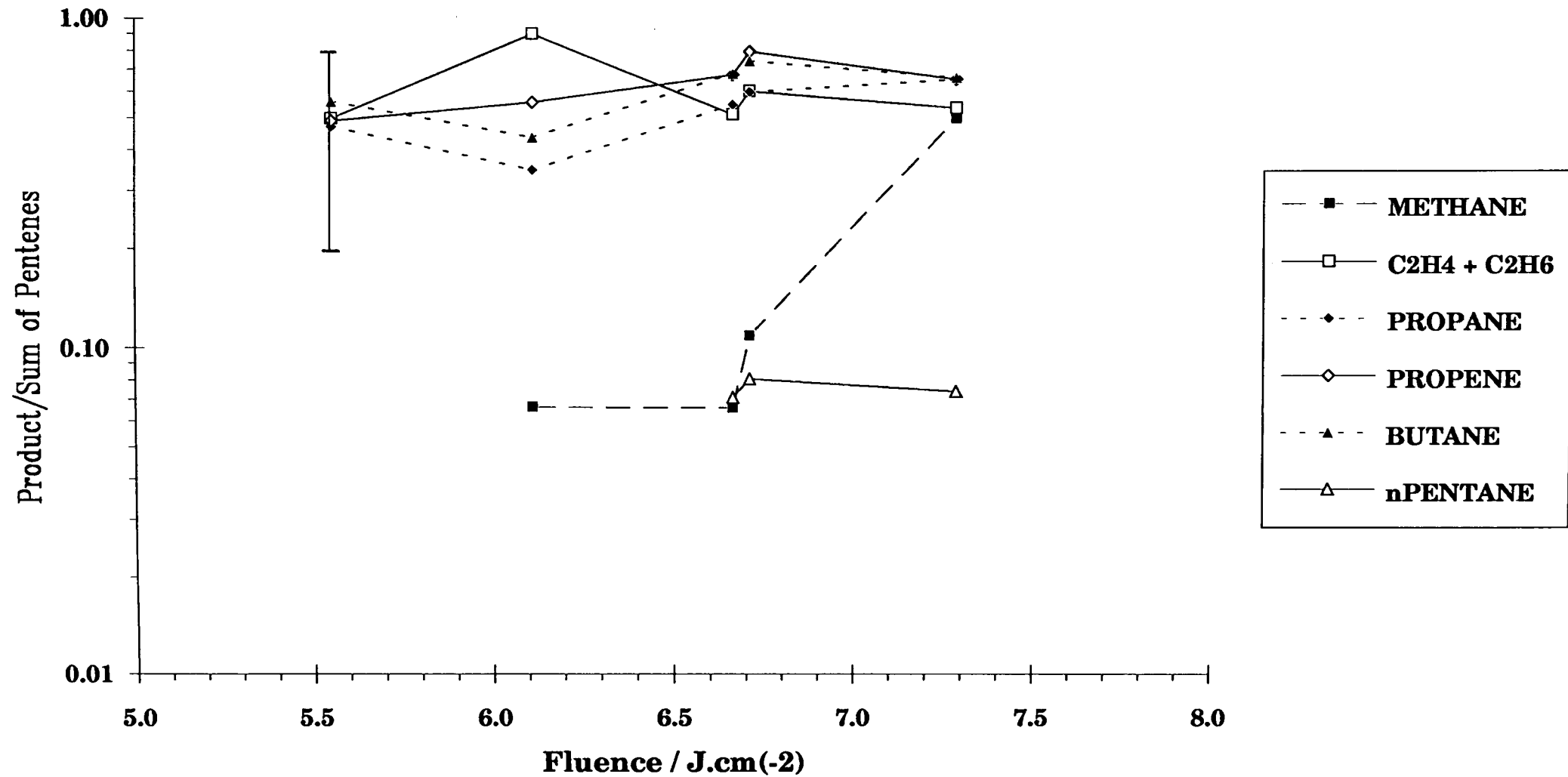
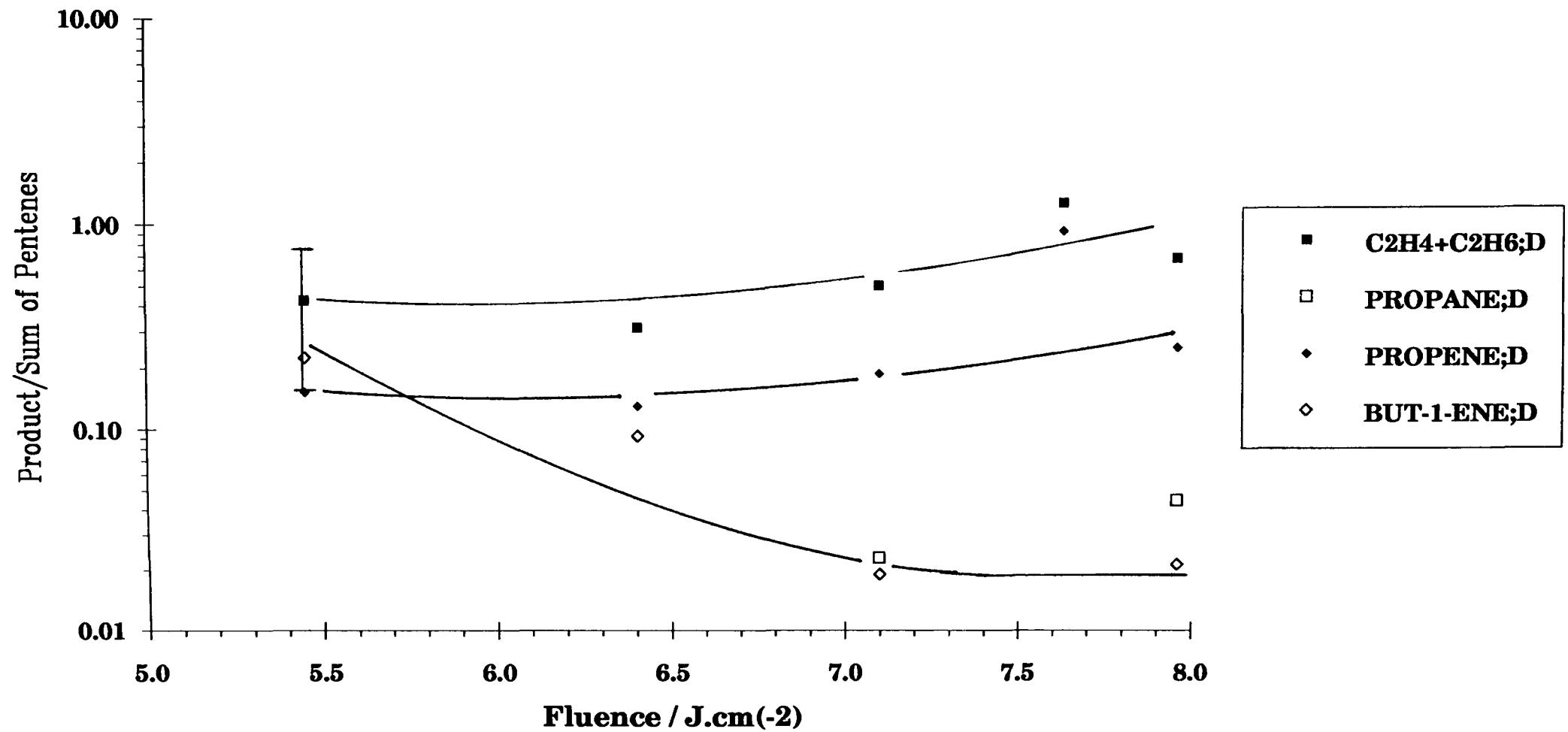


**Fig. 4.5-4 Pentan-2-ol: Ratio of product to the sum of pentenes (raw data) as a function of fluence for reactant diluted with cyclohexane (D suffix), 50 mtorr total pressure**



ECLIPSED CONFORMS

STAGGERED / SKEWED CONFORMS

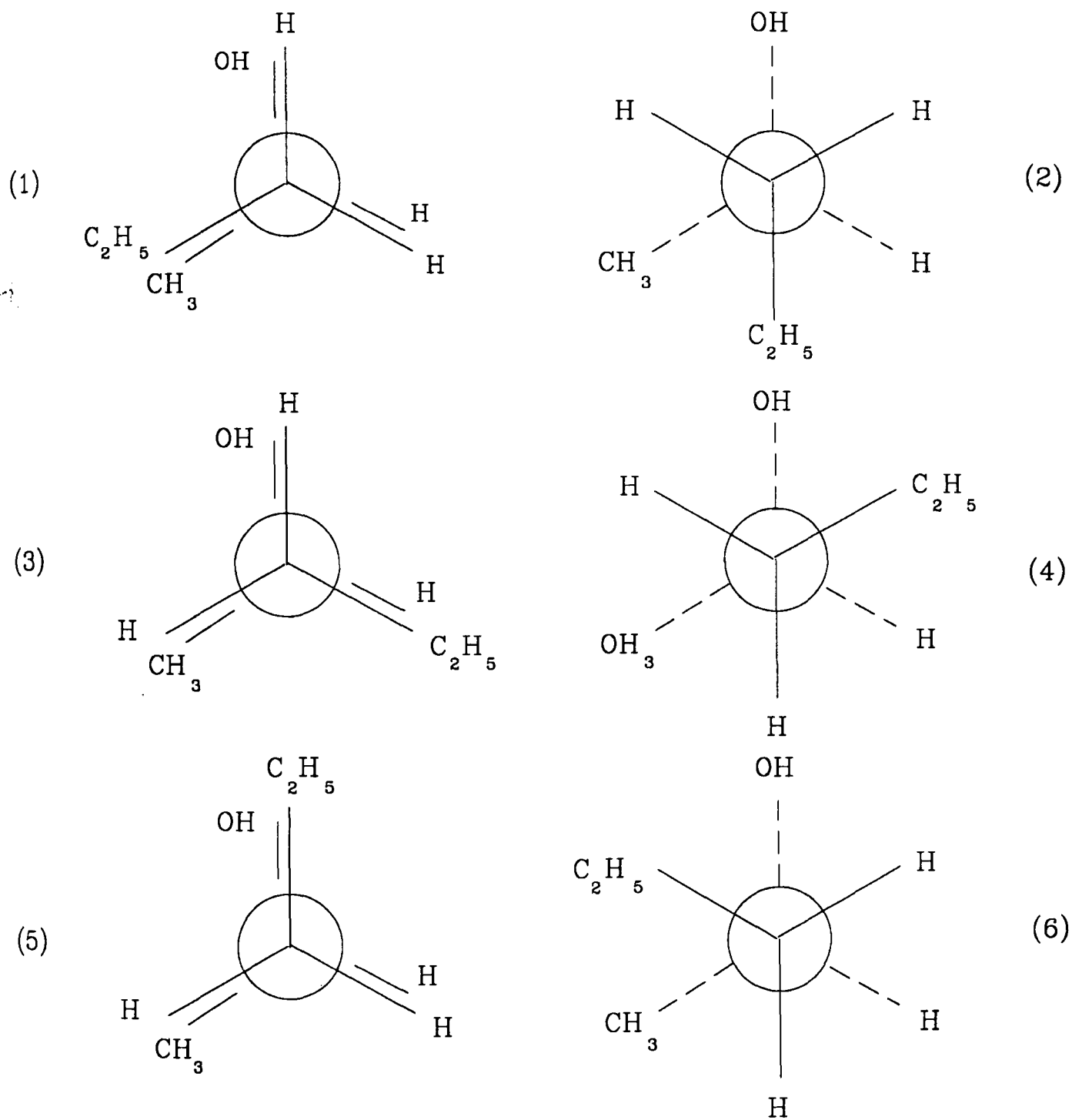
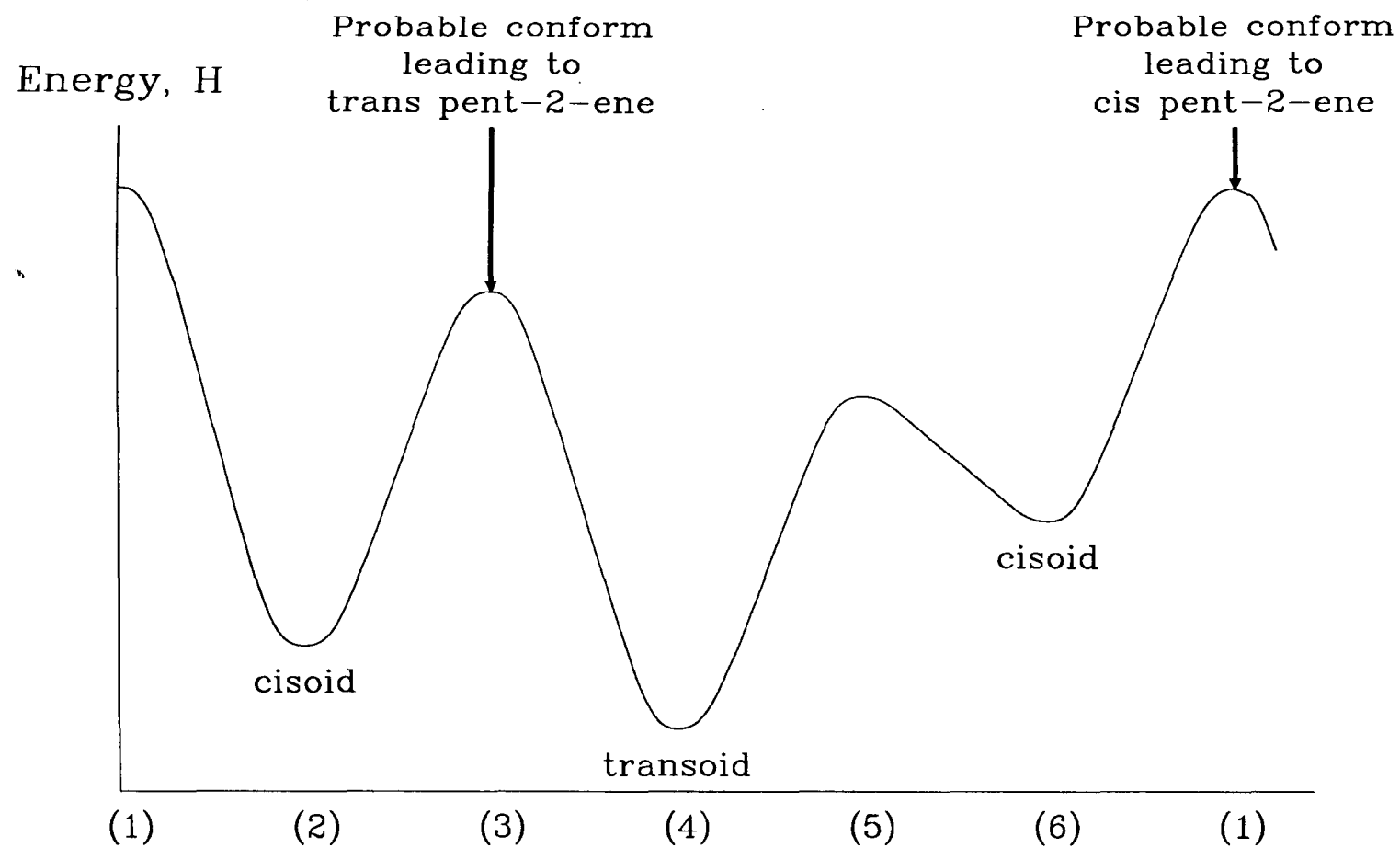


Fig. 4.5-5(a) Pentan-2-ol: Eclipsed and staggered conforms resulting from rotation about the  $C_2$  and  $C_3$  bonds



(Conform Ref.: Fig. 4.5-5(a))

Fig. 4.5-5(b) Pentan-2-ol: Schematic diagram showing energy as a function of rotation angle about the  $C_2$  and  $C_3$  bond

At all fluences, the products in decreasing importance are pent-1-ene, butane, C<sub>2</sub>, propene, and propane (all exhibiting similar yields), *trans*-pent-2-ene then *cis*-pent-2-ene, and finally, for the higher fluences only, there are traces of methane, n-pentane and an unidentified product of weight corresponding closely to a C<sub>6</sub> product. The ethane/ethene ratio was found to be 1/2.88 at a fluence of 6.1 J/cm<sup>2</sup>.

Thus it is clear that fragmentation is occurring at all fluences and there is no great change in fragmentation or elimination with fluence.

#### 4.5.2 Effect of Diluent

Pentanol was diluted with cyclohexane to a ratio of 1/9.18 and was irradiated under constant pressure, collision-free, conditions (50 mtorr total; the average reactant pressure used for these constant pressure experiments was 4.99 ± 0.05 mtorr). The results are presented in Figs. 4.5-1, -2 and -4. Fig. 4.5-1 illustrates that the diluent causes an increase in raw yield of the dehydration products, for mid to high fluences. At low fluences the conclusion can not be generalised; the *cis*-olefin yield increases, the *trans*-olefin decreases and the 1-olefin remains unchanged. The diluent has no significant effect on the ratio of the dehydration products to the sum of those products (Fig. 4.5-2).

In terms of minor product production, the addition of a diluent reduces both the number of products and the yield. This would be consistent with the hypothesis that the addition of cyclohexane to pentan-2-ol results in more efficient decomposition via the dehydration channel. Neither methane, nor n-pentane were detected, and the C<sub>4</sub> product was identified as but-1-ene rather than butane. The addition of the diluent also revealed some differences in the relative importance of the product, with data for the pure product. The yields at the lowest fluence (5.45 J/cm<sup>2</sup>) listed in decreasing order are now found to be pent-1-ene, C<sub>2</sub>, but-1-ene,

then *trans*-pent-2-ene, *cis*-pent-2-ene, and propene all in similar quantities. The order is much the same at  $6.7\text{J}/\text{cm}^2$ , except that but-1-ene becomes the most minor product, and at the highest fluence of  $8.0\text{J}/\text{cm}^2$  it is  $\text{C}_2$ , pent-1-ene, propene, *trans*-pent-2-ene, *cis*-pent-2-ene, propane and but-1-ene. As a ratio to the sum of the primary (pentene) products,  $\text{C}_2$  and propene were found to have the same trend with fluence.

#### 4.5.3 Pressure Dependence

On analysing the raw data for the variation of product yields with pressure (at a constant, moderate fluence of  $(6.76 \pm 0.04)\text{J}/\text{cm}^2$ ), the products can clearly be split into four groups as described below. These groups reflect the manner in which the products are formed. Absolute yields are presented in Figs. 4.5-6 and 4.5-8, while Figs. 4.5-7 and 4.5-9 show the yields relative to the sum of the dehydration channel products; Table 4.5-2 summarises the values of the ratios of the pentenes to the sum of the pentenes. In general, it is seen that there is little change in the relative yields of the pentenes with pressure; that most of the minor products increase relative to the pentenes as the pressure increases; and that the most important minor products are propene, and the sum of ethane and ethene. The four groups are:

- (i) Pent-1-ene, *trans*- and *cis*-pent-2-ene have shallow minima at a pressure of 0.15 torr (Fig. 4.5-6), pent-1-ene and *cis*-pent-2-ene being the major products at low pressure. Their combined yields, however, still dominate over all other yields at all measured pressures. The ratios of their yields with respect to each other hardly varies with pressure. There is a slight convergence as the pressure increases (Fig. 4.5-7). This group of products results from the molecular dehydration channels.
- (ii) Propene and ethene (plus ethane), have deep minima at pressures between roughly 0.09 torr and 0.2 torr (Fig. 4.5-8, dotted lines). They are

**Fig.4.5-6 Pentan-2-ol: Effect of pressure on yield (raw data) for pure reactant irradiated at a fluence of  $6.76 \pm 0.04 \text{ J.cm}^{-2}$**

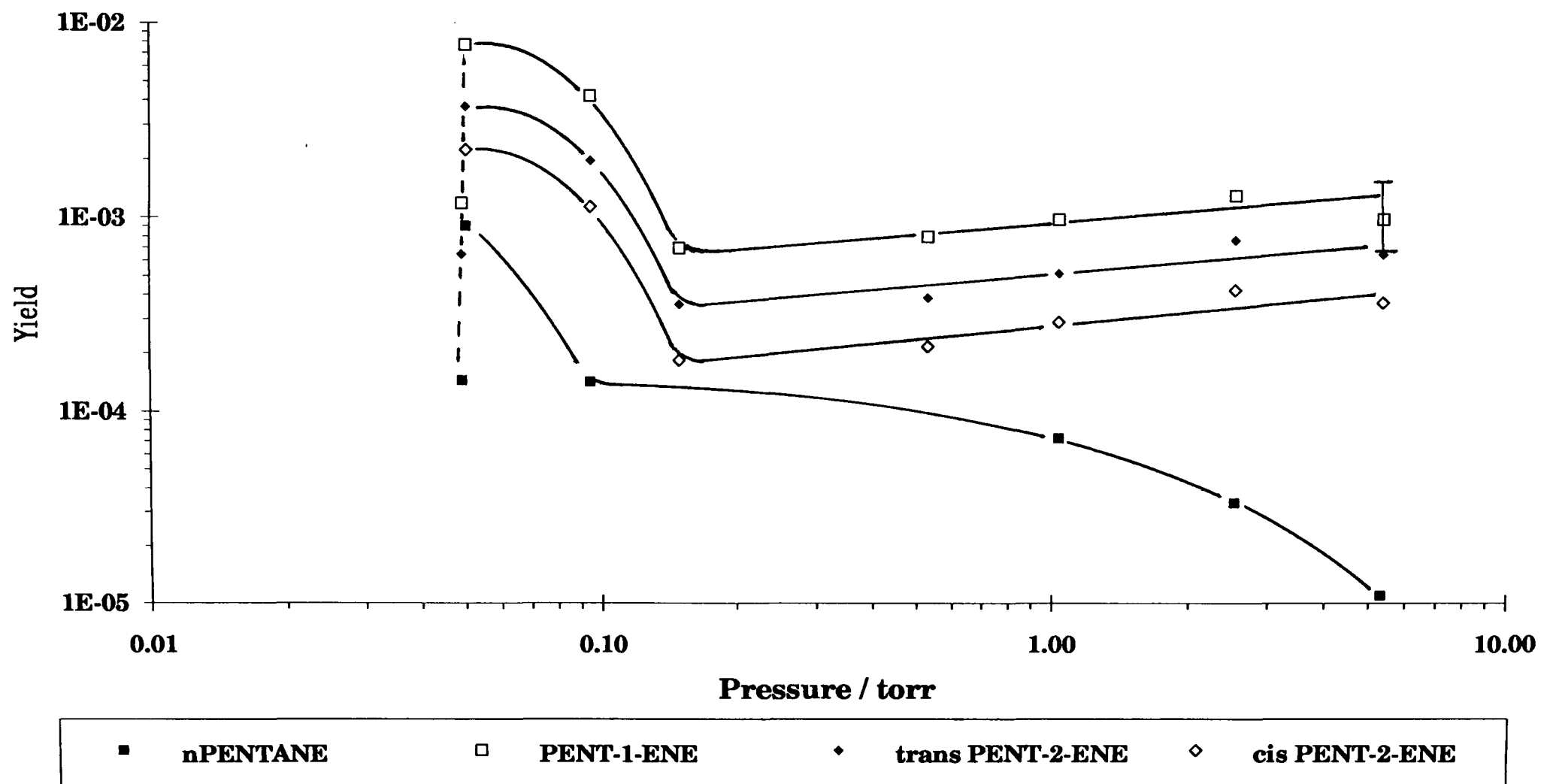


**Fig.4.5-7 Pentan-2-ol: Effect of pressure on yield ratio of the product to the sum of pentenes (raw data), for pure reactant irradiated at a fluence of  $6.76 \pm 0.04 \text{ J.cm}^{-2}$**

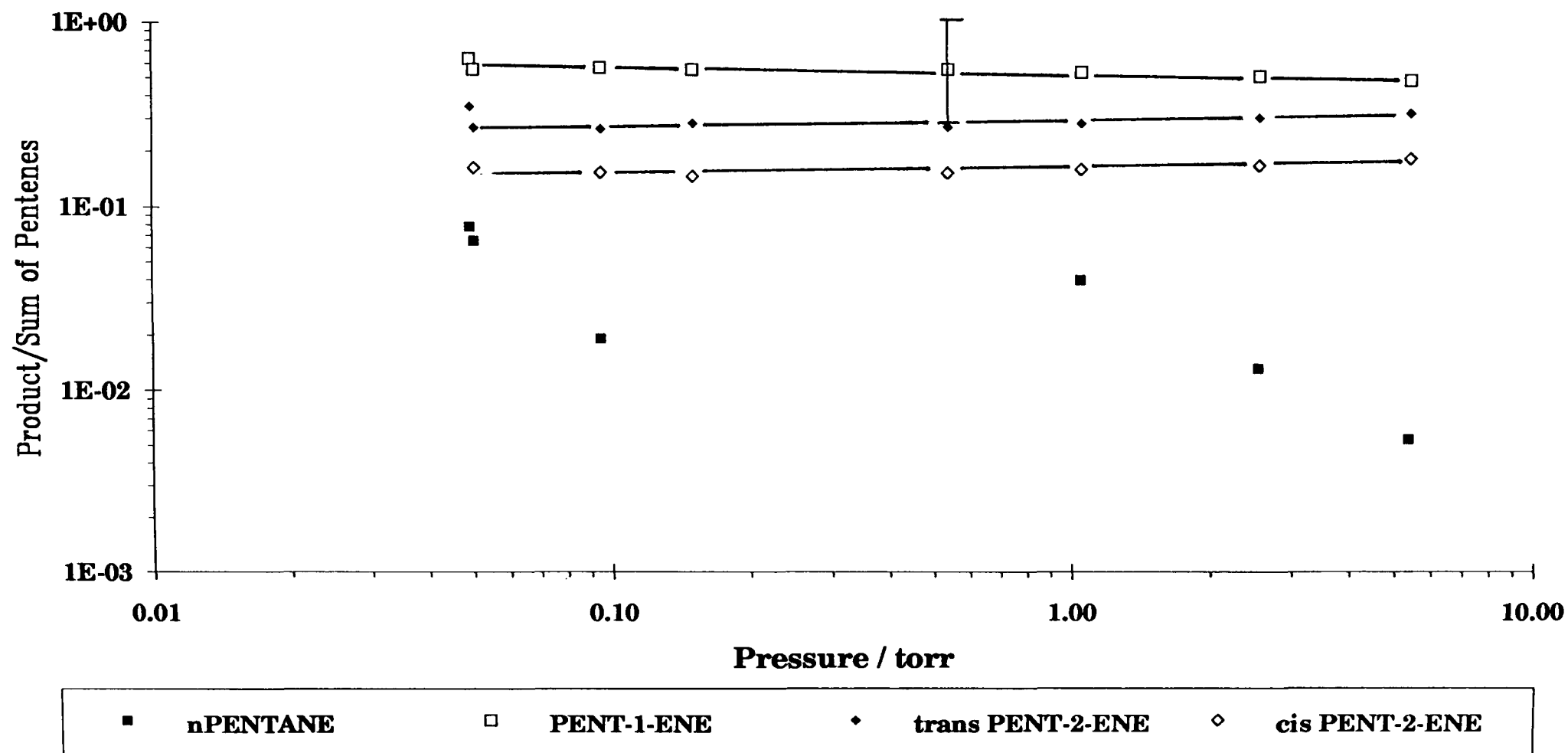


**Fig. 4.5-8 Pentan-2-ol: Effect of pressure on secondary product yield (raw data) for pure reactant irradiated at a fluence of  $6.76 \pm 0.04$  J.cm(-2)**

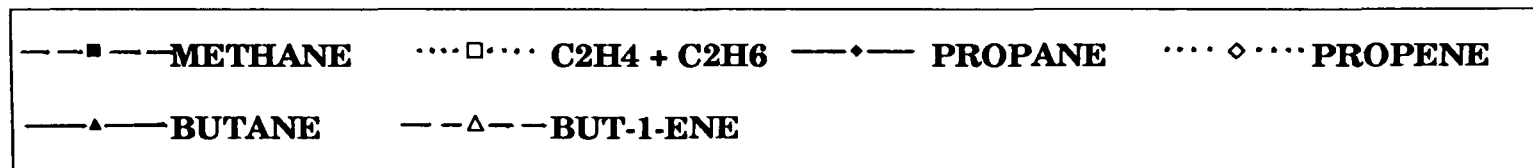
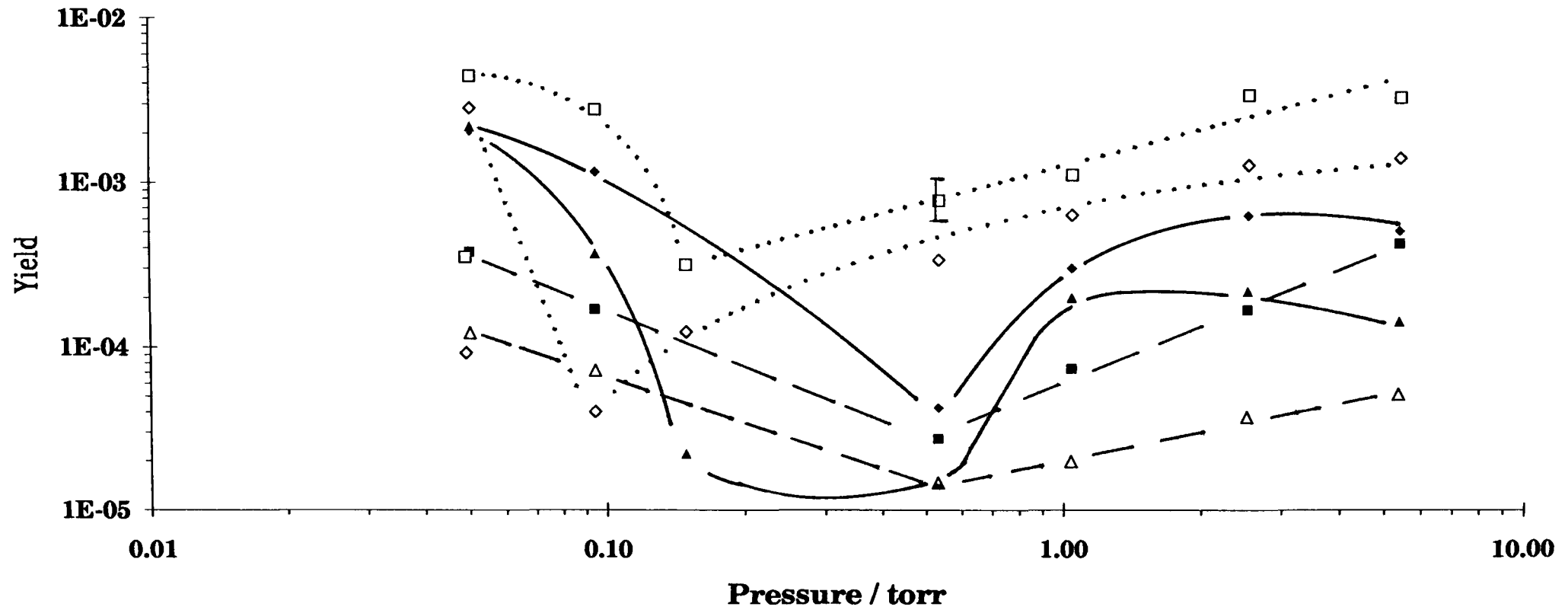
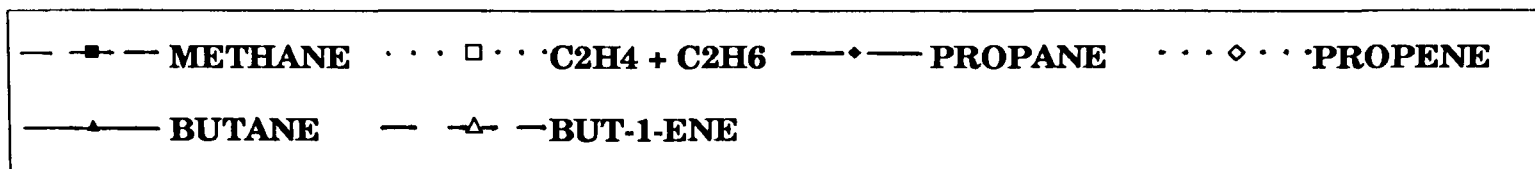
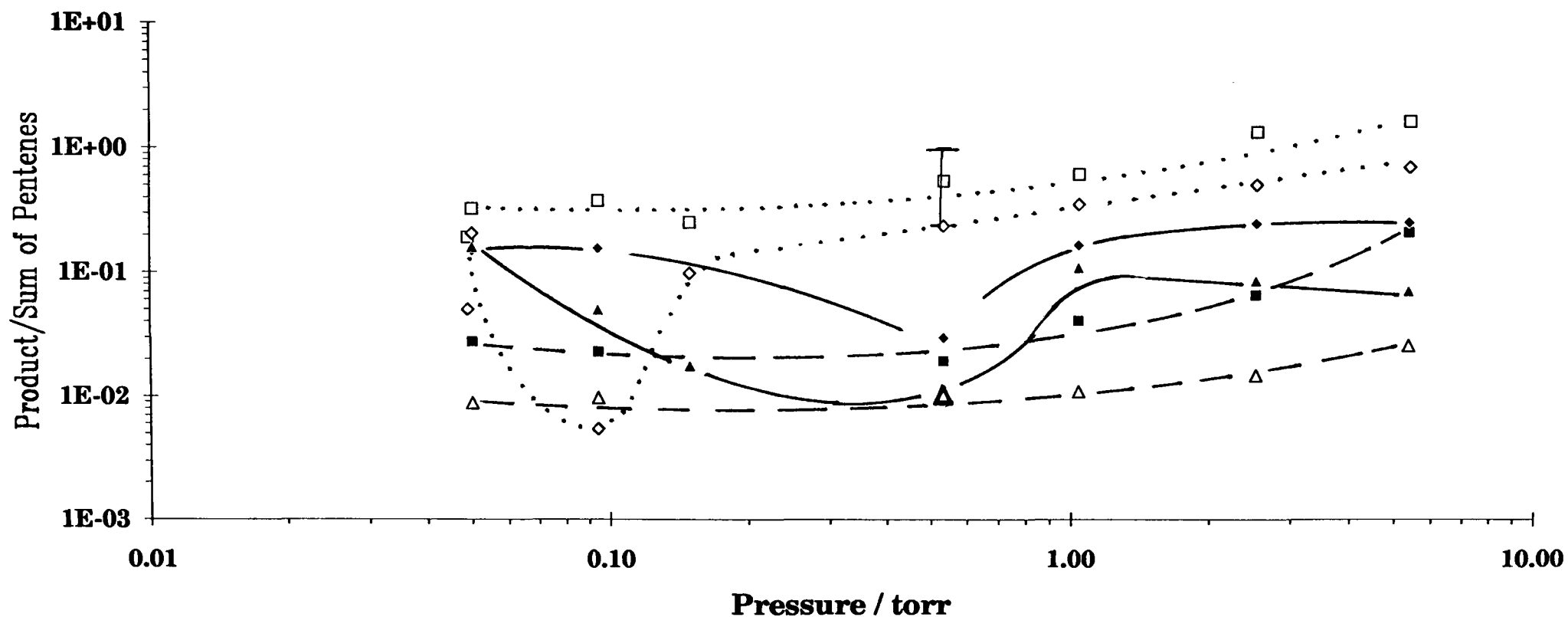


**Fig. 4.5-9 Pentan-2-ol: Effect of pressure on secondary product yield ratio of the product to the sum of pentenes (raw data), for pure reactant irradiated at a fluence of  $6.76 \pm 0.04 \text{ J.cm}^{-2}$**



Pentanol Pressure / torr	Fluence and Stability / J.cm(-2)	Ratio of Product to Sum of Butenes		
		pent-1-ene	trans pent-2-ene	cis pent-2-ene
0.049	6.86 +/- 0.03	0.6447	0.3553	-
0.050	6.96 +/- 0.05	0.5623	0.2733	0.1644
0.094	6.62 +/- 0.04	0.5751	0.2696	0.1553
0.149	6.82 +/- 0.01	0.5622	0.2887	0.1491
0.530	6.74 +/- 0.03	0.5691	0.2758	0.1550
1.036	6.59 +/- 0.03	0.5487	0.2893	0.1620
2.518	6.75 +/- 0.02	0.5213	0.3086	0.1701
5.320	6.69 +/- 0.04	0.4910	0.3254	0.1835

**Table 4.5-2** Pentan-2-ol: Ratios of the primary products to the sum of the primary products resulting from irradiation at a average moderate fluence of ((6.76 +/- 0.04 J.cm(-2)) with the R26 (9 μm) laser line

the major products at high pressure competing very effectively with production of the dehydration products. Their ratios with respect to the sum of the primary products are very similar to each other in trend (Fig.4.5-8, dotted lines); above 0.15torr,  $Y \propto P^{1.00}$ . It is the conclusion of this work, that propene and ethene result from the same kinds of *radical* reactions (i.e. disproportionation, decomposition, and molecular dehydration (see the following Discussion)).

- (iii) Propane, methane, butane and but-1-ene have deep minima at approximately 0.5torr (Fig.4.5-8, solid and dashed lines). The ratios of methane and but-1-ene with respect to the sum of the primary products are very similar (Fig.4.5-9, dashed lines), as are those for propane and butane (Fig.4.5-9, solid lines). Methane and but-1-ene are not quite as dependent on reactant pressure as propane and but-1-ene. It is the conclusion of this work (see the following Discussion) that the formation of both propane and but-1-ene depend on the radicals that result from the same carbon-carbon fission steps; the same is true of butane and propane, and, to some degree, also of methane.
- (iv) *n*-Pentane whose yield, unlike the others, strongly decreases with pressure over the entire measured pressure range (Fig.4.5-6), and competes more and more ineffectively with production of the dehydration products (Fig.4.5-7). It is possible that the reaction rate for the channel leading to *n*-pentane may be very slow, so collisions have a strong degrading effect on yield. Or, pentane production may rely on a radical species which preferentially contributes to another product as the pressure increases. Then again, pentane may be a thermal (post-pulse) product, and the deactivating effect of collisions causes more excited parent molecules to stay below the activation energy as the pressure of pentanol is further increased. It is the conclusion of this work, that *n*-pentane is formed through

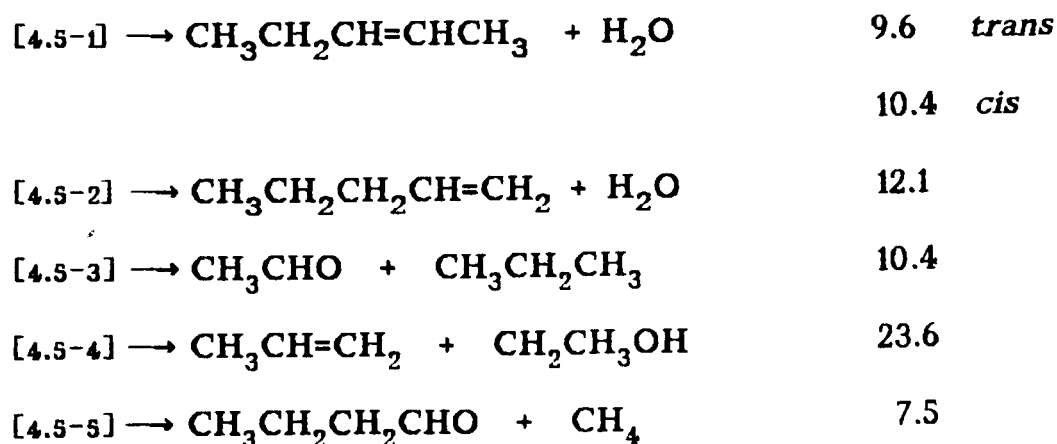
recombination of radicals required for the more efficient formation of propene and ethene; i.e. the formation of the group (iv) product is in direct competition with the formation of the group (ii) products (see the following Discussion).

#### 4.5.4 Discussion

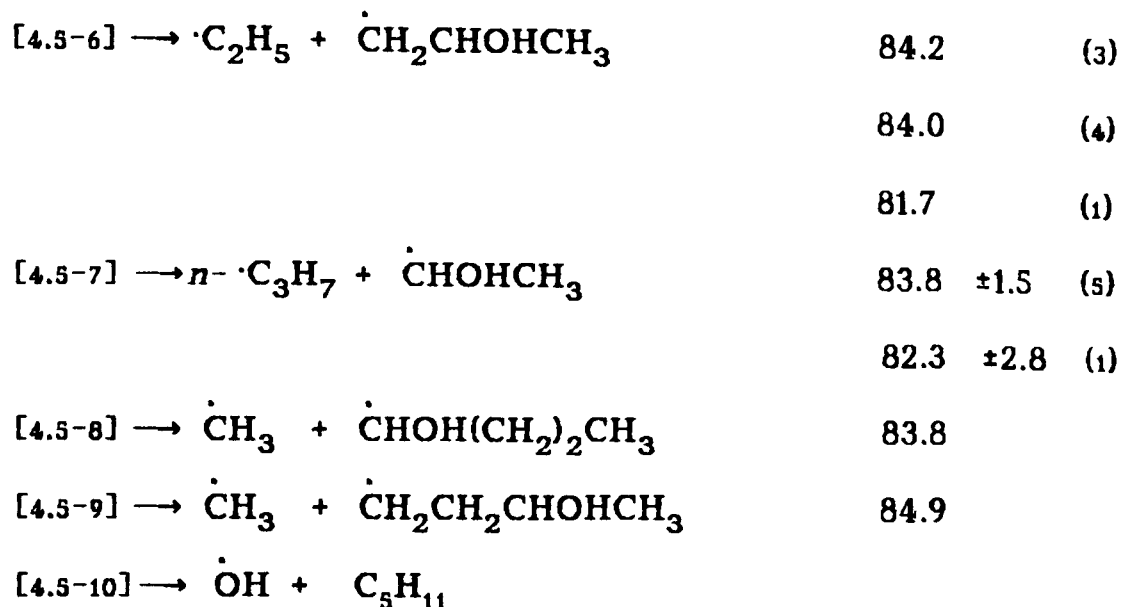
Listed below are some decomposition paths (molecular elimination and bond fission) with related heats of reaction for pentan-2-ol, which, *a priori*, may be accessible with IR irradiation. According to Fig.1.4-4, excitation to 2.3 times that of the dissociation energy is allowable. An extensive literature search did not yield Arrhenius parameters for pentanol. However, an extrapolation of Danen's analysis (23) above the previously predicted propanol (Section 4.2) and known *t*-butanol (Section 4.3) values, gives  $E_a \sim 57$  kcal/mol for the least energetic (dehydration) channel of pentanol. The maximum likely overexcitation is therefore roughly 131 kcal/mol. Hence, with no further reaction, all the listed reactions [4.5-1] through to [4.5-10] will be possible (for fission reactions,  $\Delta H$  values are similar to the activation energies). These and further reactions will be possible if the total activation energy does not exceed 131 kcal/mole.

$$\frac{\Delta H_{300}^{\circ}}{\text{kcal.mol}^{-1}}$$

Molecular Elimination:

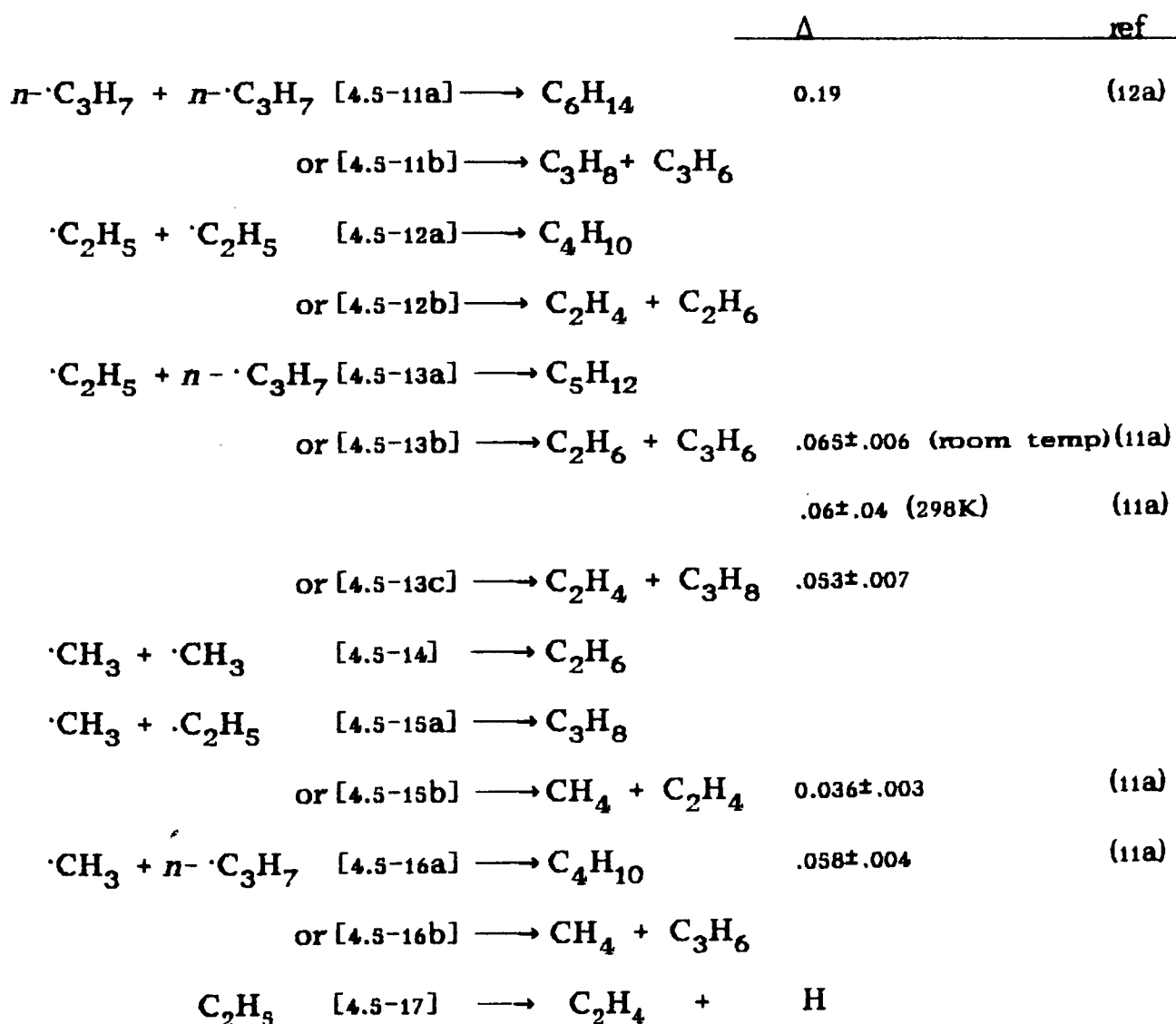


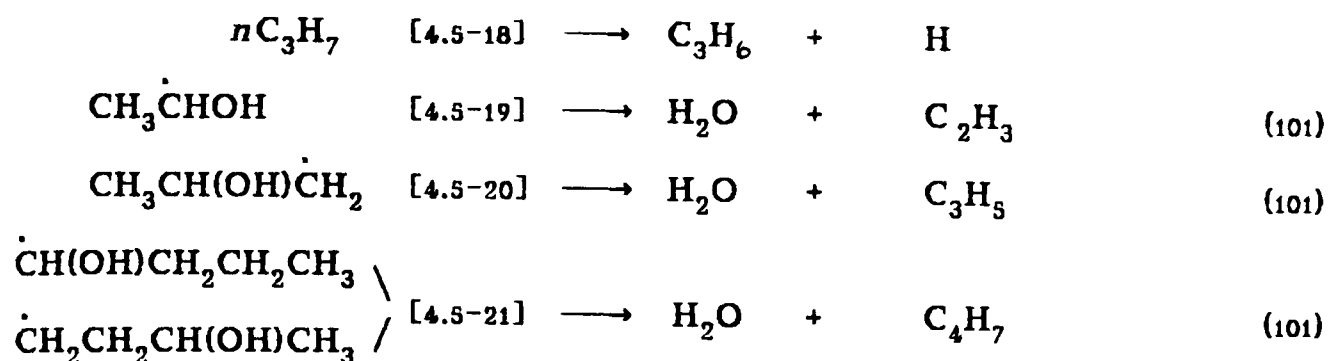
**Bond Fission:**



The energies have not been worked out for the breaking of C-H, C-O, or O-H bonds, since it was shown for ethanol, propan-2-ol, butan-2-ol and hexan-2-ol that these are typically 91, 92 and 103 kcal/mol respectively.

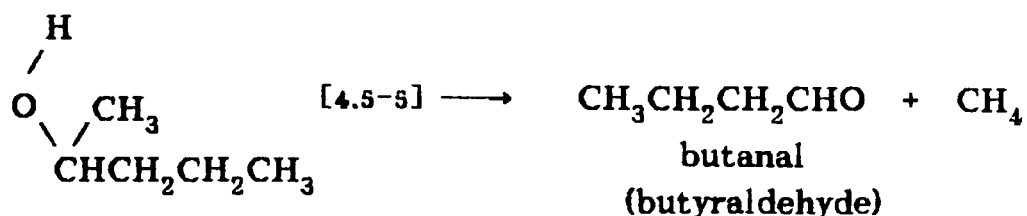
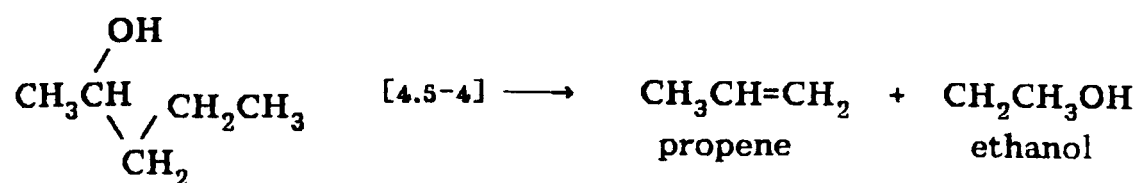
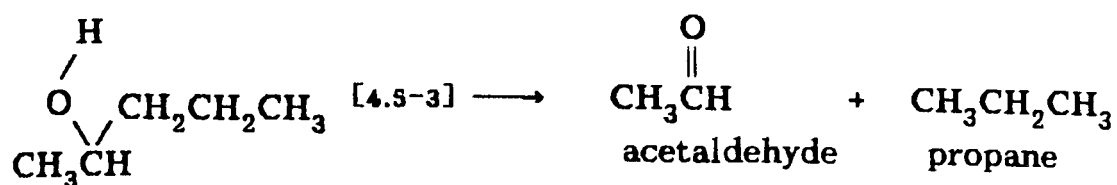
Subsequent radical reactions may be expected to form the following products:





The reaction paths [4.5-6], [4.5-7], and [4.5-8] leading to production of ethyl, *n*-propyl, and methyl radicals (respectively) have very similar heats of reaction. There are, however, two channels which lead to the production of methyl radicals, so their production is likely to be favoured. Consequently, one would expect reaction [4.5-14] to occur in statistical preference to reactions [4.5-15] and [4.5-16], which in turn would be preferable to reactions [4.5-11] through to [4.5-13]. It is thus not surprising that the yields are in the order  $\text{C}_2\text{H}_6 > \text{C}_3\text{H}_8 > \text{C}_4\text{H}_{10} > \text{C}_5\text{H}_{12} > \text{C}_6$ .

The results have clearly shown that the primary reaction paths are those of molecular dehydration, and minor products are not insignificant. Although the minor products can be well accounted for by radical reactions (shown above), it may also be true that some of the products are a result of further molecular channels. For example, by analogy to recent work on doped ethanol by Goodale *et al.* (81), a concerted molecular elimination of the methyl group as in [4.5-5] (or perhaps in this instance also of the propyl group [4.5-3]) with the hydrogen of the hydroxyl can be expected. Four-centred, molecular elimination reactions [4.5-3] to [4.5-5] would produce acetaldehyde ( $\text{CH}_3\text{CHO}$ ) and propane; propene and ethanol; and methane and butanal ( $\text{CH}_3\text{CH}_2\text{CH}_2\text{CHO}$ ), as shown below. If produced with high enough energy, the ethanol by-product may decompose to produce ethene. Propane, propene, ethane and ethene were readily detected in this work.



It is not possible to isolate the precise mechanism for the production of the minor products, because it is an extremely complex trade-off between all of the suggested mechanisms. However, because of the similarities in trends, the activation energy,  $E_a$ , of the path leading to propane can be said to be the same as that leading to butane (Fig.4.5-3); and  $E_a$  for  $C_2$  production is the same as for propene (Fig.4.5-4). This reasoning is analagous to that previously used (9) and was discussed towards the end of Section 4.3.5 where it was first applied to this work (9c).

In summary, the origin of the products observed as a result of laser irradiation of pentan-2-ol may be explained as follows:

**Pentenes:** The primary reaction paths have been shown to involve the concerted elimination of the hydroxyl with a  $C_1$ , [4.5-2], or  $C_3$ , [4.5-1], hydrogen; both paths occur, leading to pent-1-ene and pent-2-ene production. The dominant path is that which leads to the 1-olefin, even though this product is the least thermodynamically stable. It is believed that pent-2-ene isomerises after decomposition of the pentan-2-ol.

**Ethene** production may arise in one of three ways, all involving radicals:

(a) by disproportionation of ethyl radicals (produced in [4.5-6]) through reactions [4.5-12b], [4.5-13c], or [4.5-15b].

(b) by further decomposition of ethyl radicals as in [4.5-17] for which  $\Delta H^\circ \sim 40$  kcal/mol (see Table 4.2-1). The total energy requirement of the complete path ([4.5-3] followed by [4.5-17]) is  $\sim 124$  kcal/mol, just inside of the allowable limit as discussed earlier.

(c) by hydrogen abstraction of vinyl radicals, which arise, as in step [4.5-19], by water elimination from the  $\text{CH}_3\text{CHOH}$  radicals generated by carbon-carbon fission in step [4.5-4]. This type of reaction was first proposed by Zhitneva *et al.* (101).

**Ethane** is most obviously formed by recombination of methyl radicals [4.5-14] generated by the carbon-carbon fission processes [4.5-8] and [4.5-9]. Possible disproportionation reactions are those of  $\text{C}_2\text{H}_5$  with  $\text{C}_2\text{H}_5$ , as in [4.5-12b], and with  $n\text{-C}_3\text{H}_7$  as in [4.5-13b].

**Propene** may be formed in three ways:

(a) by disproportionation of  $\text{C}_3\text{H}_7$  with  $\text{C}_3\text{H}_7$  [4.5-11b],  $\text{C}_2\text{H}_5$  [4.5-13b], or  $\text{CH}_3$  [4.5-16b].

(b) by further decomposition of propyl radicals as in [4.5-18] for which  $\Delta H^\circ \sim 34$  kcal/mol (see Table 4.2-1). The total energy requirement of the complete path ([4.5-7] followed by [4.5-18]) is  $\sim 118$  kcal/mol, inside of the allowable limit as discussed earlier.

(c) analogously to ethene, it could arise by hydrogen abstraction from propenyl radicals which are themselves generated, as in the water elimination step [4.5-20], from  $\text{CH}_3\text{CH}(\text{OH})\text{CH}_2$  radicals produced in step [4.5-6].

**Propane** is probably formed by recombination of methyl radicals (produced in [4.5-8] and [4.5-9]) with ethyl radicals (from step [4.5-6]) through reaction [4.5-15a]. Disproportionation reactions involving propyl radicals as in [4.5-11b] and methyl and ethyl radicals as in [4.5-13c], are also possible; the propyl radicals are produced in the carbon-carbon fission step [4.5-7]. Also, by analogy to the production of methane from ethanol, propan-2-ol, and butan-2-ol, a possible, path for pentan-2-ol would also be the four-centred, molecular elimination reaction [4.5-3]. As implied by the discussion of  $\text{CH}_4$  production from pentan-2-ol, discussed below, it is likely that this molecular process only occurs to a small extent compared with methyl and ethyl radical recombination.

**Butane** is most likely to be formed from recombination reactions; through reaction [4.5-12a] which involves ethyl radicals formed in step [4.5-6]; and through reaction [4.5-16a] which involves methyl and propyl radicals formed at steps [4.5-8&9] and [4.5-7] respectively. Since the high pressure yields are in the order  $\text{C}_2\text{H}_6 > \text{C}_3\text{H}_8 > \text{C}_4\text{H}_{10} > \text{C}_5\text{H}_{12} > \text{C}_6$ , this is consistent with a greater production of methyl radicals than ethyl radicals which is as to be expected on statistical grounds.

**Methane** could conceivably arise by methyl abstraction. Possible disproportionation reactions are those of  $\text{CH}_3$  with  $\text{C}_2\text{H}_5$  as in [4.5-15b], and with  $n\text{-C}_3\text{H}_7$  as in [4.5-16b]. However, the concerted molecular elimination of the methyl group by the H of the OH group to give methane, was the reaction proven by Goodale *et al.* (81) to account for methane from doped ethanol: by analogy, the same molecular elimination process for pentan-2-ol is more likely to be the source of methane also producing butanal ( $\text{CH}_3\text{CH}_2\text{CH}_2\text{CHO}$ ) [4.5-5]. Since this molecular channel is expected to contribute largely to the yield of methane, and since the analagous channel is

expected to contribute to the same degree to the yield of ethene, from the low amount of  $\text{CH}_4$  produced relative to  $\text{C}_2\text{H}_6$ , it is likely that this process is unimportant compared with carbon-carbon fission processes.

*n-Pentane* is likely to be a result of recombination of an ethyl radical (produced from the carbon-carbon fission step [4.5-6]) with a propyl radical (produced from the carbon-carbon fission step [4.5-7]) as in [4.5-13a].

*But-1-ene* most likely arises from the radical, other than  $\text{CH}_3$ , formed in the carbon-carbon fission processes [4.5-8] and [4.5-9]; elimination of water from the radicals will give butenyl (as in [4.5-21]) which will form but-1-ene after hydrogen abstraction.

One other possible, but insignificant, source of butene is the pentyl radical generated by the C-O fission in step [4.5-10] (analogous to the formation of propene from butanol via step [4.3-9]). It is the results of butanol that indicate, by similarity, that the reaction [4.5-10] is likely to be insignificant.

$\text{C}_6$ , although not clearly identified, is likely to be hexane, formed from the recombination of *n*-propyl radicals. This conclusion is based on the evidence that recombination and disproportionation reactions exist for all other combinations (pairs) of  $\text{CH}_3$ ,  $\text{C}_2\text{H}_5$  and *n*- $\text{C}_3\text{H}_7$  radicals as described above.

With the exception of the small observed amount of  $\text{CH}_4$  and possibly a small amount of  $\text{C}_2\text{H}_6$ , all these other products are well accounted for by the occurrence of carbon-carbon fission processes occurring alongside the main water elimination channel which produces the pentenes.

## 4.6 PENTAN-3-OL

Multi-longitudinal mode pulses irradiated pentan-3-ol at 1.85Hz on the line  $R_{14}$  (10 $\mu$ m). Products were identified as methane, ethane, ethene, propane, propene, butane, but-1-ene, pent-1-ene, and *trans*- and *cis*-pent-2-ene. Other minor peaks (one of which lay on the trace between but-1-ene and the pent-2-enes) could not be identified. The Pye and Carlo chromatograph conditions were the same as for pentan-2-ol.

The irradiating wavelength is strongly absorbed by pent-2-enes (not pent-1-ene): the low signal absorption cross-section  $\sigma = 8.9 \times 10^{-20}$  cm<sup>2</sup>/molecule. A high pressure mixture (0.199 torr) of *trans*- and *cis*-pent-2-ene, was irradiated for 1665 pulses at high fluence (11.23 $\pm$ 0.03 J/cm<sup>2</sup>). A 4.1% conversion to the 1-olefin isomer was noted, together with production of ethene, but-1-ene and n-pentane totalling 0.04%. High pressure, high fluence runs on pentanol were not carried out for longer than 500 pulses. Thus for all experimental conditions, it was shown that secondary decomposition of pent-2-enes was negligible compared to the amount actually produced.

### 4.6.1 Fluence Dependence

Information was gathered on the variation of product yields as the fluence was altered using undiluted sample pressures of nominally 50 mtorr. The average sample pressure was 50 mtorr, and the standard error of the distribution about this average was 0.4 mtorr. The accumulated data was unsuitable for deconvolution (Fig.4.6-1). *Trans*-pent-2-ene was the only detected product at the lowest fluence of 2.1 J/cm<sup>2</sup>, but both isomers were measured above 5.8 J/cm<sup>2</sup>. Figure 4.6-2 displays the yield as a ratio to the sum of the primary, dehydration products. Fragmentation becomes evident at 8 J/cm<sup>2</sup> with the presence (in decreasing order) of ethene, methane and

**Fig. 4.6-1 Pentan-3-ol: Effect of fluence, R14 (10  $\mu\text{m}$ ), on pentene yield (raw data) for pure reactant**

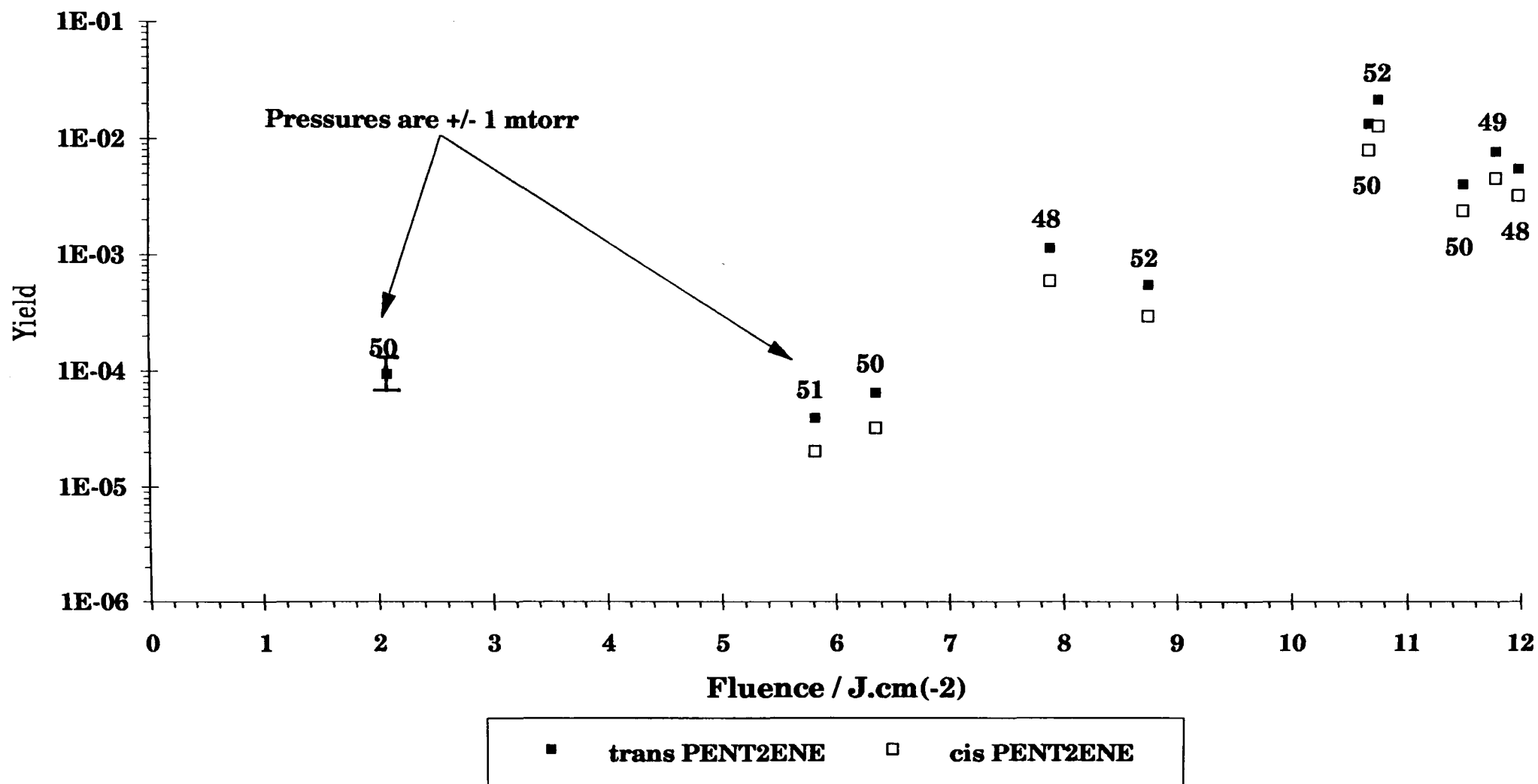
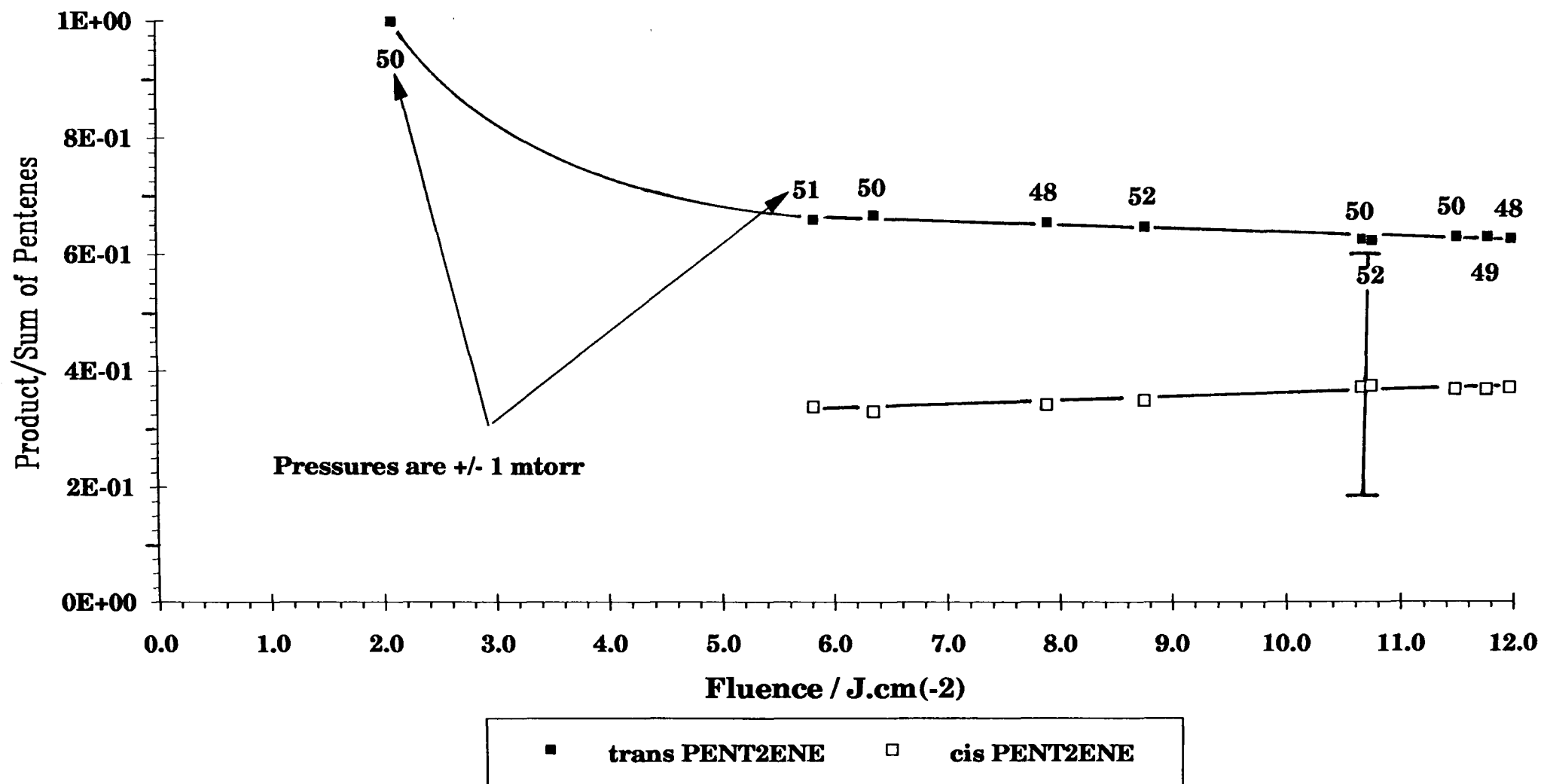


**Fig. 4.6-2 Pentan-3-ol: Effect of fluence, R14 (10  $\mu\text{m}$ ), on the yield ratio of product to sum of pentenes (raw data) for pure reactant**



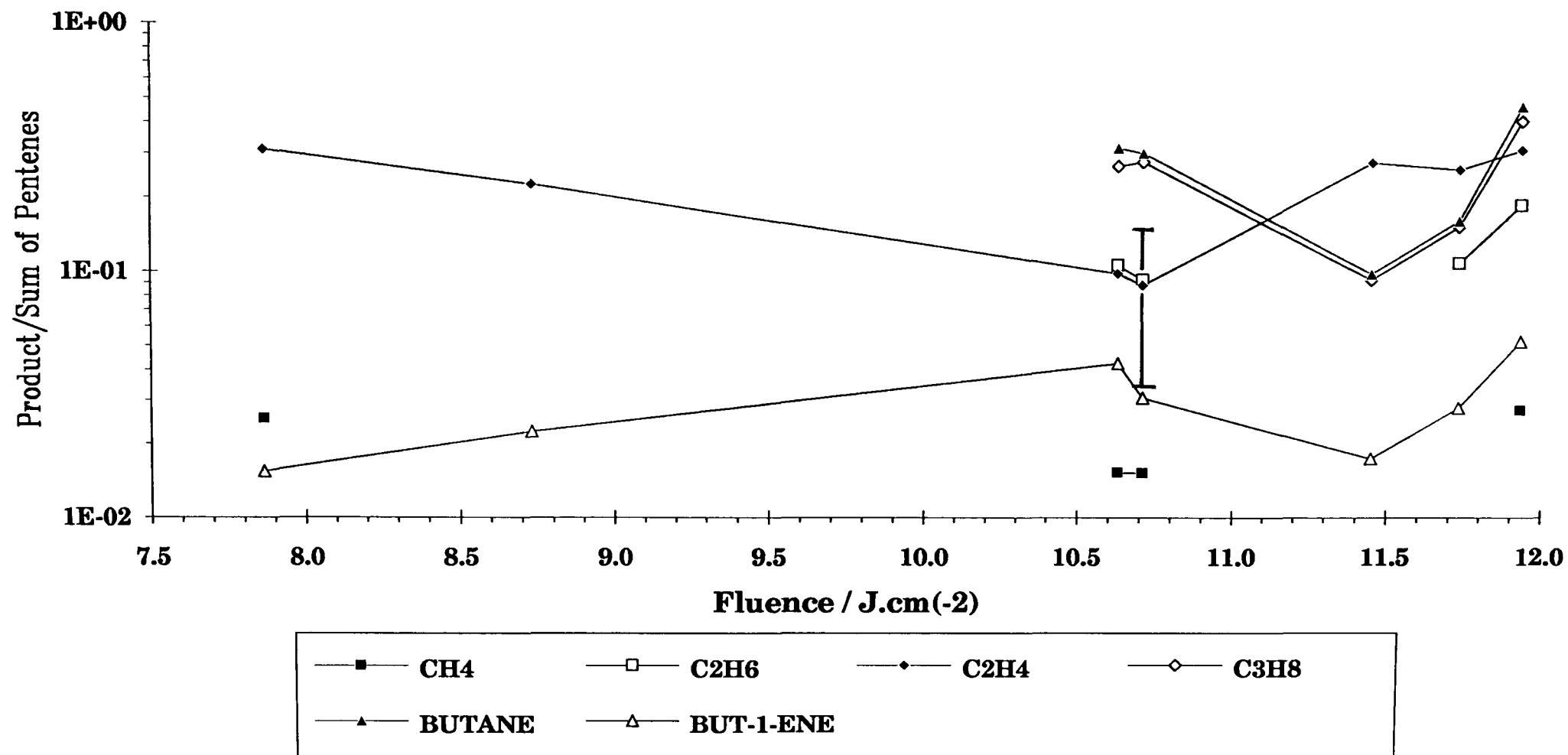
but-1-ene (Fig.4.6-3): this order is dependent on fluence. At the highest fluences ( $>11 \text{ J/cm}^2$ ) the list of fragments in decreasing order is propane and butane (in equal quantities); ethene, ethane, but-1-ene and methane (plus others not identified); propene was detected at fluences  $>10.6 \text{ J/cm}^2$  in amounts about 0.03 of those of propane which makes it the least important identified product.

There is a slight convergence in the yields of Fig.4.6-2 as the fluence increases. At the maximum fluence of  $11.9 \text{ J/cm}^2$  the ratio *trans*-pent-2-ene:*cis*-pent-2-ene is 63%:37%. The apparent local drop in primary product yield starting at around  $8 \text{ J/cm}^2$  coincides with the first detection of minor products, and may indicate that one of the "new" minor product channels competes directly with the dehydration channel. Analogously to the detailed discussion on conformers for butan-2-ol, rotations about  $\text{C}_2\text{-C}_3$ , and  $\text{C}_3\text{-C}_4$ , are the processes which result in unimolecular dehydration and the formation of pent-2-ene isomers. The observed proportion of *trans*-pent-2-ene to *cis*-pent-2-ene, will be related to the energy difference of the conformers.

The yields per pulse were independent of the number of pulses for the majority of products; an indication that the products are primary. Only propene appeared to result from secondary decomposition (accumulating with each pulse), but too great an importance should not be placed on this finding, since propene lay on the tail of the propane GLC peak and propane was a factor of 100 greater i.e. there is more uncertainty in the measurement of propene.

The *trans/cis* ratio is found to be  $\approx 1.90$  over the fluence range  $4\text{-}12 \text{ J/cm}^2$ . while the statistical ratio gives unity. The observed ratio, which is probably

**Fig. 4.6-3 Pentan-3-ol: Effect of fluence, R14 (10  $\mu\text{m}$ ), on the yield ratio of product to the sum of pentenes (raw data) for 50 mtorr of pure reactant**



nearer the equilibrium value, suggests some post-pulse thermal isomerisation. Although some conversion to pent-1-ene could occur at high fluence since pent-2-ene absorbs the irradiating wavelength, it is unlikely, for little of the 2-olefin is produced under normal conditions.

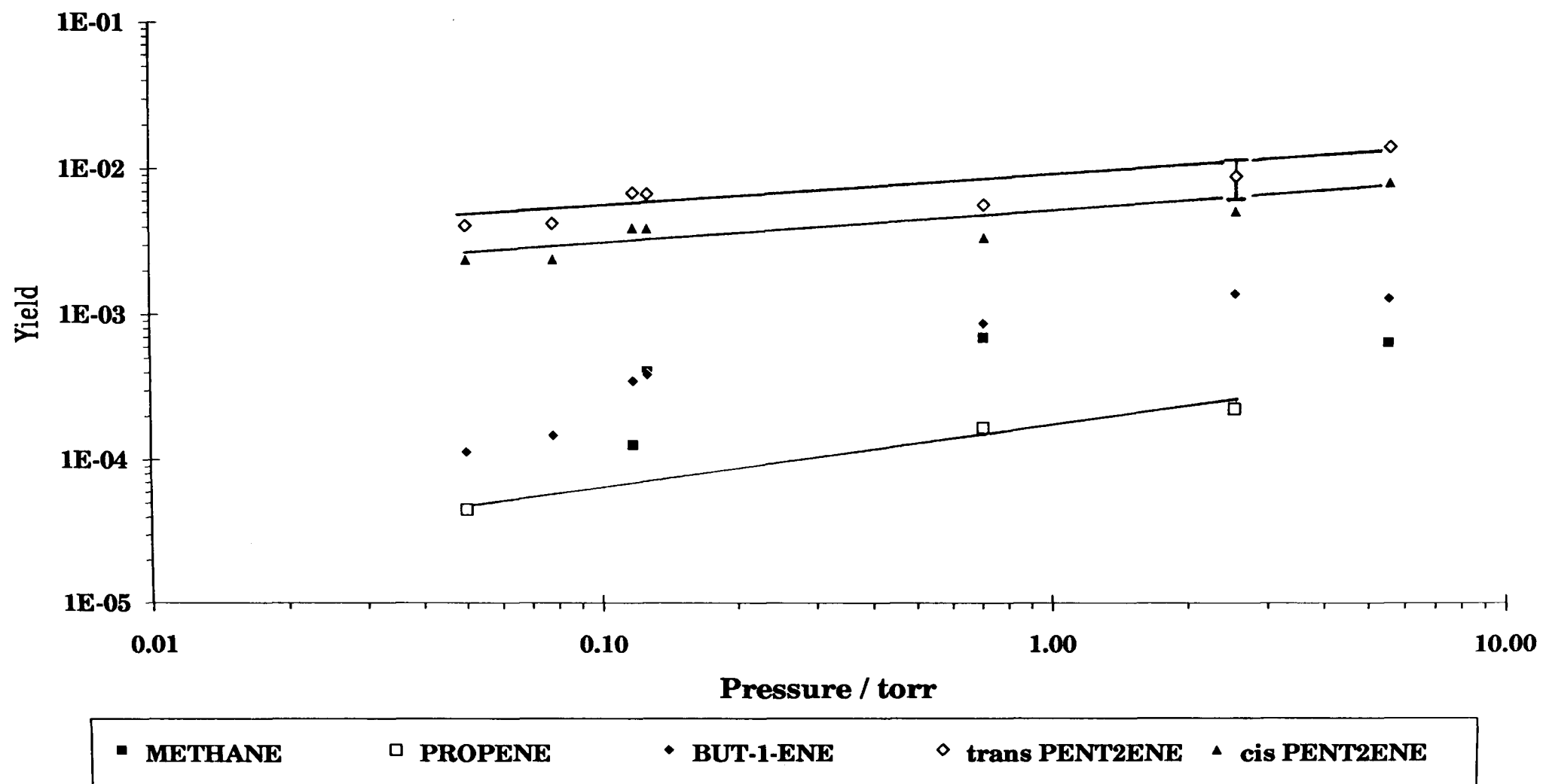
#### 4.6.2 Pressure Dependence

Experiments run under conditions of constant, high fluence ( $11.3 \text{ J/cm}^2$ ) are represented in terms of undeconvoluted data in figures 4.6-5 and 4.6-6. The average fluence was  $11.29 \text{ J/cm}^2$ , and the standard error of the distribution about this average was  $0.05 \text{ J/cm}^2$ . The pent-2-ene isomers are the major products at low pressure and maintain a constant ratio with respect to each other over the pressure range. At high pressures (7 torr), ethene and ethane are the dominant products.

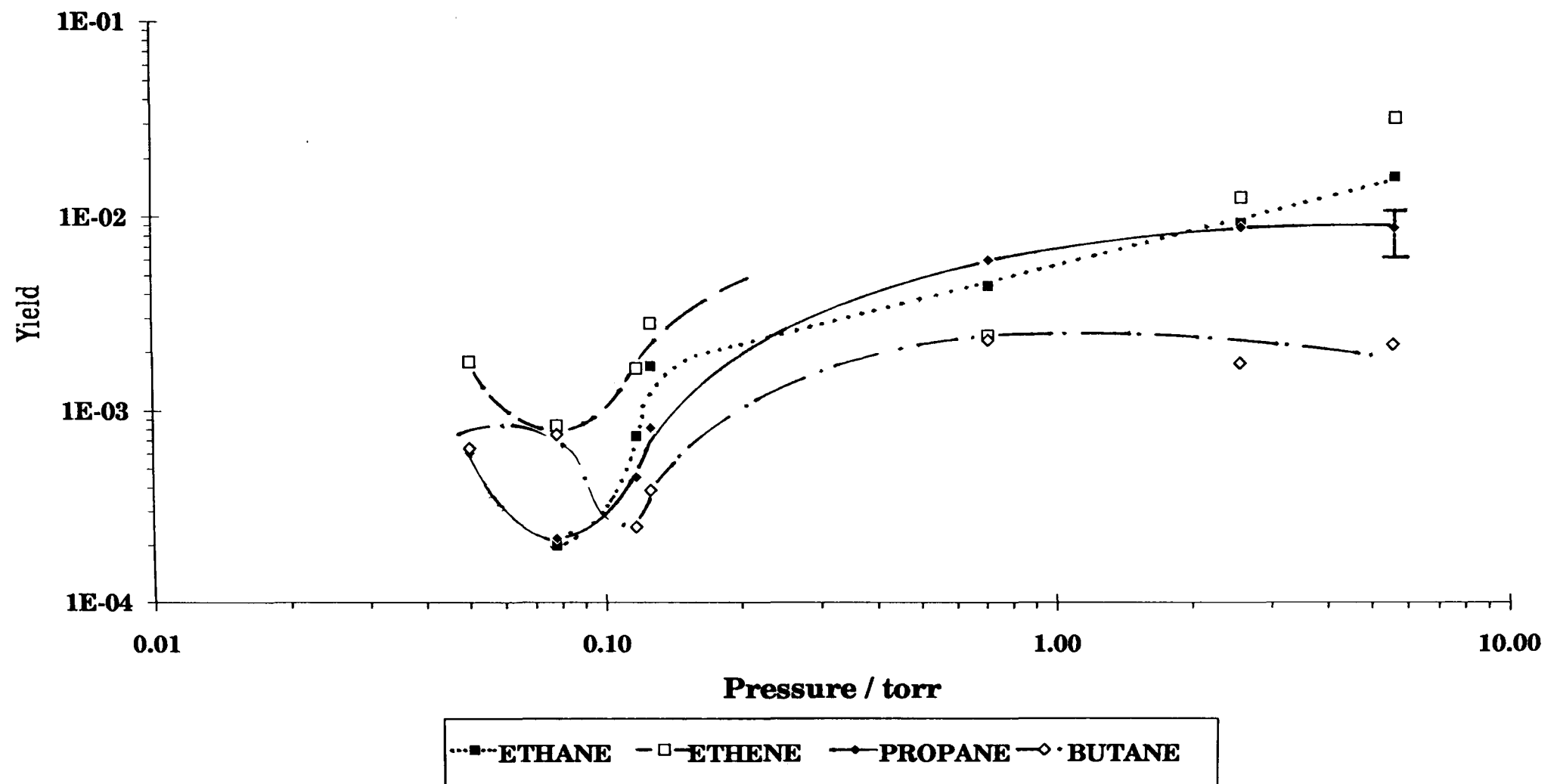
#### 4.6.3 Discussion

Listed below are some decomposition paths (molecular elimination and bond fission) with related heats of reaction for pentan-3-ol, which, *a priori*, may be accessible with IR irradiation. As explained in Section 4.5, the activation energy for unimolecular dehydration is approximately  $57 \text{ kcal/mol}$ , and the likely excitation above the dissociation limit is approximately  $131 \text{ kcal/mol}$ . Hence, as before, with no further reaction, all the listed reactions [4.6-1] through to [4.6-3] including C-H, C-O and O-H bond fission channels, will be allowed (for fission reactions,  $\Delta H$  values are similar to the activation energies). These and further reactions will be possible if the total activation energy does not exceed  $131 \text{ kcal/mole}$ .

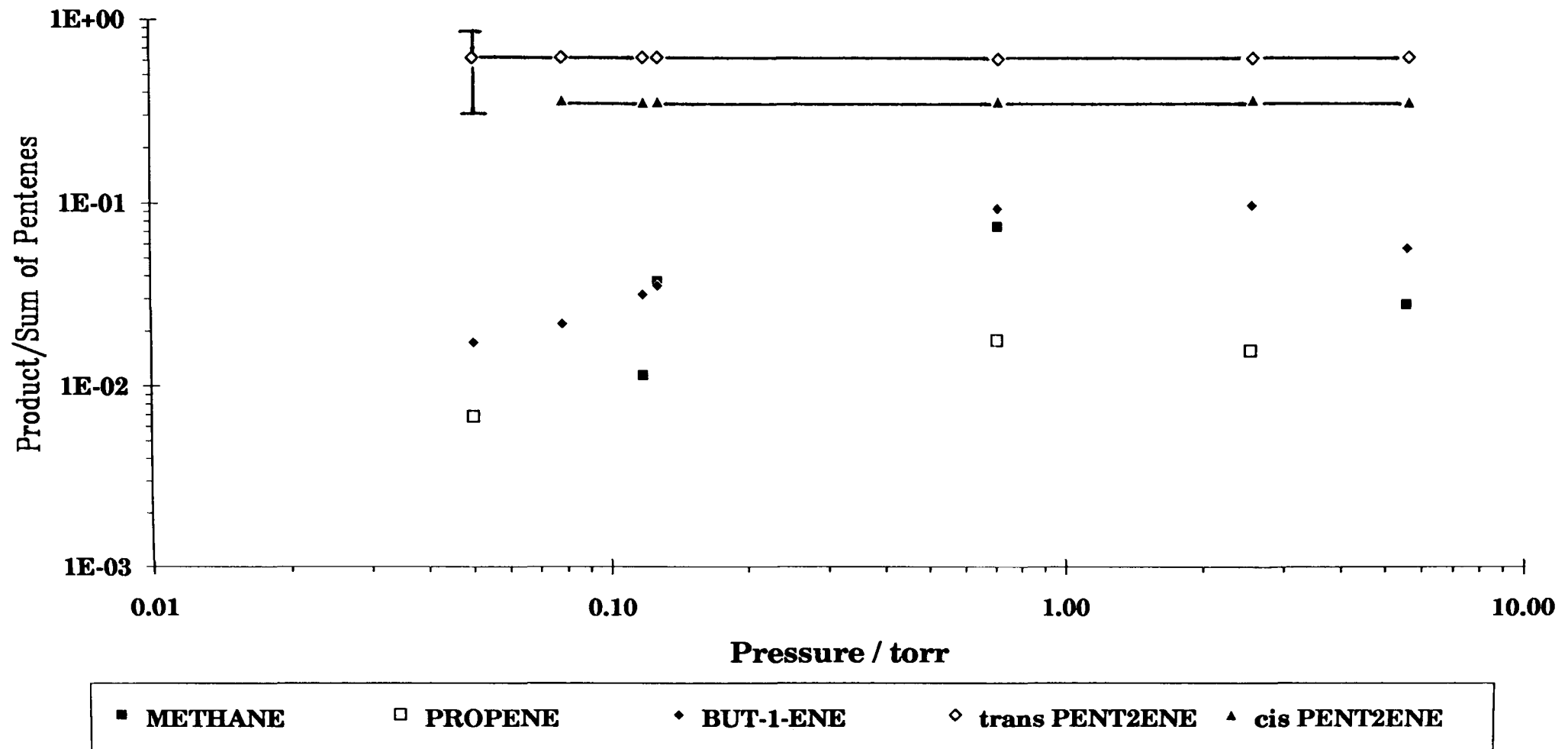
**Fig. 4.6-5(a) Pentan-3-ol: Effect of pressure on yield (raw data) for pure reactant irradiated at a fluence of 11.3 J.cm(-2)**



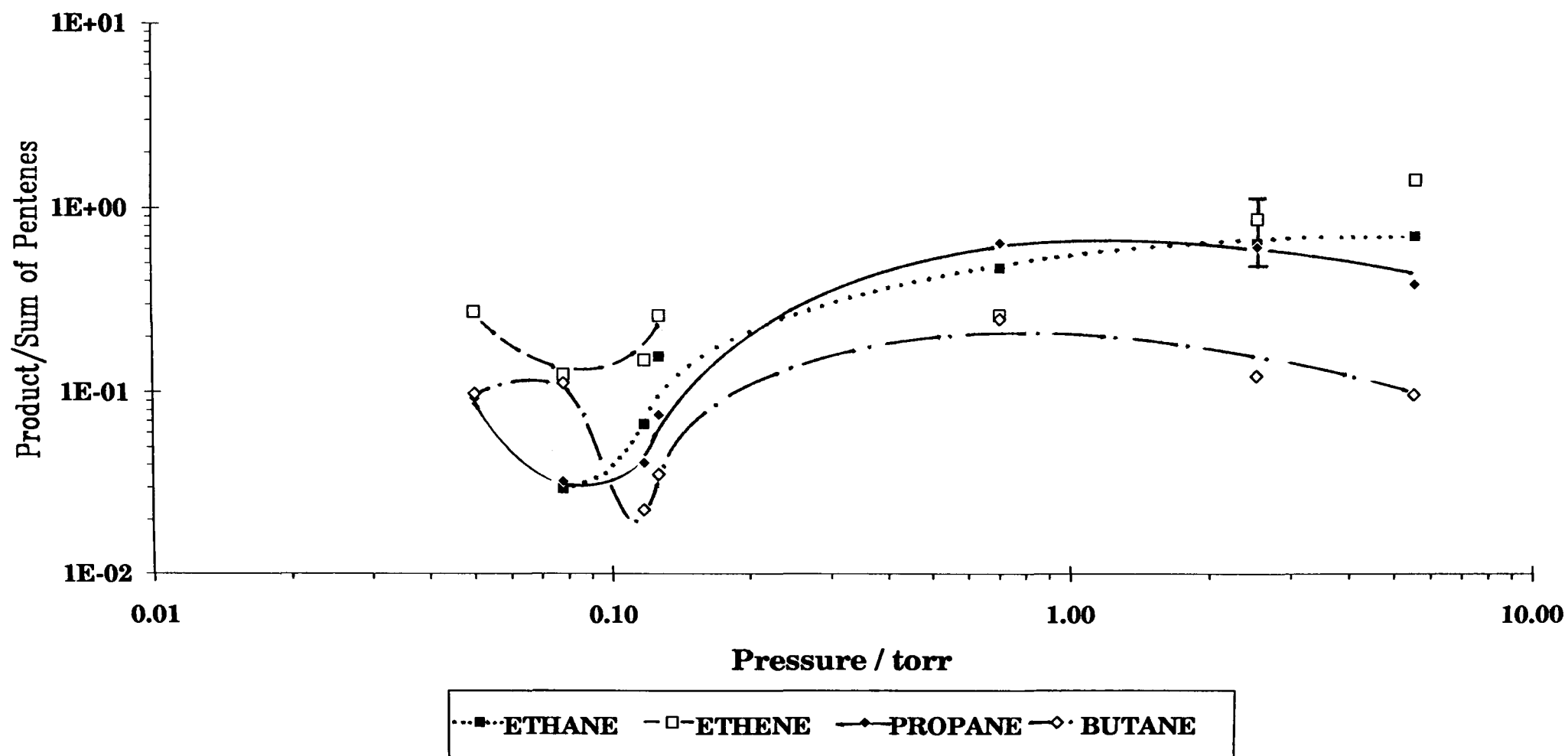
**Fig. 4.6-5(b) Pentan-3-ol: Effect of pressure on yield (raw data) for pure reactant irradiated at a fluence of  $11.3 \text{ J.cm}^{-2}$ .**

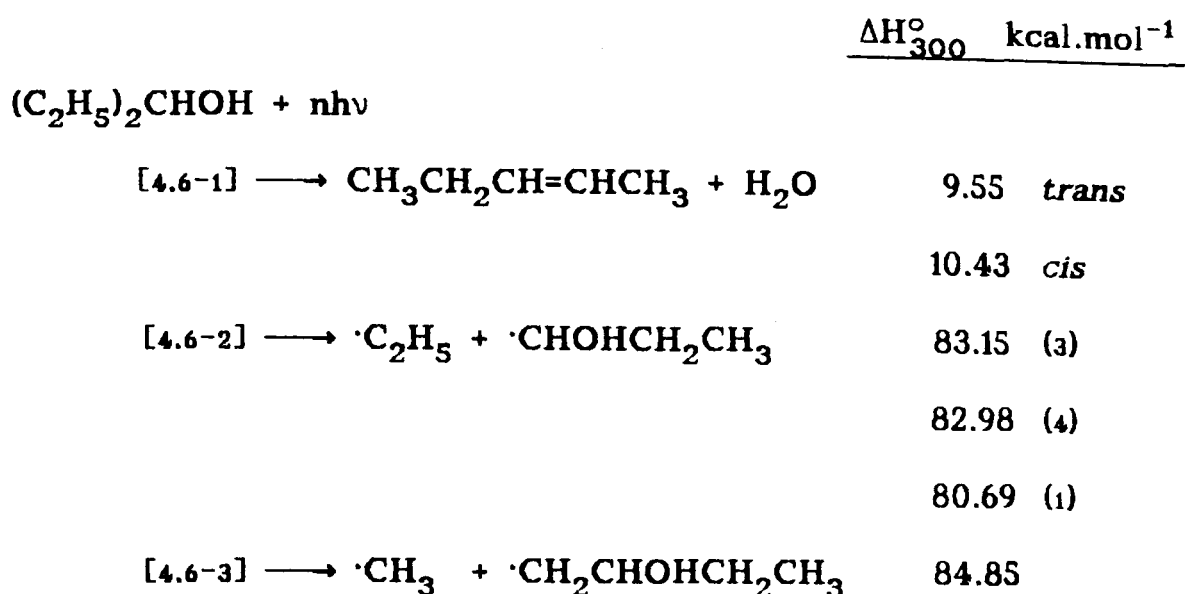


**Fig. 4.6-6(a) Pentan-3-ol: Effect of pressure on the yield ratio product to the sum of pentenes (raw data) for pure reactant irradiated at a fluence of 11.3 J.cm(-2)**

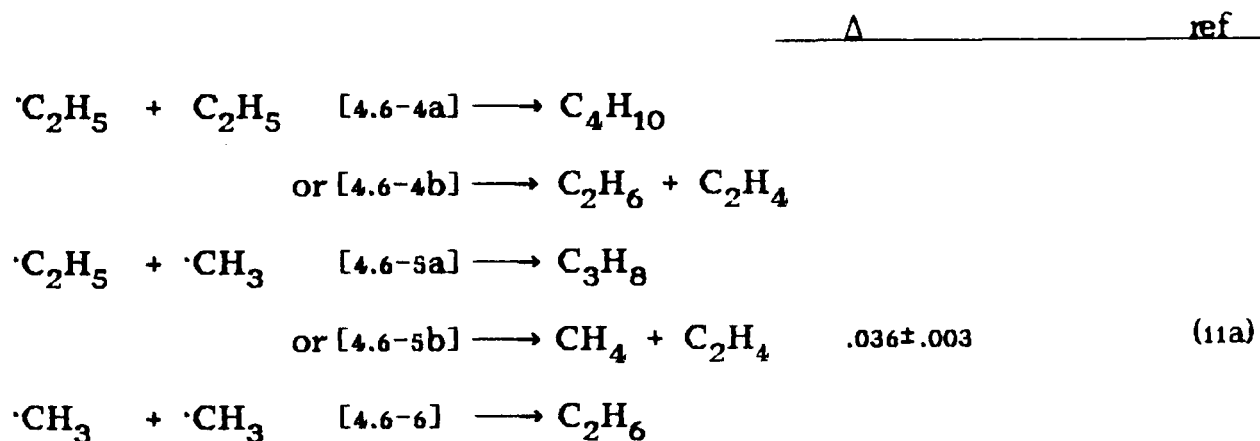


**Fig. 4.6-6(b) Pentan-3-ol: Effect of pressure on the yield ratio product to the sum of pentenes (raw data) for pure reactant irradiated at a fluence of 11.3 J.cm(-2)**





Because of the symmetry, each of the above mechanisms can occur by the breaking of two separate bonds. The energies have not been worked out for the breaking of C-H, C-O, or O-H (leading to pentyl radicals) bonds, since it was shown for ethanol, propan-2-ol, butan-2-ol and hexan-2-ol that these are typically 91, 92, 103 kcal/mol respectively. The following is a list of possible alkyl recombination reactions:



Much of the discussion presented under pentan-2-ol is again applicable here: primarily that isolation of the precise mechanism of minor product formation is not possible, because it is likely to be a complex trade-off between all previously suggested mechanisms and even additional unimolecular reactions (outlined later).

In summary, the products of pentan-3-ol can be explained as follows. The low fluence products will be described first followed by additional products found at high fluence (see listing at beginning of Section 4.6.1).

**Pent-2-ene.** Molecular dehydration is the primary path; elimination of the OH occurs with a C<sub>2</sub> or C<sub>4</sub> hydrogen, and because of molecular symmetry, both paths produce the pent-2-ene isomers.

**Ethene** is the major other product for most of the fluence range (Fig.4.6-3) and at high pressures (Fig.4.6-6). It is likely to arise from step [4.6-6], which is recombination of the methyl radicals produced from the carbon-carbon fission step [4.6-3], and also by disproportionation of two ethyl radicals as in step [4.6-4b], and of a methyl and ethyl radical as in step [4.6-5b]; the ethyl radicals arise from the carbon-carbon fission step [4.6-2].

**Methane** could also arise from these methyl radicals by hydrogen abstraction, and by disproportionation of a methyl and ethyl radical as in step [4.6-5b].

**But-1-ene** may arise from the other radical formed in step [4.6-3]; elimination of water from CH<sub>2</sub>CH(OH)C<sub>2</sub>H<sub>5</sub> gives butenyl which will give but-1-ene by hydrogen abstraction.

**Propane** is likely to arise from step [4.6-5a] which is the recombination of a methyl radical (formed from the carbon-carbon fission step [4.6-3]) with an ethyl radical (formed from the fission step [4.6-2]).

**Butane** also arises from recombination, as in step [4.6-4a], of the ethyl radicals produced in step [4.6-2].

**Ethane** could arise from these ethyl radicals by hydrogen abstraction, and by disproportionation of two ethyl radicals as in step [4.6-4b].

**Propene** may arise from the other radical formed in step [4.6-2]; elimination of water from  $\text{CH}(\text{OH})\text{C}_2\text{H}_5$  gives propenyl which will give propene by hydrogen abstraction.

Although not apparently necessary to explain the products for pentan-3-ol, since they have all been accounted for above, there follows a short description of additional unimolecular reactions that may occur (shown in Fig. 4.6-7). They are introduced, because it was recently found for ethanol that unimolecular channels (other than the main dehydration channel) were more abundant than previously thought. Rotation about the two identical bonds  $\text{C}_1\text{-C}_2$  and  $\text{C}_4\text{-C}_5$  might lead to production of propanol and ethene as shown in step [4.6-11]. An additional source of but-1-ene may be caused by a concerted elimination of the methyl group by the hydroxyl group as in [4.6-8], and ethane by concerted elimination of the ethyl group by the hydrogen of the hydroxyl group as in [4.6-10] respectively. Recent work on doped ethanol by Goodale *et al.* (81), proved the existence of a concerted molecular elimination of the methyl group. By analogy, the argument for [4.5-10] is strengthened. The final suggestion is elimination of water as in

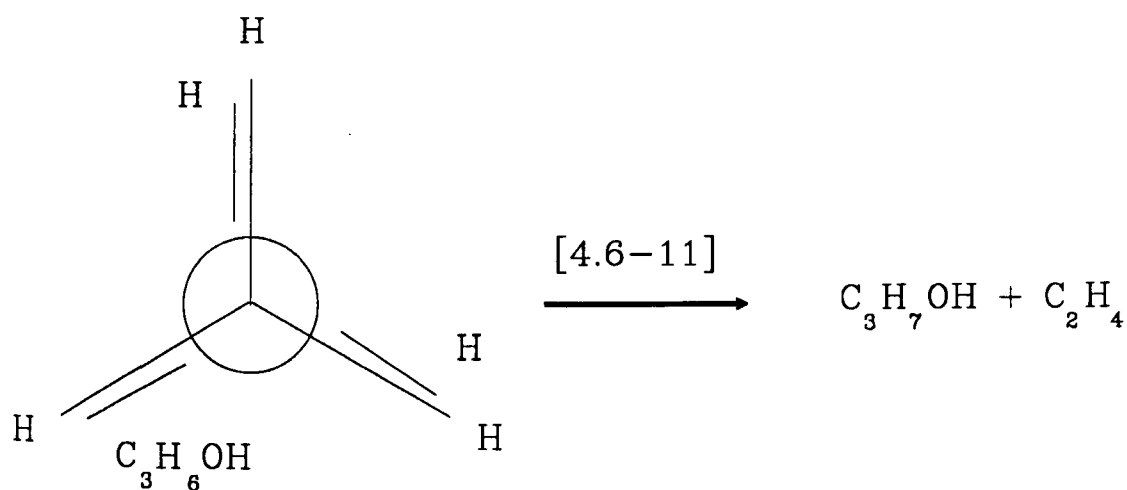
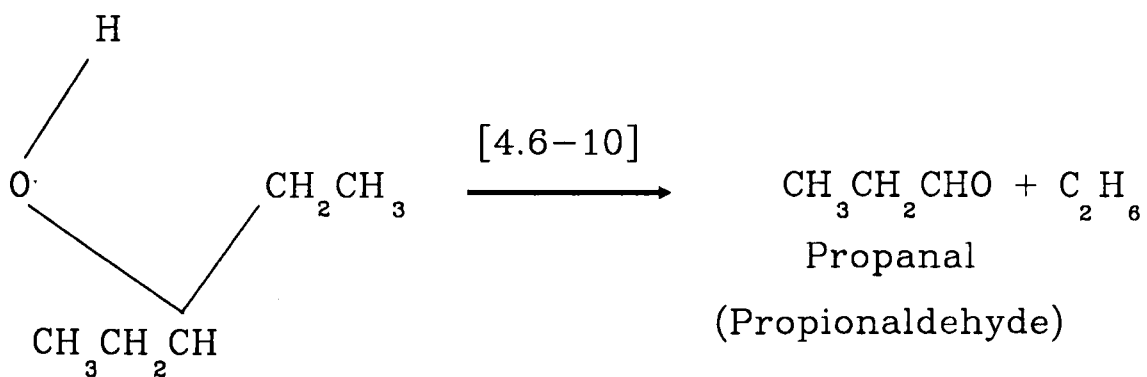
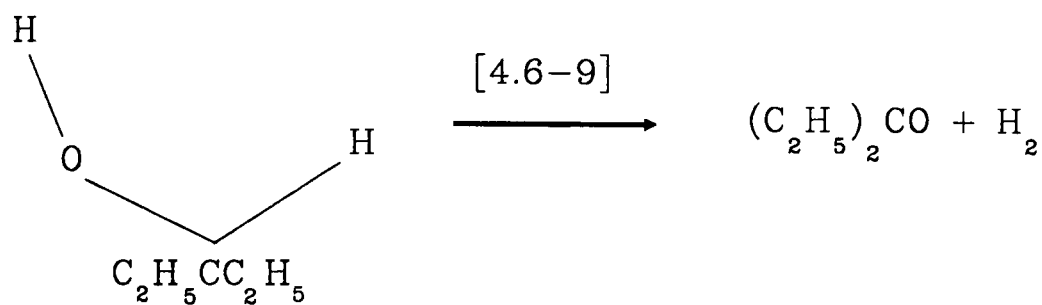
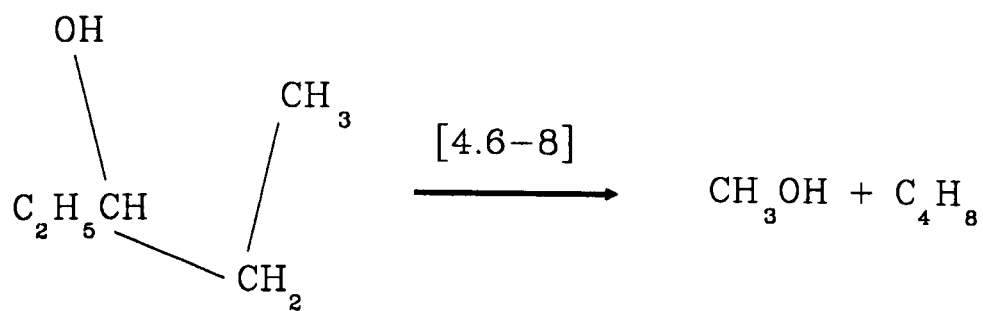


Fig. 4.6-7 Additional 4-centred unimolecular reactions for Pentan-3-ol

step [4.6-9], and is the only additional channel for which products were not measured.

Finally, because butane and propane are formed in nearly equal quantities (Fig.4.6-3) it implies that their reaction paths are equally probable, and hence it is concluded that the activation energy and A factor for the formation of these products are similar. Since they are formed through [4.6-4a] and [4.6-5a] respectively, then  $E_a$  will be roughly 84kcal/mol (the  $\Delta H$  of bond fission for [4.6-2 and -3]), and A (typically for radical reactions) will be  $10^{16}$ . Therefore, since  $E_a$  and A of these channels are both greater than for the primary channel, then butane and propane will become important, as observed, at high fluence.

## 4.7 HEXAN-2-OL

The major products expected, as a result of unimolecular dehydration, are hex-1-ene, and *cis*- and *trans*- hex-2-ene. Multi-longitudinal mode pulses were used to irradiate pure hexanol at a rate of 111 shots/min on the line P<sub>20</sub>(9μm). Over the course of the work, the products which were identified were methane, ethane, ethene, propane, propene, butane, but-1-ene, pentane, pent-1-ene, pent-2-ene, n-hexane, hex-1-ene, and *trans*- and *cis*-hex-2-ene. There were also traces of acetylene and a product which could not be identified, but which was estimated to have a retention time of a C<sub>8</sub> or C<sub>9</sub> hydrocarbon. Both the Pye and Carlo GLC conditions were the same as those used for the pentanols, except that the Pye oven temperature was increased to 50°C.

### 4.7.1 Fluence Dependence

Samples of pure hexanol, of nominally 50 mtorr pressure, were irradiated over a range of fluences (Fig.4.7-1 to 4.7-3). Decomposition was difficult being achieved only for fluences above 7.5 J/cm<sup>2</sup>, a region for which the discrete attenuating abilities of the various salt flats meant that only three data points could be taken. Fig.4.7-1 shows the yield of the dehydration channel in absolute form, while Figs.4.7-2 and 4.7-3 show all the yields as a ratio to the sum of the dehydration channel products. A list of products in order of priority is dependent on fluence. At the lowest fluence, the list (in decreasing order) is hex-1-ene, *trans*-hex-2-ene, *cis*-hex-2-ene, propene, hexane and butane. At the highest fluence the dominant products (listed in decreasing order) are hex-1-ene, ethene, propene, *trans*-hex-2-ene, hexane and *cis*-hex-2-ene, there being a mere factor of 3.2 difference between the yields of the first and last product. Fragmentation clearly contributes greatly to the decomposition.

**Fig. 4.7-1 Hexan-2-ol: Effect of fluence, P20 (9  $\mu\text{m}$ ), on yield (raw data) for pure reactant**

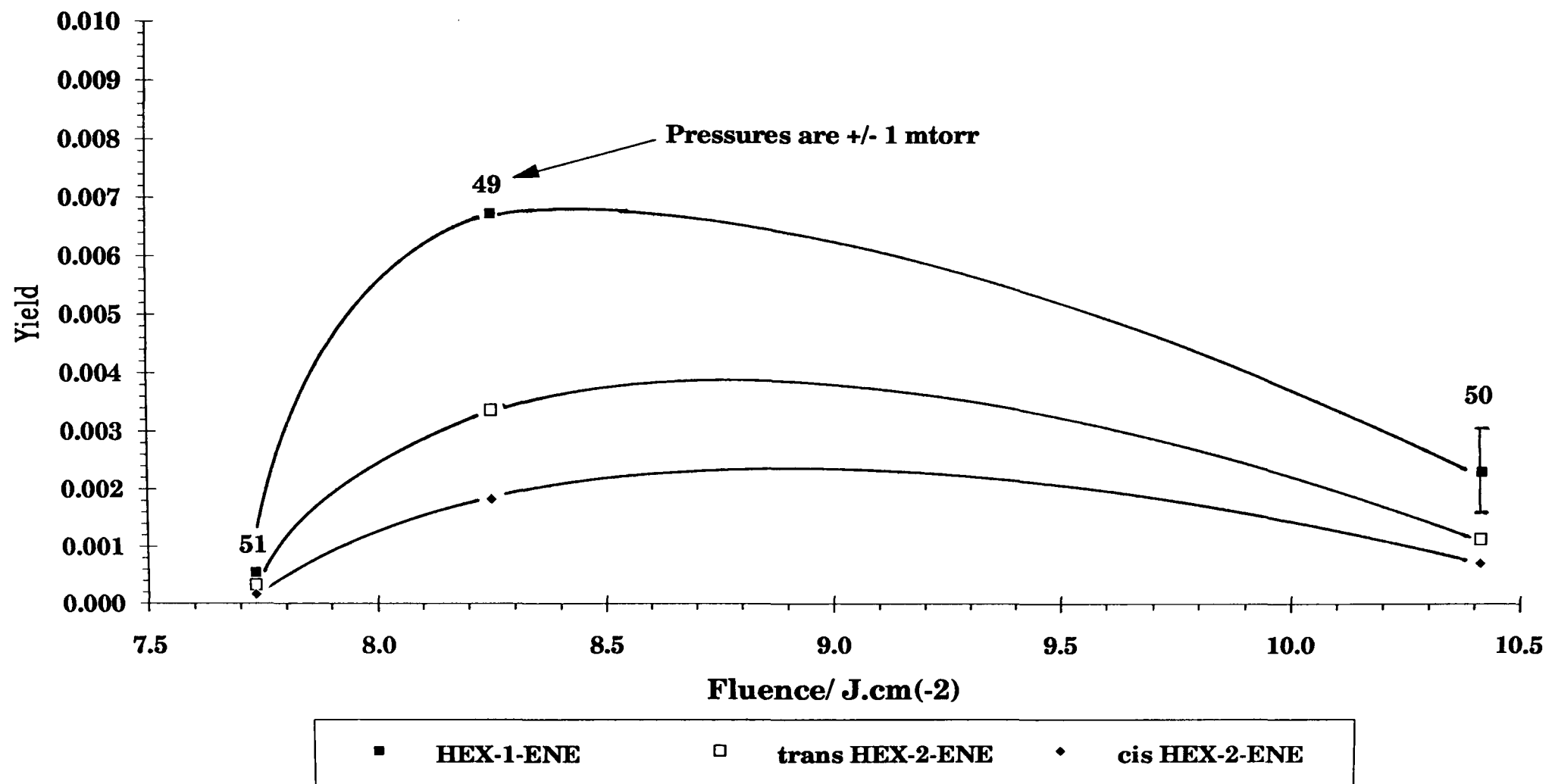


**Fig. 4.7-2 Hexan-2-ol: Effect of fluence, P20 (9  $\mu\text{m}$ ), on the yield ratio of product to the sum of hexenes (raw data) for a pure reactant**

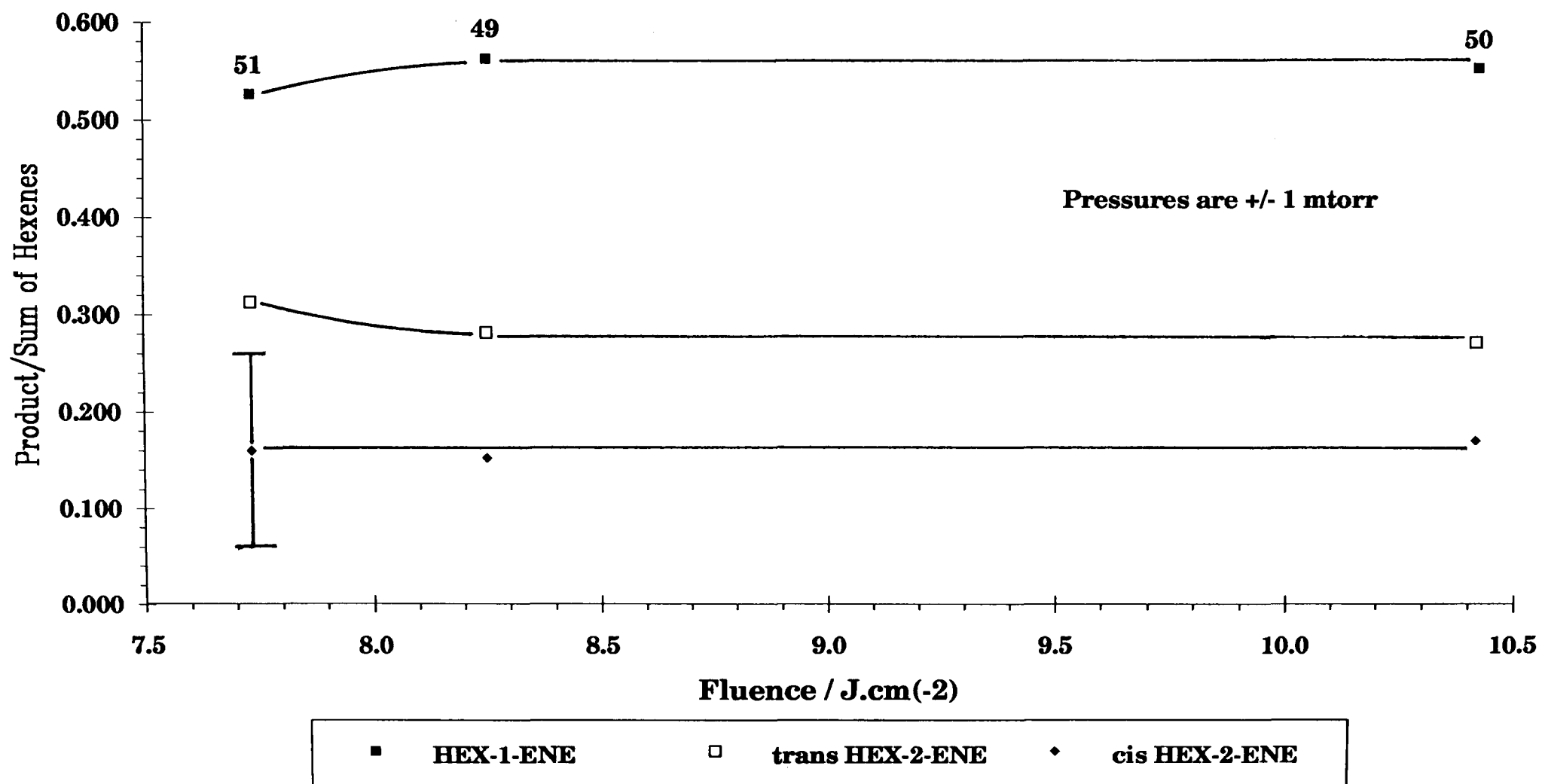
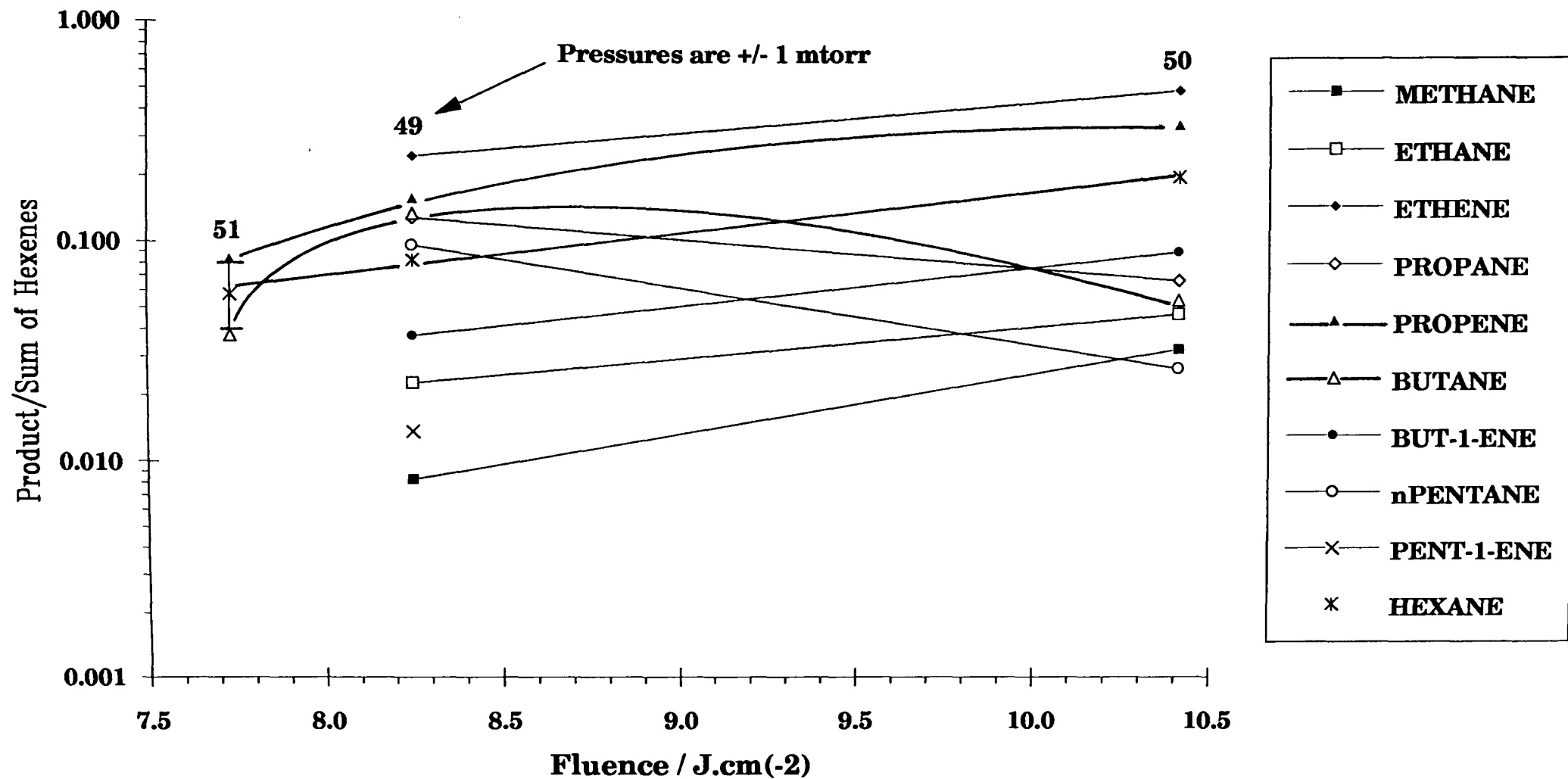


**Fig. 4.7-3 Hexan-2-ol: Effect of fluence, P20 (9  $\mu\text{m}$ ), on the yield ratio of product to the sum of hexenes (raw data) for a pure reactant**



#### 4.7.2 Pressure Dependence

The effect of reactant pressure on product yield was investigated using conditions of high fluence; the fluence range was  $9.36 \pm 0.02 \text{ J/cm}^2$  to  $10.41 \pm 0.04 \text{ J/cm}^2$ , for pressures in the range  $0.05 \rightarrow 1.6 \text{ torr}$ . The yield of hexenes showed a minimum at  $0.6 \text{ torr}$ . When expressed as a ratio to the sum of the dehydration products, there is shown to be very little variation with pressure (Fig.4.7-4) for the dehydration products (these ratios were shown in Fig.4.7-2 not to be so dependent on fluence).

Other products are expressed as a proportion to the sum of the dehydration products in Figs. 4.7-5 and 4.7-6. All the products may be considered to belong to one of three groups as described below. The trend of products within each group is similar which would lead to the conclusion that the mechanism(s) of formation for each product within a group is of the same type (or combination); for example, clearly all the products of group (i) are a result of dehydration. Furthermore, as is reviewed in detail in the Discussion section, the alkenes (group (ii)) are typically explained to be as a result of radical disproportionation reactions and decomposition of hot radicals, while the the alkanes (group (iii)) are explained to arise primarily from radical recombination reactions, but also from radical disproportionation and molecular elimination reactions. Thus, there is likely to be some competing reactions between groups (ii) and (iii). The groups are:

- i) the dehydration products which vary hardly at all with pressure.
- ii) the alkenes which typically have the lowest proportions around  $0.8 \text{ torr}$ .  
Generally the yields dominate over those in group (iii) and at times also over (i).
- (iii) the alkanes which typically have a peak at  $0.8 \text{ torr}$ , and minima at  $0.1 \text{ torr}$ . At the peak, all the alkane ratios are approximately equal to

**Fig. 4.7-4 Hexan-2-ol: Effect of pressure on the yield ratio of product to the sum of hexenes (raw data) for a pure reactant at P20 (9  $\mu\text{m}$ )**

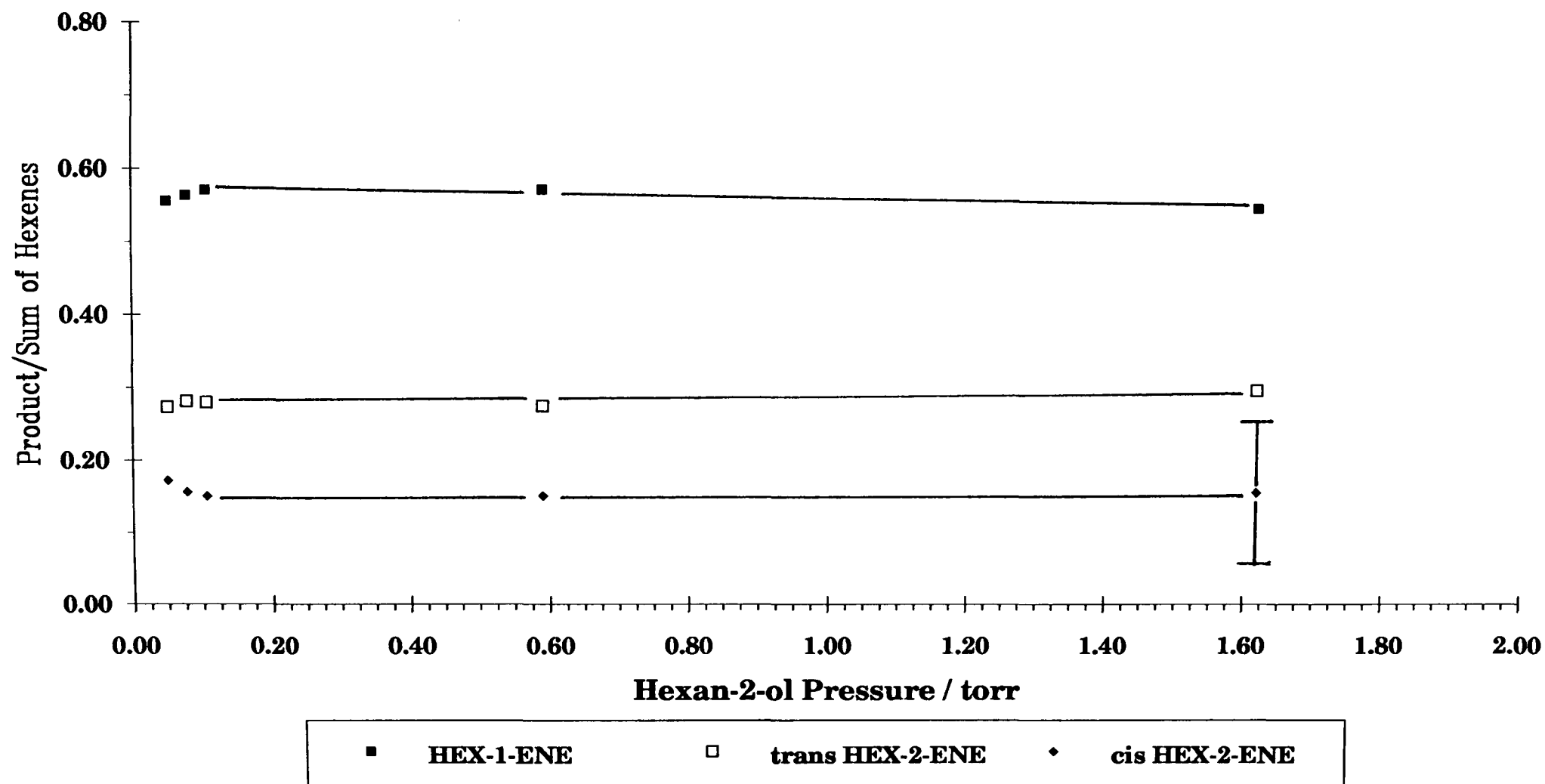


**Fig. 4.7-5 Hexan-2-ol: Effect of pressure on the yield ratio of product to the sum of hexenes (raw data) for pure reactant at P20 (9  $\mu\text{m}$ )**

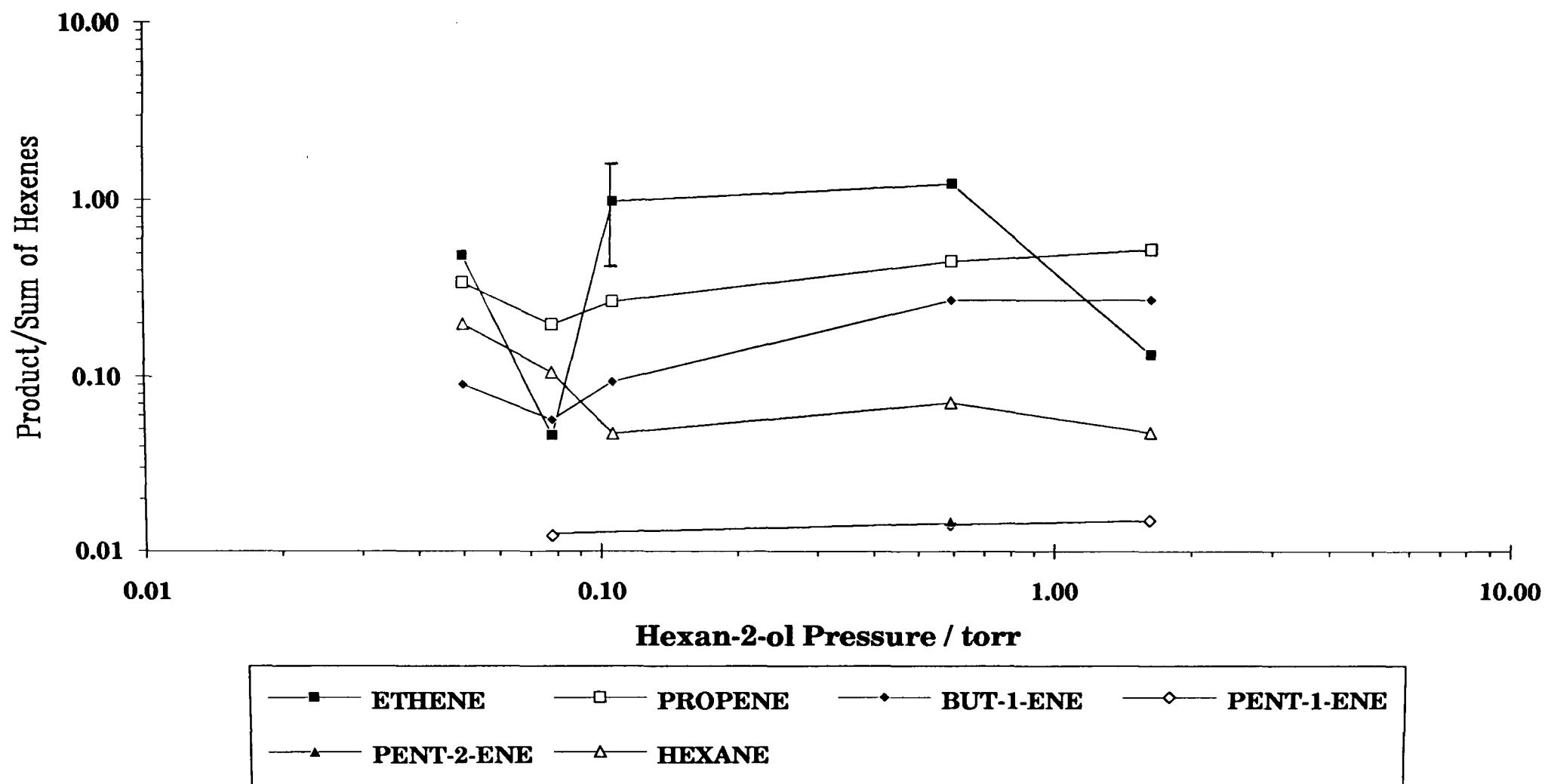
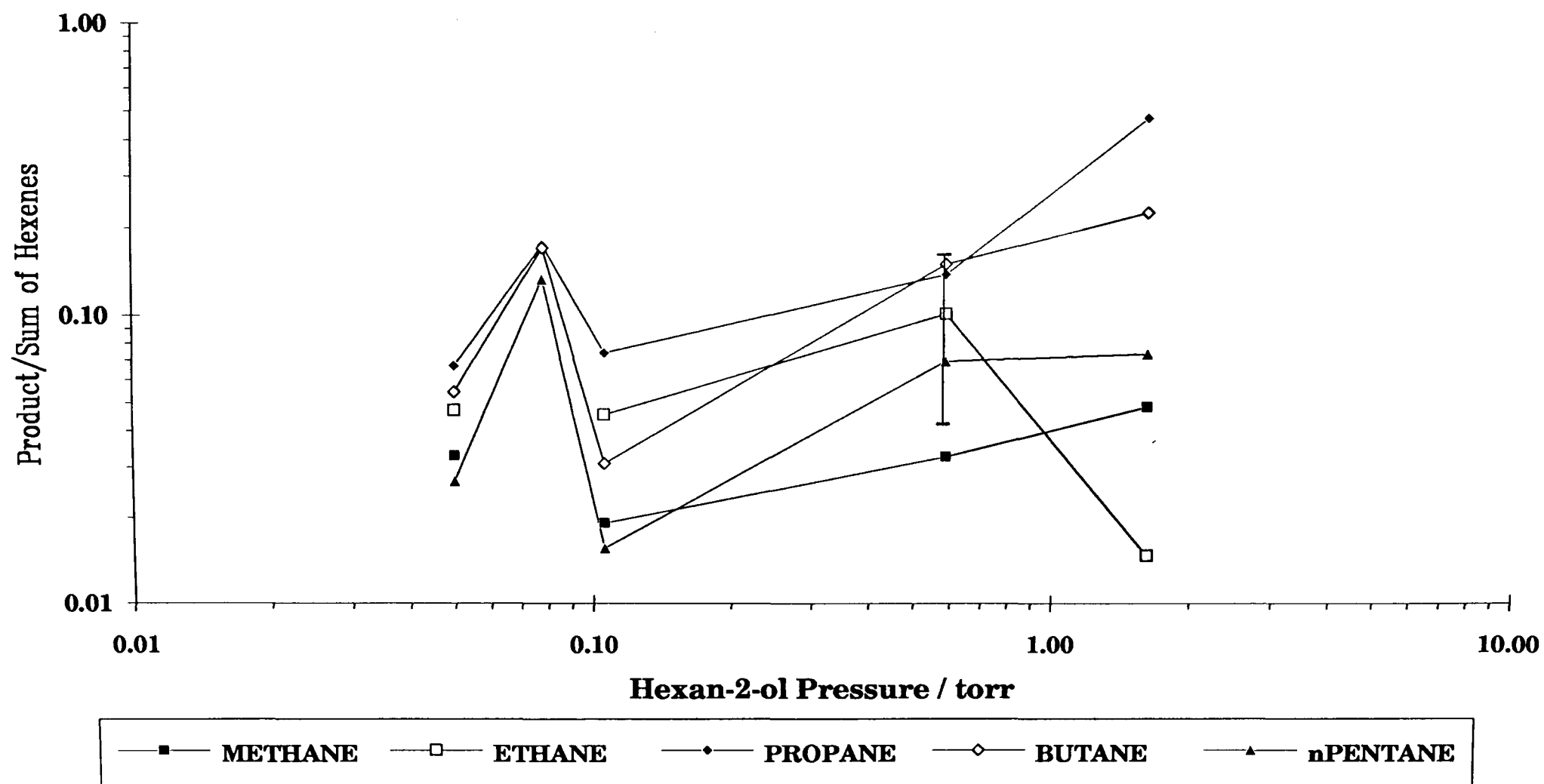


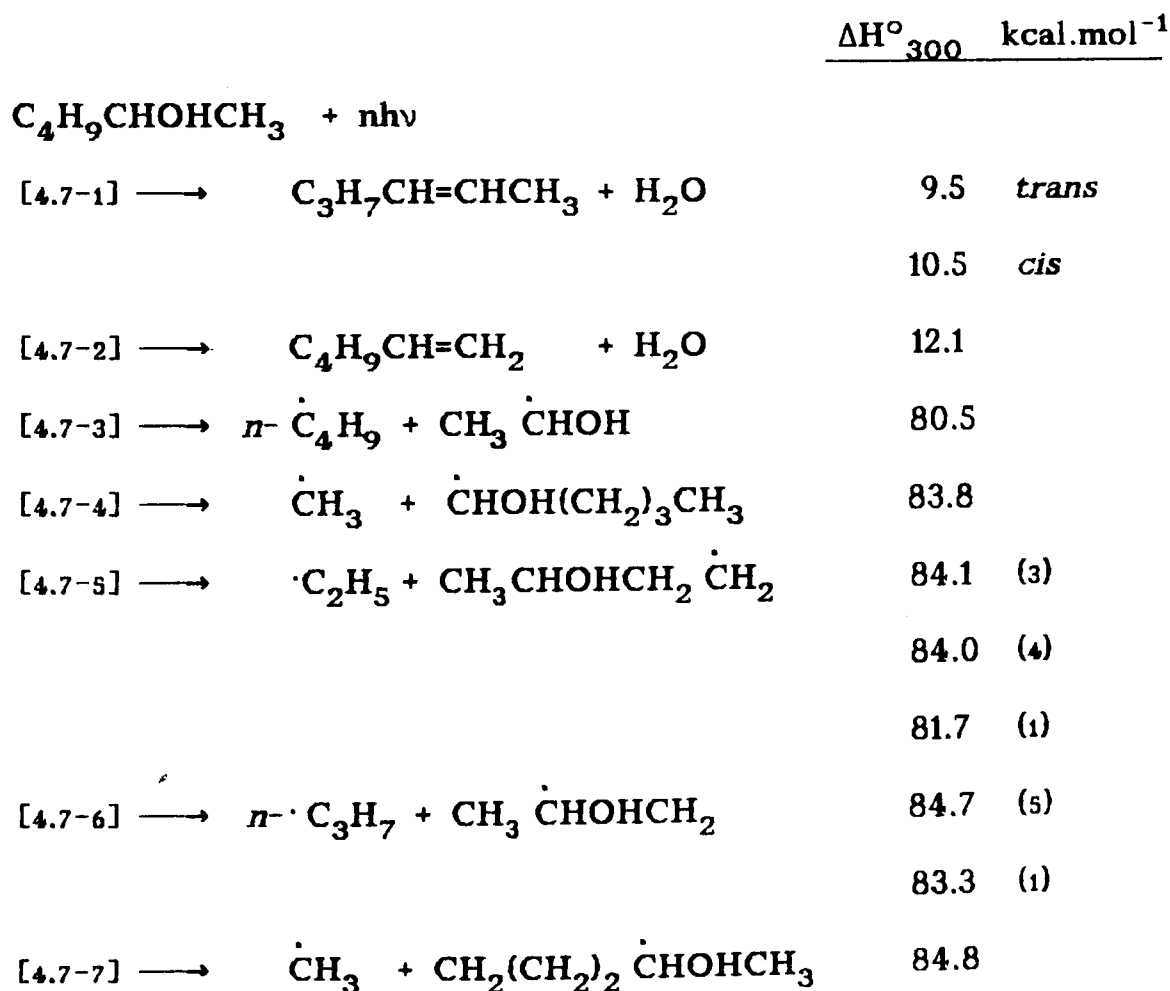
**Fig. 4.7-6 Hexan-2-ol: Effect of pressure on the yield ratio of product to the sum of hexenes (raw data) for pure reactant, at P20 (9  $\mu$ m)**

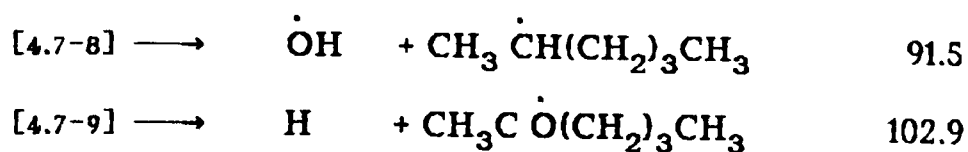


each other, and to the yield of *cis*-hex-2-ene. The peak corresponds to the minima in group (ii) products.

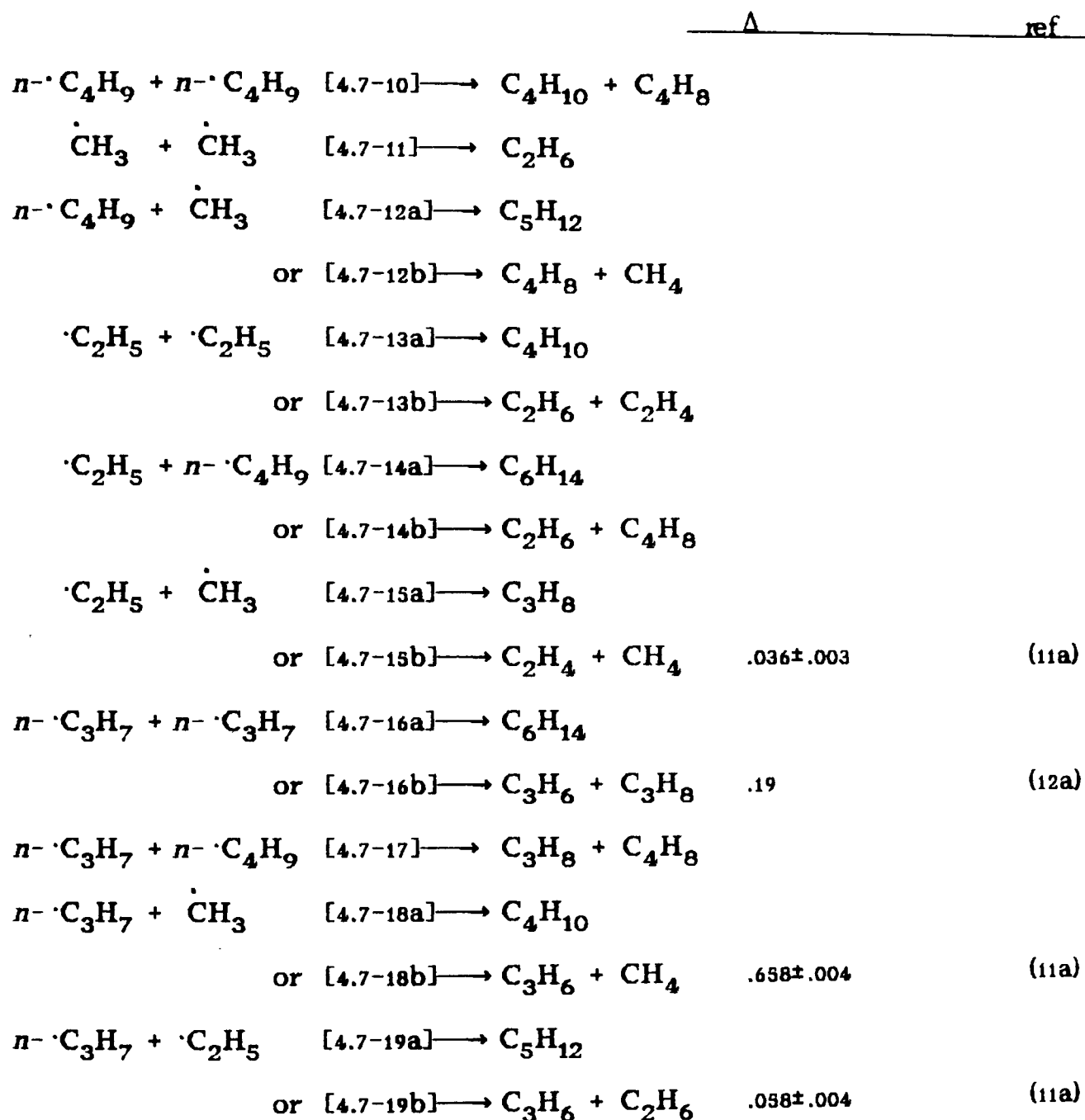
### 4.7.3 Discussion

Listed below are some decomposition paths (molecular elimination and bond fission) with related heats of reaction for hexan-2-ol, which, *a priori*, may be accessible with IR irradiation. An extensive literature search did not yield any Arrhenius parameters. Based on discussions on the choice of activation energies for alkanols covered in the previous sections, a reasonable estimate for the dehydration channel of hexanol would be 52 kcal/mol. Figure 1.4-4 shows that excitation to 2.6 times the activation energy is likely i.e. to 135 kcal/mol. Hence with no further reaction, all the listed reactions [4.7-1] through to [4.5-9] will be allowed (for fission reactions,  $\Delta H$  values are similar to the activation energies). These and further reactions will be possible if the total activation energy does not exceed 135 kcal/mole.

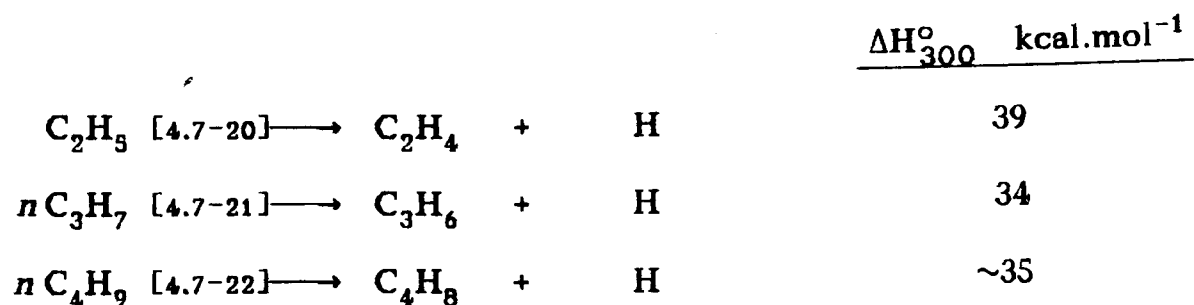




Subsequent radical recombination may be expected to form the following products:



Possible radical decomposition reactions for hexan-2-ol will be:



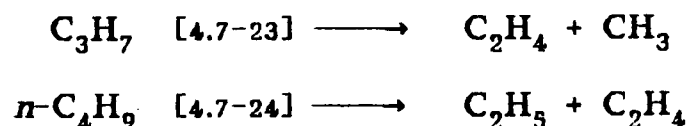
As shown in Table 4.2-2 the activation energy for [4.7-20] has been found to be 42 kcal/mol (27,100,103) and the A factor to be  $10^{13.5} \text{ s}^{-1}$  (103). The heats of reaction were estimated using the Group Contribution Method (Appendix A4).

The drop in yield of dehydration products with fluence (Fig.4.7-1) is surprising. It may possibly be due to the increasing role of other channel(s), which while having a higher activation energy than the dehydration channel, may also have a significantly higher frequency factor; reactions initiated by bond fission may be the cause since their preexponential factor is in the order of  $10^{16} \text{ s}^{-1}$  (24)(27) compared to  $10^{13} \text{ s}^{-1}$  for the dehydration channel: Between 8 and  $10 \text{ J/cm}^2$  the proportions of all product yields to the dehydration channel yields increase with fluence, except those of the alkanes propane, butane and *n*-pentane (Fig.4.7-3).

This work has demonstrated that while molecular dehydration is the primary channel, further channels are significant, and can produce products totalling over 70% of the primary channel yield (at roughly  $8.5 \text{ J/cm}^2$  - Fig.4.7-3). The OH is eliminated with either a  $\text{C}_1$  hydrogen to form hex-1-ene, or a  $\text{C}_3$  hydrogen to form hex-2-ene isomers. As is illustrated in Fig.4.7-2, close to the threshold fluence for decomposition, a convergence of *trans*-hex-2-ene and hex-1-ene is noted. Otherwise there is very little variation with fluence; at the maximum fluence of  $10.4 \text{ J/cm}^2$  hex-2-ene:*trans*-:*cis*- is 55%:27%:17%. Statistical and conformational analysis was discussed in detail in section 4.3 on butanol. Using the same argument one would have again expected a 60%:20%:20% split. The proportions are indeed approximately in this order, but the indications are that the H attached to the the third carbon has a greater affinity for reaction in hexan-2-ol than for butan-2-ol.

The channels additional to those of dehydration are primarily bond fission (later, in the discussion of methane and butane, two further molecular elimination channels will be proposed, [2.7-23] and [2.7-24]). The role of fission reactions [4.7-3] to [4.7-9] is discussed below.

The product distribution shown in Fig.4.7-3 can be largely explained based on a comparison between the likelihood of radical formation, and annihilation. The expected radicals caused by bond fission are methyl, ethyl, propyl, and butyl radicals [4.7-4&-7;-3;-5;-6]. The activation energies for bond fission leading to these radicals are similar, so they might be expected to be formed in approximately the same quantities. However, statistically methyl production will dominate. Furthermore, because activation energies for decomposition (via reactions [4.7-20;-21;-22]) are similar for each of these radicals, the resultant alkenes (ethene, propene, and butene) would also be expected to be formed in approximately the same quantities. The graph shows this simple analysis is not true, and indicates that there are further (or even alternative) channels contributing to the production of ethene, propene, and butene, in order that ethene dominates, as observed, at fluences above 8J/cm<sup>2</sup>. Some suggestions for alternative decomposition paths for the propyl and butyl radicals are:



These paths have an activation energy of approximately 35kcal/mol, and provide extra channels for C<sub>2</sub>H<sub>4</sub> production.

If there is very efficient decomposition of hot radicals, then there must be a low yield from competing radical recombination and disproportionation paths. Since reactions involving decomposition of hot radicals are likely to become more efficient as the fluence increases then ethene, propene and but-1-ene yields will increase with fluence, while product yields formed from the

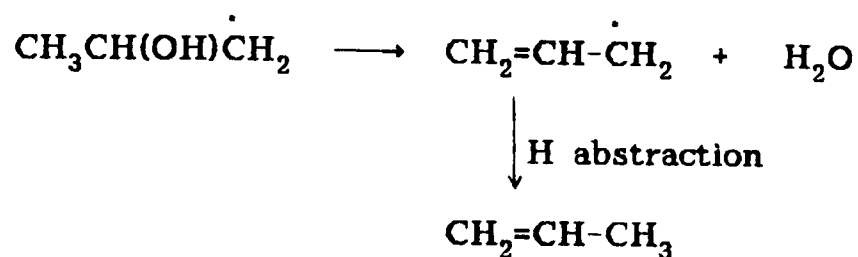
competing recombination and disproportionation paths will decrease. The results are consistent with this scenario in that ethene, propene and but-1-ene increase with fluence while propane, butane, and *n*-pentane decrease; these alkanes cannot be explained as products of decomposition of hot radicals, but can be explained by radical recombination and disproportionation paths. The increase of ethane with fluence is also consistent with the above scenario, since it is probably derived from methyl recombination for which competing reactions from decomposition of hot methyls is unlikely. However, the rise in hexane yield with fluence is inconsistent with the scenario, for its formation can only be explained by radical recombination reactions [4.7-14a] and [4.7-16a].

Not to be ruled out is the possibility of further four-centred unimolecular reactions such as the concerted reaction of the hydroxyl hydrogen with the butyl and methyl groups, leading to the production of butane and methane.

In summary, the importance of the initial carbon-carbon fission reactions, compared with elimination of water, is apparent in hexan-2-ol. Decomposition of hot radicals appears to be an important mechanism. Radical recombination and disproportionation reactions are also important, supplementing each product yield to varying degrees; it is quite extensive for methyl radical recombination. Furthermore, molecular elimination reactions are possible in addition to the main dehydration channel. The products may be explained thus:

**Hexenes:** The primary reaction paths have been shown to involve the concerted elimination of the hydroxyl with a C<sub>1</sub>, [4.7-2], or C<sub>3</sub>, [4.7-1], hydrogen, leading to hex-1-ene and hex-2-ene production. The dominant path is that which leads to the 1-olefin, even though this product is the least thermodynamically stable.





**But-1-ene** has two possible paths

(a) from disproportionation reactions of  $n\text{-C}_4\text{H}_9$  radicals (formed in the carbon-carbon fission step [4.7-3]) with other radicals (namely  $\text{CH}_3$ ,  $\text{C}_2\text{H}_5$ ,  $\text{C}_3\text{H}_7$ , and  $\text{C}_4\text{H}_9$  given by steps [4.7-12b,-14b,-17, & -10] respectively).

(b) from decomposition of hot  $n\text{-C}_4\text{H}_9$  as in step [4.7-22]. This will compete with carbon-carbon fission of the radical (that gives  $\text{C}_2\text{H}_4 + \text{C}_2\text{H}_5$  as in [4.7-24]), which probably has somewhat lower activation energy than step [4.7-22], and with fission of the radical to give  $\text{CH}_3 + \text{CH}_3\text{CH}=\text{CH}_2$ , which been found to have an activation energy of 33kcal/mol (104).

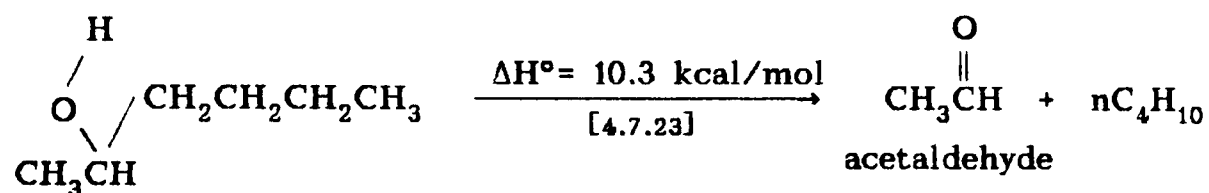
**n-Hexane** is probably formed by recombination of the propyl radicals (as in step [4.7-16a]) that result from the carbon-carbon fission step [4.7-6]. It could also be formed by recombination of ethyl and butyl radicals (as in step [4.7-14a]) which result from the fission steps [4.7-3] and [4.7-5].

**n-Pentane** arises from recombination of the ethyl and propyl radicals (as in step [4.7-19a]) that result from the carbon-carbon fission steps [4.7-5] and [4.7-6] respectively, and similarly from recombination of butyl and methyl radicals (as in step [4.7-12a]) that result from the fission steps [4.7-3] and [4.7-7].

**Propane** most likely arises from recombination of the methyl and ethyl radicals (as in step [4.7-15a]) that result from the carbon-carbon fission steps [4.7-4] and [4.7-5]. Other possibilities are through disproportionation

of two propyl radicals (as in step [4.7-16b]), and of propyl and butyl radicals (step [4.7-17]).

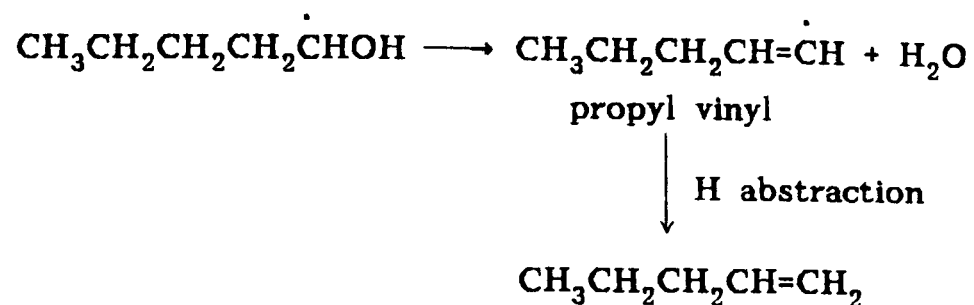
**Butane** is likely to arise from ethyl radical recombination [4.7-13a] and propyl and methyl radical recombination, the radicals being formed from carbon-carbon fission in steps [4.7-5, -6, & -4] respectively, although there may also be a contribution from a further four-centred unimolecular reaction [4.7-23] shown below. This last reaction is a concerted reaction of the hydroxyl hydrogen with the butyl group, and is analagous to a concerted reaction with the methyl group of ethanol which has recently been proven to occur by Goodale *et al.* (81).



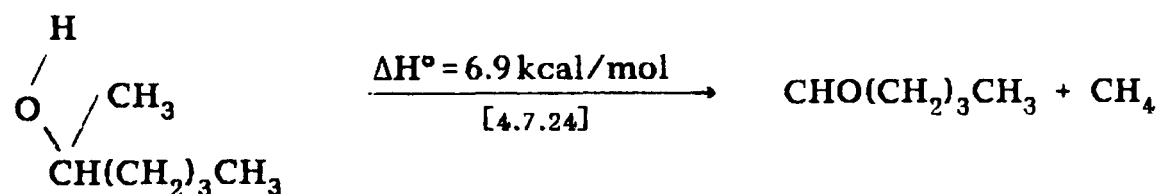
In addition there are disproportionation reactions involving butyl radicals, [4.7-10]

**Ethane** most likely arises from methyl radical recombination (step [4.7-11]), but also results from disproportionation reactions of  $\text{C}_2\text{H}_5$  radicals (formed in the carbon-carbon fission step [4.7-5]) with other radicals (namely  $\text{C}_2\text{H}_5$ ,  $\text{C}_3\text{H}_7$ , and  $\text{C}_4\text{H}_9$  given by steps [4.7-13b, -19b, & -14b] respectively).

**Pent-1-ene** may possibly form from the larger radical that results from the carbon-carbon fission step of [4.7-4] as shown below. This is analagous to the type of reaction that was used to explain the formation of ethene.

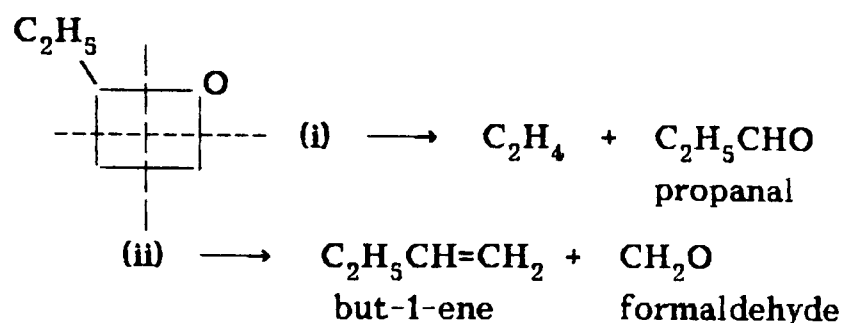


**Methane** most likely results from a four-centred unimolecular reaction [4.7-24] shown below, and similar to that used to explain butane. This reaction is a concerted reaction of the hydroxyl hydrogen with the neighbouring methyl group, and is analagous to a concerted reaction with the methyl group of ethanol which has recently been proven to occur by Goodale *et al.* (81).



#### 4.8 3,3-DIMETHYLOXETANE

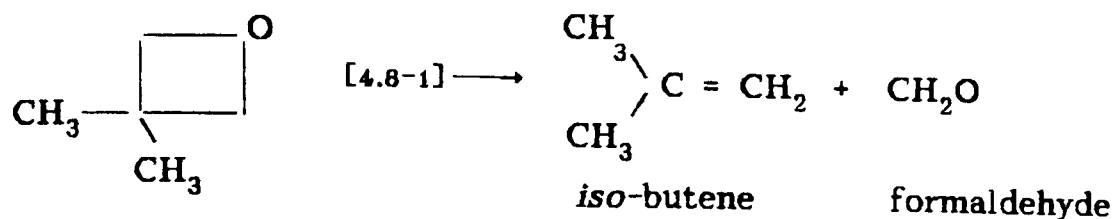
At the onset of this research, it was intended to investigate further laser induced decomposition of oxetane and its mono- and bi-alkyl substituted derivatives. In particular, to study the branching ratio between the two major decomposition channels (i) and (ii), as for example in the case of 2-ethyloxetane:



Shaw (6) studied the laser photolysis of oxetane, 2,2-dimethyloxetane and 2-methyloxetane. For the unsymmetric molecules laser photolysis was found to increase the proportion of reaction occurring by the higher energy channel compared with thermolysis. Although initially it was planned to extend the work of Shaw to a number of other oxetanes, only 3,3-dimethyloxetane could be synthesized with sufficient purity, within the time available. Since this is a symmetric molecule, only one decomposition channel is observed and hence the information available is limited.

3,3-Dimethyloxetane was irradiated at a rate of 113 shots/min. The extent of decomposition was investigated at two different wavelengths, corresponding to the laser transitions  $R_{24}(10\mu\text{m})$  and  $P_{24}(10\mu\text{m})$ . The effect of diluent was monitored for both wavelengths, but the effect of pulse type was only investigated for  $R_{24}(10\mu\text{m})$ .

The expected molecular channel [4.8-1], was previously shown by thermolysis (82) to have an activation energy  $E_a = 60.7 \text{ kcal/mol}$  and an A factor of  $10^{15.58} \text{ s}^{-1}$ .



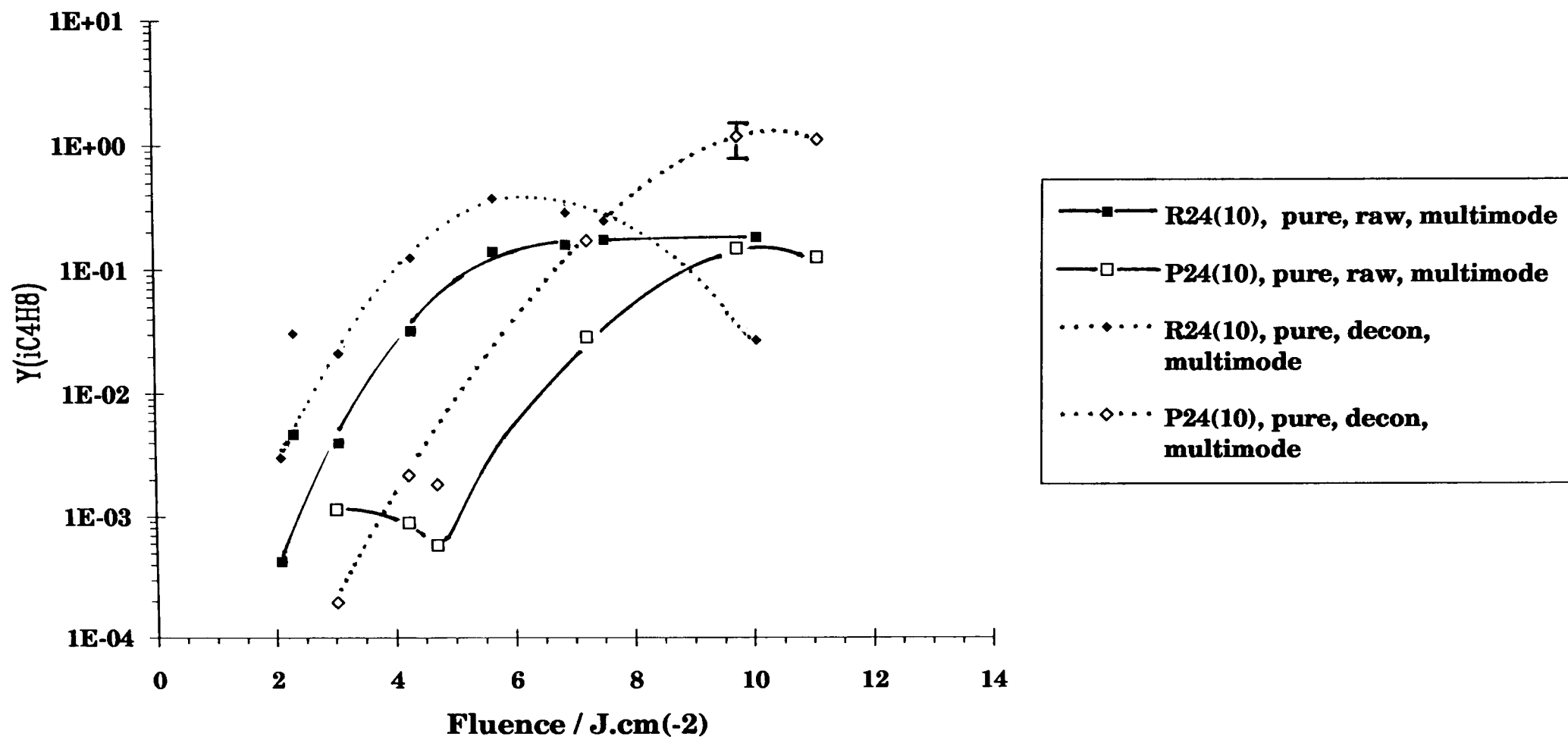
Over the course of this work, the major product was identified as *iso*-butene while other products were identified as methane, ethane, ethene, propane, propene, butane. One additional peak is thought to be propyne (methyl acetylene), occurring on the GLC trace between propene and butene, and in amounts as equally significant as those of propane; there was very roughly triple the amount of propene compared to that of propane and of propyne. The doubt in the labelling of the propyne product is merely because there was no sample of propyne available with which to confirm its GLC retention time. Further heavier hydrocarbon products (i.e.  $\gt C_4$ ) were seen to exist, but remained unidentified. There was no attempt made to detect formaldehyde.

Both Carlo and Pye GLCs were used for the product analysis. Column and flow conditions were the same as when both were used for butan-2-ol (Section 4.3). The Pye oven was kept at 40°C, and over the course of the work, the Carlo oven temperature was set either at 30°C or 40°C.

#### 4.8.1 Fluence Dependence

The dependence of the yield of *iso*-butene on fluence is shown in Fig. 4.8-1 for both irradiation lines. Sample pressures were nominally 50 mtorr, and pulses were multimode. The data is shown in both raw and deconvoluted ("decon.") form. Overall, there is an increase in yield with fluence. There is also a roll-off at the high fluences; the low point for  $P_{24}$  at high fluence is assumed to be a spurious result of the deconvolution process. The roll-off of the  $P_{24}$  data may be related to saturation of the irradiated volume: as the fluence increases, the shoulders of the gaussian intensity profile extending

**Fig. 4.8-1 3,3-Dimethyloxetane: The variation of yield with fluence, at different wavelengths, showing the effect of deconvolution of the raw data**



outwards from the bounds of the elected cylindrical "irradiated volume" become sufficiently intense to cause decomposition, consequently the yield is seen to reach and even exceed 100%. In general, deconvolution increases the yields.

Figure 4.8-2 ((a) and (b)) provides a comparison of the deconvoluted trends with fluence for five different sets of conditions; total sample pressures were nominally 50mtorr. The deconvoluted data of Fig.4.8-1 is replotted here as Series (i) and (ii):

- (i)  $R_{24}(10\mu\text{m})$  laser transition, pure reactant, multi-longitudinalmode pulse.
- (ii)  $P_{24}(10\mu\text{m})$  laser transition, pure reactant, multi-longitudinalmode pulse.
- (iii)  $R_{24}(10\mu\text{m})$  laser transition, dilute reactant, multi-longitudinalmode pulse.
- (iv)  $R_{24}(10\mu\text{m})$  laser transition, dilute reactant, single-longitudinalmode pulse.
- (v)  $P_{24}(10\mu\text{m})$  laser transition, dilute reactant, multi-longitudinalmode pulse.

Thus effects of irradiation line, diluent, and pulse type can be determined. Compare Series (i) with (ii) to establish the effect of irradiating wavelength (Fig.4.8-2(a)). To look at the effects of diluent, compare (i) with (iii), and (ii) with (v) (Fig.4.8-2(a)). The effect of pulse type is seen by comparing (iii) with (iv) (Fig.4.8-2(b)). The effect of diluent on the comparison of the effect of irradiation line may be seen by comparing the differences of (i) and (ii), against those of (iii) and (v) (Fig.4.8-2(a)). The effects of diluent and pulse type are discussed in Sections 4.8-2 and 4.8-3.

The effect of irradiation line is observed to be as follows. The high fluence roll-off observed in Fig.4.8-1 is seen to be strongest for the  $R_{24}$  data. For both pure and dilute conditions (multimode pulse) the  $R_{24}$  yields are the larger than for  $P_{24}$ . This is a result of greater absorption by  $R_{24}$  (see Ch. 3).

**Fig. 4.8-2(a) 3,3-Dimethyloxetane: The variation of deconvoluted yield with fluence, showing the effect of irradiating line (Series (i) and (ii)), and dilution (Series (i) and (iii), and (ii) and (v))**

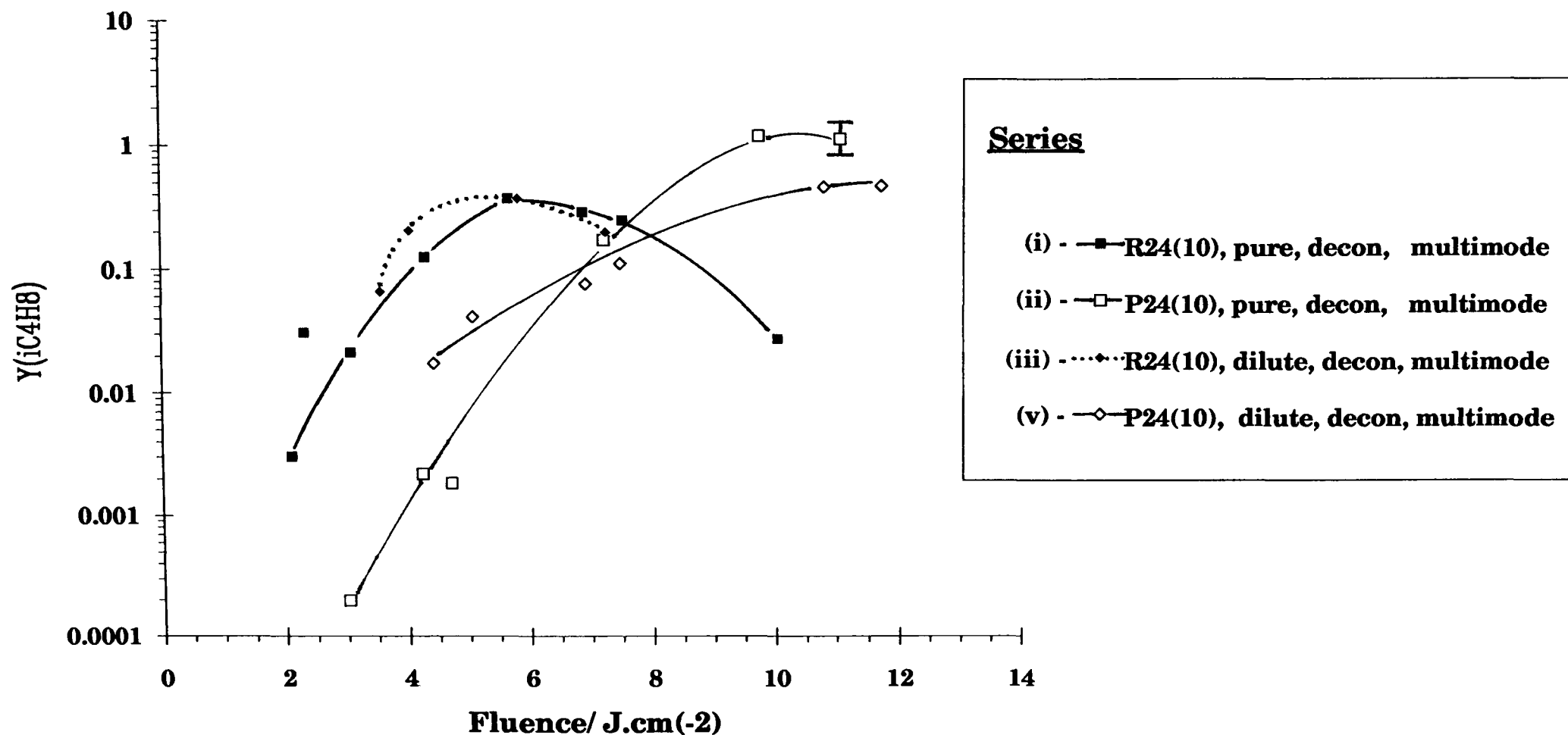
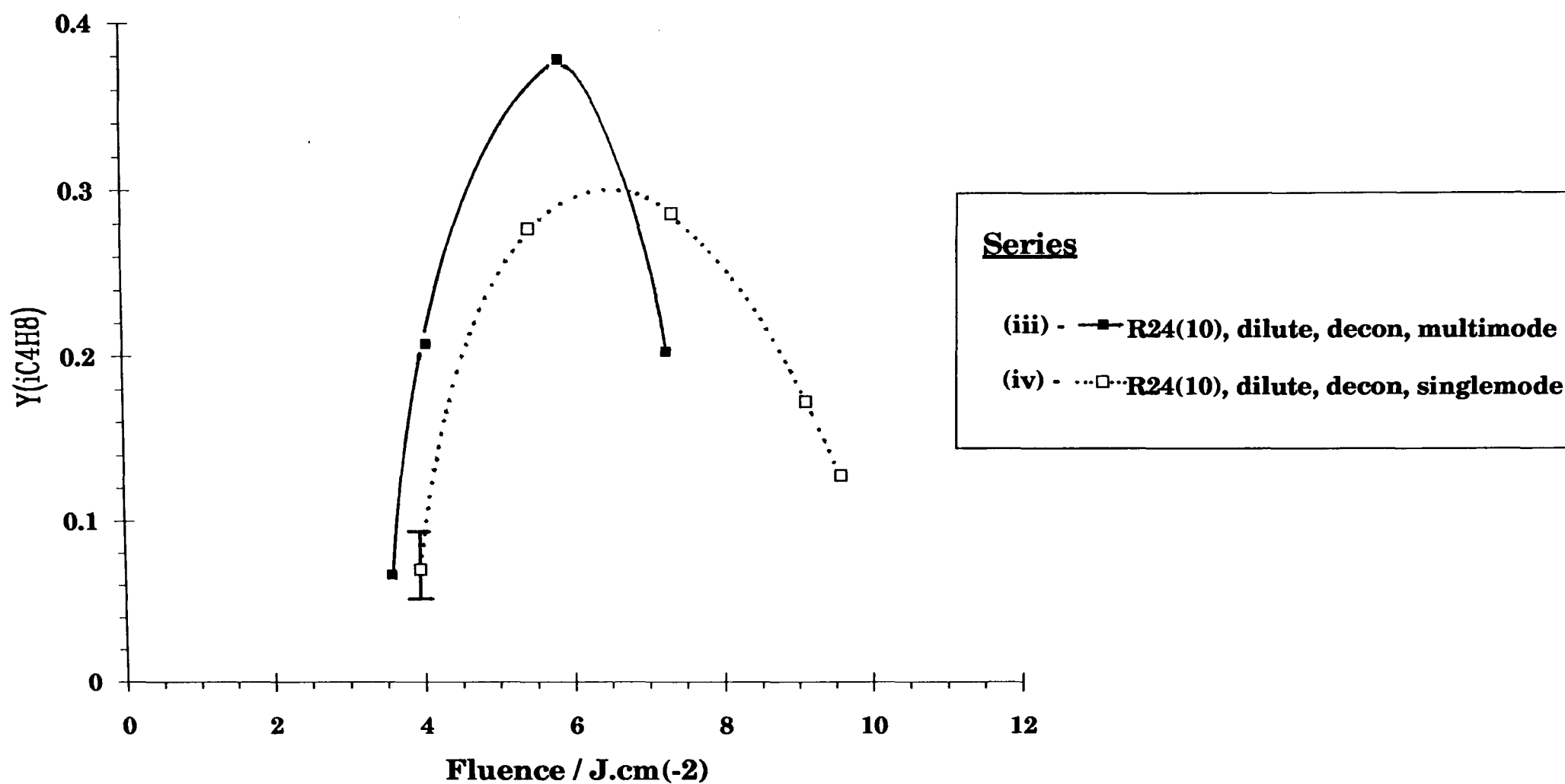


**Fig. 4.8-2(b) 3,3-Dimethyloxetane: The effect of pulse type on the variation of deconvoluted yield with fluence**



Minor products were not detected after irradiation with the  $P_{24}$  line, while for the  $R_{24}$  line, traces were detected, but at high fluence only (for conditions of dilute reactant, and singlemode and multimode pulses). Traces were more evident for the pure reactant irradiated by the  $R_{24}$  line.

#### 4.8.2 Effect of Diluent

Cyclohexane was added in excess to 3,3-dimethyloxetane to a ratio 8.86:1, and total pressures of 50mtorr were irradiated, in turn, with both laser transition frequencies and pulse types (Series (i) and (iii), and (ii) and (v) of Fig.4.8-2(b)). For the  $R_{24}$  data, the overall shape of trends with fluence for the two sets of data are approximately similar demonstrating that the diluent has had little effect. For  $P_{24}$  the results are inconclusive as to the effect of diluent on yield. Any effect is possibly masked by scatter: the  $P_{24}$  results appear to have shown that the dilution reduces the sensitivity of the yield to fluence changes.

#### 4.8.3 Effect of Pulse Type

The effects on decomposition of the pulse type (single-longitudinalmode versus multi-longitudinalmode) was investigated using the  $R_{24}(10\mu\text{m})$  laser transition only (Series (iii) and (iv), Fig.4.8-2). The optimum mixture for the low pressure tube of the hybrid TEA laser was found to be 10%(CO<sub>2</sub>):10%(N<sub>2</sub>):80%(He) forming a total pressure of 10torr. Overall, the multimode pulses give greater yields; using the multimode data as the baseline, there was found to be a maximum drop of 73% to the singlemode data at roughly 4J/cm<sup>2</sup>. The fact, that multimode pulses facilitate decomposition, is evidence that the *intensity* of the pulse has an effect on the rate of decomposition of 3,3-dimethyloxetane.

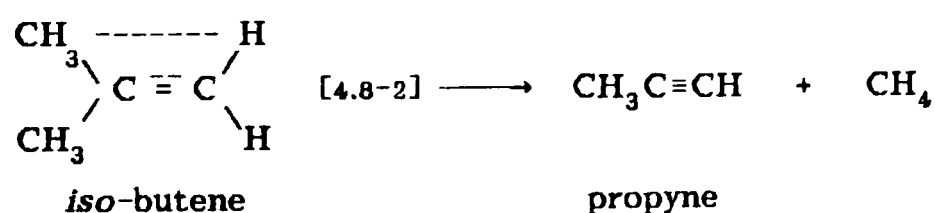
#### 4.8.4 Pressure Dependence

The dependence of isobutene yield with pressure is such that it increases with increasing pressure to roughly 0.2 torr then remains constant at about 38%, as shown in Fig. 4.8-3.

Minor product formation is very evident at pressures greater than 50 mtorr, although their yields are very small (<0.5%) compared to that of *iso*-butene.

#### 4.8.5 Discussion

No attempt was made to carry out a detailed analysis of the minor products of this heterocyclic system. A few suggestions can be made, however, as to the formation of methane, ethane, propene and propyne; four of the seven identified minor products. For example, *propyne* and *methane* may be the result of a unimolecular four-centred decomposition of the primary product *iso*-butene [4.8-2]. Unfortunately, there was no experimental analysis carried out to check the susceptibility of *iso*-butene to laser decomposition.



Also, bond fission of the reactant to give methyl radicals [4.8-3], provides the reserves for *ethane* and *methane* production through recombination and hydrogen abstraction respectively.

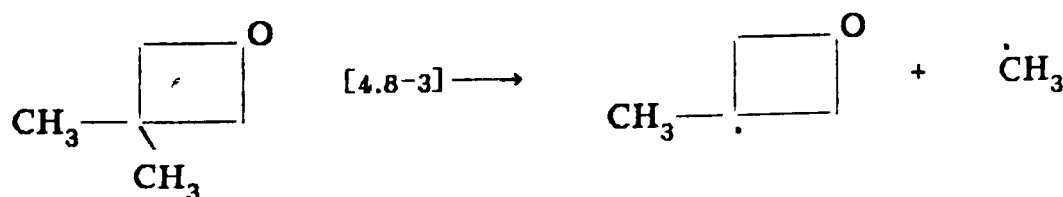
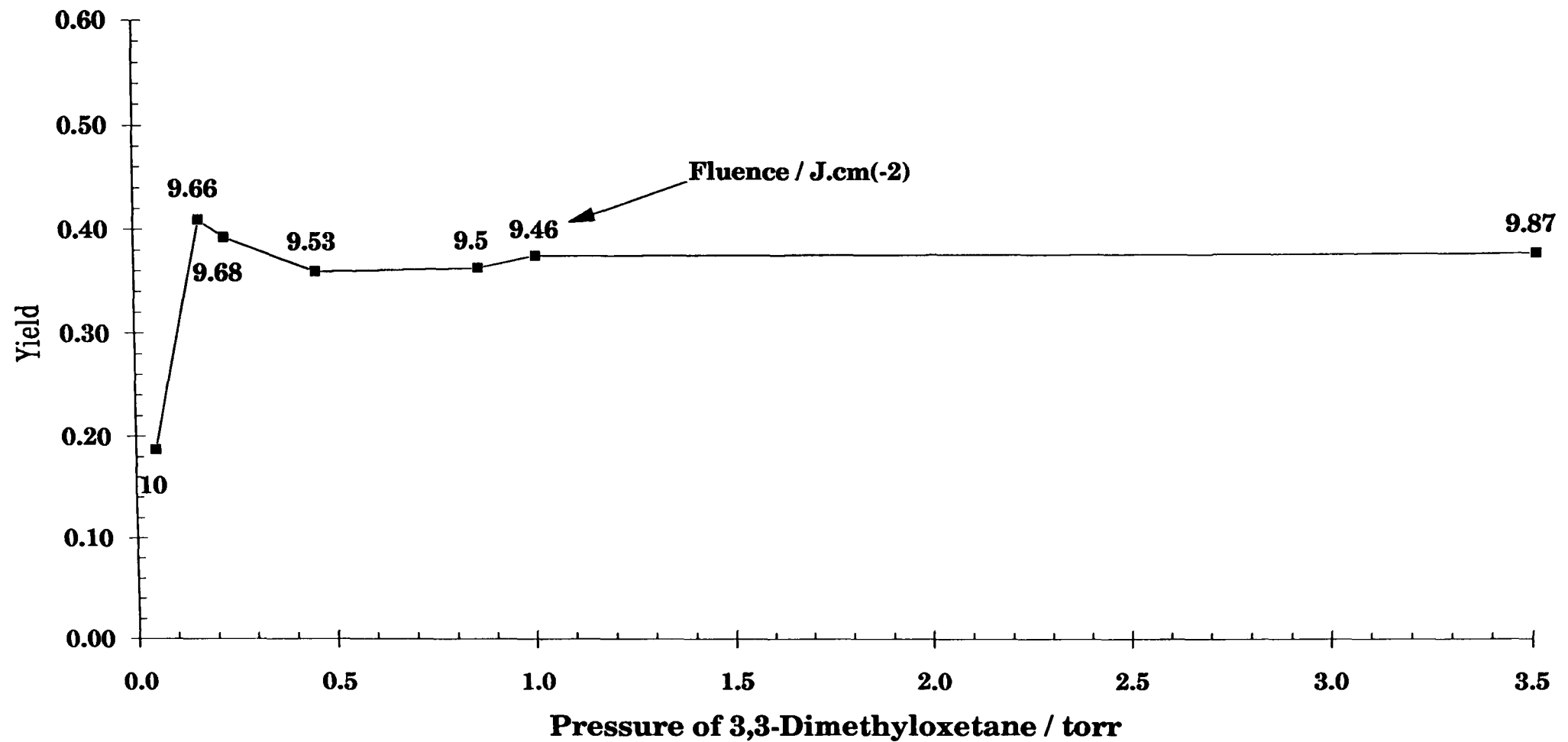
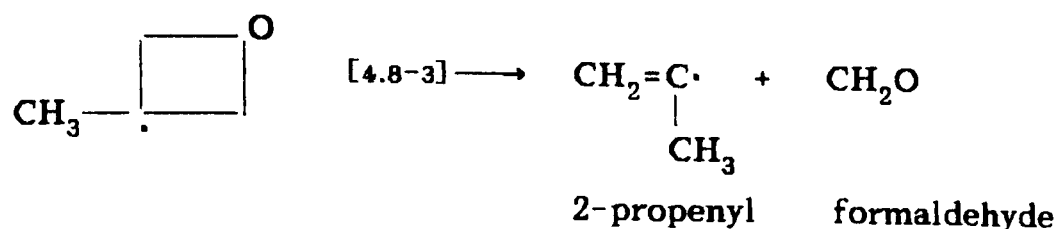


**Fig. 4.8-3 3,3-Dimethyloxetane: The variation of isobutene yield with pressure of reactant (raw data) for fluences in the range 9.45 to 10.00 +/- 0.02 J/cm(2) on R24 (10 μm)**



In turn, the cyclic radical of [4.8-3] could rearrange to give the 2-propenyl radical [4.8-4], which then could form *propene* by hydrogen abstraction.



Furthermore, *formaldehyde* has been shown to undergo a chain decomposition in the presence of methyl radicals or H atoms, forming primarily H<sub>2</sub> and CO (84). In turn, H<sub>2</sub> may react with propene to give *propane*.

Formaldehyde and *iso*-butene were detected by Cohoe *et al.* (82) after thermolysis of 3,3-dimethyloxetane (400-450°C) 10mmHg pressure), in agreement with the stoichiometry of [4.8-1]. Unlike for oxetane thermolysis, no appreciable evidence of chain decomposition was found. It was established that the increase in rate constant due to the dimethylation of oxetane in the 3 position was near to that observed for dimethylation of cyclobutane. Furthermore, the Arrhenius factor of [4.8-1] was comparable in magnitude, to the preexponential factor of various alkyl derivatives of cyclobutane (85).

Cohoe *et al.* were unable to determine whether or not the ring cleavage was a concerted process, or whether the C-O, and C-C bonds broke in succession forming biradical intermediates. There is also insufficient evidence in this work to make that conclusion.

In summary, laser photolysis of 3,3-dimethyloxetane has confirmed that the primary reaction channel is ring cleavage leading to *iso*-butene. Very small yields of minor products have been detected.

## 4.9 SUMMARISING DISCUSSION

As one progresses through the alkanol homologous series, it is observed that production of the major products can always be explained in terms of a molecular elimination channel i.e. one of dehydration. Also the number of minor products and their yields both increase, such that these yields may become comparable to those of the major products. For example, twelve minor products were identified after irradiation of hexan-2-ol, with the propene yield being half of that of *cis*-hex-2-ene; whereas for ethanol, there are only six minor products, with ethane being a factor of ten less than ethene.

It is believed that most of the 'minor' products arise as a consequence of carbon-carbon fission processes, with minor contributions due to molecular elimination. As the number of carbon atoms in the molecule increases, the probability of C-C fission compared with elimination of water involving the single OH group, is expected to increase simply for statistical reasons. The increase in the yield and variety of 'minor' products is thus a natural consequence of the increase in the length of the alkyl chain.

The proposed major, and minor, molecular elimination reaction paths involve cyclic transition states. Since the breaking and formation of more than one bond is implied, it would be reasonable to make the assumption that at least a partial intramolecular redistribution of the deposited laser energy occurs. This is the same conclusion as that reached by Danen *et al* (22) for ethyl acetate ( $\text{CH}_3\text{CO}_2\text{CH}_2\text{CH}_3$ ), which decomposed *via* a six-centred transition state to give  $\text{CH}_3\text{CO}_2\text{H} + \text{CH}_2=\text{CH}_2$  in amounts greater than that expected if produced via a thermal route. Clearly, a further indication of the occurrence of laser energy redistribution is the range of unimolecular carbon-carbon fission processes.

	Fluence/ J.cm <sup>-2</sup>	1-olefin/ total olefin	trans-2/ total olefin	cis-2/ total olefin	1-olefin/ 2-olefin	2-olefin/ 1-olefin	trans/cis
<b>Butan-2-ol</b>							
pure	7.0	0.6792	0.2177	0.1631	1.78	0.56	1.33
dilute	7.3	0.5946	0.2151	0.1903	1.47	0.68	1.13
pure	9.7*	0.6095	0.2169	0.1735	1.56	0.64	1.25
dilute	9.7*	0.6245	0.2030	0.1725	1.66	0.60	1.18
<b>Pentan-2-ol</b>							
dilute	7.1	0.5586	0.2685	0.1730	1.27	0.79	1.55
pure	7.3*	0.5730	0.2502	0.1767	1.34	0.75	1.42
dilute	8.0*	0.5717	0.2719	0.1564	1.33	0.75	1.74
<b>Pentan-3-ol</b>							
pure	7.3	-	0.6550	0.3450	-	-	1.90
pure	11.9*	-	0.6309	0.3691	-	-	1.71
<b>Hexan-2-ol</b>							
pure	7.3	curve not yet at plateau					
pure	10.3*	0.5520	0.2729	0.1564	1.29	0.78	1.74
<b>Statistical Prediction</b>							
		-	-	-	1.50	0.67	1.00
<b>Thermodynamic equilibrium ratios (butan-2-ol) at 1500 K</b>							
	-	0.762	0.138	0.101	3.19	0.31	1.37

**Table 4.9-1**

Olefin product ratios for butan-2-ol, pentan-2-ol, pentan-3-ol and hexan-2-ol. Actual experimental data is presented for the plateau region at a fluence of around 7J.cm<sup>-2</sup> and at the maximum detected fluence (\*). Where mentioned, the diluent was cyclohexane (diluent + reactant = 50 mtorr total pressure).

T / K	$\Delta G_r^\circ / \text{kcal.mole}^{-1}$			% Product		
	but-1-ene	cis-but-2-ene	trans-but-2-ene	but-1-ene	cis	trans
300	17.19	15.84	15.15	2.43	23.33	74.24
1000	63.07	63.35	62.66	32.29	28.04	39.67
1500	97.20	99.43	98.50	76.16	10.06	13.78

**Table 4.9-2** Gibbs function and calculated % of dehydration products.

The expected major products, following irradiation of the secondary alkanols heavier than propan-2-ol, were alkene isomers and their yields have been illustrated in ratio form. There is a strong similarity between the raw data results. For those plotted against fluence (Figs. 4.3-5, 4.5-2, 4.6-2, 4.7-2), it is evident that (at high fluence) the proportions are in the order of 60% 1-alkene and 40% total *cis*- and *trans*-2-alkene. The absolute values are tabulated for clarity (Table 4.9-1).

Theoretical equilibrium ratios of the butenes can be calculated from equation (4.0-1):

$$\ln K - \frac{\Delta S^\circ}{R} = \frac{-\Delta H^\circ}{RT} \quad (4.0-1)$$

where K is the 'equilibrium constant' given by the particular isomer ratio, R is the molecular gas constant, T the temperature (in K),  $\Delta S^\circ$  is the entropy change and  $\Delta H^\circ$  the enthalpy change for the relevant process, e.g. *cis*-2-olefin  $\rightarrow$  *trans*-2-olefin. The equilibrium product ratios for the butenes were calculated at three temperatures, (room temperature (300K), 1000K, and 1500K) using the tabulated Gibbs function,  $\Delta G^\circ$ , values (90) (Table 4.9-2) and applying the alternative form of equation 4.0-1 given in equation 4.0-2:

$$\Delta G^\circ = -RT \ln K \quad (4.0-2)$$

The results are shown in Table 4.9-2. It is clear, that equilibrium product ratios do not resemble the observed ratios, except in the case of the *trans*-but-2-ene to *cis*-but-2-ene ratio for 1500 K, which is fairly near the experimental ratio.

It seems clear that at high levels of excitation, the elimination of water *via* the three H atoms on the terminal C atom to give the 1-alkene, or *via* the

two H atoms on C<sub>3</sub> to give the 2-alkene, occurs on a statistical basis, leading to a 1-alkene/2-alkene ratio in the region of 3:2. However, the *trans*-2-alkene/*cis*-2-alkene ratio is closer to the expected equilibrium value at high temperatures, which implies that *cis*→*trans* isomerisation of the 2-alkene occurs *after* its production from the alkanol. As expected from thermodynamic statistics, there is always an excess of the *trans*-isomer over the *cis*.

Finally, there is a similarity between the trends of the yield ratios of the product yields (secondary alkanols and pentan-3-ol) with variation of pressure. These ratios are, for the most part, independent of pressure, though there appears to be a convergent trend towards the highest pressures (Figs. 4.3-9, 4.5-9, 4.6-6, 4.7-6).

## 5. - DISCUSSION

This final chapter considers, in more detail, the results of the absorption experiments. In addition, some points of concern are raised about roles of physical effects that have not previously been considered. Finally, there are some recommendations for further work.

### *Absorption cross-section.*

It was concluded in Section 3.8, that as the fluence approaches zero, the absorption cross-section tends towards its low signal, broadband value. This conclusion was drawn primarily from high pressure data of methanol and propan-2-ol, and low pressure (~50 mtorr) data of butan-2-ol, pentan-2-ol, pentan-3-ol, hexan-2-ol, and to a degree also of 3,3-dimethyloxetane. The data was not otherwise obtainable in the region where the gradient of the  $\sigma$  vs.  $F$  curve should change, in order to reach  $\sigma_{\text{broadband}}$  at 'zero' fluence.

The absorption cross-section traditionally used, and applied, in this thesis, is a bulk, or gross value which is rather difficult to visualise and, therefore, to predict, interpolate or extrapolate. More meaningful are the inter-vibrational level cross-sections,  $\sigma_{ij}$ . For a particular molecule,  $\sigma_{ij}$  may increase, decrease or remain constant with increasing vibrational level. Unlike the bulk cross-sections, these 'microscopic' cross-sections do not depend on fluence.

It is from a simple rate equation that  $\sigma_{ij}$  is defined as being independent of intensity,  $I$ , namely (19) (for collision-free conditions):

$$\frac{dN_i}{dt} = I \sum_j \sigma_{ij} N_j - I \sum_j \sigma_{ji} N_i \quad (5.1-1)$$

where  $N_i$  is the population of level  $i$ , and  $\sigma_{ij}$  is the absorption cross-section ( $j \rightarrow i$ ) for  $i > j$  (and the emission cross-section if  $i < j$ ).

Danen *et al.* (76) attempted to predict the bulk absorption cross-section from  $\sigma_{ij}$  values using a "large" molecule (i.e. having  $\sim 6$  atoms other than H or halogens) master equation involving absorption and emission rates proportional to the laser intensity as in Eq.5.1-1. The following Table is the author's attempt to draw some conclusions from the data on the alkanols based on visual comparison with the trends predicted by Danen.

Danen predicted the fluence variation of the net absorption cross-section based on several cases of the variation of the microscopic absorption cross-section with the level of excitation (all with stimulated emission):

- (a) increasing microscopic absorption cross-section with excitation level.
- (b) constant microscopic absorption cross-section.
- (c) decreasing microscopic cross-section with excitation level.

The following table summarises the comparisons made between the trends observed for  $\sigma$  vs  $F$  for each reactant at low pressure (nominally 50mtorr) and lowest applied fluence, studied in this work, and theoretical curves plotted by Danen *et al.* in reference (76). It is recognised that the models were intended for "large" molecules ie. incoherent excitation (no discrete levels), and high density of states, permitting used of a simplified mathematical model.

REACTANT	$\langle \sigma \rangle$
METHANOL	c
ETHANOL	c
PROPAN-2-OL	c
BUTAN-2-OL	b
PENTAN-2-OL	b
PENTAN-3-OL	b
HEXAN-2-OL	b
3,3-DIMETHYLOXETANE	c (b)

The classification of the molecules in this way is fraught with difficulties. The difference of the predicted curves for cases b and c is one of degree, since both curves have the same general shape, and hence assignments must be viewed with some caution. The basic assumptions involved in the model, with molecules reaching the quasicontinuum after the absorption of one photon, certainly do not apply in the case of methanol and probably do not apply to some of the other molecules. It seems preferable to conclude that the microscopic absorption cross-sections of these molecules do not increase with increasing levels of excitation.

#### *Other considerations*

Briefly introduced in this section are a few points that might be worthy of further consideration. The extent of work required to investigate and answer these questions is of such great magnitude, that it is beyond the scope of this particular thesis. Indeed, from a recent conversation with personnel from the Atomic Energy of Canada Ltd., Chalk River Laboratories (91), the author has learned that most of these topics are only now being reviewed, and with the aim of incorporating them into current computer models. The purpose then, is to alert the reader that work is ongoing in these areas. The topics of interest are:

(i) the interpretation of "absorption cross-section", (already discussed).

(ii) the role of a non-uniform density of reactant caused by compression and rarefaction of the opto-acoustic effect. Do the local pressure increases tend to exaggerate collision induced effects?

(iii) the role of polarisation effects induced by the electromagnetic field. Are molecules most susceptible to absorption (and hence decomposition) when their dipoles are aligned to the laser electromagnetic field? If so, the fraction of absorbing molecules within the irradiated volume will be even smaller. It has been theoretically established thus far, that polarisation of the reactant molecules by the laser beam, will only produce noticeable effects at extremely high fluences (higher than those used here), when selection rules break down (91).

## 5.1 FUTURE WORK

In general, the author would recommend that future researchers in this field should try to incorporate a real-time detection system into their experimental set-up eg. fluorescence. It would also be advantageous to control the fluence with a continuously variable attenuator: there is such a device on the market which has a negligible effect on beam pointing angle (ie. 15  $\mu$ rad beam deviation) (92).

This research has demonstrated the importance of the role played by radicals particularly in the decomposition of the larger molecules; the contribution to the product ratios by these channels cannot be neglected. The products formed by the radical processes may be common to a second process, since there is also evidence of the presence of previously unexpected molecular paths. Interpretation of the results would be greatly eased if some time could be spent on looking at the effect of various radical scavengers on product ratios.

In attempting to complete a worthwhile comparison of absorption and decomposition within an homologous series, the author notes that there are some gaps in the results which could have only otherwise been filled if the data acquisition process had been more automated eg. with a gas chromatograph chart integrator, and oscilloscope data acquisition board for the OA signal. The use of these devices would have *dramatically* improved the speed and accuracy of both acquisition and analysis. The author believes there was (and still is) valuable information to be gleaned about the variation of absorption with wavelength and fluence, and would recommend to other researchers, that in the absence of labour saving devices, they should concentrate on fewer reactant gases in order to more thoroughly review these parameters.

Of a more minor consideration is the data which could easily be gathered on the speed of sound in the chosen reactant gas. These values are not all available, and may become particularly useful when photochemical theories become so complex, as to consider the pressure change effects on the irradiated volume caused by of the compression and rarefaction of the OA pulse.

There are clear indications that molecular decomposition channels are more prolific in IR laser photochemistry than previously expected, particularly with respect to alkanols. Researchers at Chalk River (81) have carried out some very important work, which may help to sort out the role of fission reactions from the minor molecular channels. This is being accomplished by doping ethanol with deuterium, and is an extension of the work carried out by Back *et al.* The author would like to see this method extended to other alkanols.

Finally, there is some evidence that fine structure may exist in the variation of product yield with pressure (ethanol) and even fluence (ethanol, and 3,3-dimethyloxetane); and there may also be anomalies in the variation of the average number of absorbed photons per molecule with pressure (methanol, propanol, butanol, hexanol, and 3,3-dimethyloxetane). Anomalous observations have previously made of the yield against pressure data of oxetane (6) and cyclobutanone (28) and of the  $\langle n \rangle$  versus fluence data of  $\text{OsO}_4$  (105), and were found to be more noticeable at low fluence (6,28). Furthermore, yields for the larger molecules seem to be very sensitive to fluence variations. The author would suggest some detailed work using an energy stabilised laser, and a continuously variable attenuator.

## REFERENCES

- 1 *"Handbook of Chemistry and Physics"*; Ed. Weast R.C., CRC Press (1981)
- 2 BENSON S.W., *"Thermochemical Kinetics"*, J. Wiley & Sons, New York, (1968) 2nd Ed.
- 2b BENSON S.W. and O'NEAL H.E., *"Unimolecular Reactions. Kinetic Data on Gas Phase Unimolecular Reactions"*. Pub. National Bureau of Standards, Washington, D.C., NSRDS-NBS 21 (1970)
- 3 MACPHERSON M.T., PILLING M.J., SMITH M.J.C.,  
Chem. Phys. Lett. **94** 430 (1983)
- 4 HASE W. and SCHLEGEL H., J. Phys. Chem. **86** 3901 (1982)
- 5 TSANG W., J. Am. Chem. Soc. **107** 2872 (1985)
- 5b ARROWSMITH P. and KIRSCH L.J.,  
J. Chem. Soc. Faraday Trans. **74**, 3016 (1978)
- 6 SHAW C.J., Ph.D. Thesis, University of Hull (1984)
- 7 BHATNAGAR R., Ph.D. Thesis, University of Hull (1979)
- 8 GANDINI A., BACK R.A., J. Photochem. **18** 241 (1982)
- 9 BACK R.A., EVANS D.K., McALPINE R.D., VERPOORTE E.M., IVANKO M., GOODALE J.W., ADAMS H.M., Can. J. Chem. **66** 857 (1988)
- 9b BACK R.A. *et. al.*, Preparatory notes for Ref. 9.
- 9c BACK R.A., National Research Council of Canada, Private Comm.
- 10 LEITE S.R.A., ISOLANI P.C., RIVEROS J.M., Can. J. Chem. **62** 1380 (1984)
- 11a KONDRATIEV V.N., *"Rate Constants of Gas Phase Reactions"* Ed. Fristrom R.M., Nat. Bur. of Standards, U.S. Dept. of Commerce, (1972)
- 11b KERR J.A. & MOSS S.J., CRC Press, *"Handbook of Bimolecular & Termolecular Gas Reactions Vol. II"*.
- 12a ADACHI H., BASIO N., Int. J. Chem. Kinet. **13** 376 (1981)
- 12b AMBARTZUMYAN R.V., GOROKTOV Y.A., LETOKHOV V.S., MAKAROV N., PURETSKY A.A., Sov. Phys. JETP **44** 231 (1976)

- 13 FUSS W., COTTER T.P., Appl. Phys. **12** 265 (1977)
- 14 LYMAN J.L., ROCKWOOD S.D., FREUND S.M.,  
J. Chem. Phys. **67** 4545 (1977)
- 15 LIN S.T., LEE S.M., RONN A.M., Chem. Phys. Lett. **53** 260 (1978)
- 16 AVATKOV O.N., BAGRATASHVILI I.N., KNYAZER I.N., KOLOMISKY  
Y.R., LETOKHOV V.S., RYABOV E.A., Sov. J. Quant. Elec. **7** 412 (1977)
- 17 BACK M.H., BACK R.A., Can. J. Chem., **57**, 1511 (1979)
- 18 DANEN W.C., JANG J.C., "*Multiphoton Infrared Excitation and Reaction;  
Laser Induced Chemical Processes*", Ed. Steinfeld J I; Plenum Press (1981)
- 19 HOLBROOK K.A., ROONEY J.J., J. Chem. Soc. **38** 247 (1965)
- 20 FEISER L.F. and FEISER M.F., "*Organic Chemistry*",  
Heath and Company, Boston (1956)
- 21 SHIRLEY D.A., "*Organic Chemistry*",  
Holt, Rinehart and Winston, U.S.A. (1964)
- 22 DANEN W.C., MUNSLOW W.D., SETSER D.W.,  
J. Am. Chem. Soc. **99** 6961 (1977)
- 23 DANEN W.C., J. Am. Chem. Soc. **101** 1187 (1979)
- 24 TSANG W., Int. J. Chem. Kinet. **8** 193 (1976)
- 25 YAMABE T., KOIZUMI M., YAMASHITA K., TACHIBANA A.,  
J. Am. Chem. Soc. **106** 2255 (1984)
- 26 TSANG W., J. Chem. Phys. **40** 1498 (1964)
- 27 ZHITNEVA G.P. and MARKINA I.A.,  
UDC 535.217; 0018-1439/88/2206-0456; 1989 Plenum Pub. Corp. **22** 456  
(1988)
- 28 JOHN P., HUMPHRIES M.R., and HARRISON R.G.,  
CLEO '83, Baltimore, Maryland, paper WJ4
- 29 HAMILTON D.C., Ph.D. Thesis, University of Hull (1975)
- 30 GONDHALEKAR A., HOLZHAUER E., HECKENBERG N.R.,  
Phys. Lett. A **64** 229 (1973)

- 31 GONDHALEKAR A, HECKENBERG N R, HOLZHAUER E  
IEEE J. Quant. Elec., **QE 11**, 103 (1975)
- 32 BLACK J.G., KOLODNER P., SHULTZ M.J., YABLONOVITCH E.,  
BLOEMBERGEN N., Phys. Rev. A, **19** 704 (1979)
- 33 BARNARD J.A., Trans. Farad. Soc. **55** 947 (1959)
- 34 DYER P.E., BISHOP M., TAIT B.L., J. Phys. E. **20** 82 (1987)
- 35 DANEN W.C., RIO V.C., SETSER D.W.,  
J. Am. Chem. Soc. **104** 5431 (1982)
- 36 CHIN S.L., EVANS D.K., McALPINE R.D., SELANDER W.N.,  
Appl. Opt. **21** 65 (1982)
- 37 DYER P.E., JAMES D.J., RAMSDEN S.A., J. Phys. E. **5** 1162 (1972)
- 38 RAOUF D.N., PhD Thesis, University of Hull (1987)
- 39 WEULERSSE J.M., GENIER R., Appl. Phys. **24** 363 (1981)
- 40 LEO R.M., HAWKINS H.L., JOHN P., HARRISON R.G.,  
J. Phys. E: Sci. Instrum. **13** 658 (1980)
- 41 PARKER J.G., RITKE D.N., J. Chem. Phys. **59** 3713 (1973)
- 42 DEWHURST R.J., Private Communication
- 43 FRIED A., BERG W.W., Opt. Lett. **8** 160 (1983)
- 44 ROSENGREN L.G., Appl. Opt. **14** 1960 (1975)
- 45 TAM C.A., *"Ultrasensitive Spectroscopic Techniques"*, Academic Press,  
N.Y. (1983)
- 46 FRAIM F.W., MURPHY P.V., FERRAM R.J.,  
J. Acoust. Soc. Am. **53** 3713 (1973)
- 47 MORSE P.M., *"Vibration and Sound"*, McGraw-Hill (1936)
- 48 WAKE R.W., AMER N.M., Appl. Phys. Lett. **34** 379 (1979)
- 49 FUSS W., KOMPA K.L., Prog. Quant. Electr. **7** 117 (1981)
- 50 LETOKHOV V.S., Phys. Today **30** 23 (1977)
- 51 BLOEMBERGEN N., YABLONOVITCH E., Phys. Today **31** 23 (1978)

- 52 SCHULTZ P.A., SUBDO A.S., KRAJNOVITCH D.J., KWOK H.S.,  
SHEN Y.R., LEE Y.T., *Annu. Rev. Phys. Chem.* **30** 379 (1979)
- 53 LETOKHOV V.S., *"Nonlinear Laser Chemistry"*, Springer-Verlag (1983)
- 54 BELL A.G., *Proc. Am. Ass. Adven. Sci.* **29** 115 (1880)
- 55 TYNDALL J.G., *Proc. R. Soc. Lond.* **31** 307 (1881)
- 56 VIENGEROV M.L., *Dokl. Akad. Nauk. SSSR* **19** 687 (1938)
- 57 GORELIK G., *Dokl. Akad. Nauk. SSSR* **54** 779 (1946)
- 58 DEWEY C.F., KAMM R.D., HACKETT C.E.,  
*Appl. Phys. Lett.* **23** 633 (1973)
- 59 BEADLE B.C., DONOGHUE B.R., AERE Harwell, Private Comm. (1980)
- 60 KREUZER L.B., *"The Physics of Signal Generation and Detection"*, from  
*"Optoacoustic Spectroscopy and Detection"* (Ch.1), Ed. PAO Y.H.,  
Academic Press (1977)
- 61 DEWEY C.F., *"Design of Optoacoustic Systems"* from *"Optoacoustic  
Spectroscopy and Detection"* (Ch.2), Ed. PAO Y.H., Academic Press  
(1977)
- 62 ROBINSON P.J., HOLBROOK K.A., *"Unimolecular Reactions"*,  
Wiley-Interscience (1972)
- 63 AMBARTZUMIAN R.V., CHERALIN N.V., DOLJIKOV N.S.,  
LETOKHOV V.S., RYABOV E.A., *Chem. Phys. Lett.* **25** 515 (1974)
- 64 ISENER N.R., MERCHANT V., HALLSWORTH R.S., RICHARDSON M.C.,  
*Can. J. Phys.* **51** 1281 (1973)
- 65 LYMAN J.L., LEARY K.M., *J. Chem. Phys.* **69** 1858 (1978)
- 66 CHERALIN N.V., DOLJIKOV N.S., LETOKHOV V.S., LOKHAM V.N.,  
SHIBANOV A.N., *Appl. Phys.* **18** 191 (1977)
- 67 SCHOLES W.A., *Lasers and Applications* **6** 58 (1987)
- 68 QUICK C.R., WITTIG C., *J. Chem. Phys.* **69** 4201 (1978)
- 69 BEADLE B.C., DONOGHUE B.R., AERE Harwell, Private Comm. (1980)
- 70 COX D.M., *Opt. Commun.* **24** 336 (1978)

- 71 EVANS D.K., McALPINE R.D., ADAMS H.M.,  
Israel J. Chem. **24** 187 (1984)
- 72 SEDER T.A., WEITZ E., Chem. Phys. Lett. **104** 545 (1984)
- 73 BACK R.A., EVANS D.K., ADAMS H.M., Can. J. Chem. **62** 1525 (1984)
- 74 WALLER I.M., EVANS D.K., McALPINE R.D., Appl. Phys. B. **32** 75 (1983)
- 75a JANG-WREN J.C., SETSER D.W., FERRERO J.C., J. Phys. Chem. **89** 414  
(1985)
- 75b STONE J., THIELE E., GOODMAN M.F., STEPHENSON J.C., KING D.S.,  
J. Chem. Phys. **73** 2259 (1980)
- 76 *"Laser Induced Chemical Processes"*  
Ed. Steinfeld J.I., Plenum Press (1981)
- 77 HIRSCHFELDER J.O., CURTIN C.F., BIRD R.B., *"Molecular Theory of  
Gases and Liquids"* J. Wiley & Son (1st ed., 2nd printing)
- 78 HOLBROOK K.A., SHAW C.J., OLDERSHAW G.A., DYER P.E.,  
Int. J. Chem. Kinet. **18** 1215 (1986)
- 79 BARNES A.J., HALLAM H.E., Trans. Faraday Soc. **66** 1932 (1970)
- 80 BIALKOWSKI S.E., GUILLORY W.A., J. Chem. Phys. **67** 2061 (1977)
- 81 GOODALE J.W., EVANS D.K., IVANCO M., McALPINE R.D.,  
*"The Mechanism of the Infrared Laser Induced Multiphoton  
Decomposition of Ethyl Alcohol"*, Atomic Energy of Canada Research  
Company, Chalk River Nuclear Laboratories
- 82 COHOE C.F., WALTERS W.D., J. Phys. Chem. **71** 2326 (1967)
- 83 Intentionally blank
- 84 LONGFIELD J.E., WALTERS W.D., J. Am. Chem. Soc. **77** 6098 (1955)
- 85 ZUPAN M., WALTERS W.D., J. Phys. Chem. **67** 1845 (1963)
- 86 HOLBROOK K.A., PALMER J.S., Trans. Faraday Soc. **46** 114 (1950)
- 87 HEARNE G.W., EVANS T.W., YALE H.K., HOFF M.C.,  
J. Am. Chem. Soc. **75** 1392 (1953)
- 88 BARNARD J.A., HUGHES H.W.D., Trans. Faraday Soc. **56** 55 (1960)

- 89 McRAE G.A., YAMASHITA A.B., GOODALE J.W.,  
J. Chem. Phys. **92** 5997 (1990)
- 90 API Tables (1952)
- 91 McCRAE G.A., Atomic Energy of Canada Ltd., Chalk River Laboratories,  
Private Communication
- 92 BENNET K., BYER R.L., Appl. Opt. **19** 2408 (1980)
- 93 SIEGMAN, "*Lasers*", University Science Books (Mill Valley, Ca.) (1986)
- 94 SVELTO O., "*Principles of Lasers*" 2nd ed., Plenum Press (N.Y) (1982)
- 95 GERRY E.T., LEONARD D.A., App. Phys. Lett. **8** 227 (1966)
- 96 WILHOIT R.C., ZWOLINSKI B.J.,  
*The NBS tables of chemical and thermodynamic properties.*  
J. Phys. Chem. Ref. Data **2** (1973)
- 97 HOLBROOK K.A., "*Current Aspects of Unimolecular Reactions*",  
Eyre & Spottiswoode Ltd, Thanet Press (Margate) (1982)
- 98 O'SHEA D., CALLEN W.R., RHODES W.T., "*An Introduction to Lasers  
and their Applications*", Addison-Wesley Pub. Co.
- 99 HULL D.M., STEWART A., "*Laserbeam Profiles - Principles and  
Definitions*", Lasers & Applications, November 75 (1985)  
HULL D.M., STEWART A., "*Laserbeam Profiles - Equipment and  
Techniques*", Lasers & Applications, November 71 (1985)
- 100 PRATT G., RODGERS D., J. Chem. Soc., Faraday Trans. 1, **75** 1089 (1979)
- 101 ZHITNEVA G.P., MARKINA I.A., PSHEZHETSKII S.Ya.,  
High Energy Chemistry **21** 544 (1987)
- 102 U.S. Nat. Bur. Stand., Circular 461 (1947)
- 103 as for 100
- 104 HOLBROOK K.A., Chem. Soc. Rev. 163 (1986)
- 105 AMBARTZUMIAN R.V., KNYAZEV I.N., LOBKO V.V., MAKAROV G.N.,  
PURETZKY A.A., Appl. Phys. **19** 75 (1979)
- 106a HALL R.B., KALDOR A., J. Chem. Phys. **70** 4027 (1979)

- 106b ASHFOLD M.N.R., HANCOCK G., *"Gas Kinetics and Energy Transfer"*,  
A Specialist Periodical Report, Ed. P.D. Ashmore & R.J. Donovan,  
Royal Society of Chemistry, London, **4** 73 (1980)
- 107 BHATNAGAR R., DYER P.E., OLDERSHAW G.A.,  
Chem. Phys. Lett. **61** 339 (1979)

## APPENDIX

## A1 – Determination of the Speed of Sound from Optoacoustic Traces

The optoacoustic traces from the work carried out on 2,2-dimethyloxetane in the 1.5 m long cell were analysed and obvious resonances were identified. The dominant frequencies measured were 1.1 kHz, 6.99 kHz and 17 kHz. To use the Bessel function approach described in Section 1.3.3 to calculate the speed of sound  $v_s$ , the source of these resonances must be established. It is helpful to begin with an idea of the speed which may be attained as follows: The speed of a compressional wave  $v_s$  in a gas of density  $\rho$  and pressure  $p$  is given by

$$v_s = \sqrt{\frac{\gamma p}{\rho}} \quad \text{A1}$$

where  $\gamma = C_p/C_v$

$C_p$  and  $C_v$  being the specific heats at constant pressure and volume respectively. For an ideal gas

$$\frac{p}{\rho} = \frac{RT}{m}$$

where  $m$  is the kg molecular weight. So Eq. A1 becomes

$$v_s = \sqrt{\frac{\gamma RT}{m}} \quad \text{A2}$$

Thus the speed of sound is independent of pressure but proportional to  $\sqrt{T}$ . Values of  $v_s$  for the gases used in this work are presented in Table 2.3-1. Since for polyatomics  $\gamma$  typically falls in the range 1.2-1.3, then for 2,2-dimethyloxetane (molecular weight 86 g.mole<sup>-1</sup>)  $v_s$  is found to be in the range 186-194 ms<sup>-1</sup>. Choosing an average value of 190 ms<sup>-1</sup>, the cell acoustic resonances can then be predicted.

The longitudinal mode of a cylindrical cell is given by

$$f_j = \frac{v_s n_z}{2l} \quad (\text{from Eqs. 1.3-1, -2})$$

The lowest order mode will be for  $n_z=1$ , which gives  $f=6.3\text{kHz}$ . While this is approximately the value of an observed frequency (6.99kHz), the author is hesitant to assign it as a longitudinal resonance. Such resonances are not expected because the absorption is too weak.

The transverse modes have frequencies  $f_j$  of

$$f_j = \frac{v_s \alpha_{mn}}{2a} \quad (\text{from Eqs. 1.3-1 and -3})$$

(where  $m$  now signifies a transverse resonance mode rather than the molecular mass). The radius of the 1.5cm cell,  $a$ , is 1cm so the possible frequencies are

$mn$	$\alpha_{mn}^{(47)}$	$f_j / \text{kHz}$
00	0	0
01	1.220	11.6
10	0.586	5.6
11	1.697	16.1
12	2.717	25.8
20	0.972	9.2
02	2.233	21.2

The condition  $m=n=0$  describes the expansion of the thermal pulse at zero frequency. For a centred beam, which is the condition of all the work in this thesis, azimuthal resonances should not be excited, and therefore frequencies for which  $m$  is non-zero are highly unlikely. It will be noted however, that

none of the above resonant frequencies fit very well with those observed, even those for  $m_n$  of 01 and 02 which were most likely.

The validity of using a value for the speed of sound in 2,2-dimethyloxetane of  $190 \text{ ms}^{-1}$  was verified by measuring the time interval between the laser pulse trigger, and the arrival of the first acoustic transient signal. Readings from the signals from For the 1.5cm long, 1cm radius cell, this gave  $v_s = 186 \text{ ms}^{-1}$  with an uncertainty of as much as  $\pm 20 \text{ ms}^{-1}$ , while those for the 8cm long, 11mm radius cell (Fig.2.2-1), give  $v_s = 192 \text{ ms}^{-1}$ . Note for the longer cell the microphone to centre-of-cell distance was 20.58mm, and this distance was used in the  $v_s$  calculation. These values are in excellent agreement, and within 5% of the theoretical value.

So while the 7kHz resonance may be attributed to a longitudinal mode ( $n=1$ ) it is nevertheless unlikely. Furthermore since none are radial resonances, all the observed frequencies must be attributed to microphone resonances. Clearly, calculation of the speed of sound from the cell resonances is not possible, because at low pressures the microphone resonances mask them. Under such circumstances, it would be better to rely solely on the measurement of the time of arrival of the first pulse, a technique which for best accuracy requires as short an oscilloscope timebase as possible, precise triggering by the laser.

## A2 - Energy Absorbed (Differential Ratio Method)

In the differential ratio method for calibration of the OA signal (Fig.2.3-1), the energy absorbed by the gas is given by;

$$\begin{aligned} E_{abs} &= E_{in} - E_{out} && [A2.1] \\ &= E_{in} (1 - T) \end{aligned}$$

where  $T = E_{out}/E_{in}$

and  $T = V_{2F}/V_{2E} = (S_2 T_1 T_3^2 R_2 T E_o) / (S_2 T_1 T_3^2 R_2 E_o)$

also  $V_{1F}/V_{1E} = V_{1E}/V_{1F} = 1$

therefore  $T = (V_2/V_1)_F / (V_2/V_1)_E$

from Eq.A2.1:

$$E_{abs} = E_{in} \{ 1 - [(V_2/V_1)_F / (V_2/V_1)_E] \} \quad [A2.2]$$

Now  $E_o'$  rather than  $E_{in}$  will be measured (via a calibration to  $V_1$ ) and

$$E_{in} = T_3 E_o'$$

### A3 - Molecular Diffusion from the Focal Volume

A simple analysis of molecular diffusion from the focal volume (used in the experiments which used a uniform beam) is as follows: From Table 5.1-1, the time-interval between collisions when the pressure is 50mtorr (i.e. for 'collision-free' experiments) is typically 1.6 $\mu$ s. Under these conditions, during the time of the laser pulse, a molecule will move freely through space without colliding; therefore, movement out of the laser beam is by free movement rather than diffusion.

Also from Table 5.1-1, the mean speed ( $\langle c \rangle = ((8RT)/(\pi m))^{0.5}$ ), at 293 K, range from 250 - 370 m.s<sup>-1</sup>, but take  $\langle c \rangle = 291$  m.s<sup>-1</sup> for butanol as a typical value. As described in Section 2.1.2, the typical full basewidth of the laser pulses used for this work was 490 ns (50 ns FWHM). In this time, this typical molecule moves 0.14 mm. The fraction of molecules lying within 0.14 mm of the beam edge (beam radius 0.52 mm), constitute a percentage of;

$$\frac{(0.52)^2 - (0.38)^2}{(0.52)^2} \times 100\% \approx 47\%$$

Only half of these (~24%) will be moving away from the volume, and less than half of the molecules initially within the focal volume, might leave during the pulse. This amount is not considered to be a problem, since, for this work, the tail of the pulse contained so little energy. Repeating the same calculation, but using the time interval given by the basewidth of the gain-switched spike (~200 ns), reveals that only <11% of molecules leave the focal volume during that critical time. Wittig (68) calculated a figure of 12% for his focussed system, and comparison with yields obtained with shorter laser pulses, showed no difference, thus illustrating the insignificance of 'diffusion' effects.

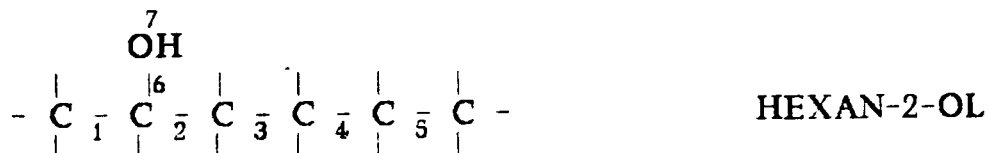
In conclusion, diffusion did not occur during the collision-free experiments. Furthermore, free movement, of the molecules from the focal volume, is considered to be insignificant.

## A4 - The Group Contribution Method

Reference is made in the main body of the text, to the formation of radicals by the breaking of the molecular bonds. In some instances the bond dissociation energy,  $D$ , for a particular bond is available from tables (1), but frequently it must be calculated, and the calculation requires knowledge of heats of formation for the free radicals *viz.*:

$$D(R-X) = \Delta H_f^0(\cdot R) + \Delta H_f^0(\cdot X) - \Delta H_f^0(RX)$$

In some instances, such as for  $\cdot CH_3$ ,  $\Delta H_f$  is available from tables (1,2,2b). But more often than not it too must be calculated, and that is when the Group Contribution Method (GCM) becomes invaluable. A "group" may be considered to be a polyvalent atom in a molecule connected to two or more ligands together with all of the ligands. The GCM of calculating heats of formation is fully described in references (2) and (2b). It is sufficient for the purposes of this thesis though to work through a particularly simple application: it has not been necessary to involve corrections for example for hindered rotations, ring structures, or non-bonded interactions (2,2b). The bonds of most interest to hexanol in this work are labelled 1 to 7 in the drawing below.



The groups that are considered to make up hexan-2-ol are:

GROUPS	$\Delta H_f^0/\text{kcal.mol}^{-1}$
2 x (C-H <sub>3</sub> C)	2 x (-10.1)
C-HOC <sub>2</sub>	-7.00
O-HC	-37.88
3 x (C-C <sub>2</sub> H <sub>2</sub> )	3x -4.93
$H_f(C_6H_{13}OH)$	-79.87

Consistent with the definition of a "group", these have been derived by taking each C and O atom, but not H, in the molecule (written as C- and O-), and considering which other atoms are immediately attached to it. For example, the first carbon in the chain has attached to it three H and the second C; hence the notation is C-H<sub>3</sub>C. The same principle may be applied to radicals. Table A4-1 lists the results of calculations required for this work. The accuracy of these calculations is not necessarily as is implied in the table viz. to 2 dec. places. As a guide, calculations were carried out for experimentally determined values. For example, while  $\Delta H_f^0(\text{iso-propyl})$  was calculated as 20.79 kcal.mol<sup>-1</sup>, other values of 20.7 (NBS), 21.0 (2), 22.6±1.8 (1) and 24.01±0.50 (5) kcal.mol<sup>-1</sup> may be found in the references. As a further example,  $\Delta H_f^0(\cdot C_2H_5)$  is calculated as 25.74 kcal.mol<sup>-1</sup>, whereas references give 25.9±1.3 (1), 28.19 (4 Hase via Tsang), and 28.36 ± 0.4 (3) kcal.mol<sup>-1</sup>, and the calculation of  $\Delta H_f^0(H)$  gives 52.6 kcal.mol<sup>-1</sup> compared to a value of 52.103 ± .001 kcal.mole<sup>-1</sup> (1). There is good reason, therefore, only to read the calculated values to two significant figures. Furthermore, there is an indication from the more recent experimental results (5.4), that the calculations may provide values that are a little on the low side.

BOND	Do /kcal.mole(-1)	RADICAL	DELTA (Ho) /kcal.mole(-1)
$\dot{\text{O}}-\text{C}$	-0.12	$(\text{CH}_3)\dot{\text{C}}\text{H}(\text{CH}_2)(\text{CH}_3)$	12.34
$\dot{\text{C}}-\text{COH}$	32.76	$(\text{CH}_3)\text{CH}\dot{\text{O}}(\text{CH}_2)(\text{CH}_3)$	-19.13
		$(\text{CH}_2)(\text{CH}_3)\dot{\text{C}}\text{HOH}$	-20.15
		$\dot{\text{C}}\text{HOH}(\text{CH}_2)_2(\text{CH}_3)$	-25.1
		$(\text{CH}_3)\text{CHOH}(\dot{\text{C}}\text{H}_2)$	-19.14
		$(\text{CH}_3)\text{CHOH}(\text{CH}_2)(\dot{\text{C}}\text{H}_2)$	-24.09
		$\dot{\text{C}}\text{HOH}(\text{CH}_2)_3(\text{CH}_3)$	-30.05
		$(\dot{\text{C}}\text{H}_2)(\text{CH}_2)_2(\text{CH}_3)$	15.84
		$(\text{CH}_3)\dot{\text{C}}\text{H}(\text{CH}_2)_3\text{CH}_3$	2.44
		$(\text{CH}_3)\text{C}\dot{\text{O}}(\text{CH}_2)_3\text{CH}_3$	-29.03

**Table A4-1:** Values obtained from group contribution method calculations, for use in further group contribution method calculations.

## A5 - Effect of Collisions on Absorption Linewidth

In this Appendix, the effect of collision broadening on the absorption linewidth of the irradiated molecules is considered, using ethanol as a typical molecule. As a further example, the linewidth values are compared against those for CO<sub>2</sub> and for typical CO<sub>2</sub> laser gas mixes.

The net rate of excitation for molecules subjected to laser irradiation is generally described by the overall rate equation

$$dN_{i+1} = \frac{-dN_{i+1}}{dt} \Big|_{\text{spon}} + \frac{-dN_i}{dt} \Big|_{\text{stim up}} + \frac{-dN_{i+1}}{dt} \Big|_{\text{stim down}} \quad (\text{A5-1})$$

Clearly, decomposition is probable when the downward transitions (spontaneous and stimulated relaxation) do not successfully compete with the upward transitions (stimulated excitation).

Molecules affected by the processes of the two parts of the stimulated component shown below (up and down transitions) (93), exhibit oscillations that are fully coherent in phase and amplitude with the applied signal. The net process is said to be COHERENT.

$$\frac{-dN_{i+1}}{dt} \Big|_{\text{stim down}} = k n(t) N_{i+1}(t)$$

$$\frac{dN_{i+1}}{dt} \Big|_{\text{stim up}} = k n(t) N_i(t)$$

where  $k$  is a constant for a particular wavelength, and  $n(t)$  is proportional to the applied signal intensity (W/cm<sup>2</sup>).

The radiative (eg. fluorescence) and non-radiative components of the spontaneous decay term are both INCOHERENT processes: ie the oscillations are not in phase with the applied signal. An example of non-radiative decay is intra-molecular energy transfer (v-v) and inelastic collisions. The result is thermalisation of the molecules. Depending on conditions, the degree may be more or less than the radiative

$$\left. \frac{dN_{i+1}}{dt} \right|_{\text{spont}} = -\gamma_{i+1,i} N_{i+1}(t)$$

$$\gamma_{i+1} = \gamma_{\text{rad}} + \gamma_{\text{nr}}$$

Therefore Eq.(5.1-1) becomes

$$k n(t) \times [N_1(t) - N_2(t)] - \gamma_{21} N_2(t)$$

The relationship of  $N_i$ ,  $N_{i-1}$  and  $N_{i+1}$  can be well described as a Boltzmann if it is suspected that the gas is in thermal equilibrium.

The absorption linewidth/bandwidth is the resultant of coherent and incoherent processes, each having a particular degree of effect depending on the conditions at that time. If the dominant processes are coherent, then the linewidth will be inhomogenously broadened, by which it is meant that each molecule does not see the same energy perturbation. The type of condition that would encourage such broadening is when a molecule, small enough to have discrete energy levels, is irradiated at collision-free pressure: rotational hole-burning often (but not always) results from the coherent transitions.

At higher pressures, collisions cause dephasing between the simultaneous applied signal (upward transition) and stimulated absorption (downward transition) ie. collisions remove coherency and cause homogenous broadening of the absorption linewidth. Transitions in the quasicontinuum are also characterised by incoherent interactions. If there is no bottleneck in the

discrete section, and incoherent interactions dominate (because of very few discrete levels), and collision transition rates and unimolecular dissociation rates are negligible, then the linear rate equation (5.1-1) stated earlier is applicable.

The extent of doppler broadening from a centre frequency  $\nu_{ao} = \omega_{ao}/2\pi$  for gas molecules of rest-mass  $M$ , and temperature  $T$  is given by the FWHM of a gaussian curve,  $\Delta\omega_d$  (93,94):

$$\Delta\omega_d = \omega_{ao} \sqrt{\frac{(8 \ln 2) kT}{Mc^2}}$$

where  $Mc^2$  is the rest-mass energy of the molecules, and  $k$  and  $c$  take the usual definition of the Boltzmann constant and speed of light respectively. The Doppler linewidth,  $\Delta\nu_d$  is then given by  $\Delta\omega_d/(2\pi)$ . In eV,  $kT$  at room temperature is 25meV, while the rest mass energy of a single proton is  $\sim 10^9$ eV. Thus the fractional doppler broadening for ethanol (molecular weight 46)  $\Delta\omega_d/\omega_{ao} \sim \sqrt{((8.5 \times 25 \times 10^{-3})/46 \times 10^9)} = 1.7 \times 10^{-6}$ ; which is similar to that of  $CO_2$  (molecular weight 44),  $1.8 \times 10^{-6}$  giving  $\Delta\nu_d(C_2H_5OH) \sim 48$  MHz and  $\Delta\nu_d(CO_2) \sim 50$  MHz i.e. the doppler linewidths of the ethanol and  $CO_2$  systems are essentially identical.

The collision broadened linewidth  $\Delta\nu_c$  for a  $CO_2$  laser is given by (94):

$$\Delta\nu_c = 7.58 (\psi_{CO_2} + 0.73\psi_{N_2} + 0.64\psi_{He}) P (300/T)^{0.5} \text{ MHz} \quad (A5-2)$$

where  $\psi$  are the fractional partial pressures of the gas mixture, and  $P$  is the total pressure (in torr). For a typical mix  $CO_2 : N_2 : He$  of 2.4:1.2:4.9,  $\Delta\nu_c/\text{torr}$  is 5.4 MHz, and  $\Delta\nu_c \approx \Delta\nu_d$  at roughly 9 torr (for atmospheric pressures,  $\Delta\nu_c \sim 4$  GHz). Fig. A5-1 confirms these calculations with actual

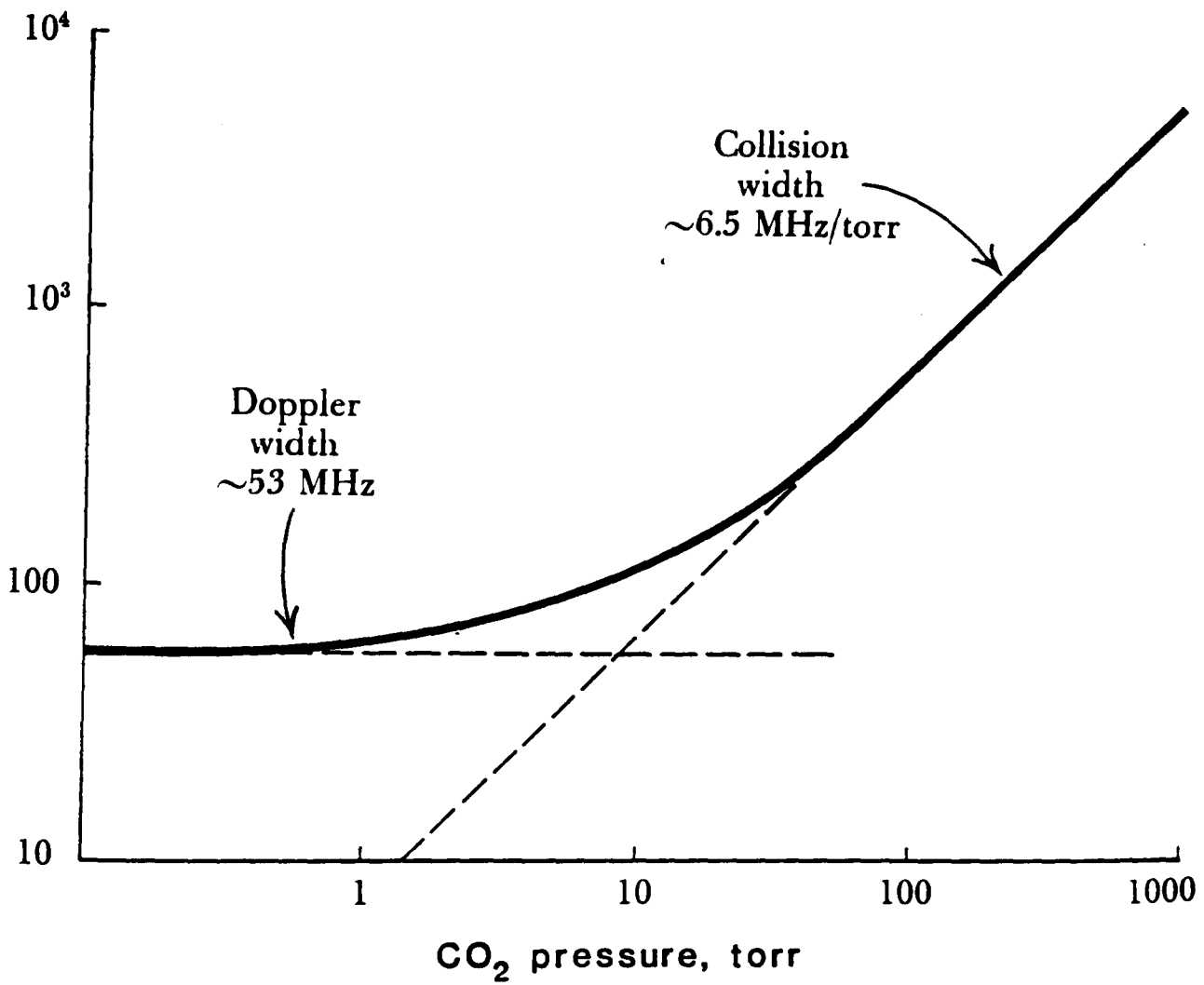


Fig. A5-1 Linewidth versus pressure in a typical CO<sub>2</sub> laser mix from Ref. 93

measurements from unspecified CO<sub>2</sub> :N<sub>2</sub> :He concentrations (94,95). From Eq. (A5-2), it is established that  $\Delta\nu_c$ /torr for **pure** CO<sub>2</sub> is of similar magnitude viz. 7.6MHz, and that in this case  $\Delta\nu_c \approx \Delta\nu_d$  at roughly 7torr. The similarity between an ethanol system and CO<sub>2</sub> system will now be established. The more general formula for the FWHM collision broadened linewidth  $\Delta\nu_c$  is a lorentzian curve given by (94):

$$\Delta\nu_c = \frac{1}{\pi\tau_c} = \frac{Z}{\pi} \quad (\text{A5-3})$$

where  $\tau_c$  is the average time between collisions (ie. mean free time), and the collision frequency,  $Z$ , is the average number of collisions per unit time for 1 torr of gas; note that the pressure for these calculations must be in Nm<sup>-2</sup> (1 torr = 133.3Nm<sup>-2</sup>). From Table A5-1, for ethanol  $\Delta\nu_c$  at 1torr is 3.4MHz. Since  $Z$  is proportional to the pressure,  $\Delta\nu_d \approx \Delta\nu_c$  at a pressure of 14torr. The same equation and table for CO<sub>2</sub> gives  $\Delta\nu_c=2.8\text{MHz}$ , with  $\Delta\nu_d \approx \Delta\nu_c$  at a pressure of 18torr. These CO<sub>2</sub> numbers are a factor of two different from those obtained through Eq. A5-2, yet both are the FWHM linewidths.

Even though there is consequently an element of doubt (factor of 2) about  $\Delta\nu_c$  for ethanol, the conclusion is clear-cut: that is, for mid-band absorption of molecules used in this work, collision broadening of the absorption linewidth typically dominates at higher pressures than used here.

Table A5-1

Calculations for collision diameters,  $\sigma$ , collision frequency, Z, and collision interval. Pressures are calculated for when the interval between collisions is 600ns (basewidth pulse length), and 1 $\mu$ s. Collision free conditions are expected when the collision interval is 1 $\mu$ s.

Gas	molar mass /g.mole(-1) Ref. (1)	$\langle c \rangle$ /m.s(-1)	$\sigma$ /nm Ref. (77)	Z (at 1 torr) /10(7). collisions.s(-1)	collision interval (at 1 torr) /ns	pressure for which there is a 0.6 $\mu$ s collision interval /mtorr	collision-free pressure (using 1 $\mu$ s collision interval) /mtorr	$\sigma$ /nm	notes
methanol	32.04	443.01	0.359	0.837	119	199.10	119.46		
ethanol	46.07	369.44	0.446	1.077	93	154.69	92.81		
propanol	60.11	323.43	use C3H8	1.233	81	135.13	81.08	0.51	C3H8
butanol	74.12	291.26	use nC4H10	1.068	94	156.11	93.67	0.5	nC4H10
pentanol	88.15	267.08	use nC5H12	1.317	76	126.52	75.91	0.58	nC5H12
hexanol	102.18	248.07	use nC6H14	1.266	79	131.64	78.99	0.59	nC6H14
3,3DMO	86.13	270.19	use 0.6	1.426	70	116.87	70.12	0.6	estimate based on cyclohexane
CO2	44.01	377.99	0.4	0.887	113	187.96	112.78		
cyclohexane	84.16	273.34	0.61	1.491	67	111.77	67.06		
ethanol:CO2 (1:8.96)	23.04		0.380	0.873	115	190.84	114.50	Empirical formula for mixed gases: $\sigma_{ij} = 0.5(\sigma_i + \sigma_j)$ and reduced mass $m^* = Ma.Mb/(Ma+Mb)$	
ethanol:cycloC6H14(1:9)	29.77		0.485	1.434	70	116.24	69.75		
propanol:cycloC6H14 (1:9)	35.07		0.56	1.460	69	114.19	68.52		
butanol:cycloC6H14 (1:9.63)	39.41		0.555	1.451	69	114.89	68.94		
pentanol:cycloC6H14 (1:9.18)	43.05		0.595	1.462	68	113.98	68.39		
hexanol..no dilution for yield tests									
3,3DMO:cycloC6H14 (1:8.77)	42.57		0.605	1.468	68	113.56	68.14		

## Notes.

1. Values for  $\sigma$  were taken from Ref. (77), though for most alkanols  $\sigma$  could not be found. In those cases, for an order of magnitude calculation, the associated alkane value (from (77)) is used.
2. According to Ref. (6), Z for 2,2DMO (at 125ns pulse length) is 1.37E7 torr(-1)s(-1). The estimate of  $\sigma$  for 3,3DMO therefore seems reasonable.

$$\langle c \rangle = \sqrt{\frac{8 RT}{\pi m}}$$

$$z = \sqrt{2} \pi \sigma^2 \langle c \rangle n$$

- $\langle c \rangle$  = average thermal velocity  
R = universal gas constant  
T = temperature  
m = molar mass  
n = number of molecules per unit volume